Cassini RPWS Instrument Calibrations

FLT Unit

Department of Physics and Astronomy
The University of Iowa
Iowa City, IA 52242

2003

Prepared by:

G. B. Hospodarsky, Operation Engineer	Date

Approved by:

D. L. Kirchner, Project Engineer	Date
R. L. Huff, Engineering Group Manager	Date
W. S. Kurth, Operation Manager	Date
D. A. Gurnett, Principal Investigator	Date

Document Revision Page

TABLE OF CONTENTS

1.0 Introduction/Purpose/Scope

2.0 Applicable Documents
- 2.1 JPL Documents
- 2.2 UI Documents
- 2.3 CETP Documents
- 2.4 Meudon Documents
- 2.5 IRFU Documents
- 2.6 Software Documents

3.0 Overview of Cassini RPWS Instrumentation

4.0 Cassini RPWS Design Aspects

5.0 Discussion of RPWS Calibration Methods

6.0 Electric Antenna Subsystem
- 6.1 Effective Lengths
- 6.2 Base Capacitance

7.0 Magnetic Search Coil (MSC)
- 7.1 Amplitude Calibration
- 7.2 Phase Calibration
- 7.3 Noise Level

8.0 Langmuir Probe (LP)

9.0 Low Frequency Digital Receiver (LFDR)
- 9.1 End-to-End Calibration
- 9.2 Input Voltage Versus Output Data Numbers
- 9.3 Channel-to-Channel Gains
- 9.4 Filter Bandwidths - Equivalent Noise Bandwidths

10.0 Medium Frequency Receiver (MFR)
- 10.1 End-to-End Calibration
- 10.2 Input Voltage Versus Output Data Numbers
- 10.3 Channel-to-Channel Gains
- 10.4 Filter Bandwidths

11.0 High Frequency Receiver (HFR)

12.0 Wideband Receiver (WBR)

- 12.1 End-to-End Calibration
- 12.2 Frequency Response (Filter Response)
- 12.3 Gain Calibration
- 12.4 AGC Characteristics

13.0 Waveform Receiver (WFR)

- 13.1 End-to-End Calibration
- 13.2 Frequency Response (Filter Response)
- 13.3 Gain Calibration
- 13.4 AGC Characteristics
- 13.5 Phase Calibration

1.0 Purpose

The purpose of this document is to provide calibrations for the Cassini Radio and Plasma Wave Subsystem and other information important for the proper interpretation of data obtained from the instrument. These calibrations are used to convert the instrument output data to geophysical units for the purpose of data reduction and analysis.

2.0 Applicable Documents

2.1 JPL Documents

2.2 UI Documents

2.2.1 Instrument Hardware and Software Specification for the Cassini Radio and Plasma Wave Investigation

2.2.2 User Guide and Software Operations Manual

2.3 CETP Documents

2.3.1 Cassini MSC-RPWS-PFU Transfer Functions, A. Meyer, Centre d'Etudes des Environnements Terrestre et Planétaires Vélizy, CNET, Issy-les-Moulneaux, France, March, 1996

2.4 Meudon Documents

2.5 IRFU Documents

2.5 Software Documents

3.0 Overview of Instrumentation

The RPWS instrumentation consists three electric antennas, three magnetic antennas, a Langmuir probe and its associated electronics, and five specialized receivers designed to address the scientific objectives and performance requirements discussed in the two previous sections. In this section we describe each of these elements of the instrument.

3.1 Block Diagram

A simplified block diagram of the RPWS instrument is shown in Figure 3.1.1. Three monopole electric field antennas, labeled E_u, E_v, and E_w, are used to provide electric field signals

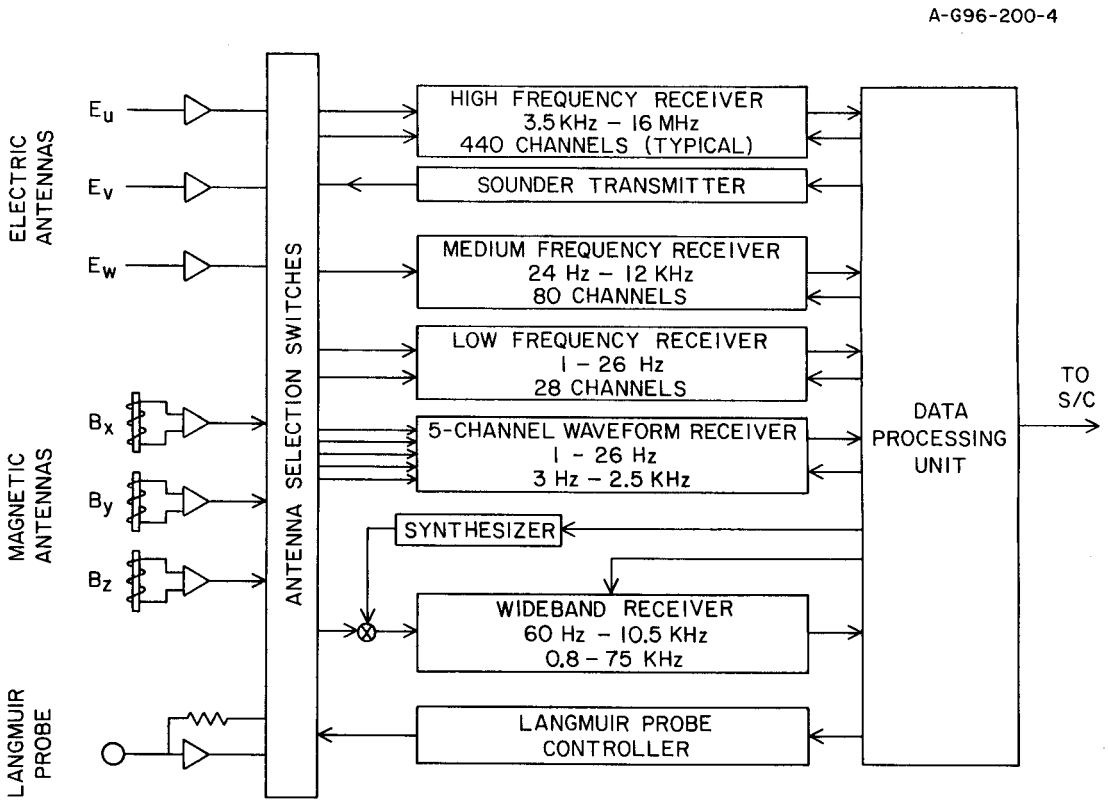

Figure 3.1.1

to the various receivers. The orientations of these three antennas relative to the x, y, and z axes of the spacecraft are shown in Figure 3.1.2. By electronically taking the difference between the voltages on the E_u and E_v monopoles, these two antennas can be used as a dipole, E_x, aligned along the x axis of the spacecraft. The E_u and E_v antennas also can be used to sound the local plasma by transmitting short pulses. In an alternate mode of operation, they can be biased and used as Langmuir probes to measure the phase velocity of density structures in the plasma. The tri-axial search coil magnetic antennas, labeled B_x, B_y, and B_z in Figure 3.1.1, are used to detect

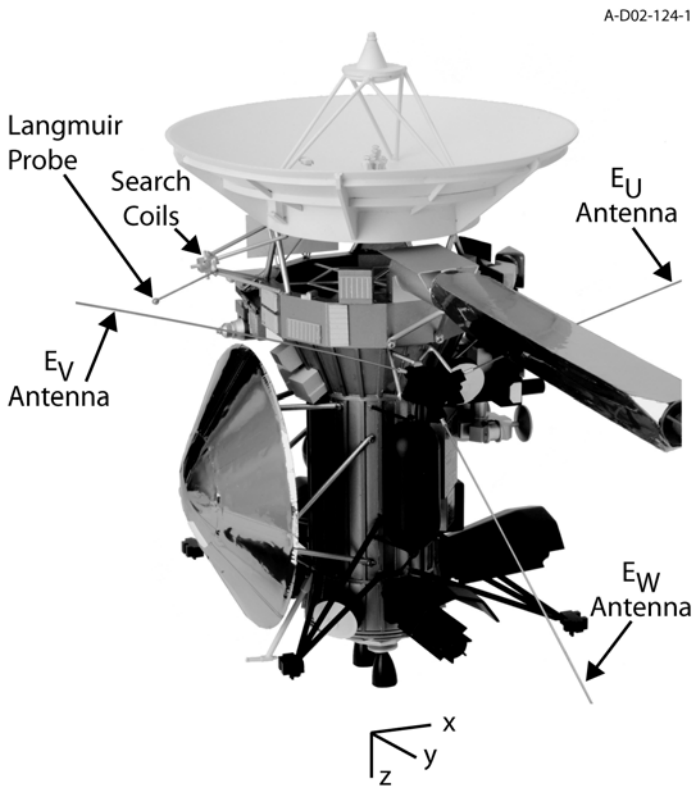

Figure 3.1.2

three orthogonal magnetic components of electromagnetic waves. The search coil axes are aligned along the x, y, and z axes of the spacecraft. The spherical Langmuir probe, shown at the bottom of the block diagram, is used for electron density and temperature measurements. Both the electric antennas and the Langmuir probe can be used to detect dust impacts.

Next, we consider the function of the five receivers shown in the middle column of the block diagram in Figure 3.1.1. These receivers are connected to the antennas described above by a network of switches in the block labeled "antenna selection switches," the details of which are not shown. The high frequency receiver (HFR) provides simultaneous auto- and cross-correlation measurements from two selected antennas over a frequency range from 3.5 kHz and 16 MHz. By switching the two inputs of this receiver between the three monopole electric antennas, this receiver can provide direction-of-arrival measurements, plus a full determination of the four Stokes parameters. The high frequency receiver includes a processor that performs all of its digital signal processing, including data compression. The high frequency receiver also includes a sounder transmitter that can be used to transmit short square wave pulses from 3.6 to 115.2 kHz. When used in conjunction with the high frequency receiver, the sounder can stimulate resonances in the plasma, most notably at the electron plasma frequency, thereby providing a direct measurement of the electron number density. The medium frequency receiver (MFR) provides intensity measurements from a single selected antenna over a frequency range from 24 Hz to 12 kHz. This receiver is usually operated in a mode that toggles every 32 seconds between the E_x electric dipole antenna and the B_x magnetic search coil, thereby providing spectral information for both the electric and magnetic components of plasma waves. The low frequency receiver (LFR) provides intensity measurements from 1 Hz to 26 Hz, typically from the E_x electric dipole antenna and the B_x magnetic antenna. The five-channel waveform receiver

(WFR) collects simultaneous waveforms from up to five sensors for short intervals in one of two frequency bands, either 1 to 26 Hz, or 3 Hz to 2.5 kHz. When connected to two electric and three magnetic antennas, this receiver provides wave normal measurements of electromagnetic plasma waves. The wideband receiver is designed to provide nearly continuous wideband waveform measurements over a bandwidth of either 60 Hz to 10.5 kHz, or 800 Hz to 75 kHz. These waveforms can be analyzed on the ground in either the temporal domain, or in the frequency domain (Fourier transformed) to provide high-resolution frequency-time spectrograms. In a special frequency-conversion mode of operation, the high frequency receiver can provide waveforms to the wideband receiver in a 25-kHz bandwidth that is tuneable to any frequency between 125 kHz and 16 MHz. Table 3.1.1 summarizes the characteristics of the five basic receivers described above.

The Langmuir probe controller shown in the block diagram is used to sweep the bias voltage of the probe over a range from -32 to +32 V in order to obtain the current-voltage characteristics of the probe, and thereby the electron density and temperature. The controller can also set the bias voltage on the E_u and E_v monopoles over a range from -10 to +10 V in order to operate them in a current collection mode for $\delta n_e/n_e$ measurements.

The RPWS data processing unit shown on the right-hand side of the block diagram consists of three processors. The first processor, called the low-rate processor, controls all instrument functions, collects data from the high frequency receiver, the medium frequency receiver, the low frequency receiver, and the Langmuir probe, and carries out all communications with the spacecraft Command and Data System (CDS). The second processor, called the high-rate processor, handles data from the wideband and five-channel waveform receivers and passes the data along to the low-rate processor for transmission to the CDS. The

third processor, called

TABLE 3.1.1

Summary of RPWS Receiver Characteristics

Receiver Section	Measurements	Spectral Range	Spectral Resolution	Temporal Resolution
High frequency Receiver (HFR)	For $E_1 = E_u, E_v$ or E_x and $E_2 = E_w$; $\|E_1\|^2$, $\|E_2\|^2$, $Re(E_1 \cdot E_2^*)$, $Im(E_1 \cdot E_2^*)$	3.5 kHz - 318 kHz 0.125-16.125 MHz	$\Delta f/f$ = 5, 10, 20% (log) Δf = 3.1 kHz - n×25 kHz (linear)	0.1 - 10 s/spectrum
Medium Frequency Receiver (MFR)	One of: E_x, E_u, E_v, E_w, B_x, B_z	24 Hz - 180 Hz 180 Hz - 1.5 kHz 1.5 kHz - 12 kHz	$\Delta f/f \simeq 13\%$ $\Delta f/f \simeq 7\%$ $\Delta f/f \simeq 7\%$	16 s/spectrum 16 s/spectrum 8 s/spectrum
Five-Channel Waveform Receiver (WFR)	Five of: E_x, E_u, E_v, E_w, B_x, B_y, B_z, LP	~1 Hz - 26 Hz 3 Hz - 2.5 kHz	0.2 Hz, typical 3.5 Hz typical	1 data set/5 min, typical, 1 data set/16 s, max
Low Frequency Receiver (LFR)	Two of: E_x, E_u, E_v, E_w, B_x, B_y, B_z, LP	~1 Hz - 26 Hz	$\Delta f/f$ = 12 %	1E + 1B spectrum/16s, typical
Wideband Receiver (WBR)	One of: E_x, E_u, E_v, E_w, B_x, LP	60 Hz - 10.5 kHz 0.8 kHz - 75 kHz	13.6 Hz, typical 109 Hz, typical	125ms/spectrum, typical

the data compression processor, is primarily used for data compression, but can also perform specialized operations such as on-board dust detection by using waveforms from the wideband receiver.

As shown in Figure 3.1.2, the RPWS hardware is mounted in several locations around the Cassini spacecraft. The main electronics package, which includes the medium frequency receiver and the digital processing unit, resides in bay 4 of the main spacecraft bus. The electric antenna deployment mechanisms and the high frequency receiver are mounted on a bracket on the +y side of the spacecraft, just below the base of the magnetometer boom. The magnetic

search coil assembly is supported by a short boom that is attached to the high gain antenna support structure on the -x side of the spacecraft. The Langmuir probe is mounted on the end of an 0.8-m hinged boom that extends outward from the magnetic search coil assembly.

3.2. Electric Antennas

The three electric monopole antennas and their deployment mechanisms were provided by Orbital Sciences Corporation. The antenna elements consist of conducting cylinders, each 10 meters long and 2.86 cm in diameter. The elements are made of beryllium-copper, silver plated on the exterior surface, and painted black on the interior for thermal control. Approximately 12% of the surface area is perforated with small holes to allow sunlight to heat the shaded side of the element in order to reduce thermal bending. The elements themselves are formed by two opposing semi-cylindrical strips with interlocking tabs. For launch, the elements are flattened and rolled onto a spool. During deployment after launch, a motor-driven deployment mechanism feeds the element through a forming channel that expands the strips into a cylindrical tube.

The physical orientations of the three elements with respect to the x, y, and z axes of the spacecraft are provided in Table 3.2.1. The E_u and E_v elements are extended symmetrically at angles of 60° with respect to the spacecraft y-z plane. The plane containing these two elements is rotated 37° with respect to the spacecraft x-y plane. These two elements can be used to provide a dipole antenna (E_x) with a tip-to-tip length of 18.52 m parallel to the spacecraft x axis. The E_w antenna is extended perpendicular to the plane formed by the E_u and E_v elements (i.e., at an angle of 37° from the spacecraft z axis). Several considerations led to this antenna configuration. First, the three monopoles provide the nearly orthogonal tri-axial configuration required for

TABLE 3.2.1

Comparison of Physical and Electrical Orientations of the Electric Antennas

Antenna†	Physical Orientation*		Electrical Orientation (Rheometry)	
	θ (deg)	ϕ (deg)	θ (deg)	ϕ (deg)
E_u	107.5	24.8	107.9	16.5
E_v	107.5	155.2	107.3	162.7
E_w	37	90	31.4	91.2

* The angle θ is the polar angle measured with respect to the spacecraft +z axis, ($\cos\theta = z/\sqrt{x^2 + y^2 + z^2}$), (and the angle ϕ is azimuth angle measured with respect to the +x axis ($\tan\phi = x/y$).

† In some previous papers [Ladreiter et al., 1995; Rucker et al., 1996], various engineering documents, and some sections of this calibration document the E_u, E_v, and E_w antenna are labeled E_{x+}, E_{x-}, and E_z. The u, v, w, notations are used in this section to avoid confusion with the spacecraft x, y, and z axes.

direction finding. Second, as previously described, the E_u and E_v elements can be operated as a dipole (E_x,), which minimizes common-mode coupling in order to provide the lowest possible level of spacecraft-generated interference. The E_u and E_v elements are also symmetric with respect to the magnetometer boom, which minimizing the effect this boom has on the dipole antenna pattern. Third, the w-axis element is rotated somewhat away from the spacecraft in order to reduce electrical coupling and interference from electrical equipment in the lower bay of the spacecraft. Fourth, the E_u and E_v elements are rotated away from the spacecraft x-y plane so that they do not interfere with the field of view of the stellar reference unit. This orientation also provides clearance for release of the Huygens probe.

The three electric antennas were deployed to their full 10-meter length during a 30-hour activity on 25 October 1997, ten days after launch. Full deployment was confirmed by both a potentiometer reading and a limit switch indication, the latter being the most reliable indication of full deployment. A brief set of measurements performed subsequent to the deployments

verified that each antenna was properly connected to the instrument and that there were no shorts to the spacecraft structure. There are no plans to retract or otherwise change the length of the elements for the duration of the mission.

Due to the complex shape of the Cassini spacecraft, the effective electrical axes of the monopole antennas differ significantly from their physical orientations. Electrical measurements using a 1:30 scale model of the spacecraft in a tank of electrolytic fluid (rheometry) were performed by Rucker et al. [1996]. These measurements show angular offsets of the electrical axes by as much as 5 to 6 degrees for the E_w antenna, and 7 to 8 degrees for the E_u and E_v antennas (see Table 4.2). Ladreiter et al. [1995] have developed an analysis technique that can be used to perform in-flight determinations of the electrical axes by using a point source with known polarization characteristics. Jupiter provides the best source for this purpose and in-flight calibrations of the electrical axes of the antennas were carried out during the Jupiter flyby, which took place in December 2000 and January 2001. Preliminary results of this calibration are given by Vogl et al. [2001]. Although this calibration occurred with the Huygens probe attached to the spacecraft, the rheometry results show that the electrical axes shift by only a small amount (less than one degree) when the probe is released.

3.3. Magnetic Antennas

The tri-axial search coil magnetic antennas were provided by CETP in Velizy, France. These antennas are mounted on a short, fixed boom just under the high gain antenna on the -x side of the spacecraft, as shown in Figure 3.1.2. The three axes of the search coils are aligned with the x, y, and z axes of the spacecraft. Each search coil utilizes 10,000 turns of 0.07 mm wire wound around a mu-metal core 25 cm long with a cross-sectional area of 15 mm^2. The

sensors have a usable frequency range of 1 Hz to 20 kHz. A flux feedback winding is used in each search coil to flatten the frequency response over the range from 30 Hz to 18 kHz. The transfer function in this frequency range is approximately 150 mV/nT. Preamplifiers are mounted at the base of the mounting boom. When the spacecraft -z axis is pointed toward the Sun, as it is whenever the spacecraft is in the inner solar system, the high gain antenna acts as a sun shade for the search coils. Two radioisotope heating units are used to provide an internal heat source for thermal control. A thermal blanketing system surrounds the assembly to minimize the radiated heat loss.

3.4. Langmuir Probe

The Langmuir probe consists of a 5-cm diameter titanium sphere mounted on the end of a 0.8-m hinged boom that folds outward from one leg of the boom that holds the search coil magnetic antenna assembly. A preamplifier is mounted near the base of the search coil boom. To minimize the influence of photoelectrons, the outermost 10.9-cm segment of the boom is made as thin as possible (diameter = 6.35 mm) and has an outer guard shield that is held at the same voltage as the probe sphere. In its deployed configuration, the probe is approximately 1.5 m from the nearest spacecraft surface. When the -z axis of the spacecraft is sun-pointed, as it is in the inner solar system, the probe is in the sunlight. The surface of the probe is coated with titanium nitride by baking at high temperature in a nitrogen atmosphere [Whalström et al., 1992]. This treatment provides a durable surface with a constant work function so that the potential of the probe surface is uniform. (If the potential varies over the surface, the current-voltage characteristic is adversely affected.) This coating effectively eliminates hysteresis effects, which can occur for other surface coatings.

The boom holding the Langmuir probe was deployed on 25 October 1997 as part of the launch sequence. Deployment was verified by noting that the probe emitted the expected photoelectron current when biased to a negative voltage (the spacecraft orientation was such that the probe was in sunlight when deployed).

As mentioned earlier, two of the electric antennas (E_u, E_v) can also be operated as Langmuir probes in a current-collecting mode. This mode is used primarily for studying plasma density variations associated with waves and turbulence. The current measurement range is 1 nA to 100 μA for positive bias voltages, and 100 pA to 100 μA for negative bias voltages.

3.5. High Frequency Receiver

The high frequency receiver consists of two sets of four analog receivers followed by a digital signal processing unit. The design is based on a similar receiver flown on the Wind spacecraft [Bougeret et al., 1995]. One set of receivers is connected to the E_w monopole. The other set of receivers can be connected either to the E_x dipole or toggled between the E_u and E_v monopoles. Three of the four receivers have fixed-frequency filters (A, B, and C) that together cover a frequency range from 3.5 to 319 kHz. Each filter covers 2.2 octaves in frequency (i.e., a factor of 4.5). Digital spectral analysis is performed within each of the three filter bands to provide 8, 16, or 32 logarithmically spaced frequency channels, yielding spectral resolutions of 20, 10, or 5%, respectively. The fourth (HF) receiver is tunable over a frequency range from 100 kHz to 16.1 MHz and has a bandwidth of 25 kHz. This receiver can be tuned in two different modes, HF1 and HF2. HF1 provides measurements over a frequency range from 100 kHz to 4.125 MHz in 25-kHz steps. HF2 provides measurements over a frequency range from 125 kHz to 16.125 MHz in 50-kHz steps. Within the 25 kHz passbands of HF1 or HF2, it is possible to

have either 1, 2, 4, or 8 linearly spaced channels, thereby giving frequency resolutions of 25, 12.5, 6.25, and 3.125 kHz. The high frequency receiver has an automatic gain control (AGC) that provides a dynamic range of about 90 dB. In addition, a switchable attenuator provides an additional 26 dB of dynamic range. At any specific gain setting of the AGC, the digital spectrum analyzer has a dynamic range of about 30 dB. Table 3.5.1 provides a summary of the basic characteristics of the high frequency receiver.

TABLE 3.5.1

Characteristics of the High Frequency Receiver

Band	Frequency Range	Frequency Steps	Frequency Resolution	Integration Times
A	3.5 kHz - 16 kHz	8, 16, or 32 (logarithmic)	20, 10, or 5 %	.125, .25, .5, 1 s
B	16 kHz - 71 kHz	8, 16, or 32 (logarithmic)	20, 10, or 5 %	.125, .25, .5, 1 s
C	71 kHz - 319 kHz	8, 16, or 32 (logarithmic)	20, 10, or 5 %	.125, .25, .5, 1 s
HF1	125 kHz - 4.125 MHz	n×25 kHz; 1, 2, 4, or 8 linear channels within 25-kHz band	3.125, 6.25, 12.5, 25, or n×25 kHz	20, 40, 80, 160 msec
HF2	125 kHz - 16.125 MHz	n×50 kHz; 1, 2, 4, or 8 linear channels within 25-kHz band	3.125, 6.25, 12.5, 25, or n×50 kHz	10, 20, 40, 80 msec

Using the two sets of receivers, complex auto- and cross-correlation measurements can be performed between the E_x dipole and E_w monopole antennas, thereby giving the amplitude and relative phase of signals detected by the two antennas. This mode of operation allows for polarization and direction-finding measurements of purely circularly polarized radio emissions such as cyclotron maser radiation. In an alternate mode of operation, the first of the two sets of receivers can be toggled rapidly between the E_u and E_v monopoles, with the second set on the E_w antenna, in order to provide direction-finding measurements.

For low frequency space-borne radio measurements, the wavelength λ is usually much

larger than the length L of the antenna. Under these conditions ($\lambda \gg L$) angular resolution is virtually nonexistent. Nevertheless, the direction to the center of the source can be obtained by comparing the amplitudes and relative phases of signals from various combinations of antennas. On a rotating spacecraft, direction-finding measurements can be performed with only two antennas. This technique was used by the Ulysses spacecraft to derive the location of Jovian low frequency radio sources with an accuracy of approximately 1 - 2° [Reiner et al., 1993; Ladreiter et al., 1994]. The main limitation of the rotating antenna technique is that the radio emission characteristics must remain essentially constant during one spacecraft rotation, which usually takes ten seconds or more. This is a serious limitation for auroral radio emissions, which often have rapid intensity variations, sometimes on time scales of a fraction of a second or less. Such rapid variations explain why the technique could be applied to only limited portions of the Jovian radio spectrum [Ladreiter et al., 1994]. Since Cassini is three-axis stabilized the rotating antenna technique obviously cannot be used. Ladreiter et al. [1995] have shown that direction-finding and full polarization information (i.e., four Stokes parameters) can be obtained with three nearly orthogonal antennas. Direction-finding and polarization measurements are strongly interdependent parameters and, ideally, measurements should be made simultaneously on all three antennas. However, since the high frequency receiver can only process signals from two antennas at a time, direction-finding and polarization measurements are made using consecutive correlation measurements with two different pairs of antennas, (E_u, E_w) and (E_v, E_w). The time between these measurements is typically 45 to 325 msec (above 125 kHz) or 250 to 2000 msec (below 125 kHz). Because of the very short time interval between successive measurements, this technique is expected to be relatively insensitive to short-term intensity variations.

The high frequency receiver utilizes digital filters that have an out-of-band rejection

greater than 45 dB. They are preceded by an anti-aliasing filter and an automatic gain control (AGC). The AGC normalizes the signal amplitude to a level that provides optimal performance for the digital signal processor. The first receiver has an input, which for simplicity we call E_1, that is selectable from either E_x, E_u, or E_v. The second receiver has an input, which we call E_2, from the E_w antenna. The digital processor provides two auto-correlations, $|E_1|^2$ and $|E_2|^2$, and two cross-correlation $\mathrm{Re}(E_1 \cdot E_2^*)$ and $\mathrm{Im}(E_1 \cdot E_2^*)$, for each frequency channel. In the normal mode of operation, a series of auto- and cross-correlation measurements is averaged in order to reduce fluctuations to the digital quantization level (1 bit = 0.375 dB). The exact number of spectrums integrated is controlled by command and depends on the detailed choices of frequency and bandwidth. The intrinsic noise level of the A, B, and C bands is 4.9×10^{-17} V^2 Hz^{-1} for the E_1 receiver and 2.5×10^{-17} V^2 Hz^{-1} for the E_2 receiver. For HF1 and HF2, these noise levels are typically double the A, B, and C noise levels due to mixer noise.

The high frequency receiver also has the capability of providing a frequency-converted signal to the wideband receiver. In the frequency conversion mode of operation, the high frequency receiver translates high frequency signals downward into a 50-kHz to 75-kHz passband, which is then sent to the wideband receiver. This passband can be shifted to any frequency between 4.125 and 16 MHz, except those centered at multiples of 50 kHz, and to any frequency between 125 kHz and 4.125 MHz.

The high frequency receiver also includes a capability to measure amplitudes in a selected frequency channel with millisecond temporal resolution. In this mode of operation any frequency between 125 kHz and 16 MHz can be selected. This capability allows very short duration signals such as lightning to be detected and can be used for envelope sampling of bursty emissions.

Since the high frequency receiver is under the control of its own processor, virtually all of the receiver parameters can be selected by command, making for an extremely flexible instrument. This flexibility allows for regular surveys of the radio frequency spectrum of Saturn at low data rates (typically about 450 bps), as well as specialized studies of short duration phenomena at very high spectral resolution (the maximum number of frequency channels across the frequency range of the receiver is approximately 3300) as well as direction-finding and full polarization measurements. To minimize the data rate for a given mode, the processor also includes both lossless (Meander code) and lossy (Rice code) compression algorithms.

3.6. Sounder Transmitter

The high frequency receiver also includes a sounder transmitter. The transmitter design is based on the Ulysses/URAP instrument [Stone et al., 1992]. In the sounder mode of operation, a short pulse consisting of a 26-V peak-to-peak square wave is transmitted on the E_x dipole antenna, and the receiver then "listens" for a resonance response from the plasma. After each pulse the transmitter frequency is increased by a small increment. This process is continued across the entire frequency range of interest, thereby producing a spectrum of the plasma resonances. When a resonance is encountered, the received signal is strongly enhanced for a short period of time after the pulse has been transmitted. The sounder can measure electron densities from 0.2 to 164 cm^{-3} ($f_{pe} \approx$ 3.6 to 115.2 kHz), and is expected to be active for a few seconds out of every 5 to 10 minutes.

The sounder can transmit in five bands over a frequency range from 3.6 kHz to 115.2 kHz. The five bands are described in Table 4-4. Each band is divided into 18 channels for a total of 90 frequencies. The default bandwidths are given in Table 3.6.1. The upper and lower

frequency limits of the frequency sweep can be selected by command.

TABLE 3.6.1

Sounder Transmission Characteristics

Band	Freq. Range (kHz)	1/Pulse Width (Hz)
1	3.6 - 7.2	200
2	7.2 - 14.4	400
3	14.4 - 28.8	800
4	28.8 - 57.6	1600
5	57.6 - 115.2	3200

Two modes of operation for the sounder are currently planned, designated PAA and AAA. Each of these two modes involves taking three measurements at the selected frequency. In the PAA (Passive Active) mode, a "passive" measurement is taken before the pulse is transmitted, and then two "active" measurements are taken; the first at a time T_0 after the pulse, and the second at a time T_1 after the first measurement. In the AAA mode, three “active” measurements are taken sequentially at time intervals of T_0, T_1, and T_2 after transmission of the pulse. The parameters T_0, T_1, and T_2 can be selected by command.

3.7. Medium Frequency Receiver

The medium frequency receiver (MFR) system is based on similar receivers flown on the ISEE, Galileo, and Polar spacecraft [Gurnett et al., 1978; 1992; 1995]. The purpose of the medium frequency receiver is to provide continuous spectral measurements over a frequency range from 24 Hz to 12 kHz, with moderate frequency and temporal resolution and a relatively low data rate. This receiver system has the capability of processing signals from the B_x, B_z, E_u, E_v, E_w and E_x, antennas. In a typical mode of operation, the receiver toggles between the E_x

dipole antenna and the B_x magnetic antenna in order to provide alternating electric and magnetic spectrums.

The medium frequency receiver consists of three frequency bands designated 1, 2, and 3, each covering a 3 octave frequency range. Band 1 is divided into 16 logarithmically spaced frequency channels ($\Delta f/f \simeq 13$ %) and bands 2 and 3 each have 32 frequency channels ($\Delta f/f \simeq 7\%$). The effective bandwidths for the three bands are given in Table 3.7.1. The frequencies are selectable using a two-stage frequency conversion scheme. Each band of the medium frequency receiver uses a mixer to convert the selected frequency to a fixed intermediate frequency (IF) filter. A second mixer then down-converts the IF signal to a baseband filter. The baseband signal is logarithmically compressed, rectified, and summed to provide a 0-5 volt DC output, and then converted to an 8-bit binary number by an analog-to-digital converter. The dynamic range of the medium frequency receiver, from the lowest signal that can be detected to the saturation level, is about 110 dB.

TABLE 3.7.1

Medium Frequency Receiver Characteristics

Band	Frequency Range	$\Delta f/f$	Effective Bandwidth (Hz)	Sweep Time (s)
1	24 - 180 Hz	13%	5.6	16
2	180 - 1500 Hz	7%	19.4	16
3	1.5 - 12 kHz	7%	139	8

The upper frequency limits of the three medium frequency receiver frequency bands are determined by three bandpass filters at the front end of the receiver. The lower frequency limits are imposed by a combination of the bandpass filters and the low frequency limit of the front end

(IF) mixer. The filter frequencies are scaled upward by a factor of eight for each successive higher band, thereby providing frequency coverage over nine octaves. The low-pass filters provide 55 dB of rejection for out-of-band signals.

3.8. Five-Channel Waveform Receiver

The five-channel waveform receiver provides simultaneous waveforms from up to five separate sensors in passbands of either 1 to 26 Hz, or 3 Hz to 2.5 kHz. The purpose of this receiver is to provide high-resolution spectral measurements and to determine the polarization and wave normal of low frequency plasma waves. When connected to the Langmuir probe (including the E_u and E_v monopoles operating in the current collecting mode), the waveform receiver can also provide $\delta n_e/n_e$ waveforms. The waveforms are sampled with 12-bit resolution once every 10 ms for the 1 to 26 Hz bands and once every 140 μs for the 26 Hz and 2.5 kHz bands. Simultaneous waveform samples from up to five receiver channels are stored in a buffer memory until they are read out via the science telemetry. The waveforms are processed on the ground to produce the auto- and cross-correlations that are needed to compute the wave normal and polarization.

The waveform receiver consists of five parallel analog input channels. The five inputs can be connected to various sensors. Table 3.8.1 summarizes the sensor selections for each of the five channels. Signals from the five sensors are routed directly to a gain select stage that has commandable gains of 0, 10, 20, or 30 dB for each receiver channel. Channels 1 and 2 have independent gain settings, but channels 3 to 5 (which are usually connected to the B_x, B_y, and B_z magnetic sensors) share the same gain control lines. The programmable gain amplifiers are similar to those used in the wideband receiver. The amplifier gains are controlled by the high

rate processor and can be operated in either a fixed gain mode or an automatic ranging mode. The output of the programmable gain amplifiers goes to a 26-Hz low-pass filter and a 3-Hz to 2.5-kHz bandpass filter. The desired analysis passband is selected by spacecraft command and the waveform outputs are sampled simultaneously by sample-and-hold circuits and converted to digital signals by a 12-bit analog-to-digital converter. The five-channel waveform receiver can also be commanded to measure one, two, three or four channels. These special modes allow greater resolution for special observations. For example, the single-channel waveform receiver mode using the 3-Hz to 2.5-kHz passband effectively allows a third wideband receiver channel in addition to the 60-Hz to 10.5-kHz and 0.8-kHz to 75-kHz channels that are included in the wideband receiver. Also, the waveform receiver provides signals to the digital processing unit in order to generate the passband for the low frequency receiver function (see Section 3.9).

TABLE 3.8.1

Waveform Receiver Input Selections

Channel	Input Selection
1	E_x dipole, E_u*
2	E_w, E_v*
3	B_x, Langmuir probe*
4	B_y
5	B_z

* Operating in Langmuir probe (current collecting) mode

Since the primary purpose of the five-channel waveform receiver is to provide the amplitude and relative phase of the five measured field components, each receiver channel must have known amplitude and phase responses. To achieve the required performance, all five low-pass passive filters have been carefully matched and are phase-stable to within a one degree between 1 Hz and 2.5 kHz.

3.9. Low Frequency Receiver

In order to have continuous spectral information in the frequency range from 1 Hz to 26 Hz, waveforms from the five-channel waveform receiver are Fourier transformed by the data compression processor in the digital processing unit. The three-channel mode (E_x, E_w, B_x) of the five-channel waveform receiver is used, although typically only two of these channels, E_x and B_x, are analyzed, thereby providing simultaneous electric and magnetic spectrums. Processor speed limits the temporal resolution between successive spectrums to about 16 seconds. The Fourier transform processing utilizes a 512-point waveform to produce a 256-frequency component spectrum with 0.2-Hz resolution. To minimize the data volume and to produce a spectrum with resolution similar to that produced by the medium frequency receiver, the linear components of the spectrum are binned to form a logarithmically spaced spectrum with 32 frequencies covering a frequency range from 0.2 to 26 Hz.

3.10. Wideband Receiver

The wideband receiver is similar to the wideband receivers previously used on the Voyager, Galileo, Polar, and Cluster spacecraft, and provides high-resolution electric and magnetic field waveform measurements in passbands of either 60 Hz to 10.5 kHz, or 0.8 to 75 kHz. The wideband receiver also serves as the front end for the on-board dust detection function. The data compression processor (described below) is used to search the waveforms for the signature of dust impacts.

The wideband receiver processes signals from a single selected sensor (either E_u, E_v, E_x, E_w, B_x, or Langmuir probe). To provide the capability for obtaining waveforms at higher frequencies, the wideband receiver input can be connected to the frequency conversion output

from the high frequency receiver (see Section 3.5).

The instantaneous dynamic range of the wideband receiver is 48 dB. Because of the expected large dynamic range of the input signals, a set of discrete gain amplifiers and an automatic gain control are used to amplify the signal to the proper level in steps of 10 dB over a range of 0 dB to 70 dB. This system provides a total dynamic range of over 100 dB for the wideband receiver. The feedback loop in the automatic gain control has a time constant of 0.1 seconds. However, gain updates are only made prior to a waveform capture. Since waveform captures typically occur once per multiple of 125 ms, the effective gain update can be much slower than 0.1 s. The output from the discrete gain amplifiers goes to the two bandpass filters (60 Hz to 10.5 kHz or 0.8 kHz to 75 kHz). The output of the selected bandpass filter is sent to an 8-bit analog-to-digital converter. The sampling rate is 27,777 samples/s for the 10-kHz channel and 222,222 samples/s for the 75-kHz channel.

3.11. Data Processing Unit

The RPWS data processing unit uses three microprocessors, the low-rate processor (LRP), the high-rate processor (HRP), and the data compression processor (DCP), to perform the tasks necessary for the instrument operation. These processors are responsible for collecting the science and housekeeping data, data formatting and data compression, and provide the interface to the spacecraft command and data system.

The tasks and responsibilities of the three processors are as follows. The low-rate processor is considered the primary processor since it has the sole interface with the Cassini spacecraft via the bus interface unit (BIU). It also provides the interface to the high frequency receiver, the interface and control for the medium frequency receiver and the analog

housekeeping analog-to-digital converter, and the control for the antenna motor subsystem. The high-rate processor is used to control the waveform and wideband receivers, and the Langmuir probe instrument. The high-rate processor contains a data compression chip for compression of waveform signals. The data compression processor contains a dedicated math processor and is used only for data processing tasks, such as data compression. This processor performs the on-board dust-detection and also the Fourier transforms for the low frequency receiver.

The essential elements of each of the three processors are an 80C85 microprocessor, two or more random access memory chips, and one or two read-only memory chips. The 80C85 runs with a 3-MHz clock and is used in the expanded configuration which uses an address latch to give a full 16-bit address bus and a bi-directional buffer to expand the data bus. Each processor can communicate with the other two processors via the interprocessor communication bus. The 80C85 has a memory address bus width of 16 bits giving a total addressing capability of 2^{16} or 64 kilobytes (kB). The memory in each of the processors consists of both a read-write memory and a read-only memory.

The low-rate and high-rate processors each have more than 64 kB of random access memory available. The low-rate processor contains 64 kB of read/write memory with 16 kB write-protected and 4 kB of read-only memory. The bus interface unit appears to the processor as an additional 16 kB of random access memory. The high-rate processor has 96 kB of random access memory. The excess memory is handled by switching memory chips under program and hardware control.

All communication with the spacecraft is over a redundant 1-MHz bi-directional serial data bus conforming to MIL STD 1553. The interface is implemented via a bus interface unit.

3.12. Mass, Power, and Telemetry

The RPWS has a total mass of 37.68 kg and requires a power of 16.38 W in its fully operational science modes. This power value does not include a momentary ~3 W increase when the bus interface unit is active. By project policy, this bus interface power is allocated to the command and data system and not to the science instrument. Mass and power breakdowns for the various elements of the instrument are provided in Table 3.12.1.

TABLE 3.12.1

Summary of RPWS Physical Characteristics

Element	Mass (kg)	Power (peak W)	Volume (cm^3)	Location
Main Electronics	5.59	5.09	41.7×17.8×16.8	Main Bus, Bay 4
Antenna Bracket Assembly	29.77	11.14	61×67×67	Upper shell structure of Bay 4
Magnetic Search Coils	1.05	0	30×30×30	1-m boom attached to high gain antenna support structure
Magnetic Search Coil Preamps	0.28	0.1	12.6×3.2×8.8	Base of search coil boom
Langmuir Probe	0.85	0	74.3×10×11.5	0.8-m boom on search coil boom
Langmuir Probe Preamp	0.135	0.05	8.7×9×4.8	Base of search coil boom
Total	37.68	16.38		

Because of its many different receivers, operating modes, and because of the use of several different data compression schemes, the RPWS has a highly variable science telemetry rate. In all of the defined telemetry modes that include RPWS science telemetry, there are four data pickup rates, or rates at which the RPWS can send data to the command and data system.

These rates are 30.464, 60.928, 182.784, and 365.568 kbps. However, because of limitations on the Cassini solid state recorder data volume as well as limits on the total data volume that can be telemetered to the ground in any given day, the RPWS can utilize such high data rates only occasionally and for relatively short periods of time. Therefore, a number of different observing modes have been defined that use minimal data rates for basic survey information and utilize the higher data rates for special observations, usually involving the wideband or five-channel waveform receivers. In the usual case where the actual science telemetry rate is less than the current telemetry mode's data pickup rates, RPWS outputs "zero-length" packets that are discarded by the command and data system to reduce the net data production rate.

The basic low-rate survey mode we have defined generates approximately 1 kbps before compression. Based on limited in-flight experience to date, the actual data rate in this mode after compression is about 700 bps. However, since most of the compression techniques used are data content dependent, it is not clear that this compressed data rate is representative of what will be encountered at Saturn. In addition to the continuous low-rate observations, the RPWS survey includes occasional wideband receiver samples (typically about one minute every couple hours) that are essential to the interpretation of the lower resolution data. On average, these high rate samples add approximately 600 bps to the RPWS survey rate. Typical observation modes that require higher data rates include the 75-kHz wideband receiver observations which generate close to 360 kbps before compression, the maximum duty cycle mode of the five-channel waveform receiver in the 2.5-kHz bandpass which generates approximately 130 kbps before compression, the low-duty cycle mode of the 10-kHz wideband receiver measurements which generates approximately 30 kbps before compression, and the high-resolution temporal and/or spectral modes of the high frequency receiver which generate data rates up to about 4 kbps.

Because of the uncertainty in the compression factors and data volume allocations imposed due to the limited downlink and onboard storage, the RPWS has the ability to monitor its actual data volume and compare it to a model. In the case where the actual data production is exceeding the model, various steps can be taken to decrease the data rate. For example, the rate at which waveform samples are acquired by the five-channel waveform receiver can be slowed down. This approach is effective when no wideband data are being acquired. During wideband receiver operations, the effective data rate can be reduced by decreasing the duty cycle of the wideband data. For example, instead of acquiring a 2048-sample data set once every 125 ms, a data set could be acquired every 250 ms.

4.0 Cassini RPWS Design Aspects

To achieve the scientific objectives of the Cassini mission, the instrumentation must have certain design and performance characteristics. This section gives the rationale for the RPWS instrument design and describes the performance required to achieve the scientific objectives described in the previous section. The topics discussed include: (1) field sensors, (2) frequency ranges, (3) frequency and time resolutions, and (4) sensitivities and dynamic ranges.

4.1 Field Sensors

A basic question that arises in the design of all radio and plasma wave instruments is what types of antennas should be used, electric or magnetic, and in each case, how many field components should be detected. For measurements of radio waves at frequencies well above the local characteristic frequencies of the plasma (i.e., above the electron cyclotron frequency and the electron plasma frequency), the propagation is essentially unaffected by the local plasma. At these frequencies, it is not necessary to measure both the electric and magnetic fields, since they have a constant known ratio, $E = cB$. In principle, it does not matter whether the electric field or the magnetic field is measured. However, for various reasons, both electrical and mechanical, it turns out that an electric antenna can operate at much higher frequencies and with a much greater sensitivity than a magnetic antenna of comparable size and weight [Gurnett, 1998]. Therefore, for high frequency radio measurements, such as for SKR and SEDs, an electric dipole antenna is preferred. For plasma waves, which occur at lower frequencies, near or below the electron cyclotron frequency and the electron plasma frequency, the situation is more complicated. Plasma waves can be either electrostatic, with no magnetic field, or electromagnetic, with both an electric field and a magnetic field. Although an electric antenna can detect both types of

waves, the only way to conclusively distinguish an electrostatic wave from an electromagnetic wave is to use both an electric antenna and a magnetic antenna. If a wave can be detected with both an electric antenna and a magnetic antenna, then it is an electromagnetic wave. If it can be detected with an electric antenna, but not with a magnetic antenna, then it is an electrostatic wave. A major shortcoming of the Voyager plasma wave instrument, which used only an electric antenna, was the inability to distinguish electrostatic waves from electromagnetic waves. Therefore, for plasma wave measurements (i.e., at frequencies below the electron cyclotron frequency and the electron plasma frequency) both electric and magnetic antennas should be used.

Next we consider the number of components to be measured. The Voyager electric field antenna consisted of two cylindrical elements mounted in a V configuration, see Scarf and Gurnett [1977] and Warwick et al. [1977]. For the plasma wave instrument the two elements were used as a dipole, and for the radio astronomy instrument they were used as two orthogonal monopoles. Although the V configuration provided a limited capability to perform polarization measurements, no capability existed for performing direction-finding measurements. Since the RPWS scientific objectives require accurate determinations of source positions, as well as polarization measurements, it is essential that the RPWS be able to perform both direction finding (i.e., wave normal, $\mathbf{k}$) and polarization measurements of high frequency radio signals (i.e., $f > f_{ce}$ and $f > f_{pe}$). Since at high frequencies the electric field is always perpendicular to the wave normal ($\mathbf{E} \cdot \mathbf{k} = 0$), the wave normal direction can be determined by measuring the plane of rotation of the electric field (provided the wave is not linearly polarized). Therefore, the RPWS must include full three-axis electric field measurements. The easiest way to achieve this is to use three orthogonal electric monopoles. In the low frequency plasma wave part of the spectrum ($f <$

f_{pe} or $f < f_{ce}$), it is also important to carry out wave normal measurements. Unfortunately, when the anisotropic effects of the plasma are considered, the wave normal of an electromagnetic wave cannot be determined from electric field measurements. From Poisson's equation, $\nabla \cdot \mathbf{E} = \rho$, one can see that because the charge density, ρ, in a plasma is in general not zero, the electric field is no longer perpendicular to the wave normal, $\mathbf{E} \cdot \mathbf{k} \neq 0$. Fortunately, Maxwell's equation $\nabla \cdot \mathbf{B} = 0$ always implies that $\mathbf{B} \cdot \mathbf{k} = 0$. Therefore, to make wave normal measurements in the low frequency plasma wave part of the spectral three-axis magnetic field measurements are required. In addition, to assure that electrostatic waves can be detected and to resolve the ambiguity in the direction of propagation (i.e., along $\mathbf{k}$ or $-\mathbf{k}$), electric field measurements are also required, although these do not necessarily have to be three-axis measurements. In addition to electric field measurements, it is also useful to have the capability to measure electron density fluctuations in the plasma wave frequency range. This capability is easily achieved by biasing the electric antenna element with a known fixed bias current (as though it were a Langmuir probe). With this bias condition, it can be shown that the voltage variations on the element are proportional to the fractional electron density variation, $\delta n_e / n_e$. For electrostatic waves simultaneous measurements of both the electric field and the electron density variation can provide information on the wavelength of the wave [Kelley and Mozer, 1972; Wahlund et al., 1998].

4.2. Frequency Ranges

To decide on the frequency ranges required for the electric and magnetic field measurements, we must consider the characteristic frequencies of the radio and plasma wave phenomena to be studied in the vicinity of Saturn. The frequency ranges and spectrums of all

radio and plasma wave phenomena known or predicted to occur in the vicinity of Saturn are summarized in Figures 4.2.1, 4.2.2 and 4.2.3. Figure 4.2.1 shows a model of the electron plasma frequency, f_{pe}, and electron cyclotron frequency, f_{ce}, as a function of radial distance near the equatorial plane on the dayside of Saturn; and Figures 4.2.2 and 4.2.3 show representative electric and magnetic field spectrums at a radial distance of 10 R_S . First, we consider the upper limit of the frequency range. Two high frequency limits must be considered, one for the electric field and the other for the magnetic field. The high frequency limit for the electric field is determined by the highest radio emission frequency of interest, and the high frequency limit for the magnetic field is determined by the highest plasma wave frequency of interest. As can be seen in Figure 4.2.1, lightning from Saturn's atmosphere (SEDs) has the highest frequencies.

Figure 4.2.1

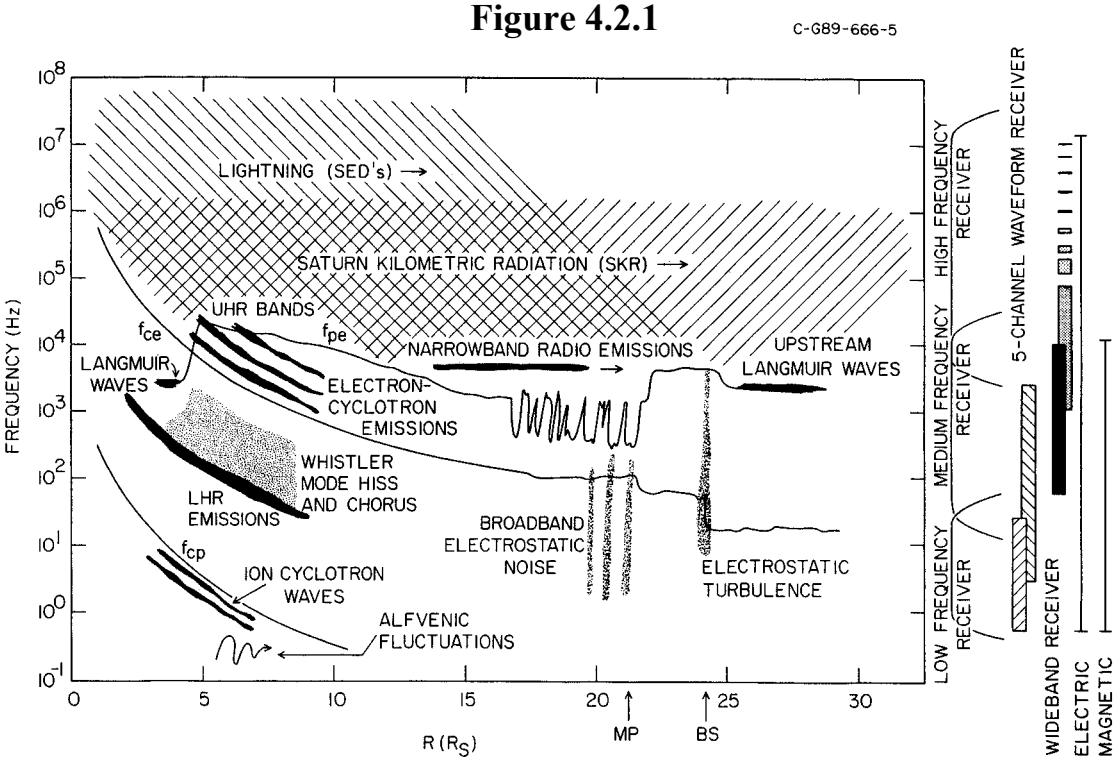

Figure 4.2.2

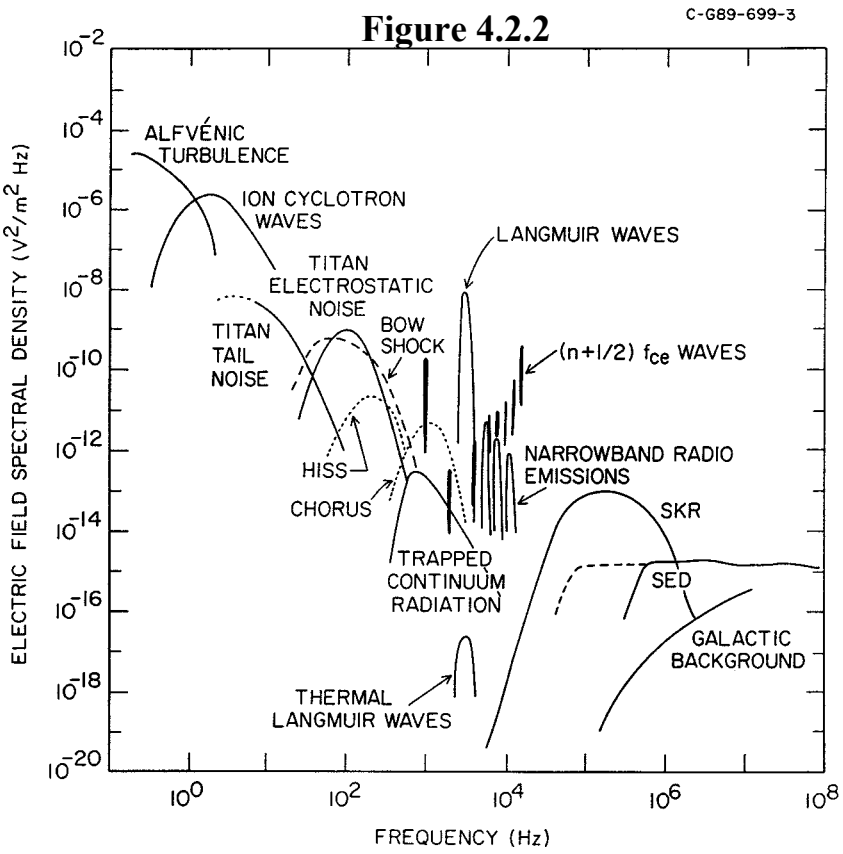

Figure 4.2.3

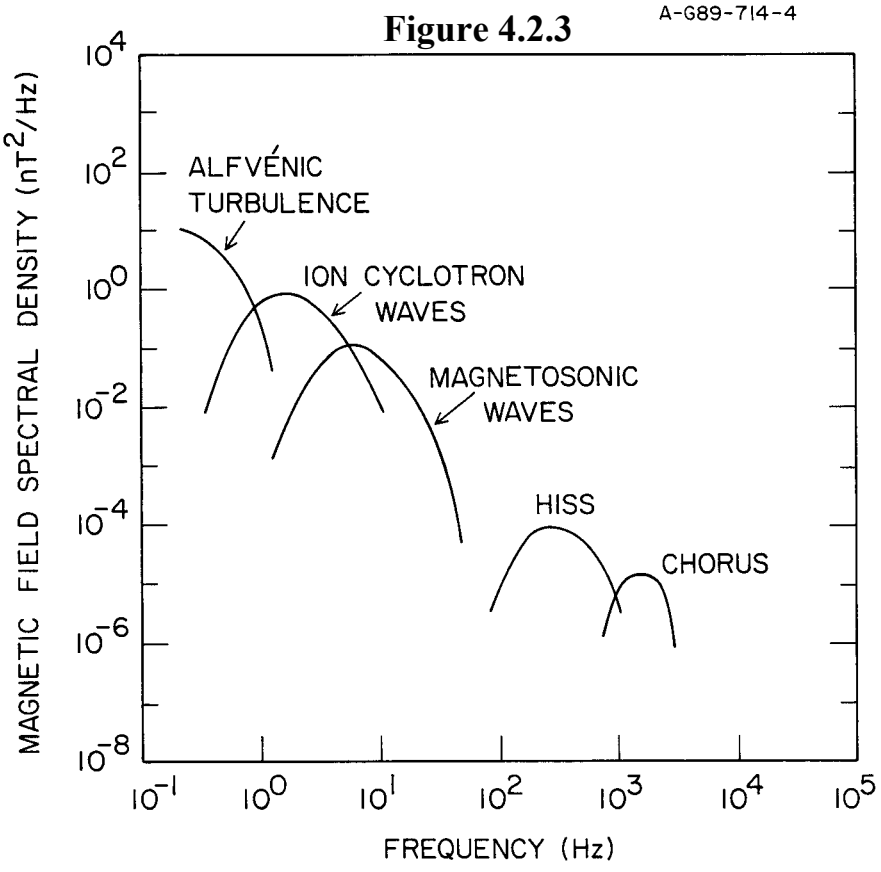

From the Voyager observations it is known that the SED spectrum extends up to at least 40 MHz. Since the shape of the high frequency part of the SED spectrum is already known [Zarka and Pedersen, 1983], we do not plan to make electric field measurements as high as 40 MHz. Our primary objectives relative to SEDs are to monitor the long-term occurrence of lightning and to study variations in the low frequency cutoff imposed by Saturn's ionosphere. For these purposes it is only necessary to measure the SED spectrum to frequencies slightly greater than the maximum ionospheric cutoff frequency. Since the maximum plasma frequency of the dayside ionosphere is typically about 5 MHz, we have selected 16 MHz as the upper frequency limit for the electric field measurements. Since the ionospheric cutoff frequency varies as $f_{cutoff} = f_{pe}/\cos\theta$, where θ is the angle of incidence, this upper frequency limit allows the detection of lightning over a large range of incidence angles, approximately $0 \leq \theta \leq 70°$.

For the upper frequency limit of the magnetic field measurements we must consider the highest plasma wave frequency that is likely to be encountered in Saturn's magnetosphere. Asdiscussed earlier, magnetic field measurements have two main purposes: (1) to distinguish electrostatic waves from electromagnetic waves, and (2) to determine the wave normal direction of electromagnetic waves. During the baseline tour, the periapsis radial distance is expected to be in the range from about 4 to 6 R_S, and the apoapsis is in the range from about 20 to 130 R_S. As can be seen from Figure 4.2.1, the whistler mode, which is the highest frequency electromagnetic plasma wave mode that is likely to be of interest, is generally in the range from 3 to 10 kHz, with a maximum of about 12 kHz. Based on this magnetic field model we have selected 12 kHz as the upper limit for the magnetic field measurements. This allows magnetic field measurements with a simple tri-axial search coil magnetometer, which can be easily designed to respond to frequencies up to 12 kHz. In selecting this upper limit we realize that it

will not be possible to detect the magnetic field of certain plasma wave modes that occur at frequencies above 12 kHz. For example, during the Titan flybys UHR emissions are expected to extend up to frequencies as high as several hundred kHz, and during Saturn Orbit Insertion (SOI), which is at about 1.3 R_S, electrostatic $(n + ½)f_c$ electron cyclotron waves could extend up to frequencies as high as several hundred kHz. However, in all of these cases we feel confident that it will be easy to identify these electrostatic modes. For example, at Titan the UHR emissions will be at frequencies of ten to several hundred kHz, well above the electron cyclotron frequency, which is the highest frequency for the whistler mode. The situation is more complicated near SOI, where whistler-mode emissions could occur at frequencies as high as 500 kHz. To provide magnetic field measurements at such high frequencies would require the use of a loop antenna [Gurnett, 1998]. Although such antennas have been flown in the past, they are large and very difficult to accommodate on the spacecraft, so a decision was made that high frequency magnetic field measurements were not justified to achieve this limited objective, given the additional resources that would be required.

Next, we consider the low frequency limit of the plasma wave spectrum. Since scientifically interesting plasma wave phenomena exist down to essentially zero frequency, the low frequency cutoff of the RPWS electric and magnetic field sensors is determined almost entirely by technical considerations. For example, conventional static field magnetometers tend to have better sensitivities than search coil magnetometers at frequencies below about 1 Hz. Since a tri-axial static field magnetometer (MAG) is included on Cassini [Southwood et al., this issue], there is no reason to extend the frequency range of the RPWS magnetic antenna below about 1 Hz. Therefore, we have adopted 1 Hz as the low frequency cutoff of the RPWS magnetic field measurements. For the electric field antennas the situation is more complicated.

The frequency response of the electronics for the electric field measurements could easily be extended below 1 Hz. However, because of sheath effects around the spacecraft body, such low frequency, quasi-static, electric field measurements require very long antennas, typically with lengths at least ten times the maximum dimension of the spacecraft body. Since such long antennas (~100 meters, tip-to-tip) could not be accommodated on Cassini due to spacecraft dynamics considerations, we have arbitrarily defined the low frequency cutoff of the RPWS electric field measurements to be the same as for the magnetic field measurements (i.e., 1 Hz).

4.3. Frequency and Time Resolutions

It is well known that the frequency and temporal structure of Saturnian radio emissions and plasma waves vary over an extremely large range [Scarf et al.,1984; Zarka, 1998]. Some types of waves, such as continuum radiation and whistler-mode hiss, have smooth continuous spectrums that can be resolved with very modest frequency and time resolution. On the other hand, certain other types of waves, such as lightning-generated whistlers, whistler-mode chorus, and cyclotron maser radiation, have extremely complicated frequency-time structures. These structures often extend down to frequency and time resolutions on the order of $\Delta f \Delta t \sim 1$. Furthermore, in some cases it is necessary to stress high frequency resolution (i.e., small Δf), such as in the analysis of plasma resonances, whereas in other cases it is necessary to stress high-time resolution (i.e., small Δt), such as in the analysis of lightning and dust impacts. Resolving these conflicting demands is one of the main challenges that must be faced in designing a radio and plasma wave investigation.

What little is known about the fine structure of radio emissions and plasma waves at Saturn comes almost entirely from the Voyager measurements. The Voyager plasma wave

instrument had a 16-channel spectrum analyzer spanning the frequency range from 10 Hz to 56 kHz, and a wideband waveform receiver that covered the frequency range from 50 Hz to 10 kHz. The time resolution of the 16-channel measurements was 4 seconds. During selected intervals, the wideband waveform provided high-resolution 48-second "snapshots" of the electric field waveform with a sample rate of 28,800 samples/sec. However, the number of wideband frames that could be transmitted was severely limited by data rate considerations. The Voyager planetary radio astronomy instrument, which made measurements from 20 kHz to 40 MHz, had somewhat better frequency resolution ($\Delta f/f \sim 1$ to 5 percent), but relatively poor time resolution (~6 seconds/sweep). Although the radio astronomy instrument also included a high-rate mode that allowed rapid (millisecond) sampling of a selected channel, again the amount of high-rate data collected was severely limited.

Since it is highly likely that radio emissions and plasma waves in Saturn's magnetosphere have fine-scale structures comparable to those observed in the Earth's magnetosphere, it is important that the RPWS instrument be designed with sufficient frequency and time resolution to resolve these structures. In particular, the RPWS should provide a substantial improvement relative to the Voyager radio and plasma wave instruments. Our basic approach to achieving this goal is to make measurements on two widely different frequency and time scales: nearly continuous low-rate spectral measurements with a frequency resolution on the order of a few percent and a time resolution on the order of a few seconds, and short-duration high-rate wideband waveform measurements with frequency and time resolutions approaching the limit, $\Delta f \Delta t \sim 1$. To provide flexibility, the frequency and time resolution of the low-rate measurements must be controlled by a reprogrammable microprocessor, so that they can be changed to accommodate unexpected results. The high-rate wideband waveform measurements

will allow us to produce high resolution frequency-time spectrograms. Since the entire waveform is transmitted to the ground, these measurements have the advantage that the frequency and time resolution of the spectral processing can be adjusted during the ground processing to provide the optimum resolution for the phenomena being investigated, the only limit being that $\Delta f \Delta t \gtrsim 1$. To provide high-resolution measurements of high frequency radio emissions, the waveform receiver must also have a frequency conversion mode of operation that can provide waveform measurements in selected frequency bands at high frequencies. This mode of operation will allow us to determine whether SKR has fine structure comparable to terrestrial AKR. Such high-resolution measurements of SKR will provide fundamental constraints on the mechanism by which these radio emissions are generated.

4.4. Sensitivities and Dynamic Ranges

The RPWS instrument must have sufficient sensitivity to detect the weakest signals of interest in the vicinity of Saturn, and still have adequate dynamic range to respond to the strongest signals without saturating. Figures 4.2.2 and 4.2.3 show the range of electric and magnetic field strengths that must be measured for various phenomena in the vicinity of Saturn. For some phenomena, such as the SKR and SED events, the intensities vary considerably. In these cases, the spectrums were selected from periods of relatively high intensity at a radial distance of 10 R_S. As can be seen, the intensities vary over a wide range. For electric fields the spectral densities that must be measured range from a minimum of about 10^{-18} $V^2m^{-2}Hz^{-1}$ at 10^6 Hz, to a maximum of about 10^{-6} $V^2m^{-2}Hz^{-1}$ at 1 Hz, a total range of 120 dB. For the magnetic field the spectral densities that must be measured range from a minimum of about 10^{-7} nT^2Hz^{-1} at 10^3 Hz to a maximum of about 10^1 nT^2Hz^{-1} at 1 Hz, a total range of 80 dB. Since it is very

difficult to achieve a total dynamic range of 120 dB, special techniques must be used to accommodate this very large range of signal strengths. For example, since the intensities tend to increase toward lower frequencies, the gain near the front end of the receiving system must be decreased at low frequencies in order to avoid saturation when strong low frequency signals are present. Also, since digital waveforms typically cannot accommodate such large dynamic ranges, automatic gain control systems must be used for all waveform measurements. These and a variety of other techniques must be used in order to assure that the instrument can perform reliable measurements over the large range of field strengths illustrated in Figures 4.2.2 and 4.2.3.

5.0 RPWS Calibration Methods

An extensive series of amplitude calibrations, frequency responses, phase calibrations, and instrument performance checks were carried out on the RPWS prior to launch, both before and after integration on the spacecraft. These tests and calibrations were performed at room temperature (25°C), -20°C, and 40°C. While there are calibration signals available in the instrument for in-flight calibration purposes, these are mainly used to check for drifts due to aging or radiation exposure. The primary calibration information to derive physical units (spectral density, etc.) is derived from the prelaunch tests.

5.1. Calibration Procedure

5.1.1. Electric Antennas

Each of the RPWS electric antennas is connected to an amplifier located in the high frequency receiver. In the long wavelength regime where the wavelength is much greater than the tip-to-tip length of the antenna, L, the potential between the two elements of an electric dipole is given by $\Delta V = E L_{eff}$, where L_{eff} is a quantity called the effective length [Gurnett, 1998]. This relation ignores the presence of any electrical load. For a dipole consisting of collinear elements, to a very good approximation L_{eff} is one-half the tip-to-tip length of the antenna. For a V configuration, L_{eff} is the distance between the geometric centers of the two elements. Taking into account the 120° included angle between the two elements of the E_x dipole and the finite distance between the roots of the two elements, the effective length of the Cassini E_x dipole is $L_{eff} = 9.26$ m. Next we must consider the effect of an electrical load on the antenna. At frequencies above a few tens of Hz, where the antenna impedance is primarily capacitive, the ratio of the output voltage to the input voltage is given by a simple capacitive

divider,

$$\frac{V_{out}}{E\ L_{eff}} = \frac{C_A}{C_A + C_L} \quad . \tag{1}$$

In the above equation C_A and C_L are the antenna and load capacities, respectively. For a cylindrical antenna, to a good approximation, the antenna capacity is given by

$$C_A = \frac{2\pi\varepsilon_0(L/2)}{[\ell n(L/2a) - 1]} \tag{2}$$

where L/2 is the length of the element, a is the radius of the element and ε_o is the permittivity of free space. For L/2 = 10 m and a = 0.014 m, C_A = 100.2 pF.

The load capacity can be considered to be the sum of two parts: (1) the base capacity, which consists of the internal capacities of all circuits and mechanical structures connected to the base of the antenna; and (2) the capacity between the antenna and the spacecraft structure. Since the electric antenna cannot be fully extended in-flight configuration while the spacecraft is on the ground, there is no way to directly measure the capacitance between the antenna and the spacecraft structure. Thus, the total base capacitances listed in Table 5-1 only give lower limits to the load capacities. Another, and perhaps better way to estimate the load capacities is to determine the half-wavelength resonance frequency of the antenna. This resonance frequency is shifted downward by a small amount due to the load capacity. During the instrument checkout in December 1998 and January 1999, a sharp peak was observed in the E_x dipole noise level at 8.5 MHz (see the discussion of noise levels in Section 14.1). This peak is due to the half-wave resonance. An antenna modeling program was then used with an accurate representation of the spacecraft geometry to determine the load capacitance required to place the resonant frequency

at 8.5 MHz. The resulting value was C_L = 150 pF. This is our best current estimate of the load capacity for the E_x antenna. Using the capacitive divider relation above with C_A = 100.2 pF and C_L = 150 pF gives a loading loss of 7.9 dB for the E_x antenna. Chapter 6 discusses the calibration of the electric antenna in more detail.

Due to the complex shape of the Cassini spacecraft that acts as the ground plane for these antennas, the electrical axes of the antennas are expected to be rotated significantly from their physical orientations [Rucker et al., 1996]. Radio signals from Jupiter were used as a calibration source during the Cassini flyby of Jupiter in late 2000 and early 2001 to determine the electrical axes of the antennas. The orientations of the antenna axes can be determined by inverting the direction-finding software, using the direction to Jupiter as the source direction. Preliminary results from this calibration are given by Vogl et al. [2001]. Additional antenna calibrations are scheduled on approach to Saturn and while in orbit after the Huygens probe is released.

Electric field calibrations of the receivers were performed by applying signals with known amplitudes at the preamplifier inputs and relating the input signal strength with the resulting telemetry value. As described below, the telemetry values from the various receivers are related to the input signal strength either via a set of look-up tables or through an analytical function that fits ground calibration data.

5.1.2. Magnetic Antennas

The sensitivity, frequency response, phase response, and noise levels of the magnetic search coil antennas were calibrated at a low-noise magnetic field observatory near Chambon La Foret, France. The calibrations were performed using a Helmholtz coil driven by a known AC current source to produce a magnetic field with a known magnitude and phase. The thermal

blankets were installed in order to account for any conductivity effects that the blanket may have on the sensor response. The resulting data relate input field strength to the voltage at the magnetic preamplifier output. Additional calibrations were then used to relate the voltage input to the various receivers to an output telemetry value. Combining these two steps provides an overall end-to-end calibration of the magnetic field measurements. This calibration was verified through a series of tests performed with the search coil antennas connected to the RPWS instrument after integration on the spacecraft. An end-to-end check of the phase response was also carried out after integration on the spacecraft. Noise levels were measured on the spacecraft by placing the search coils in a μ-metal chamber, which shields the sensors from external noise sources. See Chapter 7 for a more detailed discussion of the calibration of the magnetic search coils.

5.1.3. High Frequency Receiver

The calibration of the high frequency receiver was performed at Meudon, France. Sine wave and white noise sources with known spectral properties were applied to the input of the electric antenna amplifiers and the corresponding telemetry values were recorded. The calibration data were then fit to analytical models for each of the receiver bands. From these models, the telemetry values can be converted to physical units. A series of tests was then performed after integration of the instrument on the spacecraft, to verify the high frequency receiver calibrations. See Chapter 11 for a more detailed discussion of the calibration of the HFR.

5.1.4. Medium Frequency Receiver

The medium frequency receiver uses compressors with a piecewise-linear approximation to a logarithmic amplitude response. Over the range of amplitudes, the response of each compressor consists of a series of five distinct linear segments that deviate slightly from a true logarithmic response. Because the compressors for each of the three bands have different amplitude sensitivity characteristics, the amplitude response of each compressor must be measured separately. This was accomplished by applying a signal to the input of the electric antenna preamplifier at the center frequency of the filter channel for each Band [Band 1 (channel 8), Band 2 (channel 16) and Band 3 (channel 10)]. The amplitude was stepped in 2 dB increments to cover the complete amplitude range of the receiver.

Since all the frequency channels of a given medium frequency receiver band utilize the same logarithmic compressors, it is only necessary to measure the amplitude response at one frequency channel for each band. The amplitude responses for the remaining channels can be obtained by calibrating the gain through the entire system as a function of frequency at a fixed amplitude. This calibration is called a channel-to-channel gain test. By combining the amplitude response with the channel-to-channel gain calibration, a complete set of calibrated look-up tables can be produced that convert the output telemetry values to signal strengths at the preamplifier inputs.

The frequency response of the three filters used in the medium frequency receiver was also determined by sweeping a sine wave signal over frequency while monitoring the output of a fixed channel. See Chapter 10 for a more detailed discussion of the calibration of the MFR.

5.1.5. Low Frequency Receiver

The low frequency receiver employs onboard fast Fourier transform processing of one or two channels of the five-channel waveform receiver to produce spectrums over a frequency range from 1 Hz to 26 Hz. The calibration of the low frequency receiver involved both amplitude and frequency calibrations. The amplitude calibration is similar to the medium frequency receiver amplitude calibration. A signal was applied to the input of the electric antenna amplifier at the center frequency of every fourth Fourier frequency component. The amplitude was then stepped in 2 dB increments to cover the complete amplitude range of the receiver.

The sensitivity of the low frequency receiver varies from channel to channel across the band. These frequency variations affect the calibration. A channel-channel gain test, similar to that performed on the medium frequency receiver, was conducted for each of the gain states of the low frequency receiver. This test was performed by applying an input signal of fixed amplitude to the input of the electric preamplifiers, and sweeping the signal from the lowest frequency channel of the low frequency receiver to the highest frequency channel. A combination of the amplitude response and the channel-channel gain measurements is then used to complete the calibration of the low frequency receiver for each gain state. See Chapter 9 for a detailed discussion of the calibration of the LFDR.

5.1.6. Wideband and Five-Channel Waveform Receivers

The response of the wideband and five-channel waveform receivers was determined by applying signals of known frequency and amplitude to the electric preamplifiers, and determining the gain factors required to convert the telemetry values into physical units. These

gain factors provide calibrations for both the time-series waveform and the spectrum produced by a Fourier transform of the waveform. The amplitude response of the wideband and five-channel waveform receivers was determined for each gain state, and for every filter mode. The frequency and phase response of the wideband receiver and the five-channel waveform receiver was determined by applying input signals of fixed amplitude to the input of the individual receivers, and sweeping the signal across the frequency band of the receiver. End-to-end calibration checks were performed by repeating the frequency response test and by applying an input signal of white noise with known spectral properties to the input of the electric and magnetic preamplifiers. See Chapter 12 for a discussion of the WBR calibration, and Chapter 13 for a discussion of the WFR calibration.

6.0 Electric Antennas

The RPWS Electric antennas extend radially from the RPWS Antenna Bracket located about 1.1m below the magnetometer boom.

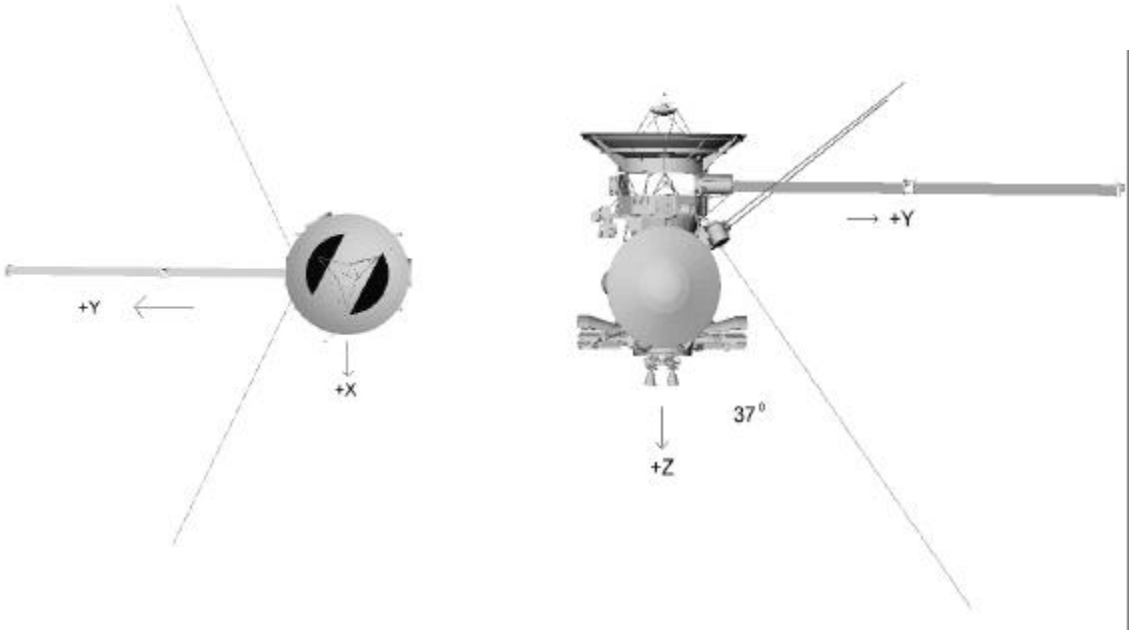

Top View Side View

Figure 6.0 Cassini Spacecraft

The RPWS uses three 10m long antenna elements. The element mounting configuration is shown in Fig. 6.1. The two upper elements are mounted with an angle of 120 degrees between them and form the X antenna. The centerlines of the two X axis elements are parallel but separated by 13.66cm. The third antenna is mounted at a 90° angle to the plane of the X axis antennas 37° from the spacecraft +Z axis. The mechanisms were aligned at assembly and shims determined for each mechanism to provide the required 1° (+/-.5° from centerline) alignment accuracy.

Physically the antennas are constructed of 2.86cm (1.125") diameter tubes of .098mm (.004") beryllium copper alloy. The elements have a thermal finish of bright polished silver plate externally and black thermal paint internally. The surface is perforated with small holes allowing solar radiation from about 12% of the sunlit element area to shine through and warm the shaded side of the element. This lowers the thermal differential across the element to decrease mechanical oscillations driven from thermal input. At the base of each antenna element spring loaded guide rollers contact the element as it enters the deployment mechanism. These rollers supply a spring constant for small movements of the antenna and should decrease the mechanical deadband of the antenna to zero for the purposes of the attitude control system.

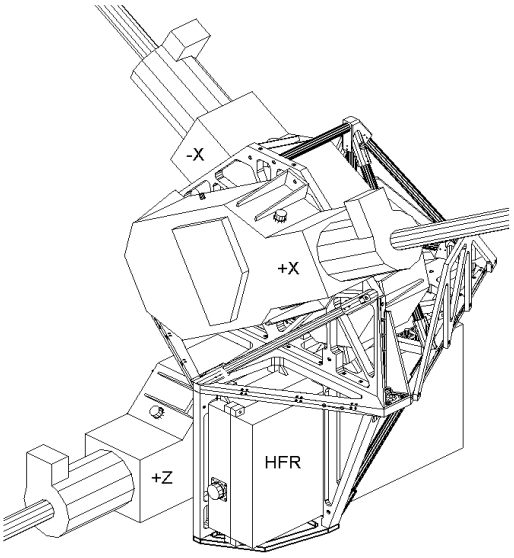

Figure 6.1 RPWS Antenna Bracket

The elements are formed from two interlocking strips of metal. At the tabs which occur at 1 inch intervals, there is no perforation. The area taken up by these non-perforated sections amounts to approximately 1 square cm per tab, or 2 sq cm per inch of length. The total exposed conductor area per element is 7993 sq cm plus the area of the tip mass at 17sq cm for a total of 8010 sq cm.

The Z axis antenna angle and position takes it past one of the RTG power sources and sun shades. The RTG and a section of antenna were mocked up in the lab and the element to was measured. This test indicates there is approximately 3pF of capacitance between the RTG and the antenna. The power bus to RTG capacitance was measured on an inert RTG and a flight RTG by placing known impedances in series with a signal generator and noting the amplitude division and phase shift. This test shows that there is on the order of 17,000pF between the RTG case and the main power bus. As a result, significant coupling of power bus noise to the Z antenna exists. To decrease the noise levels, the spacecraft has relays which will allow the RTG cases to be shorted to ground.

The exit snout of the antenna mechanisms is painted with Z307 black conductive paint, with a .1 inch insulating gap between the paint and the element. Thermal blankets cover up to the outer rim of the exit snout leaving a total area of 28.94 sq cm of paint exposed to the plasma. Figure 6.2 details the paint pattern of the exit snout. The conductivity of the black paint is 100-100,000 ohms/sq in.

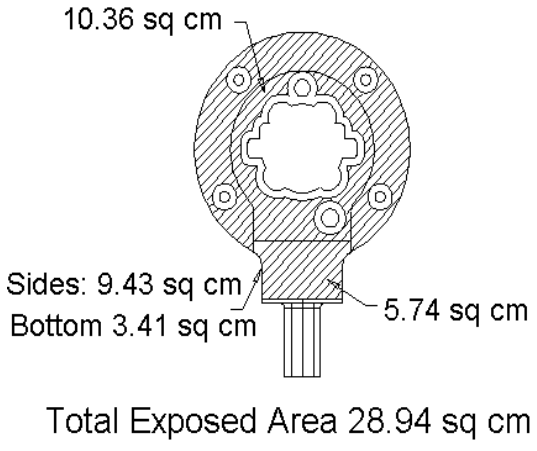

Figure 6.2 Conductive Paint

6.1 Physical Properties

The antenna elements have the following physical properties:

Mass/unit length	91.5g/m	
Natural frequency	.18Hz	(Includes effect of tip mass)
Damping	.37%	
Tip mass	34g	

6.2 Base Capacitance (in pF)

A. Measured

Mechanism	005 (+Z)	006 (-X)	007 (+X)
	50.7±.2	50.8±.2	50.4±.3
Coax Capacitance			
	37.4±.4	34.3±.4	34.7±.3
HFR Input Capacitance			
	Ez	Ex-	Ex+
	17.6	28.0	33.8
Total	**105.7±.6**	**113.1±.6**	**118.9±.6**

DC Isolation Element to Case >500Megohms

B. Calculated

The measured values take into account only the internal antenna capacitances. Capacitance from the antenna element to the S/C structure is ignored. To estimate the total antenna base capacitance, the effect of the base capacitance on the resonant frequency of the antenna is observed. The antenna resonance frequency as indicated by the peak of the galactic background radiation is observed to be at 8.5 MHz. Using an antenna modeling program with an accurate representation of the geometry, it is found that a value of 150 pF is required to resonate the antennas at 8.5 MHz.

6.3 Effective length

Geometrically, assuming perfectly straight elements, the center to center distance of the X axis booms is 9.26m. Because the +X element has a 13.66cm offset in the +Y direction, the geometric center to center line would form an angle of .85° between the antenna axis and the X axis in the X-Y plane.

Given that the antenna capacitance per element is given by:

$$C_{Ant}=2\pi\varepsilon_o l/(\ln(l/a)-1)$$

where ϵo is given by 8.85E-12, l=10m, and a=.0143m (.5625 in.), then:

$$C_{Ant}=100.2\text{pF}$$

There will be a loss expected of 8db from the capacitive voltage division due to the base capacitance calculated at 150 pF.

7.0 Magnetic Search Coil (MSC)

The Cassini RPWS magnetic sensor (MSC) consists of three search coil magnetometers mounted in a triaxial fixture. The search coil array is mounted on a boom ~1 meter from the spacecraft, and is oriented such that the measurement axes of the search coils are aligned with the principle axes of the spacecraft (Bx aligned with the spacecraft x axis, By aligned with the spacecraft y axis, and Bz aligned with the spacecraft z axis). The location and orientation of the search coil magnetometers are shown in Figure 3.1.2. Each sensor axis consists of a mu-metal core 27 cm long wound with 10,000 turns of fine wire, each search coil magnetometer responds to dB/dt over a frequency range of ~1 Hz to ~12.6 kHz. The search coils were built at the Centre d'Etudes des Environnements Terrestre et Planétaires.

7.1 Amplitude Calibration

The stand-alone calibrations of the RPWS search coil magnetometers were performed A. Meyer at the Centre d'Etudes des Environnements Terrestre et Planétaires using a drive coil in a mu-metal box and verified using a transmitting loop at a low noise location. These calibrations are summarized in the reference in Section 5.1.2, and are reproduced here as Tables 7.1.1, 7.1.2, and 7.1.3, and Figures 7.1.1, 7.1.2, and 7.1.3. Figures and Tables 7.1.1, 7.1.2, and 7.1.3 show the transfer function response for the Bx, By, and Bz search coils.

The End-to-End calibrations for each receiver is given in the individual receiver sections. These End-to-End calibrations were determined by combining the search coil calibration and the receiver calibrations, and verified by a series of tests with the search coils attached to the spacecraft, but in the mu-metal box.

Figure 7.1.1 Bx Search Coil Transfer Function

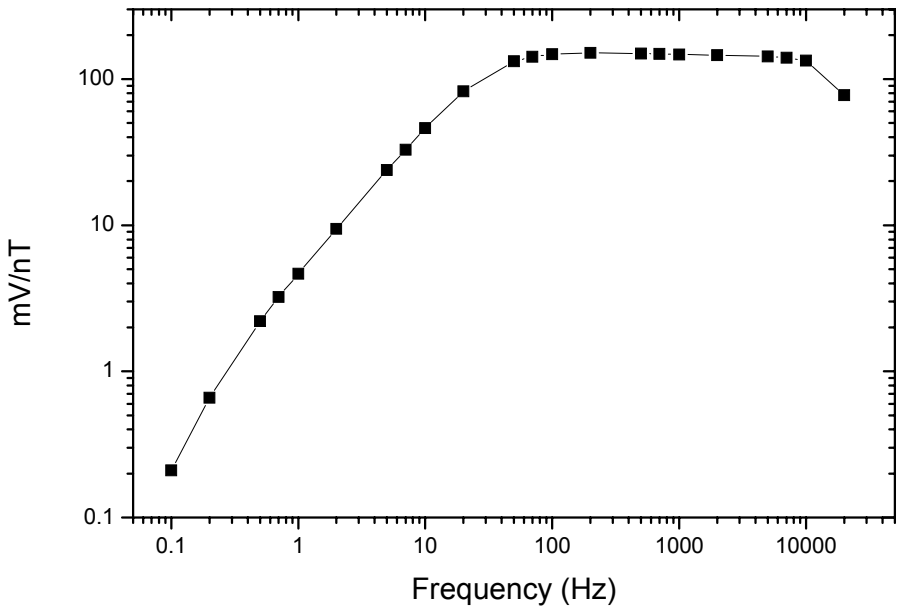

Table 7.1.1
Bx SEARCH COIL

Frequency (Hz)	Output (mV/nT)	Output (dBv/nT)	Output (Phase °)
0.1	0.21	-73.75	153.6
0.2	0.66	-63.63	135.6
0.5	2.20	-53.16	111.7
0.7	3.22	-49.83	105.2
1	4.66	-46.64	100.1
2	9.43	-40.51	92.5
5	23.85	-32.45	83.7
7	32.81	-29.68	79.7
10	46.13	-26.72	74.2
20	82.51	-21.67	59.0
50	132.43	-17.56	32.4
70	142.23	-16.94	23.7
100	148.08	-16.59	16.1
200	150.66	-16.44	6.7
500	149.28	-16.52	0.2
700	148.42	-16.57	-1.6
1000	147.40	-16.63	-3.4
2000	146.05	-16.71	-8.0
5000	142.56	-16.92	-20.2
7000	139.96	-17.08	-27.9
10000	133.81	-17.47	-40.5
20000	77.45	-22.22	-93.2

Figure 7.1.2 By Search Coil Transfer Function

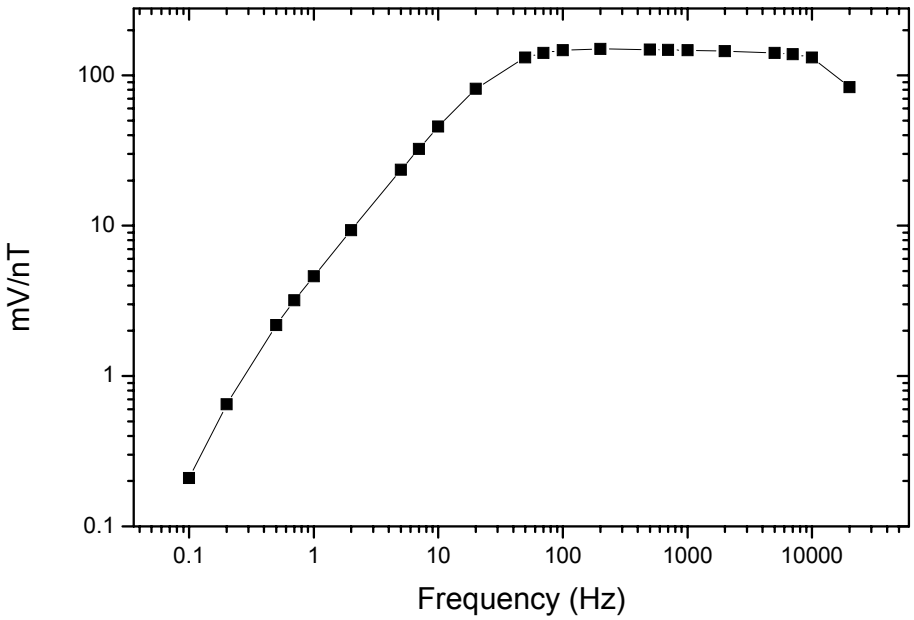

Table 7.1.2By
SEARCH COIL

Frequency (Hz)	Output (mV/nT)	Output (dBv/nT)	Output (Phase °)
0.1	0.21	-73.66	153.4
0.2	0.65	-63.68	135.2
0.5	2.18	-53.25	111.4
0.7	3.19	-49.93	105.0
1	4.60	-46.75	99.9
2	9.31	-40.62	92.5
5	23.55	-32.56	83.7
7	32.40	-29.79	79.7
10	45.60	-26.82	74.2
20	81.56	-21.77	59.2
50	131.37	-17.63	32.4
70	141.25	-17.00	23.8
100	147.06	-16.65	16.2
200	149.80	-16.49	6.8
500	148.42	-16.57	0.1
700	147.74	-16.61	-1.7
1000	146.72	-16.67	-3.6
2000	144.88	-16.78	-8.4
5000	140.93	-17.02	-21.2
7000	138.04	-17.20	-29.4
10000	131.07	-17.65	-42.8
20000	83.37	-21.58	-91.9

Figure 7.1.3 Bz Search Coil Transfer Function

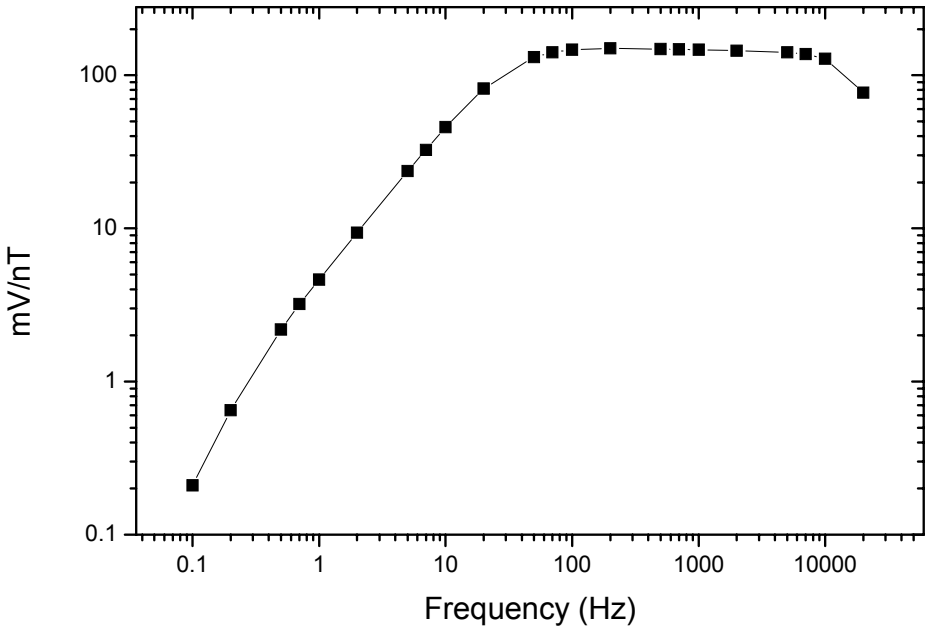

Table 7.1.3
Bz SEARCH COIL

Frequency (Hz)	Output (mV/nT)	Output (dBv/nT)	Output (Phase °)
0.1	0.21	-73.67	153.8
0.2	0.65	-63.71	135.4
0.5	2.18	-53.23	111.7
0.7	3.20	-49.89	105.3
1	4.62	-46.71	100.1
2	9.36	-40.57	92.5
5	23.66	-32.52	83.6
7	32.55	-29.75	79.7
10	45.81	-26.78	74.2
20	81.85	-21.74	59.0
50	131.22	-17.64	32.3
70	141.25	-17.00	23.7
100	147.06	-16.65	16.1
200	149.62	-16.50	6.6
500	148.08	-16.59	0.1
700	147.23	-16.64	-1.7
1000	146.55	-16.68	-3.6
2000	144.88	-16.78	-8.5
5000	140.77	-17.03	-21.7
7000	137.40	-17.24	-30.2
10000	127.79	-17.87	-44.8
20000	76.82	-22.29	-94.3

7.2 Phase Calibration

The stand-alone phase calibrations of the RPWS search coil magnetometers were performed A. Meyer at the Centre d'Etudes des Environnements Terrestre et Planétaires using a drive coil in a mu-metal box and verified using a transmitting loop at a low noise location. These calibrations are reproduced here as Figures 7.2.1, 7.2.2, and 7.2.3, and show the phase response for the Bx, By, and Bz search coils with respect to frequency.

Figure 7.2.1 Bx Search Coil Phase

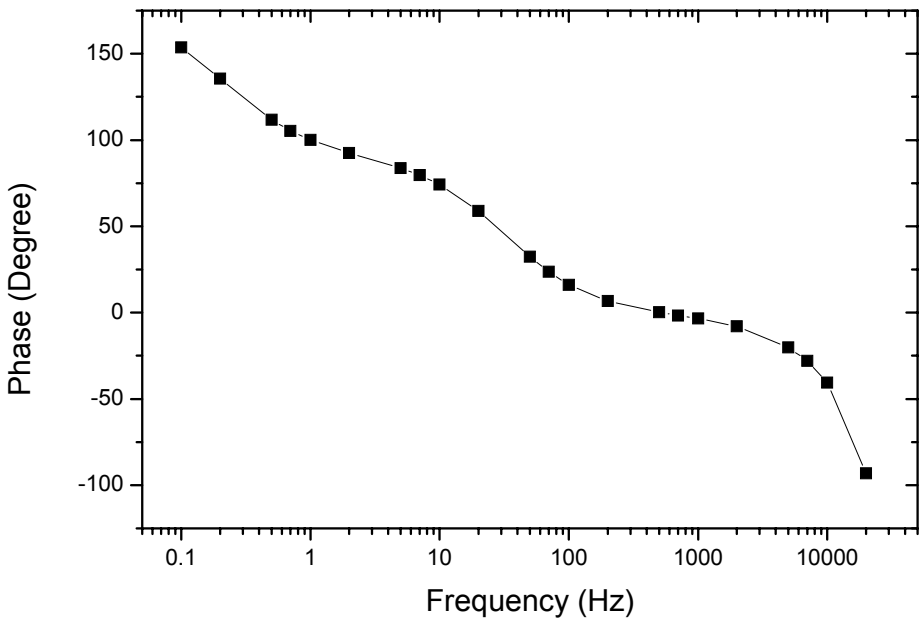

Figure 7.2.1 By Search Coil Phase

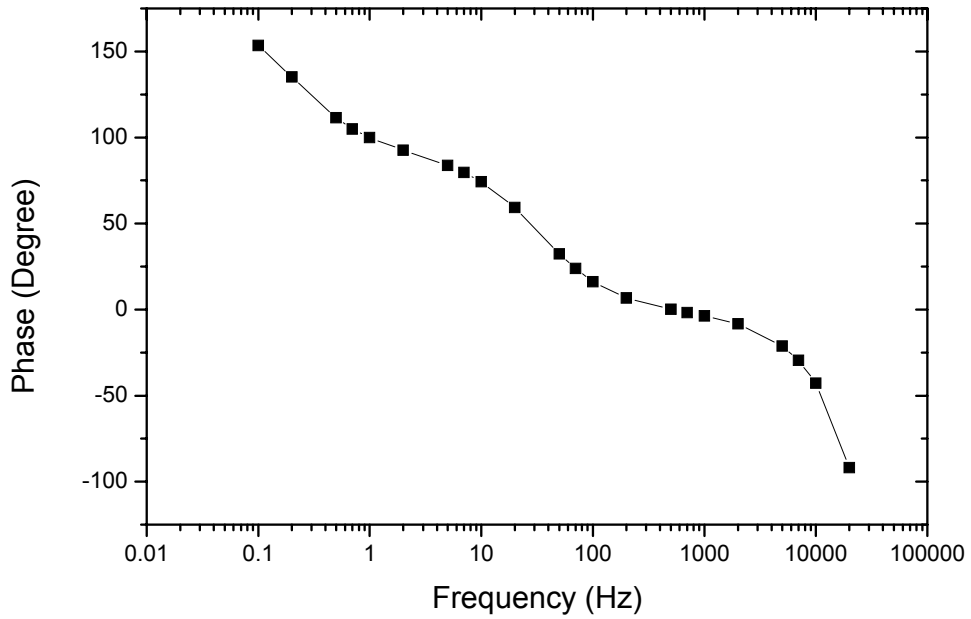

Figure 7.2.1 Bz Search Coil Phase

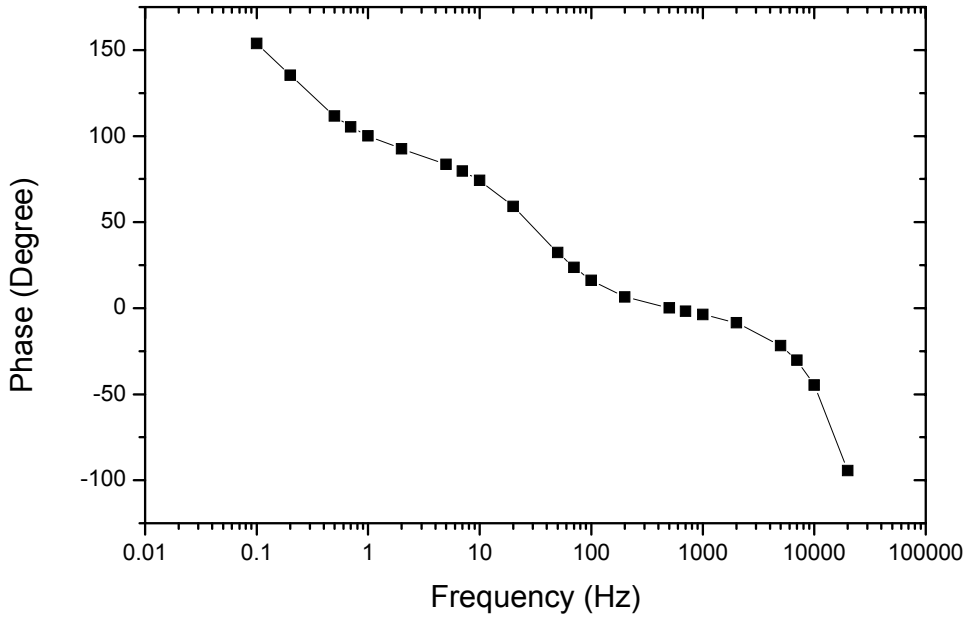

7.3 Magnetic Search Coil Noise Levels

Table 7.3.1 show the measured noise levels for the search coil and preamplifier during bench testing. The in-flight noise level will be discussed in the individual receiver sections.

Table 7.3.1 SEARCH COIL BENCH NOISE LEVELS

Frequency (Hz)	Bx Sensitivity $nT/Hz^{1/2}$	By Sensitivity $nT/Hz^{1/2}$	Bz Sensitivity $nT/Hz^{1/2}$
0.1	2.67E-01	1.98E-01	3.16E-01
0.2	5.95E-02	5.20E-02	8.16E-02
0.5	1.23E-02	1.02E-02	1.39E-02
0.7	6.83E-03	5.94E-03	7.32E-03
1	3.98E-03	3.69E-03	4.24E-03
2	1.62E-03	1.82E-03	1.74E-03
5	6.39E-04	6.62E-04	6.47E-04
7	4.65E-04	4.84E-04	4.41E-04
10	3.30E-04	3.44E-04	3.18E-04
20	1.47E-04	1.55E-04	1.53E-04
50	7.01E-05	6.63E-05	6.87E-05
70	4.59E-05	4.99E-05	4.94E-05
100	3.69E-05	3.82E-05	3.61E-05
200	1.95E-05	2.21E-05	2.31E-05
500	1.61E-05	1.64E-05	1.76E-05
700	1.62E-05	1.60E-05	1.69E-05
1000	1.63E-05	1.77E-05	1.69E-05
2000	1.66E-05	1.71E-05	1.71E-05
5000	1.87E-05	1.87E-05	2.10E-05
7000	2.21E-05	2.16E-05	2.40E-05
10000	2.82E-05	2.98E-05	3.44E-05
20000	8.63E-05	8.18E-05	8.93E-05

8.0 Langmuir Probe

8.1 Introduction

The RPWS Langmuir Probe (LP) instrument for Cassini consists of one spherical probe on a stiff boom, a boom root preamplifier, interface circuitry for the cylindrical plus and minus antennas, and an electronics board located in the RPWS electronics box. The LP can be used to estimate a number of fundamental plasma parameters, among which the electron density is usually the most requested parameter. The LP instrument is designed to measure the *dc* and *ac* variations of the electrical current to a dedicated spherical probe, but also in a limited time sharing mode make use off the minus and plus RPWS cylindrical antenna for additional interferometer measurements. From these measured currents it is possible to derive the following physical parameters.

Electron density (N_e)
Electron temperature (T_e)
Density variations up to 10 kHz ($\delta n/n$)
Effective ion temperature over mean ion mass (T_i/m_i)
UV intensity (photoelectron flux) mostly from Ly-α
Spacecraft potential (U_{sc})
Dust impacts on spacecraft

The accuracies of these parameters have been estimated to about 10% for the electron density and about 20% for the other parameters from the in-flight commissioning as well as during the inter-instrument calibrations made during the Earth flyby in 1998. The instrument will be operative during a significant part of the Saturn tour in a wide range of physical environments. The accuracy of each parameter under various conditions may therefore vary somewhat. Measurements are expected to be possible down to as low plasma densities as 1 cm^{-3}, depending somewhat on solar activity conditions.

A bias voltage sweep of up to ±32V referred to the satellite ground can be made on the dedicated spherical probe to obtain most of the physical parameters defined above. In *ac* mode the bias voltage will be set manually or automatically to a level determined by the local plasma parameters obtained by a sweep or pre-estimated from mission parameters. The cylindrical antenna bias is limited to ±12V in order to fulfill the satellite potential drift requirement.

The scientific capabilities of the instrument proposal and the design parameters are given in Table 1. The comparison show that the instrument performs as original proposed in most ways. The design drivers for the instrument have been the capability to cover up to five decades of electron and ion density ranges, and to provide *ac* density variations from all probes to the RPWS wave analyzers WBR and WFR.

Table 1. LP scientific instrument performance (proposal vs. calibration results)

Instrument proposal			Calibration results	
Quantity	Measurement range.	Frequency range	Measurement range	Frequency range
Sphere DC	±5 dec (1nA-100uA)	0-10Hz	±6 dec (±6.5 at 20C)	0-6Hz
Sphere AC	50-0.1% mod	0-10kHz	100-0.05% min	0-6kHz
Sphere Sweep	±50 V	1kHz	±32 V	1kHz
±5 Cylp DC	±5 dec (1nA-100uA)	2.5kHz at 1uA	±5 dec (1nA-100uA)	2.7kHz at 1uA
Cylp Bias	±10 V	---	±12 V	---

From calibration point of view the instrument consists of several modules with unique transfer functions. The contact surface between plasma and sensor, the preamplifier or cylinder probe electronics interface, the analogue signal processing, the buffers for *ac* signals distribution to RPWS wave analyzers, multiplexes, bias circuitry, filter and the ADC, and the controller unit are all modules which will be addressed in this document. For detailed information on the interconnections between modules see the block diagram in Figure 1.

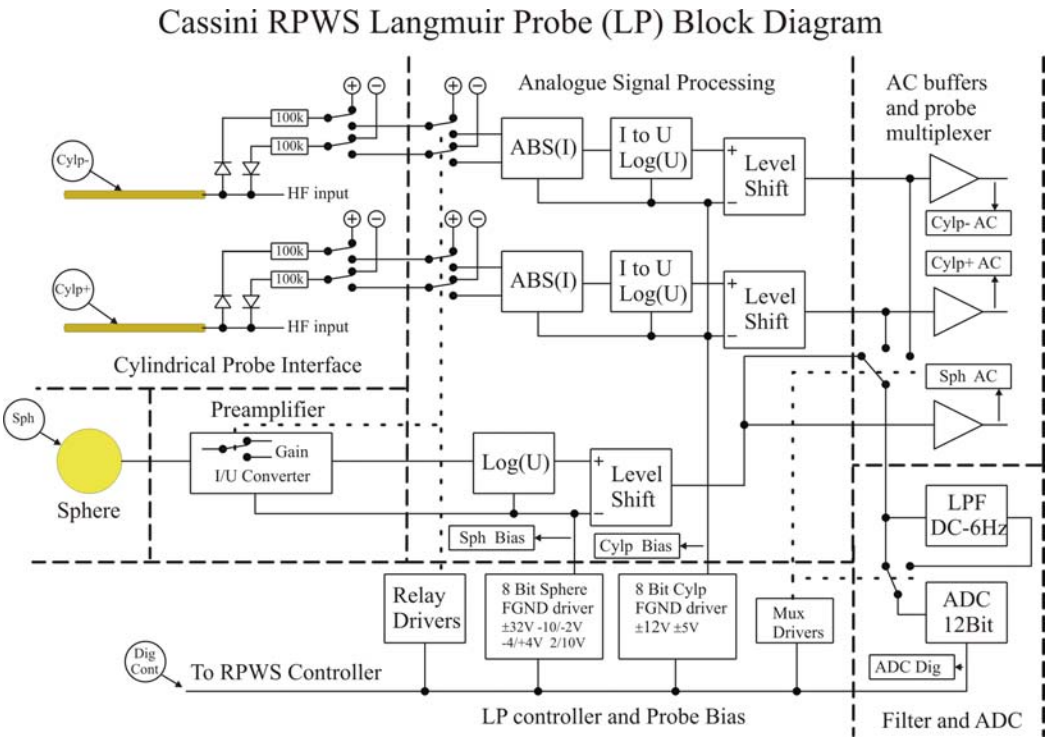

Figure 1. Langmuir Probe block diagram.

Extensive calibration has been carried out on the LP assembly as well as the LP integrated into the complete RPWS. The main reference calibration was performed on the stand-alone LP assembly in Uppsala before delivery to RPWS. On satellite level only a few tests have been carried out to verify correct operation of the instrument. Details are shown in the block diagram of main input (encircled) and output (in a box) quantities used to establish proper transfer functions.

The Calibration fulfill the following purposes:

- To verify instrument performance in relation to scientific requirements.
- To obtain the transfer functions for the instrument, and adequate information for conversion of TM to physical units.
- To determine drift of parameters due to temperature changes.

8.2 Dedicated spherical probe mechanical drawings

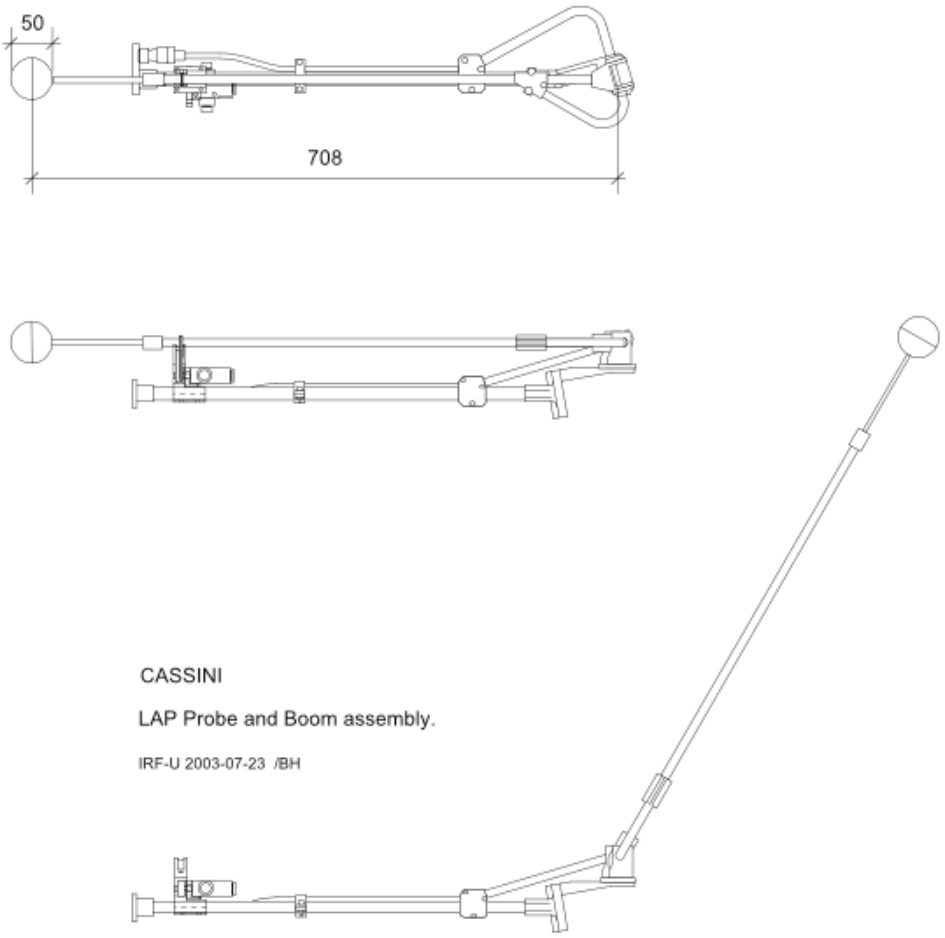

Figure 2. Dedicated Langmuir Probe assembly mechanical configuration before and after deployment.

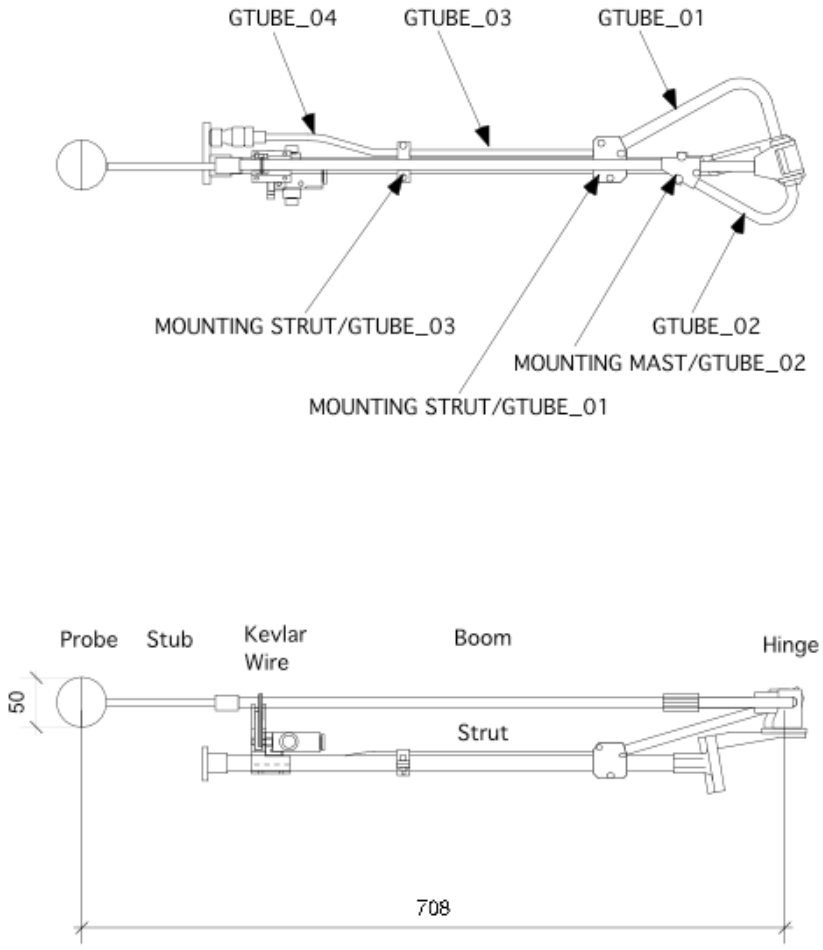

Figure 3. Dedicated Langmuir Probe mechanical labeling.

8.2.1 Spherical probe

The spherical probe sensor is situated on top of a stiff boom 1.2 m from the spacecraft body when deployed. For calibration purposes a cable and probe simulator was used to replace the boom assembly.

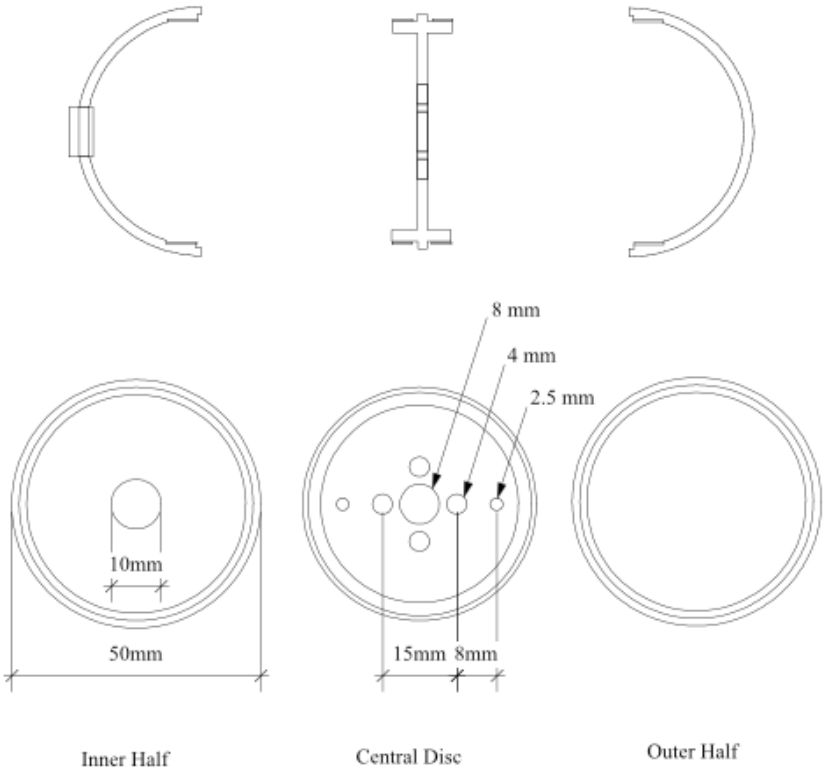

Figure 4. Dedicated Langmuir Probe sensor.

8.2.2 Spherical probe low frequency calibration.

In Figure 5 a generic test set-up for *dc* calibrations is shown. The Keithley 220 current generator feed current to the preamplifier via a boom cable. The resulting voltage on the input of the ADC and the digital ADC output is collected by the controller and stored in the calibration file. The controller also operates the current generator to form a closed loop calibration sequence. Heavy filtering of the 220 mains supply is needed to ensure a low noise environment required for low current measurements.

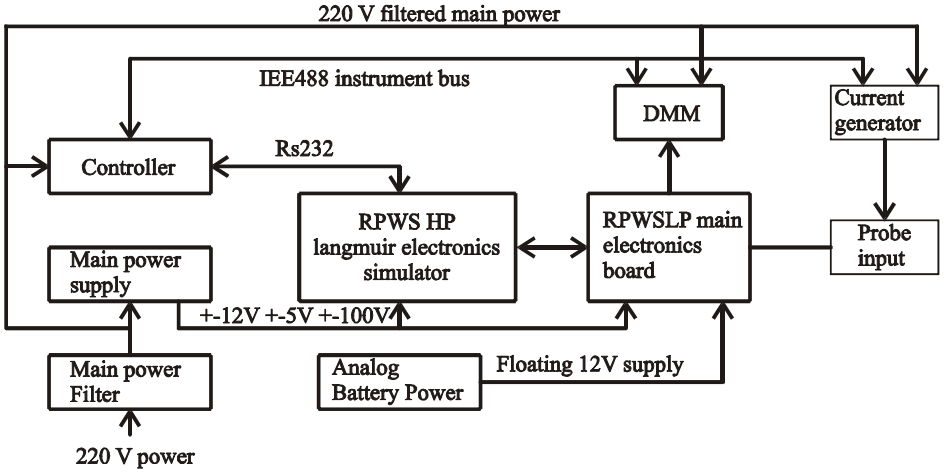

Figure 5. The *dc* test set-up.

8.3.1.2 Converting telemetry values to physical units.

The proper physical units for the spherical probe measurements will be obtained using a physical parameters model applied to the in-flight measured probe current vs. bias (not given here). The *dc* probe current to TM unit conversion is given by calibration curves in 8.3.1.3.

8.3.1.3 Spherical probe *dc* calibration.

The calibration output data are stored in files with a unique file name describing the calibration type and at which temperature it was made.

Table 2. File name identification:

Character position	Description
1	Spherical probe
2	P = positive input current N = negative input current
3	Current
4,5	LG = low preamplifier gain HG = high preamplifier gain
6,7	LF = 6Hz filter HF = No filter
8-12	Temperature in deg. Celsius.

Table 3. Data file format:

Column	Description
1	Input current to probe (Amp)
2	Digitized data from LP 12bit ADC (0-4095 -5 to 5 V)
3	Input voltage to ADC (Voltage –5 to 5 V)

Spherical probe *dc* current calibration plots:

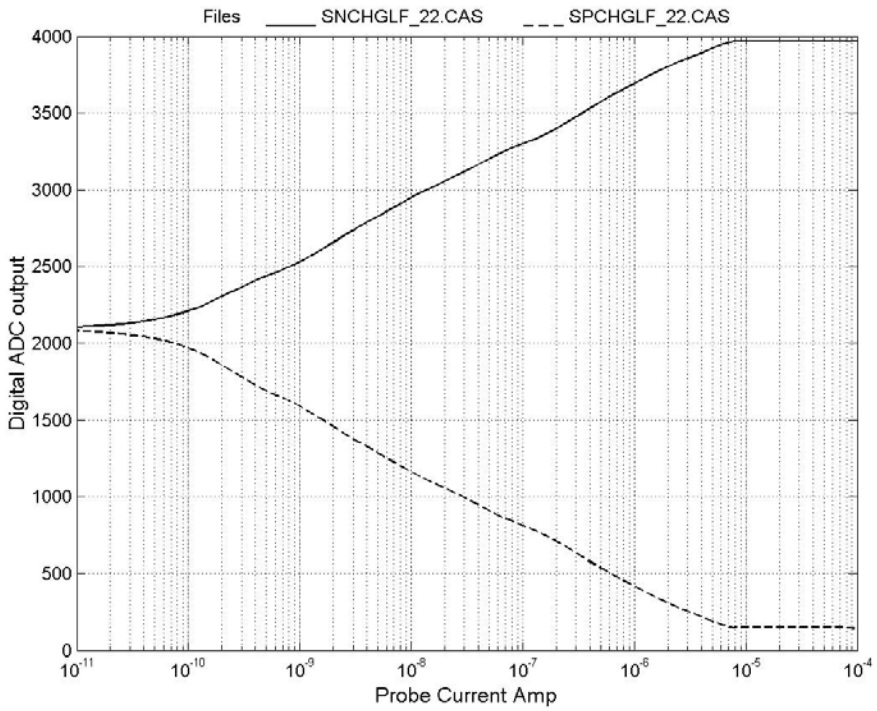

Figure 6. The *dc* transfer function from Sph to ADC dig. (See block diagram) Preamplifier at high gain, pos. and neg. input current, 6 Hz filter, and 22C.

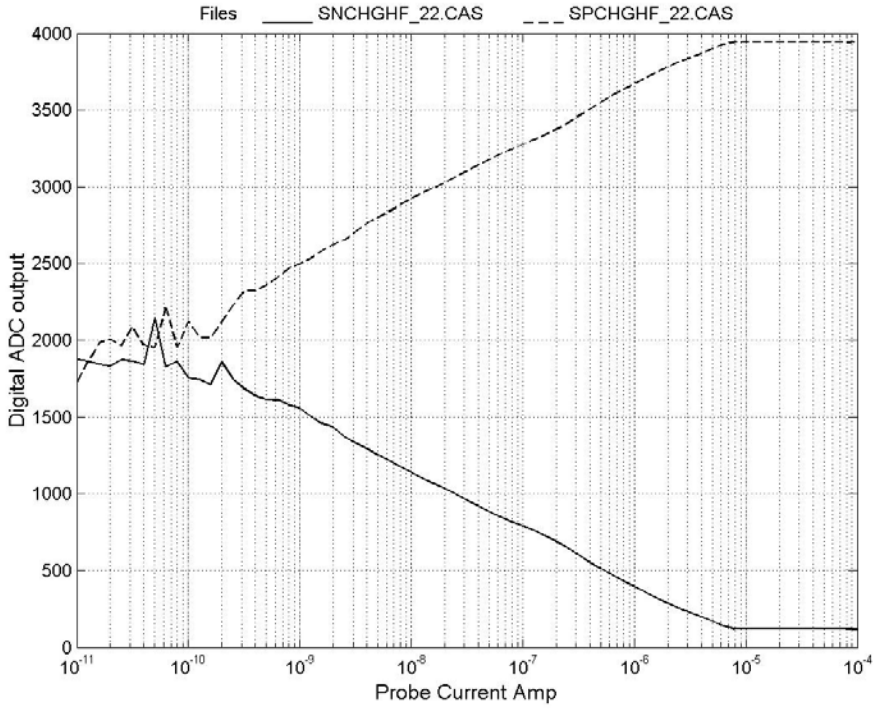

Figure 7. The *dc* transfer function from Sph to ADC dig. (See block diagram) Preamplifier at high gain, pos. and neg. input current, without filter, and 22C.

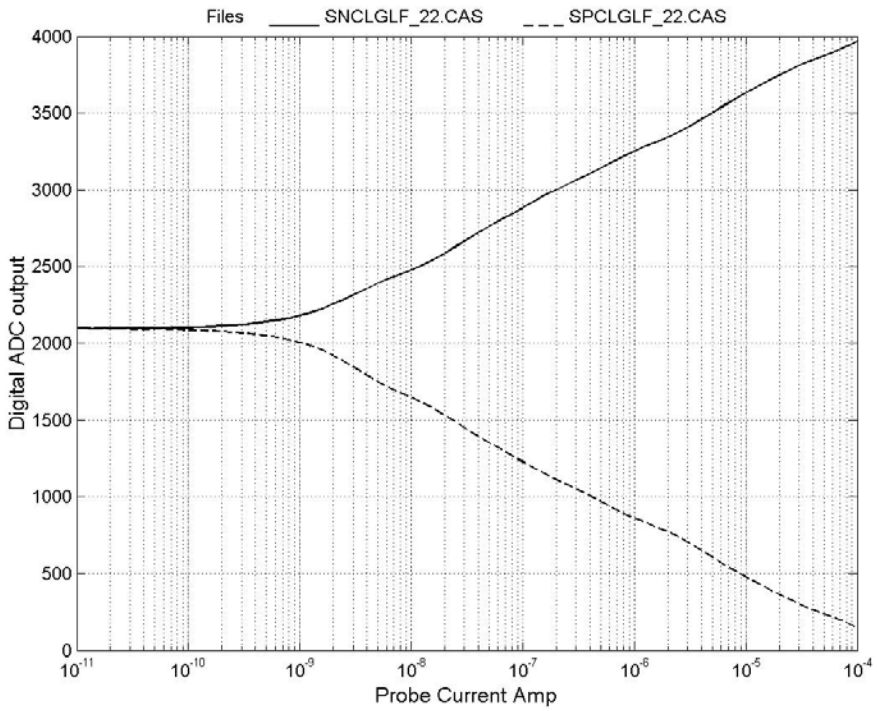

Figure 8. The *dc* transfer function from Sph to ADC dig. (See block diagram) Preamplifier at low gain, pos. and neg. input current, 6Hz filter, and 22C.

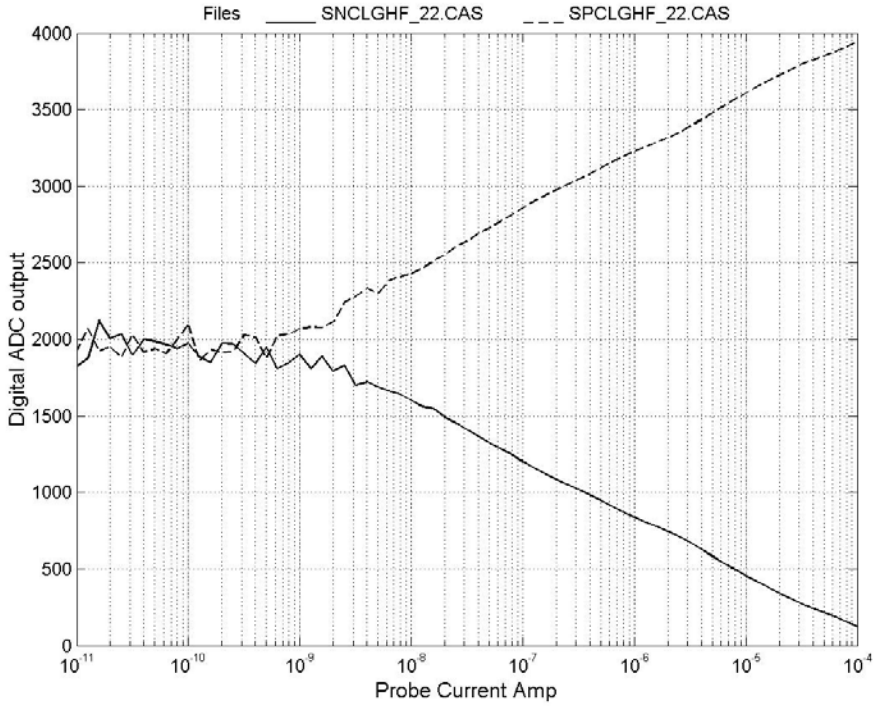

Figure 9. The *dc* transfer function from Sph to ADC dig. (See block diagram) Preamplifier at low gain, pos. and neg. input current, without filter, and 22C.

Table 4. List of files for the *dc* spherical probe calibration:

Temperature	Fig No.	Positive Current	Negative Current
22C	1	SPCHGLF_22.CAS	SNCHGLF_22.CAS
	2	SPCHGHF_22.CAS	SNCHGHF_22.CAS
	3	SPCLGLF_22.CAS	SNCLGLF_22.CAS
	4	SPCLGHF_22.CAS	SNCLGHF_22.CAS
-20C		SPCHGLF_-20.CAS	SNCHGLF_-20.CAS
		SPCHGHF_-20.CAS	SNCHGHF_-20.CAS
		SPCLGLF_-20.CAS	SNCLGLF_-20.CAS
		SPCLGHF_-20.CAS	SNCLGHF_-20.CAS
0C		SPCHGLF_0.CAS	SNCHGLF_0.CAS
		SPCHGHF_0.CAS	SNCHGHF_0.CAS
		SPCLGLF_0.CAS	SNCLGLF_0.CAS
		SPCLGHF_0.CAS	SNCLGHF_0.CAS
40C		SPCHGLF_40.CAS	SNCHGLF_-20.CAS
		-	-
ADC input voltage only		SPCLGLF_-20.CAS	SNCLGLF_-20.CAS
		-	-

8.3.1.4 ADC filter characteristic.

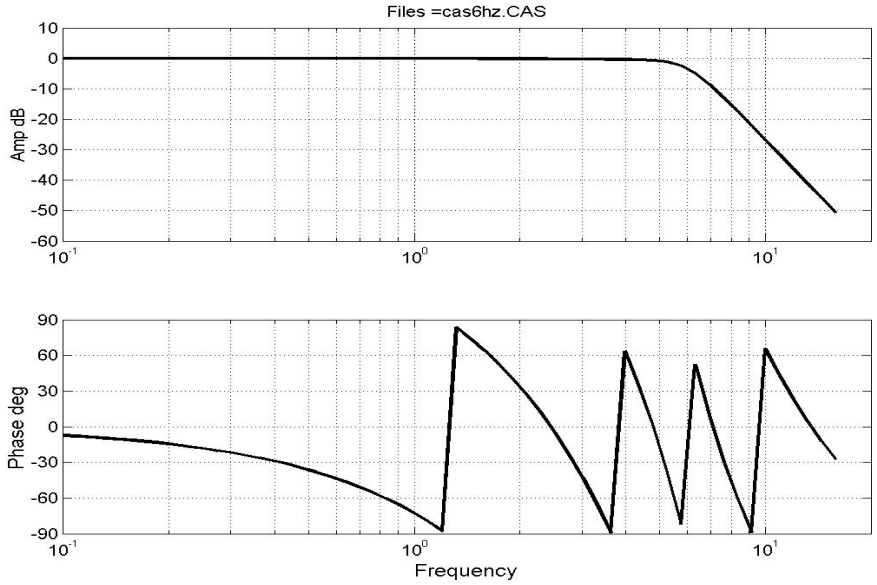

Figure 10. ADC input aliasing filter response.

8.2.3 Spherical probe high frequency calibration

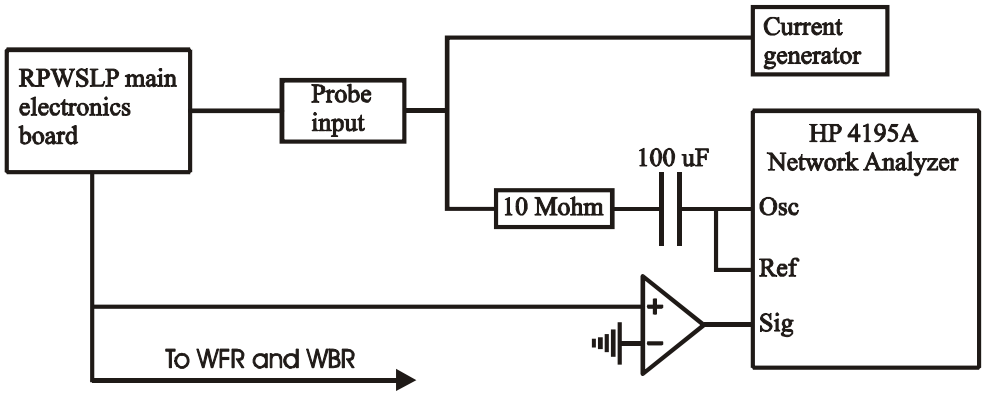

Figure 11. The *ac* test set-up.

Figure 11 show the test set-up used for the *ac* calibration. The transfer function from Sph to Sps *ac* is determined in this calibration (see block diagram).

Adding a constant current from the current generator to the *ac* current from the Network Analyzer generates an *ac* modulated current on the input of the probe. It should be noted that the input impedance for the preamplifier is in the order of a few Ohm at frequencies up to 10kHz. That is why the voltage output from the Network Analyzer is converted, via the resistor, to a defined the *ac* current at the input of the preamplifier. Half the *ac* p-p current divided by the *dc* current define the modulation (m), which is used as the main input parameter for this calibration. The modulation is defined as:

$$m = (I_{ac,p\text{-}p}/2)/I_{dc}$$

8.2.3.1 Converting telemetry values to physical units

The conversion from modulation (m) to mean output voltage (V_{rms}) is covered by this calibration. The estimate of signal power from modulation values requires a scientific model, which is not included here.

8.2.3.2 HF calibration tests / results for the WFR and WBR LP output.

Output voltage rms. vs. input m and the noise floor for a constant *dc* current is given by the MX plots. Those quantities can also be extracted from the frequency response calibration (S) plots and the *dc* Diff calibration. As the logarithmic factor varies with the input *dc* current the Diff calibration must be used if accuracy better than ±1.5 dB is required.

In the Modulation calibration (MX plots) the frequency is 660 Hz and m is varied from 50% to 0.05% in seven steps. The resulting instrument response is stored on paper plots (see figure 12).

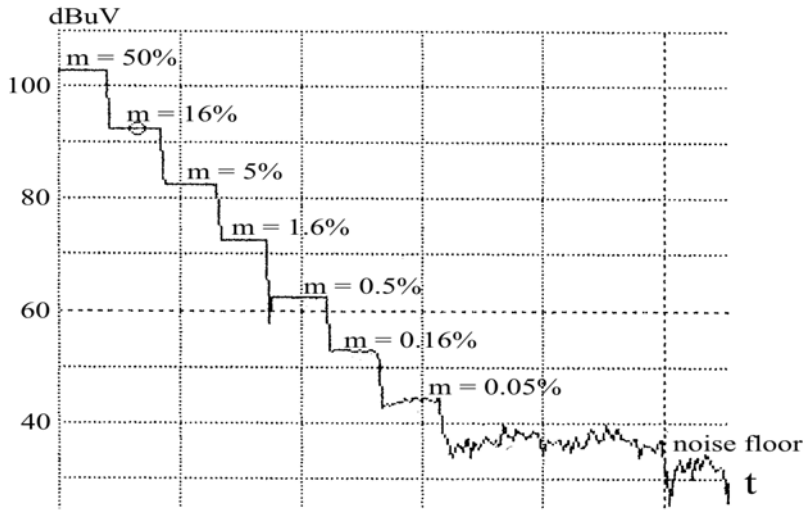

Figure 12. M1 modulation plot. I_{dc} = +10 nAmp

The output voltage can be obtained from the following equation

$$\log(V_{out}) = k + \log(m)$$

where k = -0.625 for an average of M1 to M15 levels.

Table 5. List of M plots:

Plot No.	File name	Input current	Preamp. Gain	Noise floor (<m)
1	m01.tif	+10nA	high	0.01%
2	m01.tif	+1nA	high	0.1%
3	m02.tif	-1nA	high	0.1%
4	m03.tif	-10nA	high	0.01%
5	m03.tif	+100nA	high	0.005%
6	m04.tif	+100nA	low	0.005%
7	m04.tif	+10nA	low	0.01%
8	m05.tif	+1uA	low	0.001%

The preamplifier is the dominating pole in the path from probe to LP output to WFR and WBR, and the frequency response is given by its gain. The 3dB point is 6kHz for high gain and 8kHz for low gain and independent on input current. Figure 13 show the frequency response for high gain and Figure 14 show the response for low gain.

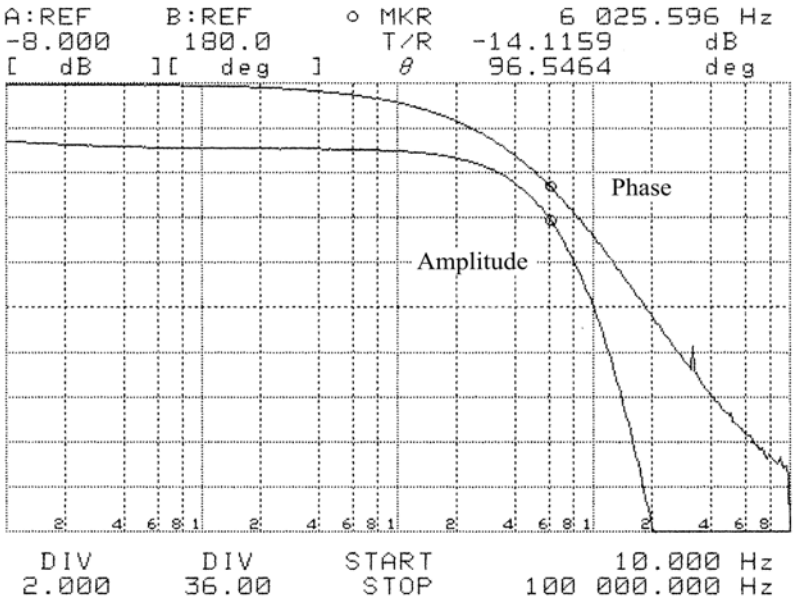

Figure 13. Frequency response for the Spherical probe output to the RPWS wave receivers. High gain, m = 10% and I_{DC} = 100nA.

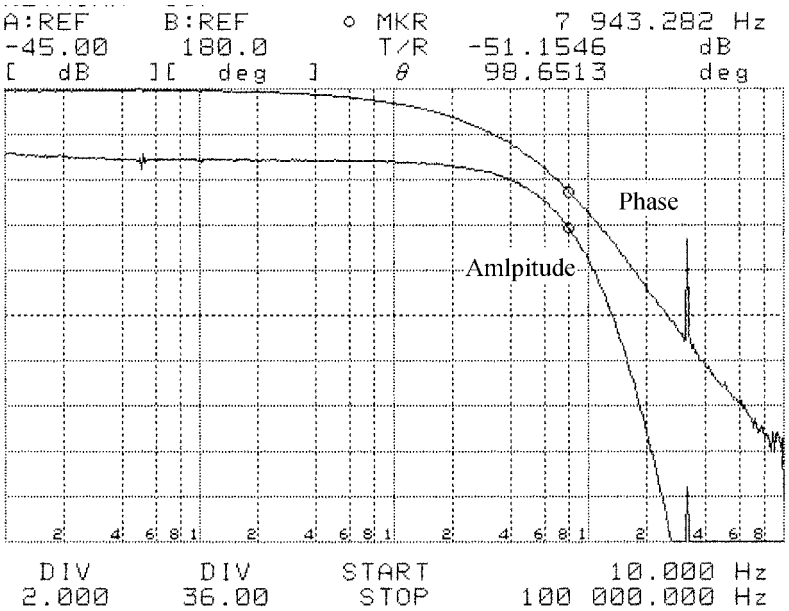

Figure 14. Frequency response for the spherical probe output to the RPWS wave receivers. Low gain, m = 10% and I_{dc} = 10nA.

Table 6. List of S plots:

Plot No.	File name	m %	Input DC current	Preamp. gain
1	S1_2.tif	10	1uA	High
2	S1_2.tif	10	100nA	High
3	S3_4.tif	10	10nA	High
4	S3_4.tif	10	1nA	High
5	S5_6.tif	10	-1nA	High
6	S5_6.tif	10	-10nA	High
7	S7_8.tif	10	-100nA	High

8	S7_8.tif	10	-1uA	High
9	S9_13.tif	10	10uA	Low
11	S11_15.tif	10	100nA	Low
13	S9_13.tif	10	-10uA	Low
15	S11_15.tif	10	-100nA	Low

8.3.3 Sphere probe bias voltage

The LP spherical probe bias voltage is under RPWSHR processor control. The Bias voltage can be set to 256 levels in four ranges. FUL covers a bias range from –33V to +31V in 256 steps and is used for sweeping and fixed bias. LOW, MID, and HIG have a range of 8 V in 256 steps and are centered around –6V, 0, and +6 respectively. They are used for fine sweeps around zero input current and sweep in low plasma temperatures. This calibration gives the transfer function from Dig Com to Sph Bias (see block diagram).

Figure 15, 16, 17, and 18 show plots of bias voltage vs. digital 8 bit word input from RPWS HP for FUL, LOW, MID, and HIG respectively at 22C.

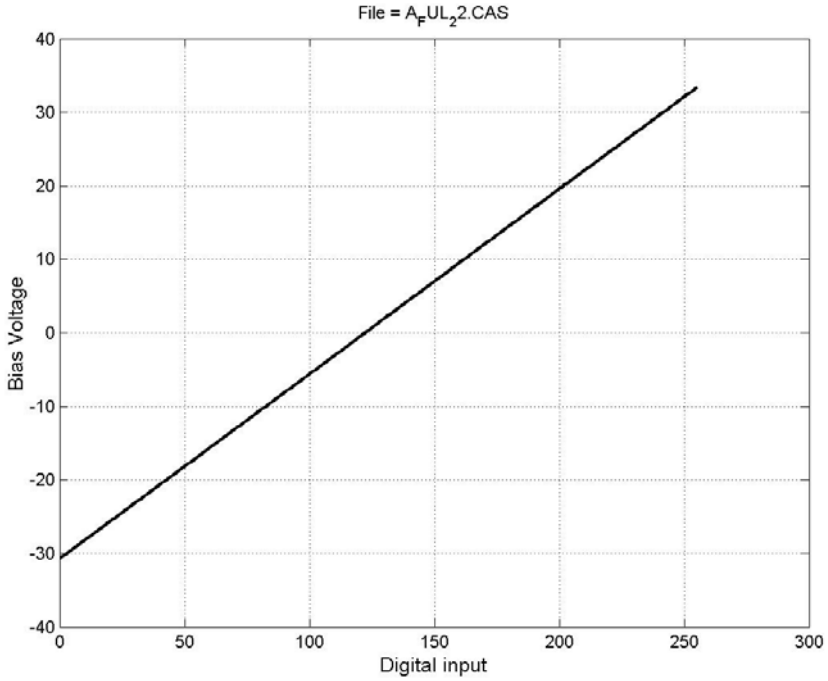

Figure 15. LP spherical probe full bias range.

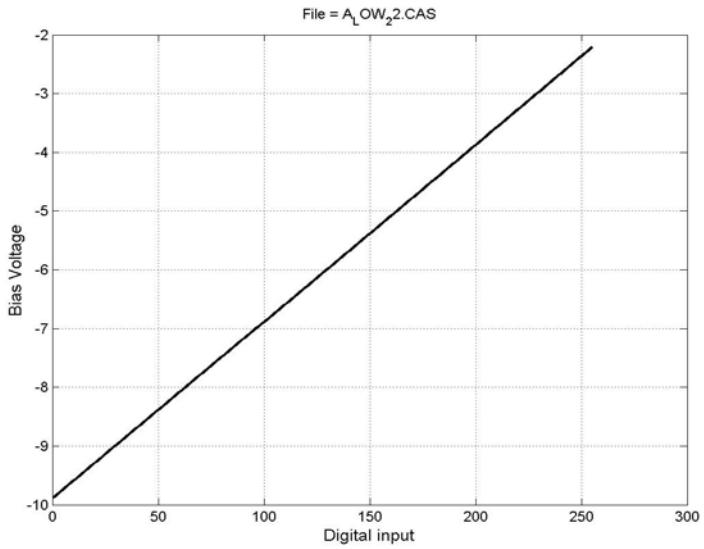

Figure 16. LP spherical probe low bias range.

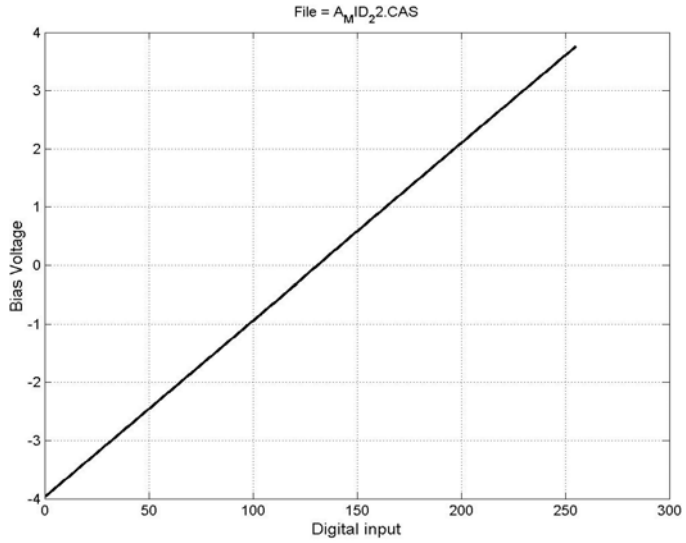

Figure 17. LP spherical probe middle bias range.

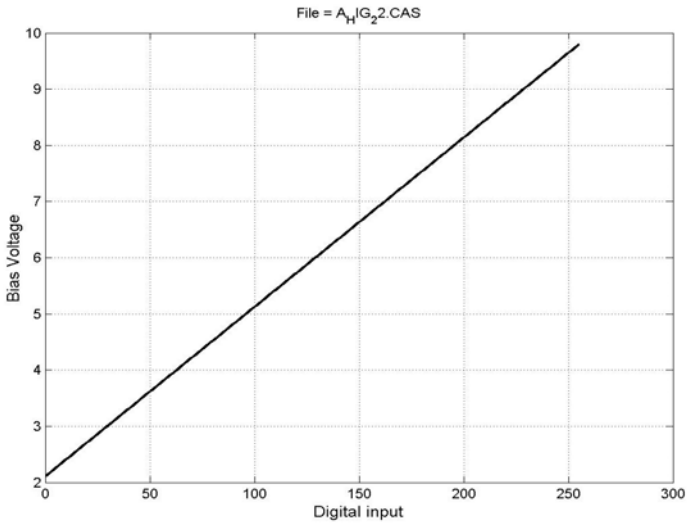

Figure 18. LP spherical probe high bias range.

Table 7. List of Spherical probe bias calibration files.

Temp.	File name FUL	File name LOW	File name MID	File name HIG
-20C	A_FUL_-20.CAS	A_LOW_-20.CAS	A_MID_-20.CAS	A_HIG_-20.CAS
0C	A_FUL_0.CAS	A_LOW_0.CAS	A_MID_0.CAS	A_HIG_0.CAS
22C	A_FUL_22.CAS	A_LOW_22.CAS	A_MID_22.CAS	A_HIG_22.CAS
40C	A_FUL_40.CAS	A_LOW_40.CAS	A_MID_40.CAS	A_HIG_40.CAS

8.4 Cylindrical probes

The LP cylindrical probes (cylp) are two of the three long antenna used by the HFR for E-field measurements from a few Hz to 10MHz. The LP is connected to –cylp and +cylp via two relays, a diode and a 100kohm resistor used for high voltage protection. The bias voltage is restricted to ±10V at the sensor due to satellite environment requirements.

8.4.1 Low frequency calibration

This Calibration is performed using the same test set-up as for the spherical probe *dc* calibration. The transfer functions from –Cylp and +Cylp to ADC Dig are obtained from this calibration (see block diagram).

8.4.1.1 Converting telemetry values to physical units

The proper physical units for the cylindrical probe measurements will be obtained using a physical parameters model applied to the in-flight measured probe current vs. bias (not given here). The *dc* probe current to TM unit conversion is given by calibration curves in 8.4.1.2.

8.4.1.2 Cylindrical probe *dc* calibration tests/results

The calibration output data are stored in files with a unique file name describing the calibration type and at which temperature it was made.

Table 8. File name identification:

Character position	Description
1,2	PC = Positive Cylp.
3,4	PC = positive input current NC = negative input current
5,6	LF = 6Hz filter HF = No filter
7,11	Temperature in deg. Celsius.

Table 9. Data file format:

Column	Description
1	Input current to probe (Amp)
2	Digitized data from LP 12bit ADC (0-4095 -5 to 5 V)

3	Input voltage to ADC	(Voltage –5 to 5 V)

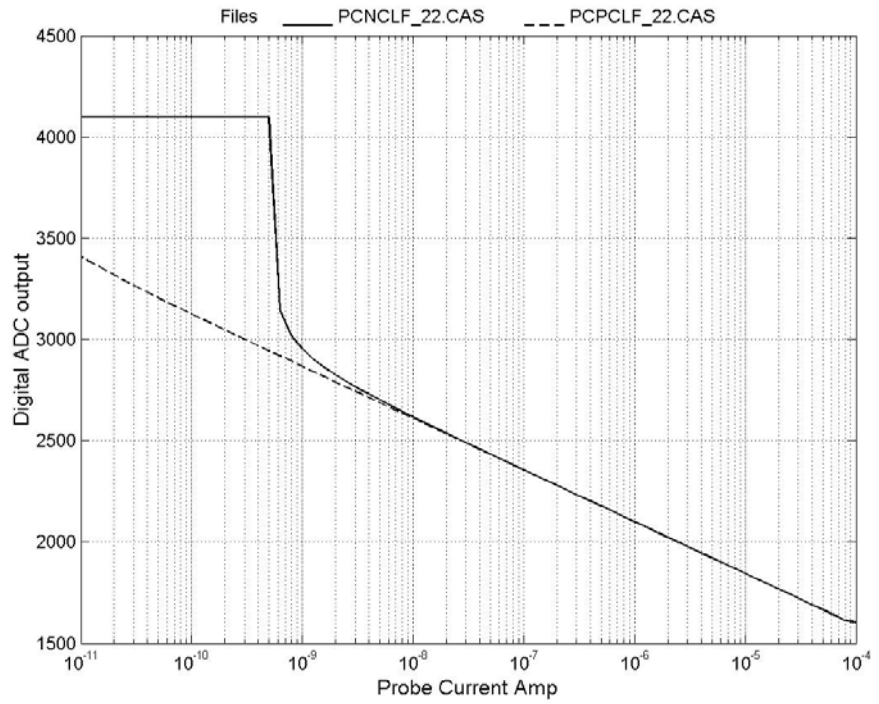

Figure 19. + Cylindrical probe *dc* calibration curves for 22C. 6Hz filter connected.

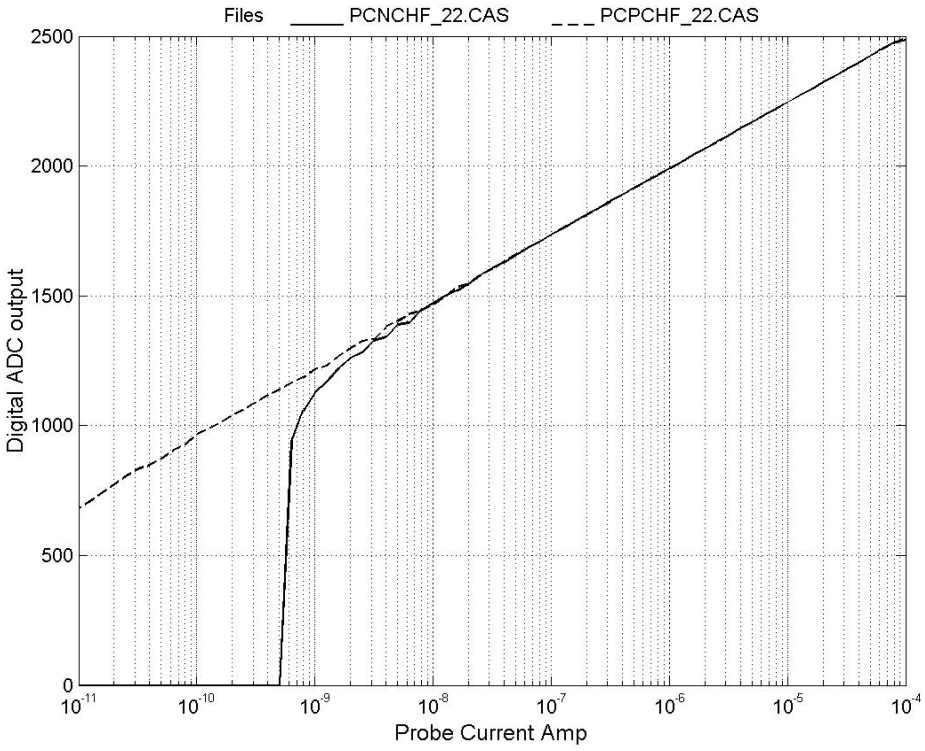

Figure 20. + Cylindrical probe *dc* calibration curves for 22C. No filter connected.

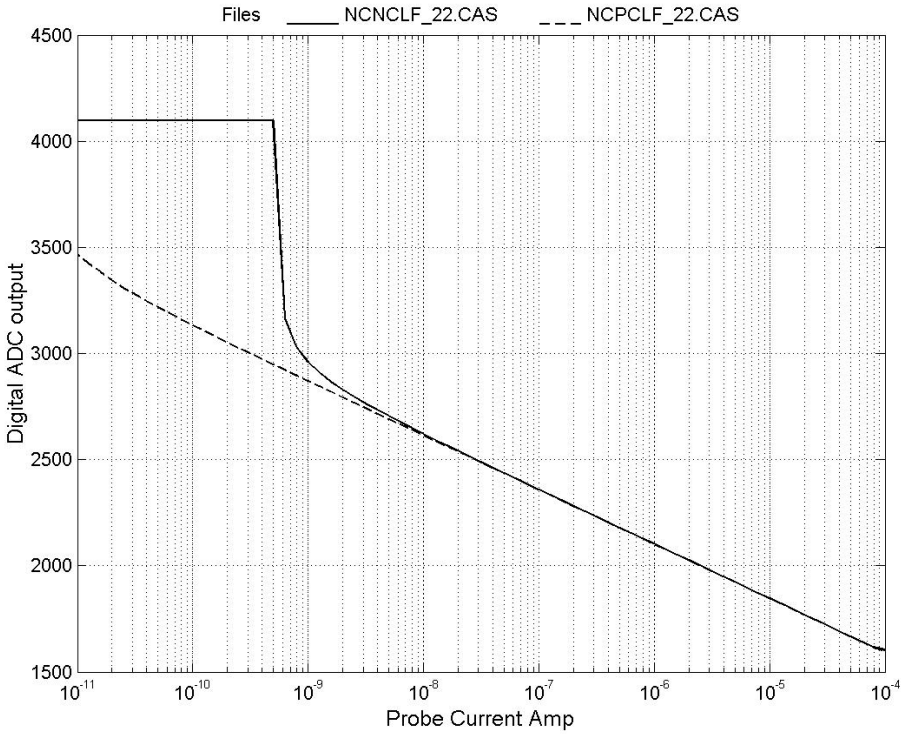

Figure 21. - Cylindrical probe *dc* calibration curves for 22C. 6Hz filter connected.

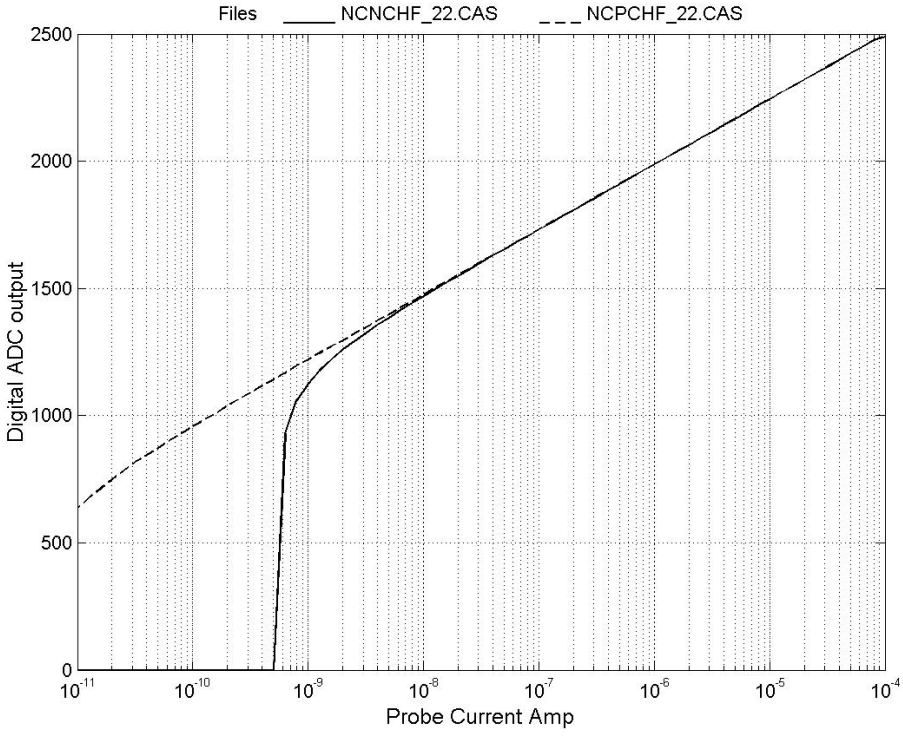

Figure 22. - Cylindrical probe *dc* calibration curves for 22C. No filter connected.

Table 10. List of files for the *dc* Cylindrical probe calibration:

Temperature	Cylp.	Positive Current	Negative Current
22C	neg	NCPCLF_22.CAS	NCNCLF_22.CAS
	neg	NCPCHF_22.CAS	NCNCHF_22.CAS
	pos	PCPCLF_22.CAS	PCNCLF_22.CAS
	pos	PCPCHF_22.CAS	PCNCHF_22.CAS
-20C	neg	NCPCLF_-20.CAS	NCNCLF_-20.CAS
	neg	NCPCHF_-20.CAS	NCNCHF_-20.CAS
	pos	PCPCLF_-20.CAS	PCNCLF_-20.CAS
	pos	PCPCHF_-20.CAS	PCNCHF_-20.CAS
0C	neg	NCPCLF_0.CAS	NCNCLF_0.CAS
	neg	NCPCHF_0.CAS	NCNCHF_0.CAS
	pos	PCPCLF_0.CAS	PCNCLF_0.CAS
	pos	PCPCHF_0.CAS	PCNCHF_02.CAS
40C	neg	NCPCLF_40.CAS	NCNCLF_40.CAS
	--	--	--
ADC input voltage only	pos	PCPCLF_40.CAS	PCNCLF_40.CAS
	--	--	--

8.4.2 High frequency calibration.

As for the spherical probe m will be the main input parameter for all cylindrical probe HF calibrations. Unlike the spherical probe logarithmic processor the cylindrical processor have a constant logarithmic factor for the range of interest and the transfer functions can be obtained form the flat part of the NC and PC frequency response plots. The test set-up is the same as for the spherical probe (see Figure 5). The cylindrical probes frequency response is depending on the input current and range from a few Hz to tens of kHz.

8.4.2.1 Converting telemetry values to physical units.

The conversion from m to V_{rms} output voltage is covered by this calibration. The estimate of signal power from m values requires a scientific model, which is not included here.

8.4.2.2 Cylindrical probes HF calibration tests/results.

The output voltage from the cylindrical probe to WBR is given by the same equation as for the spherical probe. Figure 23 and 24 show the frequency response for +100nA and –100nA current input to the negative cylindrical probe and Table 10 lists the frequency response obtained from all NC and PC plots. The relationship is given by

$$\log(V_{out}) = k + \log(m)$$

where k = -0.648 obtained from plot NC5, NC6, PC5 and PC6.

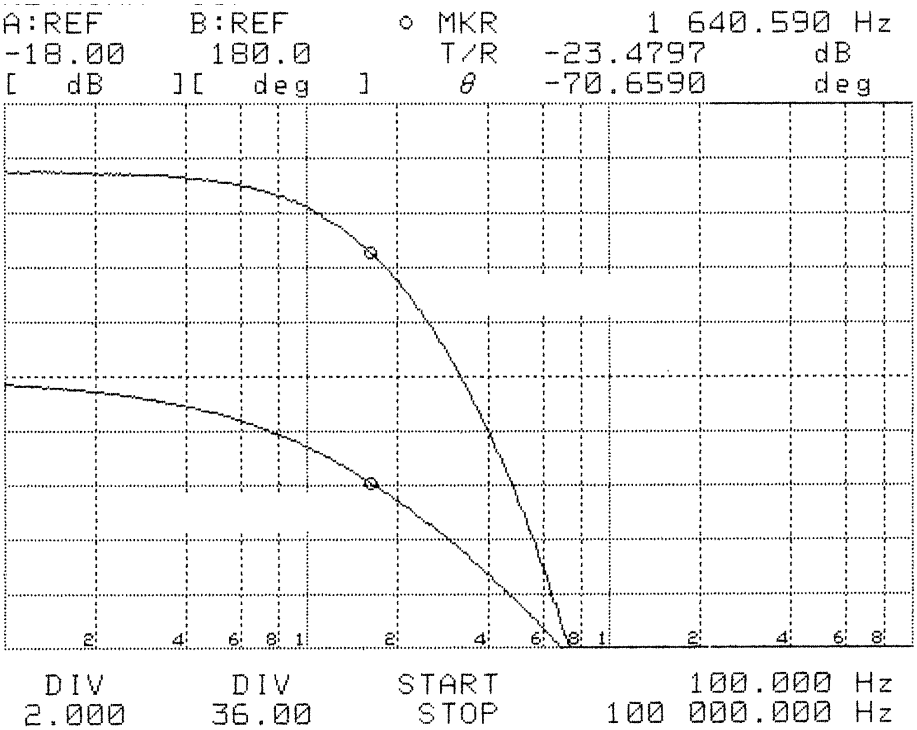

Figure 23. –Cylindrical probe frequency response at 100nA input current.

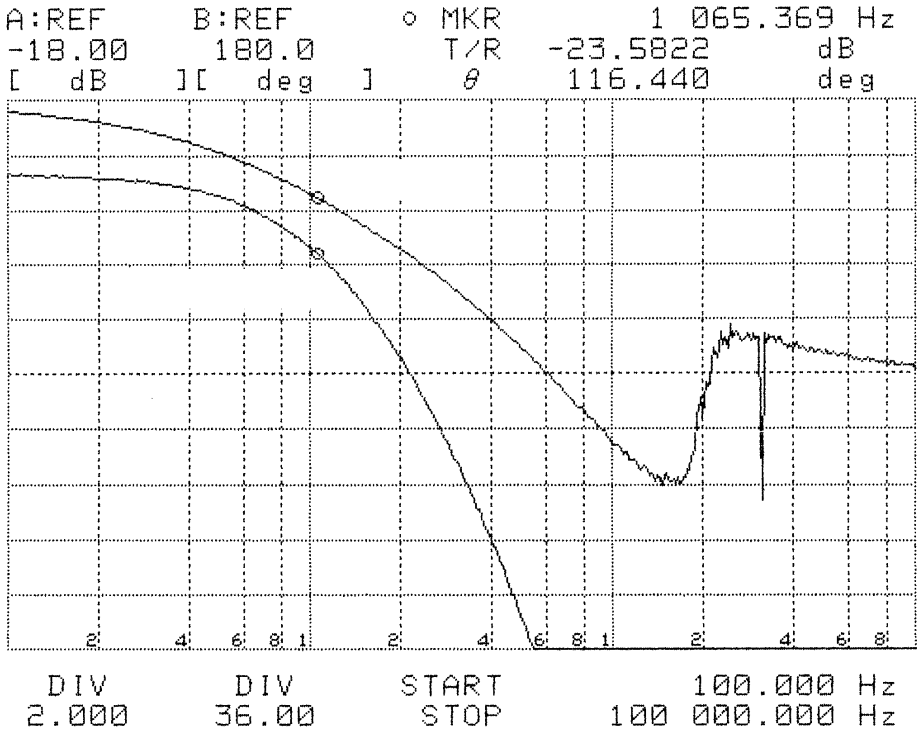

Figure 24. –Cylindrical probe frequency response at -100nA input current.

Table 10. List of NC and PC plots.

Plot No	File name	3dB cut off freq.	Input current
NC8	NC8.tif	2750Hz	1uA
NC5	NC4_5.tif	1650Hz	100nA
NC2	NC1_2.tif	216Hz	10nA

NC1	NC1_2.tif	20Hz	1nA
NC7	NC6_7.tif	3050Hz	-1uA
NC6	NC6_7.tif	1070Hz	-100nA
NC3	NC3.tif	148Hz	-10nA
NC4	NC4_5.tif	31Hz	-1nA
PC8	PC8_7.tif	3160Hz	1uA
PC5	PC5_6.tif	1290Hz	100nA
--	--	--	10nA
PC1	PC1_4.tif	26Hz	1nA
PC7	PC8_7.tif	2950Hz	-1uA
PC6	PC5_6.tif	1080Hz	-100nA
--	--	--	-10nA
PC4	PC1_4.tif	35Hz	-1nA

8.4.3 ±Cylindrical probe bias voltage.

The cylindrical probe bias can be operated in two ranges, ±10 V and ±5V, with 256 steps in each range. To find the actual probe bias the voltage drop over the 100kohm resistor in series with the diode need to be subtracted. This calibration gives the bias voltage at the driver end. Figure 25 and 26 show plots of the two ranges at 22C.

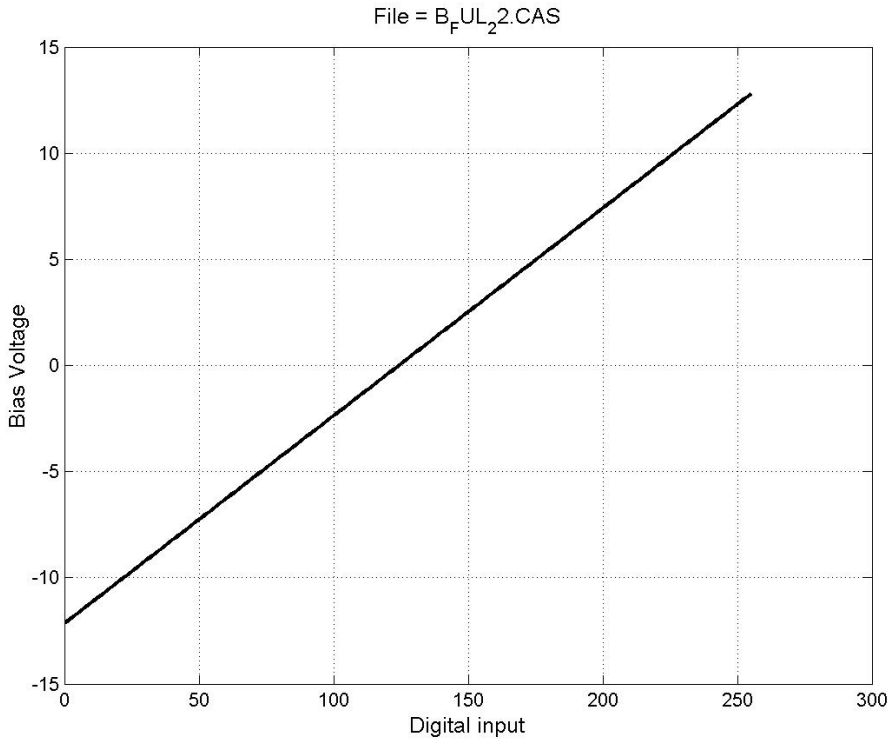

Figure 25. ±Cylindrical probe full bias range at 22C

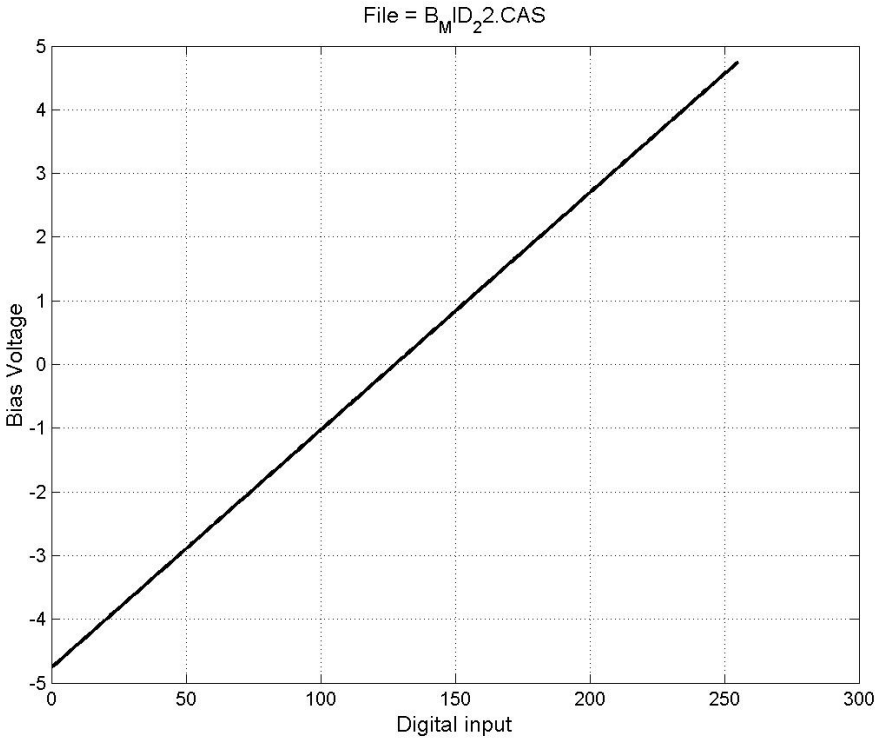

Figure 26. ±Cylindrical probe middle bias range at 22C.

Table 11. List of Cylindrical probe bias calibration files.

Temp.	File name FUL	File name MID
-20C	B_FUL_-20.CAS	B_MID_-20.CAS
0C	B_FUL_0.CAS	B_MID_0.CAS
22C	B_FUL_22.CAS	B_MID_22.CAS
40C	B_FUL_40.CAS	B_MID_40.CAS

9.1 LFDR Subsystem Description

The Low Frequency Digital Receiver (LFDR) employs onboard FFT processing of one or two channels of the Wave Form Receiver (WFR) to produce a 1 Hz to 27 Hz spectrums which can be transmitted to the ground.

9.1.1 General LFDR Characteristics

The Low Frequency Digital Receiver combines hardware and software functions to provide an onboard spectrum analysis of low frequency signals. The hardware receiver which is used is the Waveform Receiver (WFR, see Section 13). Normally the WFR is configured in low band mode (also called 40 Hz mode) to provide waveform data sets to the LFDR software, but the high band mode could be configured as well. The calibrations described in this document apply only to the low band mode. In this mode a waveform is captured and an FFT performed on the data. Normally the waveform is of length 512, but it is also possible to command the LFDR to process WFR snapshots of length 256 or 1024, if more or less frequency resolution is desired. The calibrations in this document are valid for the default length of 512 samples, but they could easily be extended to the other snapshot lengths. Regardless of snapshot length, the data is processed by the on-board software as follows:

1) The data, which are 12-bit values ranging from 0 to 4095, is averaged. The average is subtracted from all data values, leaving data with no DC component.

2) The data is scanned for maximum and minimum values, and using these the data is pre-scaled. The data is multiplied by the largest factor of 2 which will still leave the data as 12-bit items. This pre-scale factor is included in the output data packet, and is referred to as the digital gain factor.

3) A Hanning (or Hahn) window is applied to the data. This reduces edge effects and sidelobe spreading.

4) A Fast Fourier Transform is performed on the data. After the FFT, all data above 26 Hz is ignored. For the 512 sample snapshot size, this implies that FFT bins 1 through 133 are used. Note that the center frequency of each of these FFT bins is 100*i/512, where i varies from 1 through 133, so that these frequencies vary from 0.195 Hz through 25.977 Hz.

5) The FFT output for each bin is squared and these individual output values (which are proportional to power) are summed using a pseudo-logarithmic mapping function. The mapping function can be commanded to be strictly linear, but the default is logarithmic. The number of output channels is programmable, but the default is 32. For this number of channels, the “logarithmic” mapping function is given in Table 9.1.1.1 (assuming an input snapshot size of 512).

Table 9.1.1.1 LFDR Logarithmic Frequency Mapping Function.

LFDR Step Number	FFT Bin Numbers Included	LFDR Center Frequency (Hz)
1	1	0.195
2	2	0.390
3	3	0.586
4	4	0.781
5	5	0.977
6	6	1.172
7	7	1.367
8	8	1.563
9	9	1.758
10	10	1.953
11	11	2.148
12	12	2.344
13	13	2.539
14	14	2.734
15	15	2.930
16	16	3.125
17	17	3.320
18	18	3.515
19	19	3.711
20	20-21	4.004
21	22-25	4.590
22	26-29	5.371
23	30-34	6.250
24	35-39	7.227
25	40-46	8.398
26	47-53	9.766
27	54-62	11.328
28	63-72	13.184
29	73-84	15.332
30	85-98	17.871
31	99-115	20.898
32	116-133	24.316

6) Using this mapping function, the squares of the FFT output bins are summed. The square root of the sum is taken, producing 32 values proportional to the voltage in each LFDR frequency bin.

7) The values are then mapped to a floating point representation, which requires a byte for each value. The floating point number can be represented by EEEMMMMM, where the upper three bits are an exponent and the lower 5 bits are a mantissa. The exponent is a number ranging from 0 through 7, and the mantissa is a number ranging from 0 through 31. The value can be recovered by using the equation:

$$\text{Value} = (2^{\text{Exponent}}) * \text{Mantissa} + \text{Base(Exponent)}$$

where Base(Exponent) is:

Base(0) = 0
Base(1) = 32
Base(2) = 96
Base(3) = 224
Base(4) = 480
Base(5) = 992
Base(6) = 2016
Base(7) = 4064

This floating point representation is given in the form of a lookup table in Table 9.1.1.2. The 8-bit floating point representation is referred to as Data Number in this table, and the value is referred to as Counts.

8) The 32 bytes of data are packetized along with information about the sensor, the hardware gain state, the WFR channel number, the frequency band selection (40 Hz or 2.5 kHz), and the digital gain factor.

Figure 9.1.1.1 summarizes the stages of the LFDR processing.

Table 9.1.1.2 LFDR Data Number to Counts Lookup Table

DN (Hex)	LFDR Counts (Decimal)							
00	0	1	2	3	4	5	6	7
08	8	9	10	11	12	13	14	15
10	16	17	18	19	20	21	22	23
18	24	25	26	27	28	29	30	31
20	32	34	36	38	40	42	44	46
28	48	50	52	54	56	58	60	62
30	64	66	68	70	72	74	76	78
38	80	82	84	86	88	90	92	94
40	96	100	104	108	112	116	120	124
48	128	132	136	140	144	148	152	156
50	160	164	168	172	176	180	184	188
58	192	196	200	204	208	212	216	220
60	224	232	240	248	256	264	272	280
68	288	296	304	312	320	328	336	344
70	352	360	368	376	384	392	400	408
78	416	424	432	440	448	456	464	472
80	480	496	512	528	544	560	576	592
88	608	624	640	656	672	688	704	720
90	736	752	768	784	800	816	832	848
98	864	880	896	912	928	944	960	976
a0	992	1024	1056	1088	1120	1152	1184	1216
a8	1248	1280	1312	1344	1376	1408	1440	1472
b0	1504	1536	1568	1600	1632	1664	1696	1728
b8	1760	1792	1824	1856	1888	1920	1952	1984
c0	2016	2080	2144	2208	2272	2336	2400	2464
c8	2528	2592	2656	2720	2784	2848	2912	2976
d0	3040	3104	3168	3232	3296	3360	3424	3488
d8	3552	3616	3680	3744	3808	3872	3936	4000
e0	4064	4192	4320	4448	4576	4704	4832	4960
e8	5088	5216	5344	5472	5600	5728	5856	5984
f0	6112	6240	6368	6496	6624	6752	6880	7008
f8	7136	7264	7392	7520	7648	7776	7904	8032

Figure 9.1.1.1

RPWS LOW-FREQUENCY DIGITAL RECEIVER (LFDR)

(DATA PROCESSING FLOW)

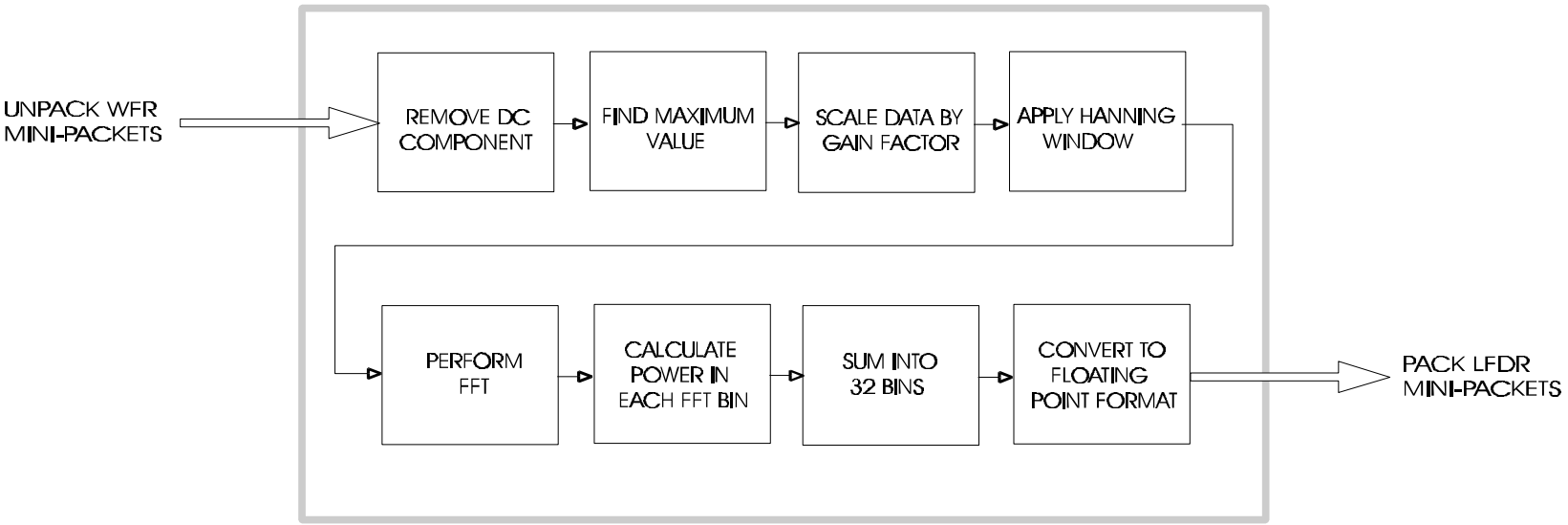

9.1.2 LFDR Format and Computational Aspects

When operating in LFDR mode, the DCP must receive data in the form of WFR mini-packets (raw, unpacked and unsegmented). There are 3 possible sample set lengths: N = 256, 512, or 1024. Since the 40-Hz WFR data is sampled at 100 Hz, the frequency resolutions for these lengths are 0.390 Hz, 0.195 Hz, and 0.098 Hz respectively. This length is commandable, and the LFDR code reconfigures the FFT accordingly. For a longer sample length, a longer computation time is required. The current estimates for the computation times are:

FFT length 256:	2.34 seconds
FFT length 512:	4.80 seconds
FFT length 1024:	10.74 seconds

These times were measured using a "lightly-loaded" DCP running at 3 MHz (i.e., the same speed as the Flight Unit). Only the Real-Time Kernel and the necessary I/O modules were running in addition to the FFT module. Since for normal operations the DCP will be running compression code also, no more than 50 % of available time should be dedicated to the LFDR process. For example, if it were desired to get 2 spectra, one for Ex and one for Bx, every 10 seconds, this could be done. The computation time, using a length 512 FFT would be 9.60 seconds for the two FFT's. But this would not leave much time for compression and other DCP responsibilities. So the FFT length would have to be decreased to 256, resulting in a total LFDR computation time of 4.68 seconds for the two FFT's and a processor load of 4.68/10.00 or 47% processor use.

9.1.3 LFDR Input Options

Any combination of WFR channels can be specified as the inputs to the FFT process. These are Ex, Ez, Bx, By, and Bz. The default mode is (Ex,Bx). Each channel is actually processed independently of the others, and a separate mini-packet is output to the telemetry for each channel.

9.1.4 LFDR Output Options

The output of the FFT is truncated above 26 Hz. This means for 1024-point mode 266 FFT bins are used for the output, for 512-point mode 133 FFT bins are used for the output, and for 256-point mode 67 FFT bins are used for the output. The number of output channels M is a commandable parameter. The FFT bins up to 26 Hz are "lumped together" into the M output channels, using either a linear mapping or a logarithmic mapping function. Typically for the lower FFT bins, the FFT bin size is too wide to do a logarithmic mapping. In other words, the logarithmic mapping function would imply fractional bins, and only integral bins are allowed in the approximation. In this case the FFT bin value is output directly without a mapping function, and there is a one-to-one mapping (actually a linear, not a log, map). The choice of a log or linear

function is commandable. The following example of the two mapping functions illustrates how the log function becomes linear at the lower end of the sample range:

For N = 512 and M = 32, ΔF = 0.195 Hz. However according to E.Oran Brigham, "The Fast Fourier Transform And Its Applications", the 3-dB bandwidth for a single FFT bin when using a Hanning window is 1.4 x ΔF.

Output Channel #	Log Mode FFT bin #'s	Center Freq(Hz)	3-dB BW(Hz)	BW / Center Freq.	Linear Mode FFT bin #'s
1	1	0.195	0.273	140.00%	1-4
2	2	0.390	0.273	70.00%	5-8
3	3	0.586	0.273	46.59%	9-12
4	4	0.781	0.273	34.96%	13-17
5	5	0.977	0.273	27.94%	18-21
6	6	1.172	0.273	23.29%	22-25
7	7	1.367	0.273	19.97%	26-29
8	8	1.563	0.273	17.47%	30-33
9	9	1.758	0.273	15.53%	34-37
10	10	1.953	0.273	13.98%	38-42
11	11	2.148	0.273	12.71%	43-46
12	12	2.344	0.273	11.65%	47-50
13	13	2.539	0.273	10.75%	51-54
14	14	2.734	0.273	9.99%	55-58
15	15	2.930	0.273	9.32%	59-62
16	16	3.125	0.273	8.74%	63-67
17	17	3.320	0.273	8.22%	68-71
18	18	3.515	0.273	7.77%	72-75
19	19	3.711	0.273	7.36%	76-79
20	20-21	4.004	0.469	11.71%	80-83
21	22-25	4.590	0.859	18.71%	84-87
22	26-29	5.371	0.859	15.99%	88-91
23	30-34	6.250	1.055	16.88%	92-96
24	35-39	7.227	1.055	14.60%	97-100
25	40-46	8.398	1.445	17.21%	101-104
26	47-53	9.766	1.445	14.80%	104-108
27	54-62	11.328	1.836	16.21%	109-112
28	63-72	13.184	2.031	15.41%	113-116
29	73-84	15.332	2.285	14.90%	117-121
30	85-98	17.871	2.813	15.74%	122-125
31	99-115	20.898	3.398	16.26%	126-129
32	116-133	24.316	3.594	14.78%	130-133

9.1.6 Logarithmic Compression of LFDR Amplitude Values

The FFT bins are combined by squaring the amplitudes for a group of FFT bins, adding the squared amplitudes, and taking the square root of the sum of squares. The resulting value is proportional to the signal voltage in that frequency band. The value can be a 13-bit number, since the raw time series data is 12-bit. It is then log-compressed to an 8-bit value, which is output to the telemetry.

The logarithmic compression function has a maximum error of 0.5 parts per 32, since 5 bits are used to express the mantissa, and rounding gives an additional bit of accuracy. Hence the error is on the order of 1%. The compression function is given as follows:

Bits D7-D5, Exponent
Bits D4-D0, Mantissa
Value = (2^{Exponent}) * Mantissa + Base(Exponent)

where Base(Exponent) is:

Base(0) = 0
Base(1) = 32
Base(2) = 96
Base(3) = 224
Base(4) = 480
Base(5) = 992
Base(6) = 2016
Base(7) = 4064

9.1.6 LFDR Mini-packet Format

For each channel processed, there is an LFDR mini-packet produced. This requires 2 bytes for the mini-packet header, 2 bytes for the Spacecraft Time, and 2 bytes for the LFDR status field (channel #, gain setting, Log/lin mode, etc.). Hence for an LFDR mini-packet holding 32 output channels, there is an overhead of 6/32 or 19%. Obviously for longer channel lengths the percentile overhead decreases.

9.1.7 LFDR Error Conditions and Error Handling

The following error conditions are possible during the LFDR process:

1) The data set length delivered to the FFT program is not one of its preferred lengths (256, 512, or 1024). In this case, the default length of 512 is used. If any part of a data set is lost or corrupted in the transfer of data from the HRP to the DCP, then the entire data set must be discarded. If any 12-bit data value in the raw data set has high bits set (i.e., is greater than 12 bits) then the high bits are masked off and the data is used as if it were normal. When an error

condition does not prevent data analysis, then the mini-packet produced will have a bit to flag the suspect data set.

2) Round-off error results in loss of amplitude resolution at low amplitudes. Total dynamic range is only about 60 dB, instead of the 72 dB hoped for. Also there is an aliasing effect caused by the interaction between round-off error and the use of an N/2 length real-only FFT to speed up the calculation of the length N FFT. This aliasing effect shows up as frequency components above 25 Hz wrapping around the 25 Hz frequency point and showing up as lower frequencies. This effect is about 60 dB down, so a maximum amplitude signal only shows up with a barely measurable FFT component.

   To alleviate the round-off problem, a floating point algorithm was considered but rejected. A compromise was reached by adding a "pre-scale" function, which multiplies the amplitudes by some power of 2 (up to 1024). The exact factor is determined by scanning the raw data for the maximum value. High amplitude data is not scaled at all, low amplitude is scaled by as much as 60 dB (1024). The pre-scale power of 2, a number from 0 to 10, is sent in the LFDR mini-packet header. Note that the calculation times for the different lengths of FFT has increased and it is now necessary to either decrease the number of samples in the FFT analysis to 256, or else decrease the frequency of the LFDR snapshots from 10 seconds to 20 seconds.

9.2.1 Converting LFDR telemetry Values to Physical Units

In this section, the procedure for obtaining a calibrated data value from a raw LFDR measurement is described. For the specifics about the LFDR mini-packet structure, see the Users' Guide and Software Operations Manual.

1) The LFDR data numbers should all be converted to counts using either the formula in Section 9.1 or the lookup Table 9.1.1.2.

2) The digital scale factor should be applied to all the counts. The mini-packet contains a 4-bit field, called the digital gain factor (DGF). All counts should be divided by 2^{DGF}, yielding adjusted counts.

3) The hardware gain state should be noted from the mini-packet. Using this gain state, the correct calibration factor table should be selected, from Tables 9.3.2.1 (corresponding to gain state 00) through 9.3.2.4 (corresponding to gain state 30). The adjusted counts for each LFDR step should be divided by the corresponding step's calibration factor from the selected table. This yields volts rms in that LFDR bin. This is the voltage difference Vdiff between the Ex+ and Ex- antennas.

4) The Tables 9.3.2.1 through 9.3.2.4 are appropriate for the Ex dipole input. Once the voltage Vdiff is found, the sensor-dependent conversion factor must be used to adjust the voltage. The voltage difference between the Ex+ antenna and the Ex- antenna is given the symbol VDEx. Since the voltage difference Vdiff calculated in steps 1 through 3 is for the voltage difference between Ex+ and Ex-, no conversion is necessary for VDEx. VDEx is equal to Vdiff. The voltage between the Ex+ antenna and spacecraft ground is given the symbol VEx+. The voltage between the Ex- antenna and spacecraft ground is given the symbol VEx- . The voltage between the Ez antenna and spacecraft ground is given the symbol VEz. The voltage out of the Bx magnetic preamp is given the symbol Vbxpa. The voltage out of the By magnetic preamp is given the symbol Vbypa. The voltage out of the Bz magnetic preamp is given the symbol Vbzpa. Figure 9.2.1.1 shows the location of these voltages. The conversion factors and their symbols are listed below. The conversion factors convert the Vdiff values to the voltage at the various sensors.

Symbol	Factor	
CF+ex	1.0	Conversion factor for a monopole using the the Ex+ antenna
CF-ex	1.0	Conversion factor for a monopole using the the Ex- antenna
CFez	1.0	Conversion factor for the Ez antenna
Cfbx	24.0	Conversion factor for the Bx Search Coil
Cfby	24.0	Conversion factor for the By Search Coil
Cfbz	24.0	Conversion factor for the Bz Search Coil

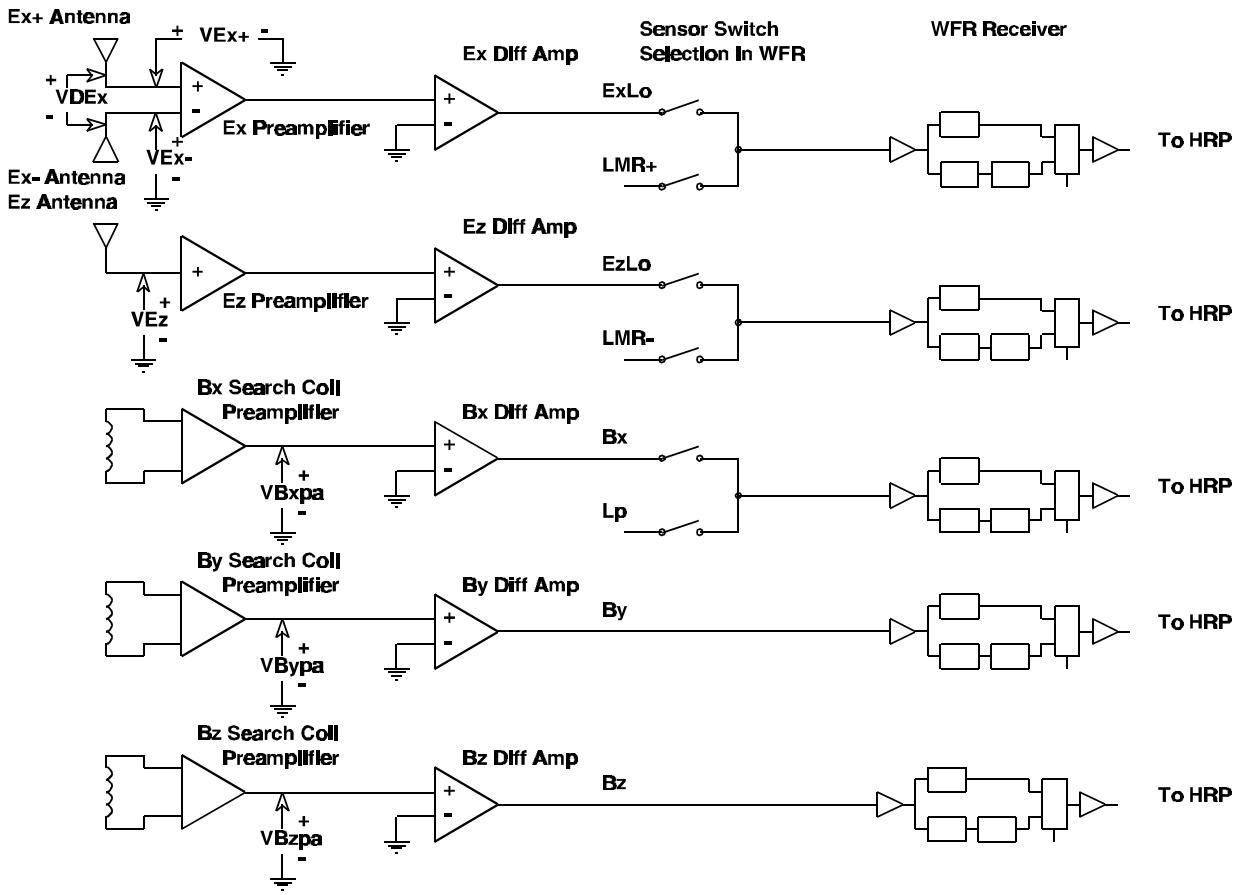

Figure 9.2.1.1

Sensor to WFR Diagram

wfr-sig.blk

The formulas for converting the Vdiff value to the sensor input voltage are:

VDEx	=	Vdiff	(units are volts rms)
VEx+	=	(CF+ex)*(Vdiff)	
VEx-	=	(CF-ex)*(Vdiff)	
VEz	=	(CFez)*(Vdiff)	
Vbxpa	=	(CFbx)*(Vdiff)	
VBypa	=	(CFby)*(Vdiff)	
VBzpa	=	(CFbz)*(Vdiff)	

5) From the mini-packet information, the sensor is noted. For the the Search Coils, the voltages at the outputs of the Search Coil preamplifiers must now be converted to nanotesla. Table 9.2.1.1 contains the conversion factors for the three Search Coils at each of the 32 LFDR center frequencies. These factors were derived by using a cubic spline interpolation on the Search Coil calibration data given in Section 7. Since the Search Coil calibrations are frequency-dependent, the value corresponding to the step of interest should be chosen. This conversion factor is given the symbol of CBxnt for the Bx Search Coil, CBynt for the By Search Coil, and CBznt for the Bz Search Coil. Their units are V/nT. To convert from voltage at the output of the Bx Search Coil preamplifier, VBxpa must be divided by CBxnt. Likewise, to convert from voltage at the output of the By Search Coil preamplifier, VBypa must be divided by Cbynt. And similarly, to convert from voltage at the output of the Bz Search Coil preamplifier, VBzpa must be divided by Cbznt. This is shown in the following equations:

NTBx	=	Vbxpa / CBxnt	(units are nT rms)
NTBy	=	Vbypa / Cbynt	
NTBz	=	Vbzpa / CBznt	

NTBx is the field detected by the Bx Search Coil, NTBy is the field detected by the By Search Coil, and NTBz is the field detected by the Bz Search Coil. At this point we have meaningful physical units. For the electric antennas we have the voltage measured at the antenna elements. For the magnetic sensors we have the magnetic field in nanotesla at the sensors. Next the magnitude of the electric field for the electric antennas can be obtained. The voltages at the antennas are divided by the effective antenna length. This produces units of volts per meter. Here the effective antenna lengths are defined as the physical distances between the geometric centers of the antennas for the Ex dipole, and the geometric center for the Ez antenna. The effective length for the Ex+ to Ex- dipole antenna configuration is given the symbol LExdelta. The Ex+ monopole effective length is given the symbol L+Ex. The Ex- monopole effective length is given the symbol L-Ex. The Ez monopole is given the symbol LEz. See section 5.1 for a more detailed discussion of the effective lengths of the antennas.

Effective Antenna Length in Meters for various mode configurations

Antenna	Effective Length (meters)	Configuration
LExdelta	8.66	dipole
L+Ex	5.00	monopole
L-Ex	5.00	monopole
LEz	5.00	monopole

The electric antenna field on the Ex dipole is represented by VMExdelta, the electric field on the Ex+ monopole by VM+Ex, the electric field on the Ex- monopole by VM-Ex, and the electric field on the Ez monopole by VMEz. The following equations show the method for calculating the electric antenna field on the antenna in volts per meter. These equations do not include effects due to stray capacitive divider effects between the antennas and the spacecraft.

VMExdelta = (VDEx) / (Lexdelta)
VM+Ex = (Vex+) / (L+Ex)
VM-Ex = (Vex-) / (L-Ex)
VMEz = (Vez) / (LEz)

6) Finally, the power spectral density can be obtained by squaring the field strength and dividing by effective bandwidth EBW. The theoretical bandwidth is 1.5*Df for LFDR steps 1 through 19 (i.e., single FFT bin channels), and approximately N*Df for higher LFDR channels (where N is the number of FFT bins included in the sum). More precise estimates of the effective bandwidths are given in Section 9.3.3. The EBW for the step of interest should be selected from Table 9.3.3.2, in the column labeled "Average Noise Bandwidth".

7) The spectral density of the signal on the Ex dipole is represented by Exdeltasd, the Ex+ monopole antenna by +Exsd and the -Ex antenna by -Exsd. The following equations show the method for calculating the electric antenna spectral density on the antennas in volts rms squared per meters squared per Hertz.

Exdeltasd = $(VMExdelta)^2$ / EBW
+Exsd = $(VM+Ex)^2$ / EBW
-Exsd = $(VM-Ex)^2$ / EBW
Ezsd = $(VMEz)^2$ / EBW

The spectral density of the signal from the Bx sensor is represented by Bxd. The spectral density of the signal from the By sensor is represented by Byd. The spectral density of the signal from the Bzd sensor is represented by Bzd. The following equations show the method for calculating the magnetic spectral density at the magnetic sensors in nanotesla squared per Hertz.

$$Bxd = NTBx^2 / EBW$$
$$Byd = NTBy^2 / EBW$$
$$Bzd = NTBz^2 / EBW$$

Table 9.2.1.1 LFDR Search Coil Conversion Factors.

LFDR Step Number	LFDR Center Frequency (Hz)	Bx Conversion Factor (V/nT)	By Conversion Factor (V/nT)	Bz Conversion Factor (V/nT)
1	0.195	0.00064	0.00063	0.00063
2	0.39	0.00163	0.00161	0.00161
3	0.586	0.00264	0.00262	0.00262
4	0.781	0.00362	0.00358	0.00359
5	0.977	0.00455	0.00449	0.00451
6	1.172	0.00547	0.00540	0.00542
7	1.367	0.00640	0.00631	0.00634
8	1.563	0.00733	0.00723	0.00727
9	1.758	0.00826	0.00816	0.00820
10	1.953	0.00920	0.00909	0.00913
11	2.148	0.01015	0.01002	0.01008
12	2.344	0.01110	0.01096	0.01102
13	2.539	0.01205	0.01190	0.01197
14	2.734	0.01301	0.01285	0.01292
15	2.930	0.01396	0.01379	0.01386
16	3.125	0.01492	0.01473	0.01481
17	3.320	0.01587	0.01567	0.01575
18	3.515	0.01682	0.01661	0.01669
19	3.711	0.01776	0.01754	0.01763
20	4.004	0.01917	0.01893	0.01903
21	4.590	0.02195	0.02167	0.02178
22	5.371	0.02554	0.02522	0.02533
23	6.250	0.02947	0.02910	0.02924
24	7.227	0.03382	0.03340	0.03356
25	8.398	0.03907	0.03860	0.03878
26	9.766	0.04511	0.04459	0.04480
27	11.328	0.05176	0.05117	0.05140
28	13.184	0.05923	0.05856	0.05881
29	15.332	0.06728	0.06651	0.06679
30	17.871	0.07596	0.07508	0.07537
31	20.898	0.08507	0.08410	0.08439
32	24.316	0.09389	0.09284	0.09311

9.2.2 Examples of Converting LFDR telemetry Values to Physical Units

Three examples of conversions from raw LFDR telemetry data values to science units are given below.

1) Let the LFDR sensor be the Ex dipole. Let the DGF be 3 and let the hardware gain state be gain state 20. Let the telemetry value for step 18 of the LFDR be 97 decimal (61 hexadecimal). Using Table 9.1.1.2, we see that this floating point representation corresponds to 232 LFDR counts. Using the digital gain factor, we find that adjusted counts are $232 / 2^{DGF} = 232 / 2^3 = 232 / 8 = 29$. Now consulting the calibration factor table for gain state 20, Table9.3.2.3, we see that for LFDR step 18 the calibration factor is 41864 counts per Vrms. Hence the voltage Vdiff at frequency 3.515 Hz is Vdiff = 29 / 41864 = 6. $93x10^{-4}$ Vrms. Since the tables were produced from Ex dipole calibration tests, VDEx is equal to Vdiff. Since the LFDR sensor is the Ex dipole, the effective antenna length is 8.66 meters. Then the electric field strength is

$$\begin{aligned} \text{VMExdelta} &= (\text{VDEx}) / (\text{Lexdelta}) \\ &= 6.93x10^{-4} \text{ Vrms} / 8.66 \text{ meters} \\ &= 8.00x10^{-5} \text{ Vrms / meter} \end{aligned}$$

VMExdelta is now squared and divided by the effective bandwidth of LFDR step 18 to obtain the spectral density of the signal on the Ex dipole antenna at 3.515 Hz. The effective bandwidth is found in Table 9.3.3.2 to be 0.2045 Hz.

$$\begin{aligned} \text{Exdeltasd} &= (\text{VMExdelta})^2 / \text{EBW} \\ &= (8.00x10^{-5} \text{ Vrms / meter})^2 / 0.2045 \text{ Hz} \\ &= 3.13x10^{-8} \text{ Vrms}^2 / \text{meter}^2 \text{ Hz} \end{aligned}$$

2) Let the LFDR sensor be the Ez antenna. Let the DGF be 7 and let the hardware gain state be gain state 00. Let the telemetry value for step 32 of the LFDR be 167 decimal or A7 hexadecimal. Noting that for this value the Mantissa is 7 and the Exponent is 5, we calculate the Value for counts with the equation:

$$\begin{aligned} \text{Value} &= (2^{\text{Exponent}}) * \text{Mantissa} + \text{Base(Exponent)} \\ &= (2^5) * 7 + 992 \\ &= 32 * 7 + 992 \\ &= 1216 \quad \text{counts} \end{aligned}$$

Using the digital gain factor, we find that adjusted counts are

$1216 / 2^{DGF} = 1216 / 2^7 = 1216 /128 = 9.5$ counts.

Now consulting the calibration factor table for gain state 00, Table 9.3.2.1, we see that for LFDR step 32 the calibration factor is 7185 counts per Vrms. Hence the voltage Vdiff at frequency 24.316 Hz is Vdiff = 9.5 / 7185 = 1.32×10^{-3} Vrms. Since the tables were produced from Ex dipole calibration tests, the voltage at the Ez antenna is:

$$\begin{aligned} Vez &= (Cfez)*(Vdiff) \\ &= 1.00 * 1.32 \times 10^{-3} \text{ Vrms} \\ &= 1.32 \times 10^{-3} \text{ Vrms} \end{aligned}$$

Since the LFDR sensor is the Ez monopole, the effective antenna length is 5.00 meters. Then the electric field strength is

$$\begin{aligned} VMEz &= (VEz) / (Lez) \\ &= 1.32 \times 10^{-3} \text{ Vrms} / 5.00 \text{ meters} \\ &= 2.64 \times 10^{-4} \text{ Vrms / meter} \end{aligned}$$

VMEz is now squared and divided by the effective bandwidth of LFDR step 32 to obtain the spectral density of the signal on the Ez monopole antenna at 24.316 Hz. The effective bandwidth is found in Table 9.3.3.2 to be 2.6172 Hz.

$$\begin{aligned} Ezsd &= (VMEz)^2 / EBW \\ &= (2.64 \times 10^{-4} \text{ Vrms / meter})^2 / 2.6172 \text{ Hz} \\ &= 2.67 \times 10^{-8} \text{ Vrms}^2 / \text{meter}^2 \text{ Hz} \end{aligned}$$

3) Let the LFDR sensor be the Bx Search Coil. Let the DGF be 8 and let the hardware gain state be gain state 30. Let the telemetry value for step 20 of the LFDR be 208 decimal. Using Table 9.1.1.2, we see that this floating point representation corresponds to 3040 LFDR counts. Using the digital gain factor, we find that adjusted counts are 3040 / 2^{DGF} = 3040 / 2^8 = 3040 / 256 = 11.875 counts. Now consulting the calibration factor table for gain state 30, Table 9.3.2.4, we see that for LFDR step 20 the calibration factor is 77930 counts per Vrms. Hence the voltage Vdiff at frequency 4.004 Hz is Vdiff = 11.875 / 77930 = 1.52×10^{-4} Vrms. Since the tables were produced from Ex dipole calibration tests, the voltage at the Bx preamplifier is:

$$\begin{aligned} VBxpa &= (Cfbx)*(Vdiff) \\ &= 24.00 * 1.52 \times 10^{-4} \text{ Vrms} \\ &= 3.66 \times 10^{-3} \text{ Vrms} \end{aligned}$$

Since the LFDR sensor is the Bx Search Coil, the conversion factor CBxnt = 0.01917 V/nT from Table 9.2.1.1 must be used to calculate magnetic field strength. Then the magnetic field strength at 4.004 Hz is

$$\begin{aligned} NTBx &= (VBxpa) / Cbxnt \\ &= 3.66\times10^{-3}\ Vrms / 0.01917\ V/nT \\ &= 1.91\times10^{-1}\ nT \end{aligned}$$

NTBx is now squared and divided by the effective bandwidth of LFDR step 20 to obtain the spectral density of the signal on the Bx Search Coil at 4.004 Hz. The effective bandwidth is found in Table 9.3.3.2 to be 0.2871 Hz.

$$\begin{aligned} Bxd &= (NTBx)^2 / EBW \\ &= (1.91^{-1}\ nT)^2 / 0.2871\ Hz \\ &= 1.27\times10^{-1}\ nT^2 / Hz \end{aligned}$$

9.3.1 Input Voltage Versus Output Data Numbers

In this section, the results for the LFDR 2-dB calibration tests are presented and interpreted. The relationships between the LFDR raw counts (after expanding the floating point format and applying the digital gain factor) and the voltage at the Ex preamplifier inputs are presented. Differential signals of known amplitude are applied to the preamplifier inputs at the center frequency of several steps of the LFDR. The oscillator level is maintained at a constant 1Vrms while an adjustable attenuator and a low frequency isolation buffer are placed between the oscillator and the Eu differential amplifier input. The stimulus amplitude is adjusted in 2 dB steps from 0 dBv (dB relative to 1Vrms) to -126 dBv. See Figure 9.3.1.1 for the stimulus setup.

The amplifiers are linear, and to find out the calibration factors, a linear least squares fit was performed on the data in the linear region. Two measurements are taken for each amplitude setting and both are included in the least squares fit. The raw data counts are then plotted as a function of dBv and the least squares linear fit shown also. The room temperature 2-dB results are shown in Figures 9.3.1.2 through 9.3.1.9. The -20°C 2-dB results are shown in Figures 9.3.1.10 through 9.3.1.14. The +40°C 2-dB results are shown in Figures 9.3.1.15 through 9.3.1.22.

The results relating input voltage to the data counts of the above process, for each step and for each gain state, is shown in Table 9.3.1.1. The results are also given for hot and cold temperatures for comparison. However, these simply illustrate that the room temperature results are adequate for calibration. These tables, along with the Channel-to-Channel gain test results (Section 9.3.2) are used to produce a calibration factor for all 32 LFDR steps and at all 4 gain states.

One note about the room temperature plot for LFDR Step 1: there are interference noise spikes about 20 dB above the noise floor for attenuations greater than 40 dB. It has been determined that these noise spikes occur whenever the MFR switches its input sensor from the Bz to the Ex sensor. It is noted that these noise spikes do not occur in the LFDR Step 1 plot at -20° C. For that test, the MFR was not toggling between antennas. In flight the LFDR will be configured to avoid taking data during the time of the MFR antenna switch.

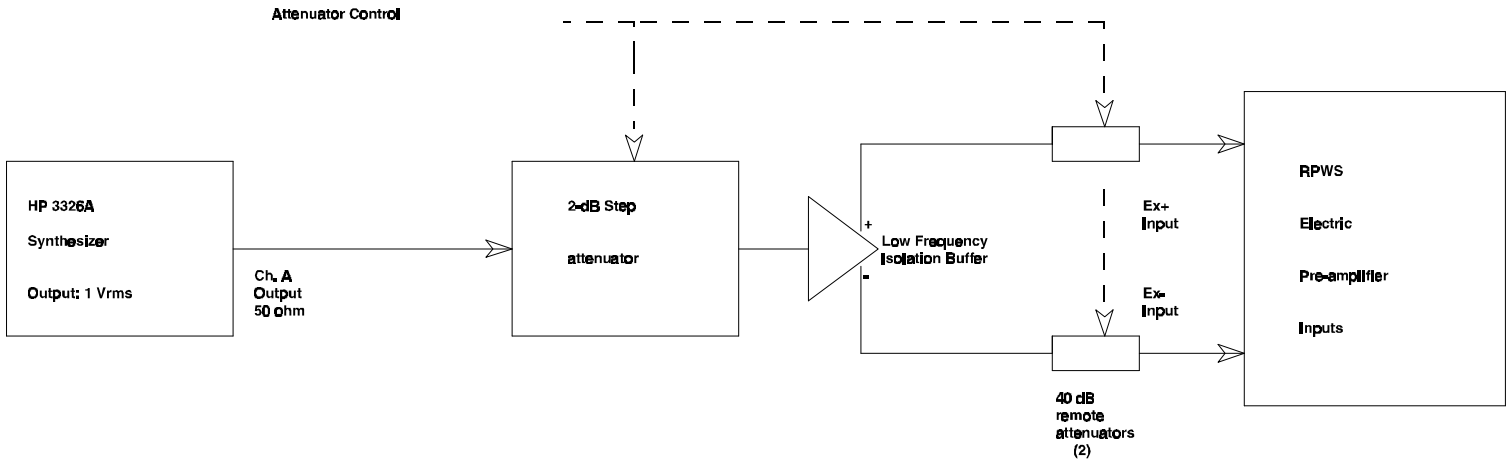

Figure 9.3.1.1

LFDR 2dB Calibration Stimulus Configuration

Figure 9.3.1.2

LFDR Amplitude Response

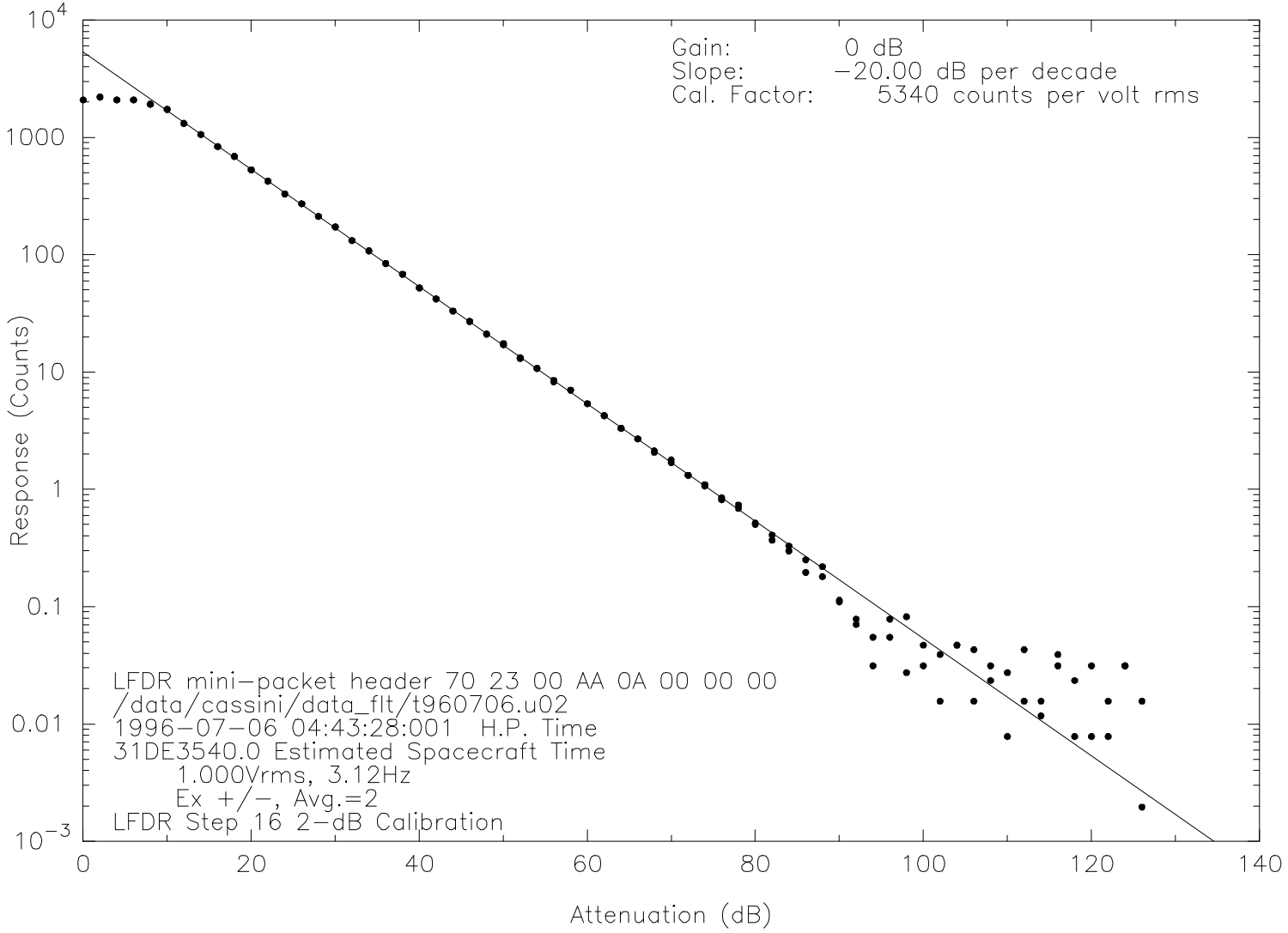

Figure 9.3.1.3

LFDR Amplitude Response

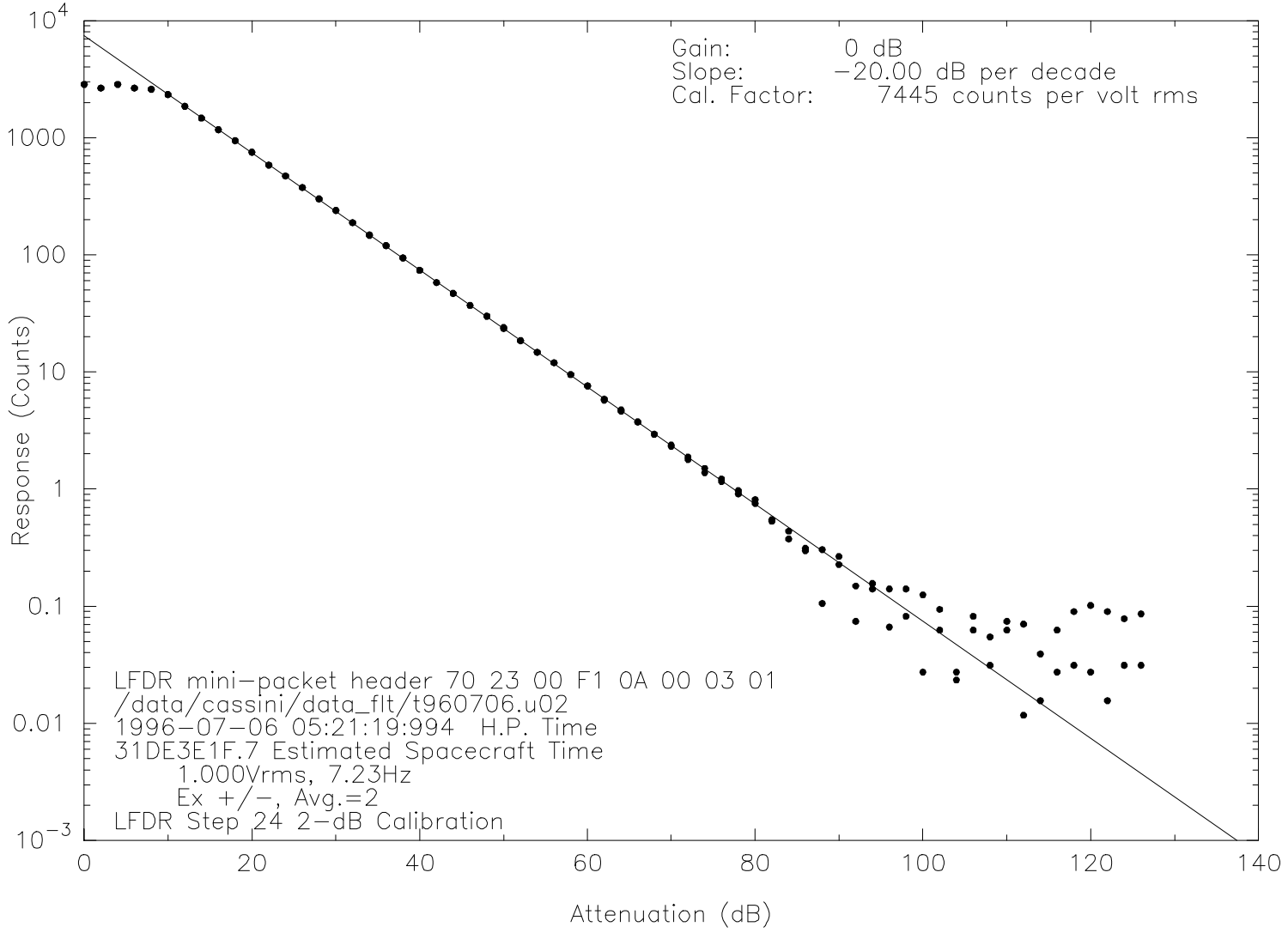

Figure 9.3.1.4

LFDR Amplitude Response

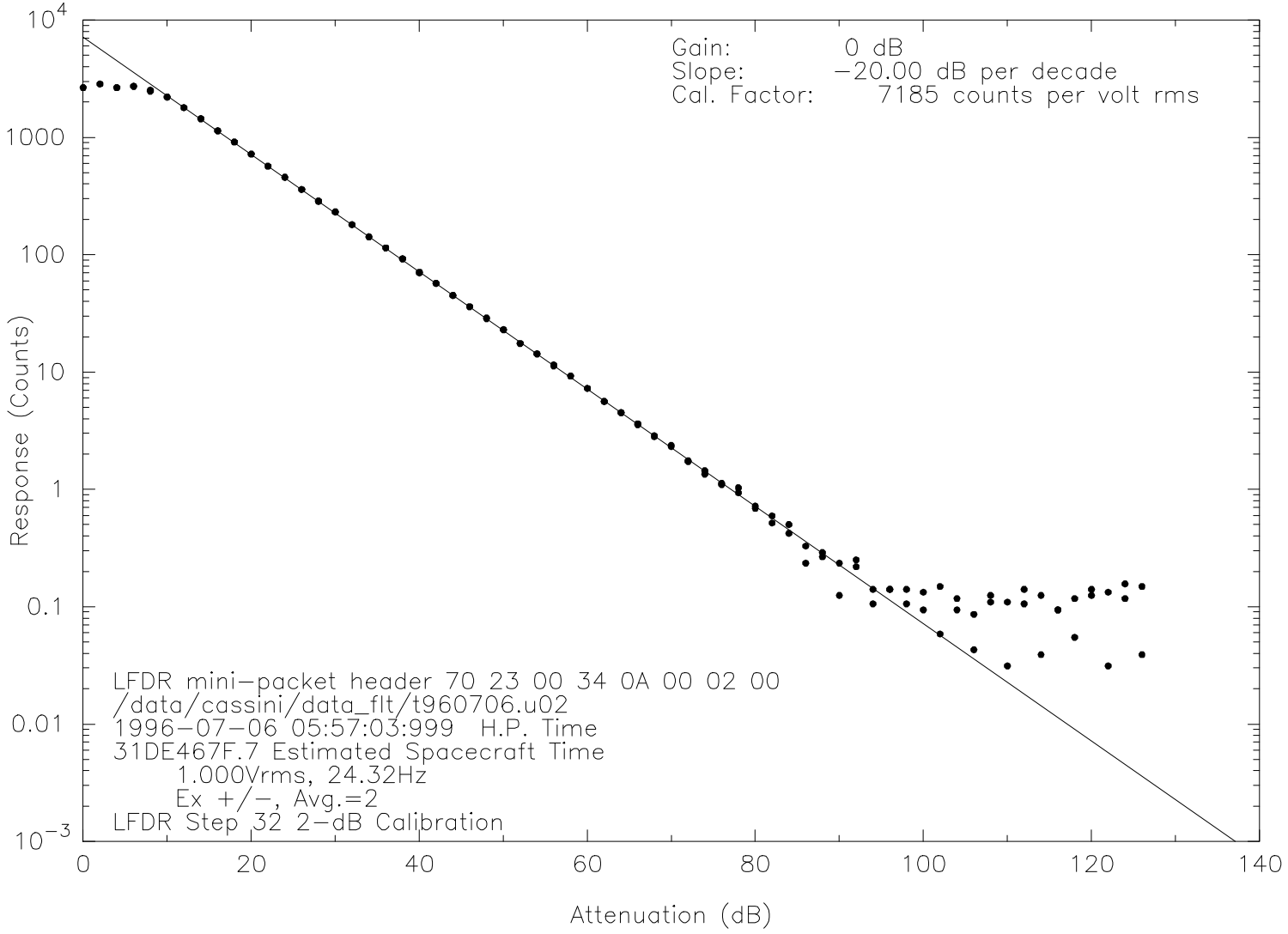

Figure 9.3.1.5

LFDR Amplitude Response

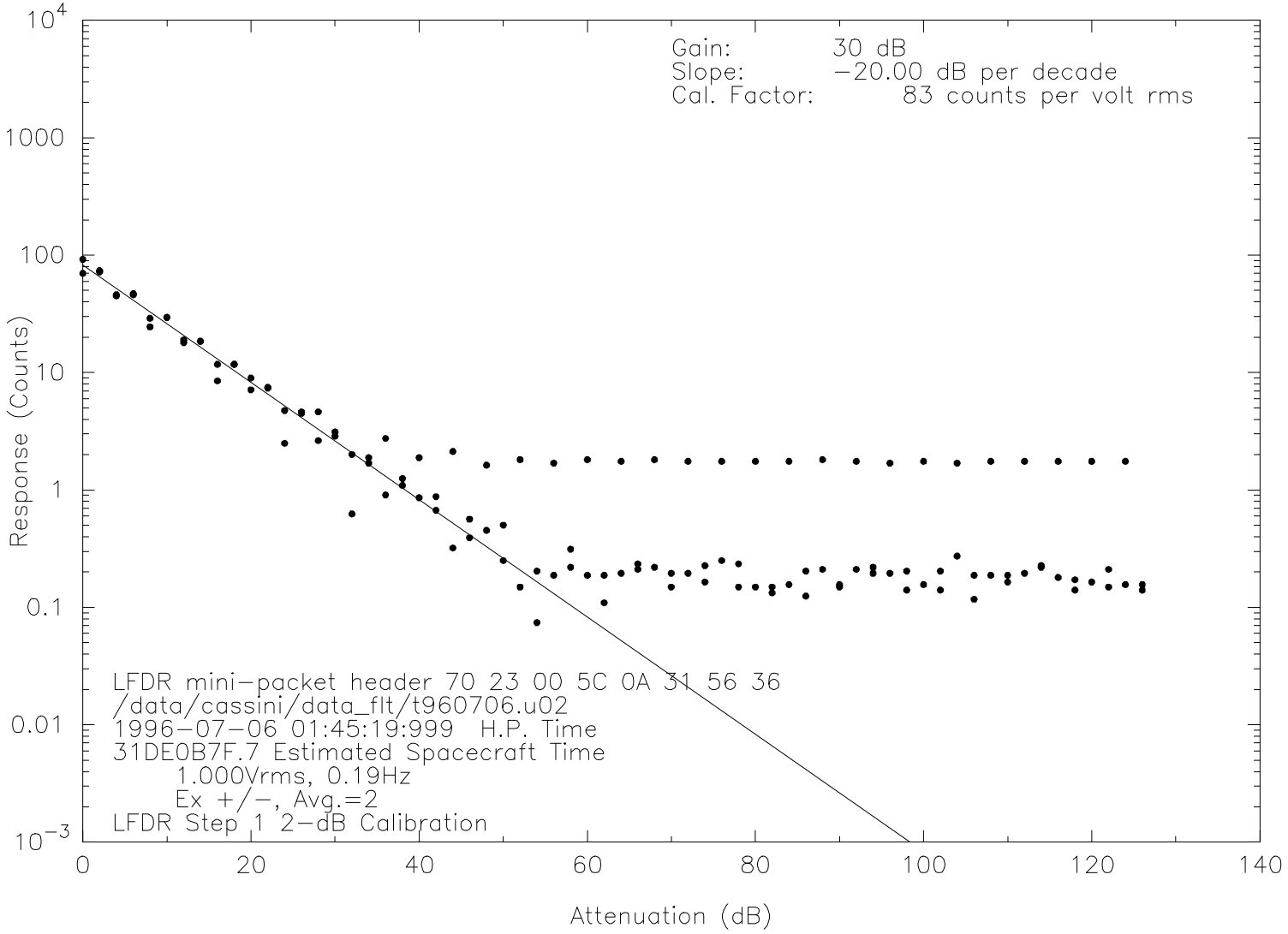

Figure 9.3.1.6

LFDR Amplitude Response

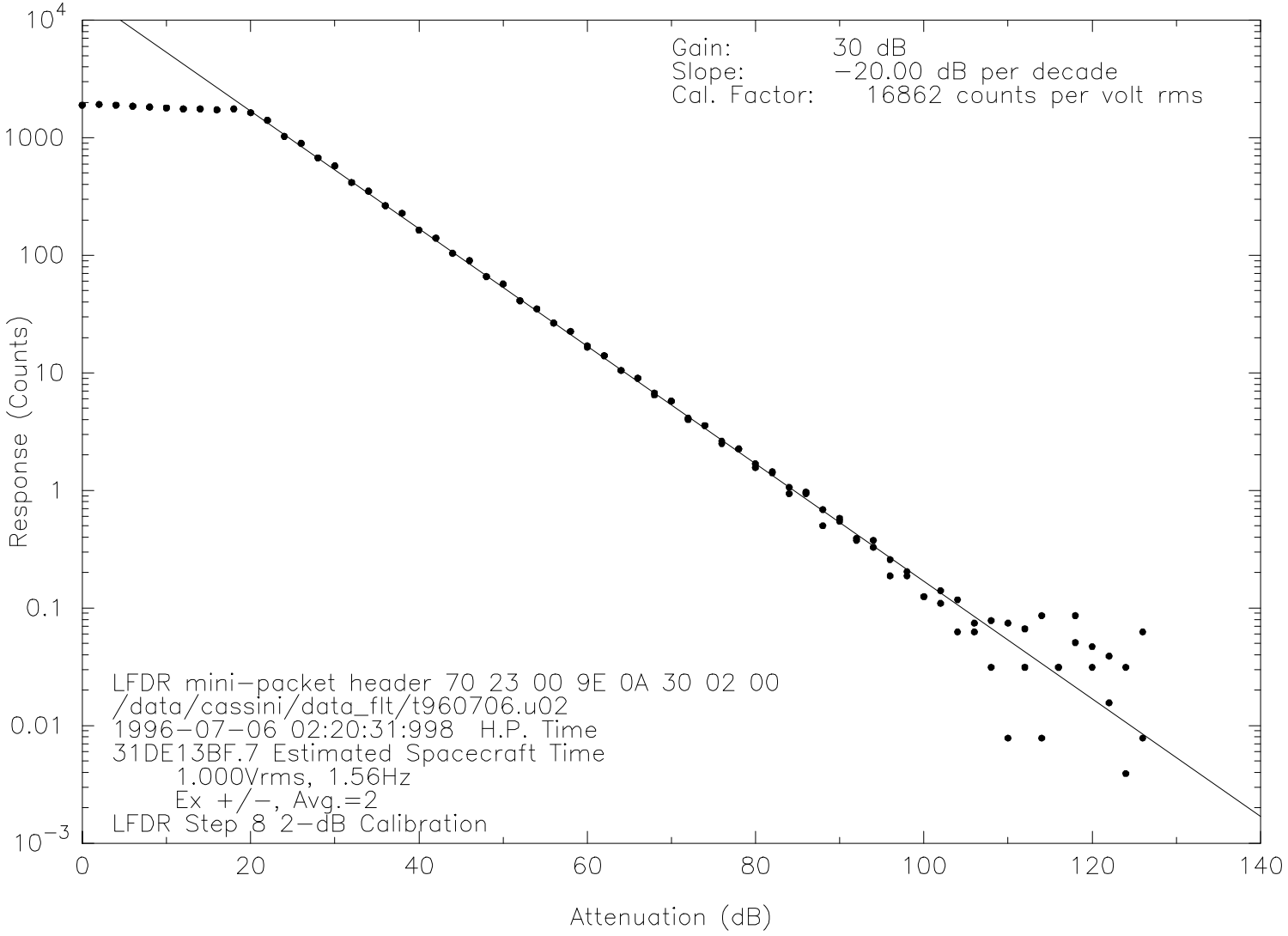

Figure 9.3.1.7

LFDR Amplitude Response

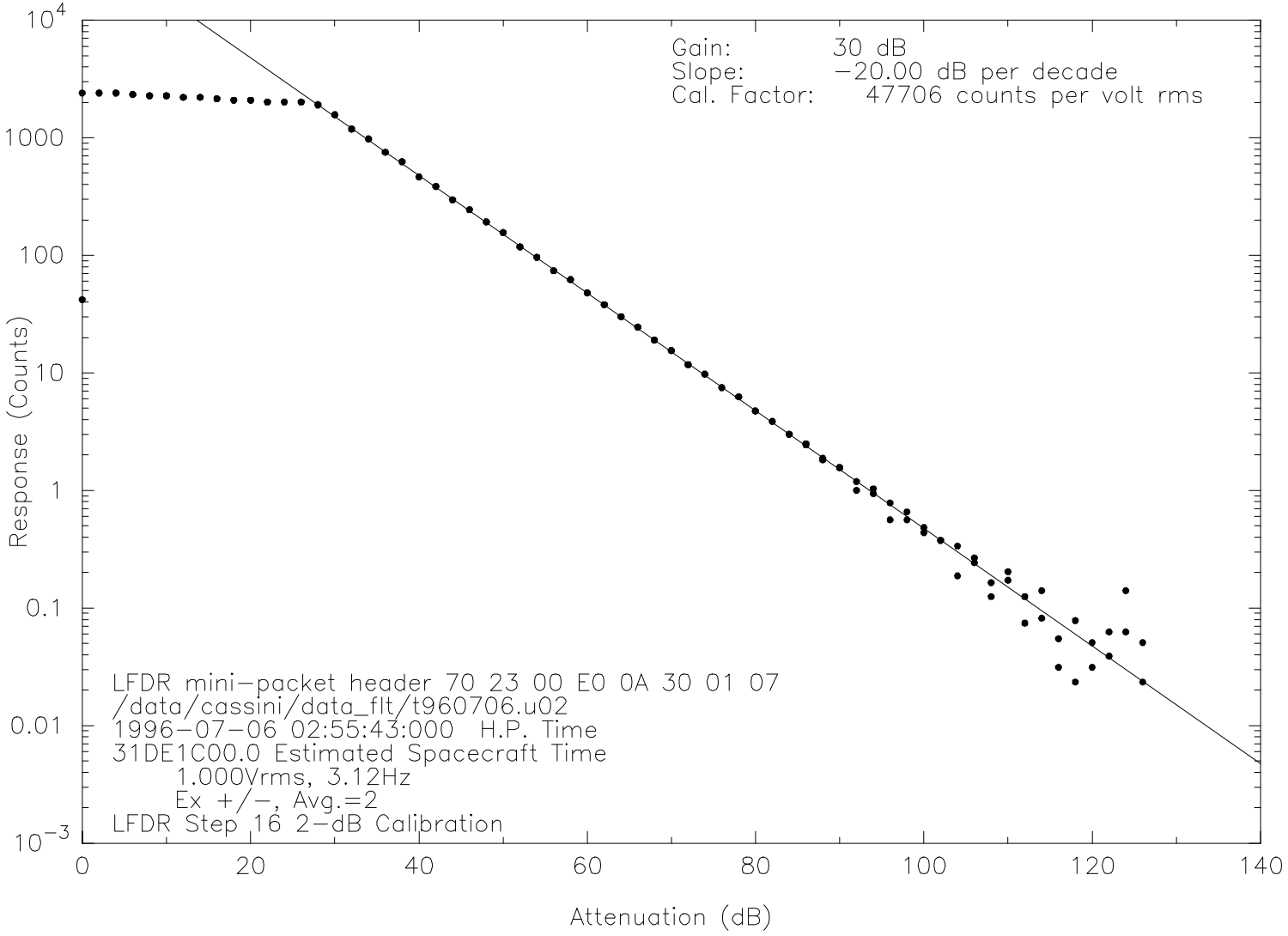

Figure 9.3.1.8

LFDR Amplitude Response

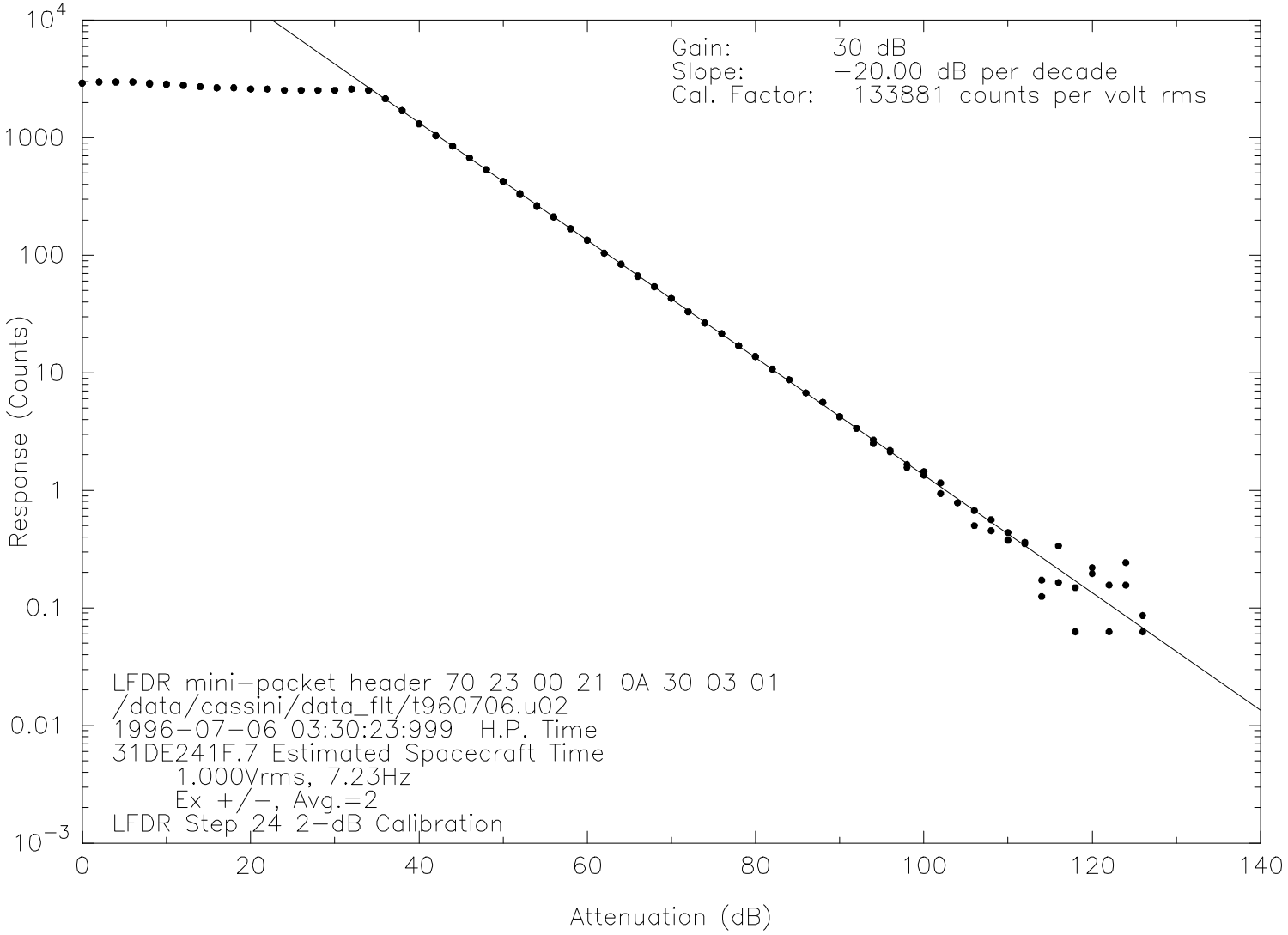

Figure 9.3.1.9
LFDR Amplitude Response

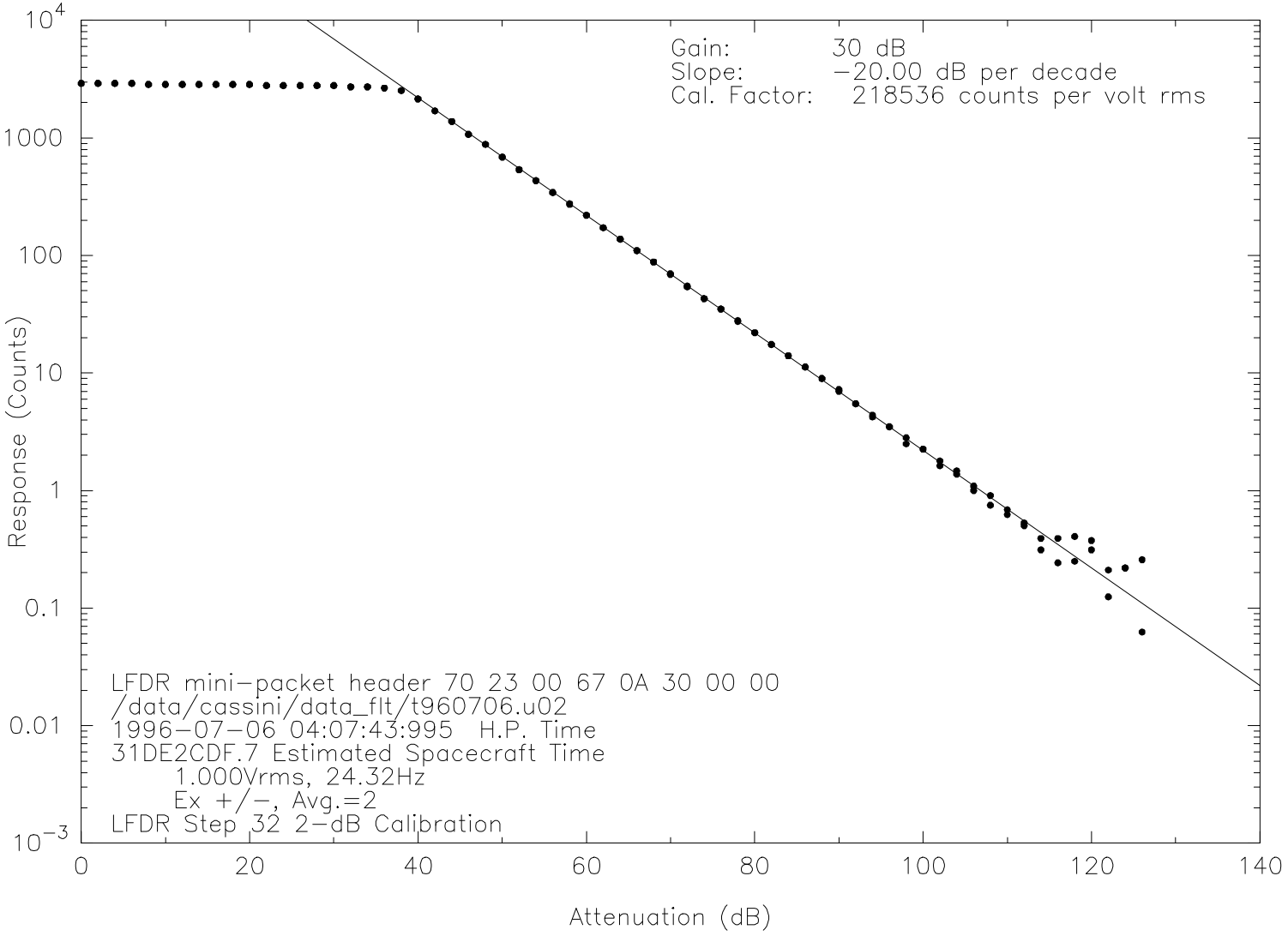

Figure 9.3.1.10
LFDR Amplitude Response

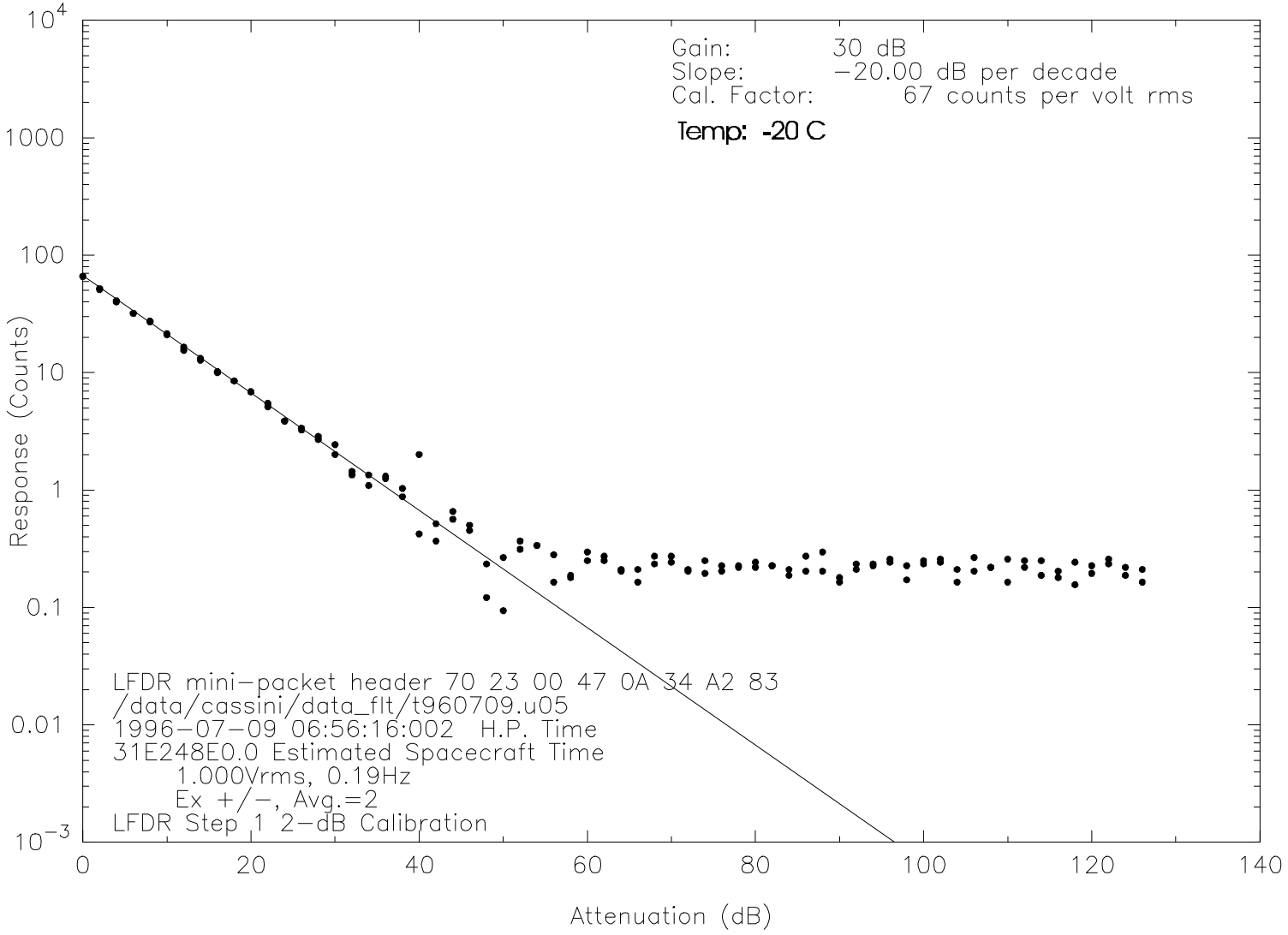

Figure 9.3.1.11

LFDR Amplitude Response

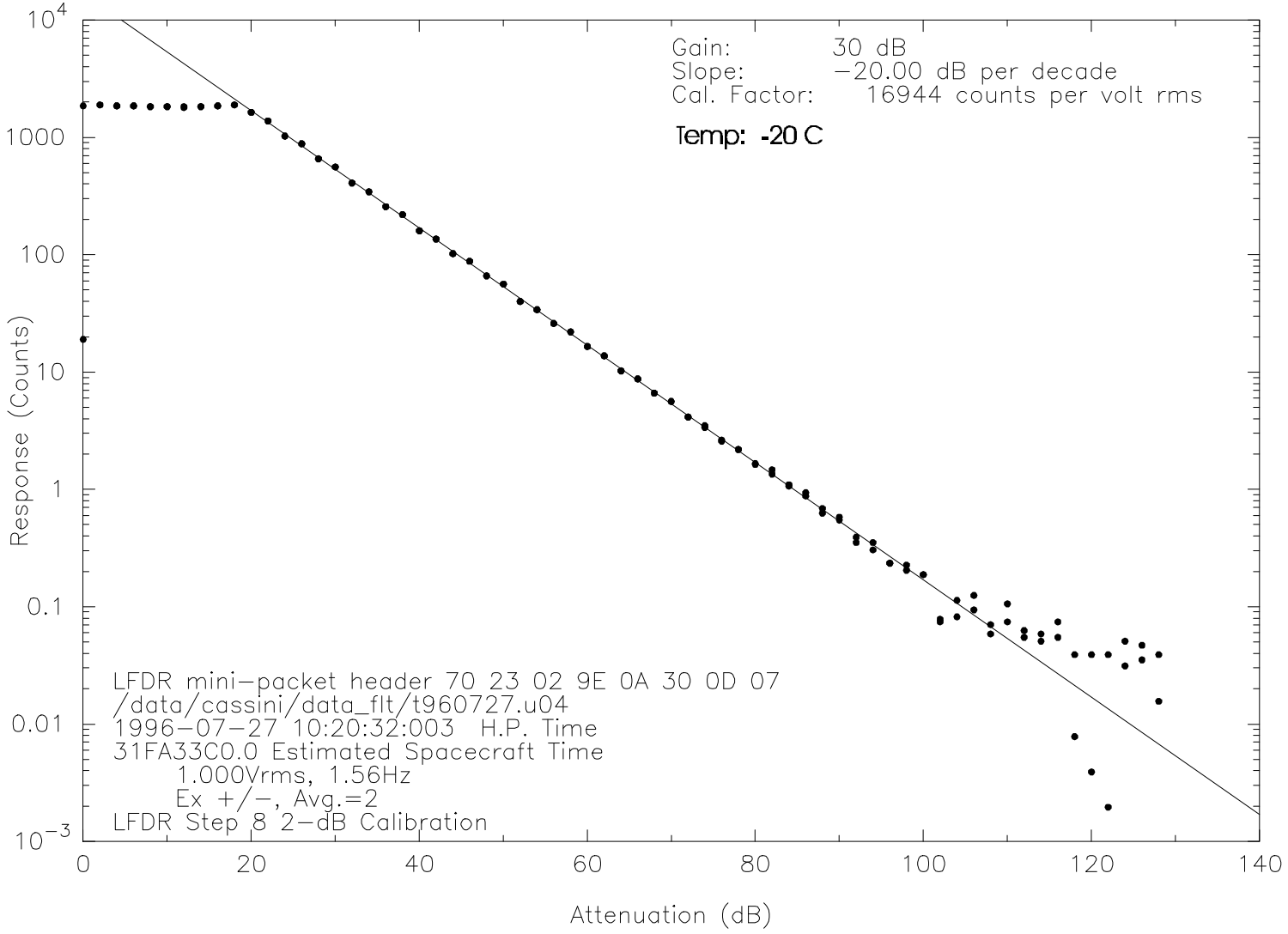

Figure 9.3.1.12
LFDR Amplitude Response

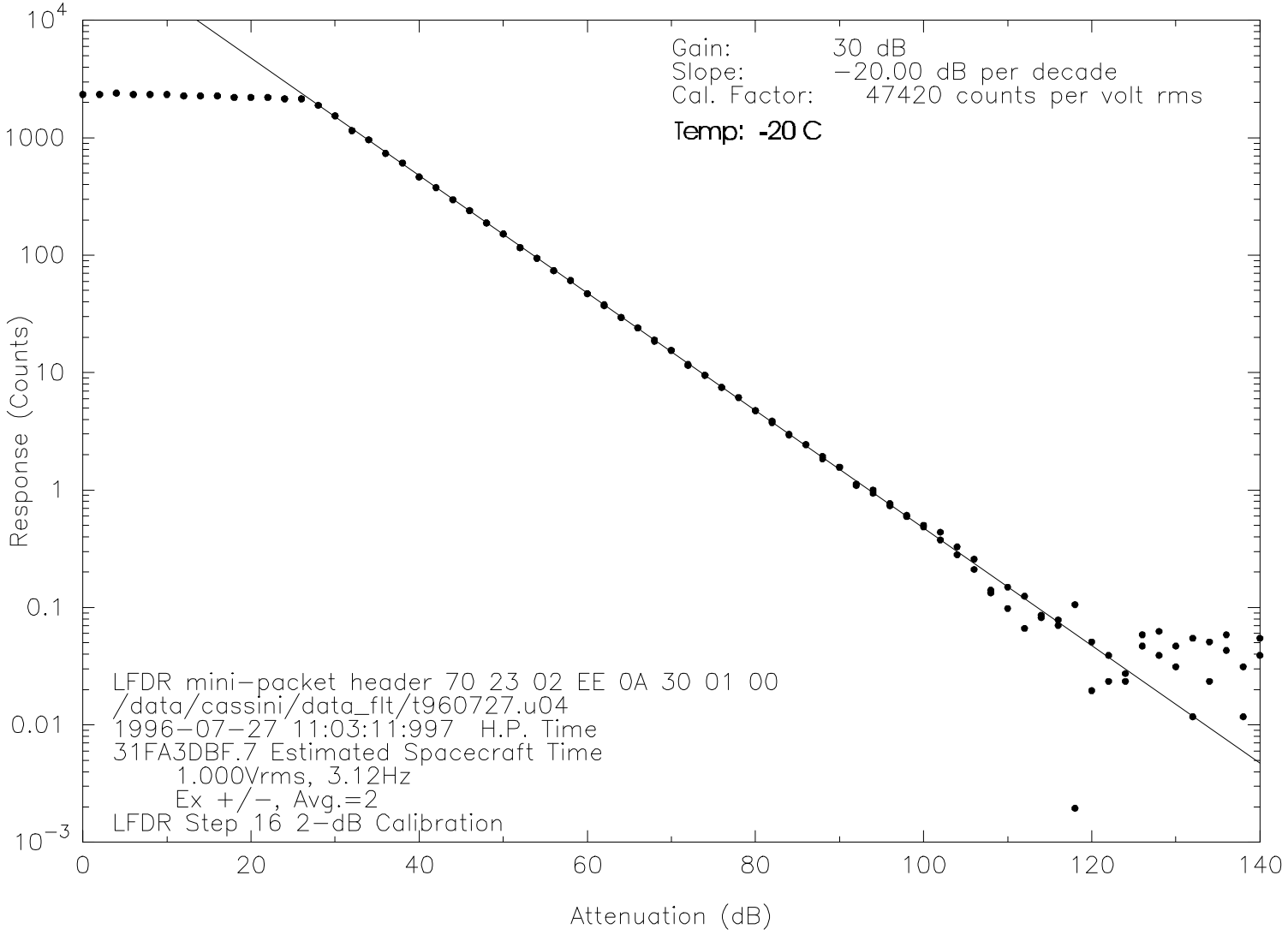

Figure 9.3.1.13

LFDR Amplitude Response

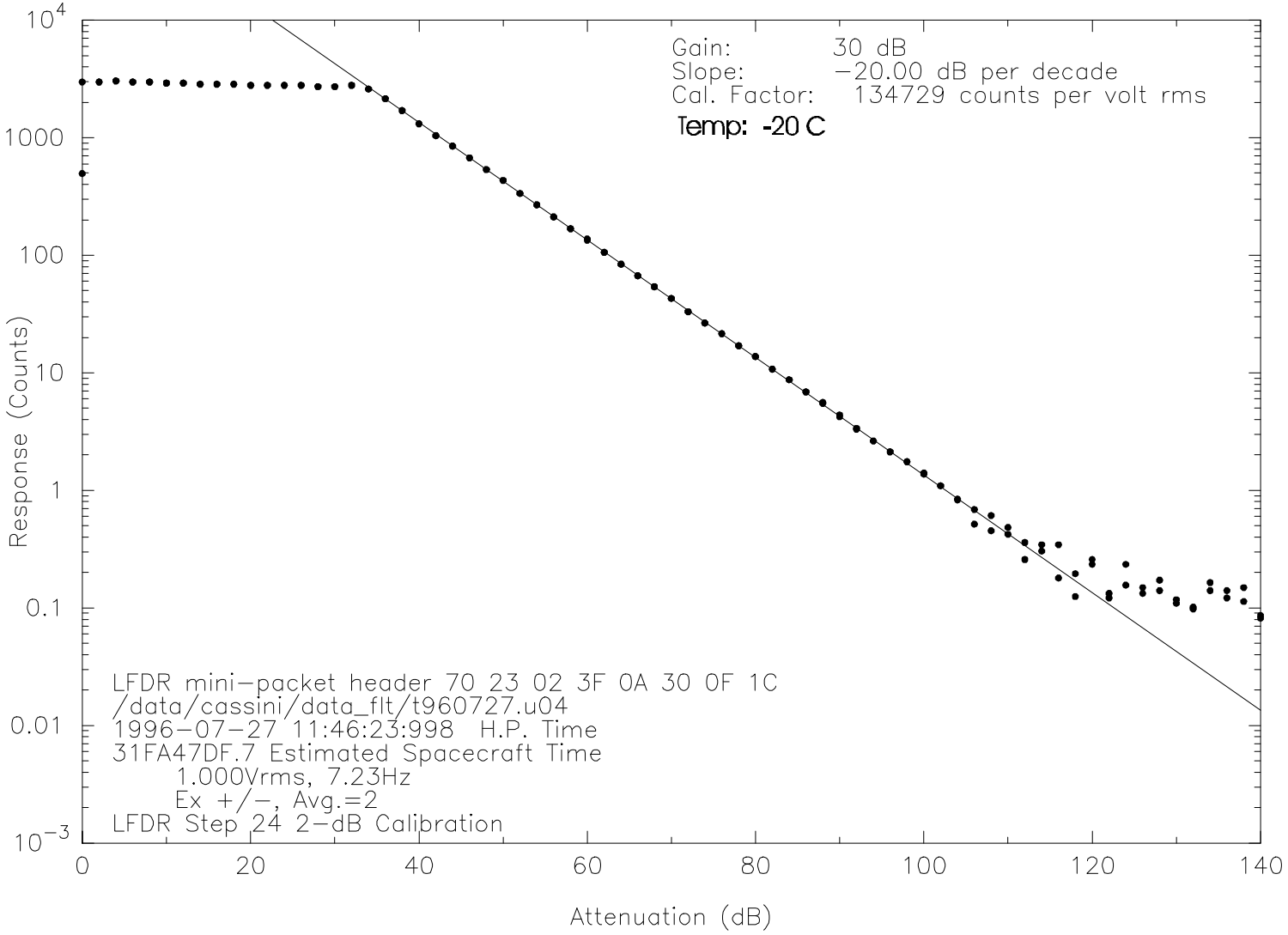

Figure 9.3.1.14
LFDR Amplitude Response

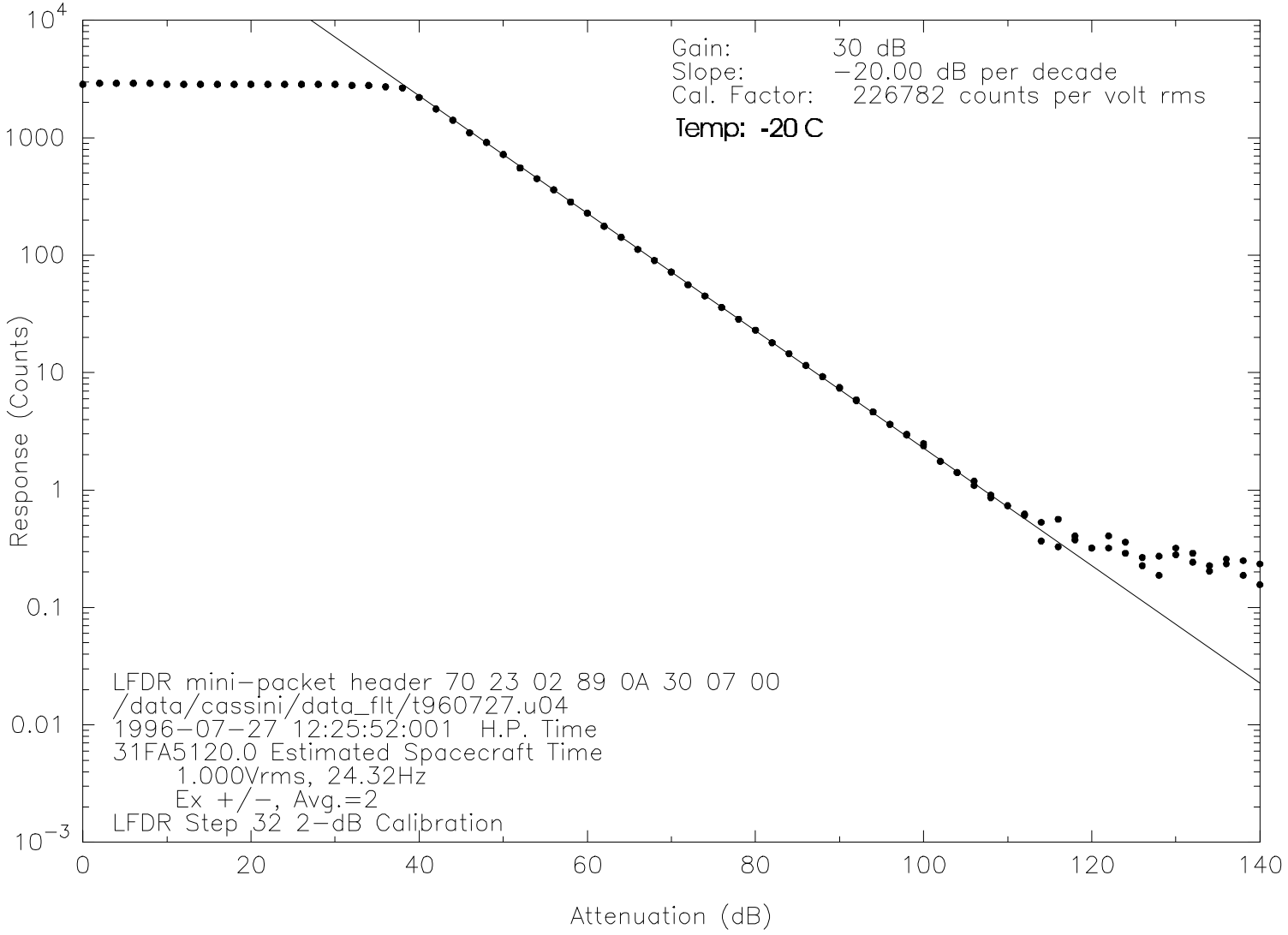

Figure 9.3.1.15

LFDR Amplitude Response

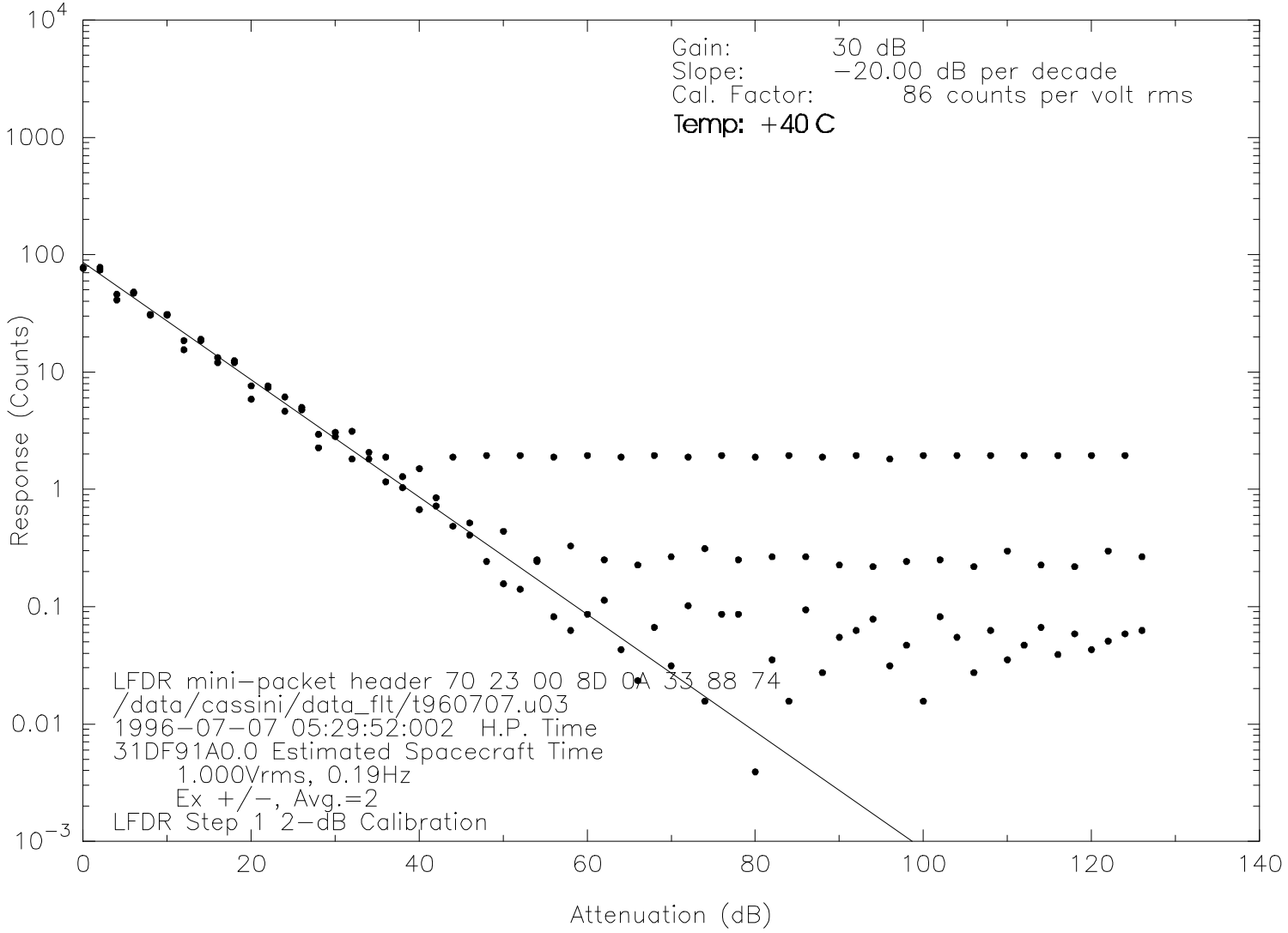

Figure 9.3.1.16

LFDR Amplitude Response

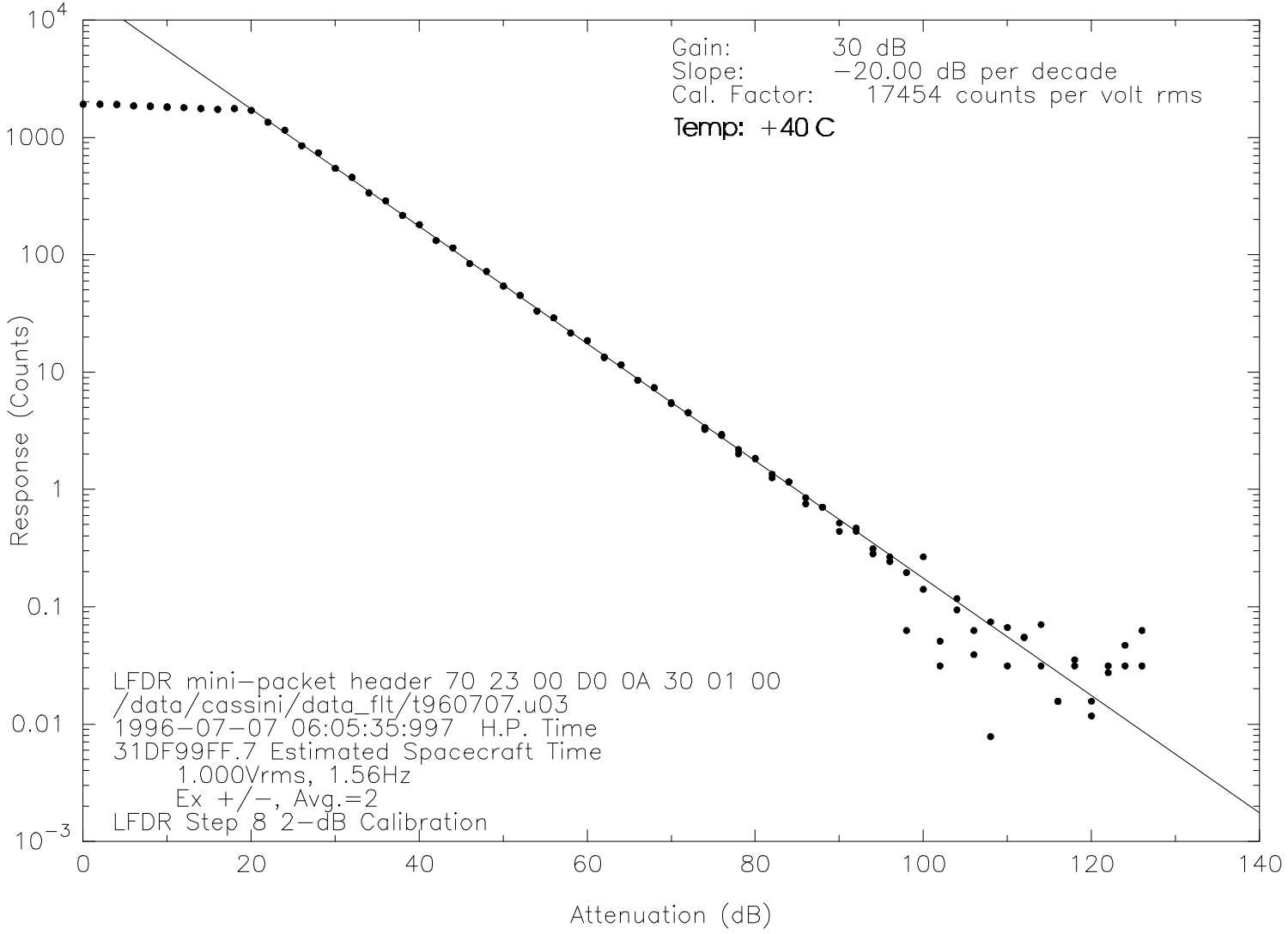

Figure 9.3.1.17
LFDR Amplitude Response

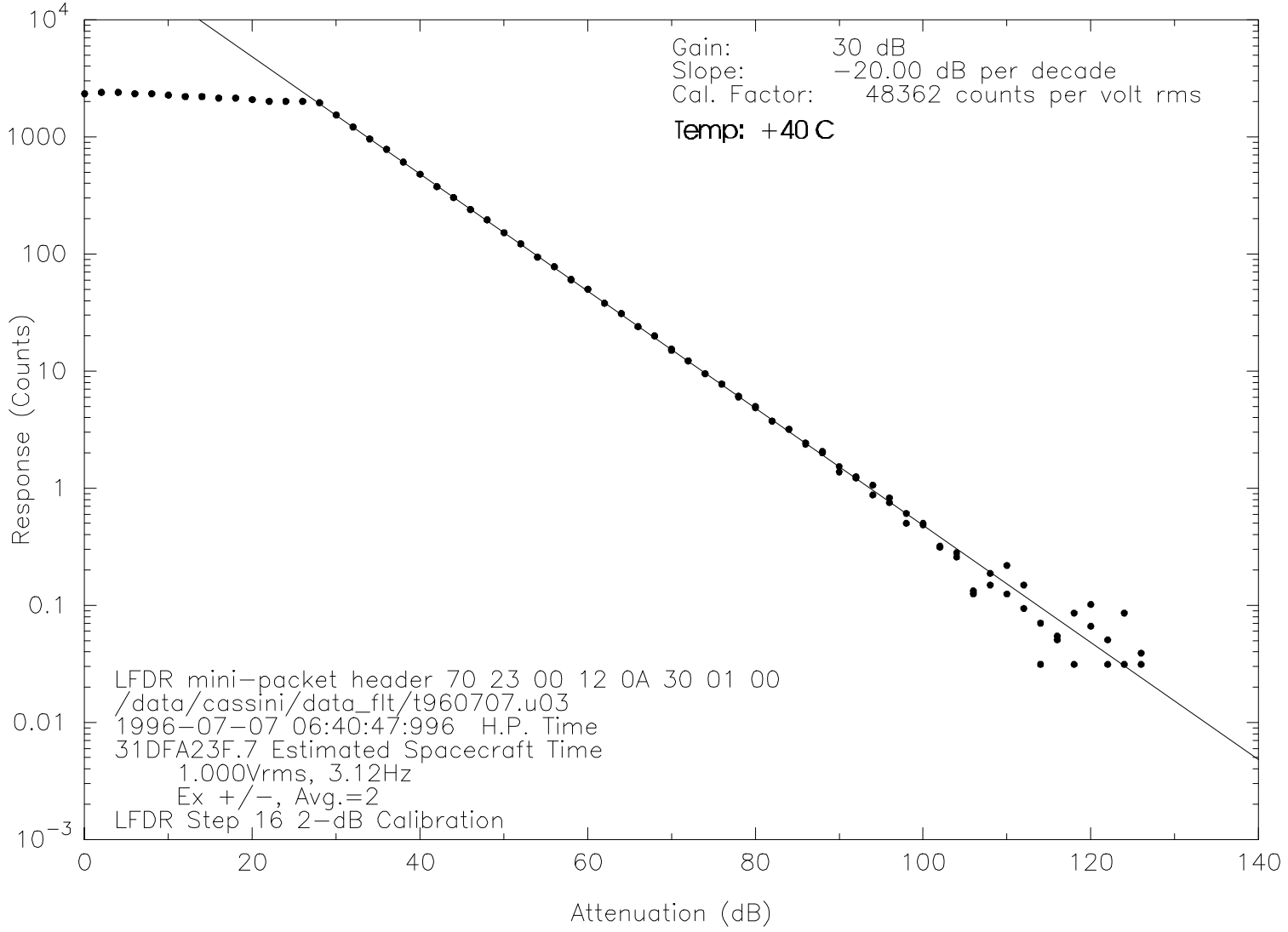

Figure 9.3.1.18

LFDR Amplitude Response

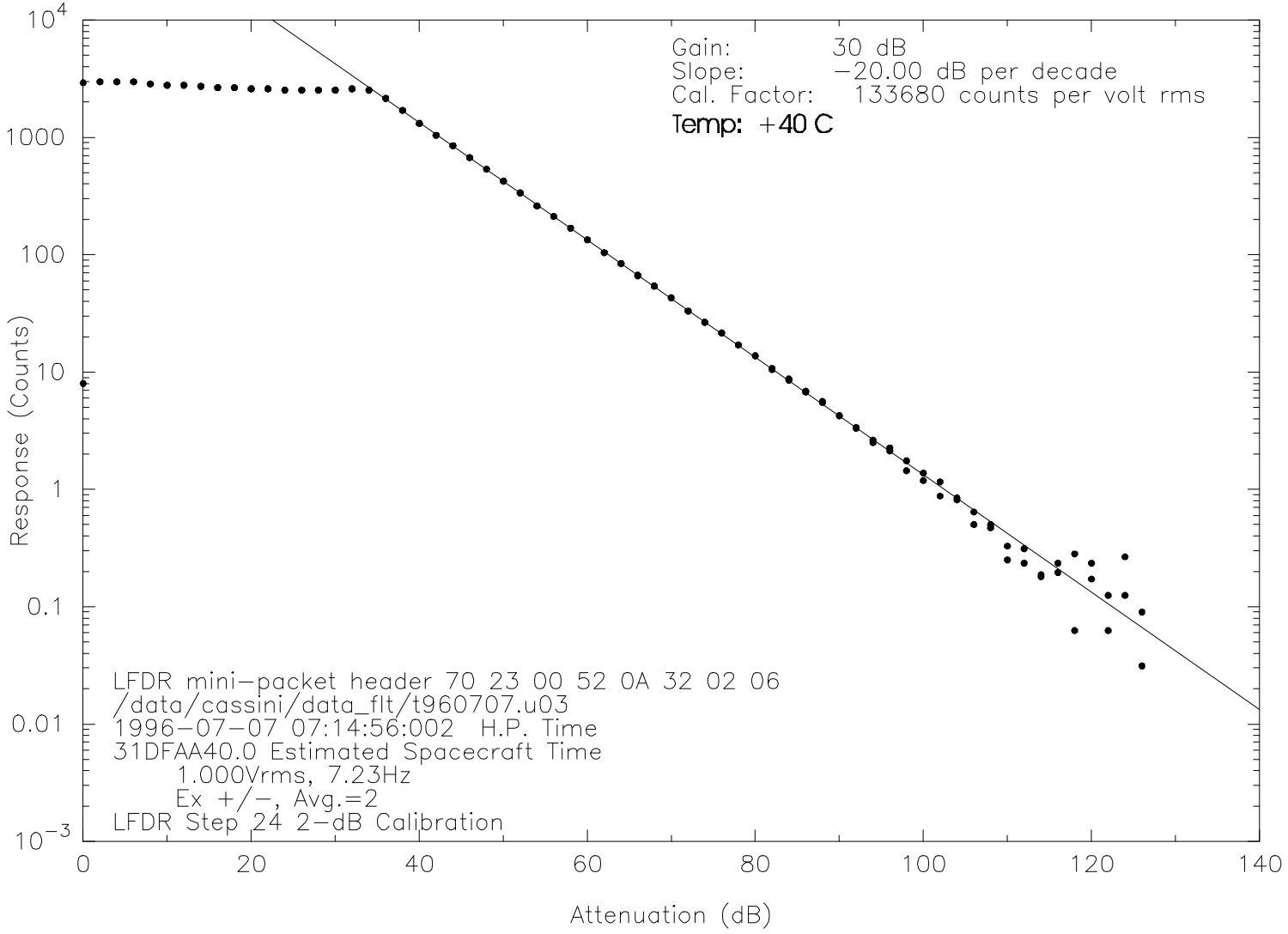

Figure 9.3.1.19
LFDR Amplitude Response

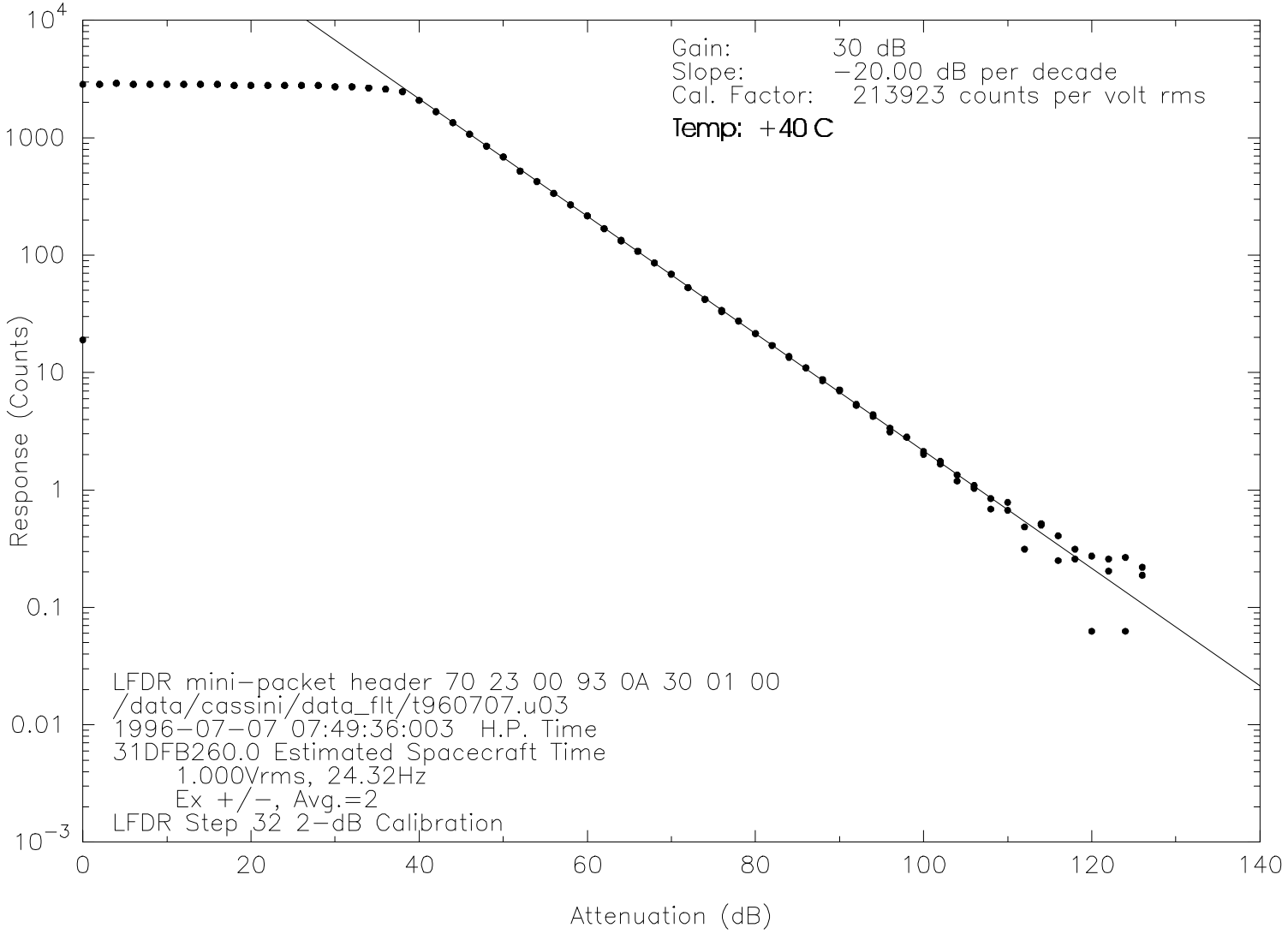

Figure 9.3.1.20

LFDR Amplitude Response

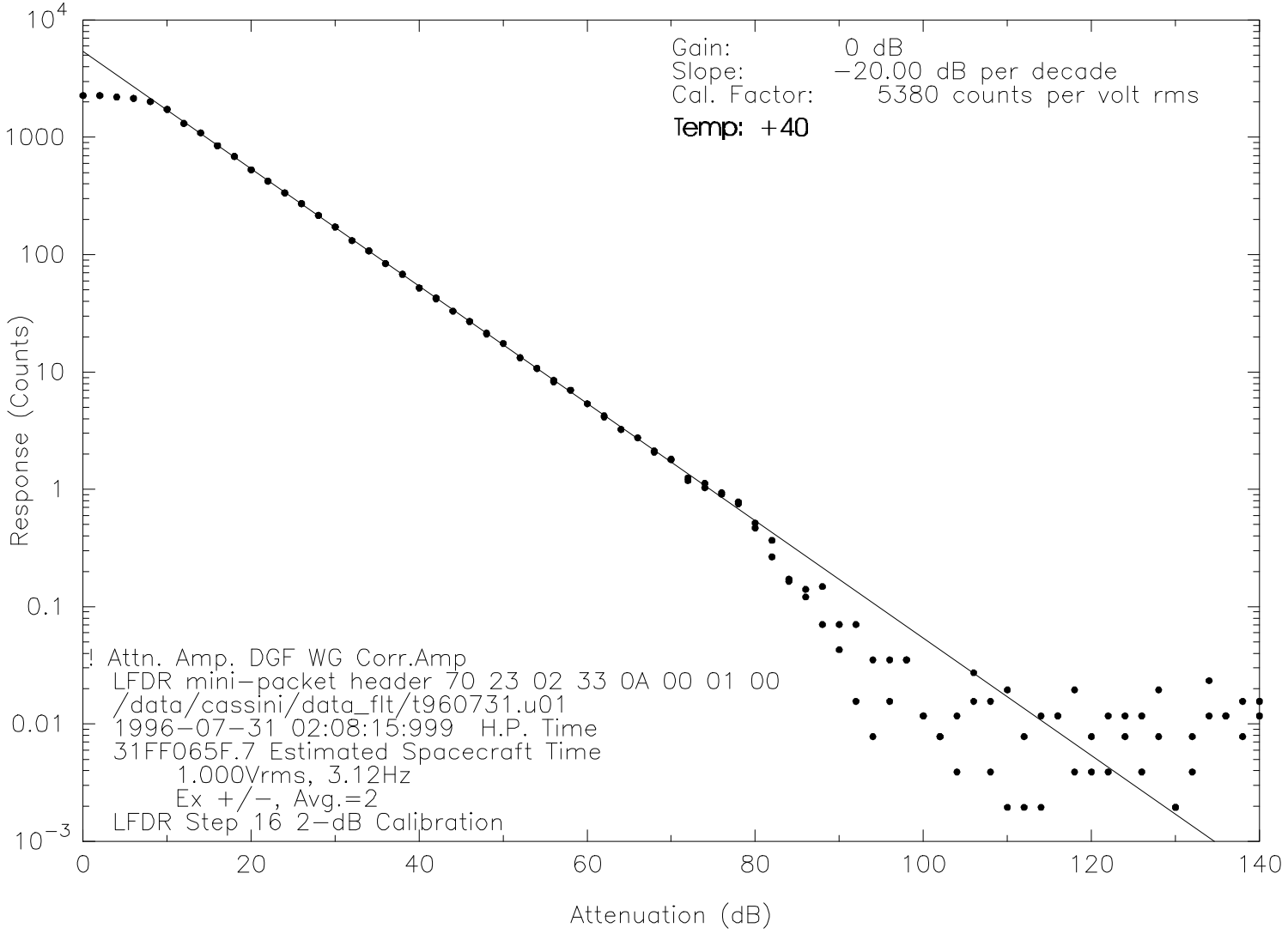

Figure 9.3.1.21
LFDR Amplitude Response

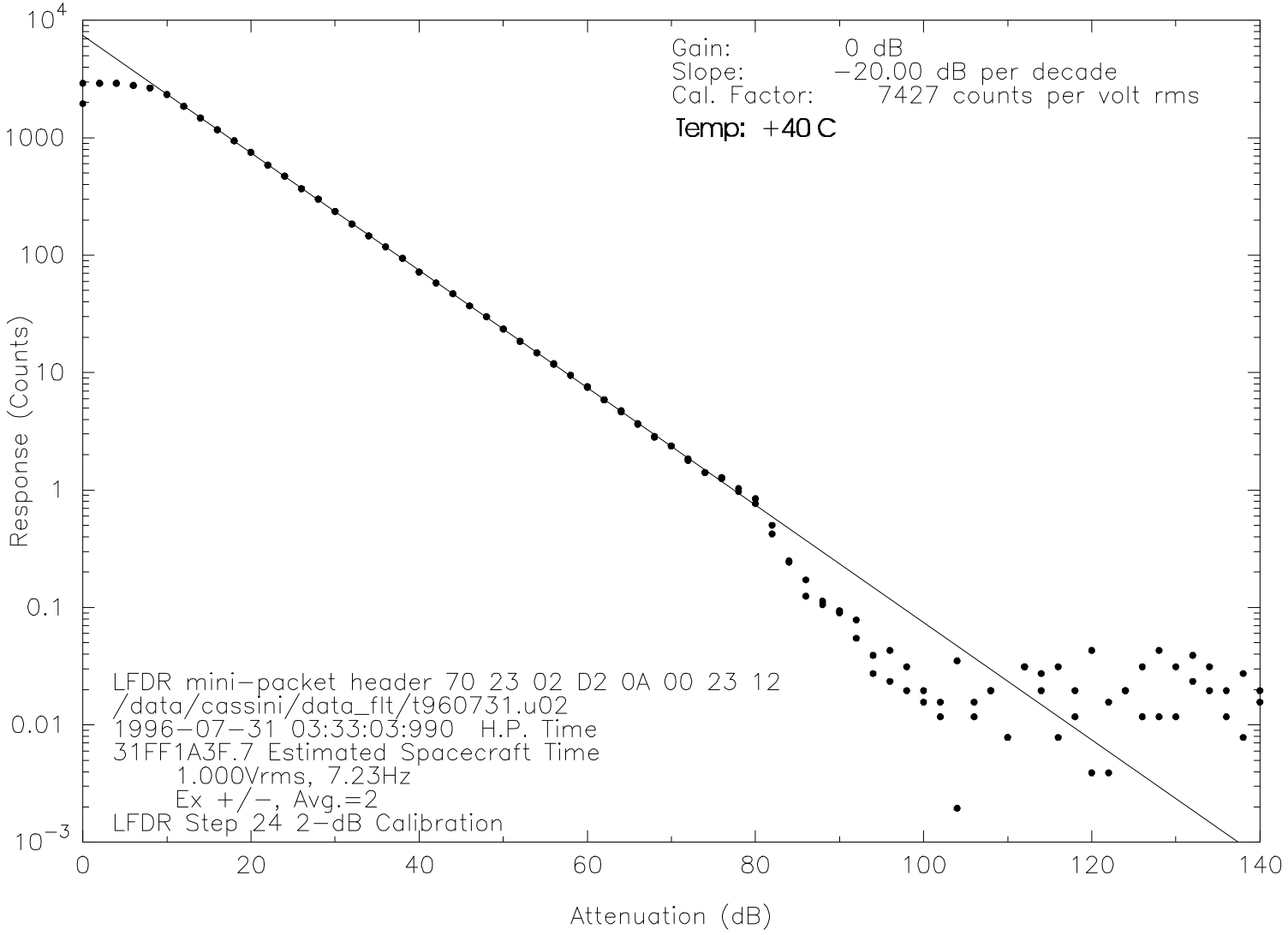

Figure 9.3.1.22
LFDR Amplitude Response

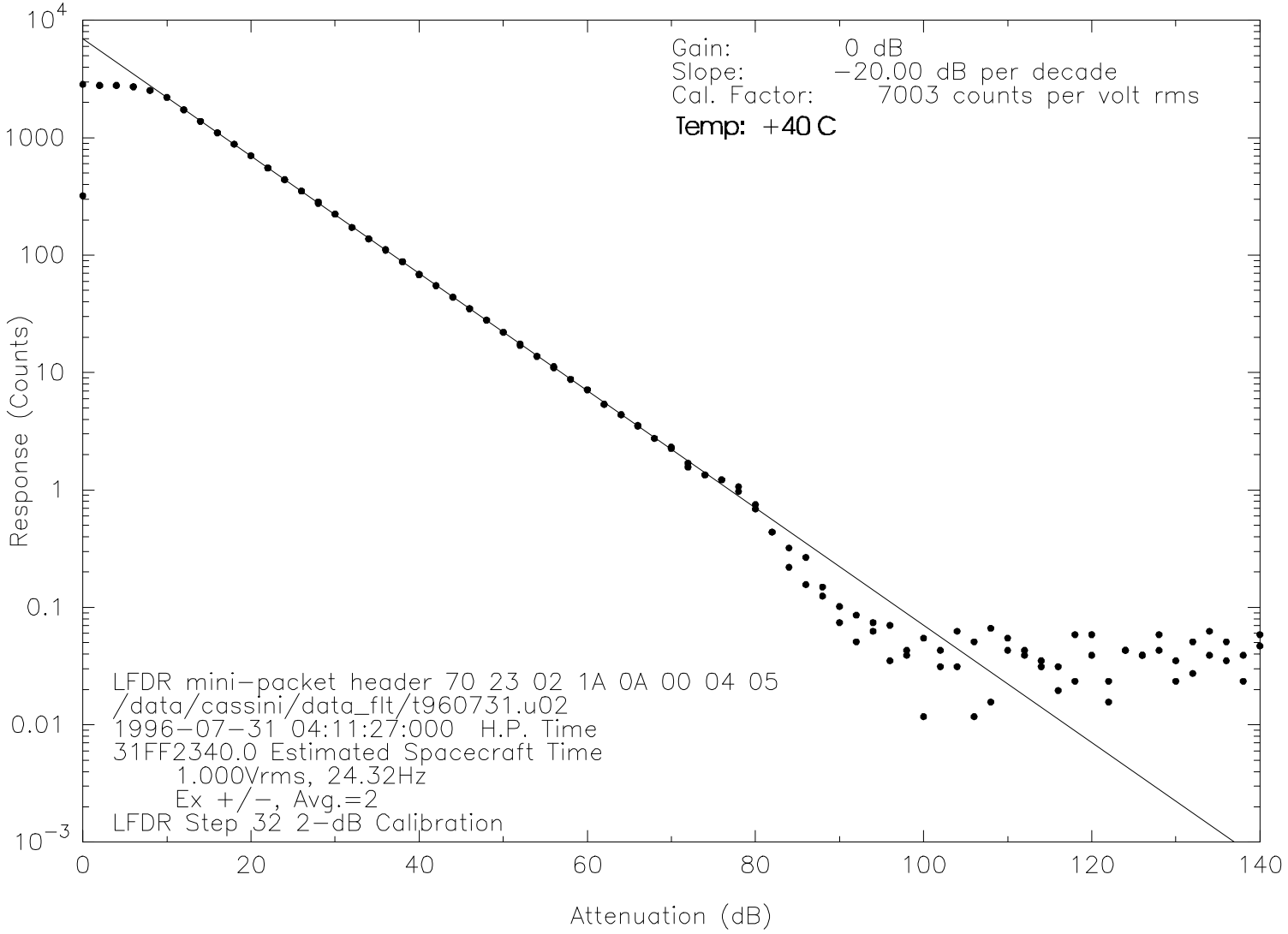

Table 9.3.1.1 LFDR Counts-to-Volts$_{RMS}$ Calibration Factor Table

Temperature	Gain State	LFDR Step	Frequency (Hz)	Calibration Factor
24° C	0	16	3.12	5340 counts/ Vrms
24° C	0	24	7.23	7445 counts/ Vrms
24° C	0	32	24.32	7185 counts/ Vrms
24° C	30	1	0.195	83 counts/ Vrms
24° C	30	8	1.56	16862 counts/ Vrms
24° C	30	16	3.12	47706 counts/ Vrms
24° C	30	24	7.23	133881 counts/ Vrms
24° C	30	32	24.32	218536 counts/ Vrms
-20° C	30	1	0.195	67 counts/ Vrms
-20° C	30	8	1.56	16944 counts/ Vrms
-20° C	30	16	3.12	47420 counts/ Vrms
-20° C	30	24	7.23	134729 counts/ Vrms
-20° C	30	32	24.32	226782 counts/ Vrms
40° C	0	16	3.12	5380 counts/ Vrms
40° C	0	24	7.23	7427 counts/ Vrms
40° C	0	32	24.32	7003 counts/ Vrms
40° C	30	1	0.195	86 counts/ Vrms
40° C	30	8	1.56	17454 counts/ Vrms
40° C	30	16	3.12	48362 counts/ Vrms
40° C	30	24	7.23	133680 counts/ Vrms
40° C	30	32	24.32	213923 counts/ Vrms

9.3.2 Channel-to-Channel Gains

The sensitivity of the LFDR varies from step to step across the band. Variations of insertion losses and filter roll-off, especially in the programmable gain amplifiers, affect the calibrations. Because of the significant dependence upon frequency, the programmable gain amplifiers do not actually provide the nominal gains which the gain state implies, except at frequencies above about 20 Hz. The programmable gain amplifiers have approximately 1-pole filters with the following nominal break frequencies:

Gain State	Nominal 3-dB Frequency (Hz)
0 dB	0.4
10 dB	1.1
20 dB	3.5
30 dB	13.0

Additionally, a high-pass filter proceeds the programmable gain amplifiers, and this HPF has a sharp roll-off below the nominal break frequency of 1 Hz. The effects of this filter and the gain amps are combined in the channel-to-channel gain calibrations.

The channel to channel gains are performed by stimulating at the center frequency of each step at a fixed amplitude of -60 dBv. The ratios between the amplitudes for unknown steps and known steps can be used to produce calibration factors for the steps for which no 2-dB calibration was run. The stimulus setup for the channel-to-channel gains test is shown in Figure 9.3.1.1. Figure 9.3.2.1 and Tables 9.3.2.1 through 9.3.2.4 show the channel-to–channel gains for each of the LFDR gain settings. One thing to notice in the channel-to-channel gains plots is the abrupt increase at LFDR step 20. This is due to the fact that for step numbers 1 through 19, one and only one FFT bin is included in the measurement. Above that point each LFDR step includes more than one FFT bin, so the effects of the Hanning window become apparent: the effective bandwidth is 1.5 FFT bins for Hanning-windowed data. This effect will be calibrated out when the effective noise bandwidth is included in the calculation to give spectral density.

The channel-to-channel gains results for the LFDR are presented for room temperature (+24° C) only, since the variation with temperature is negligible, as noted in Section 9.3.1.

Figure 9.3.2.1: LFDR Channel−Channel Gain

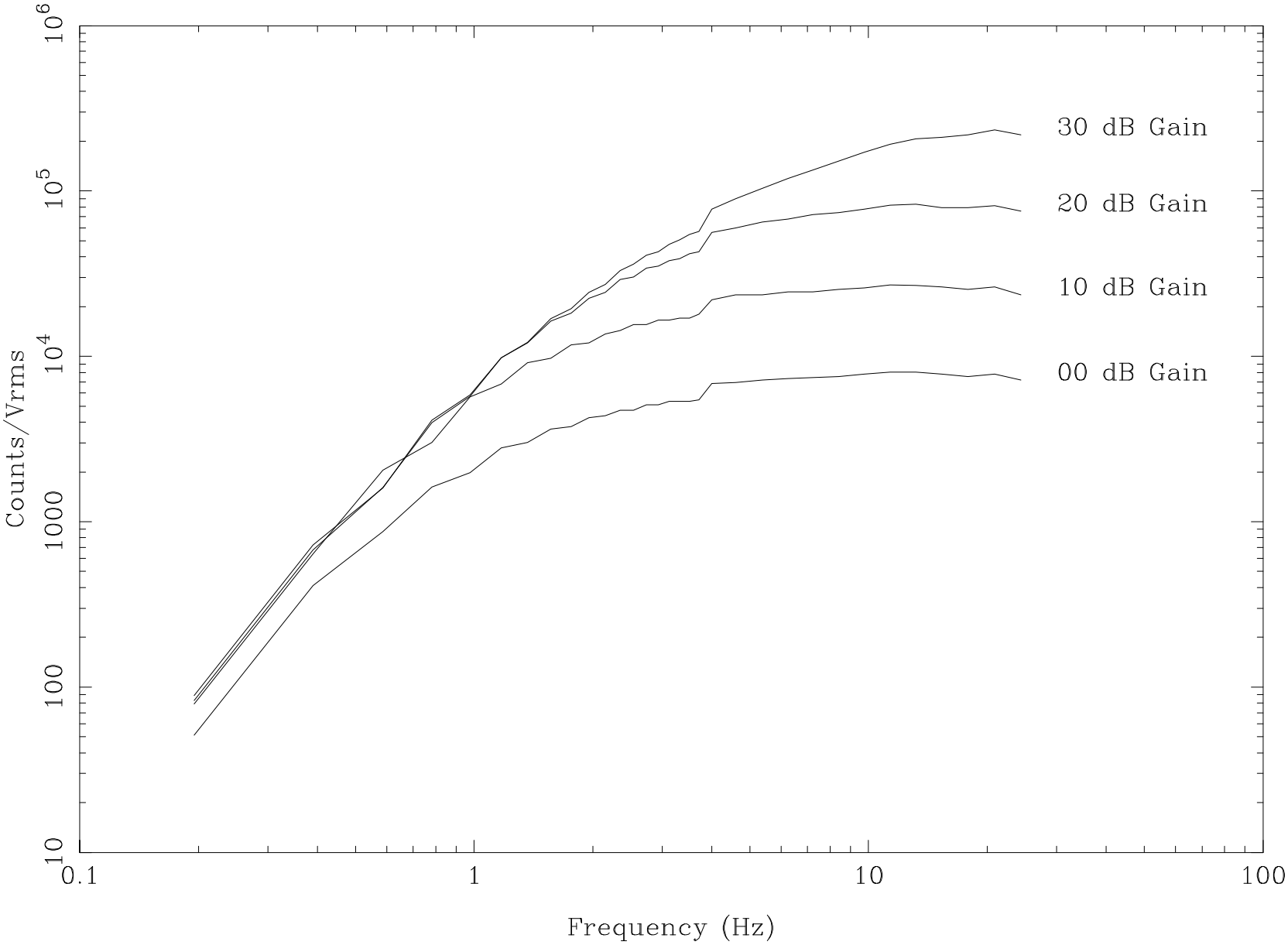

Table 9.3.2.1 LFDR Channel-to-Channel Gain results for 0-dB Gain State

Temperature	Gain State	LFDR Step	Frequency (Hz)	Average Ch-Ch counts	Cal. Factor counts / Vrms
24° C	0	1	0.195	< noise level	51
24° C	0	2	0.390	0.4219	410
24° C	0	3	0.586	0.8984	872
24° C	0	4	0.781	1.672	1623
24° C	0	5	0.977	2.031	1972
24° C	0	6	1.172	2.875	2791
24° C	0	7	1.367	3.094	3004
24° C	0	8	1.563	3.750	3641
24° C	0	9	1.758	3.875	3762
24° C	0	10	1.953	4.375	4248
24° C	0	11	2.148	4.500	4369
24° C	0	12	2.344	4.875	4733
24° C	0	13	2.539	4.875	4733
24° C	0	14	2.734	5.250	5097
24° C	0	15	2.930	5.250	5097
24° C	0	16	3.125	5.500	5340
24° C	0	17	3.320	5.500	5340
24° C	0	18	3.515	5.500	5340
24° C	0	19	3.711	5.625	5461
24° C	0	20	4.004	7.000	6835
24° C	0	21	4.599	7.125	6957
24° C	0	22	5.371	7.375	7201
24° C	0	23	6.250	7.500	7323
24° C	0	24	7.227	7.625	7445
24° C	0	25	8.398	7.750	7567
24° C	0	26	9.766	8.000	7811
24° C	0	27	11.328	8.250	8055
24° C	0	28	13.184	8.250	8037
24° C	0	29	15.332	8.000	7794
24° C	0	30	17.871	7.750	7550
24° C	0	31	20.898	8.000	7794
24° C	0	32	24.316	7.375	7185

Table 9.3.2.2 LFDR Channel-to-Channel Gain results for 10-dB Gain State

Temperature	Gain State	LFDR Step	Frequency (Hz)	Average Ch-Ch counts	Cal. Factor counts / Vrms
24° C	10	1	0.195	< noise level	79
24° C	10	2	0.390	0.6797	637
24° C	10	3	0.586	2.188	2049
24° C	10	4	0.781	3.219	3015
24° C	10	5	0.977	6.063	5679
24° C	10	6	1.172	7.250	6792
24° C	10	7	1.367	9.750	9134
24° C	10	8	1.563	10.38	9719
24° C	10	9	1.758	12.50	11710
24° C	10	10	1.953	12.88	12061
24° C	10	11	2.148	14.63	13700
24° C	10	12	2.344	14.75	14360
24° C	10	13	2.539	16.00	15577
24° C	10	14	2.734	16.00	15577
24° C	10	15	2.930	17.00	16551
24° C	10	16	3.125	17.00	16551
24° C	10	17	3.320	17.50	17038
24° C	10	18	3.515	17.50	17038
24° C	10	19	3.711	18.50	18011
24° C	10	20	4.004	22.00	21980
24° C	10	21	4.599	23.50	23479
24° C	10	22	5.371	23.50	23479
24° C	10	23	6.250	24.50	24478
24° C	10	24	7.227	24.50	24478
24° C	10	25	8.398	25.50	25477
24° C	10	26	9.766	26.00	25977
24° C	10	27	11.328	27.00	26976
24° C	10	28	13.184	27.00	26820
24° C	10	29	15.332	26.50	26324
24° C	10	30	17.871	25.50	25330
24° C	10	31	20.898	26.50	26324
24° C	10	32	24.316	23.75	23592

Table 9.3.2.3LFDR Channel-to-Channel Gain results for 20-dB Gain State

Temperature	Gain State	LFDR Step	Frequency (Hz)	Average Ch-Ch counts	Cal. Factor counts / Vrms
24° C	20	1	0.195	< noise level	89
24° C	20	2	0.390	0.7734	724
24° C	20	3	0.586	1.703	1595
24° C	20	4	0.781	4.375	4098
24° C	20	5	0.977	6.250	5855
24° C	20	6	1.172	10.50	9836
24° C	20	7	1.367	12.88	12061
24° C	20	8	1.563	17.50	16394
24° C	20	9	1.758	19.50	18267
24° C	20	10	1.953	24.00	22482
24° C	20	11	2.148	26.00	24357
24° C	20	12	2.344	30.00	29208
24° C	20	13	2.539	31.00	30181
24° C	20	14	2.734	35.00	34076
24° C	20	15	2.930	36.00	35049
24° C	20	16	3.125	39.00	37970
24° C	20	17	3.320	40.00	38944
24° C	20	18	3.515	43.00	41864
24° C	20	19	3.711	44.00	42838
24° C	20	20	4.004	56.00	55950
24° C	20	21	4.599	60.00	59947
24° C	20	22	5.371	65.00	64943
24° C	20	23	6.250	67.50	67440
24° C	20	24	7.227	72.00	71936
24° C	20	25	8.398	74.00	73934
24° C	20	26	9.766	78.00	77931
24° C	20	27	11.328	82.00	81927
24° C	20	28	13.184	84.00	83441
24° C	20	29	15.332	80.00	79468
24° C	20	30	17.871	80.00	79468
24° C	20	31	20.898	82.00	81454
24° C	20	32	24.316	76.00	75494

Table 9.3.2.4 LFDR Channel-to-Channel Gain results for 30-dB Gain State

Temperature	Gain State	LFDR Step	Frequency (Hz)	Average Ch-Ch counts	Cal. Factor counts / Vrms
24° C	30	1	0.195	< noise level	83
24° C	30	2	0.390	0.7188	673
24° C	30	3	0.586	1.719	1610
24° C	30	4	0.781	4.250	3981
24° C	30	5	0.977	6.125	5738
24° C	30	6	1.172	10.50	9836
24° C	30	7	1.367	13.00	12178
24° C	30	8	1.563	18.00	16862
24° C	30	9	1.758	20.75	19438
24° C	30	10	1.953	26.00	24356
24° C	30	11	2.148	29.00	27167
24° C	30	12	2.344	34.00	33102
24° C	30	13	2.539	37.00	36023
24° C	30	14	2.734	42.00	40891
24° C	30	15	2.930	44.00	42838
24° C	30	16	3.125	49.00	47706
24° C	30	17	3.320	52.00	50627
24° C	30	18	3.515	56.00	54521
24° C	30	19	3.711	58.50	56955
24° C	30	20	4.004	78.00	77930
24° C	30	21	4.599	90.00	89920
24° C	30	22	5.371	104.0	103908
24° C	30	23	6.250	119.0	118894
24° C	30	24	7.227	134.0	133881
24° C	30	25	8.398	152.0	151865
24° C	30	26	9.766	172.0	171847
24° C	30	27	11.328	192.0	191829
24° C	30	28	13.184	208.0	206616
24° C	30	29	15.332	212.0	210589
24° C	30	30	17.871	220.0	218536
24° C	30	31	20.898	236.0	234430
24° C	30	32	24.316	220.0	218536

9.3.3 Filter Bandwidths

In this section detection bandwidth calibration data for the LFDR are presented. There are two ways to evaluate detection bandwidth. One is to measure the frequency response of the filter. A sinusoidal stimulus is swept over the filter passband and the response of the receiver is noted. The other method is to determine the effective bandwidth by noting the receiver response to a white noise stimulus. In the following paragraphs, both methods are discussed and filter bandwidth data are presented for the LFDR filters.

9.3.3.1 Filter Frequency Response Curves

The shapes of the LFDR digital filters are shown in Figures 9.3.3.1.1 and 9.3.3.1.2. For these tests, a tone of fixed amplitude (-60 dB Vrms) was swept over the frequency range from 0.1 Hz to 30 Hz in steps of 0.1 Hz. The stimulus was injected into the Ex dipole inputs. The output of all LFDR steps was measured at each frequency (see Figure 9.3.1.1 for a diagram of the test setup). Tests were run at room temperature only. The results are shown for the 30-dB gain state in Figure 9.3.3.1.1, and for the 0-dB gain state in Figure 9.3.3.1.2. For the LFDR steps consisting of one and only one FFT bin, i.e., those with a center frequency less than 4 Hz, one can note that the overlap agrees quite well with the theoretical prediction for a Hanning window. This theoretical overlap is 6 dB down for adjacent steps. The deviations from this theoretical filter shape are probably due to the high-pass filter roll-off of the gain amplifiers. The higher LFDR steps show sharper roll-off.

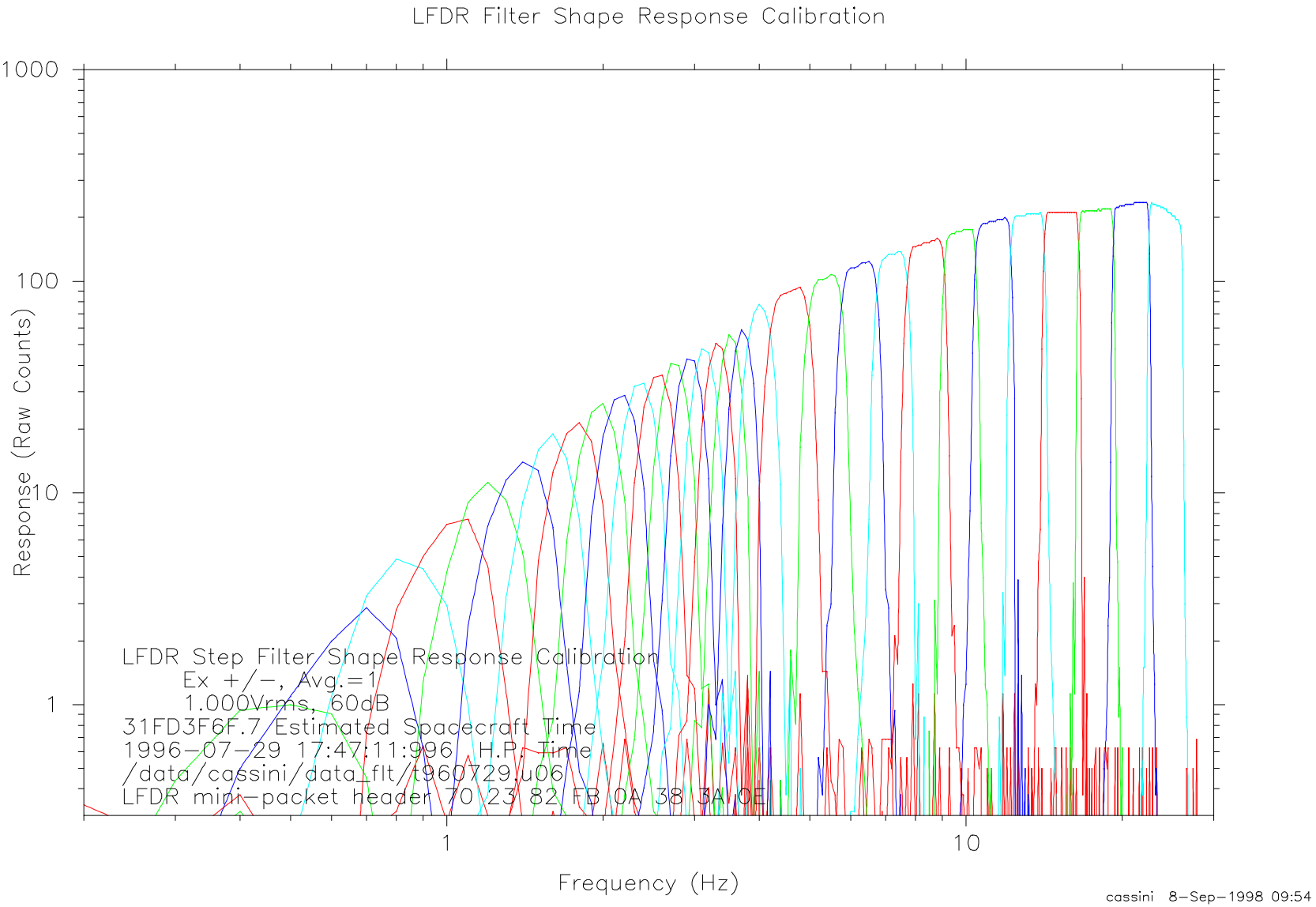

Figure 9.3.3.1.1: LFDR Filter Frequency Response at 30 dB Gain

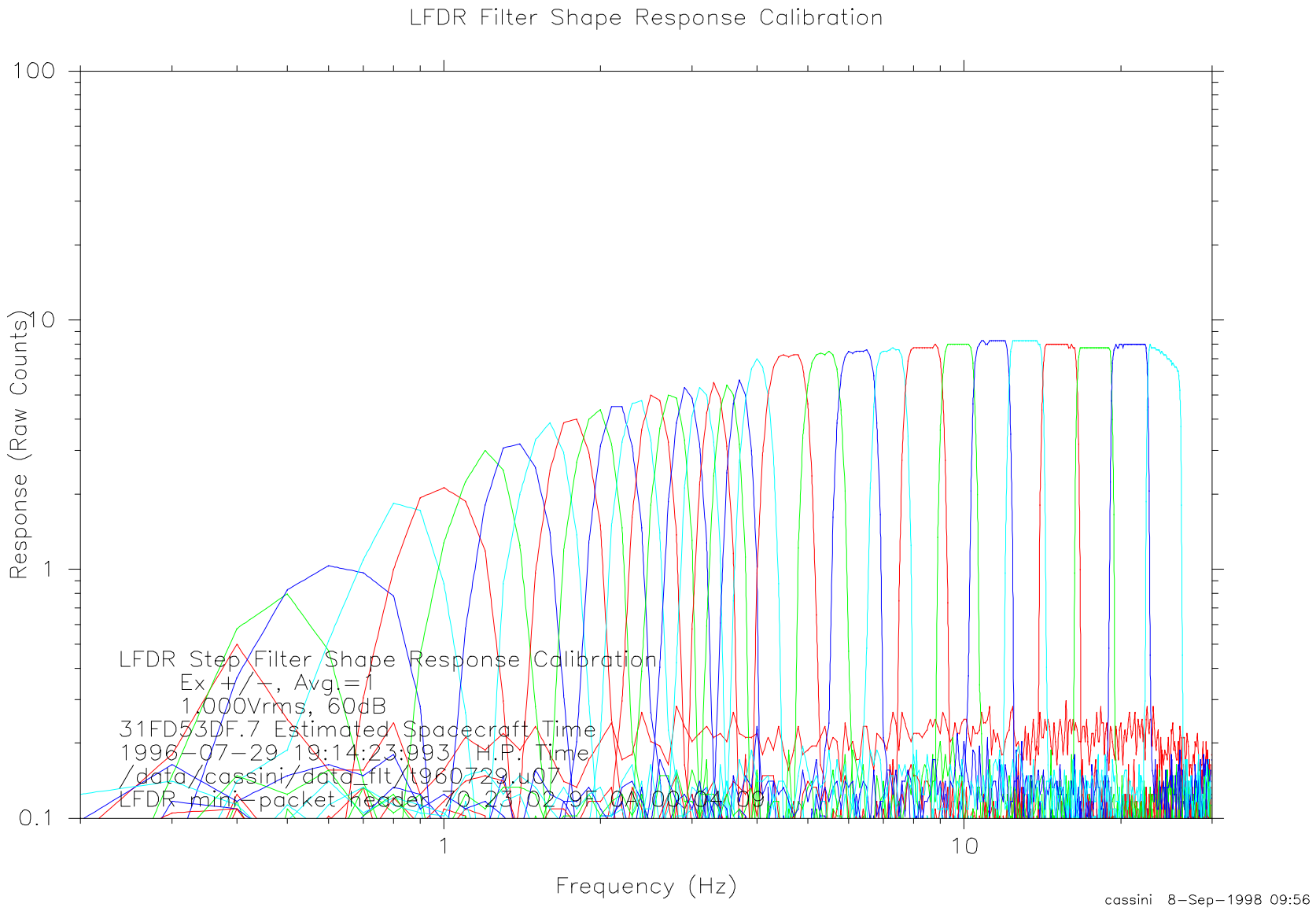

Figure 9.3.3.1.2: LFDR Filter Frequency Response at 0 dB Gain

9.3.3.2 Effective Bandwidths

Here we determine the effective bandwidth of the LFDR by observing the receiver response to a white noise stimulus. These white noise tests were conducted on June 29, 1996, at room temperature. The stimulus configuration is shown in Figure 9.3.2.2.1. The noise source used was the Hewlett Packard 8057A Precision Noise Generator, which is a pseudo-random noise generator which closely approximates Gaussian amplitude distribution. It is the best noise source for low frequency applications. To produce very low frequency noise, an external clock input of 5 kHz was used. According to the specification, with this configuration the nominal output is 1.563 Vrms (with the 50 ohm load) over a nominal bandwidth of 259.6 Hz. This would give a nominal spectral density of 9.41×10^{-3} V_{rms}^2/Hz, or -20.26 dBv/$Hz^{1/2}$. Several measurements were made with the HP3585 Spectrum Analyzer (which can measure as low as 20 Hz), and a typical measurement is show in Figure 9.3.2.2.2. The spectral density which will be used to determine the noise bandwidths is -21.5 dBv/$Hz^{1/2}$.

The white noise generator output was run through the low-frequency driver of the GSE and the attenuation stepped from 0 dB to 120 dB in 2 dB increments. At each attenuation 10 measurements of the LFDR data were taken. Simultaneously the Low-Band Waveform Receiver took several measurements for comparison. It is desired that the receiver be operating in the linear region; for this reason attenuations less than 40 dB were discarded, since the receiver is near clipping (with the 30 dB gain state active). Also for LFDR channels 8 through 19, attenuations greater than 80 dB are discarded since this is near noise floor. For the higher channels 20-32 (frequencies at 4 Hz and above), attenuations as high as 94 dB were used in the analysis. For the lowest channels (1-7), the response is very poor, hence the data was not used in the analysis. Since for all the lower channels 1-19 it is the case that one and only one FFT bin is included in the measurement, it follows that their bandwidths are all the same. Therefore one bandwidth was obtained for these channels by averaging the individual bandwidths determined for channels 8 through 19. For the high frequencies, averages of similar channels were used to determine the bandwidth. It is believed that the deviations from the theoretical bandwidths cited in Section 9.2.1 are due to the high-pass filter roll-off in the gain amplifiers.

Over the linear range of interest, an rms average was done using the 10 measurements obtained at each attenuation. Then a least squares linear fit was done on these rms averages to obtain the best fit, knowing that for each 20 dB of attenuation, a corresponding decrease of a factor of ten should occur in the measured LFDR counts. The raw data and least squares fit analysis results are shown in Figures 9.3.3.2.3 through 9.3.3.2.27. Those results are summarized in Table 9.3.3.2. It is recommended that the Average Noise Bandwidth be used in calculating spectral density.

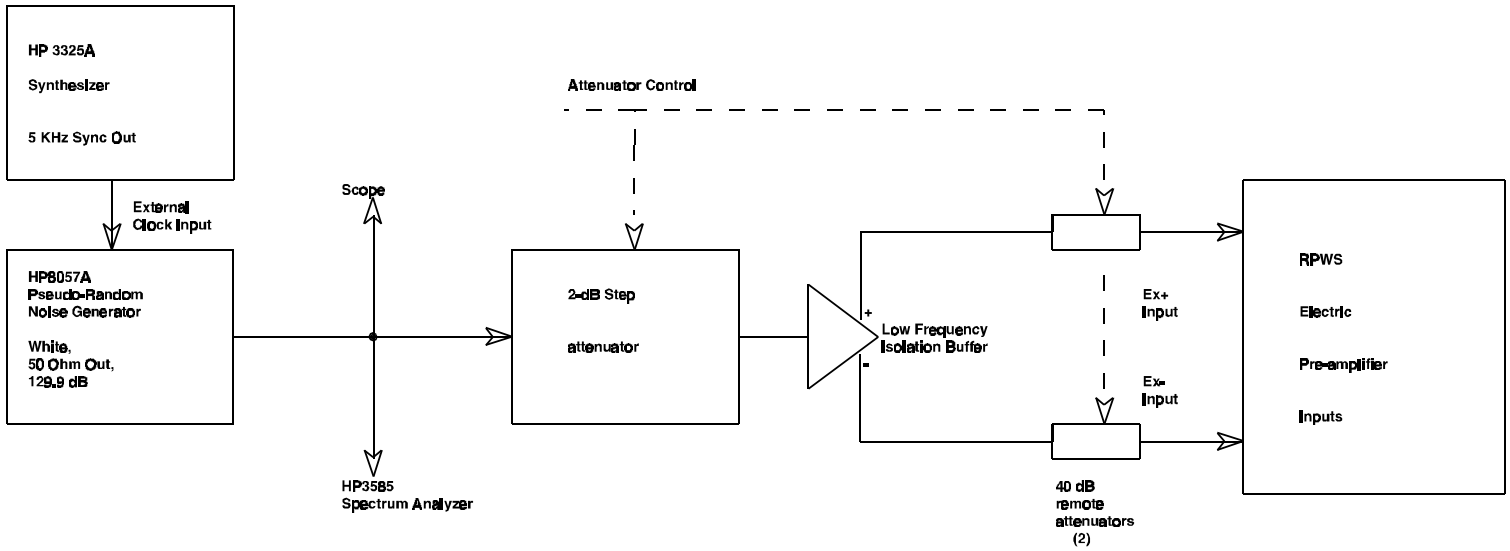

Figure 9.3.3.2.1

LFDR White Noise Response Stimulus Configuration

Figure 9.3.3.2.2: HP8535 Spectrum Analyzer Display
LFDR White Noise Test

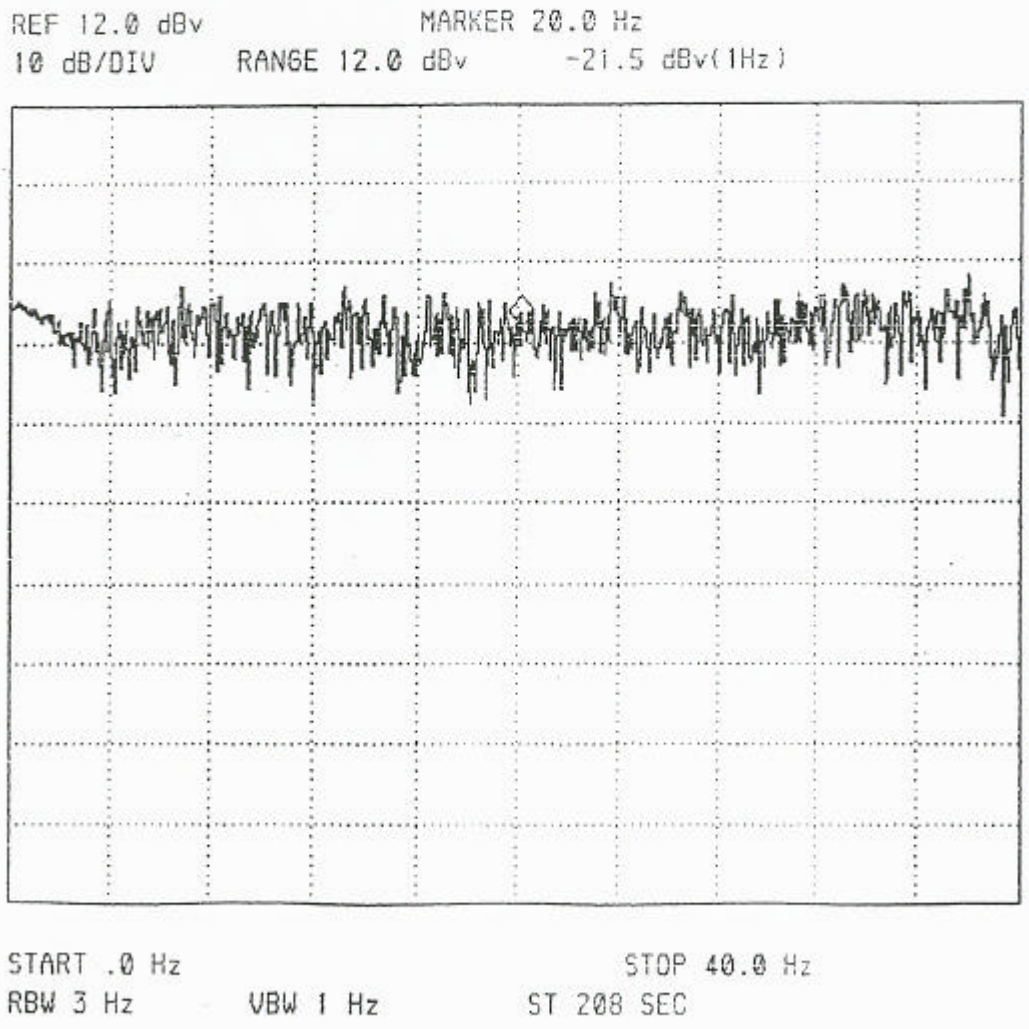

Table 9.3.3.2 LFDR Equivalent Noise Bandwidths.

LFDR Step Number	LFDR Center Frequency (Hz)	FFT Bin Numbers Included	Measured Noise Bandwidth (Hz)	Average Noise Bandwidth (Hz)
1	0.195	1	---	0.2045
2	0.390	2	---	0.2045
3	0.586	3	---	0.2045
4	0.781	4	---	0.2045
5	0.977	5	---	0.2045
6	1.172	6	---	0.2045
7	1.367	7	---	0.2045
8	1.563	8	0.2075	0.2045
9	1.758	9	0.2154	0.2045
10	1.953	10	0.2085	0.2045
11	2.148	11	0.2072	0.2045
12	2.344	12	0.1982	0.2045
13	2.539	13	0.2026	0.2045
14	2.734	14	0.1767	0.2045
15	2.930	15	0.2114	0.2045
16	3.125	16	0.1984	0.2045
17	3.320	17	0.2193	0.2045
18	3.515	18	0.2040	0.2045
19	3.711	19	0.2044	0.2045
20	4.004	20-21	0.2871	0.2871
21	4.590	22-25	0.5628	0.5719
22	5.371	26-29	0.5809	0.5719
23	6.250	30-34	0.7354	0.7373
24	7.227	35-39	0.7391	0.7373
25	8.398	40-46	1.0520	1.0429
26	9.766	47-53	1.0338	1.0429
27	11.328	54-62	1.3182	1.3182
28	13.184	63-72	1.4466	1.4466
29	15.332	73-84	1.8386	1.8386
30	17.871	85-98	2.0797	2.0797
31	20.898	99-115	2.5488	2.5488
32	24.316	116-133	2.6172	2.6172

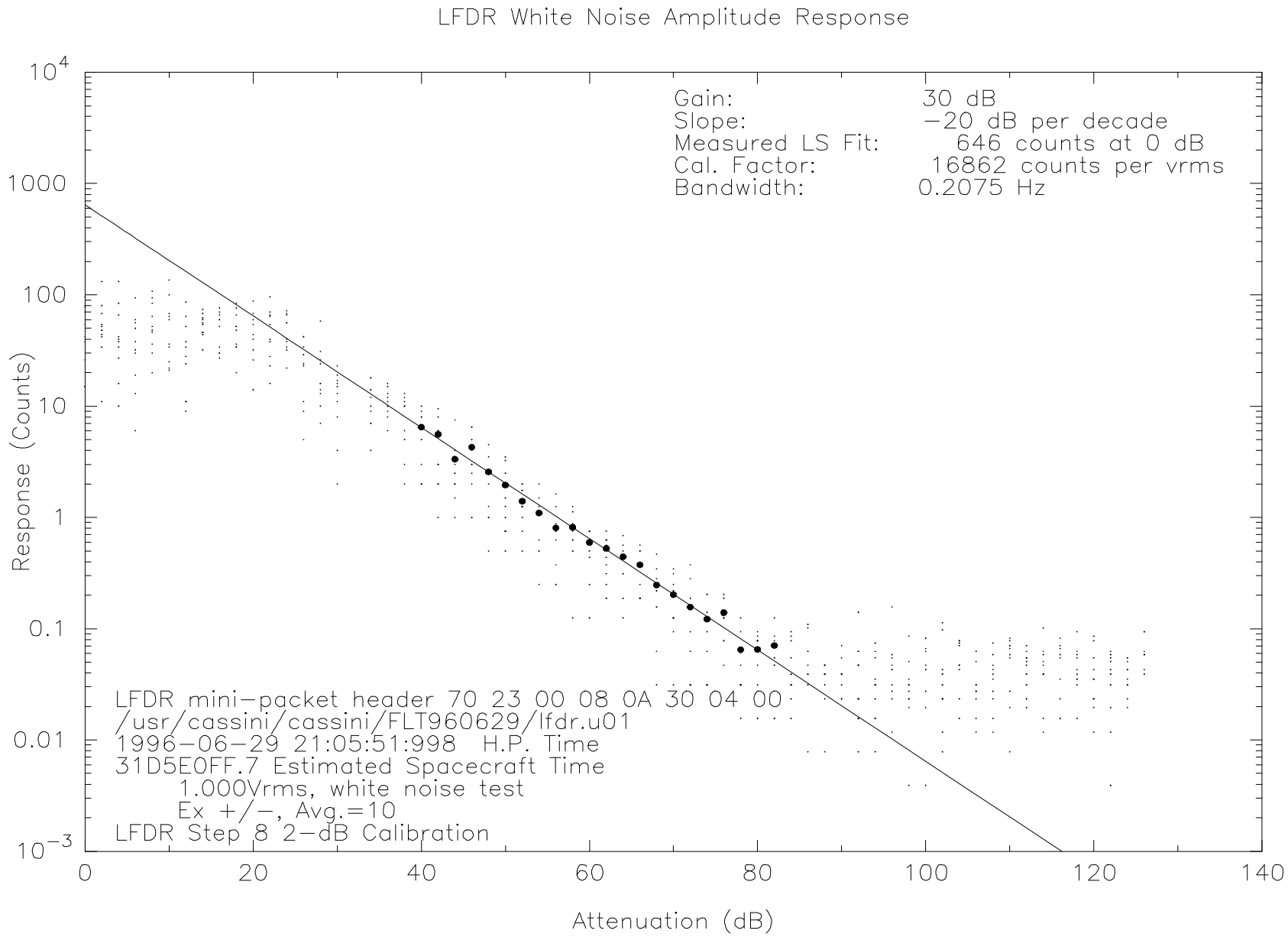

Figure 9.3.3.2.3: LFDR Step 08 Noise Bandwidth

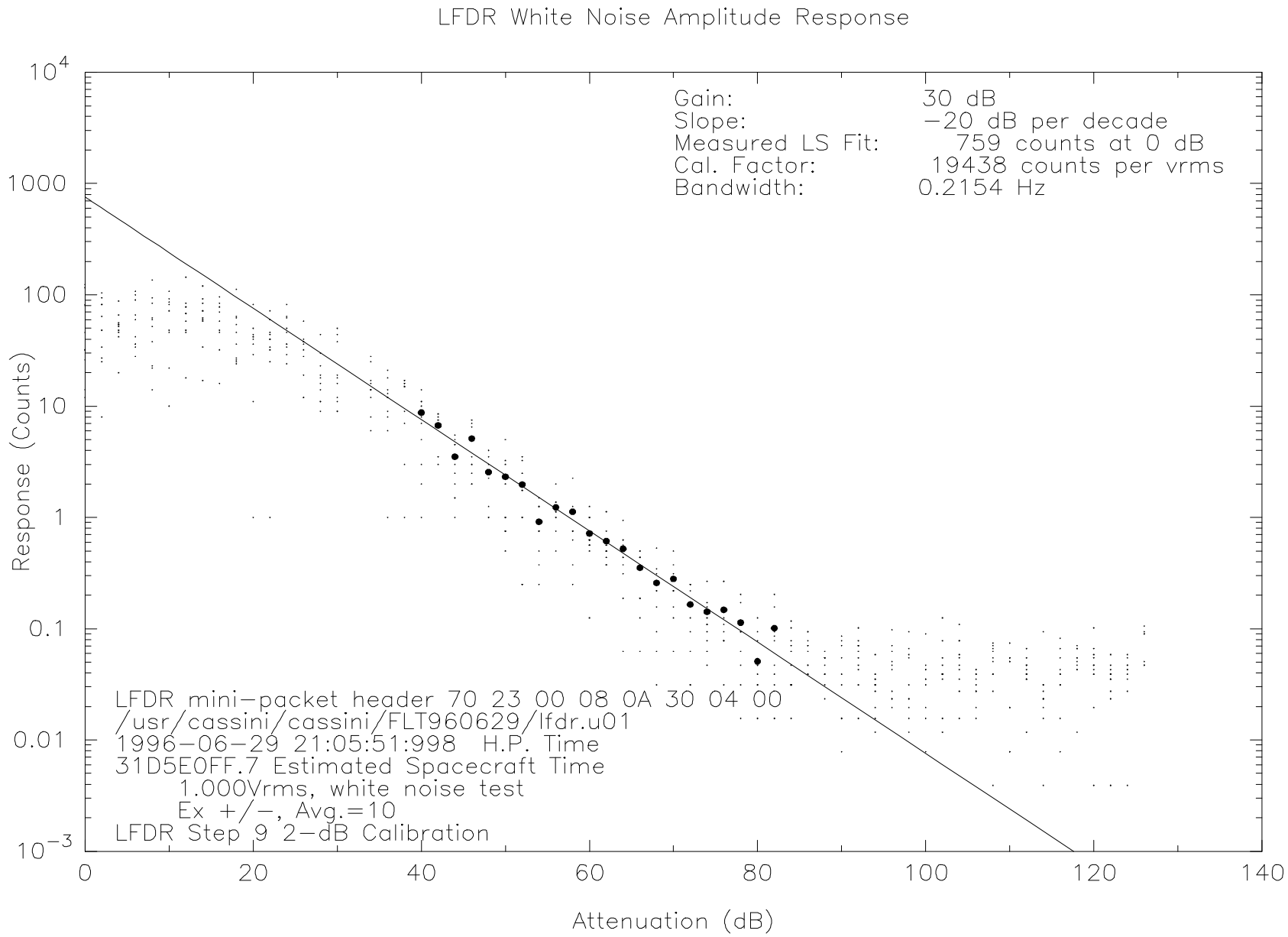

Figure 9.3.3.2.4: LFDR Step 09 Noise Bandwidth

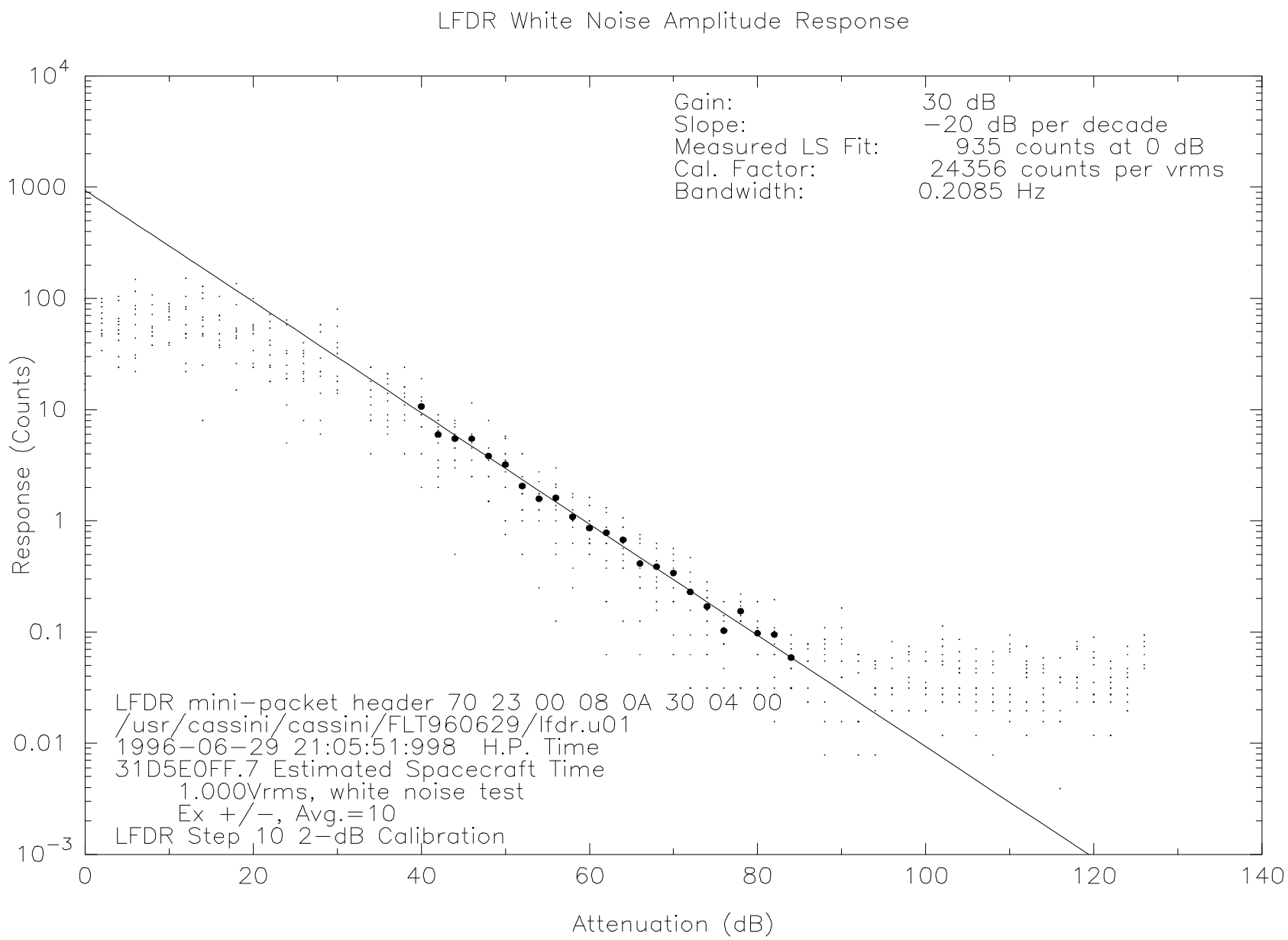

Figure 9.3.3.2.5: LFDR Step 10 Noise Bandwidth

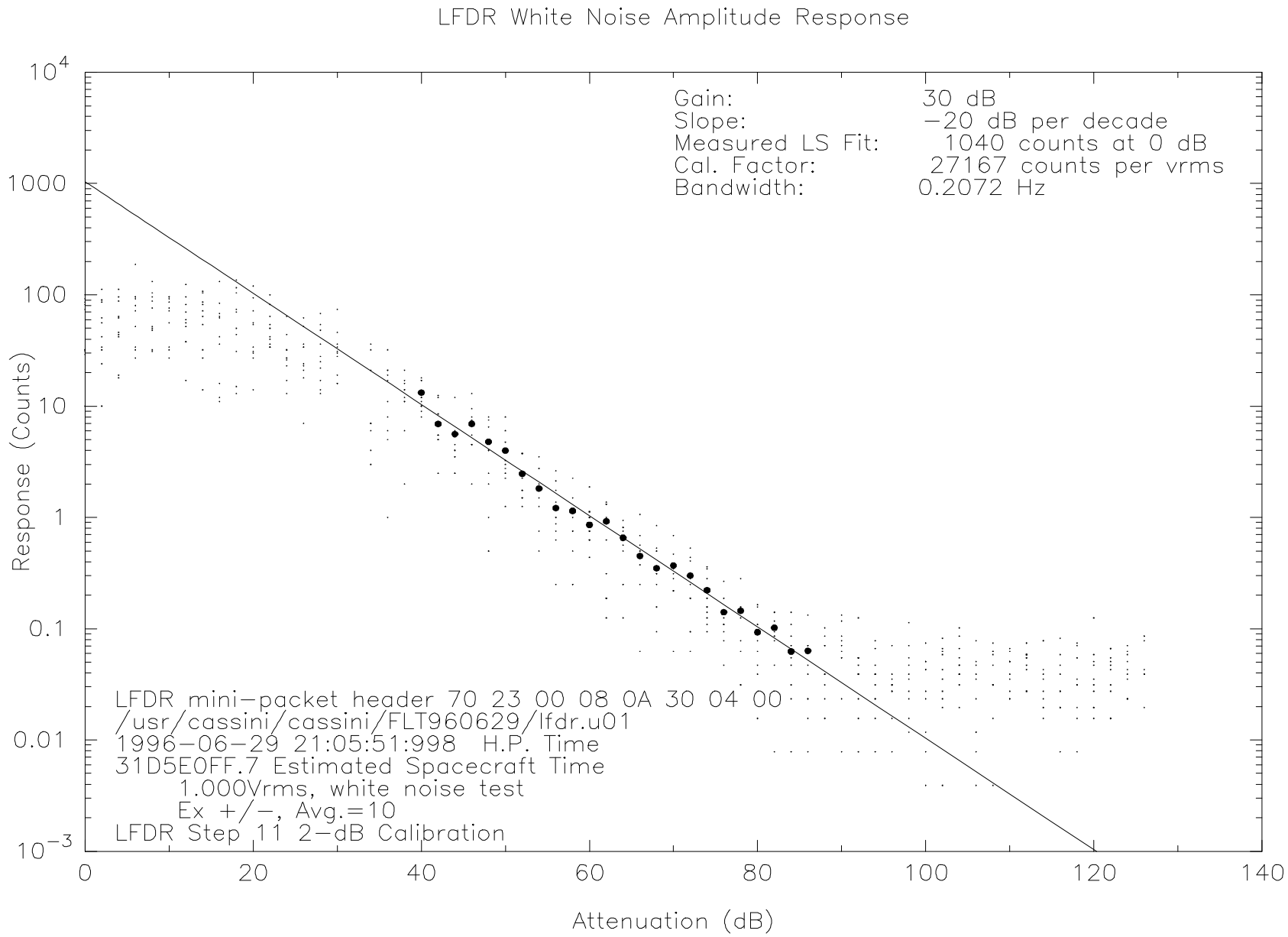

Figure 9.3.3.2.6: LFDR Step 11 Noise Bandwidth

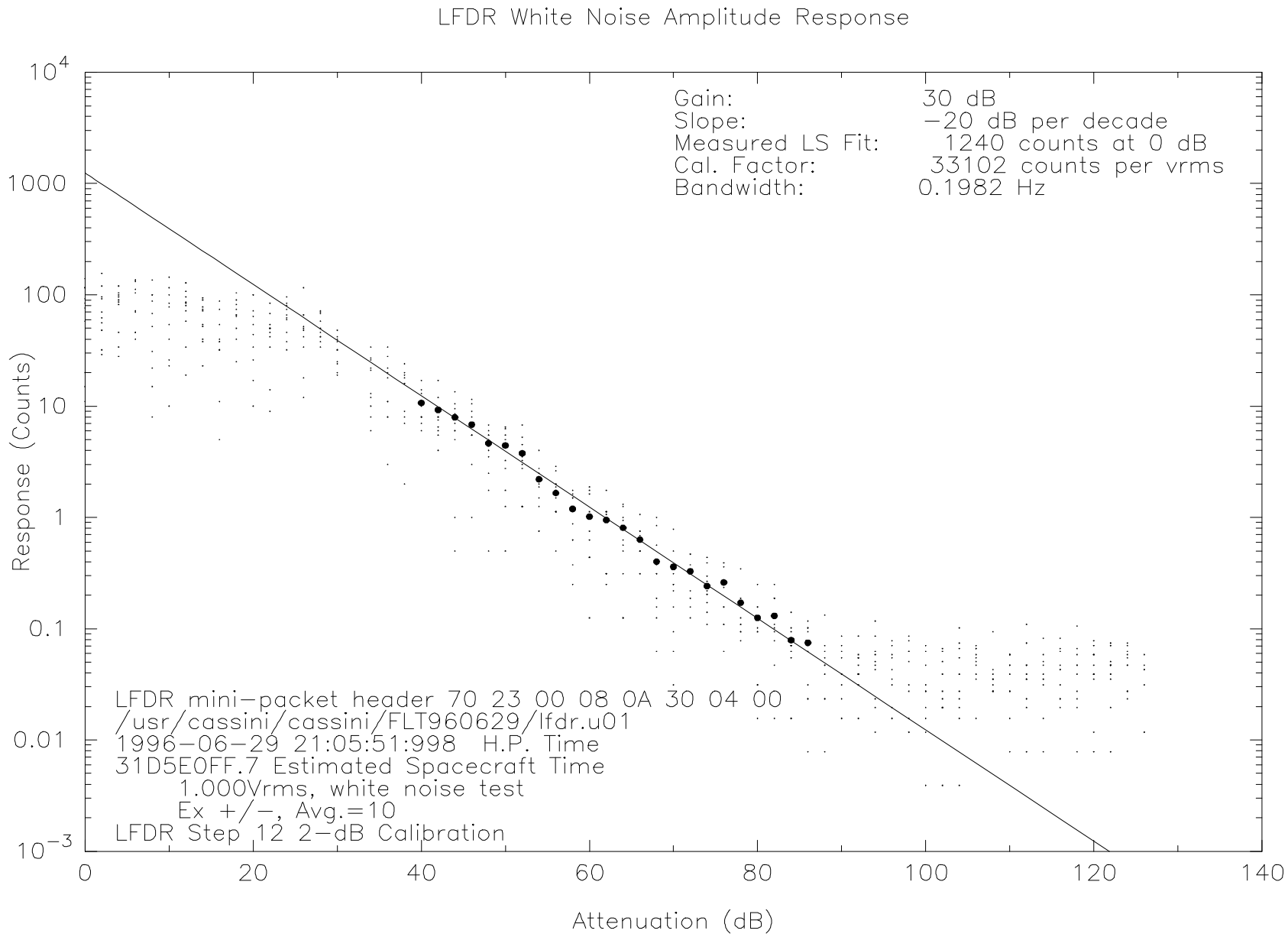

Figure 9.3.3.2.7: LFDR Step 12 Noise Bandwidth

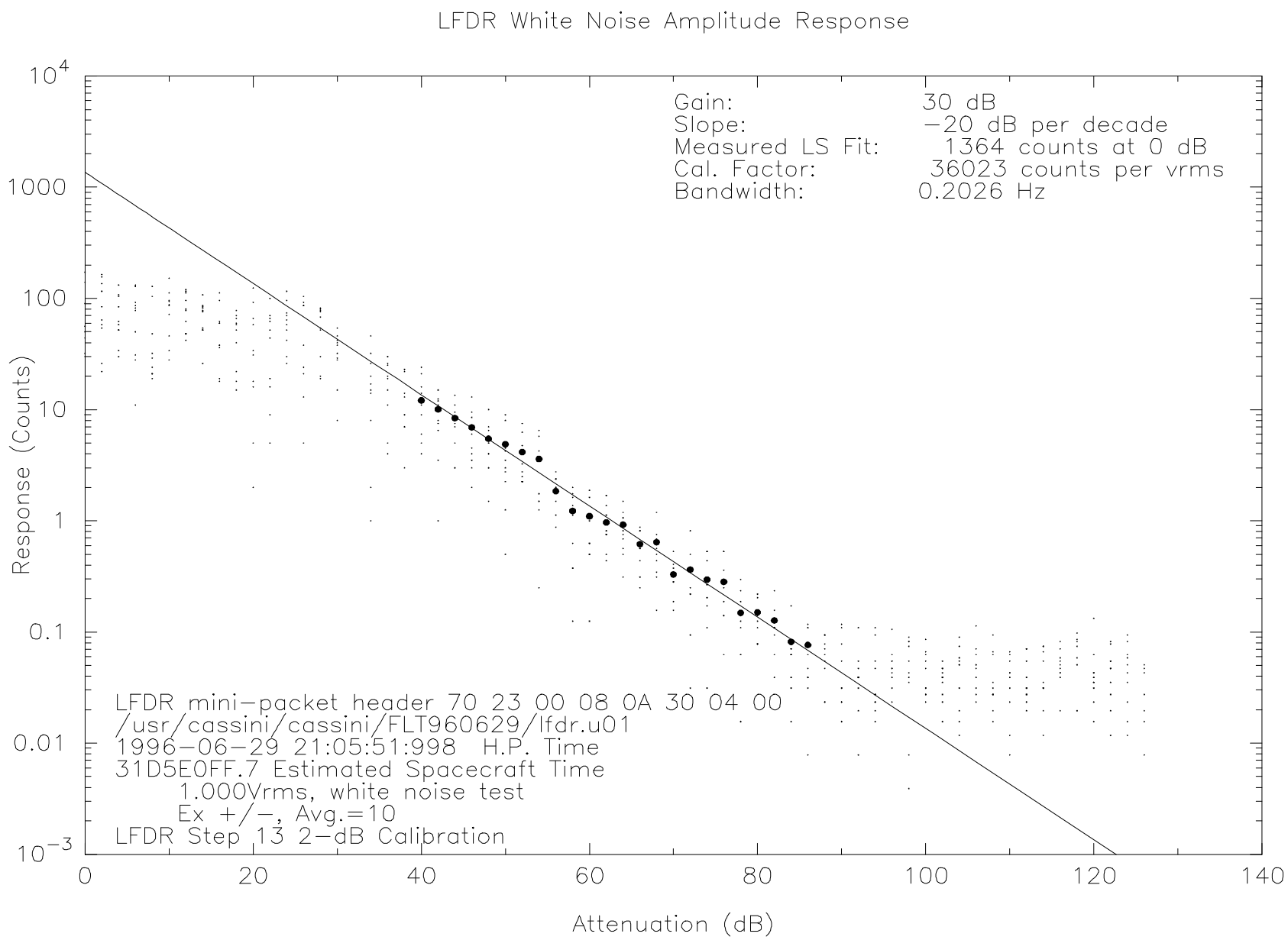

Figure 9.3.3.2.8: LFDR Step 13 Noise Bandwidth

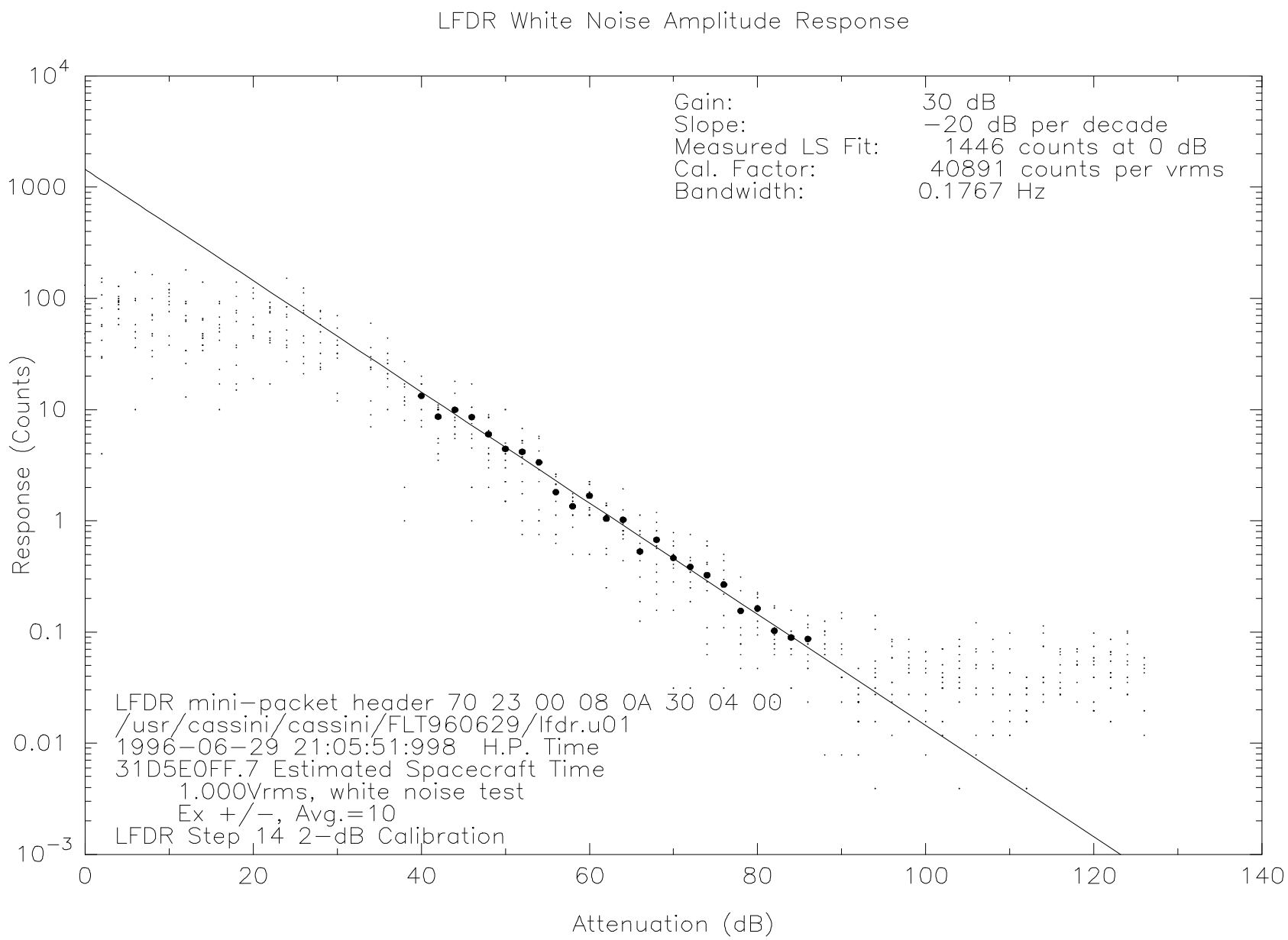

Figure 9.3.3.2.9: LFDR Step 14 Noise Bandwidth

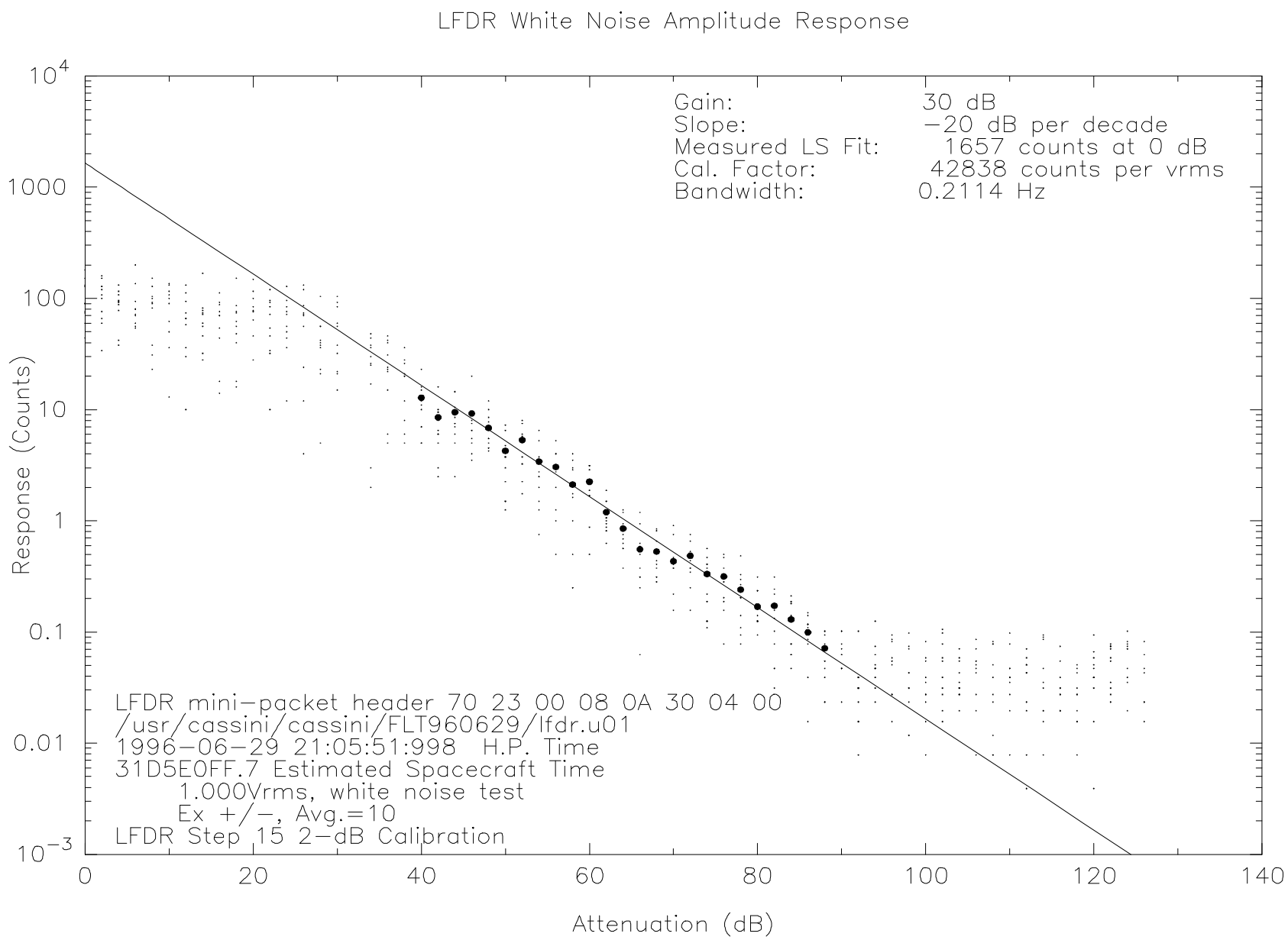

Figure 9.3.3.2.10: LFDR Step 15 Noise Bandwidth

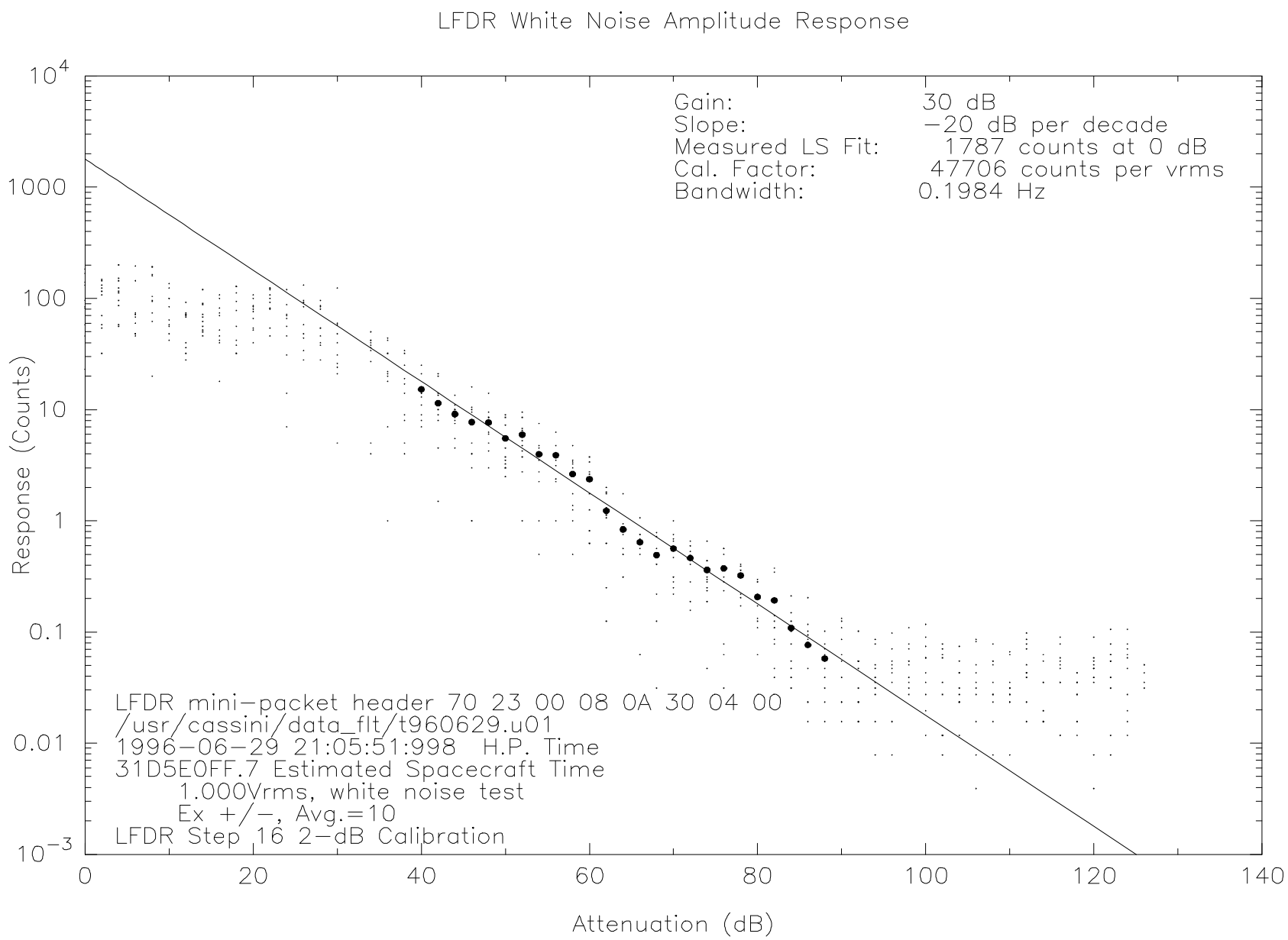

Figure 9.3.3.2.11: LFDR Step 16 Noise Bandwidth

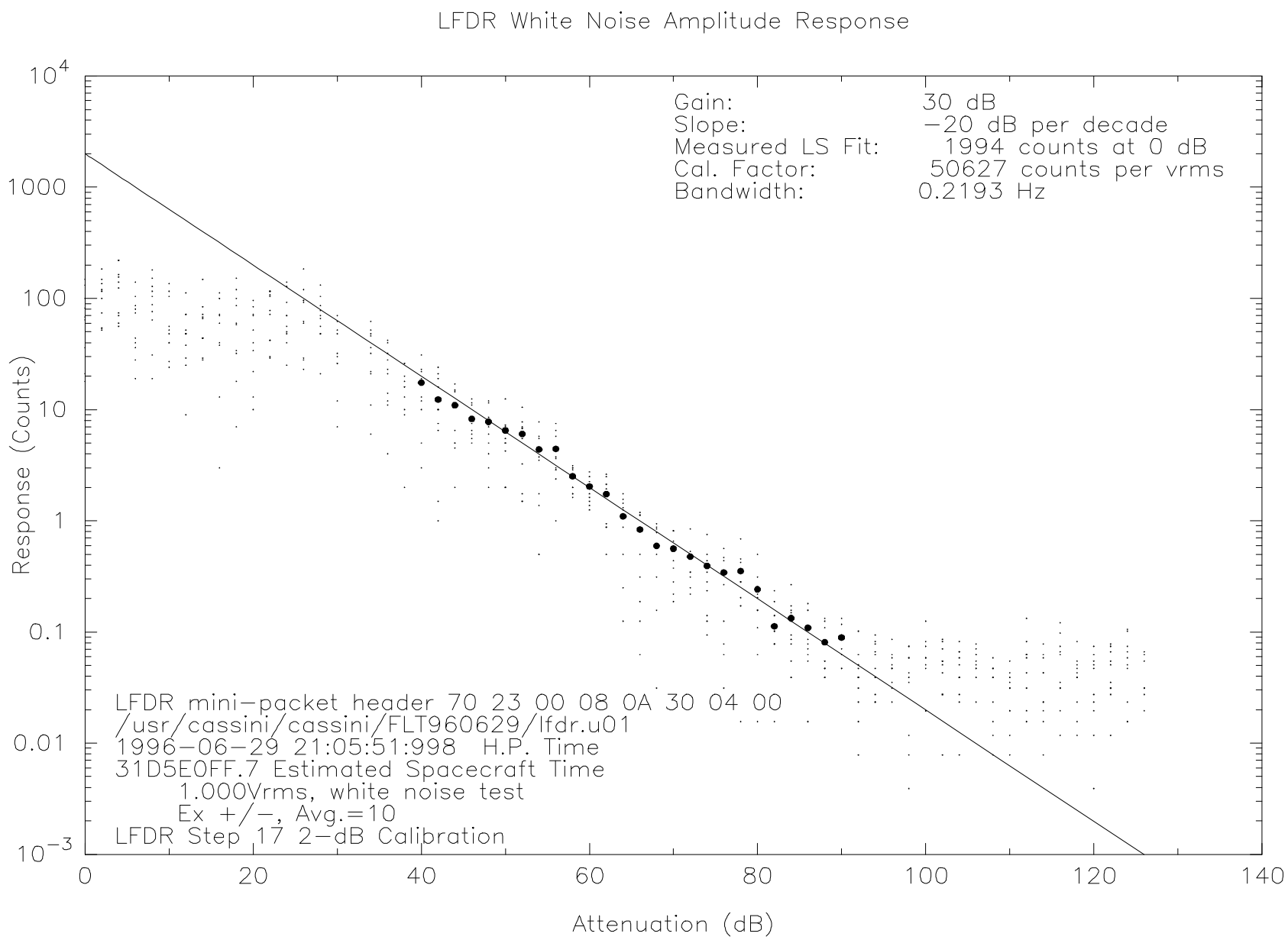

Figure 9.3.3.2.12: LFDR Step 17 Noise Bandwidth

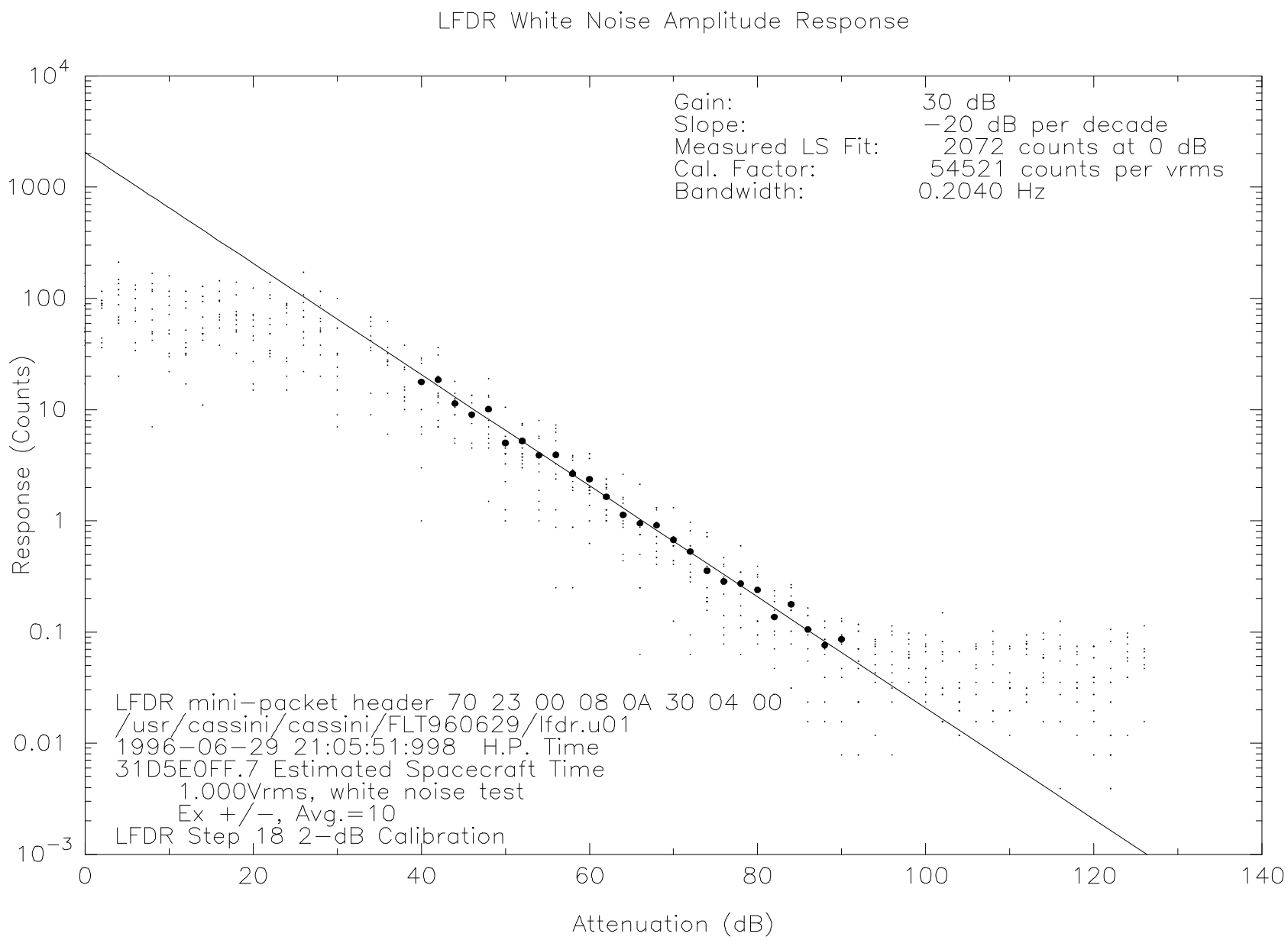

Figure 9.3.3.2.13: LFDR Step 18 Noise Bandwidth

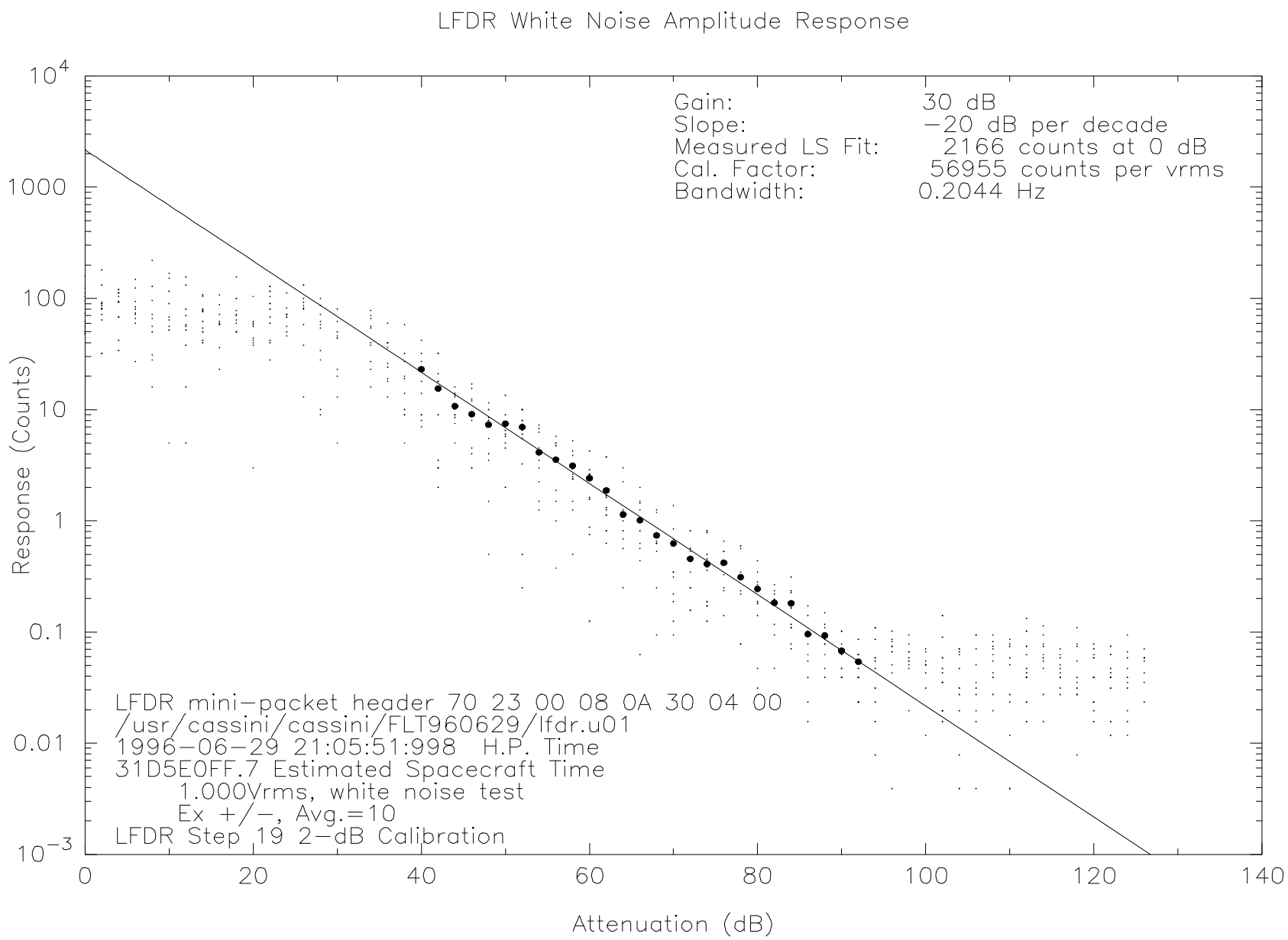

Figure 9.3.3.2.14: LFDR Step 19 Noise Bandwidth

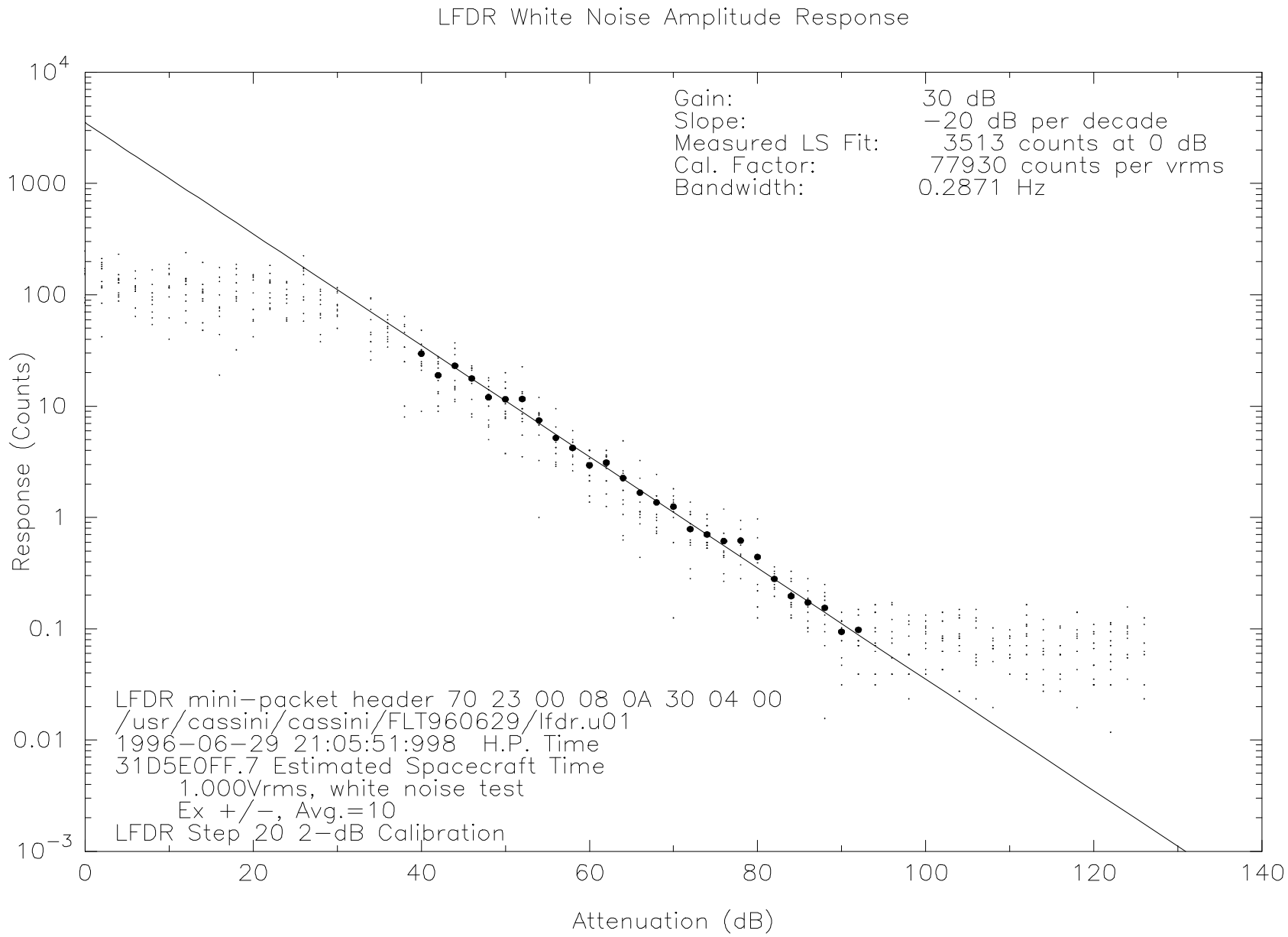

Figure 9.3.3.2.15: LFDR Step 20 Noise Bandwidth

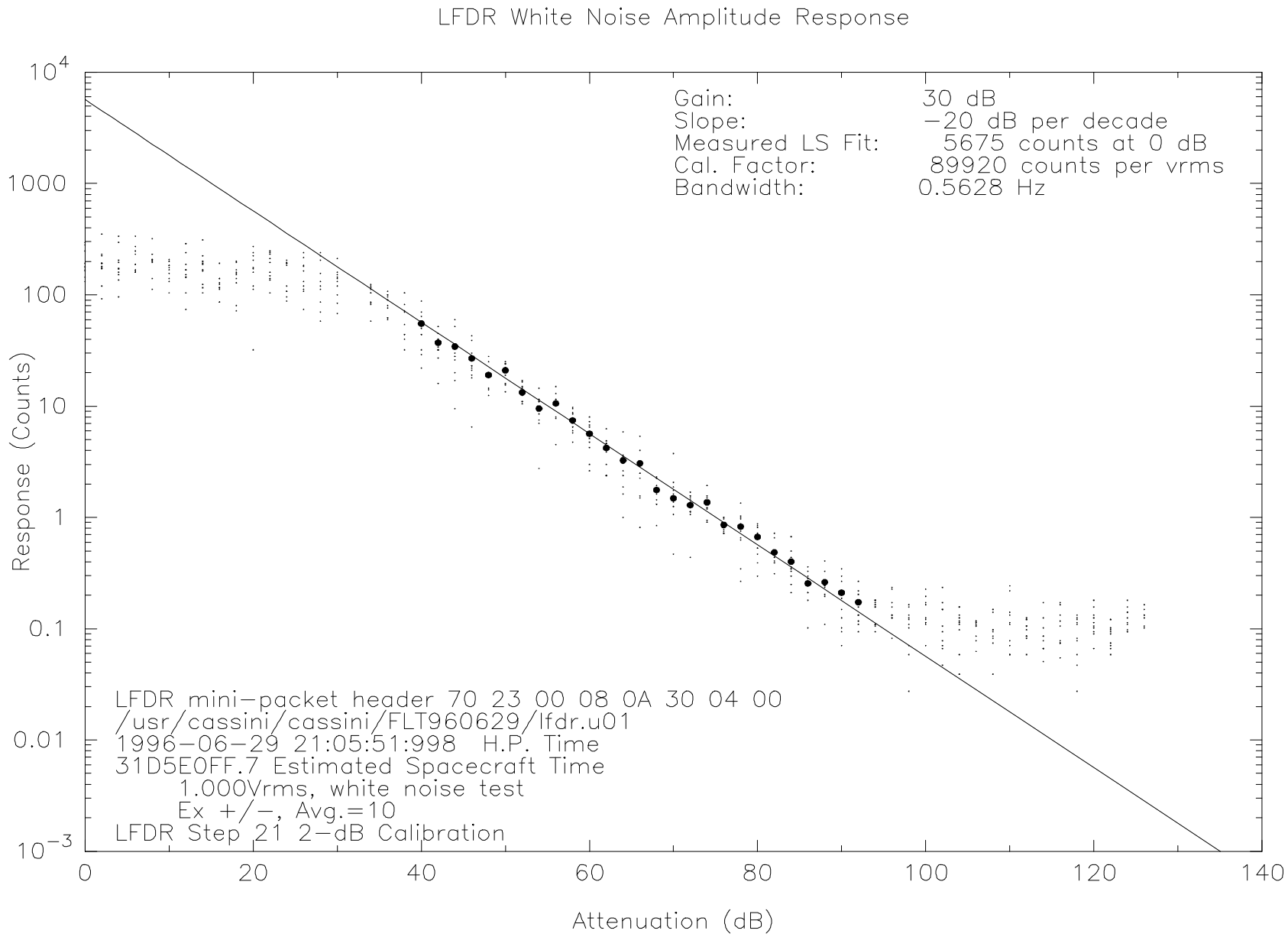

Figure 9.3.3.2.16: LFDR Step 21 Noise Bandwidth

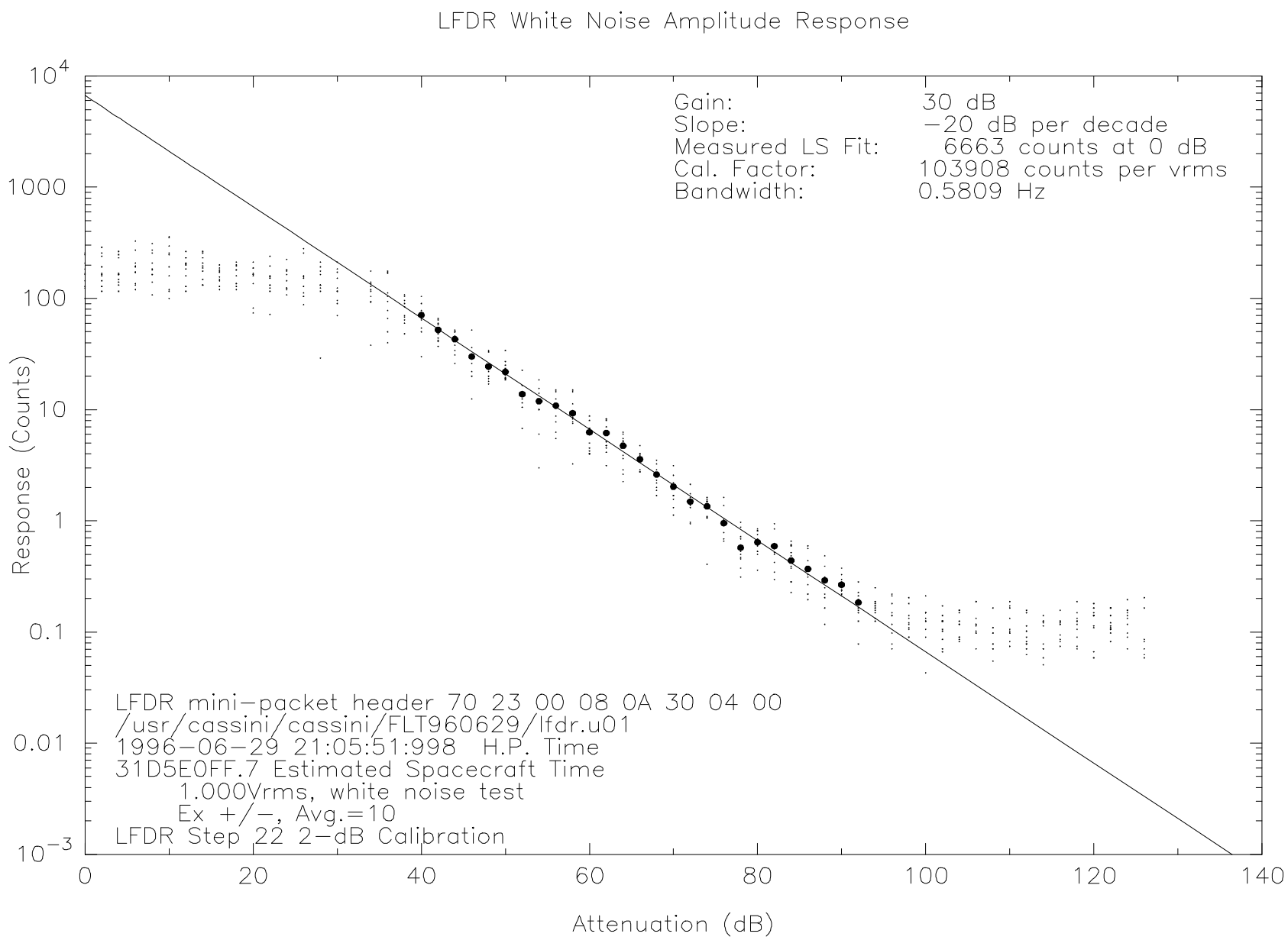

Figure 9.3.3.2.17: LFDR Step 22 Noise Bandwidth

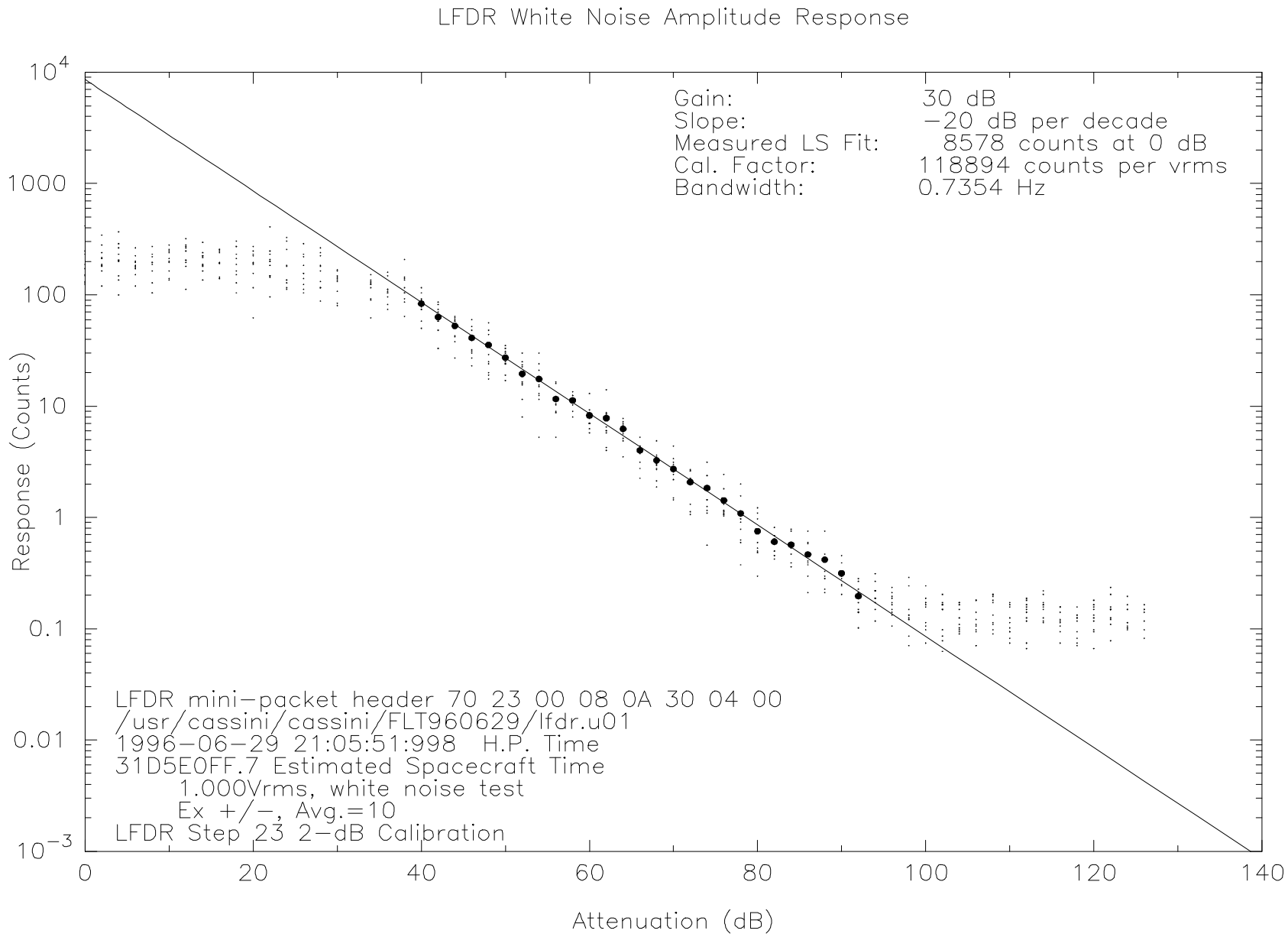

Figure 9.3.3.2.18: LFDR Step 23 Noise Bandwidth

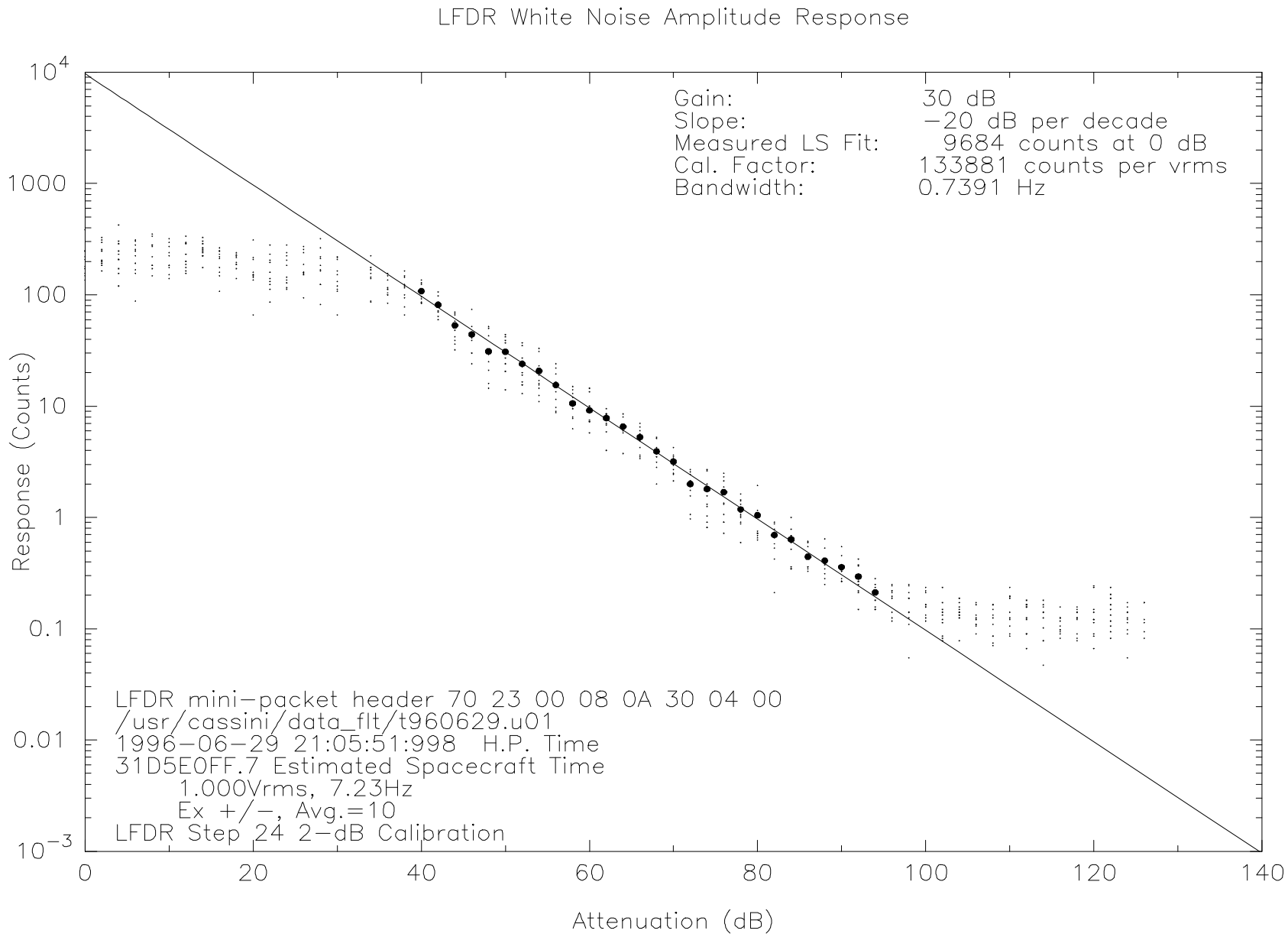

Figure 9.3.3.2.19: LFDR Step 24 Noise Bandwidth

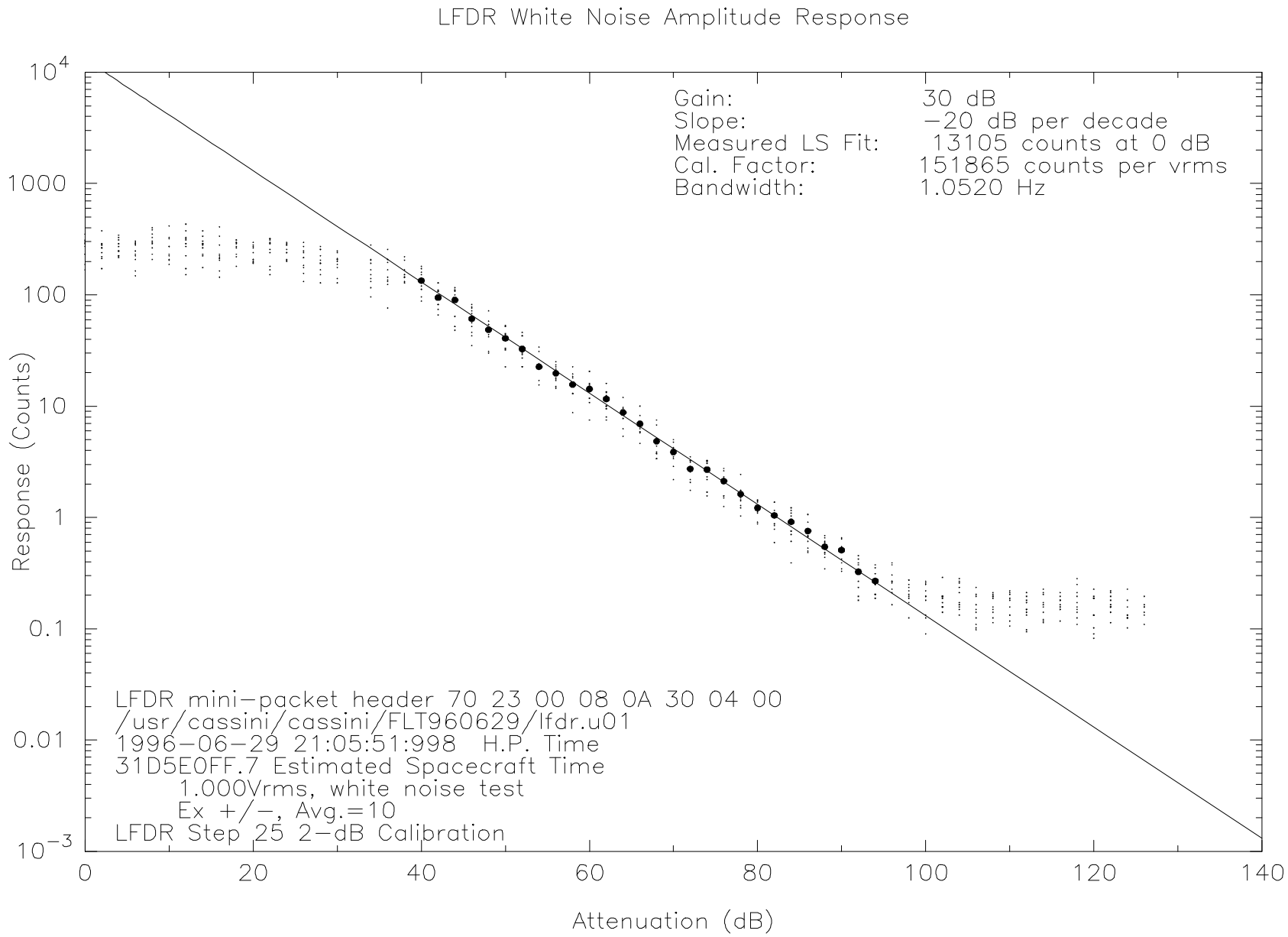

Figure 9.3.3.2.20: LFDR Step 25 Noise Bandwidth

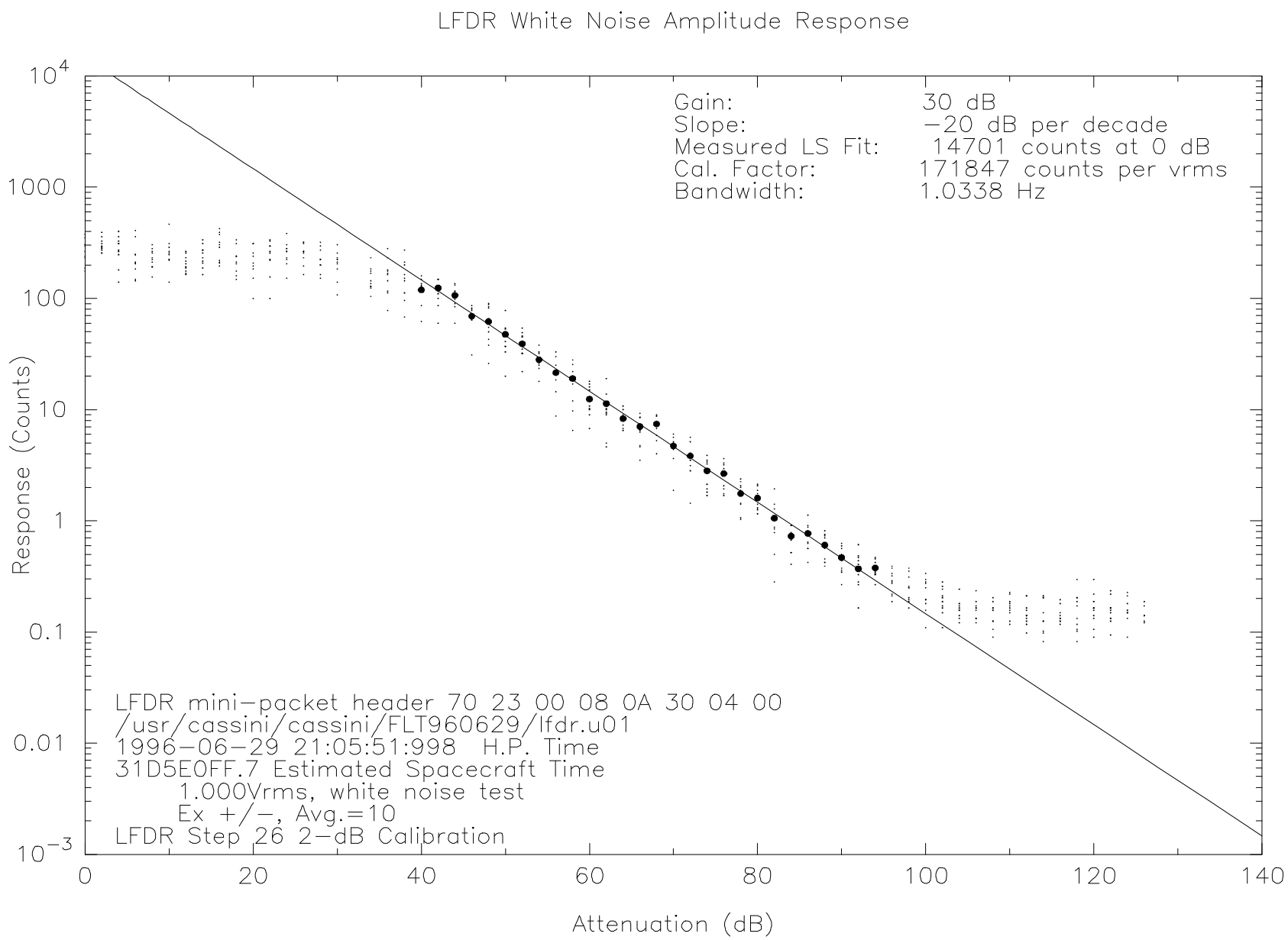

Figure 9.3.3.2.21: LFDR Step 26 Noise Bandwidth

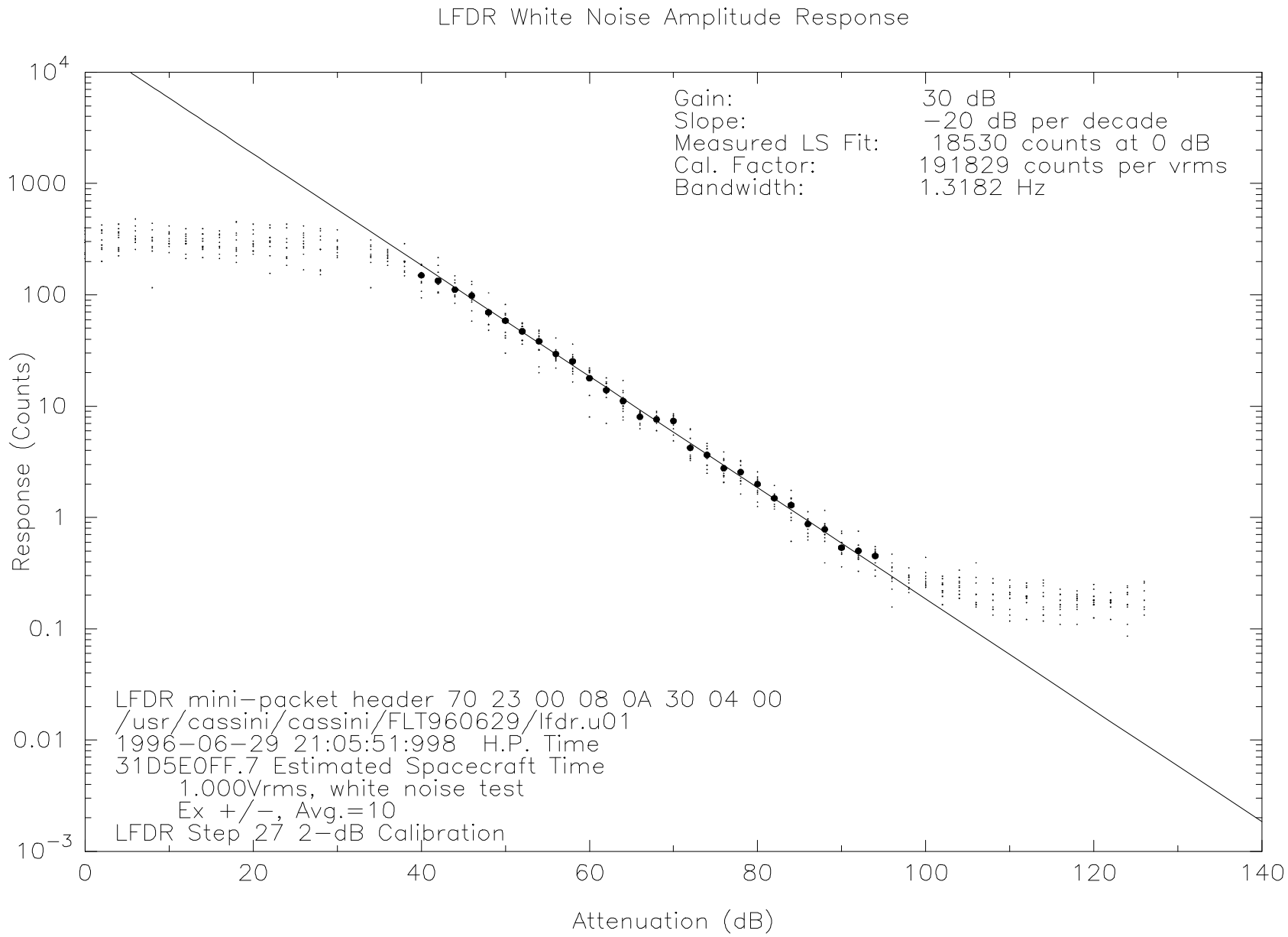

Figure 9.3.3.2.22: LFDR Step 27 Noise Bandwidth

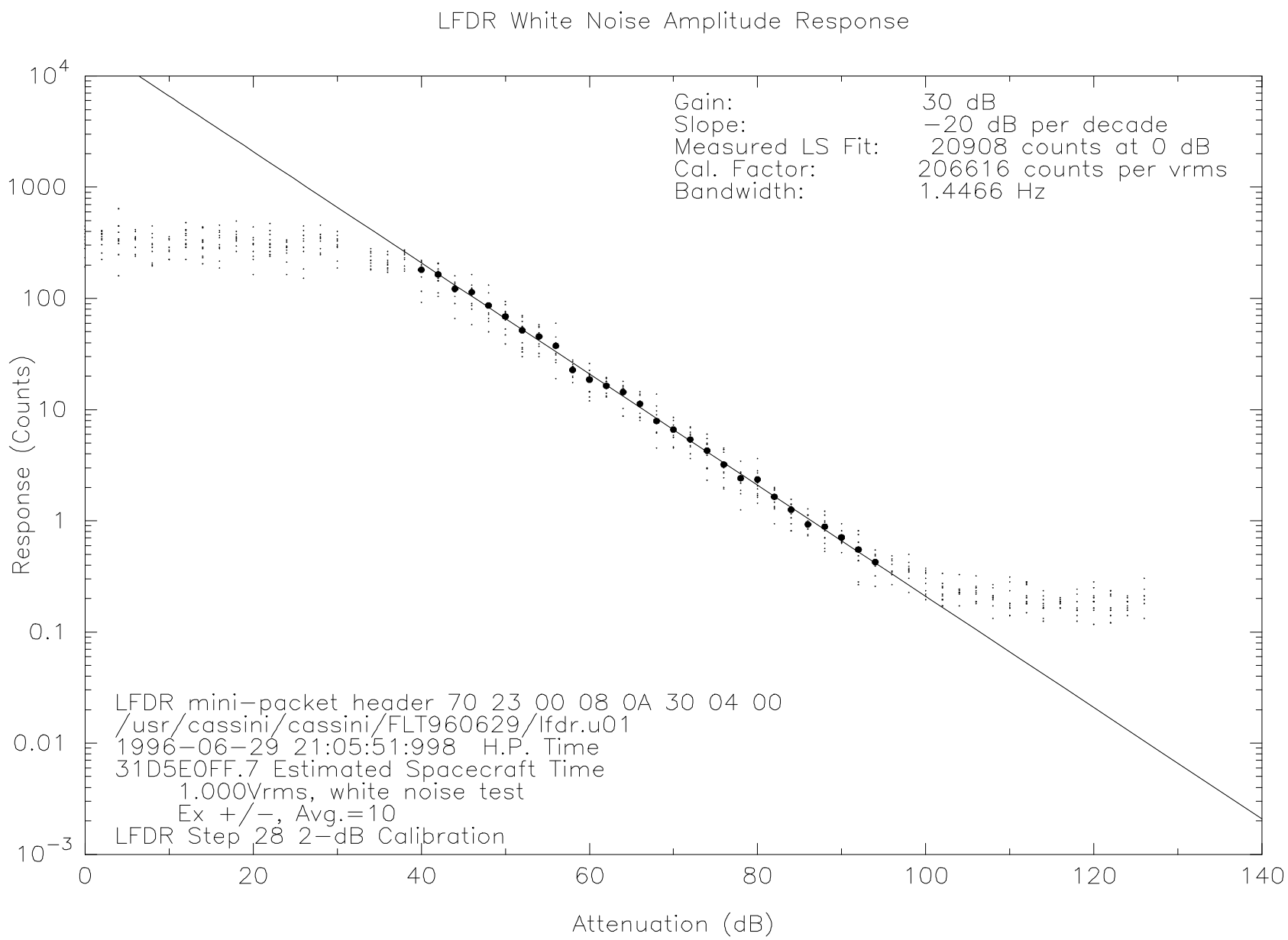

Figure 9.3.3.2.23: LFDR Step 28 Noise Bandwidth

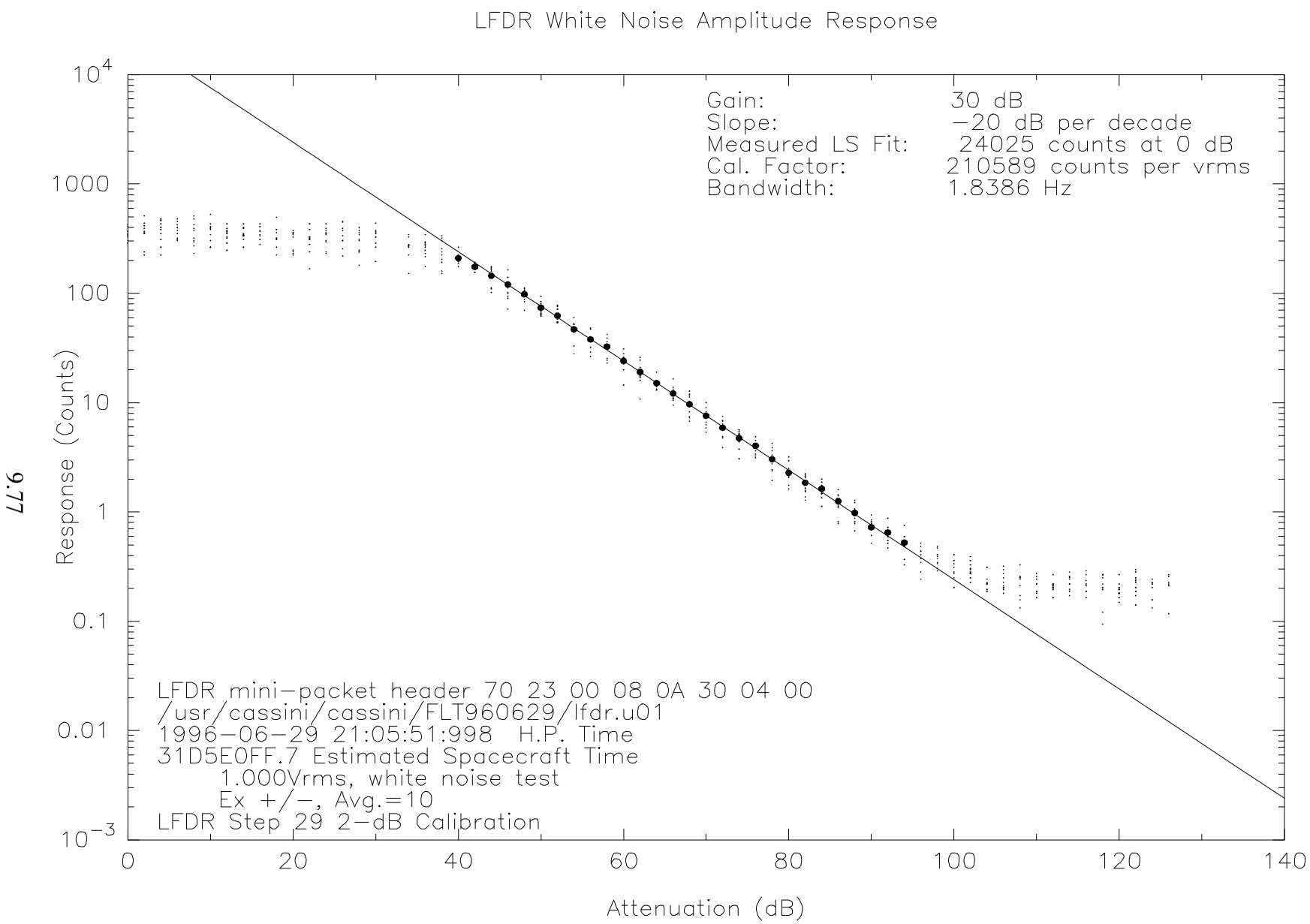

Figure 9.3.3.2.24: LFDR Step 29 Noise Bandwidth

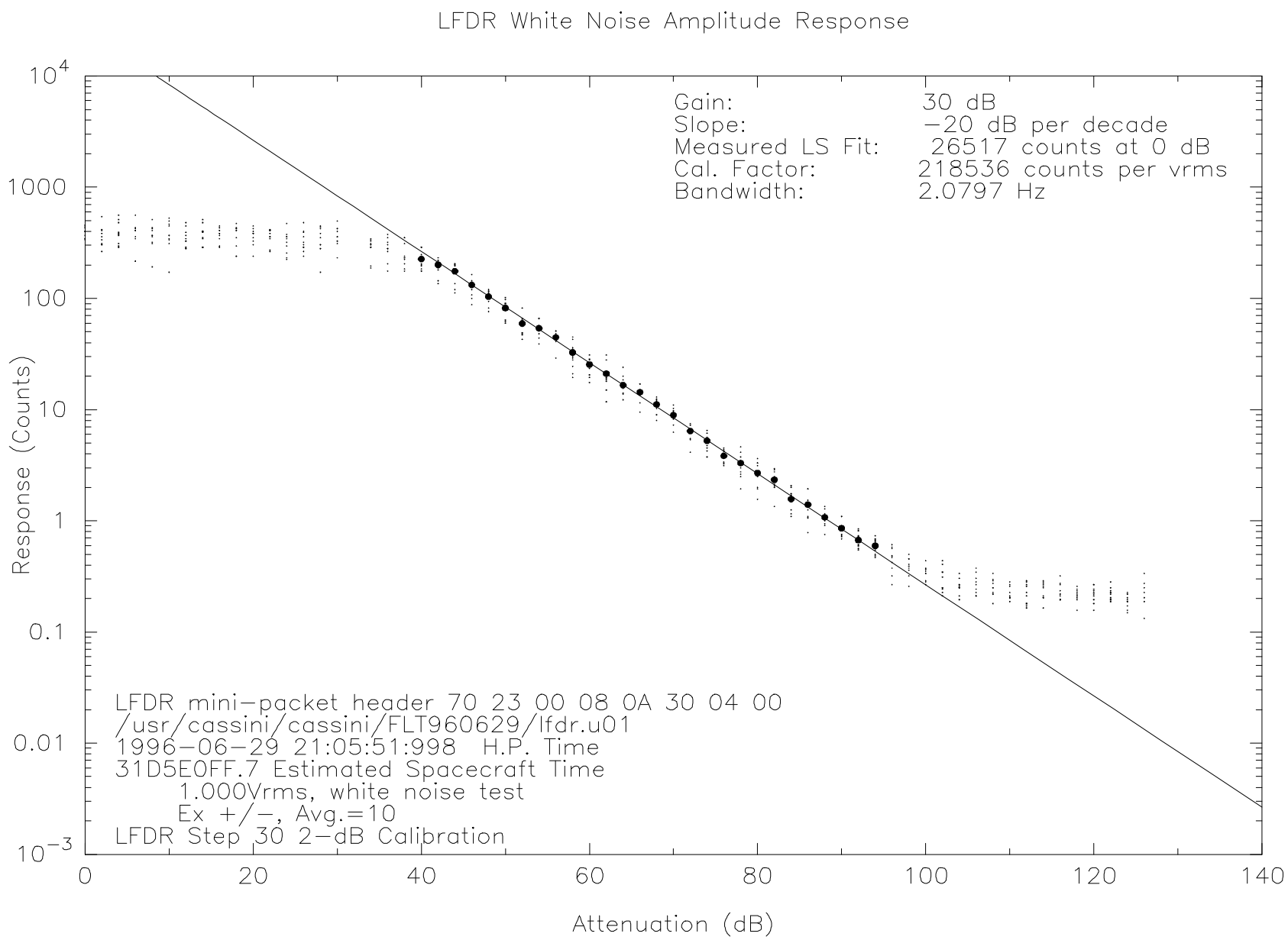

Figure 9.3.3.2.25: LFDR Step 30 Noise Bandwidth

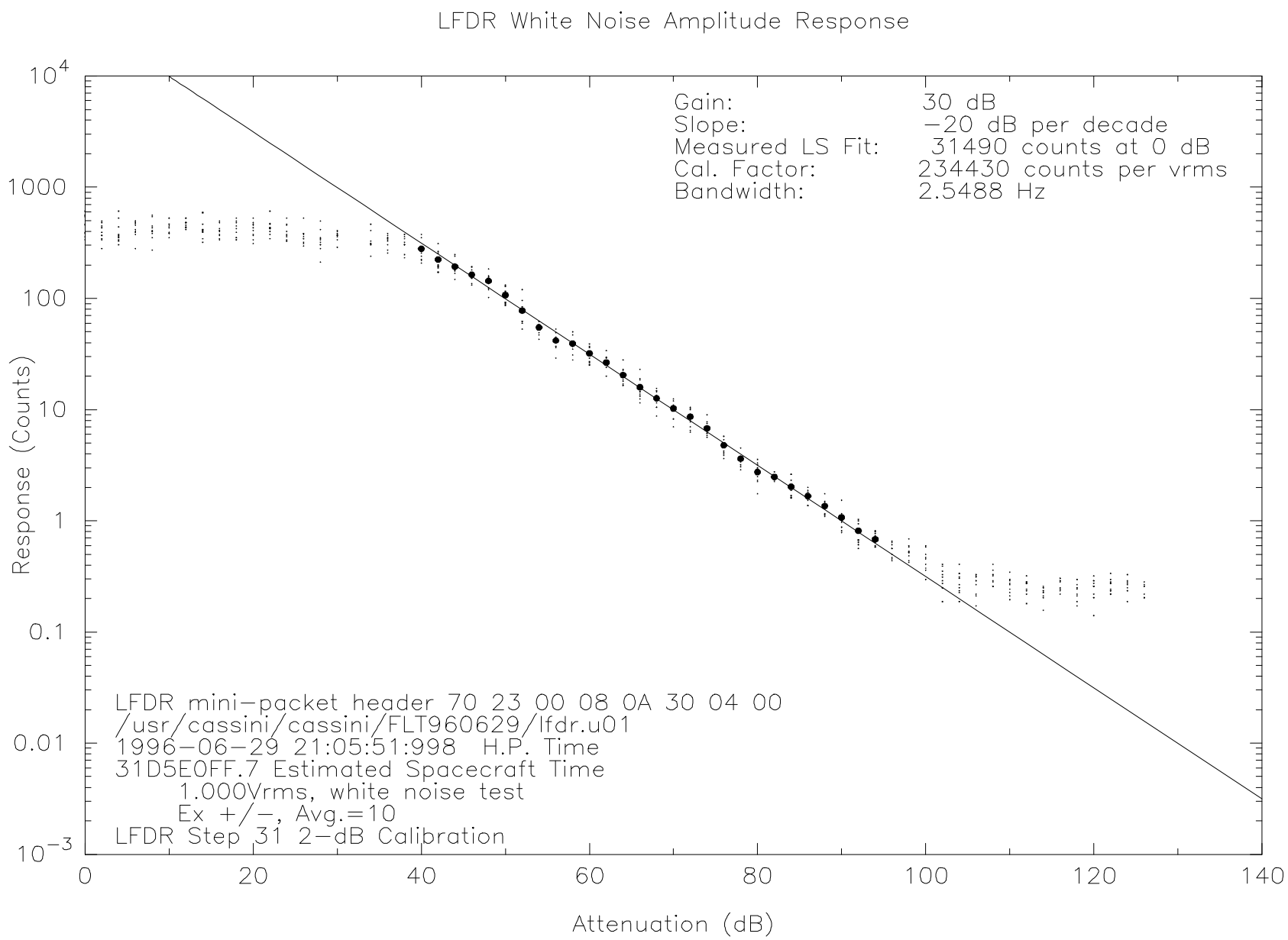

Figure 9.3.3.2.26: LFDR Step 31 Noise Bandwidth

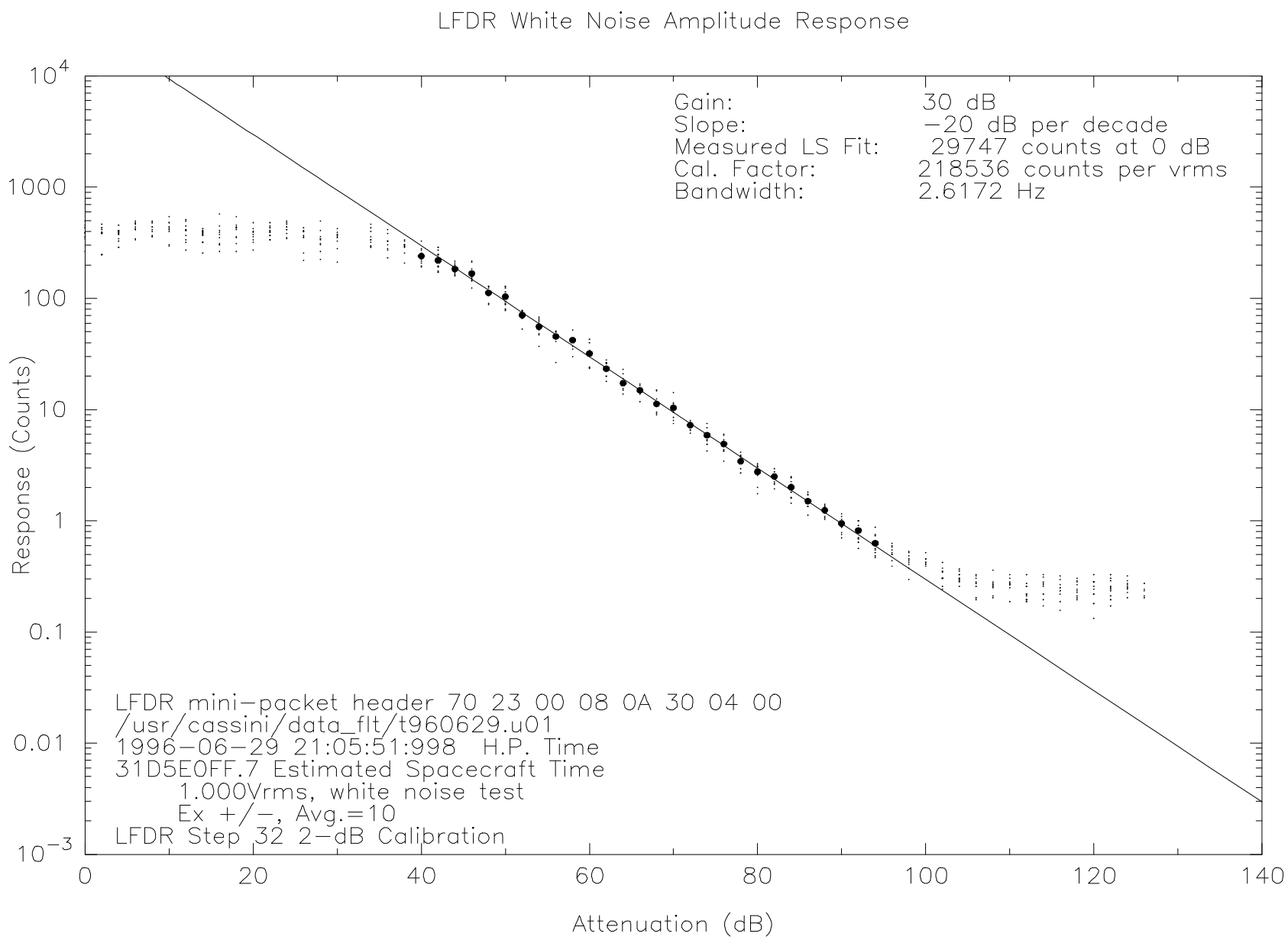

Figure 9.3.3.2.27: LFDR Step 32 Noise Bandwidth

9.3.4 LFDR In-Flight Noise Levels

For an estimate of the LFDR noise levels, data was taken both before and after the electric boom deployment on October 10,1997. Those results are presented in this section.

Figure 9.3.4.1 and Table 9.3.4.1 show the pre-deployment noise level for the Ex dipole (red line) and the post-deployment noise level (green line). The shot noise on the antenna is 10 to 20 dB above the receiver noise floor for all frequencies above 1 Hz. For the two LFDR channels below 0.5 Hz, the noise floor of the Ex dipole is not visible above the receiver noise floor, since the receiver noise floor is so high. The interference lines at 8 Hz and 24 Hz are no longer visible after deployment.

Figure 9.3.4.2 and Table 9.3.4.2 show the pre-deployment noise level for the Ez monopole (red line) and the post-deployment noise level (green line). The shot noise on the antenna is 10 to 20 dB above the receiver noise floor for all frequencies. For the two LFDR channels below 0.5 Hz, it is not understood why the receiver noise floor is lower than that of the Ex dipole; it is possible that antenna switching transients caused the elevated noise floors in the Ex dipole data. Again, the interference lines at 8 Hz and 24 Hz are no longer visible after deployment.

Figure 9.3.4.3 and Table 9.3.4.3 show the Bx search coil post-deployment noise level (green line). For the two LFDR channels below 0.5 Hz, the receiver noise floor obscures the Bx sensor noise floor. The interference lines at 8 Hz and 24 Hz are still visible after deployment.

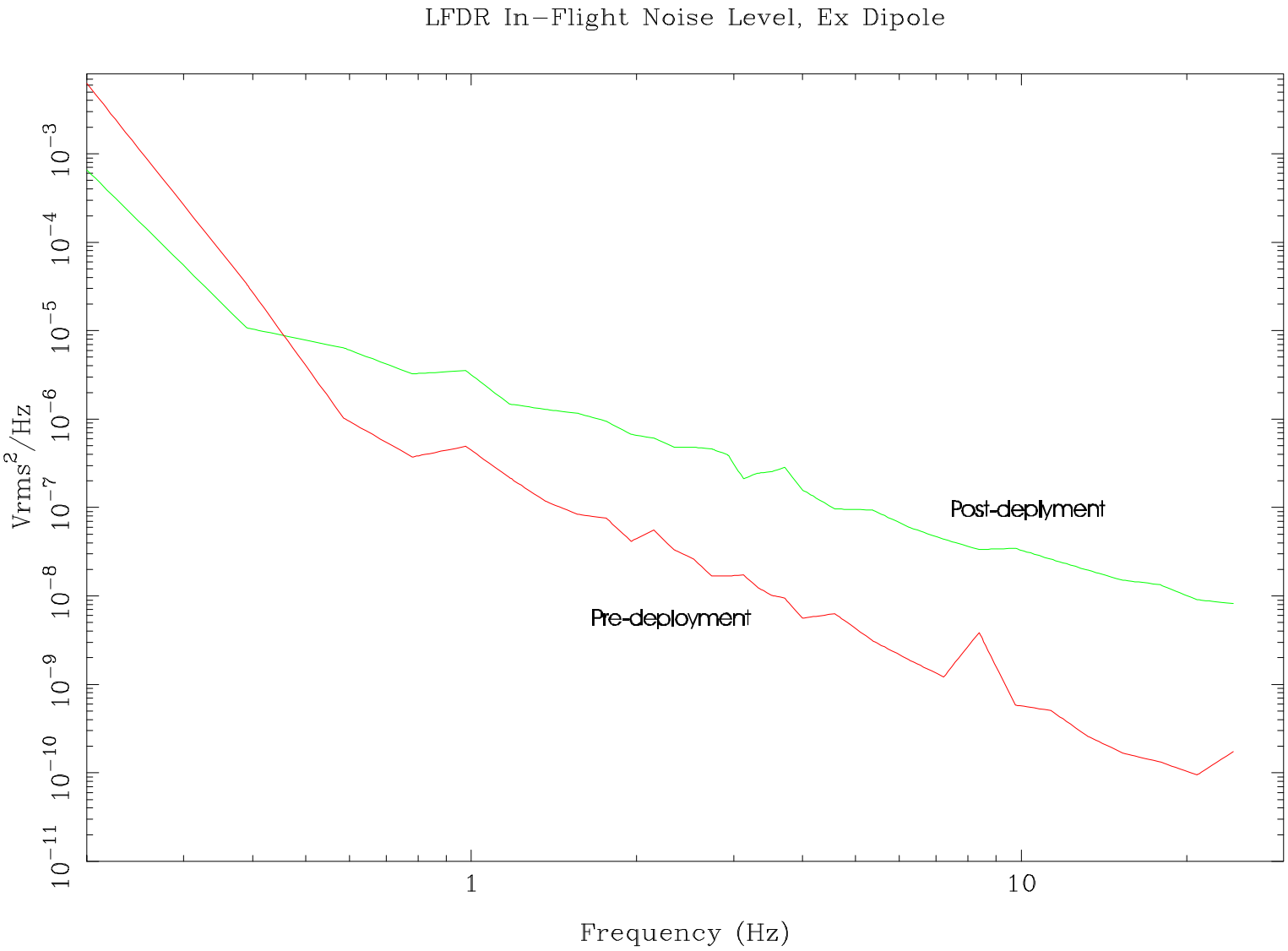

Figure 9.3.4.1: LFDR Ex Dipole Noise Levels

Table 9.3.4.1 LFDR In-Flight Noise Level, Ex Dipole

Frequency (Hz)	Pre-Deploy Noise Level V^2/Hz	Post-Deploy Noise Level V^2/Hz
0.195	7.637e-03	7.677e-04
0.391	3.382e-05	1.080e-05
0.586	1.033e-06	6.387e-06
0.781	3.733e-07	3.239e-06
0.977	4.920e-07	3.566e-06
1.172	2.166e-07	1.474e-06
1.367	1.178e-07	1.284e-06
1.562	8.324e-08	1.165e-06
1.758	7.642e-08	9.439e-07
1.953	4.136e-08	6.781e-07
2.148	5.611e-08	6.093e-07
2.344	3.326e-08	4.818e-07
2.539	2.607e-08	4.846e-07
2.734	1.671e-08	4.628e-07
2.930	1.692e-08	3.960e-07
3.125	1.721e-08	2.106e-07
3.320	1.250e-08	2.440e-07
3.516	1.012e-08	2.542e-07
3.711	9.497e-09	2.867e-07
4.004	5.619e-09	1.575e-07
4.590	6.259e-09	9.601e-08
5.371	3.135e-09	9.406e-08
6.250	1.891e-09	6.006e-08
7.227	1.217e-09	4.377e-08
8.398	3.840e-09	3.351e-08
9.766	5.837e-10	3.446e-08
11.328	5.051e-10	2.597e-08
13.184	2.604e-10	1.972e-08
15.332	1.661e-10	1.496e-08
17.871	1.334e-10	1.335e-08
20.898	9.459e-11	9.027e-09
24.316	1.730e-10	8.187e-09

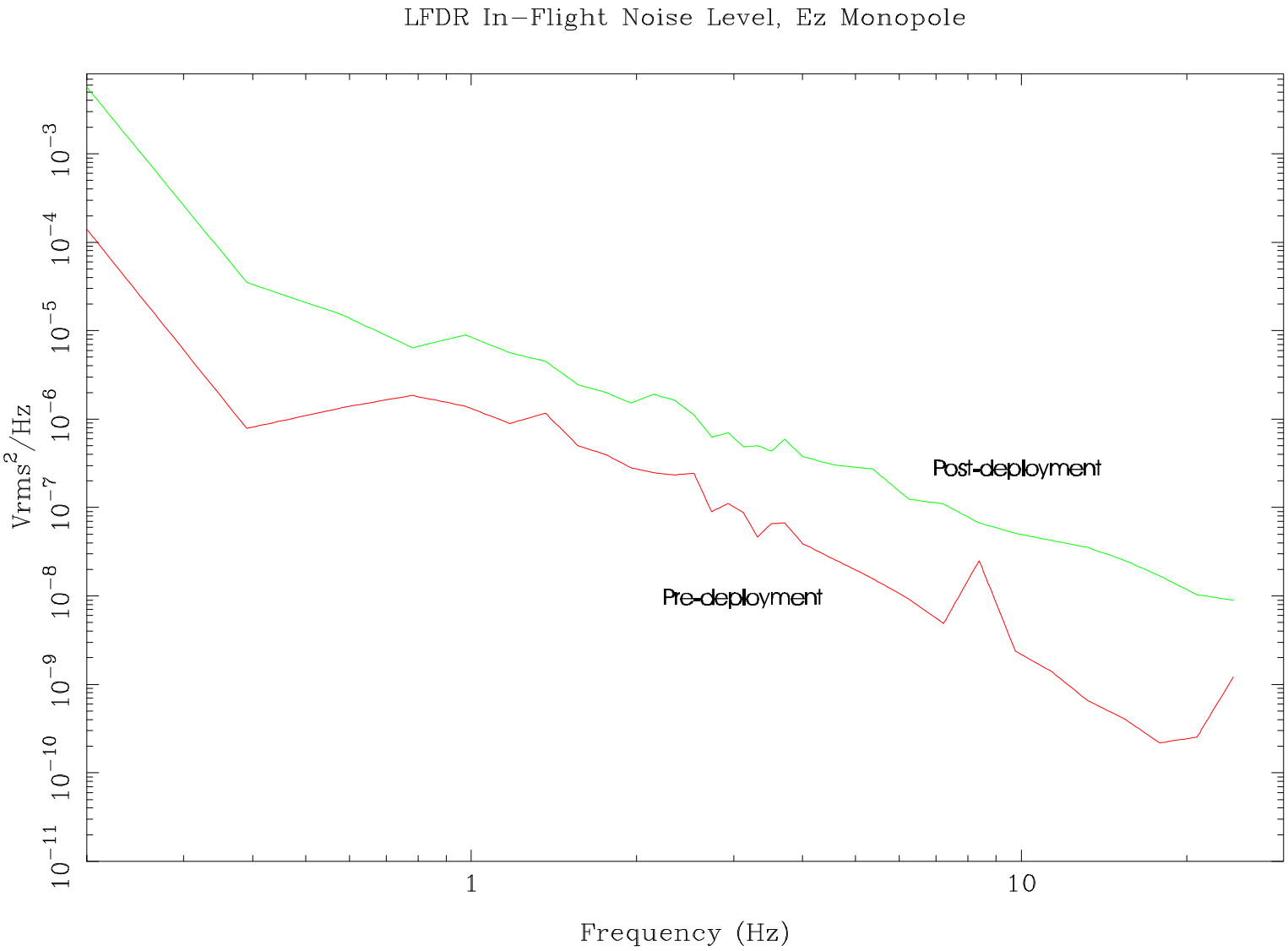

Figure 9.3.4.2: LFDR Ez Monopole Noise Levels

Table 9.3.4.2 LFDR In-Flight Noise Level, Ez Monopole

Frequency (Hz)	Pre-Deploy Noise Level V^2/Hz	Post-Deploy Noise Level V^2/Hz
0.195	1.704e-04	6.865e-03
0.391	7.871e-07	3.498e-05
0.586	1.363e-06	1.490e-05
0.781	1.852e-06	6.416e-06
0.977	1.409e-06	9.013e-06
1.172	8.874e-07	5.647e-06
1.367	1.167e-06	4.537e-06
1.562	5.052e-07	2.444e-06
1.758	3.958e-07	1.980e-06
1.953	2.831e-07	1.516e-06
2.148	2.490e-07	1.915e-06
2.344	2.326e-07	1.626e-06
2.539	2.454e-07	1.124e-06
2.734	8.943e-08	6.311e-07
2.930	1.105e-07	7.011e-07
3.125	8.746e-08	4.906e-07
3.320	4.618e-08	4.988e-07
3.516	6.550e-08	4.349e-07
3.711	6.727e-08	5.940e-07
4.004	3.904e-08	3.785e-07
4.590	2.574e-08	3.014e-07
5.371	1.568e-08	2.728e-07
6.250	9.234e-09	1.237e-07
7.227	4.867e-09	1.093e-07
8.398	2.498e-08	6.715e-08
9.766	2.374e-09	5.138e-08
11.328	1.407e-09	4.245e-08
13.184	6.571e-10	3.553e-08
15.332	4.154e-10	2.567e-08
17.871	2.168e-10	1.691e-08
20.898	2.527e-10	1.022e-08
24.316	1.216e-09	8.941e-09

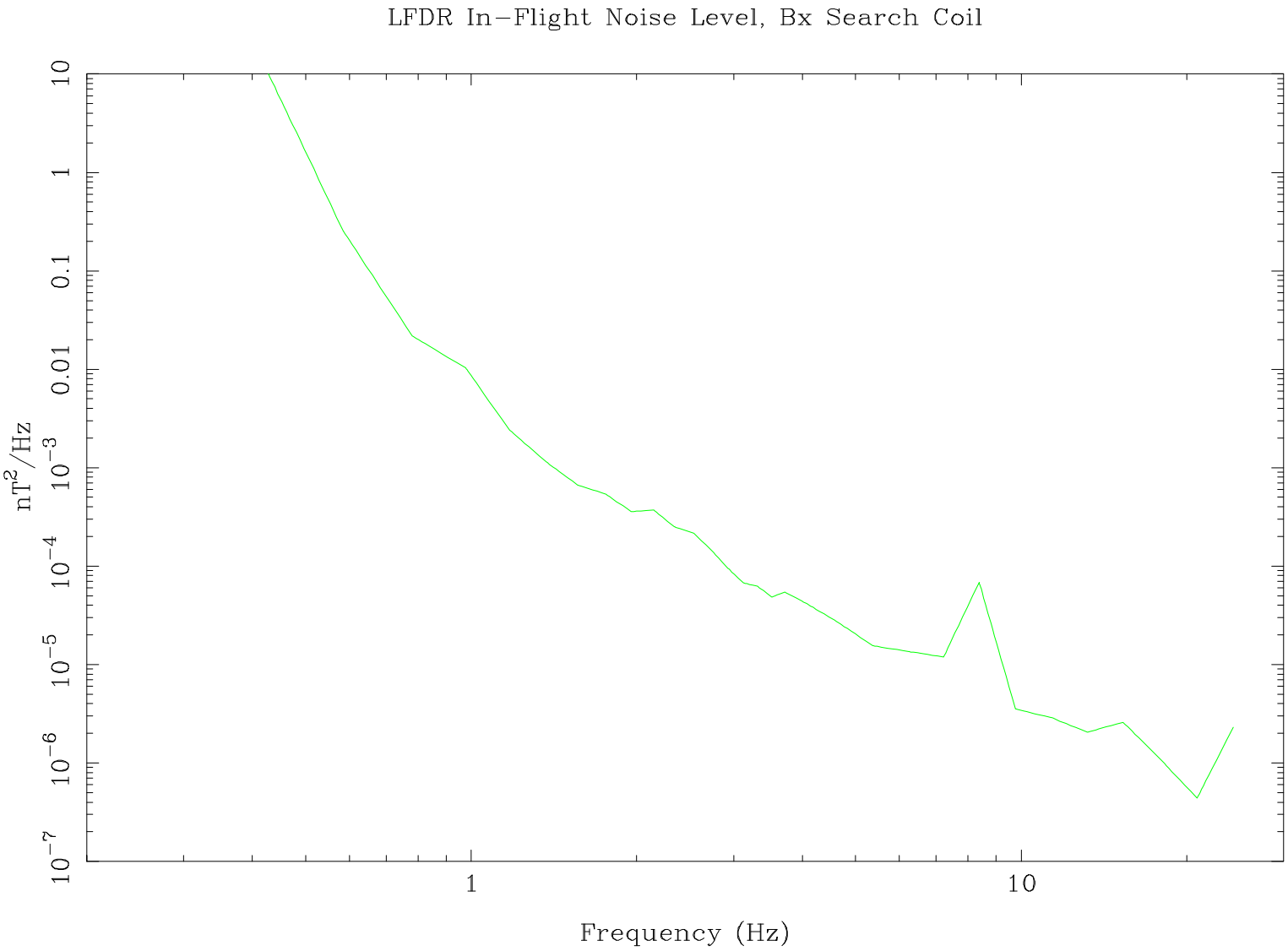

Figure 9.3.4.3: LFDR Bx Search Coil Noise Levels

Table 9.3.4.3 LFDR In-Flight Noise Level, Bx Search Coil

Frequency (Hz)	In-Flight Noise Level nT^2/Hz
0.195	7.555e+05
0.391	2.832e+01
0.586	2.495e-01
0.781	2.170e-02
0.977	1.033e-02
1.172	2.433e-03
1.367	1.159e-03
1.562	6.638e-04
1.758	5.354e-04
1.953	3.590e-04
2.148	3.704e-04
2.344	2.524e-04
2.539	2.153e-04
2.734	1.433e-04
2.930	9.530e-05
3.125	6.727e-05
3.320	6.283e-05
3.516	4.823e-05
3.711	5.396e-05
4.004	4.351e-05
4.590	2.815e-05
5.371	1.557e-05
6.250	1.347e-05
7.227	1.195e-05
8.398	6.853e-05
9.766	3.533e-06
11.328	2.908e-06
13.184	2.059e-06
15.332	2.597e-06
17.871	1.108e-06
20.898	4.400e-07
24.316	2.305e-06

10.0 Medium Frequency Receiver (MFR)

10.1 MFR Subsystem Description

This section of the RPWS Calibration Document augments the hardware overview given in Section 3 by providing a more detailed description of the Medium Frequency Receiver (MFR), a system based on designs flown on the ISEE, DE-1, Galileo, and CRRES spacecraft. The MFR processes signals from the Bx, Bz, Ex dipole, Ex+ monopole, Ex- monopole, or Ez monopole antennas, and provides electric field and magnetic field amplitude measurements over the frequency range 24 Hz to 12.6 kHz. The receiver design offers moderately good frequency and amplitude resolution, a balance in technical performance consistent with overall RPWS measurement objectives.

10.1.1 General MFR Characteristics

The MFR system sweeps over the frequency range 24 Hz to 12.6 kHz, and consists of three frequency bands each 1 octave wide. Designated 1, 2, and 3, each frequency band is divided into narrow frequency steps which are synthesized using a two-stage frequency conversion scheme. A block diagram of the MFR system is shown in Figure 10.1.1.1.

Each band uses a front end (IF) mixer to up mix the desired frequency of interest to a set frequency IF bandpass filter. A second fixed frequency (baseband) mixer down-converts the IF bandpass filter output to baseband frequencies. This baseband signal is logarithmically compressed, rectified and summed to a 0-5 volt DC output.

The primary mode of operation for the MFR is the Logarithmic Sweep mode. The Logarithmic Sweep mode provides 80 frequency steps (16 in Band 1, 32 each in Bands 2 and 3) with approximated logarithmic spacing over the frequency range of the receiver..

All 3 bands are driven from a front end buffer whose input is selectable between the Ex dipole, Ez, Bx, and Bz antennas. The LRP provides all control (antenna select, mixer reference) signals as well as processing the MFR bands 0-5.12 volts DC output signals. Regulated power for the MFR is provided by the RPWS power supply through the WFR.

Figure 10.1.1.1 RPWS MEDIUM FREQUENCY RECEIVER (MFR)

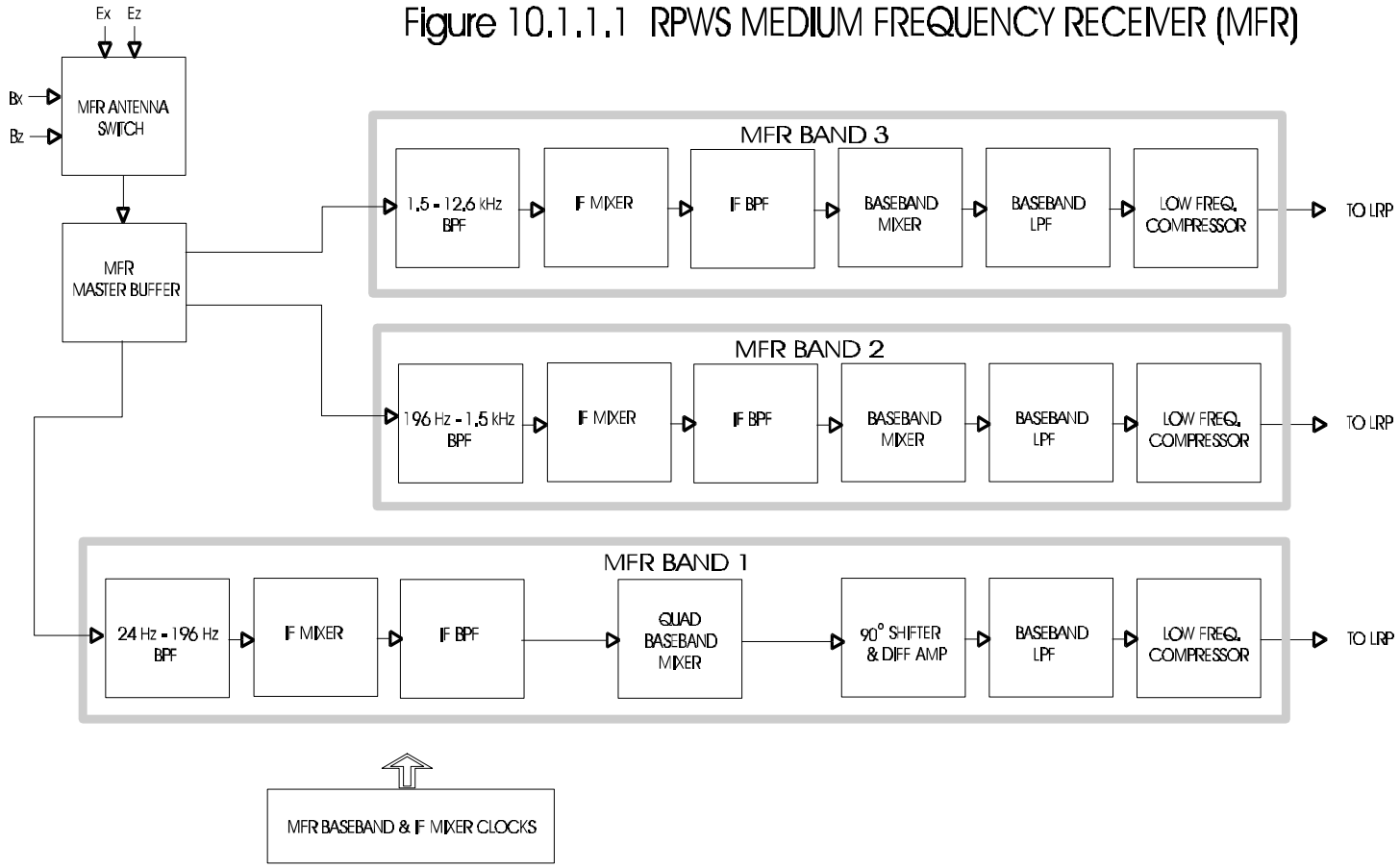

10.1.2 Frequency Bands

The upper frequency limits of the three MFR frequency bands are determined by active filters which receive signals from the sensors and associated differential amplifiers through a filter driver amplifier. Lower frequency limits are imposed by the lower limit of the front end (IF) mixer chopping frequencies. The input filter cutoffs are scaled by a factor of eight relative to each other, which provides a frequency response of three octaves for the entire MFR. The bandpass filters provide rejection of out-of-band signals, which is required by the subsequent front end (IF) mixer stage. The passbands of the input filters are as follows:

Band #	Bandwidth
1	24 Hz - 200 Hz
2	200 Hz - 1600 Hz
3	1.6 kHz - 12.6 kHz

10.1.3 Frequency Selection

The MFR uses a frequency conversion scheme to synthesize a very narrow detection passband. This narrow band is then stepped by varying the front end (IF) mixer clock signals to shift up the desired signal band into the IF filter passband. Mixed to ~2.5 times the given band's frequency limit, the signal band is passed through the IF bandpass filter which excludes extraneous components from the subsequent constant-frequency mixing stage.

Band 1, using single sideband topology, employs two separate baseband mixers which combine the IF output signal with conversion frequencies f and f shifted by 90 degrees. This conversion produces a pair of baseband signals with upper and lower sidebands superposed, but with a phase difference of 180 degrees. A quadrature phase shift network then shifts the converted signals by an additional 90 degrees so that when the signals are summed, the upper sideband components add and the lower sideband components cancel. Because of the low frequency range of Band 1, a design using the double sideband detection method would result in an extremely low detection frequency. By using the single sideband detection approach, the detected bandwidth is at a higher frequency allowing faster stepping rates. Unlike Band 1, Bands 2 and 3 do use the double sideband method (due to board space limitations and wider allowable bandwidth).

For all three MFR bands, the baseband signals are then bandpass-filtered and processed by a logarithmic compressor stage that provides a DC analog value proportional to the logarithm of the input signal. The dynamic range of each compressor is in the order of 100 dB with 1 Vrms applied ≈5.12 V DC out. These DC output values are sampled by the LRP.

For each band, the mixing frequencies needed to generate the discrete frequency steps are provided by the frequency control logic (FCL). The MFR uses separate frequency generators for

each band, allowing different stepping rates for the three bands. Because the lower frequency bands require longer time periods to stabilize at a given step before a measurement can be made, different stepping rates are needed in order to maximize the time resolution of measurements provided in each frequency band. Step selection and timing are managed by the LRP via reference clocks to the FCL. Although the MFR has the capability of being locked to a particular frequency step in any of the three bands, the normal manner of operation will be to step at regular intervals over the three frequency ranges as indicated below.

Mode	Band	Freq. Range	# Steps	Step Dwell	Sweep Time
Log	1	24 - 200 Hz	16	1 sec	16 sec
	2	200 - 1600 Hz	32	0.5 sec	16 sec
	3	1.6 - 12.5 kHz	32	0.25 sec	8 sec

The individual front end mixing frequencies for each band are selected to provide a logarithmic distribution of center frequencies. The center frequencies for the Logarithmic Sweep mode is shown in Table 10.1.3.1. Additional aspects of the MFR subsystem are discussed in detail in the following sections.

10.1.4 Mixing Signals

The MFR frequency bands are synthesized by a double conversion scheme as described earlier, with variable front-end IF mixers providing the narrow band sweep capabilities of the receiver system, and back-end mixers providing the frequency conversion to baseband. All three bands receive mixer control clocks from the LRP. These signals are level shifted, divided down and phase shifted by the MFR frequency control logic so as to provide proper control signals to the front and rear mixers.

For bands 1 and 2, front-end IF mixing signals are derived directly from a programmable digital divide-by located on the LRP board. The LRP clock signals are level and phase shifted by the MFR FCL. These signals up convert the desired narrow band of interest to a fixed IF bandpass frequency. Band 3 uses the LRP clock signal as a reference clock. This reference is multiplied up to the required Band 3 mixer (IF) frequency using a current controlled oscillator within a phase locked loop (PLL). This is required since direct digital divide by would not provide the frequency resolution required of the receivers step frequency function. The PLL oscillator signal is then level and phase shifted to provide the signal needed by the front end mixer.

All three bands' back-end (baseband) mixers use a fixed frequency set at or near the IF bandpass center frequency. The reference signal is provided by the LRP and is digitally divided and shifted to the appropriate levels on the MFR board.

Table 10.1.3.1
MFR Logarithmic Center Frequencies (Hz)

Step	Band 1	Band 2	Band 3
1	23.8910	192.1108	1536.8867
2	26.2510	214.6289	1671.8125
3	29.1468	225.9814	1785.1016
4	32.4228	237.3965	1899.1719
5	36.2695	260.4165	2083.3320
6	40.8909	272.0229	2269.5547
7	46.5109	295.4307	2316.4336
8	52.8165	307.2329	2481.5547
9	60.4319	331.0381	2648.3047
10	69.4643	355.1138	2816.7148
11	80.0469	379.4644	3011.2422
12	92.3442	404.0947	3208.0039
13	107.2421	429.0103	3432.0820
14	124.3865	454.2153	3659.0898
15	144.8837	492.5771	3992.2891
16	169.0493	518.5288	4279.2383
17		558.0356	4651.2734
18		598.2544	4813.1094
19		639.2046	5086.1094
20		680.9058	5419.2148
21		723.3794	5758.4805
22		766.6470	6162.3164
23		825.6113	6575.0586
24		870.8198	7027.5117
25		932.4595	7490.9219
26		995.7109	7997.7500
27		1060.6372	8518.0195
28		1144.2549	9120.0586
29		1213.2041	9705.6328
30		1302.0835	10165.0117
31		1375.4399	11078.0430
32		1470.0942	11799.3281

10.1.5 Control Functions

Control functions are provided by the LRP board. The LRP provides the MFR with all variable front end mixing signals, fixed back end mixing signals, antenna selects, and accepts the MFR DC outputs. The LRP controls step and timing selection for each individual band. The variable conversion frequencies are generated when the LRP loads the appropriate control codes into a counter timer interrupt chip (an 82C54 located on the LRP). These outputs are used as the reference frequencies of the MFR FCL. Band 3 uses one of the timer outputs as a phase-locked loop (PLL) reference and multiplies up this reference for use as the front end mixer clock. Bands 1 and 2 use the remaining two outputs for inputs to their level and phase shifters that subsequently provide the mixing signals for each of their respective front end (IF) mixers. The LRP supplies a 125 kHz digital level signal for the MFR logic to generate the fixed back end (baseband) mixer signals. The LRP provides a two-bit antenna select signal and MFR data (0 to 5 volts) is accepted into the LRP by an A\D converter channel.

10.1.6 Antenna Selection

The MFR system is designed to process signals from either the Ex dipole, Ez monopole, Bx searchcoil, or the Bz searchcoil antenna providing information regarding wave amplitude. The sensors to be used are connected to the MFR inputs via analog switches which are controlled by the LRP in response to spacecraft commands. The following antennas may be selectively switched to the MFR receiver inputs:

LRP Command		
MFRANT1	MFRANT0	Selected Antenna
0	0	Ex (dipole) *
0	1	Ez (monopole)
1	0	Bx (search coil)
1	1	Bz (search coil)

* It should be noted that the HFR can supply either the dipole Ex (default), or a monopole (Ex+ or Ex-) antenna to the MFR.

10.1.7 Power

The instrument power supply provides the MFR with five regulated supply voltages. The supply voltages and expected average current loads are as follows:

+12 V	13.85 mA
+6 V	25.9 mA
+5 V	8.68 mA
-6 V	23.0 mA
-12 V	9.9 mA

The total power requirement for the MFR is approximately 628 mW.

10.1.8 Data Products

The MFR provides one DC voltage output per frequency band for a total of 3 analog values. The analog parameters are scaled from 0 to 5.12 V, which corresponds to a ~100 dB dynamic range for measured signal amplitude. The lines carrying these voltages are sampled by the LRP at a rate determined by LRP software.

10.2.1 Conversion of Data Numbers to Science Units

This section describes the procedure for obtaining a calibrated data value from a MFR raw measurement.

1) First the voltage lookup tables in Section 10.3.1 should be used to convert the data number DN to a voltage represented by the symbol Vtable. Select the appropriate table corresponding to the band and step of interest. These tables are the conversions between the DN out of the instrument and the voltage difference between the Ex+ and Ex- antennas.

2) Once the voltage Vtable is found, the sensor-dependent conversion factor must be used to adjust the voltage. The voltage difference between the Ex+ antenna and the Ex- antenna is given the symbol VDEx. Since the tables in Section 10.3.1 are for the voltage difference between Ex+ and Ex- no conversion is necessary for VDEx. VDEx is equal to Vtable. The voltage between the Ex+ antenna and spacecraft ground is given the symbol VEx+. The voltage between the Ex- antenna and spacecraft ground is given the symbol VEx-. The voltage between the Ez antenna and spacecraft ground is given the symbol VEz. The voltage out of the Bx magnetic preamp is given the symbol VBxpa. The voltage out of the Bz magnetic preamp is given the symbol VBzpa. Figure 10.2.1.1 shows the location of each of these voltages.

   The conversion factors and their symbols are listed below. The conversion factors convert the Vtable values to the voltage at the various sensors.

Symbol	Factor	
CF+ex	1.0	Conversion factor for a monopole using the Ex+ antenna
CF-ex	1.0	Conversion factor for a monopole using the Ex- antenna
CFez	1.0	Conversion factor for the Ez antenna
CFbx	24.0	Conversion factor for the Bx Search Coil
CFbz	24.0	Conversion factor for the Bz Search Coil

   The formulas for converting the Vtable value to the sensor input voltage are shown below.

VDEx	=	Vtable (units are volts rms.)
VEx+	=	(CF+ex) * (Vtable)
VEx-	=	(CF-ex) * (Vtable)
VEz	=	(CFez) * (Vtable)
Vbxpa	=	(CFbx) * (Vtable)
Vbzpa	=	(CFbz) * (Vtable)

   For the electric sensors there may be frequency dependent adjustments necessary because of the interaction of the antenna with the plasma, but these are dependent upon the plasma impedance. If the user wishes to adjust for these effects, see Section 6.0.

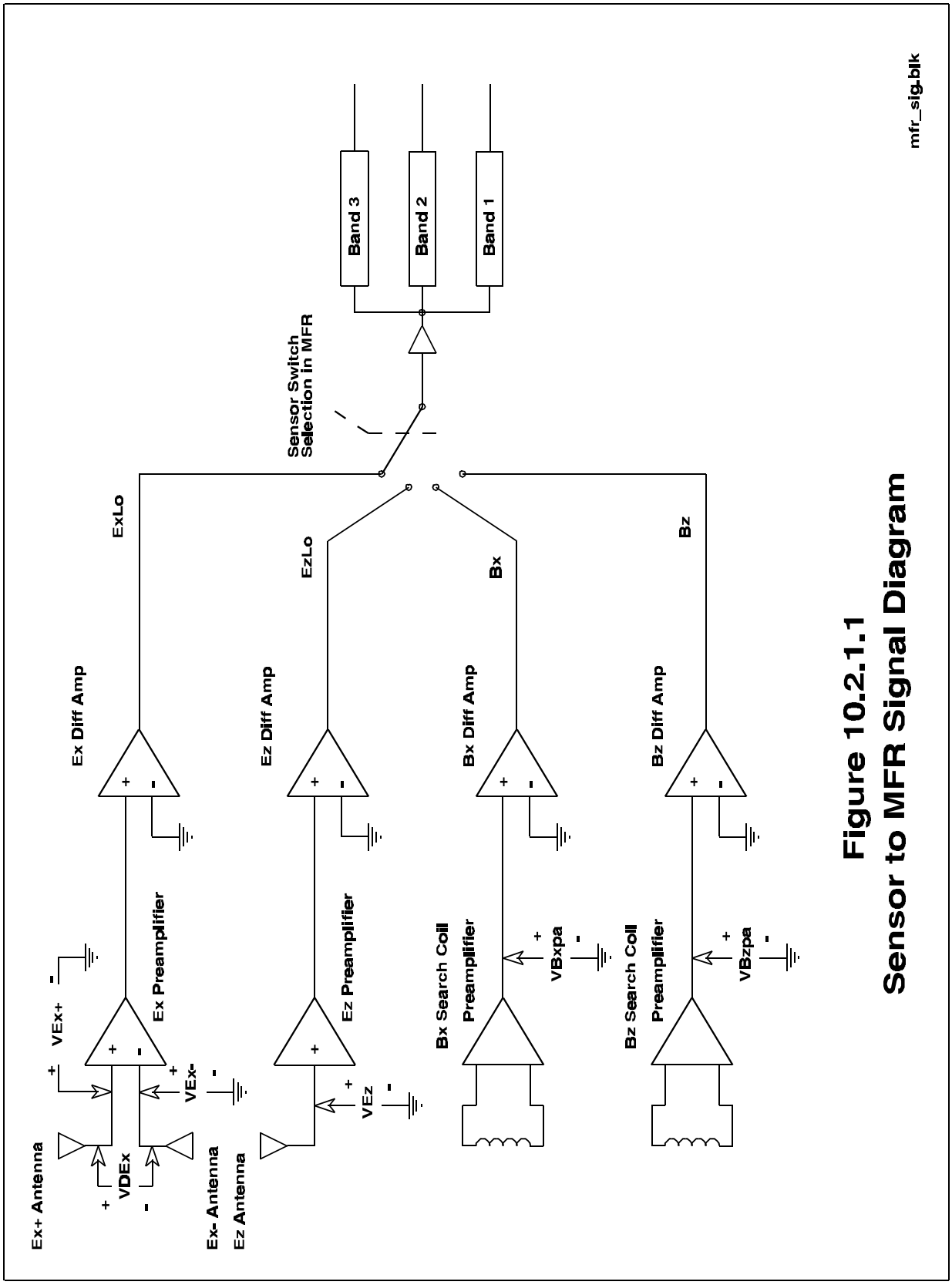

Figure 10.2.1.1
Sensor to MFR Signal Diagram

3) The voltages at the outputs of the Search Coil preamplifiers must now be converted to nanotesla. Table 10.2.1.1 contains the conversion factors for the Bx Search Coil and Figure 10.2.1.2 presents this data graphically. This conversion factor is frequency dependent and the value corresponding to the step of interest should be chosen. This conversion factor is given the symbol of CBxnt. The units of this factor are V/nT. Table 10.2.1.2 and Figure 10.2.1.3 present the conversion factors for the Bz Search Coil in tabular and graphical form. The conversion factor for the Bz Search Coil is given the symbol CBznt. It also has units of V/nT. To convert from voltage at the output of the Bx Search Coil preamplifier VBxpa must be divided by CBxnt. Likewise the voltage output of the Bz Search Coil must be divided by CBznt. This is shown in the following equations.

NTBx	=	Vbxpa / CBxnt	(units are nT rms.)
NTBz	=	Vbzpa / CBznt	

NTBx is the field at the Bx Search Coil and NTBz is the field at the Bz Search Coil. At this point, we have meaningful physical units. For the electric antennas we have the voltage measured at the antenna elements. For the magnetic sensors we have the magnetic field in nanotesla at the sensors. Next the magnitude of the electric field for the electric antennas can be obtained. The voltages at the antennas are divided by the effective antenna length. This produces units of volts per meter. Here the effective lengths are defined as the physical distances between the geometric centers of the antennas for the Ex and the geometric center for the Ez antenna. The effective length for the Ex+ to Ex- dipole antenna configuration is given the symbol Exdelta. The Ex+ monopole effective length is given the symbol L+Ex. The Ex- monopole is given the symbol L-Ex. The Ez monopole is given the symbol LEz. See Section 6.3 for a more detailed discussion of the effective length of the antennas.

Effective Antenna Length in Meters for various mode configurations

Antenna	Effective Length(in meters)	Configuration
LExdelta	8.66	dipole
L+Ex	5.0	monopole
L-Ex	5.0	monopole
LEz	5.0	monopole

The electric antenna field on the Ex dipole is represented by VMExdelta, the electric field on the Ex+ monopole by VM+Ex, the electric field on the Ex- monopole by VM-Ex and the electric field on the Ez monopole by VMEz. The following equations show the method for

calculating the electric antenna field on the antenna in volts per meter. These equations do not include effects due to the stray capacitive divider effects between the antennas and the spacecraft.

VMExdelta = (VDEx) / (LExdelta)
VM+Ex = (VEx+) / (L+Ex)
VM-Ex = (VEx-) / (L-Ex)
VMEz = (VEz) / (LEz)

4) To obtain spectral density one must square the value from Step 3 and divide by the effective bandwidth EBW. The effective bandwidth depends upon which MFR Band (1 through 3) is being used (See Section 10.3.3).

Effective Bandwidth in Hz	
MFR Band 1	5.6
MFR Band 2	19.4
MFR Band 3	139

The spectral density of the signal on the Ex dipole antenna is represented by Exdeltasd, the Ex+ monopole antenna by +Exsd and the Ex- antenna by -Exsd. The following equations show the method for calculating the electric antenna spectral density on the antennas in volts rms squared per hertz.

Exdeltasd = $(VMExdelta)^2$ / EBW
+Exsd = $(VM+Ex)^2$ / EBW
-Exsd = $(VM-Ex)^2$ / EBW
Ezsd = $(VMEz)^2$ / EBW

The spectral density of the signal from the Bx sensor is represented by Bxd. The spectral density of the signal from the Bz sensor is represented by Bzd. The following equations show the method for calculating the magnetic spectral density at the magnetic sensors in nanotesla squared per hertz.

Bxd = $NTBx^2$ / EBW
Bzd = $NTBz^2$ / EBW

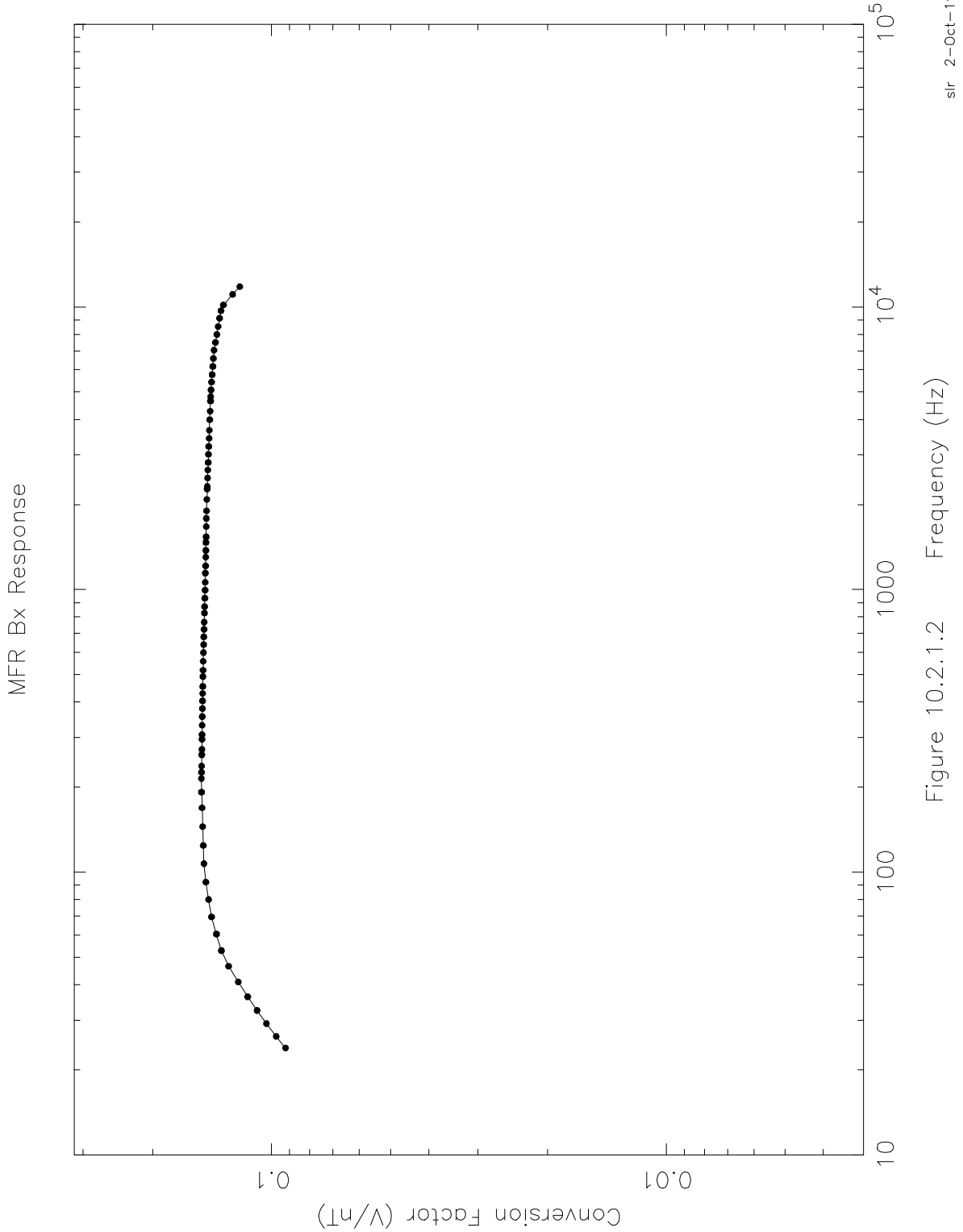

Figure 10.2.1.2

Table 10.2.1.1
Conversion Table for Cassini Search Coil Bx (MFR)

MFR Band	MFR Step	Center Freq.	CFbx V/nT	MFR Band	MFR Step	Center Freq.	CFbx V/nT	MFR Band	MFR Step	Center Freq.	CFbx V/nT
1	1	23.89	0.0922	2	1	192.11	0.1505	3	1	1536.89	0.1466
1	2	26.25	0.0973	2	2	214.63	0.1506	3	2	1671.81	0.1464
1	3	29.15	0.1030	2	3	225.98	0.1505	3	3	1785.10	0.1463
1	4	32.42	0.1088	2	4	237.40	0.1504	3	4	1899.17	0.1462
1	5	36.27	0.1149	2	5	260.42	0.1503	3	5	2083.33	0.1459
1	6	40.89	0.1215	2	6	272.02	0.1502	3	6	2269.55	0.1456
1	7	46.51	0.1285	2	7	295.43	0.1501	3	7	2316.43	0.1455
1	8	52.82	0.1340	2	8	307.23	0.1500	3	8	2481.55	0.1452
1	9	60.43	0.1379	2	9	331.04	0.1499	3	9	2648.30	0.1450
1	10	69.46	0.1420	2	10	355.11	0.1498	3	10	2816.71	0.1447
1	11	80.05	0.1444	2	11	379.46	0.1497	3	11	3011.24	0.1445
1	12	92.34	0.1468	2	12	404.09	0.1496	3	12	3208.00	0.1443
1	13	107.24	0.1483	2	13	429.01	0.1495	3	13	3432.08	0.1440
1	14	124.39	0.1489	2	14	454.22	0.1494	3	14	3659.09	0.1437
1	15	144.88	0.1495	2	15	492.58	0.1493	3	15	3992.29	0.1434
1	16	169.05	0.1500	2	16	518.53	0.1492	3	16	4279.24	0.1432
				2	17	558.04	0.1490	3	17	4651.27	0.1428
				2	18	598.25	0.1488	3	18	4813.11	0.1427
				2	19	639.20	0.1487	3	19	5086.11	0.1424
				2	20	680.91	0.1485	3	20	5419.21	0.1419
				2	21	723.38	0.1483	3	21	5758.48	0.1415
				2	22	766.65	0.1482	3	22	6162.32	0.1409
				2	23	825.61	0.1479	3	23	6575.06	0.1404
				2	24	870.82	0.1478	3	24	7027.51	0.1399
				2	25	932.46	0.1476	3	25	7490.92	0.1388
				2	26	995.71	0.1474	3	26	7997.75	0.1377
				2	27	1060.64	0.1473	3	27	8518.02	0.1366
				2	28	1144.25	0.1471	3	28	9120.06	0.1354
				2	29	1213.20	0.1470	3	29	9705.63	0.1343
				2	30	1302.08	0.1469	3	30	10165.01	0.1325
				2	31	1375.44	0.1468	3	31	11078.04	0.1255
				2	32	1470.09	0.1466	3	32	11799.33	0.1204

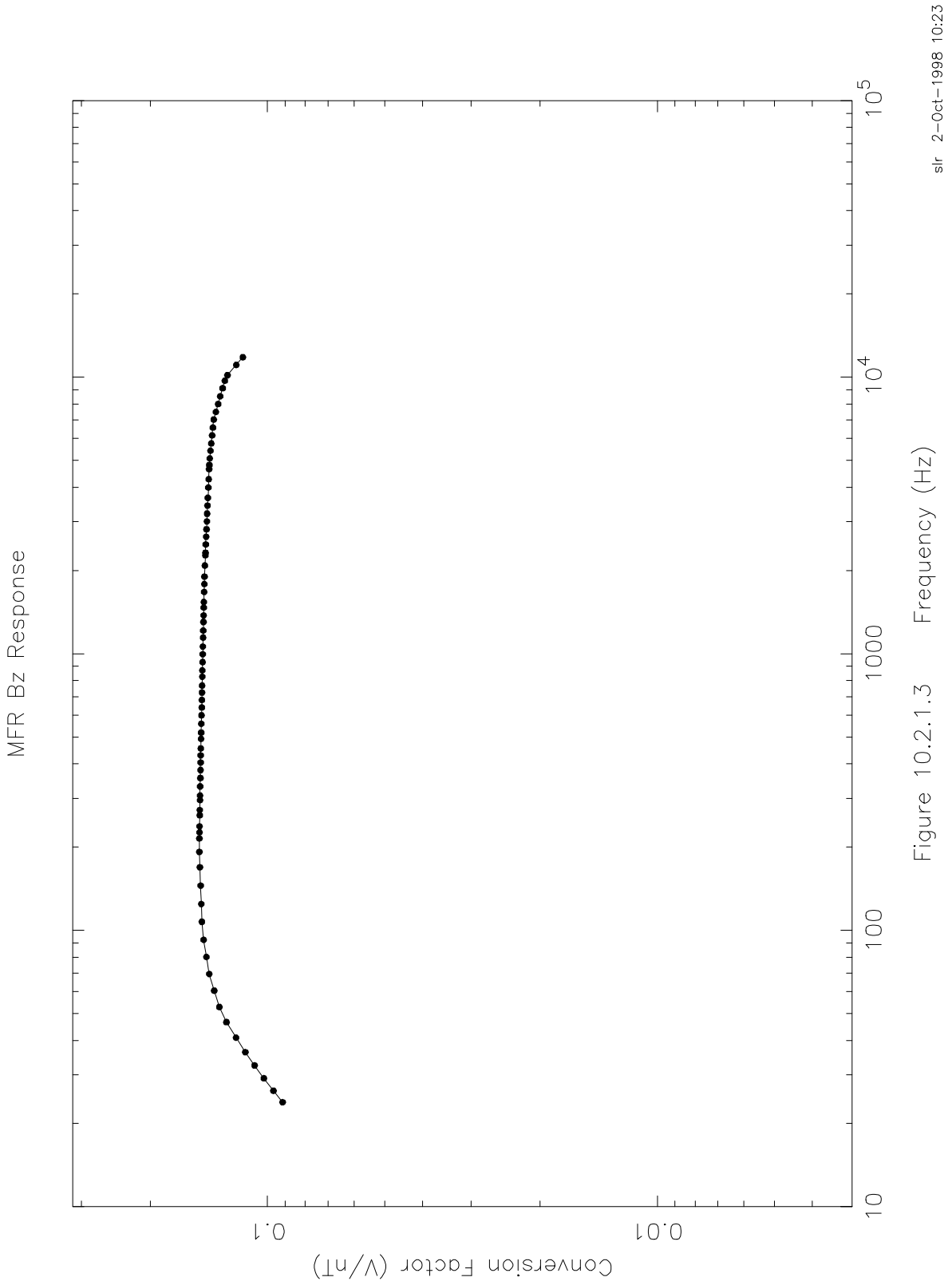

Figure 10.2.1.3

Table 10.2.1.2
Conversion Table for Cassini Search Coil Bz (MFR)

MFR Band	MFR Step	Center Freq.	CFbx V/nT	MFR Band	MFR Step	Center Freq.	CFbx V/nT	MFR Band	MFR Step	Center Freq.	CFbx V/nT
1	1	23.89	0.0914	2	1	192.11	0.1495	3	1	1536.89	0.1455
1	2	26.25	0.0965	2	2	214.63	0.1495	3	2	1671.81	0.1453
1	3	29.15	0.1021	2	3	225.98	0.1494	3	3	1785.10	0.1452
1	4	32.42	0.1079	2	4	237.40	0.1493	3	4	1899.17	0.1450
1	5	36.27	0.1139	2	5	260.42	0.1492	3	5	2083.33	0.1447
1	6	40.89	0.1204	2	6	272.02	0.1491	3	6	2269.55	0.1443
1	7	46.51	0.1273	2	7	295.43	0.1490	3	7	2316.43	0.1442
1	8	52.82	0.1329	2	8	307.23	0.1489	3	8	2481.55	0.1439
1	9	60.43	0.1369	2	9	331.04	0.1488	3	9	2648.30	0.1436
1	10	69.46	0.1410	2	10	355.11	0.1487	3	10	2816.71	0.1433
1	11	80.05	0.1434	2	11	379.46	0.1485	3	11	3011.24	0.1430
1	12	92.34	0.1458	2	12	404.09	0.1484	3	12	3208.00	0.1428
1	13	107.24	0.1473	2	13	429.01	0.1483	3	13	3432.08	0.1425
1	14	124.39	0.1479	2	14	454.22	0.1482	3	14	3659.09	0.1422
1	15	144.88	0.1484	2	15	492.58	0.1481	3	15	3992.29	0.1418
1	16	169.05	0.1490	2	16	518.53	0.1480	3	16	4279.24	0.1415
				2	17	558.04	0.1478	3	17	4651.27	0.1411
				2	18	598.25	0.1476	3	18	4813.11	0.1409
				2	19	639.20	0.1475	3	19	5086.11	0.1406
				2	20	680.91	0.1473	3	20	5419.21	0.1400
				2	21	723.38	0.1472	3	21	5758.48	0.1394
				2	22	766.65	0.1471	3	22	6162.32	0.1387
				2	23	825.61	0.1469	3	23	6575.06	0.1380
				2	24	870.82	0.1468	3	24	7027.51	0.1373
				2	25	932.46	0.1467	3	25	7490.92	0.1356
				2	26	995.71	0.1466	3	26	7997.75	0.1338
				2	27	1060.64	0.1464	3	27	8518.02	0.1321
				2	28	1144.25	0.1462	3	28	9120.06	0.1303
				2	29	1213.20	0.1461	3	29	9705.63	0.1286
				2	30	1302.08	0.1459	3	30	10165.01	0.1266
				2	31	1375.44	0.1458	3	31	11078.04	0.1203
				2	32	1470.09	0.1456	3	32	11799.33	0.1156

10.2.2 Examples of Conversions from Data Numbers to Science Units

Three examples of conversions from data numbers to science units will be performed. Examples will include the Ex+ dipole electric antennas, the Ex+ monopole electric antenna and the Bx Search Coil as sensor inputs.

1) The first example will use the Ex+ dipole as the sensor input. For this example a data number of 97 for MFR Band 3 Step 18 will be converted to V_{rms}^2 / (meter^2 * Hz). The first step is to use the look up tables in Section 10.3.1 and find the table for MFR Band 3 Step 18. In this table the value of 2.7967E-05 V_{rms} corresponds to a data number of 97. Therefore Vtable is 2.7967E-05 V_{rms}. Since the tables were produced from Ex dipole calibration tests VDEx is equal to Vtable. Next VDEx is divided by the effective length of the Ex dipole antenna (Lexdelta) to obtain the electric field, VMExdelta, in V_{rms} / meter (see Section 10.2.1, Step 3).

   VMExdelta = (VDEx) / (Lexdelta)
   = 2.7967E-05 V_{rms} / 8.66 meters
   = 3.2294E-06 V_{rms} / meter

   VMExdelta is now squared and divided by the effective bandwidth of MFR Band 3 of 139 Hz to obtain the spectral density of the signal on the Ex dipole antenna (see Section 10.2.1, Step 4).

   Spectral density on the Ex dipole = Exdelta = (VMExdelta)^2 / $EBW_{Band\ 3}$
   = (3.2294E-06 V_{rms} / meter)^2 / 139 Hz
   = 7.5029E-14 V_{rms}^2 / (meters^2 * Hz)

2) The next example uses the Ex+ monopole electrical antenna as the sensor input. For this example MFR Band 2 Step 7 with a data number of 140 was chosen. The first step is to use the MFR Band 2 Step 7 look up table in Section 10.3.1. A data number of 140 corresponds to 1.3573E-04 V_{rms}. Referring to Step 2 of Section 10.2.1 Vtable is multiplied by (CF+ex) to give the voltage on the Ex+ monopole antenna.

   VEx+ = (CF+ex) * Vtable
   = 1.0 * 1.3573e-04 V_{rms}
   = 1.3573E-04 V_{rms}

   VEx+ is now divided by the effective length of the Ex+ monopole (L+Ex) which is 5.0 meters (see Section 10.2.1, Step 3).

   (VM+Ex) = (VEx+) / (L+Ex) = 1.3573E-04 V_{rms} / 5.0 meters
   = 2.7146E-05 V_{rms} / meter

VM+Ex is now squared and divided by the effective bandwidth of MFR Band 2 of 19.4 Hz to obtain the spectral density of the signal on the Ex+ monopole antenna (see Section 10.2.1, Step 4).

Spectral density on the Ex+ monopole	=	$+Exsd = (VM+Ex)^2 / EBW_{Band\ 2}$
	=	$(2.7146E-05)^2 / 19.4$ Hz
	=	$3.785E-11 V_{rms} / (meter^2 * Hz)$

3) The last example will use the Bx Search Coil as the sensor input. For this example MFR Band 1 Step 12 with a data number of 125 was chosen. The first step is to use the MFR Band 1 Step 12 look up table in Section 10.3.1. A data number of 125 corresponds to 1.7153E-04 V_{rms}. Referring to Step 2 of Section 10.2.1, Vtable is multiplied by CFbx to give the voltage, Vbxpa, at the output of the Bx Search Coil.

Vbxpa	=	(CFbx) * (Vtable) = 24.0 * 1.7153E-04
	=	4.1167E-03 V_{rms}

Next the voltage at the output of the Bx Search Coil is converted to nT by dividing it by the conversion factor CBxnt in Table 10.2.1.1 for MFR Band 1 Step 12 (see Section 10.2.1, Step 3).

NTBx	=	Vbxpa / Cbxnt
	=	4.1167E-03 V_{rms} / 0.1468 V / nT
	=	2.8043E-02 nT_{rms}

NTBx is now squared and divided by the effective bandwidth of MFR Band 1 of 5.6 Hz to obtain the spectral density of the magnetic field at the Bx Search Coil (see Section 10.2.1, Step 4).

Spectral density at the Bx Search Coil	=	Bxd
	=	$(NTBx)^2 / EBW_{Band\ 1}$
	=	$(2.8043E-02\ nT)^2 / 5.6$ Hz
	=	$5.077E-03\ nT_{rms}^2 / Hz$

10.3.1 Amplitude Calibration (Input Voltage Versus Output Data Numbers)

This section contains the amplitude calibration of the MFR steps. The tables in this section contain the relationships between the 8-bit data numbers at the output of the log compressors and the voltage at the Ex preamplifier inputs, VDEx. Differential signals of known amplitude are applied to the Ex+ and Ex- preamplifier inputs. The drive frequency is a step near the middle of each of the three MFR bands. The steps used for the MFR bands are MFR Band 1 Step 8, MFR Band 2 Step 16 and MFR Band 3 Step 10. An adjustable attenuator and a balancing transformer with a 1:1 turns ratio are placed between the oscillator and the Ex+ and Ex- preamplifier inputs. The stimulus amplitude is adjusted in 2 dB steps from 0 dBv (dB relative to 1 V-rms.) to -140 dBv. The oscillator level is switched from 1 V-rms. to 0.01 V-rms. when the output of the stimulus is stepped from to -118 dBv to -120 dBv. The stimulus set up for the amplitude calibration is shown in Figure 10.3.1.1.

All compressors have some degree of ripple in their amplitude response and averaging is necessary. Four or more measurements are taken for each amplitude setting and these are averaged arithmetically. The averaged output data numbers are then plotted as a function of dBv and linear fits between points are used in order to associate an input voltage with each possible data number from 0 to 255.

A correction is made to each curve to take into account that the signal input to the log compressor actually consists of both the applied signal and the noise floor. This noise is made up of preamplifier noise, noise external to the instrument, and the receiver noise. This correction may be expressed as follows:

$$V(t)^2 = V(n)^2 + V(s)^2 \qquad \text{Equation 10.3.1.1}$$

V(t) is the total signal at the input to the compressor. V(n) is the background noise and V(s) is the input signal. For most of the compressors, the noise level in the system is such that none of the compressor stages are saturated with no input signal present and a straight line fit provides a value for V(n). Calibrations are run in 2 dB steps below -100 dBv for each step. From this data steps are chosen such that they are not saturating the compressor.

The result of the above process, for each MFR step, is a look up table relating input voltage to the output data number. For amplitudes higher than the saturation level of the compressor, the lookup tables are obtained by adjusting the center step 2 dB calibrations up or down using the Channel-to-Channel gain results (see Section 10.3.2). For lower amplitudes, the least squares linear fit is performed for each step. The results are presented in tabular form and in graphical form for each step, and are shown in the MFR Appendix.

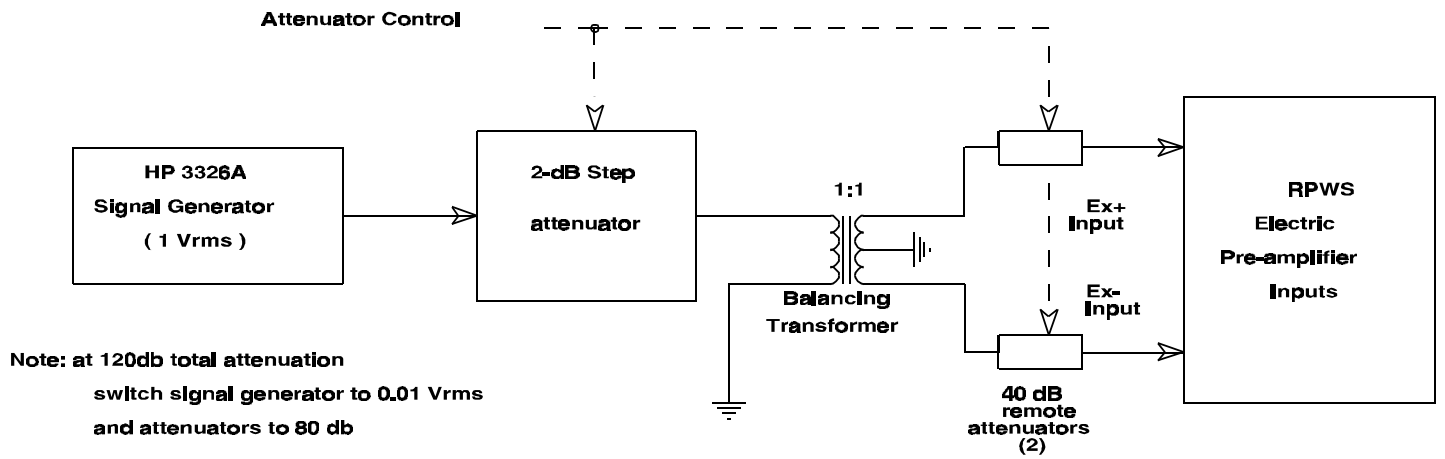

Figure 10.3.1.1

MFR 2db Calibration Stimulus Configuration

mfr_2db.blk

10.3.2 Channel-to-Channel Gains

The sensitivity of the MFR varies from step to step across the band. Variations of insertion losses and roll-off within MFR bands affect the calibrations of the steps of that band. The channel to channel gains were performed by stimulating the MFR with random noise at a fixed amplitude. If, for instance, a channel has a gain of +1dB relative to a reference channel, then the input signal of that channel is 1dB less than the reference channel input for the same output. The relative variations in random noise amplitude response were used to correct the sine wave look-up tables in Section 10.3.1. MFR Band 1 Step 8, MFR Band 2 Step 16 and MFR Band 3 Step 10 were used as the reference channels for this technique. This method adjusts for differences in the logarithmic section of the curves. The lower ends of the tables are filled in using the linear fit technique described in Section 10.3.1. The stimulus setup for the channel-to-channel gain test is shown in Figure 10.3.2.1.

The channel to channel gain test was performed using a random noise input signal. The random noise test data has interference at 60 Hz and at the 3rd, 5th and 7th harmonics of 60 Hz. This interference has been corrected for by interpolating or extrapolating from adjacent channels. The effective bandwidth calculations in Section 10.3.3 provide the correction factor between the random noise input and the sine wave input. This is because a known spectral density random noise input is used to calculate the effective bandwidth. Refer to Section 10.3.3 for details. The corrected and uncorrected channel-to-channel gains for the MFR are presented in tabular and graphical formats in Tables 10.3.2.1 and 10.3.2.2 and Figures 10.3.2.2 and 10.3.2.3.

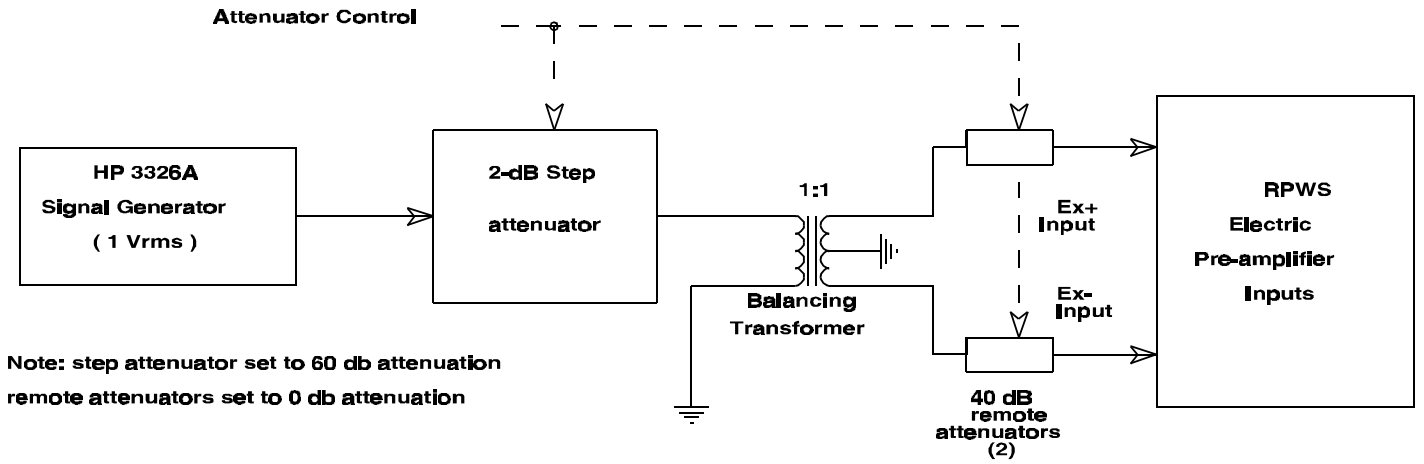

Figure 10.3.2.1

MFR Channel to Channel Gain Stimulus Configuration

mfr_chn.blk

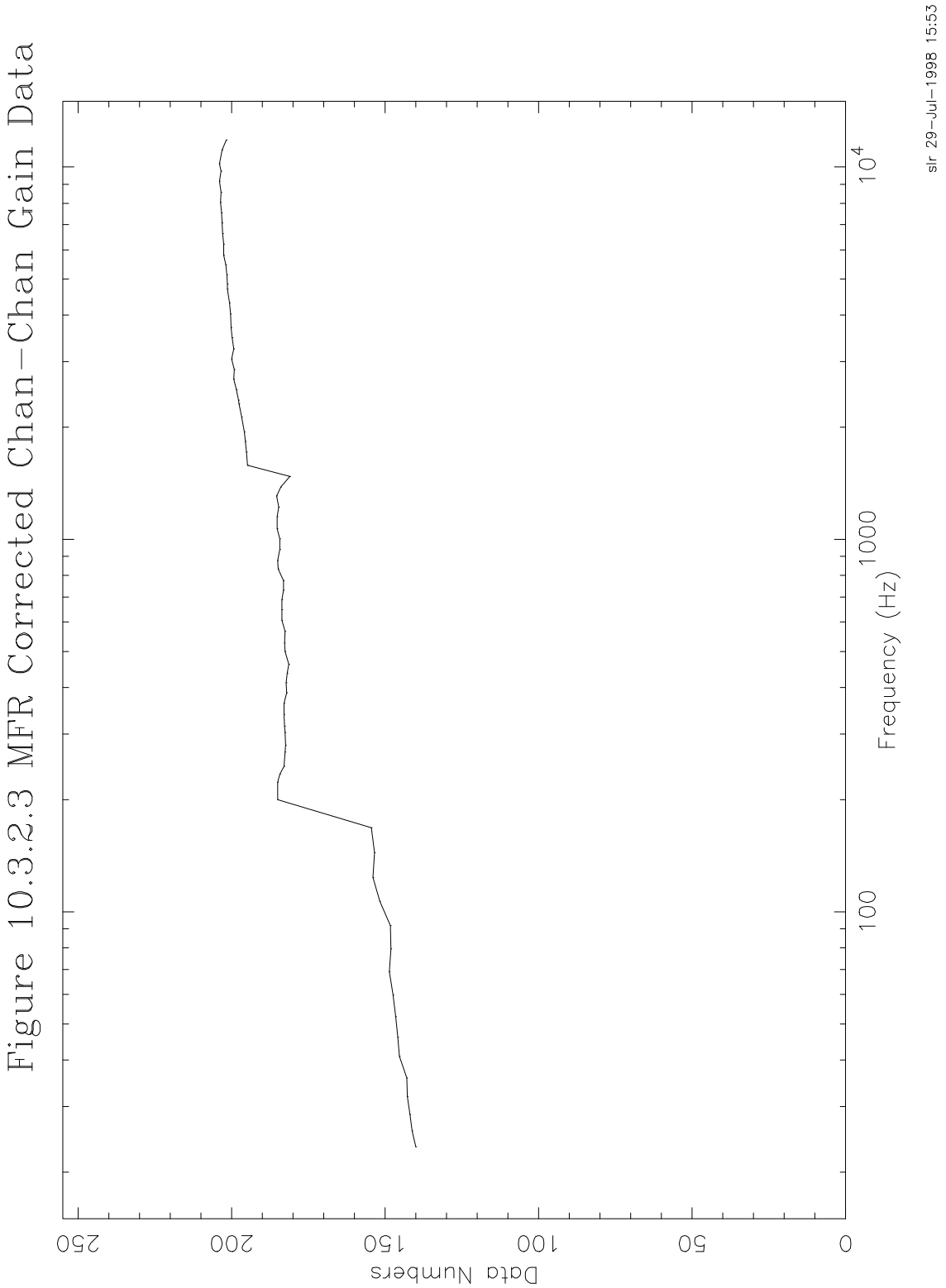
Figure 10.3.2.3 MFR Corrected Chan-Chan Gain Data
Data Numbers
0
50
100
150
200
250
Frequency (Hz)
100
1000
10^4
slr 29-Jul-1998 15:53

Table 10.3.2.2 MFR Corrected Chan-Chan Gain Data

Frequency (Hz)	Output (DN)	Frequency (Hz)	Output (DN)
2.3400E+01	1.3998E+02	9.4050E+02	1.8429E+02
2.5800E+01	1.4118E+02	1.0037E+03	1.8439E+02
2.8600E+01	1.4189E+02	1.0686E+03	1.8514E+02
3.1900E+01	1.4281E+02	1.1522E+03	1.8517E+02
3.5800E+01	1.4289E+02	1.2212E+03	1.8457E+02
4.0900E+01	1.4537E+02	1.3101E+03	1.8538E+02
4.6000E+01	1.4589E+02	1.3834E+03	1.8397E+02
5.2300E+01	1.4657E+02	1.4781E+03	1.8100E+02
5.9900E+01	1.4749E+02	1.5819E+03	1.9484E+02
6.9000E+01	1.4860E+02	1.7168E+03	1.9510E+02
7.9500E+01	1.4821E+02	1.8301E+03	1.9550E+02
9.1800E+01	1.4835E+02	1.9442E+03	1.9591E+02
1.0670E+02	1.5167E+02	2.1283E+03	1.9673E+02
1.2390E+02	1.5406E+02	2.3146E+03	1.9752E+02
1.4440E+02	1.5350E+02	2.3614E+03	1.9778E+02
1.6850E+02	1.5445E+02	2.5266E+03	1.9840E+02
2.0010E+02	1.8500E+02	2.6933E+03	1.9923E+02
2.2260E+02	1.8498E+02	2.8617E+03	1.9913E+02
2.3390E+02	1.8434E+02	3.0562E+03	1.9994E+02
2.4540E+02	1.8296E+02	3.2530E+03	1.9935E+02
2.6840E+02	1.8263E+02	3.4771E+03	1.9986E+02
2.8000E+02	1.8251E+02	3.7041E+03	2.0023E+02
3.0340E+02	1.8267E+02	4.0373E+03	2.0037E+02
3.1520E+02	1.8274E+02	4.3242E+03	2.0067E+02
3.3900E+02	1.8290E+02	4.6963E+03	2.0140E+02
3.6310E+02	1.8294E+02	4.8581E+03	2.0140E+02
3.8740E+02	1.8203E+02	5.1311E+03	2.0159E+02
4.1200E+02	1.8225E+02	5.4642E+03	2.0181E+02
4.3700E+02	1.8184E+02	5.8035E+03	2.0257E+02
4.6220E+02	1.8143E+02	6.2073E+03	2.0254E+02
5.0050E+02	1.8256E+02	6.6201E+03	2.0286E+02
5.2650E+02	1.8275E+02	7.0725E+03	2.0307E+02
5.6600E+02	1.8253E+02	7.5359E+03	2.0326E+02
6.0630E+02	1.8361E+02	8.0427E+03	2.0357E+02
6.4720E+02	1.8364E+02	8.5630E+03	2.0338E+02
6.8890E+02	1.8355E+02	9.1651E+03	2.0396E+02
7.3180E+02	1.8302E+02	9.7506E+03	2.0340E+02
7.7460E+02	1.8319E+02	1.0210E+04	2.0402E+02
8.3360E+02	1.8476E+02	1.1123E+04	2.0307E+02
8.7880E+02	1.8496E+02	1.1844E+04	2.0164E+02

Figure 10.3.2.2 MFR Uncorrected Chan-Chan Gain Data

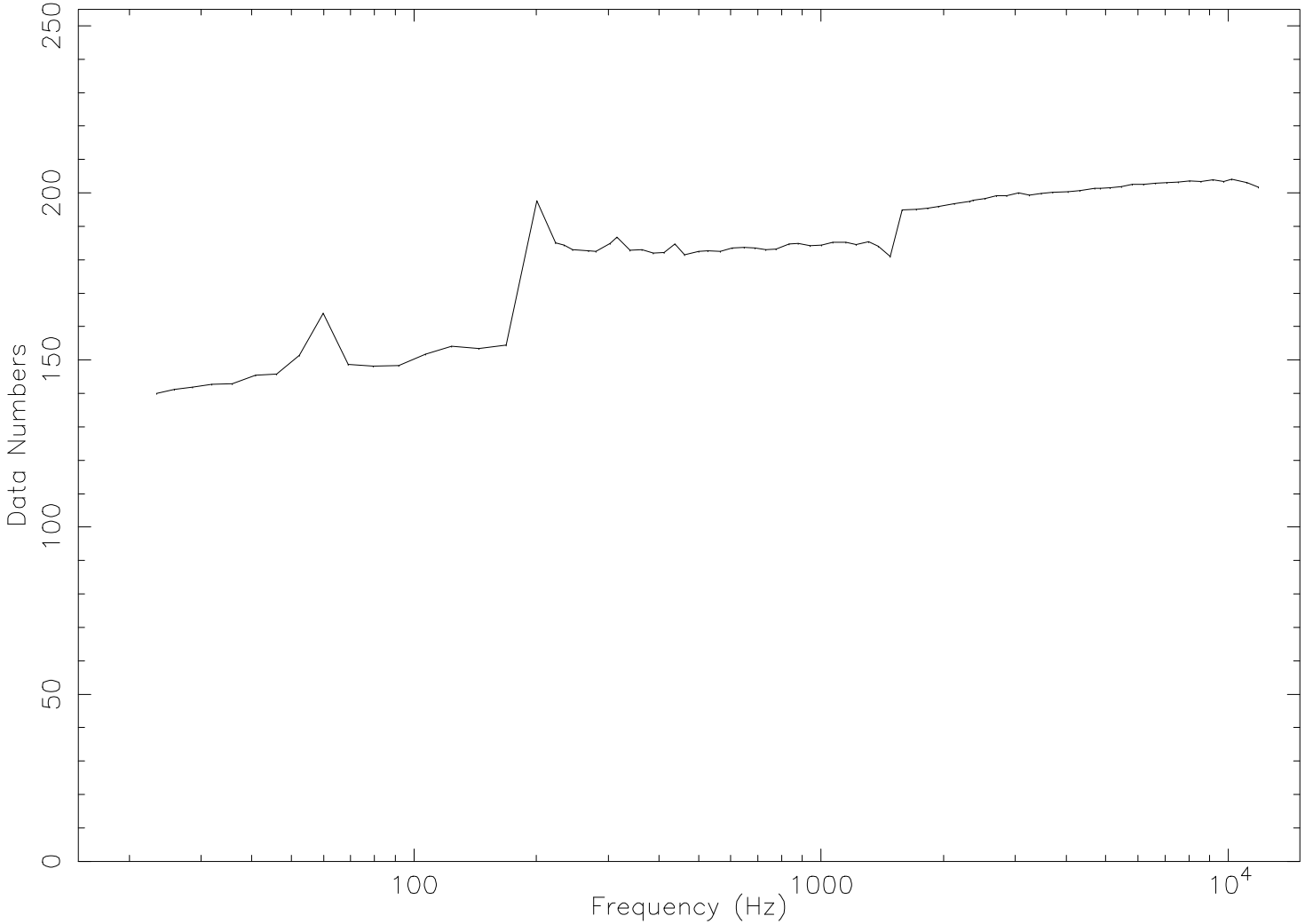

slr 29-Jul-1998 16:02

Table 10.3.2.1 MFR Uncorrected Chan-Chan Gain Data

Frequency (Hz)	Output (DN)	Frequency (Hz)	Output (DN)
2.3400E+01	1.3998E+02	9.4050E+02	1.8429E+02
2.5800E+01	1.4118E+02	1.0037E+03	1.8439E+02
2.8600E+01	1.4189E+02	1.0686E+03	1.8514E+02
3.1900E+01	1.4281E+02	1.1522E+03	1.8517E+02
3.5800E+01	1.4289E+02	1.2212E+03	1.8457E+02
4.0900E+01	1.4537E+02	1.3101E+03	1.8538E+02
4.6000E+01	1.4589E+02	1.3834E+03	1.8397E+02
5.2300E+01	1.5145E+02	1.4781E+03	1.8100E+02
5.9900E+01	1.6401E+02	1.5819E+03	1.9484E+02
6.9000E+01	1.4860E+02	1.7168E+03	1.9510E+02
7.9500E+01	1.4821E+02	1.8301E+03	1.9550E+02
9.1800E+01	1.4835E+02	1.9442E+03	1.9591E+02
1.0670E+02	1.5167E+02	2.1283E+03	1.9673E+02
1.2390E+02	1.5406E+02	2.3146E+03	1.9752E+02
1.4440E+02	1.5350E+02	2.3614E+03	1.9778E+02
1.6850E+02	1.5445E+02	2.5266E+03	1.9840E+02
2.0010E+02	1.9767E+02	2.6933E+03	1.9923E+02
2.2260E+02	1.8498E+02	2.8617E+03	1.9913E+02
2.3390E+02	1.8434E+02	3.0562E+03	1.9994E+02
2.4540E+02	1.8296E+02	3.2530E+03	1.9935E+02
2.6840E+02	1.8263E+02	3.4771E+03	1.9986E+02
2.8000E+02	1.8251E+02	3.7041E+03	2.0023E+02
3.0340E+02	1.8490E+02	4.0373E+03	2.0037E+02
3.1520E+02	1.8684E+02	4.3242E+03	2.0067E+02
3.3900E+02	1.8290E+02	4.6963E+03	2.0140E+02
3.6310E+02	1.8294E+02	4.8581E+03	2.0140E+02
3.8740E+02	1.8203E+02	5.1311E+03	2.0159E+02
4.1200E+02	1.8225E+02	5.4642E+03	2.0181E+02
4.3700E+02	1.8465E+02	5.8035E+03	2.0257E+02
4.6220E+02	1.8143E+02	6.2073E+03	2.0254E+02
5.0050E+02	1.8256E+02	6.6201E+03	2.0286E+02
5.2650E+02	1.8275E+02	7.0725E+03	2.0307E+02
5.6600E+02	1.8253E+02	7.5359E+03	2.0326E+02
6.0630E+02	1.8361E+02	8.0427E+03	2.0357E+02
6.4720E+02	1.8364E+02	8.5630E+03	2.0338E+02
6.8890E+02	1.8355E+02	9.1651E+03	2.0396E+02
7.3180E+02	1.8302E+02	9.7506E+03	2.0340E+02
7.7460E+02	1.8319E+02	1.0210E+04	2.0402E+02
8.3360E+02	1.8476E+02	1.1123E+04	2.0307E+02
8.7880E+02	1.8496E+02	1.1844E+04	2.0164E+02

10.3.3 Effective Noise Bandwidth

In this section the detection bandwidth calibration data for the MFR is presented. There are two ways to evaluate detection bandwidth. One is to measure the frequency response of the filter. A sinusoidal stimulus is swept over the filter pass-band and the response of the compressor is noted. The other method is to determine the effective bandwidth by noting the compressor response to a white noise stimulus. In the following paragraphs, both methods are discussed and filter data are presented for the MFR filters

10.3.3.1 Filter Frequency Response Curves

The sine wave frequency responses of the detection filters used in the MFR are determined by applying a differential signal fixed at 0.001 volts rms to the Ex inputs and sweeping it over the filter pass-bands. Figures 10.3.3.1.1, 10.3.3.1.2 and 10.3.3.1.3 show the curves for Band 1 Step 8, Band 2 Step16, and Band 3 Step 10, respectively, using the Ex inputs. The data is also given in tabular form in Tables 10.3.3.1.1 through 10.3.3.1.3. The MFR plots show the upper and the lower side bands. The MFR Band 1 circuit is designed to reject the lower side band. The responses for any MFR step other than the center steps are determined by making an adjustment according to the channel-to-channel gain tables presented in Section 10.3.2 of this document. The response for sensors other than the Ex+ and Ex- is determined by referring to the differential amplifier calibrations and the sensor calibrations in Sections 6.0 and 7.0 of this document to determine an appropriate factor to adjust the amplitude by. The stimulus setup is shown in Figure 10.3.3.1.4.

10.3.3.2 Effective Bandwidths

The frequency response curves shown in Section 10.3.3.1 were generated with sine wave stimuli. While this is useful for observing the filter shape and estimating the bandwidth, many actual emissions more closely approximate random noise having bandwidths wide in comparison to the filter bandwidth. It is necessary to be able to interpret the amplitude measurements in terms of the noise spectral density of the received signal. To determine the spectral density V_f^2 the following equation is used:

$$V_f^2 = V_s^2/D_f \qquad \text{Equation 10.3.3.2.1}$$

For a given output data number, the look-up tables in Section 10.3.1 can be used to find the corresponding input voltage Vs. The effective bandwidth D_f is defined to be the bandwidth which V_s^2 must be divided by to give the input voltage spectral density if the same log compressor output voltage were due entirely to a random noise input. Note that this effective bandwidth includes the effects of both the filter bandwidth and the non-ideal detection characteristics of the log compressor. If the compressor were a true rms detector (square-law device) then the effective bandwidth defined in equation 10.3.3.2.1 would be equivalent to the well-known ‘noise-

bandwidth' commonly used to characterize the bandwidth of a filter. The effective bandwidth D_f cannot be interpreted as the 'noise bandwidth' in the usual sense.

The noise bandwidth of each of the three MFR bands was determined in the following manner. A random noise signal of known density was applied to the MFR. The density was calculated by measuring the random noise amplitude before the step attenuators with a spectrum analyzer. Several readings were averaged together to improve the accuracy of the measurement. The test setup for determining the effective bandwidths of the MFR filters consists of a random noise generator with a white spectrum over the frequency range of the filters. Figures 10.3.3.2.1, 10.3.3.2.2, and 10.3.3.2.3 show the stimulus set ups used to determine the effective bandwidths. Different setups are used depending on the noise frequency range. In every case, a white noise stimulus of known power spectral density is injected into the programmable attenuator. The differential signal is applied to the Ex+ and Ex- inputs. A 2-dB calibration was performed using white noise. Large amplitude noise inputs which saturated the receiver and low level inputs at the receiver noise level were discarded. Both of these cause error in bandwidth calculation. For each amplitude number corresponding to a given spectral density, the program finds a value out of a file containing 2-dB calibration values. A computation is performed according to the expression in Equation 10.3.3.2.1 to determine the effective bandwidth. Several bandwidths, corresponding to various input noise densities, were averaged together.

Tables 10.3.3.2.1, 10.3.3.2.2, and 10.3.3.2.3 consists of 3 tables for the MFR effective bandwidths. These were calculated for the center step of each band of the MFR in logarithmic mode. The effective bandwidths are constant for any step on a given band because the same detection filters and log compressors area used in that band.

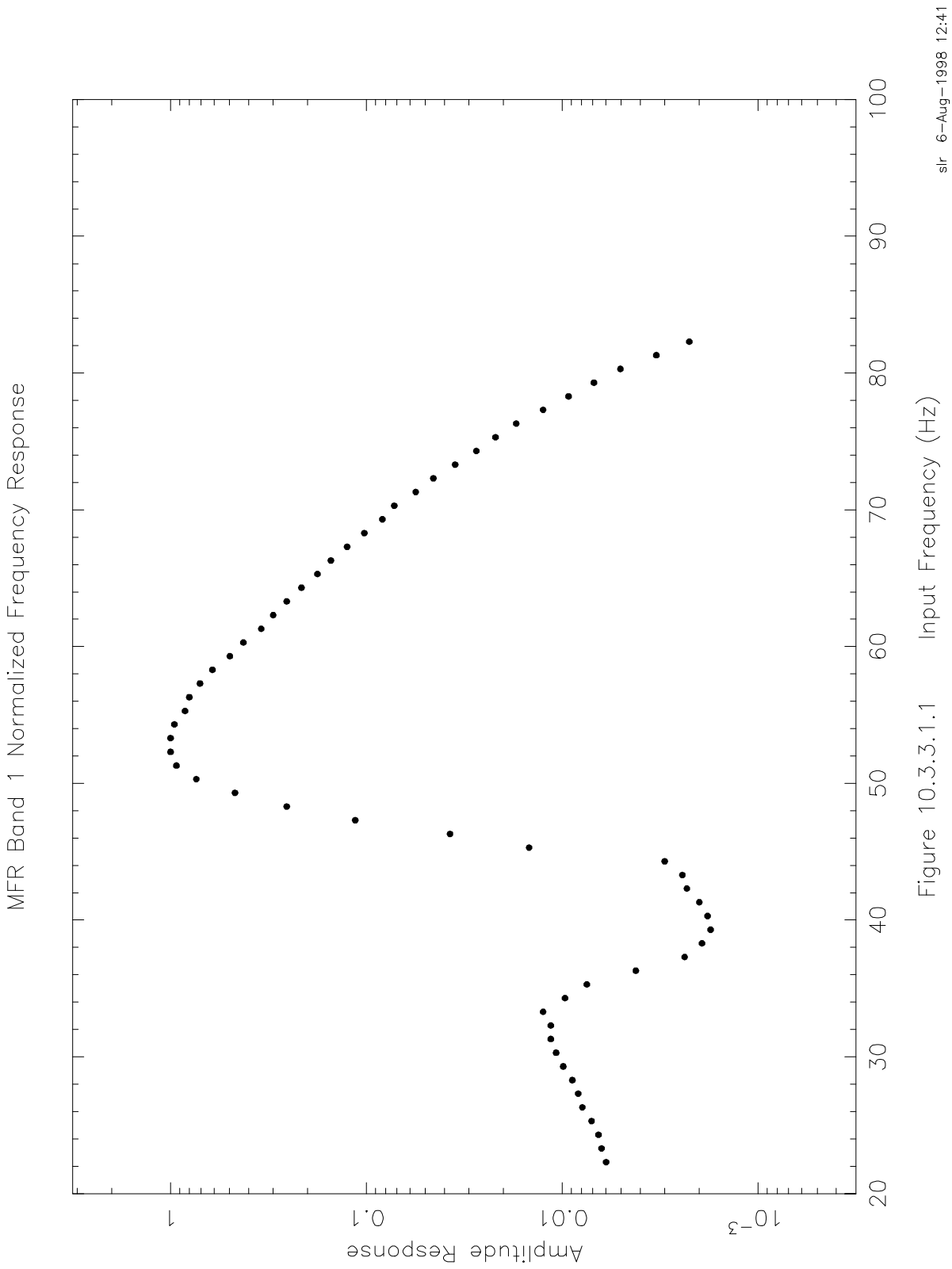

Figure 10.3.3.1.1

Table 10.3.3.1.1 MFR Band 1 Normalized Frequency Response

Frequency (Hz)	Amplitude (normalized)	Frequency (Hz)	Amplitude (normalized)
22.3000	0.0060	52.3000	1.0000
23.3000	0.0063	53.3000	1.0000
24.3000	0.0065	54.3000	0.9551
25.3000	0.0071	55.3000	0.8427
26.3000	0.0079	56.3000	0.8023
27.3000	0.0083	57.3000	0.7074
28.3000	0.0089	58.3000	0.6113
29.3000	0.0099	59.3000	0.4983
30.3000	0.0108	60.3000	0.4247
31.3000	0.0115	61.3000	0.3443
32.3000	0.0115	62.3000	0.2993
33.3000	0.0125	63.3000	0.2551
34.3000	0.0097	64.3000	0.2145
35.3000	0.0075	65.3000	0.1777
36.3000	0.0042	66.3000	0.1518
37.3000	0.0024	67.3000	0.1254
38.3000	0.0019	68.3000	0.1025
39.3000	0.0017	69.3000	0.0830
40.3000	0.0018	70.3000	0.0721
41.3000	0.0020	71.3000	0.0560
42.3000	0.0023	72.3000	0.0455
43.3000	0.0024	73.3000	0.0352
44.3000	0.0030	74.3000	0.0275
45.3000	0.0148	75.3000	0.0219
46.3000	0.0374	76.3000	0.0172
47.3000	0.1139	77.3000	0.0125
48.3000	0.2551	78.3000	0.0093
49.3000	0.4689	79.3000	0.0069
50.3000	0.7382	80.3000	0.0051
51.3000	0.9325	81.3000	0.0033

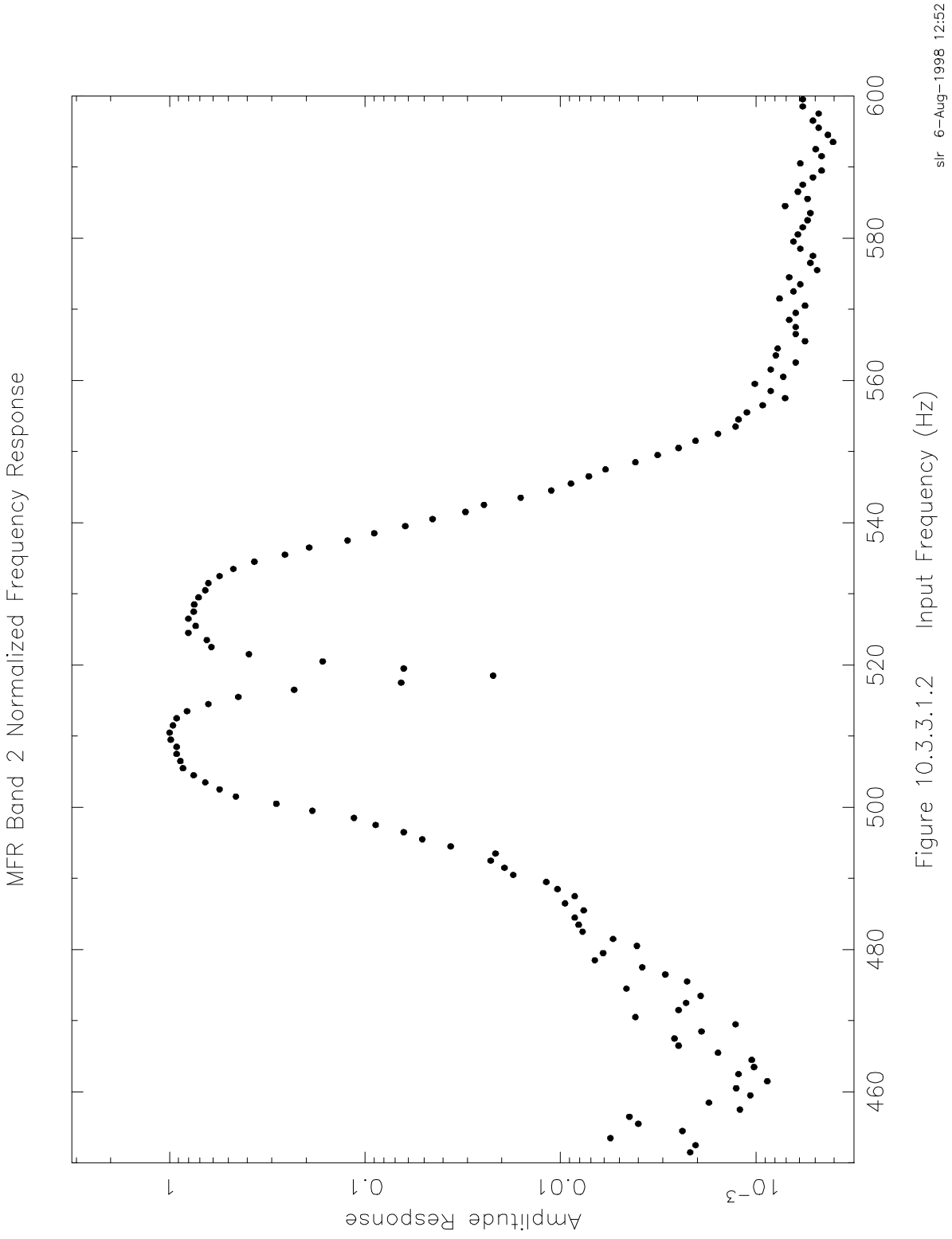

Figure 10.3.3.1.2

Table 10.3.3.1.2 MFR Band 2 Normalized Frequency Response

Frequency (Hz)	Amplitude (normalized)	Frequency (Hz)	Amplitude (normalized)	Frequency (Hz)	Amplitude (normalized)	Frequency (Hz)	Amplitude (normalized)	Frequency (Hz)	Amplitude (normalized)
451.5000	0.0022	481.5000	0.0054	511.5000	0.9602	541.5000	0.0306	571.5000	0.0008
452.5000	0.0020	482.5000	0.0077	512.5000	0.9205	542.5000	0.0247	572.5000	0.0006
453.5000	0.0056	483.5000	0.0081	513.5000	0.8146	543.5000	0.0160	573.5000	0.0006
454.5000	0.0024	484.5000	0.0085	514.5000	0.6331	544.5000	0.0112	574.5000	0.0007
455.5000	0.0040	485.5000	0.0076	515.5000	0.4450	545.5000	0.0088	575.5000	0.0005
456.5000	0.0044	486.5000	0.0095	516.5000	0.2304	546.5000	0.0072	576.5000	0.0005
457.5000	0.0012	487.5000	0.0085	517.5000	0.0654	547.5000	0.0059	577.5000	0.0005
458.5000	0.0017	488.5000	0.0104	518.5000	0.0221	548.5000	0.0041	578.5000	0.0006
459.5000	0.0011	489.5000	0.0118	519.5000	0.0634	549.5000	0.0032	579.5000	0.0006
460.5000	0.0013	490.5000	0.0175	520.5000	0.1648	550.5000	0.0025	580.5000	0.0006
461.5000	0.0009	491.5000	0.0194	521.5000	0.3927	551.5000	0.0020	581.5000	0.0006
462.5000	0.0012	492.5000	0.0228	522.5000	0.6106	552.5000	0.0016	582.5000	0.0005
463.5000	0.0010	493.5000	0.0215	523.5000	0.6448	553.5000	0.0013	583.5000	0.0005
464.5000	0.0011	494.5000	0.0365	524.5000	0.8016	554.5000	0.0012	584.5000	0.0007
465.5000	0.0016	495.5000	0.0510	525.5000	0.7349	555.5000	0.0011	585.5000	0.0005
466.5000	0.0025	496.5000	0.0634	526.5000	0.8016	556.5000	0.0009	586.5000	0.0006
467.5000	0.0026	497.5000	0.0883	527.5000	0.7530	557.5000	0.0007	587.5000	0.0006
468.5000	0.0019	498.5000	0.1139	528.5000	0.7470	558.5000	0.0008	588.5000	0.0005
469.5000	0.0013	499.5000	0.1859	529.5000	0.7108	559.5000	0.0010	589.5000	0.0005
470.5000	0.0041	500.5000	0.2840	530.5000	0.6568	560.5000	0.0007	590.5000	0.0006
471.5000	0.0025	501.5000	0.4581	531.5000	0.6331	561.5000	0.0008	591.5000	0.0005
472.5000	0.0023	502.5000	0.5548	532.5000	0.5548	562.5000	0.0006	592.5000	0.0005
473.5000	0.0019	503.5000	0.6568	533.5000	0.4716	563.5000	0.0008	593.5000	0.0004
474.5000	0.0046	504.5000	0.7530	534.5000	0.3686	564.5000	0.0008	594.5000	0.0004
475.5000	0.0023	505.5000	0.8542	535.5000	0.2572	565.5000	0.0006	595.5000	0.0005
476.5000	0.0029	506.5000	0.8807	536.5000	0.1930	566.5000	0.0006	596.5000	0.0005
477.5000	0.0038	507.5000	0.9205	537.5000	0.1228	567.5000	0.0006	597.5000	0.0005
478.5000	0.0067	508.5000	0.9205	538.5000	0.0897	568.5000	0.0007	598.5000	0.0006
479.5000	0.0061	509.5000	0.9867	539.5000	0.0622	569.5000	0.0006	599.5000	0.0006
480.5000	0.0041	510.5000	1.0000	540.5000	0.0452	570.5000	0.0006	600.5000	0.0005

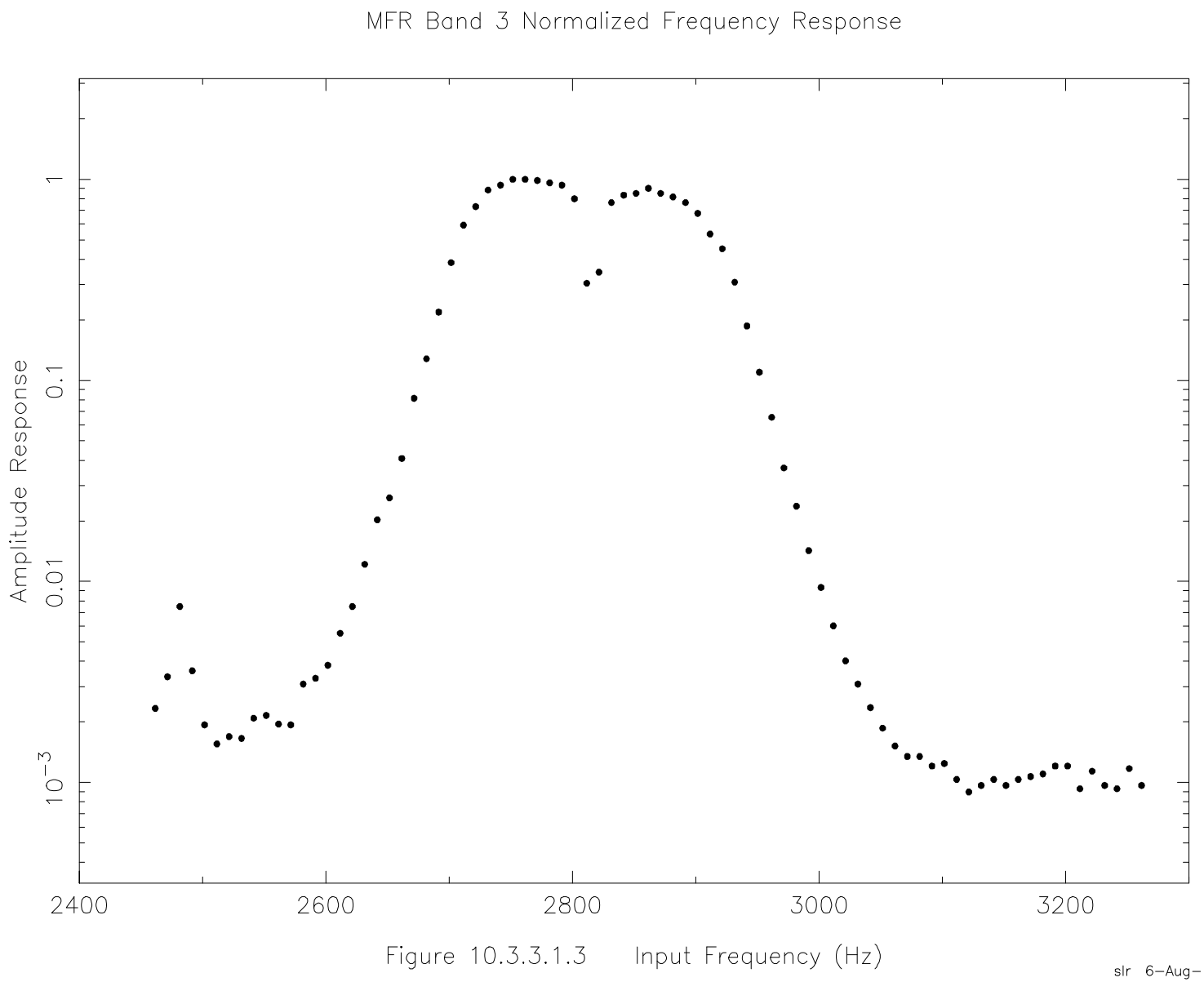

Figure 10.3.3.1.3

Table 10.3.3.1.3 MFR Band 3 Normalized Frequency Response

Frequency (Hz)	Amplitude (normalized)	Frequency (Hz)	Amplitude (normalized)
2461.7000	0.0023	2861.7000	0.9011
2471.7000	0.0034	2871.7000	0.8505
2481.7000	0.0075	2881.7000	0.8168
2491.7000	0.0036	2891.7000	0.7663
2501.7000	0.0019	2901.7000	0.6771
2511.7000	0.0016	2911.7000	0.5350
2521.7000	0.0017	2921.7000	0.4513
2531.7000	0.0017	2931.7000	0.3079
2541.7000	0.0021	2941.7000	0.1864
2551.7000	0.0022	2951.7000	0.1096
2561.7000	0.0019	2961.7000	0.0656
2571.7000	0.0019	2971.7000	0.0367
2581.7000	0.0031	2981.7000	0.0237
2591.7000	0.0033	2991.7000	0.0142
2601.7000	0.0038	3001.7000	0.0093
2611.7000	0.0055	3011.7000	0.0060
2621.7000	0.0075	3021.7000	0.0040
2631.7000	0.0122	3031.7000	0.0031
2641.7000	0.0203	3041.7000	0.0024
2651.7000	0.0260	3051.7000	0.0019
2661.7000	0.0409	3061.7000	0.0015
2671.7000	0.0814	3071.7000	0.0013
2681.7000	0.1281	3081.7000	0.0013
2691.7000	0.2186	3091.7000	0.0012
2701.7000	0.3854	3101.7000	0.0012
2711.7000	0.5917	3111.7000	0.0010
2721.7000	0.7308	3121.7000	0.0009
2731.7000	0.8842	3131.7000	0.0010
2741.7000	0.9349	3141.7000	0.0010
2751.7000	1.0000	3151.7000	0.0010
2761.7000	1.0000	3161.7000	0.0010
2771.7000	0.9865	3171.7000	0.0011
2781.7000	0.9602	3181.7000	0.0011
2791.7000	0.9349	3191.7000	0.0012
2801.7000	0.8000	3201.7000	0.0012
2811.7000	0.3044	3211.7000	0.0009
2821.7000	0.3451	3221.7000	0.0011
2831.7000	0.7663	3231.7000	0.0010
2841.7000	0.8337	3241.7000	0.0009
2851.7000	0.8505	3251.7000	0.0012

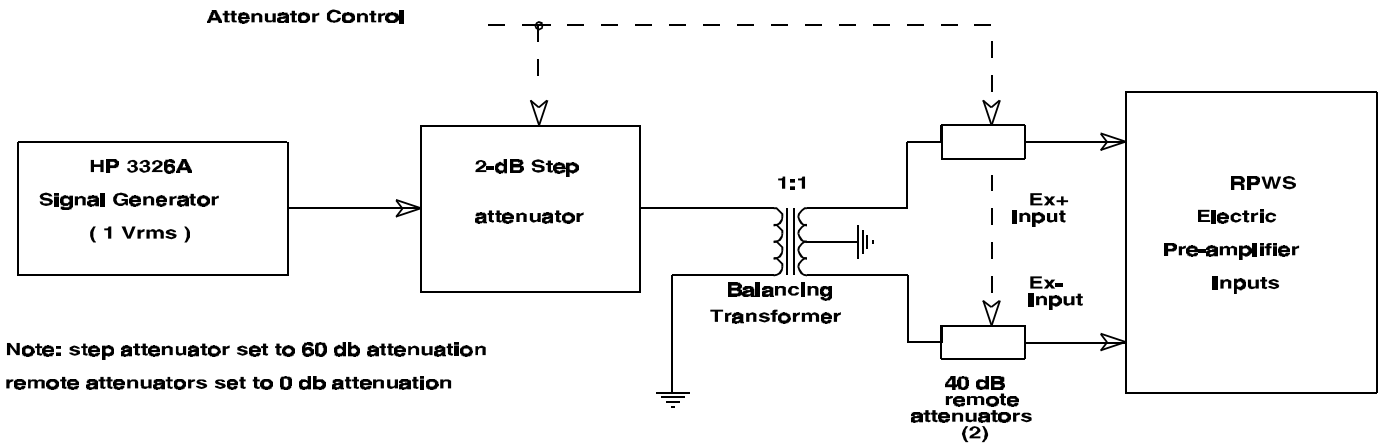

Figure 10.3.3.1.4

MFR Frequency Response Stimulus Configuration

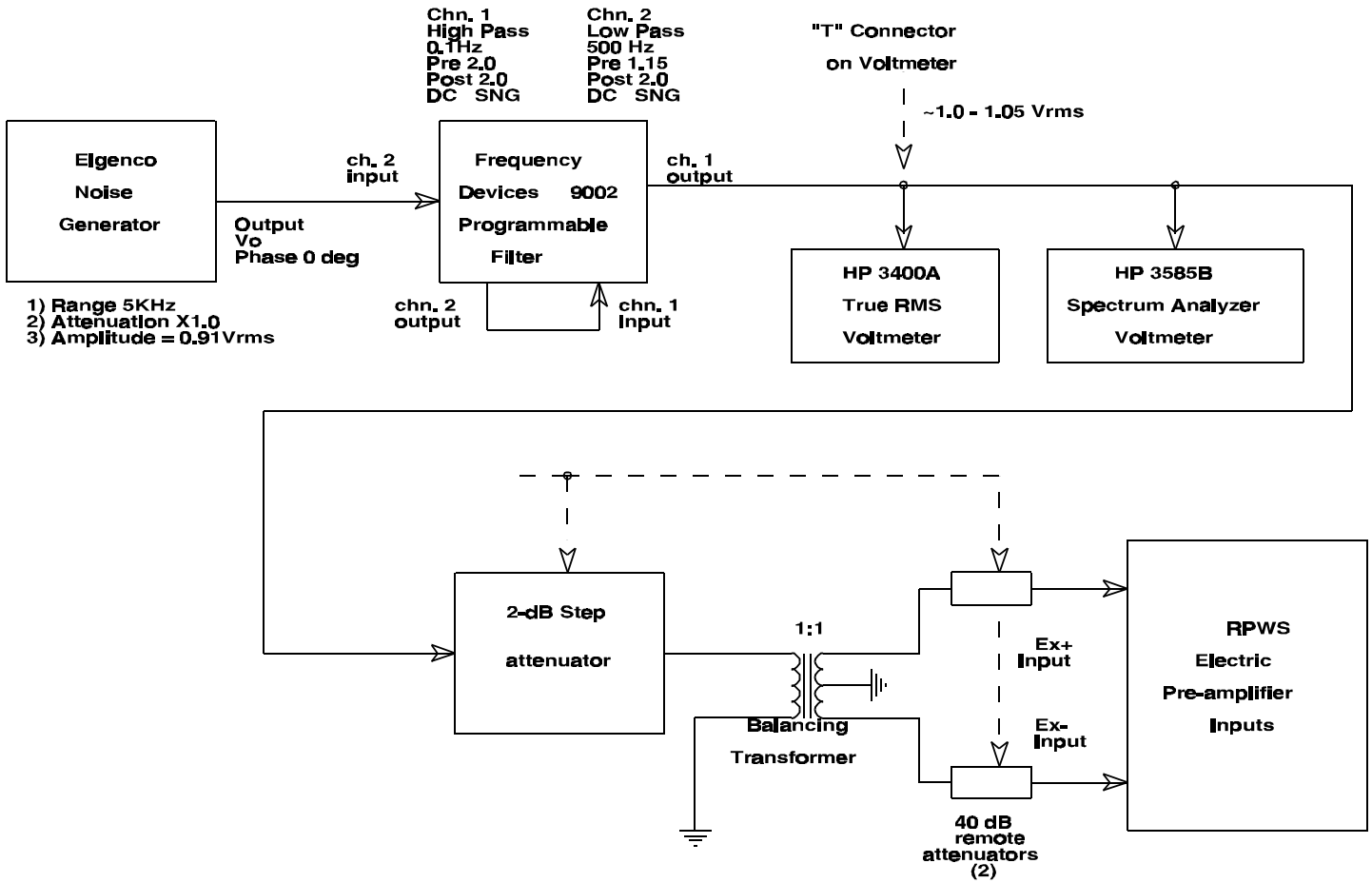

Figure 10.3.3.2.1

MFR Noise Bandwidth Calculation

Stimulus Configuration Band 1 Step 8

mfr_bw1.blk

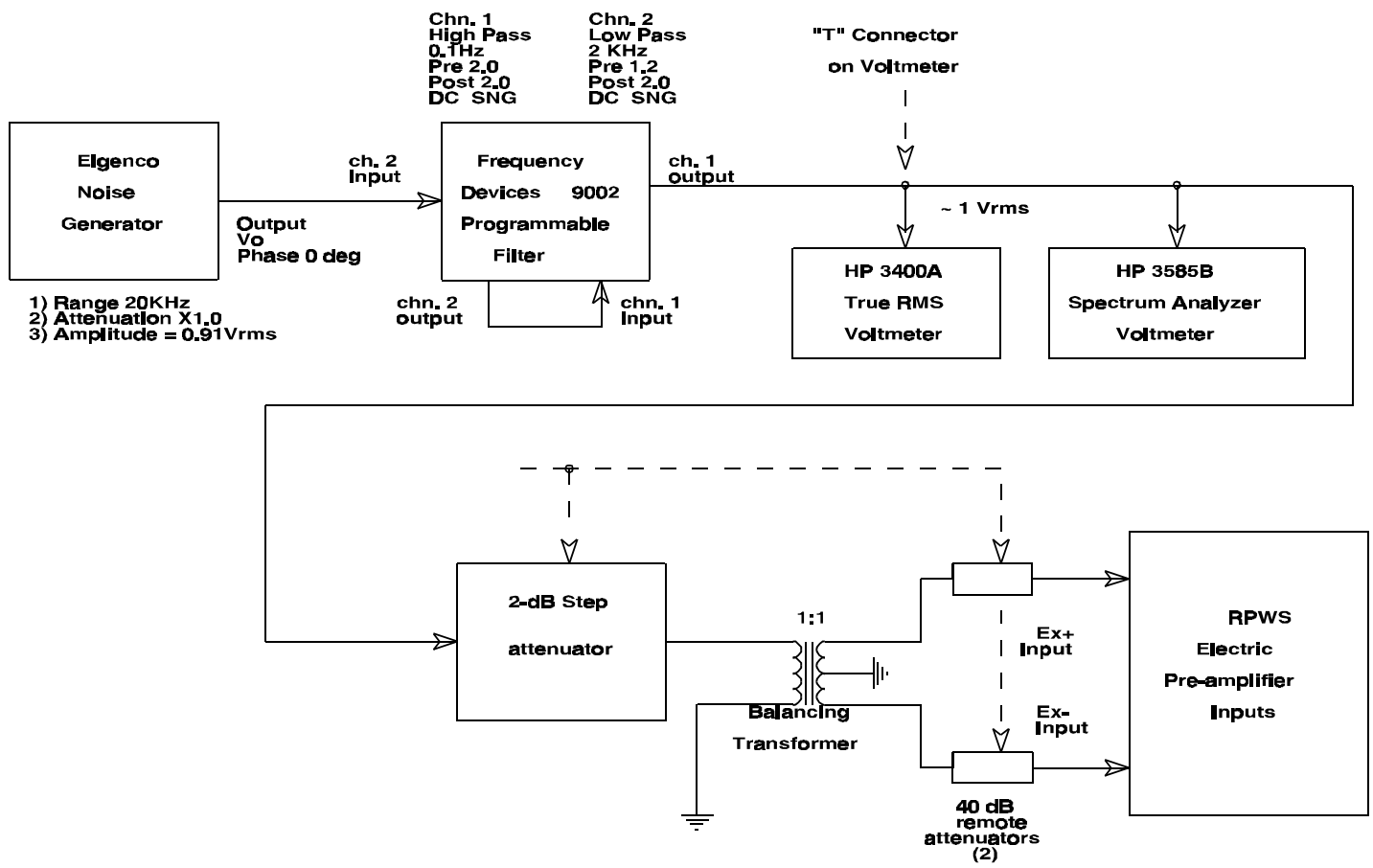

Figure 10.3.3.2.2

MFR Noise Bandwidth Calculation

Stimulus Configuration Band 2 Step 16

mfr_bw2.blk

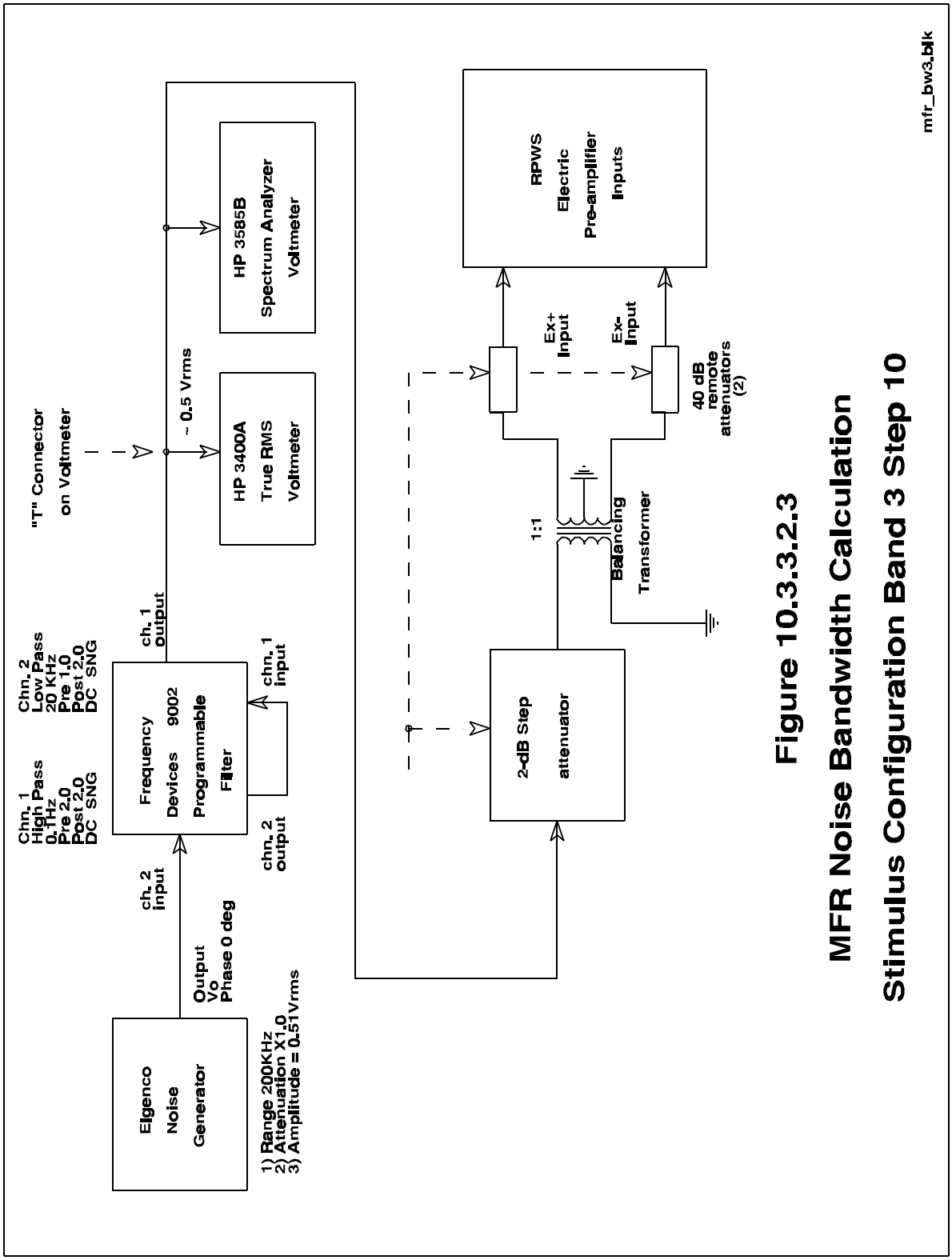

Figure 10.3.3.2.3

MFR Noise Bandwidth Calculation

Stimulus Configuration Band 3 Step 10

Table 10.3.3.2.1 MFR Band 1 Noise Bandwidth Calculation

Attenuation (dB)	Noise Bandwidth (Hz)
40.00000	3.95021
42.00000	4.71771
44.00000	5.44352
46.00000	5.45427
48.00000	4.80216
50.00000	5.57220
52.00000	5.03907
54.00000	7.46237
56.00000	7.67222
58.00000	7.13399
60.00000	5.28326
62.00000	5.48081
64.00000	5.67438
66.00000	4.45331
68.00000	5.30630
70.00000	5.45724
72.00000	7.46054
74.00000	5.65557
76.00000	5.89967
78.00000	6.08212
80.00000	4.84844

Average Noise Bandwidth = 5.65949 Hz

Table 10.3.3.2.2 MFR Band 2 Noise Bandwidth Calculations

Attenuation (dB)	Noise Bandwidth (Hz)
40.00000	23.16115
42.00000	18.32768
44.00000	20.09491
46.00000	30.10968
48.00000	19.30607
50.00000	19.76923
52.00000	19.63375
54.00000	15.33376
56.00000	12.49454
58.00000	17.21832
60.00000	25.28433
62.00000	20.03923
64.00000	28.66408
66.00000	26.96831
68.00000	18.16952
70.00000	17.46194
72.00000	11.97135
74.00000	16.02716
76.00000	15.62077
78.00000	13.97217
80.00000	17.90250

Average Noise Bandwidth = 19.40621 Hz

Table 10.3.3.2.3 MFR Band 3 Noise Bandwidth Calculation

Attenuation (dB)	Noise Bandwidth (Hz)
40.00000	126.94929
42.00000	150.54008
44.00000	117.92113
46.00000	167.13432
48.00000	170.56709
50.00000	165.75240
52.00000	183.88214
54.00000	183.68256
56.00000	168.28555
58.00000	116.19930
60.00000	104.42429
62.00000	120.06332
64.00000	123.04401
66.00000	116.88811
68.00000	152.99593
70.00000	156.18509
72.00000	109.23030
74.00000	143.60846
76.00000	106.50285
78.00000	128.32590
80.00000	103.17294

Average Noise Bandwidth = 138.82643 Hz

10.3.4 Receiver Noise Levels

10.3.4.1 In-Flight Receiver Noise Levels

In-flight noise levels of the MFR were obtained during the deployment of the electric antennas on Oct. 24-25, 1997. The noise levels were measured both with the antennas retracted, before the extension of the antennas, and after the antennas were extended. The noise levels were determined by looking for the data number with the peak number of occurrences in each channel. These peak data numbers were then converted into voltage from the amplitude tables in Section 10.3.1. The square of the voltage of each step was then divided by the effective noise bandwidth of the respective band. This noise level data is listed in Tables 10.3.4.1.1 and 10.3.4.1.2 and shown in Figures 10.3.4.1.1 and 10.3.4.1.2.

In-flight noise levels were also measured after the antennas were extended. The noise levels were also determined by looking for the data number with the peak number of occurrences in each channel. This was done during the time after the antennas were extended and when not in direction finding mode. The number of occurrences of data numbers would increase with increasing data number values. A peak number of occurrences would be reached and then the number of occurrences would decrease. The noise level is assumed to be at this peak. This is because the signals at the input to the receiver will be at the noise levels the greatest amount of time. Real signals will stay at constant levels for much less time then at the noise level. On some channels a second peak occurred greater than the first peak. The first peak was chosen as the noise level and the other peaks to be time dependent interference signals. There are times that the in-flight data is below the noise level. Data numbers below the measured noise level are handled by extending the calibration curves. The extended noise level data is listed in Tables 10.3.4.1.3 and 10.3.4.1.4 and shown in Figures 10.3.4.1.3 and 10.3.4.1.4.

The in-flight search coil noise levels were performed in the same manner as the electric antenna. The results are shown in Tables 10.3.4.1.5 and 10.3.4.1.6 and Figures 10.3.4.1.5 and 10.3.4.1.6.

10.3.4.2 Bench Level Receiver Noise Levels (Pre-flight)

A series of tests were performed on the ground before launch to determine the instrument noise level with a variety of loads across the inputs of the instrument. Figure 10.3.4.2.1 and Table 10.3.4.2.1 show the measured noise level of the MFR with a 220 pF capacitor across the input to the Ex antenna input. Figure 10.3.4.2.2 and Table 10.3.4.2.2 show the measured noise level of the MFR with a 220 pF capacitor in parallel with a 10 MΩ resistor across the input to the Ex antenna input. Figure 10.3.4.2.3 and Table 10.3.4.2.3 show the measured noise level of the MFR attached to the Bx search coil. The large signals observed at 60 Hz (and harmonics) is due to power line interference.

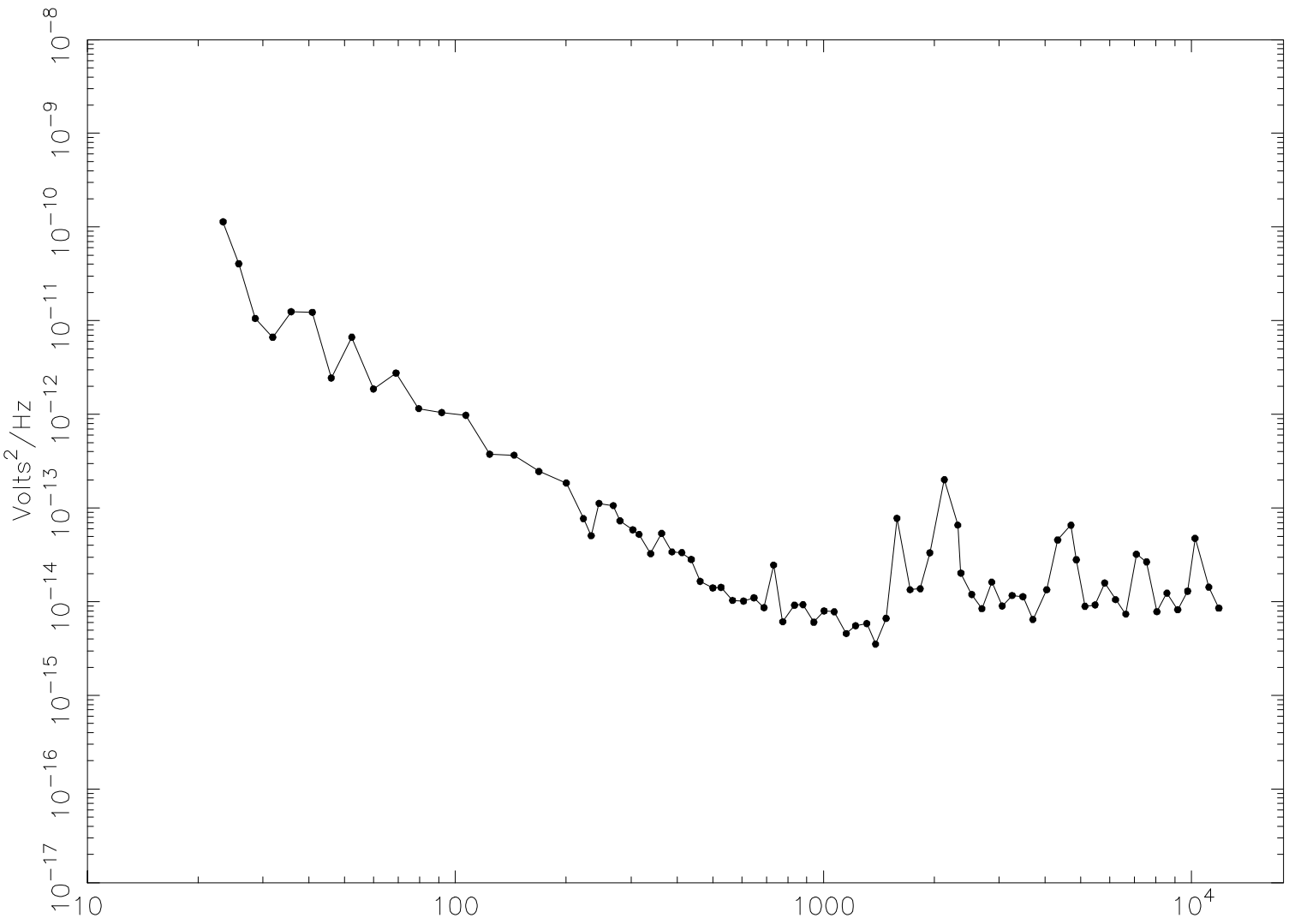

Figure 10.3.4.1.1

Table 10.3.4.1.1 MFR In-Flight ExLo Noise Plot (Antennas Retracted)

Channel	Frequency (Hz)	V^2/Hz	Channel	Frequency (Hz)	V^2/Hz
1	23.8910	1.1354e-10	41	932.4595	6.0518e-15
2	26.2510	4.0518e-11	42	995.7109	7.9681e-15
3	29.1468	1.0558e-11	43	1060.6372	7.7984e-15
4	32.4228	6.6563e-12	44	1144.2549	4.5675e-15
5	36.2695	1.2472e-11	45	1213.2041	5.5245e-15
6	40.8909	1.2282e-11	46	1302.0835	5.8439e-15
7	46.5109	2.4400e-12	47	1375.4399	3.5243e-15
8	52.8165	6.6600e-12	48	1470.0942	6.6346e-15
9	60.4319	1.8689e-12	49	1536.8867	7.7708e-14
10	69.4643	2.7574e-12	50	1671.8125	1.3394e-14
11	80.0469	1.1537e-12	51	1785.1016	1.3780e-14
12	92.3442	1.0451e-12	52	1899.1719	3.3167e-14
13	107.2421	9.7571e-13	53	2083.3320	2.0104e-13
14	124.3865	3.7530e-13	54	2269.5547	6.5814e-14
15	144.8837	3.6609e-13	55	2316.4336	2.0190e-14
16	169.0493	2.4586e-13	56	2481.5547	1.1940e-14
17	192.1108	1.8522e-13	57	2648.3047	8.4237e-15
18	214.6289	7.7150e-14	58	2816.7148	1.6227e-14
19	225.9814	5.0610e-14	59	3011.2422	9.0051e-15
20	237.3965	1.1206e-13	60	3208.0039	1.1666e-14
21	260.4165	1.0636e-13	61	3432.0820	1.1336e-14
22	272.0229	7.3057e-14	62	3659.0898	6.4628e-15
23	295.4307	5.8699e-14	63	3992.2891	1.3433e-14
24	307.2329	5.2347e-14	64	4279.2383	4.5689e-14
25	331.0381	3.2599e-14	65	4651.2734	6.5666e-14
26	355.1138	5.3664e-14	66	4813.1094	2.8069e-14
27	379.4644	3.3990e-14	67	5086.1094	8.9071e-15
28	404.0947	3.3388e-14	68	5419.2148	9.2386e-15
29	429.0103	2.8252e-14	69	5758.4805	1.5816e-14
30	454.2153	1.6498e-14	70	6162.3164	1.0529e-14
31	492.5771	1.4039e-14	71	6575.0586	7.3684e-15
32	518.5288	1.4177e-14	72	7027.5117	3.2088e-14
33	558.0356	1.0322e-14	73	7490.9219	2.6560e-14
34	598.2544	1.0136e-14	74	7997.7500	7.8360e-15
35	639.2046	1.0971e-14	75	8518.0195	1.2326e-14
36	680.9058	8.6330e-15	76	9120.0586	8.2070e-15
37	723.3794	2.4637e-14	77	9705.6328	1.2938e-14
38	766.6470	6.1046e-15	78	10165.0117	4.7480e-14
39	825.6113	9.1727e-15	79	11078.0430	1.4294e-14
40	870.8198	9.3085e-15	80	11799.3281	8.5456e-15

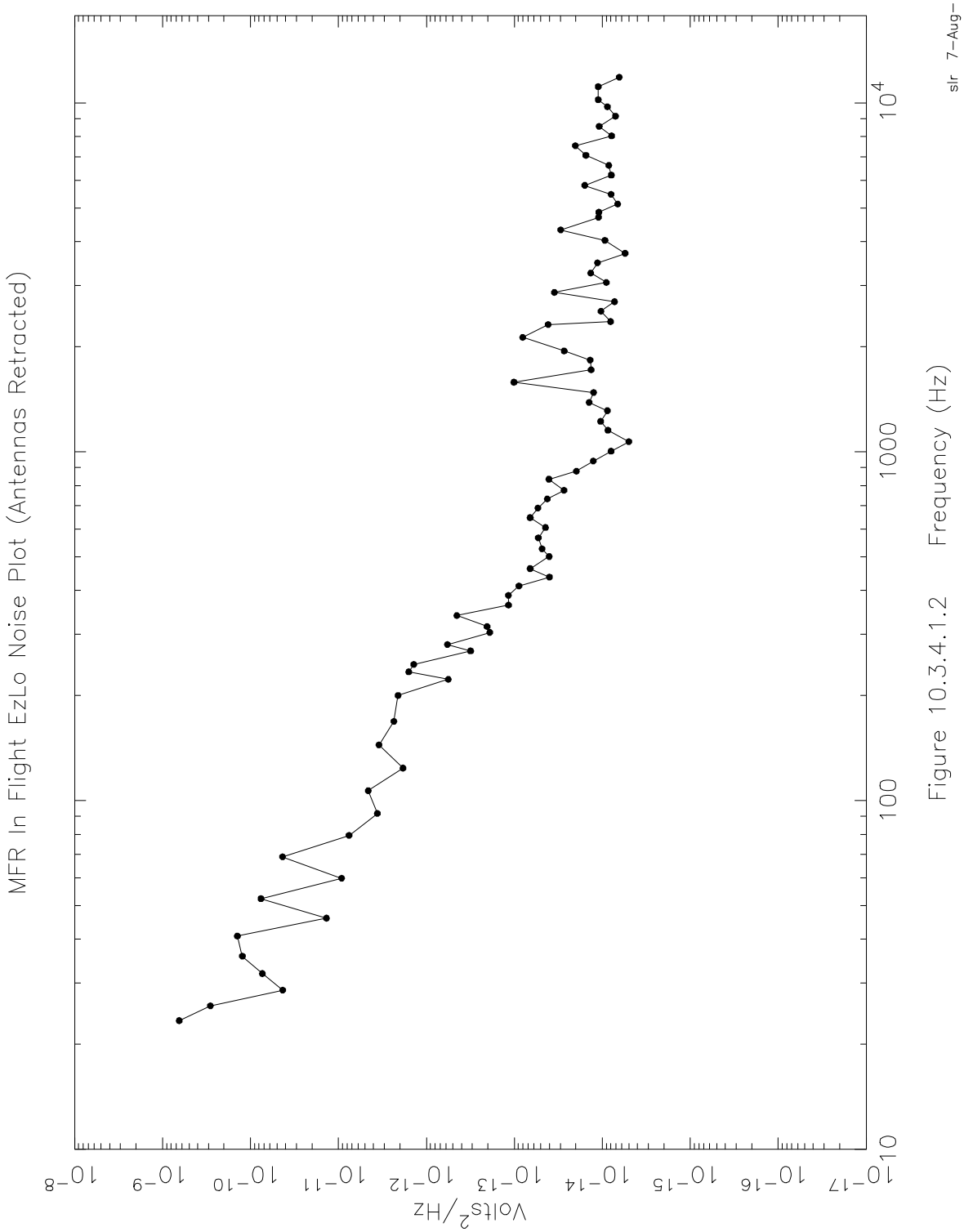

Figure 10.3.4.1.2

Table 10.3.4.1.2 MFR In-Flight EzLo Noise Plot (Antennas Retracted)

Channel	Frequency (Hz)	V^2/Hz	Channel	Frequency (Hz)	V^2/Hz
1	23.8910	6.4583e-10	41	932.4595	1.2627e-14
2	26.2510	2.8648e-10	42	995.7109	7.9681e-15
3	29.1468	4.2874e-11	43	1060.6372	4.9904e-15
4	32.4228	7.3389e-11	44	1144.2549	8.6352e-15
5	36.2695	1.2401e-10	45	1213.2041	1.0445e-14
6	40.8909	1.4093e-10	46	1302.0835	8.7299e-15
7	46.5109	1.3709e-11	47	1375.4399	1.4101e-14
8	52.8165	7.6005e-11	48	1470.0942	1.2543e-14
9	60.4319	9.2187e-12	49	1536.8867	1.0102e-13
10	69.4643	4.3276e-11	50	1671.8125	1.3394e-14
11	80.0469	7.5904e-12	51	1785.1016	1.3780e-14
12	92.3442	3.6184e-12	52	1899.1719	2.7152e-14
13	107.2421	4.5976e-12	53	2083.3320	8.0246e-14
14	124.3865	1.8400e-12	54	2269.5547	4.1397e-14
15	144.8837	3.4570e-12	55	2316.4336	8.0554e-15
16	169.0493	2.3490e-12	56	2481.5547	1.0400e-14
17	192.1108	2.0960e-12	57	2648.3047	7.2624e-15
18	214.6289	5.6508e-13	58	2816.7148	3.5095e-14
19	225.9814	1.5850e-12	59	3011.2422	9.0051e-15
20	237.3965	1.3955e-12	60	3208.0039	1.3530e-14
21	260.4165	3.1481e-13	61	3432.0820	1.1336e-14
22	272.0229	5.7636e-13	62	3659.0898	5.5068e-15
23	295.4307	1.8974e-13	63	3992.2891	9.3285e-15
24	307.2329	2.0410e-13	64	4279.2383	2.9719e-14
25	331.0381	4.5115e-13	65	4651.2734	1.1051e-14
26	355.1138	1.1650e-13	66	4813.1094	1.0962e-14
27	379.4644	1.1679e-13	67	5086.1094	6.6896e-15
28	404.0947	8.8877e-14	68	5419.2148	7.9658e-15
29	429.0103	3.9839e-14	69	5758.4805	1.5816e-14
30	454.2153	6.5997e-14	70	6162.3164	7.9083e-15
31	492.5771	4.0209e-14	71	6575.0586	8.4580e-15
32	518.5288	4.8316e-14	72	7027.5117	1.5384e-14
33	558.0356	5.3318e-14	73	7490.9219	2.0335e-14
34	598.2544	4.4316e-14	74	7997.7500	7.8360e-15
35	639.2046	6.6102e-14	75	8518.0195	1.0834e-14
36	680.9058	5.3949e-14	76	9120.0586	7.0762e-15
37	723.3794	4.2132e-14	77	9705.6328	8.7747e-15
38	766.6470	2.7207e-14	78	10165.0117	1.1117e-14
39	825.6113	4.0454e-14	79	11078.0430	1.1128e-14
40	870.8198	1.9695e-14	80	11799.3281	6.4191e-15

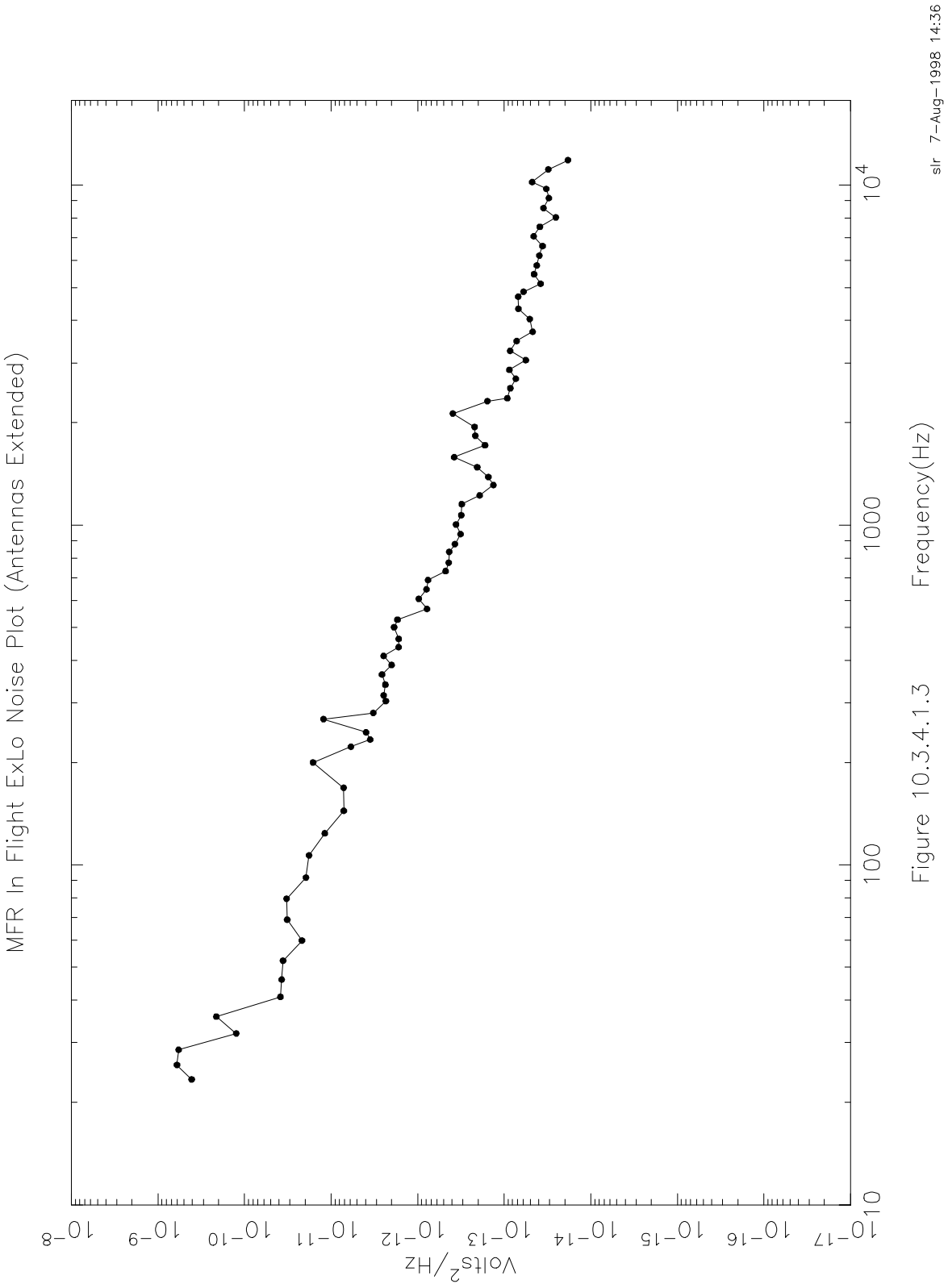

Figure 10.3.4.1.3

Table 10.3.4.1.3 MFR In-Flight ExLo Noise Plot (Antennas Extended)

Channel	Frequency (Hz)	V^2/Hz	Channel	Frequency (Hz)	V^2/Hz
1	23.8910	4.0811e-10	41	932.4595	3.1964e-13
2	26.2510	6.0413e-10	42	995.7109	3.6061e-13
3	29.1468	5.7717e-10	43	1060.6372	3.1367e-13
4	32.4228	1.2465e-10	44	1144.2549	3.0997e-13
5	36.2695	2.1238e-10	45	1213.2041	1.9161e-13
6	40.8909	3.8463e-11	46	1302.0835	1.3314e-13
7	46.5109	3.7212e-11	47	1375.4399	1.5268e-13
8	52.8165	3.5880e-11	48	1470.0942	2.0488e-13
9	60.4319	2.1751e-11	49	1536.8867	3.7918e-13
10	69.4643	3.2183e-11	50	1671.8125	1.6659e-13
11	80.0469	3.2811e-11	51	1785.1016	2.1584e-13
12	92.3442	1.9510e-11	52	1899.1719	2.1997e-13
13	107.2421	1.7957e-11	53	2083.3320	3.9318e-13
14	124.3865	1.1814e-11	54	2269.5547	1.5625e-13
15	144.8837	7.1360e-12	55	2316.4336	9.2016e-14
16	169.0493	7.1546e-12	56	2481.5547	8.4904e-14
17	192.1108	1.6191e-11	57	2648.3047	7.3338e-14
18	214.6289	5.9162e-12	58	2816.7148	8.7134e-14
19	225.9814	3.5466e-12	59	3011.2422	5.6296e-14
20	237.3965	3.9471e-12	60	3208.0039	8.5563e-14
21	260.4165	1.2268e-11	61	3432.0820	7.1924e-14
22	272.0229	3.2576e-12	62	3659.0898	4.6846e-14
23	295.4307	2.3336e-12	63	3992.2891	5.0787e-14
24	307.2329	2.4793e-12	64	4279.2383	6.8657e-14
25	331.0381	2.3636e-12	65	4651.2734	6.9076e-14
26	355.1138	2.5875e-12	66	4813.1094	5.9693e-14
27	379.4644	2.0027e-12	67	5086.1094	3.8049e-14
28	404.0947	2.4788e-12	68	5419.2148	4.5291e-14
29	429.0103	1.6639e-12	69	5758.4805	4.2108e-14
30	454.2153	1.6574e-12	70	6162.3164	3.9354e-14
31	492.5771	1.8739e-12	71	6575.0586	3.6124e-14
32	518.5288	1.7124e-12	72	7027.5117	4.5620e-14
33	558.0356	7.8100e-13	73	7490.9219	3.8777e-14
34	598.2544	9.6934e-13	74	7997.7500	2.5386e-14
35	639.2046	7.9098e-13	75	8518.0195	3.5099e-14
36	680.9058	7.5913e-13	76	9120.0586	3.0526e-14
37	723.3794	4.7622e-13	77	9705.6328	3.2634e-14
38	766.6470	4.3711e-13	78	10165.0117	4.7480e-14
39	825.6113	4.3101e-13	79	11078.0430	3.0913e-14
40	870.8198	3.7124e-13	80	11799.3281	1.8380e-14

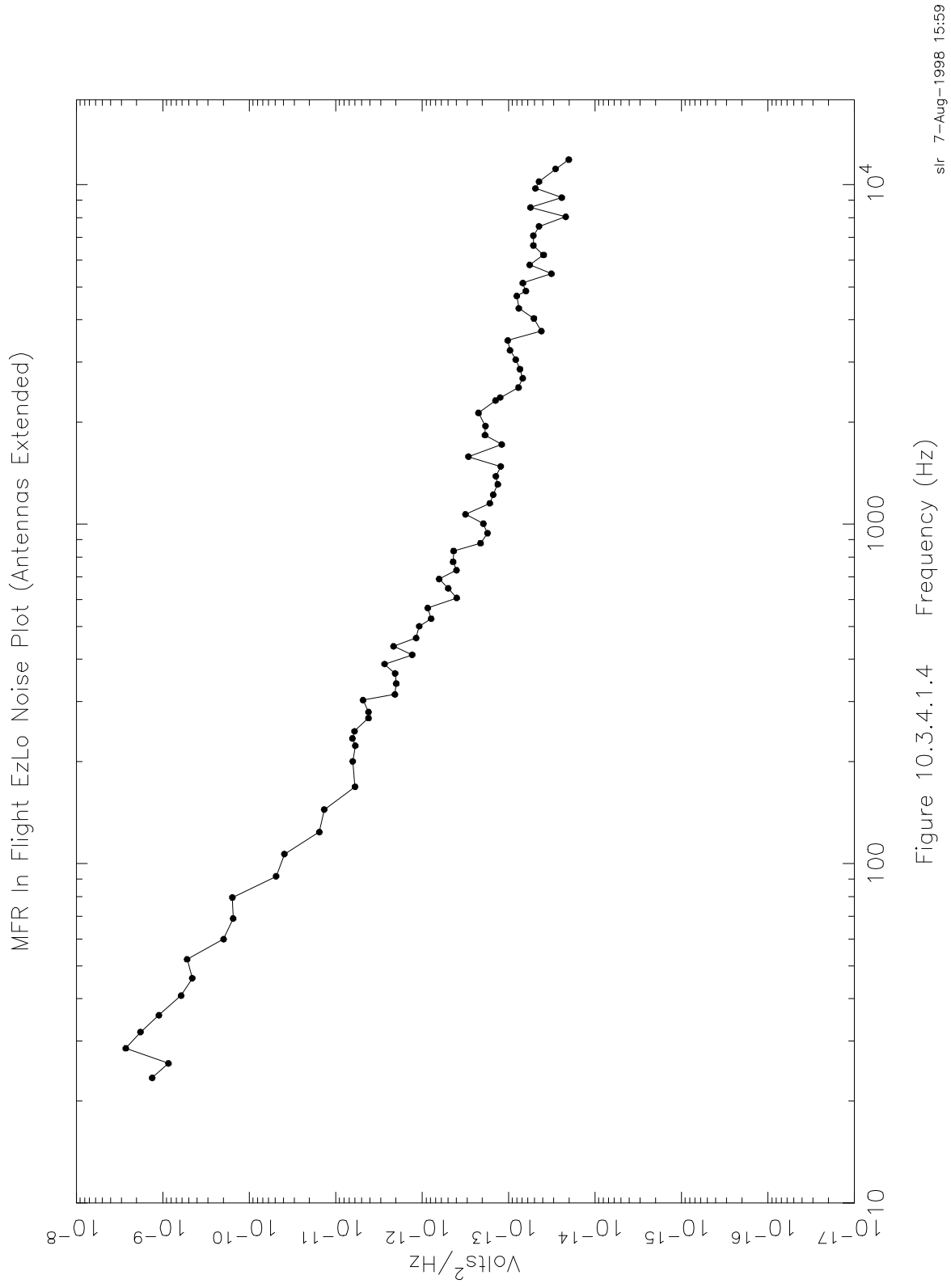

Figure 10.3.4.1.4

Table 10.3.4.1.4 MFR In-Flight EzLo Noise Plot (Antennas Extended)

Channel	Frequency (Hz)	V^2/Hz	Channel	Frequency (Hz)	V^2/Hz
1	23.8910	1.3205e-09	41	932.4595	1.7463e-13
2	26.2510	8.5894e-10	42	995.7109	1.9572e-13
3	29.1468	2.6828e-09	43	1060.6372	3.1367e-13
4	32.4228	1.8139e-09	44	1144.2549	1.6479e-13
5	36.2695	1.1104e-09	45	1213.2041	1.5071e-13
6	40.8909	6.1224e-10	46	1302.0835	1.3314e-13
7	46.5109	4.5507e-10	47	1375.4399	1.3988e-13
8	52.8165	5.2392e-10	48	1470.0942	1.2315e-13
9	60.4319	1.9753e-10	49	1536.8867	2.9194e-13
10	69.4643	1.5389e-10	50	1671.8125	1.2008e-13
11	80.0469	1.5702e-10	51	1785.1016	1.8700e-13
12	92.3442	4.8643e-11	52	1899.1719	1.8434e-13
13	107.2421	3.9302e-11	53	2083.3320	2.2221e-13
14	124.3865	1.5432e-11	54	2269.5547	1.4127e-13
15	144.8837	1.3529e-11	55	2316.4336	1.2469e-13
16	169.0493	5.9709e-12	56	2481.5547	7.6628e-14
17	192.1108	6.3376e-12	57	2648.3047	6.8599e-14
18	214.6289	5.9162e-12	58	2816.7148	7.3605e-14
19	225.9814	6.4063e-12	59	3011.2422	8.2629e-14
20	237.3965	6.0294e-12	60	3208.0039	9.6107e-14
21	260.4165	4.1584e-12	61	3432.0820	1.0198e-13
22	272.0229	4.1539e-12	62	3659.0898	4.1646e-14
23	295.4307	4.8131e-12	63	3992.2891	5.0787e-14
24	307.2329	2.0596e-12	64	4279.2383	7.6183e-14
25	331.0381	1.9877e-12	65	4651.2734	8.0039e-14
26	355.1138	2.0570e-12	66	4813.1094	6.3150e-14
27	379.4644	2.7209e-12	67	5086.1094	6.8368e-14
28	404.0947	1.3039e-12	68	5419.2148	3.1860e-14
29	429.0103	2.1406e-12	69	5758.4805	5.6788e-14
30	454.2153	1.1709e-12	70	6162.3164	3.9354e-14
31	492.5771	1.0805e-12	71	6575.0586	5.1463e-14
32	518.5288	7.8642e-13	72	7027.5117	5.1694e-14
33	558.0356	8.5808e-13	73	7490.9219	4.4314e-14
34	598.2544	3.9693e-13	74	7997.7500	2.1763e-14
35	639.2046	4.9760e-13	75	8518.0195	5.5658e-14
36	680.9058	6.3583e-13	76	9120.0586	2.4120e-14
37	723.3794	4.0019e-13	77	9705.6328	4.8754e-14
38	766.6470	4.3711e-13	78	10165.0117	4.4467e-14
39	825.6113	4.3101e-13	79	11078.0430	2.8488e-14
40	870.8198	2.1118e-13	80	11799.3281	2.0092e-14

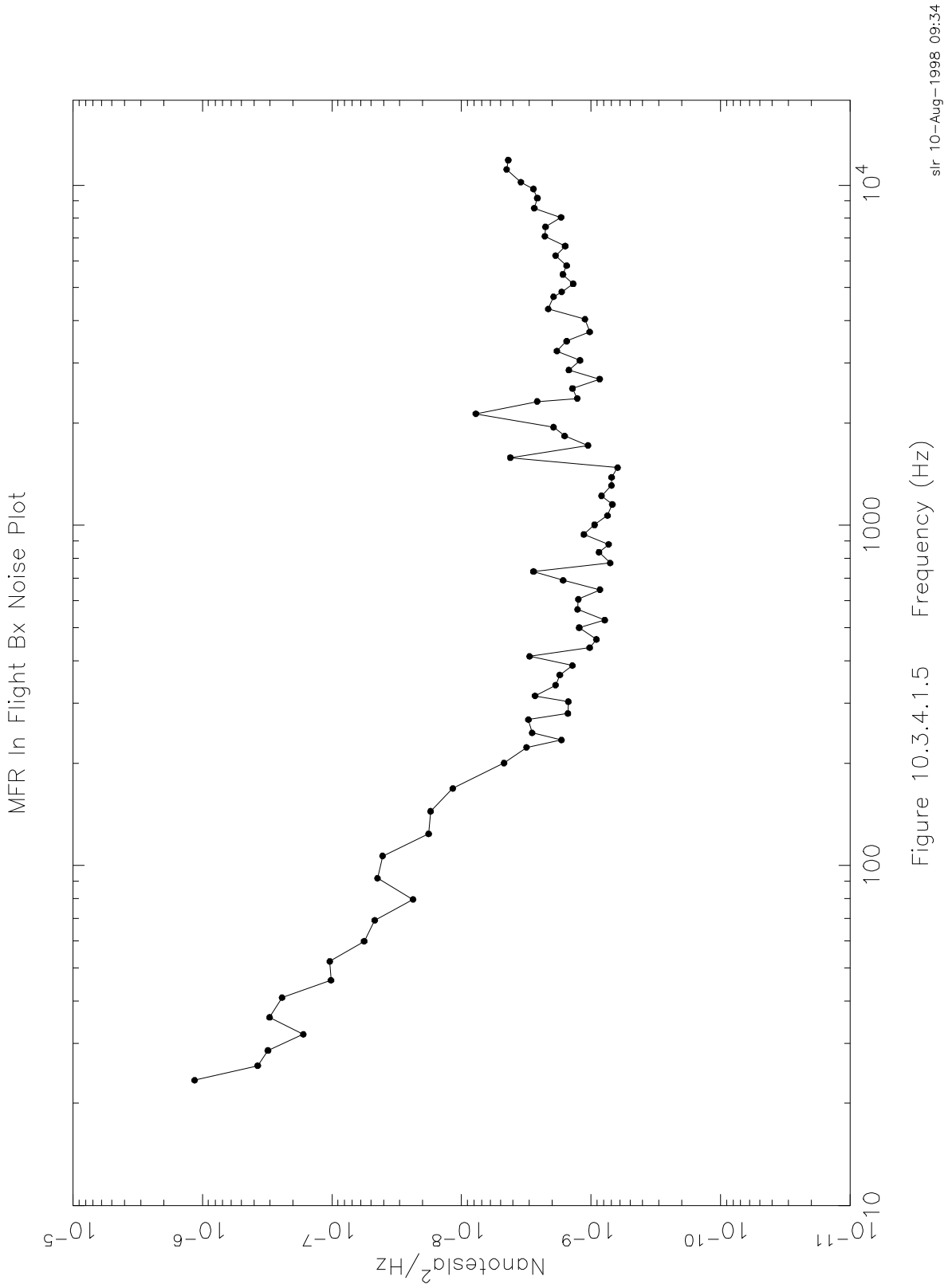

Figure 10.3.4.1.5

Table10.3.4.1.5 MFR In-Flight Bx Noise Plot

Channel	Frequency (Hz)	nT^2/Hz	Channel	Frequency (Hz)	nT^2/Hz
1	23.8910	1.1523e-06	41	932.4595	1.1378e-09
2	26.2510	3.7454e-07	42	995.7109	9.4126e-10
3	29.1468	3.1279e-07	43	1060.6372	7.4746e-10
4	32.4228	1.6671e-07	44	1144.2549	6.8548e-10
5	36.2695	3.0351e-07	45	1213.2041	8.3044e-10
6	40.8909	2.4326e-07	46	1302.0835	6.9529e-10
7	46.5109	1.0187e-07	47	1375.4399	6.9429e-10
8	52.8165	1.0431e-07	48	1470.0942	6.2471e-10
9	60.4319	5.6566e-08	49	1536.8867	4.2049e-09
10	69.4643	4.6870e-08	50	1671.8125	1.0582e-09
11	80.0469	2.3761e-08	51	1785.1016	1.6004e-09
12	92.3442	4.4587e-08	52	1899.1719	1.9488e-09
13	107.2421	4.0754e-08	53	2083.3320	7.7664e-09
14	124.3865	1.7959e-08	54	2269.5547	2.6058e-09
15	144.8837	1.7385e-08	55	2316.4336	1.2799e-09
16	169.0493	1.1700e-08	56	2481.5547	1.3926e-09
17	192.1108	4.7096e-09	57	2648.3047	8.5861e-10
18	214.6289	3.1502e-09	58	2816.7148	1.4835e-09
19	225.9814	1.6969e-09	59	3011.2422	1.2182e-09
20	237.3965	2.8536e-09	60	3208.0039	1.8366e-09
21	260.4165	3.0461e-09	61	3432.0820	1.5443e-09
22	272.0229	1.5111e-09	62	3659.0898	1.0244e-09
23	295.4307	1.5013e-09	63	3992.2891	1.1157e-09
24	307.2329	2.7097e-09	64	4279.2383	2.1414e-09
25	331.0381	1.8803e-09	65	4651.2734	1.9501e-09
26	355.1138	1.7432e-09	66	4813.1094	1.6882e-09
27	379.4644	1.3940e-09	67	5086.1094	1.3772e-09
28	404.0947	2.9860e-09	68	5419.2148	1.6506e-09
29	429.0103	1.0266e-09	69	5758.4805	1.5448e-09
30	454.2153	9.0919e-10	70	6162.3164	1.8802e-09
31	492.5771	1.2365e-09	71	6575.0586	1.5853e-09
32	518.5288	7.8362e-10	72	7027.5117	2.2740e-09
33	558.0356	1.2749e-09	73	7490.9219	2.2504e-09
34	598.2544	1.2549e-09	74	7997.7500	1.7064e-09
35	639.2046	8.5323e-10	75	8518.0195	2.7488e-09
36	680.9058	1.6440e-09	76	9120.0586	2.5965e-09
37	723.3794	2.7861e-09	77	9705.6328	2.7908e-09
38	766.6470	7.1390e-10	78	10165.0117	3.4846e-09
39	825.6113	8.7139e-10	79	11078.0430	4.4883e-09
40	870.8198	7.3234e-10	80	11799.3281	4.3636e-09

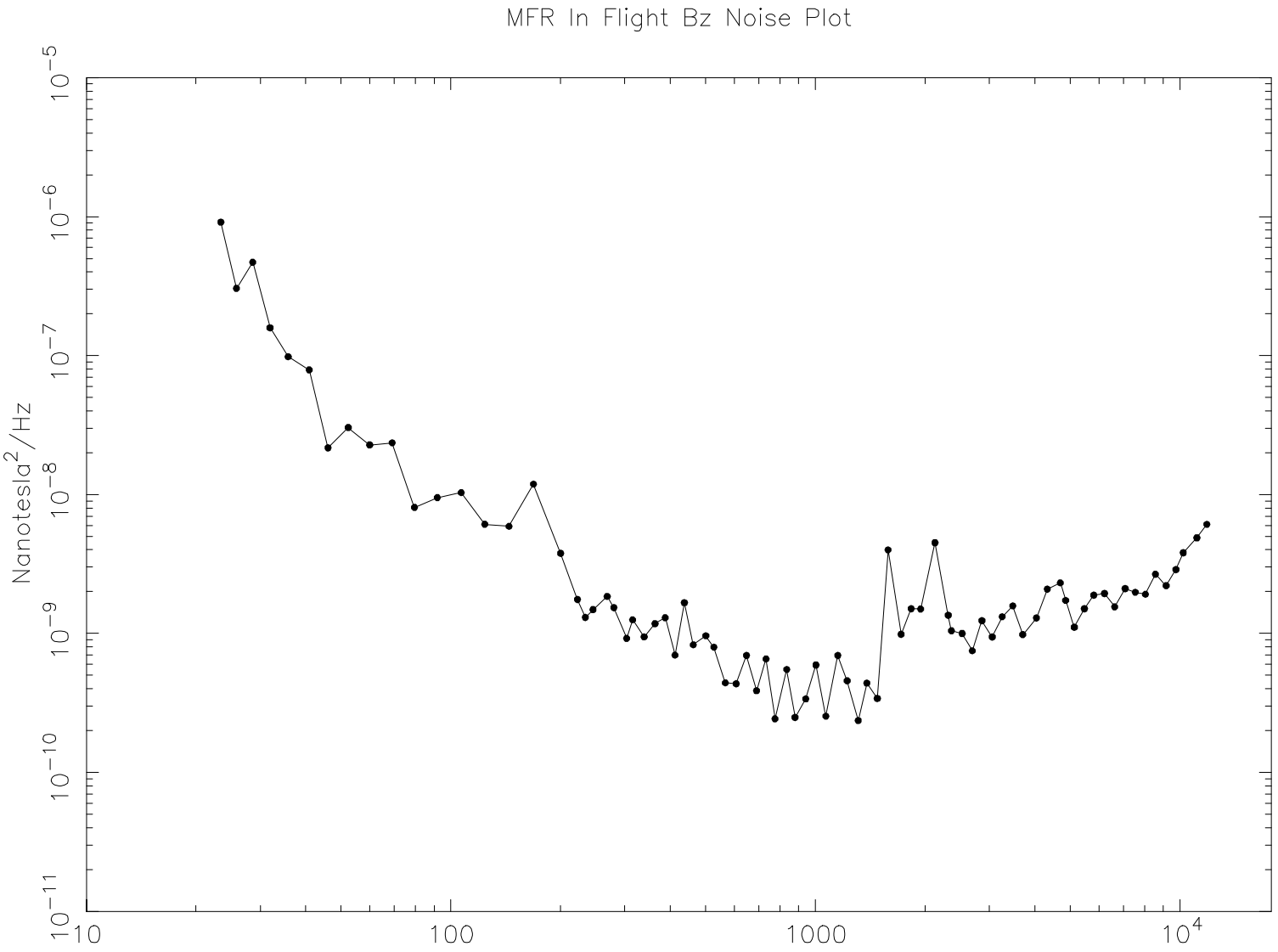

Figure 10.3.4.1.6

Table 10.3.4.1.6 MFR In-Flight Bz Noise Plot

Channel	Frequency (Hz)	nT^2/Hz	Channel	Frequency (Hz)	nT^2/Hz
1	23.8910	9.1277e-07	41	932.4595	3.3804e-10
2	26.2510	3.0419e-07	42	995.7109	5.9347e-10
3	29.1468	4.6934e-07	43	1060.6372	2.5353e-10
4	32.4228	1.5834e-07	44	1144.2549	6.9404e-10
5	36.2695	9.8221e-08	45	1213.2041	4.5673e-10
6	40.8909	7.8757e-08	46	1302.0835	2.3619e-10
7	46.5109	2.1677e-08	47	1375.4399	4.3871e-10
8	52.8165	3.0336e-08	48	1470.0942	3.4071e-10
9	60.4319	2.2778e-08	49	1536.8867	3.9897e-09
10	69.4643	2.3534e-08	50	1671.8125	9.8639e-10
11	80.0469	8.0765e-09	51	1785.1016	1.5070e-09
12	92.3442	9.4981e-09	52	1899.1719	1.5019e-09
13	107.2421	1.0332e-08	53	2083.3320	4.5017e-09
14	124.3865	6.1034e-09	54	2269.5547	1.3527e-09
15	144.8837	5.9092e-09	55	2316.4336	1.0469e-09
16	169.0493	1.1862e-08	56	2481.5547	9.9770e-10
17	192.1108	3.7693e-09	57	2648.3047	7.5012e-10
18	214.6289	1.7545e-09	58	2816.7148	1.2342e-09
19	225.9814	1.3059e-09	59	3011.2422	9.4287e-10
20	237.3965	1.4832e-09	60	3208.0039	1.3190e-09
21	260.4165	1.8473e-09	61	3432.0820	1.5776e-09
22	272.0229	1.5335e-09	62	3659.0898	9.8083e-10
23	295.4307	9.2171e-10	63	3992.2891	1.2936e-09
24	307.2329	1.2534e-09	64	4279.2383	2.0814e-09
25	331.0381	9.4531e-10	65	4651.2734	2.3160e-09
26	355.1138	1.1752e-09	66	4813.1094	1.7309e-09
27	379.4644	1.3002e-09	67	5086.1094	1.1086e-09
28	404.0947	6.9871e-10	68	5419.2148	1.5092e-09
29	429.0103	1.6640e-09	69	5758.4805	1.8866e-09
30	454.2153	8.2904e-10	70	6162.3164	1.9420e-09
31	492.5771	9.6200e-10	71	6575.0586	1.5559e-09
32	518.5288	7.9638e-10	72	7027.5117	2.1010e-09
33	558.0356	4.4088e-10	73	7490.9219	1.9805e-09
34	598.2544	4.3394e-10	74	7997.7500	1.9164e-09
35	639.2046	6.9412e-10	75	8518.0195	2.6711e-09
36	680.9058	3.8728e-10	76	9120.0586	2.2083e-09
37	723.3794	6.5521e-10	77	9705.6328	2.8832e-09
38	766.6470	2.4288e-10	78	10165.0117	3.8164e-09
39	825.6113	5.5078e-10	79	11078.0430	4.8872e-09
40	870.8198	2.4876e-10	80	11799.3281	6.0993e-09

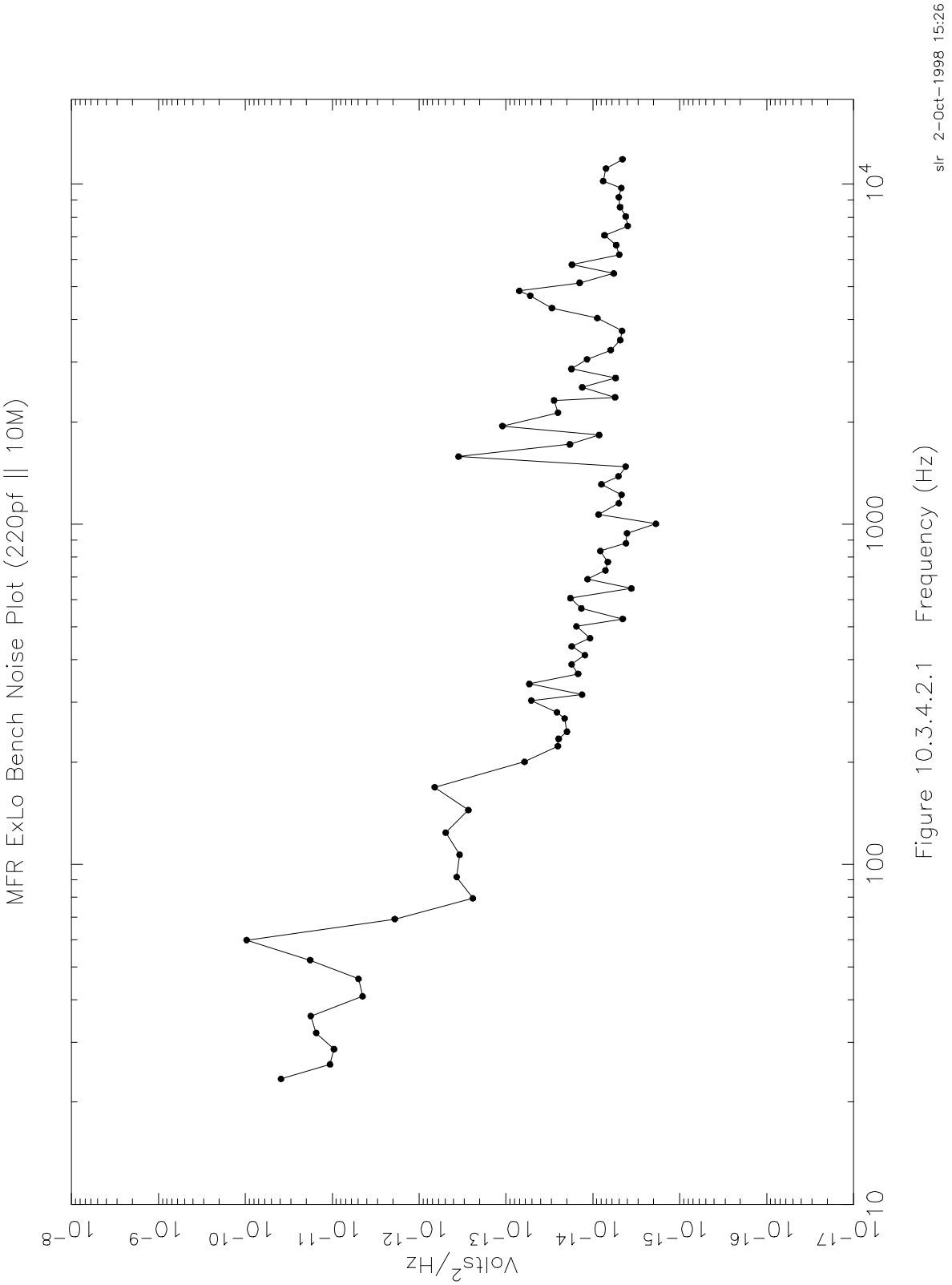

Figure 10.3.4.2.1

Table 10.3.4.2.1 MFR ExLo Bench Noise Plot (220 pF || 10 MΩ)

Channel	Frequency (Hz)	V^2/Hz	Channel	Frequency (Hz)	V^2/Hz
1	23.8910	3.8826e-11	41	932.4595	4.0367e-15
2	26.2510	1.0598e-11	42	995.7109	1.8801e-15
3	29.1468	9.5246e-12	43	1060.6372	8.5983e-15
4	32.4228	1.5304e-11	44	1144.2549	5.0360e-15
5	36.2695	1.7657e-11	45	1213.2041	4.6635e-15
6	40.8909	4.4648e-12	46	1302.0835	7.9548e-15
7	46.5109	4.9808e-12	47	1375.4399	5.0760e-15
8	52.8165	1.7952e-11	48	1470.0942	4.1985e-15
9	60.4319	9.6492e-11	49	1536.8867	3.5152e-13
10	69.4643	1.9065e-12	50	1671.8125	1.8381e-14
11	80.0469	2.4007e-13	51	1785.1016	8.4549e-15
12	92.3442	3.6885e-13	52	1899.1719	1.0964e-13
13	107.2421	3.4145e-13	53	2083.3320	2.5231e-14
14	124.3865	4.9362e-13	54	2269.5547	2.7978e-14
15	144.8837	2.7084e-13	55	2316.4336	5.5457e-15
16	169.0493	6.6306e-13	56	2481.5547	1.3224e-14
17	192.1108	6.1263e-14	57	2648.3047	5.4647e-15
18	214.6289	2.5308e-14	58	2816.7148	1.7627e-14
19	225.9814	2.4801e-14	59	3011.2422	1.1679e-14
20	237.3965	1.9852e-14	60	3208.0039	6.2201e-15
21	260.4165	2.1159e-14	61	3432.0820	4.8378e-15
22	272.0229	2.5866e-14	62	3659.0898	4.5950e-15
23	295.4307	5.1135e-14	63	3992.2891	8.8737e-15
24	307.2329	1.3298e-14	64	4279.2383	2.9541e-14
25	331.0381	5.3696e-14	65	4651.2734	5.2517e-14
26	355.1138	1.4792e-14	66	4813.1094	7.0365e-14
27	379.4644	1.7545e-14	67	5086.1094	1.4193e-14
28	404.0947	1.2339e-14	68	5419.2148	5.7480e-15
29	429.0103	1.7521e-14	69	5758.4805	1.7403e-14
30	454.2153	1.0763e-14	70	6162.3164	4.9639e-15
31	492.5771	1.5479e-14	71	6575.0586	5.3756e-15
32	518.5288	4.5320e-15	72	7027.5117	7.3359e-15
33	558.0356	1.3545e-14	73	7490.9219	3.9658e-15
34	598.2544	1.8104e-14	74	7997.7500	4.1861e-15
35	639.2046	3.5986e-15	75	8518.0195	4.8568e-15
36	680.9058	1.1516e-14	76	9120.0586	5.0310e-15
37	723.3794	7.1553e-15	77	9705.6328	4.6990e-15
38	766.6470	6.7307e-15	78	10165.0117	7.5990e-15
39	825.6113	8.1921e-15	79	11078.0430	7.0746e-15
40	870.8198	4.1560e-15	80	11799.3281	4.5642e-15

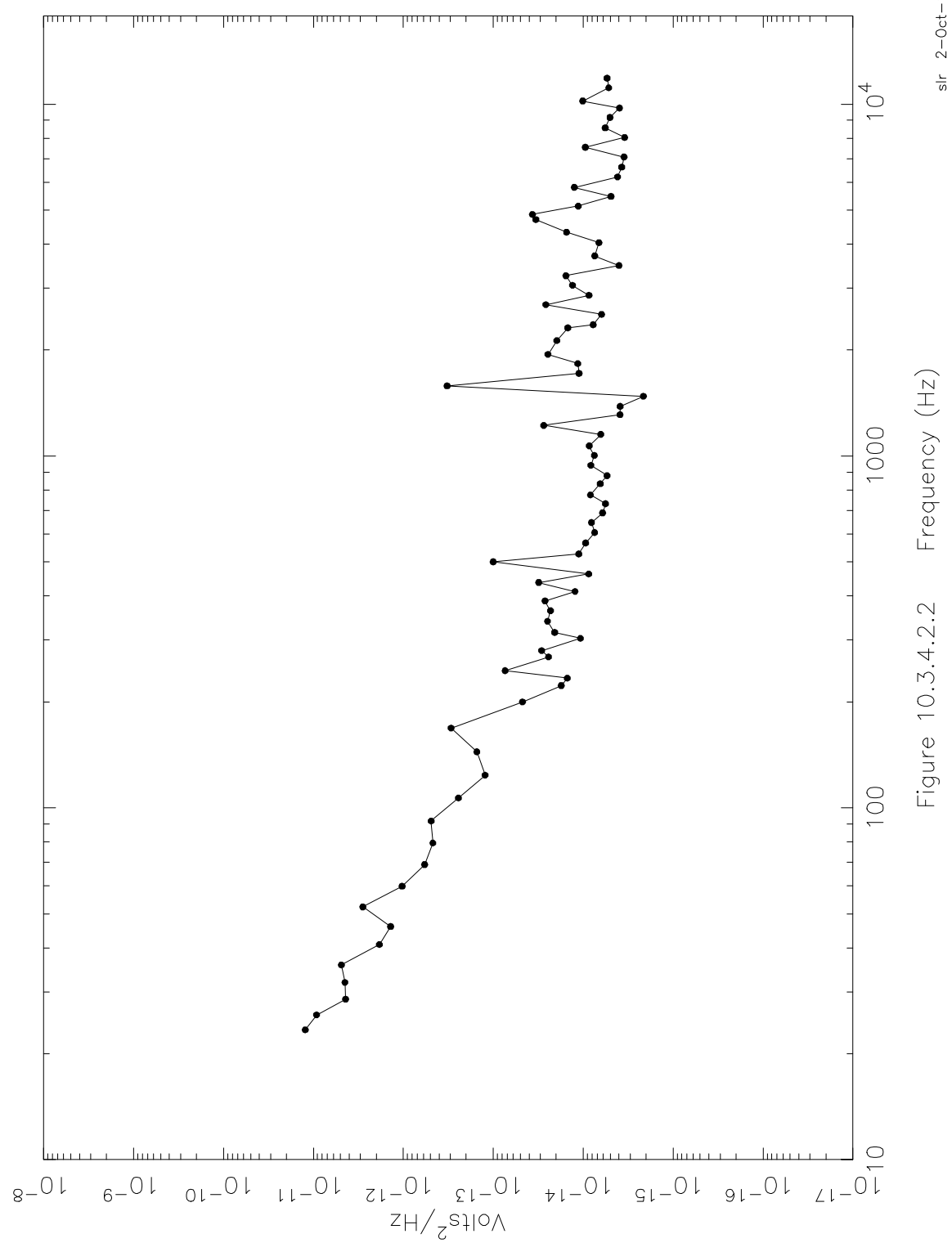

Figure 10.3.4.2.2

Table 10.3.4.2.2 MFR In-Flight ExLo Noise Plot (220pf)

Channel	Frequency (Hz)	V^2/Hz	Channel	Frequency (Hz)	V^2/Hz
1	23.8910	1.2353e-11	41	932.4595	8.2379e-15
2	26.2510	9.2171e-12	42	995.7109	7.5204e-15
3	29.1468	4.3857e-12	43	1060.6372	8.5983e-15
4	32.4228	4.4753e-12	44	1144.2549	6.3738e-15
5	36.2695	4.8878e-12	45	1213.2041	2.7507e-14
6	40.8909	1.8450e-12	46	1302.0835	3.8980e-15
7	46.5109	1.3824e-12	47	1375.4399	3.8858e-15
8	52.8165	2.8241e-12	48	1470.0942	2.1423e-15
9	60.4319	1.0326e-12	49	1536.8867	3.2676e-13
10	69.4643	5.8028e-13	50	1671.8125	1.1118e-14
11	80.0469	4.7054e-13	51	1785.1016	1.1510e-14
12	92.3442	4.9113e-13	52	1899.1719	2.4736e-14
13	107.2421	2.4447e-13	53	2083.3320	1.9642e-14
14	124.3865	1.2341e-13	54	2269.5547	1.4802e-14
15	144.8837	1.5236e-13	55	2316.4336	7.7457e-15
16	169.0493	2.9466e-13	56	2481.5547	6.2499e-15
17	192.1108	4.7442e-14	57	2648.3047	2.6021e-14
18	214.6289	1.7574e-14	58	2816.7148	8.6379e-15
19	225.9814	1.5003e-14	59	3011.2422	1.3186e-14
20	237.3965	7.3837e-14	60	3208.0039	1.5596e-14
21	260.4165	2.4289e-14	61	3432.0820	3.9982e-15
22	272.0229	2.8998e-14	62	3659.0898	7.4435e-15
23	295.4307	1.0742e-14	63	3992.2891	6.6655e-15
24	307.2329	2.0780e-14	64	4279.2383	1.5312e-14
25	331.0381	2.4962e-14	65	4651.2734	3.3612e-14
26	355.1138	2.3113e-14	66	4813.1094	3.6703e-14
27	379.4644	2.6575e-14	67	5086.1094	1.1362e-14
28	404.0947	1.2339e-14	68	5419.2148	4.8976e-15
29	429.0103	3.1150e-14	69	5758.4805	1.2575e-14
30	454.2153	8.7180e-15	70	6162.3164	4.1712e-15
31	492.5771	1.0002e-13	71	6575.0586	3.7333e-15
32	518.5288	1.1191e-14	72	7027.5117	3.5160e-15
33	558.0356	9.4059e-15	73	7490.9219	9.4714e-15
34	598.2544	7.4816e-15	74	7997.7500	3.4601e-15
35	639.2046	8.0974e-15	75	8518.0195	5.7002e-15
36	680.9058	6.0920e-15	76	9120.0586	5.0310e-15
37	723.3794	5.6536e-15	77	9705.6328	3.9485e-15
38	766.6470	8.3094e-15	78	10165.0117	1.0118e-14
39	825.6113	6.4728e-15	79	11078.0430	5.1976e-15
40	870.8198	5.4283e-15	80	11799.3281	5.4316e-15

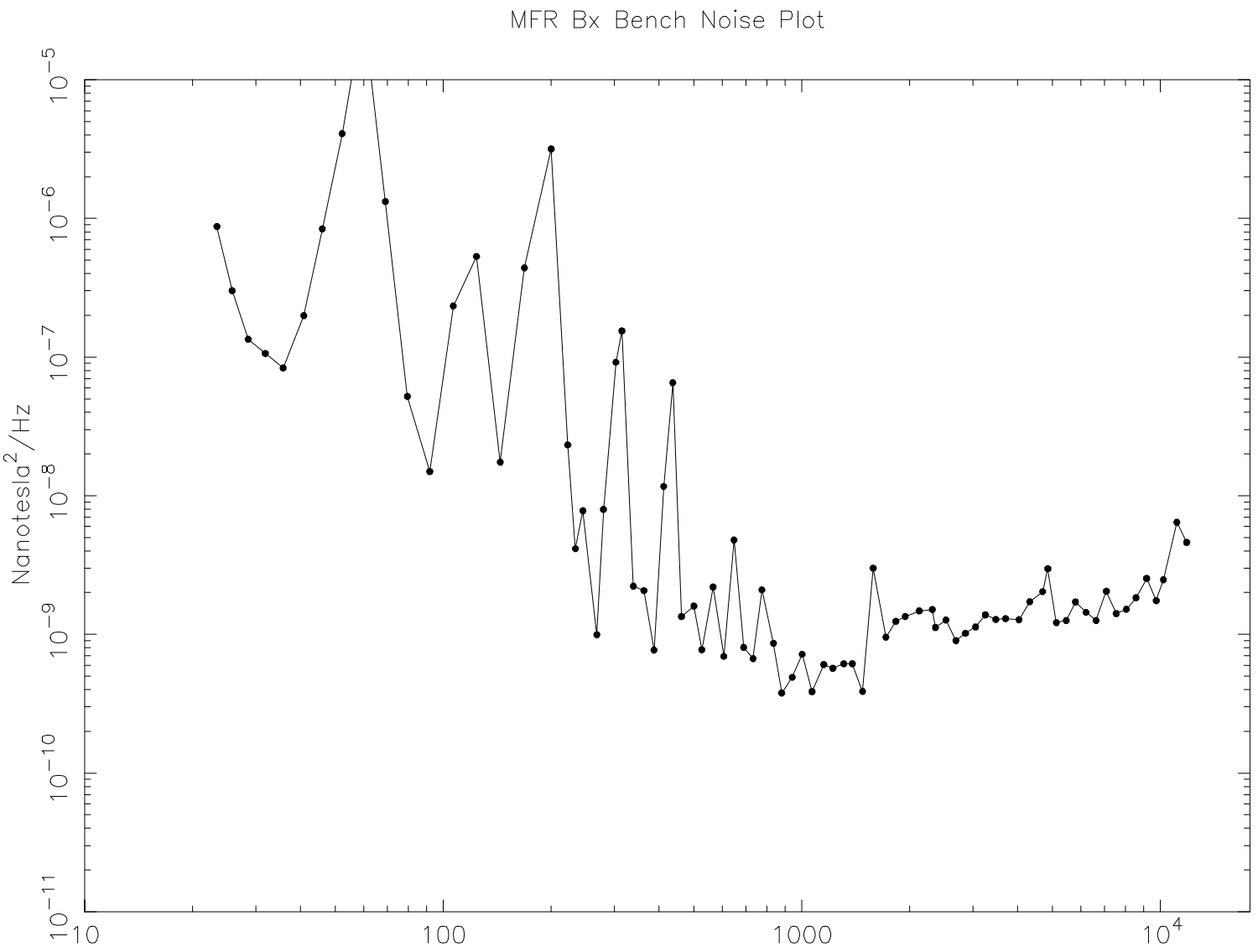

Figure 10.3.4.2.3 Frequency (Hz)

slr 2-Oct-1998 15:36

Table 10.3.4.2.3 MFR Bx Bench Noise Plot

Channel	Frequency (Hz)	nT^2/Hz	Channel	Frequency (Hz)	nT^2/Hz
1	23.8910	8.7224e-07	41	932.4595	4.9002e-10
2	26.2510	3.0116e-07	42	995.7109	7.1969e-10
3	29.1468	1.3429e-07	43	1060.6372	3.8582e-10
4	32.4228	1.0627e-07	44	1144.2549	6.0502e-10
5	36.2695	8.3312e-08	45	1213.2041	5.7067e-10
6	40.8909	1.9907e-07	46	1302.0835	6.1370e-10
7	46.5109	8.4046e-07	47	1375.4399	6.1284e-10
8	52.8165	4.0902e-06	48	1470.0942	3.8782e-10
9	60.4319	3.0581e-05	49	1536.8867	3.0074e-09
10	69.4643	1.3217e-06	50	1671.8125	9.5305e-10
11	80.0469	5.1971e-08	51	1785.1016	1.2400e-09
12	92.3442	1.4943e-08	52	1899.1719	1.3470e-09
13	107.2421	2.3355e-07	53	2083.3320	1.4771e-09
14	124.3865	5.3205e-07	54	2269.5547	1.5098e-09
15	144.8837	1.7509e-08	55	2316.4336	1.1225e-09
16	169.0493	4.3995e-07	56	2481.5547	1.2696e-09
17	192.1108	3.1684e-06	57	2648.3047	9.0248e-10
18	214.6289	2.3264e-08	58	2816.7148	1.0188e-09
19	225.9814	4.1438e-09	59	3011.2422	1.1329e-09
20	237.3965	7.7991e-09	60	3208.0039	1.3824e-09
21	260.4165	9.9422e-10	61	3432.0820	1.2838e-09
22	272.0229	7.9735e-09	62	3659.0898	1.2967e-09
23	295.4307	9.1908e-08	63	3992.2891	1.2768e-09
24	307.2329	1.5470e-07	64	4279.2383	1.7217e-09
25	331.0381	2.2296e-09	65	4651.2734	2.0345e-09
26	355.1138	2.0669e-09	66	4813.1094	2.9729e-09
27	379.4644	7.7112e-10	67	5086.1094	1.2157e-09
28	404.0947	1.1662e-08	68	5419.2148	1.2602e-09
29	429.0103	6.5289e-08	69	5758.4805	1.7143e-09
30	454.2153	1.3440e-09	70	6162.3164	1.4432e-09
31	492.5771	1.5999e-09	71	6575.0586	1.2603e-09
32	518.5288	7.7544e-10	72	7027.5117	2.0443e-09
33	558.0356	2.1965e-09	73	7490.9219	1.4152e-09
34	598.2544	6.9421e-10	74	7997.7500	1.5176e-09
35	639.2046	4.8049e-09	75	8518.0195	1.8376e-09
36	680.9058	8.0556e-10	76	9120.0586	2.5294e-09
37	723.3794	6.6836e-10	77	9705.6328	1.7510e-09
38	766.6470	2.0952e-09	78	10165.0117	2.4805e-09
39	825.6113	8.6228e-10	79	11078.0430	6.4390e-09
40	870.8198	3.7801e-10	80	11799.3281	4.6106e-09

Calibration of Flight Model #1
of Cassini-RPWS
High Frequency Receiver (HFR) / KRONOS[1]

Bob Manning

DESPA, Observatoire de Paris, Meudon

16/12/1999

[1] CNES denomination.

Table of contents

Table of contents 2
Introduction. 4
Preliminary discussion. 4
Receivers modeling. 6
  Attenuators 8
  DBcal 8
Calibration methods. 10
  GSE 10
  Specific discussion of bands ABC : 12
  Specific discussion of bands H1/2 : 12
  Phases 14
Back to measurements in physical units 15
Appendices. 17
  Data tables 17
    a123.dat 17
    ahf.dat 17
    a1hf1.dat 18
    a1hf2.dat 18
    dbcal_08.dat 19
    dbcal_16.dat 19
    dbcal_32.dat 19
    dbcalhf.dat 20
    phase8_abc.dat 21
    phase16_abc.dat 21
    phase32_abc.dat 21
    phase_hf1.dat 22
    phase_hf2.dat 22
    phase1248_hf.dat 22
  Matlab Programs. 23
    a1hf2find.m 23
    a1hf1find.m 23
    dbcal_2.m 24
    phaseabc.m 25
    phase_hf_fit.m 26
    readdata.m 27
    physique.m 27
    phasemag.m 31
    correl_phase.m 32
    fixsign.m 32
    ntodb.m 33
    fitlogeq.m 33
    fitlog.m 33
    llogntox.m 35
    llogxton.m 35
  Various files. 36
    dbcal32.txt 36
    dbcal.txt 37
    dbcal_2.txt 40
    correction_sinx_x_abc.txt 42

integration_times.txt 42
corr_integrate_times.txt 44
Files newcode 46
IDL programs 48
help_cal.pro 48
cal.pro 48
agc_db.pro 49
auto_db.pro 49
read_constants.pro 49
constants.xdr 51
prep_df.pro 51
read_phases.pro 54
phases.xdr 55

Introduction.

This document summarizes the procedures used for the calibration of the flight model of the receiver KRONOS/HFR on Cassini-RPWS. It contains all the informations allowing to convert raw data from telemetry to calibrated measurements in physical units.

Four types of files are found in the appendices :

1) data tables (*.dat), complete if not too long, with indications of the order in which data are organized.
2) Matlab programs (*.m) used for this document.
3) a few other useful files.
4) *IDL programs (*.pro) putting in practice the above tables for actual data calibration (amplitudes and phases).*[2]

Preliminary discussion.

The figure below is a very simplified sketch of the HFR, which main purpose is to identify calibration needs :

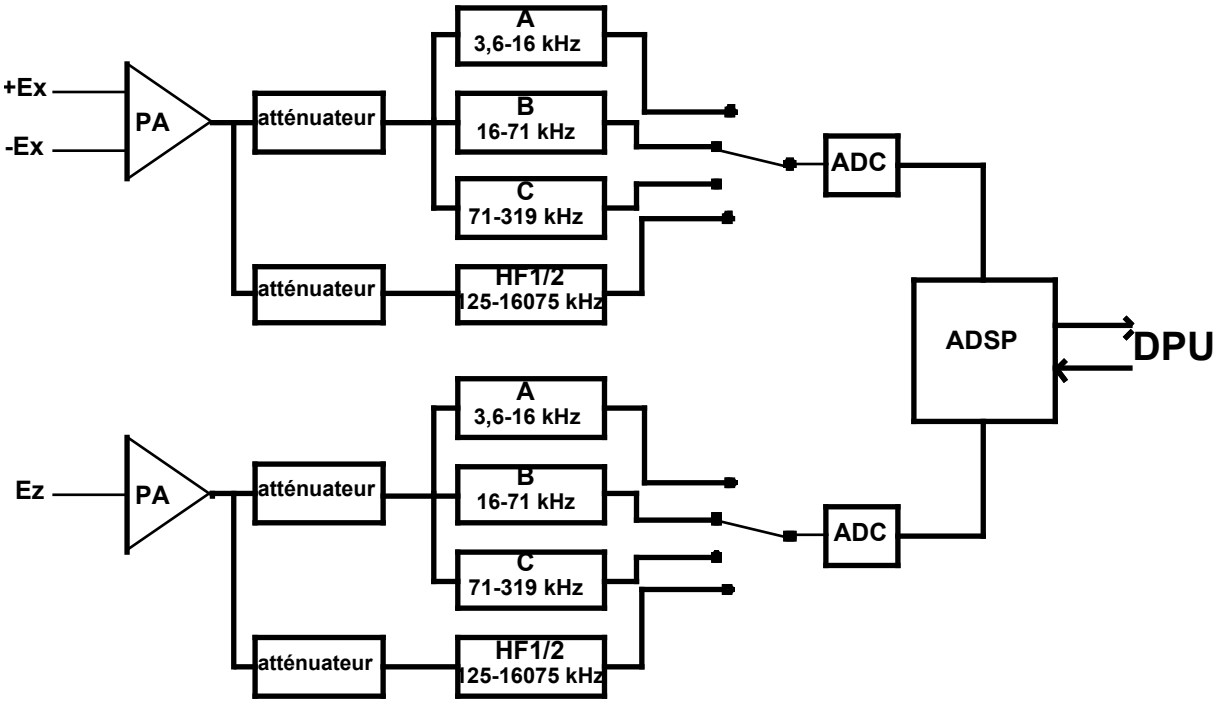

There are thus eight analog physical receivers. On the one hand, there are the 2x3 ABC receivers covering contiguous frequency ranges of relative width f_{max}/f_{min}=4.5 each. These bands are more finely analyzed by the digital analyzer (ADSP) in 8, 16, or 32 logarithmically spaced channels.

[2] added by P. Zarka (2001).

On the other hand, there are the two high frequency (HF) heterodyne receivers covering each a broad frequency range thanks to tunable oscillators and quartz filters, not shown on the figure. These receivers select an instantaneous band of 25 kHz width, a finer analysis of which is possible with the ADSP.

The calibrations mainly concern the analog part of the receivers (but the "gain" of the digital part must also be known). The receivers have a variable gain, as a function of the frequency as well as of the input level. A more complete sketch of one receiver (of ABC type, i.e. without the additional frequency shifting circuit) connected to the Ex dipole is shown below for clarity :

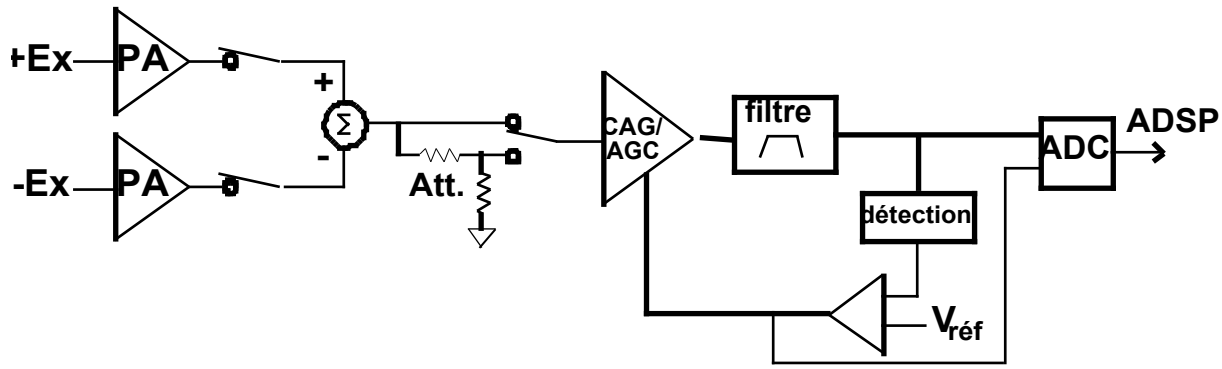

There is a preamplifier for each monopole antenna. Telecommand allows to select either one, of both in differential mode. A 30 dB attenuator may also be selected. This front-end part of the receiver has a fixed transfer function independent of the input level but may exhibit frequency dependent variations.

The following stage of the receiver has a variable gain, and is called AGC (for Automatic Gain Control). It has two purposes : amplify the signal up to a detectable level, and provide a way to measure the signal with an accuracy little dependent on the input level. The signal is amplified to a constant level of 0.5 V_{eff}. This is the optimal level for the subsequent digitization. After detection, a error-amplifying circuit retroacts on the variable gain stage so that the above fixed output level is reached (on average). The input voltage to the correction circuit is digitized in order to know the instantaneous gain. The gain response will be discussed in the next section.

The bandpass filter being part of the feedback loop restricts the frequency range to the one which will be subsequently analyzed digitally.

Digitization is performed with the ADC (Analog to Digital Converter).

The philosophy chosen for calibration and retrieval of measurement values in physical units consists of modeling separately the analog parts depending or not on signal amplitude, i.e. the AGC or the front-end of the receiver. The contribution of the digital part is taken into account automatically by the same measurements.

Receivers modeling.

Below is an example of plot of the output of a receiver as a function of the input signal. It shows a nearly linear dependency between the input voltage log(V) in dB and the continuous AGC output in telemetry points.

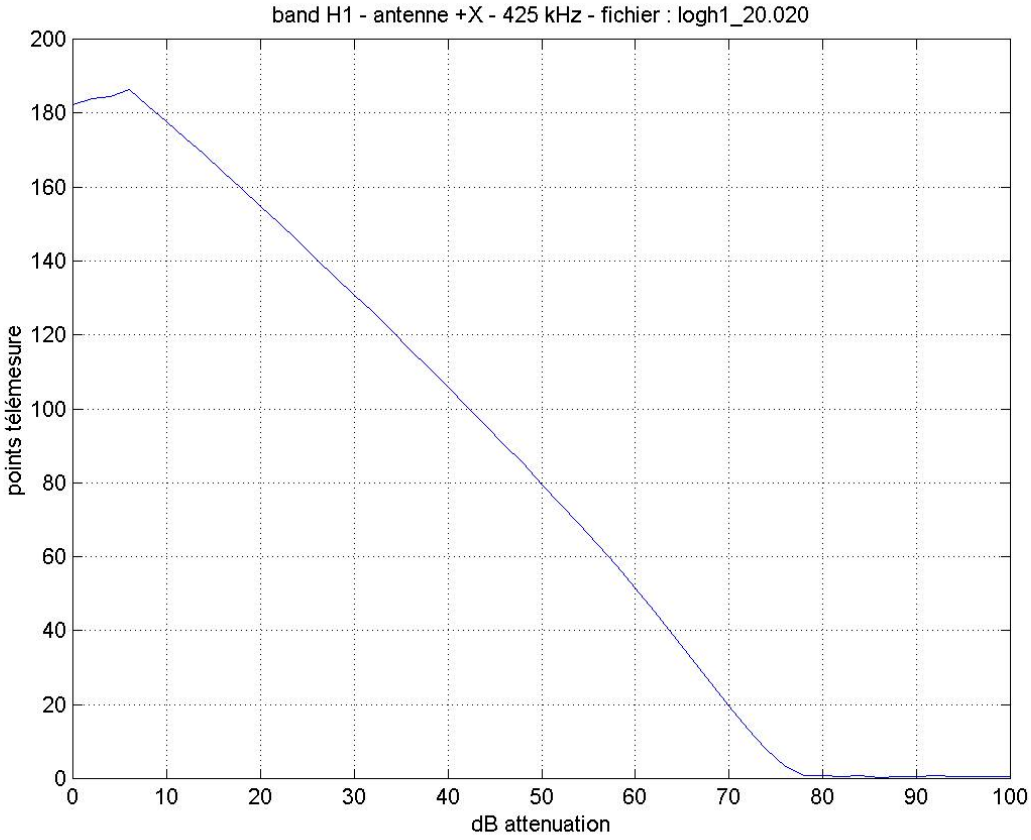

It has been shown that this curve is well described by the formula :

$$N = A_2 \cdot \log_{10}\left\{\left[10^{(A_1 - x)/10} + 10^{A_4/10}\right]^{1/4} - 1\right\} + A_3 \qquad (1)$$

In this expression, N is the telemetry level (number of points) and x represents the attenuation of the input signal in dB. We can see that A_2 defines the general slope of the curve, in points/dB/40. A_1 plays the role of the receiver's gain, in dB. A_4 represents either the receiver noise, or the constant level of an external perturbating noise. The coefficient A_3 does not have any clear significance. It could correspond to an internal receiver offset, but such an offset should not actually exist. However taking it into account may improve the quality of the fits.

A Matlab program was written to fit the values of the four coefficients A_1 to A_4. It has a graphical interface which allows to select the points to fit. An example is given in the figure below :

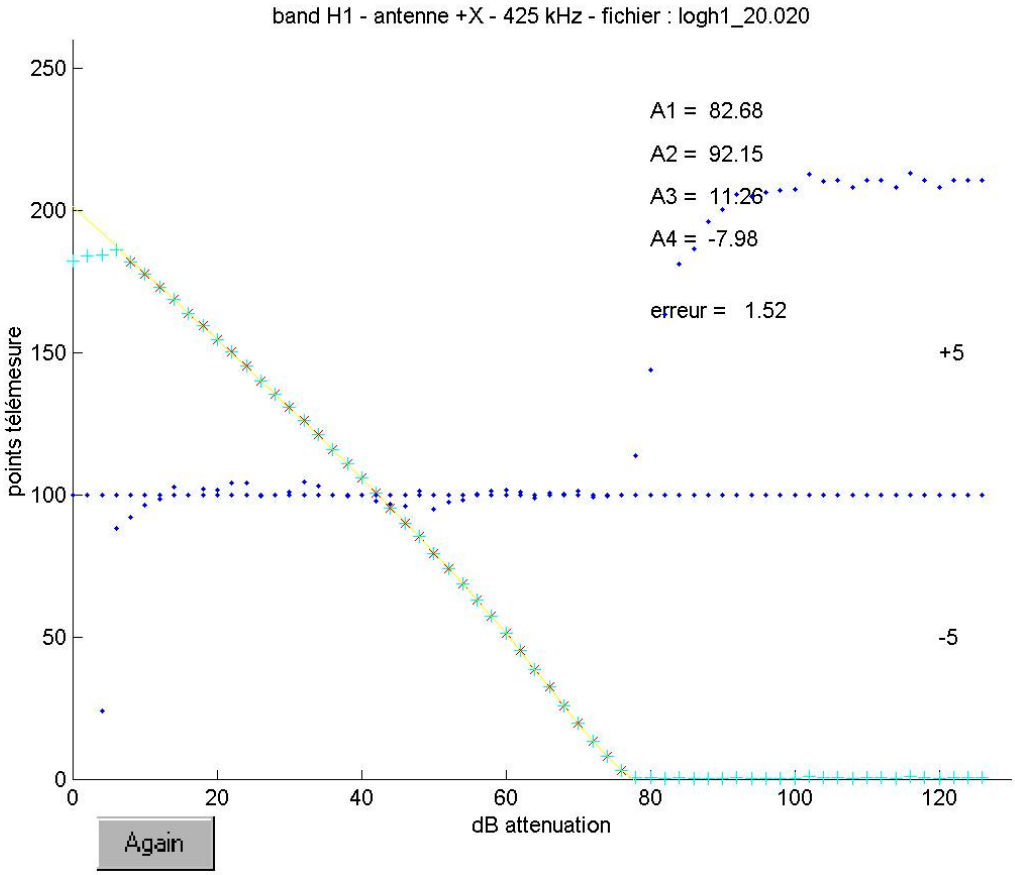

This curve was built as follows : a very stable noise generator (see discussion below) was used to feed the instrument through a programmable attenuator. 64 steps of 2 dB each have been measured. The "+" symbols represent all the raw telemetry values. The "*" symbols represent the points selected interactively for the fit. The solid line is the fitted curve. The blue dots, which refer to the ordinate scale on the right, are the residuals between the raw values and the fit. The values found for parameters A_1-A_4 are displayed.

The AGC is characterized mostly by A_2 and A_3. A_1 corresponds to the overall receiver gain, and thus to the horizontal position of the curve – a gain modification would only shift the curve to the right or to the felt. A_4 concerns the conditions at the receiver input, not the AGC.

For the ABC receivers, the A_1 coefficients are considered to be constant in the corresponding frequency ranges. Our measures characterize thus average values over the whole frequency bands. Gain variations inside a band are taken into account via the "dBcal" tables (see below). For the HF receivers, it is necessary to measure the gain at each channel center frequency.

Note that on the above two curves, the abscissa (dB attenuation) does not have any absolute reference. Actually, the "0 dB" level corresponds to a level that we will name below dBV0, minus the value of possible fixed (and known) attenuators which are part of the circuit.

Attenuators

Calibrations of the log responses (1) can be made with or without the internal fixed selectable attenuators. We have found that calibrations "with" give better results because the effect of electrical perturbations at the receiver input is reduced. We use mainly the calibrations with a variable input level in order to determine the coefficients A_2 et A_3 characterizing the AGCs.

For ABC receivers, the coefficients A_1 (characterizing the gain) are obtained through fits with "attenuator ON", and modified for the case "attenuator OFF" through a direct measurement of the attenuation performed at a constant adequate level. For these receivers, the characteristics of attenuators are thus very easy to take into account. This is because the attenuators simply consist of two resistors cabled as shown on the above synoptic sketch. Thus we found that the attenuations do not vary with frequency in the ABC bands. The values found are 30.1 dB for the Ex receiver and 30.0 dB for the Ez receiver.

For the HF receivers, implementation is more difficult, and attenuation is consequently frequency-dependent. This results in one set of coefficients A_1 per frequency, with and without attenuator.

DBcal

The previous sections only concern the analog front end of our receivers. Moreover, gain variations inside the analyzed bands are not taken into account, but only an average gain is determined. These variations will be taken into account during the analysis of the outputs of the digital analysis part, the "autos" (autocorrelations).

Let us remind that the receiver's AGC sends to the digital processor (ADSP) a signal with constant power in the band to be analyzed. The processor performs a finer spectral analysis of the signal in the band. Its "auto" outputs give the measured power in each sub-band, with a quasi-logarithmical coding of the form :

$$N = 2^E * (M + 8) \qquad (2)$$

the information being transmitted as 8-bit words [e4 e3 e2 e1 e0 m2 m1 m0].

When we send a signal with flat spectrum (white noise) at the receiver's input, we get a series of output "autos" approximately equal but not quite, because they include the variations of gain with frequency, for the analog part as well as for the digital part of the receiver. But, if the signal contains spectral variations within the band analyzed, some "autos" output will increase while others will necessarily decrease. This is illustrated in the next figure (raw "autos" outputs converted to dB, versus channel number, with variable SNR) :

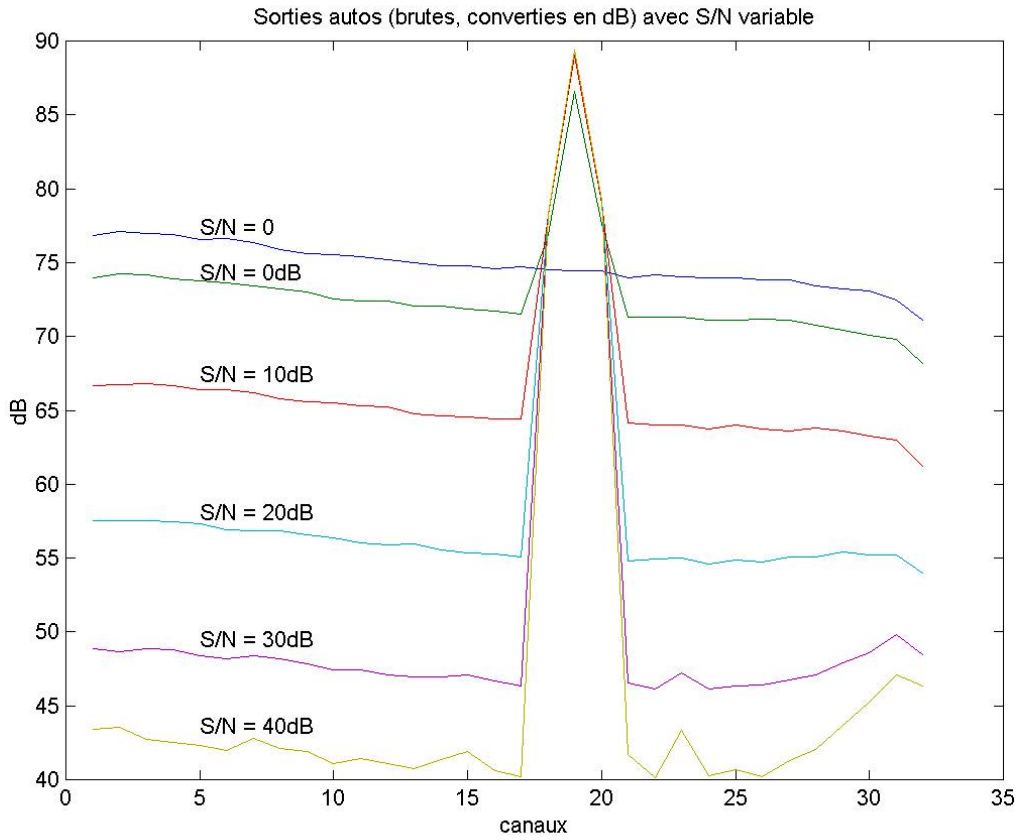

The six curves represent the output levels (converted in dB) of the Cx receiver (C band, Ex sensor – Flight Model #2), when fed by the sum of a white noise and of a sinusoid at 174 kHz. The curve labeled "S/N = 0" corresponds to a white noise input only. The curve labeled "S/N = 0dB" corresponds to a mixture of white noise plus sinusoidal signal with approximately equal powers. The other curves result from increasing attenuation applied to the noise in order to increase progressively the Signal-to-Noise Ratio (SNR).

The values for white noise alone, recorded in the best possible experimental conditions, serve as a reference called "dBcal" values (see below).

The next figure displays the same data when both AGC and dBcal are taken into account. The noise level for the cases "S/N = 0" and "S/N = 0dB" are the same and the signal level in channel #19 (corresponding to the frequency of the sinusoid) is the same in every case, except of course for "S/N = 0". Note that this example suffers two imperfections : (i) the calibration coefficients used are those of FM#1 (while the FM#2 was used for obtaining the displayed curves), and (ii) a few electrical perturbations affected the experiment.

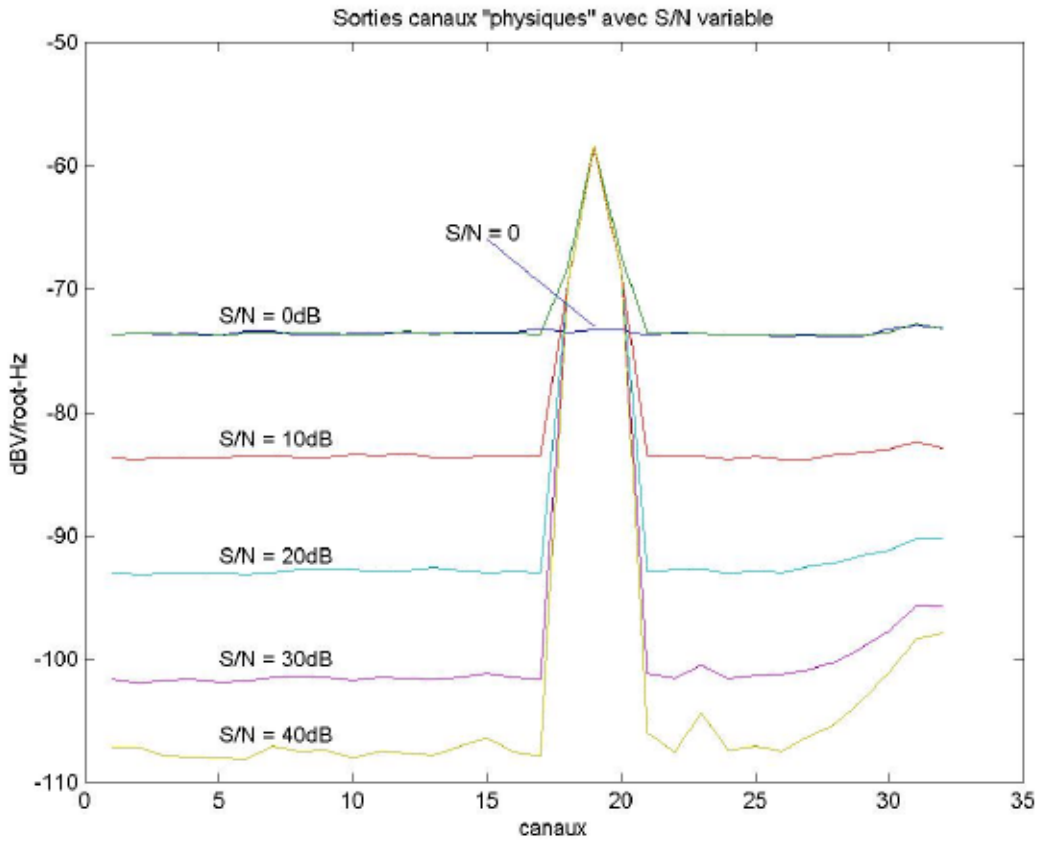

Calibration methods.

GSE

The heart of the calibration equipment is the so-called "stimuli" of the GSE (Ground Support Equipment). The stimuli are very stable and reliable generators of noise or sinusoidal signals, followed by programmable attenuators (as stable and reliable). The whole system is physically located in a bay dedicated to this application and can be entirely controlled by an external computer (PC).

The noise generator of the stimuli used is of the type "pseudo-random". Its output is a logic signal of amplitude V_c and consists of a series of '0's and '1's, with a seemingly random occurrence. The maximum frequency of switching between consecutive values if the clock frequency F_s. Vc is approximately constant but F_s changes depending on the bandwidth used. A different clock frequency is used for calibrating each receiver.

The total output power is equal to $V_c^2/4$. The distribution of the power inside the band varies as $\sin^2(x)/x^2$, with a first zero at F_s, which implies $x = \bullet * f/F_s$. As the sum of $\sin^2(x)/x^2$ between zero and infinity is equal to $\bullet/2$, and as $\sin^2(x)/x^2 \bullet 1$ for $x \bullet 0$, the noise spectral density at low frequencies is $V_c^2/4/F_s/2$ (in Volts squared per Hertz).

We refer to this spectral density as V0 or dBV0 in our formulas. A way to measure it precisely is to measure the peak-to-peak voltage with a digital oscilloscope. The results are :

Band	V_c	F_s (kHz)	dBV0
A	1,86	40	-43,6
B	1,86	180	-50,2
C	1,835	800	-56,8
H1	1,805	4800	-64,7
H2	1,55-1,7	40000	-75,2/-74,4 ‡ -74,3

Measurements performed with an accurate voltmeter gave identical results for the bands A,B,C,H1. Measurements are difficult for band H2, so that we use the method described below for better determining the spectral density in this band.

We have a good confidence for the determination of dBV0 in the H1 band. In addition, we recorded pairs of test files with identical stimulation conditions except for the H1/H2 clock, and an adequate frequency coverage ("flucthf1.020" and "flucthf.022" files). The analysis of these files shows a difference of 9,6 dB between the two generators at low frequencies. The difference in clock frequency contributes for a difference of 9,2 dB, so that we find in addition a 0,4 dB decrease of the level (i.e. ~1,7 V pour V_c), which seems reasonable. The dBV0 value for H2 band becomes thus -74,3.

The figure below displays the spectrum relative to the value of dBV0 calculated for the generator tuned to band C. The vertical dotted line at 320 kHz marks the maximum frequency of the C band.

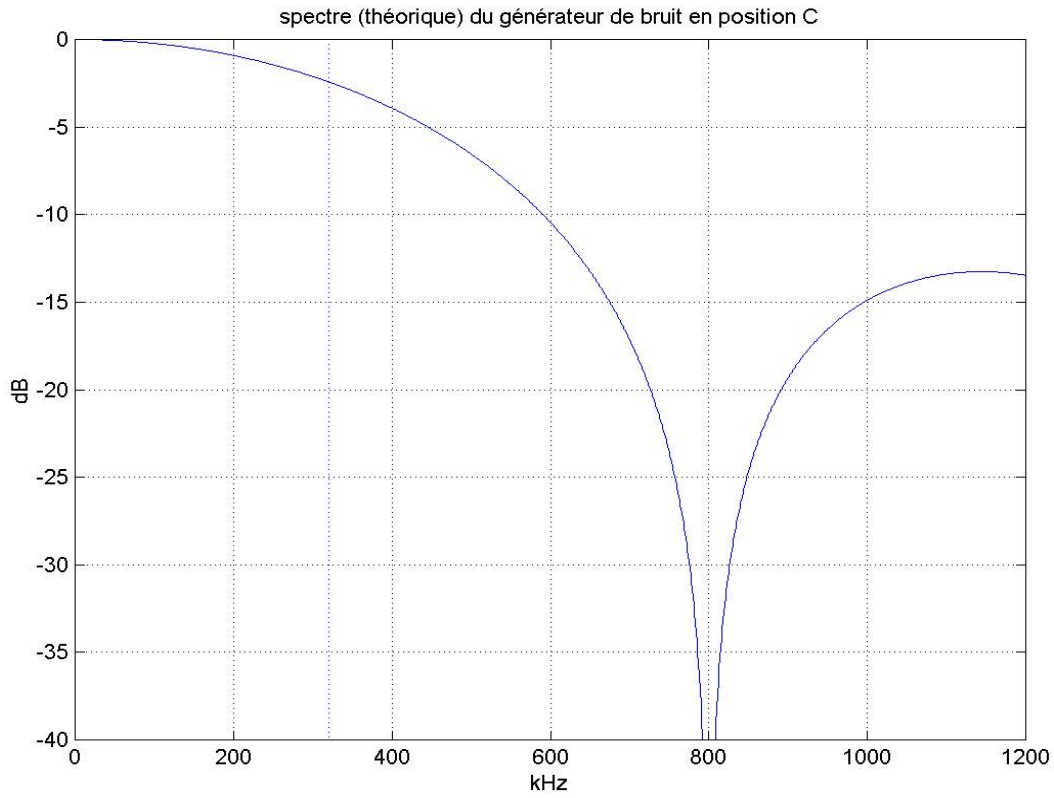

Specific discussion of bands ABC :

It must be noted that the average power in the useful (effective) band is thus not equal to dBV0. This is especially important for bands ABC, for which the whole band is analyzed simultaneously. This correction is described in the file "correction_sinx_x_abc.txt" given in appendix. The resulting final dBV0 values for ABC are thus :

```
dBV0(A) = -44.61
dBV0(B) = -51.14
dBV0(C) = -57.76
```

In the previous section, we have explained that the dBcal's correspond to "autos" outputs in the presence of white noise, i.e. with a flat spectrum. For the bands ABC, we have determined these dBcal coefficients using measurements performed with the noise generator in position "H1". This brings in a worst case error of 0,06 dB. We have used the file "fluctabc.004", with the processing described in "dbcal32.txt" (see appendix).

This latter processing corresponds to the case of 32 channels in ABC bands. For the cases of 16 and 8 channels, we have used the specific files "32filabc.002", "16filabc.001", and "8filtabc.001", with the processing using "dbcal_2.m" and continued with "dbcal_2.txt" (see appendix).

A final step is to incorporate the dBV0 in the coefficients found for the A_1 values. With the polarities used, it is necessary to subtract them, i.e. to increase them in absolute value.

Final values of A_1, A_2, and A_3 coefficients are found in the file "a123.dat" given in appendix with annotations. dBcal's are listed in files "dBcal_08.dat", "dBcal_16.dat," and "dBcal_32.dat" also reproduced in appendix.

Specific discussion of bands H1/2 :

We have explained above that the fitted coefficients A_2 and A_3 are those which characterize the AGC part of the receivers. A_1 corresponds to the receiver's gain and A_4 to ambient noise, internal or external. But the receivers H1/2 are designed so that the AGC part works at constant frequency whatever the observing frequency. We consider thus that unique values can be used for A_2 and A_3 (for X and for Z), but that A_1 must be determined for each center frequency of observation.

In order to obtain the best values for A_2 and A_3, we have performed several fittings over the whole frequency band, at selected "clean" frequencies (with little electrical perturbations). The results of these fittings is listed in the file "ahf.dat" in appendix. We have taken average values for A_2 X and Z : 96,76 and 94,81. For A_3 we have chosen "0" for both receivers. This choice is not critical because it can be compensated by small variations of A_1.

Then the frequency-dependent A_1 are determined through measurements with white noise input (and correction for sin(x)/x). We have adopted the following scheme : we have two files ("flucthf.021" and "flucthf.022") for which white noise has been injected at an adequate level and observed at all HF2 frequencies, starting from 25 kHz. The receiver was in direction-finding mode in order to measure the response of both X inputs, with and without the internal attenuator. We have used the program "a1h2find.m" (given in appendix) in order to determine the A_1 coefficients which would give the expected noise spectrum in sin(x)/x. The value found above for dBV0 (-74.3 dBV) was subtracted from the A_1 in order to simplify the processing. This value should thus not be used again in this case.

The curve of the spectral variation of A_1 versus HF2 frequency is given below. The observed undulations correspond to variations of the response of anti-image frequency filters.

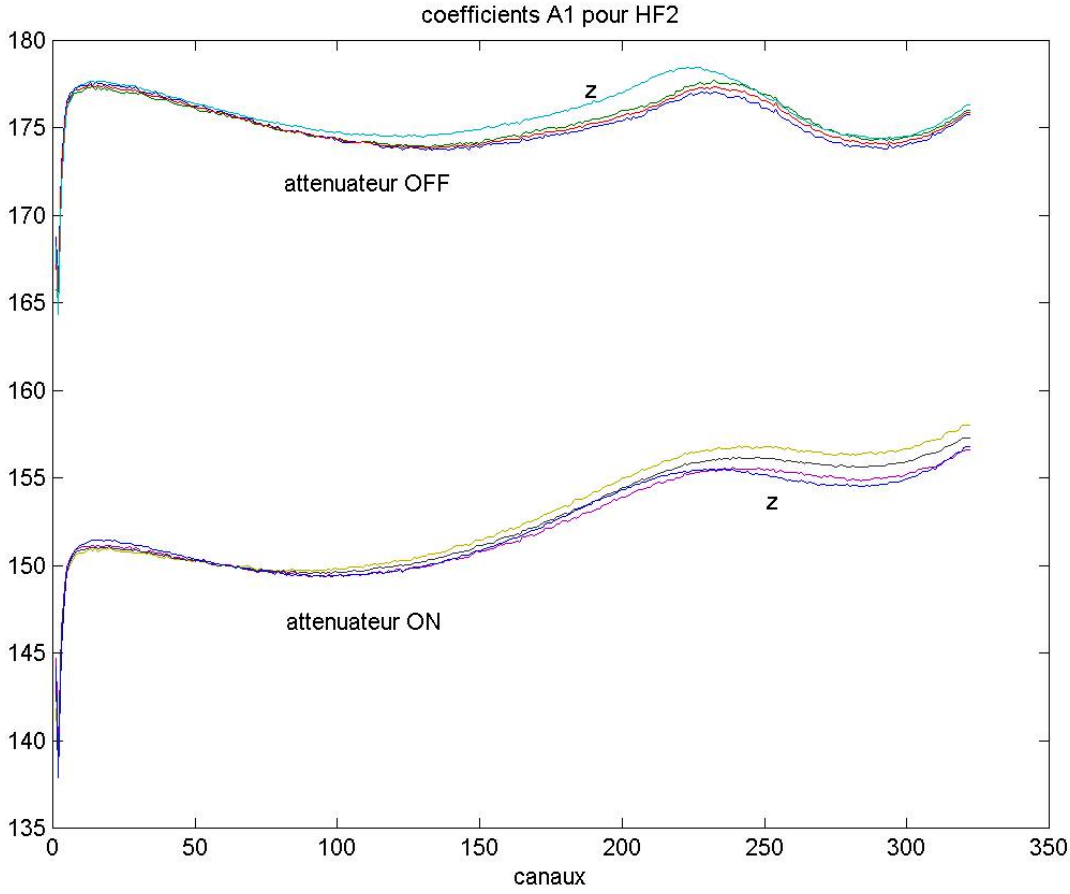

Next, A_1 values must be determined for HF1 frequencies, i.e. every 25 kHz instead of 50 kHz for HF2. It appeared to be more interesting to interpolate the A_1 values found for HF2 than to recalculate a whole new set of coefficients with different experimental data, in order to avoid small discrepancies at common frequencies. This has been done with the routine "a1hf1find.m".

As H1/2 instantaneously analyze only relatively narrow spectral bands, the dBcal's do not need to be corrected for input spectral power variations of the form

sin(x)/x within the band because the level does not vary practically over the 25 kHz width of the filter. The processing of dBcal's for a number of sub-band channels of 1, 2, 4, and 8 is identical to that applied to ABC (with data files "1filthf.001", "2filthf.001", "4filthf.001", and "8filthf.001").

Phases

It is quite easy to measure the phase shifts introduced by the receivers, i.e. the one found at the input of digitizers with identical input signals on +X and Z or -X and Z antennas, due to phase advances or delays in the analog parts of the receiver. These phase shifts are obtained as the arctangent of cross-correlation outputs with adequate input conditions. This is done by the program "phasemag.m" listed in appendix.

Data files used for ABC are "llgar20.020", "llgbr20.020", and "llgcr20.020" for the measurements without the internal attenuator, and "logata20.020", "logatb20.020", and "logatc20.020" with the attenuator. Phase differences due to the presence of the attenuator are negligible (~0,1°), so that a single table can be used in both cases. Slightly larger differences exist between +X and –X(+180°) sensors, up to 3°.

We have used the Matlab program "phaseabc.m" to determine phase shift values. This program calls the subroutine "phasemag.m". Note that the values for the +/-X dipole mode are simply arithmetic averages of the values found for +X and -X separately.

The files mentioned above only correspond to the 32 channel case. Files for 16 and 8 channels have all been recorded with the +X sensor only. Their analysis has shown that the phase shifts found for the 16 channel case are very close to arithmetic averages 2 by 2 of the 32 channel ones. So, this scheme was chosen to calculate the phases in files "phasenn_ABC.dat".

For HF1/2, two distinct calculations are necessary : one for the overall variations versus frequency (as for the A_1 coefficients), and the other for 1, 2, 4, or 8 filters. We have proceeded as follows :

We had two filed in HF2 ("flucthf.021" and "flucthf.022") covering the whole frequency range, resp. with and without the internal attenuator, with direction finding ON, and only one filter per 25 kHz band. As for ABC we have used the program "phasemag.m" to determine the phase shift. We have interpolated the results to obtain the values for frequencies 2•n•25 kHz, and simply duplicated the 25 kHz values for 0 Hz. Then, we have found interesting to fit the results with a smoothed spline curve, which has been done with the program "phase_hf_fit.m". An exempla of result from this fitting is displayed on the figure below :

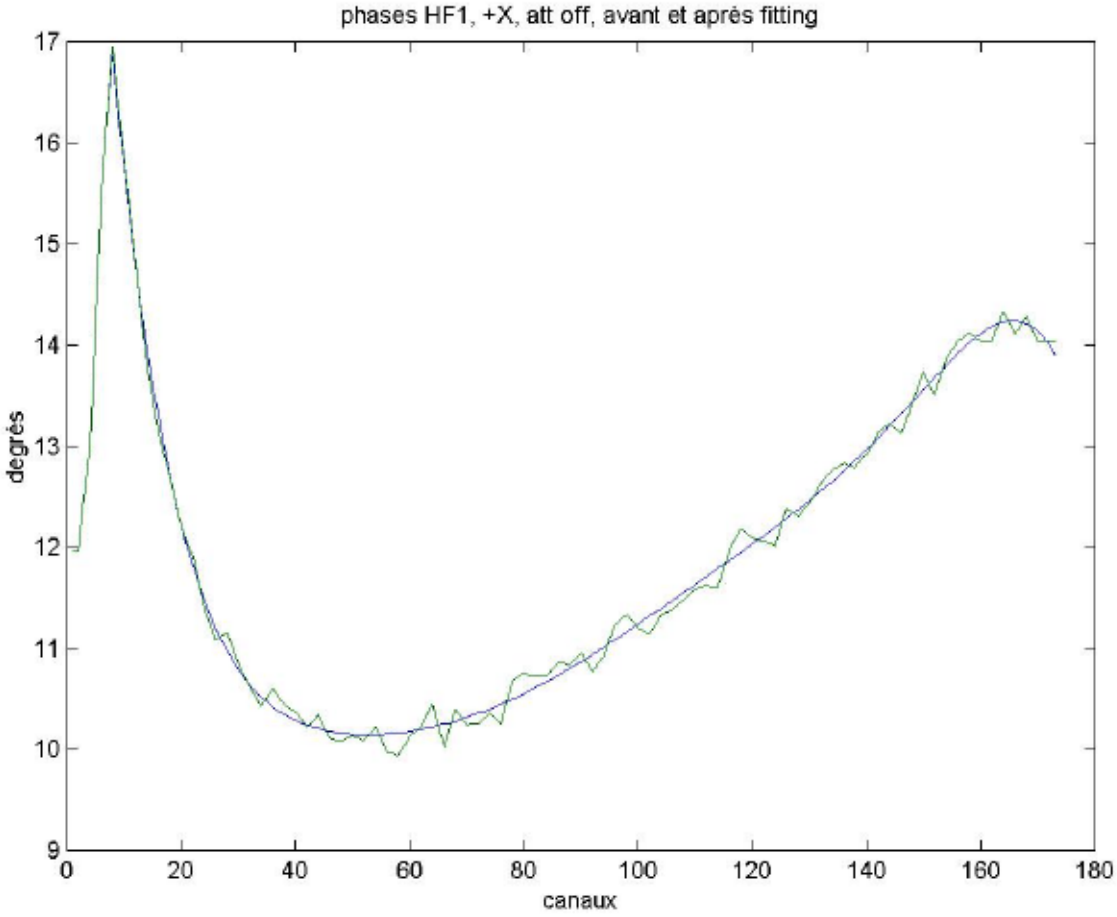

These phases are tabulated in the files "phase_hf1.dat" and "phase_hf2.dat".

To compute the phase shifts inside the 25 kHz band, we have four files recorded in nearly identical conditions except for the number of filters in the band : "1filt.001", "2filt.001", "4filt.001", and "8filt.001". We have computed each phase shift with respect to that obtained for 1 filter taken as a reference. The resulting table is in "phase1248_hf.dat".

The two types of phase shifts must be added together.

Back to measurements in physical units.

The conversion of raw TM data to measurements in physical units follows the general method described in the programs "physique.m" and "phasemag.m" or "correl_phase.m".

In a first stage, one must determine the total power in the band, or more exactly the spectral density of the white noise which would correspond to the same AGC level. This is done using the following formula (x is in dBV/• Hz), which is simply the inverse of formula (1) :

$$X = -A_1 + 40 \cdot \log_{10}[10^{(N - A_3)/A_2} + 1] \qquad (3)$$

For the case when there is no auto-correlation measurement, for example for HF1/2 with a number of filters =1, this formula gives the signal amplitude in physical units. But in general, and especially for ABC, the spectrum in the band is not white noise, thus it will be necessary to analyze the autos. As described above, the available dBcal are the auto outputs in case of a white noise. The problem is thus to compare the measured auto with these dBcal.

dBcal are expressed in dB, while auto are expressed using the 8-bit quasi-logarithmic coding described above. We must then convert the auto in dB, as done by the program "ntodb.m" in appendix, and then perform the following calculation to obtain the spectral power in each channel :

$$\text{dBV/•Hz} = X + \text{dBauto} - \text{dBcal} \qquad (4)$$

Cross-correlation data are transmitted with the same coding as autos. To compute the true correlation ratio (•), the real and imaginary cross-correlation outputs must be compared to the two corresponding auto outputs (X and Z), according to the following calculation :

$$\bullet_{real} = N_{cross\text{-}real} / (N_{auto\text{-}X} \bullet N_{auto\text{-}Z})^{1/2}$$
$$\bullet_{imag} = N_{cross\text{-}imag} / (N_{auto\text{-}X} \bullet N_{auto\text{-}Z})^{1/2} \qquad (5)$$

where N is calculated according to formula (2) [cf. "correl_phase.m" in appendix]. Also,

$$\bullet_{total} = (\bullet_{real}^{2} + \bullet_{imag}^{2})^{1/2}$$

with

$$\bullet_{real} = \bullet_{total} * \cos(\bullet + \bullet)$$
$$\bullet_{imag} = \bullet_{total} * \sin(\bullet + \bullet)$$

where • represents the phase to be measured and • the phase shift introduced by the receivers. To determine •, one has to compute the arctangent of $\bullet_{imag}/\bullet_{real}$ and then subtract the • taken from the phase shift tables.

Appendices.

Data tables.

a123.dat

A1	A2	A3	A1 (att.ON)		
166.37	73.20	-0.01	136.27	Ex	band A
164.84	73.16	3.21	134.84	Ez	" "
168.48	85.61	0.08	138.38	Ex	band B
168.70	85.03	1.31	138.70	Ez	" "
168.43	82.58	0.01	138.33	Ex	band C
169.46	82.30	0.00	139.46	Ez	" "
0	94.81	0	0	Ex	band HF
0	96.76	0	0	Ez	" "

ahf.dat

- with tests logh2_20.20

X (dipole) --

n	5n+8	F(kHz)	A1	A2	A3	A4
3	23	1175	76.65	96.74	0.00	-13.98
7	43	2175	76.30	96.55	0.00	-11.76
9	53	2675	76.00	96.50	0.00	-11.12
11	63	3175	75.79	96.70	0.00	-11.50
14	78	3925	75.45	96.89	0.00	-11.24
17	93	4675	75.36	97.15	0.00	-10.08
19	103	5175	75.46	97.11	0.00	-7.71
24	128	6425	76.18	97.06	0.01	-7.90
29	153	7675	72.86	93.51	16.05	-7.02
35	183	9175	79.80	97.31	0.00	-5.92
40	208	10425	77.74	96.21	12.65	6e4
49	253	12675	84.51	96.81	0.00	-9.40
53	273	13675	81.16	96.61	7.83	1.9e5
57	293	14675	79.88	96.11	11.43	2.7e4
62	318	15925	82.38	96.89	6.65	-3.72

-----

mean 1-8 & 10-15 = 96.76

mean 1-15 = 96.54

Z--

n	5n+8	F(kHz)	A1	A2	A3	A4
3	23	1175	77.12	94.86	0.0	-13.31
7	43	2175	76.66	94.55	0.01	-11.30
9	53	2675	76.11	94.88	0.01	-10.68
11	63	3175	75.90	94.71	0.0	-11.05
14	78	3925	75.58	94.55	0.0	-10.54
17	93	4675	75.30	95.00	0.0	-9.54
19	103	5175	75.48	94.54	0.01	-6.85
24	128	6425	75.98	94.67	0.01	-6.49
29	153	7675	77.13	95.05	0.01	-7.62
35	183	9175	79.61	95.27	0.01	-6.21
40	208	10425	76.06	93.25	16.9	1.6e+006

```
 49  253  12675  80.27  93.22   9.3    -6.93
 53  273  13675  79.45  94.16   8.9     4e+004
 57  293  14675  78.48  92.96  12.7    -4.64
 62  318  15925  83.44  95.88   0.01   -4.41
                           -----
            mean 1-10 = 94.81
            mean 1-15 = 94.50
```

a1hf1.dat

```
  +Ex     -Ex    +/-Ex     Ez     +Ex     -Ex    +/-Ex     Ez
 ------  ------  ------  ------  ------  ------  ------  ------
 168.78  165.78  167.27  168.21  144.70  141.78  143.23  144.24   f0   0
 168.78  165.78  167.27  168.21  144.70  141.78  143.23  144.24   f1  25
 167.38  165.72  166.55  166.27  142.08  140.43  141.25  141.06   f2  50
 165.99  165.66  165.82  164.33  139.46  139.08  139.27  137.87   f3  75
                             :
                             :
                             :
                             :
                             :
174.83  174.75  174.79  175.08  149.40  149.72  149.56  149.42  f171  4275
174.81  174.75  174.78  175.08  149.45  149.72  149.58  149.42  f172  4300
-----------------------------  -----------------------------
    int. attenuator OFF               int. attenuator ON
```

a1hf2.dat

```
  +Ex     -Ex    +/-Ex     Ez     +Ex     -Ex    +/-Ex     Ez
 ------  ------  ------  ------  ------  ------  ------  ------
 168.78  165.78  167.27  168.21  144.70  141.78  143.23  144.24    f0   25
 165.99  165.66  165.82  164.33  139.46  139.08  139.27  137.87    f1   75
 172.83  172.48  172.65  171.58  146.38  146.09  146.23  145.20    f2  125
 175.46  175.08  175.27  174.68  148.83  148.48  148.65  148.18    f3  175
                                    :
                             :
                             :
                             :
                             :
175.77  175.98  175.88  176.34  156.61  158.02  157.31  156.80  f320  6025
175.77  175.98  175.88  176.34  156.61  158.02  157.31  156.80  f321  6075
-----------------------------  -----------------------------
     int. attenuator OFF               int. attenuator ON
```

dbcal_08.dat

```
70.26 70.87 70.57 70.51 71.41 71.58 71.49 71.24 69.66 69.63 69.65 69.21 C0
69.92 70.26 70.09 70.21 71.92 71.98 71.95 71.84 69.14 69.11 69.12 68.84  .
69.39 69.74 69.56 69.76 71.53 71.48 71.50 71.46 68.42 68.31 68.36 68.20  .
69.06 69.40 69.23 69.29 70.58 70.55 70.57 70.56 67.73 67.68 67.70 67.65
68.87 68.99 68.93 69.08 69.39 69.40 69.40 69.40 67.16 67.16 67.16 67.20
68.85 68.89 68.87 68.92 68.43 68.43 68.43 68.42 66.94 66.93 66.94 67.10
68.93 68.82 68.88 68.81 67.38 67.38 67.38 67.37 66.71 66.68 66.69 66.87  .
67.70 67.53 67.61 67.52 65.87 65.82 65.84 65.92 65.08 65.16 65.12 65.21 C7
 +X    -X    +/-X   Z    +X    -X    +/-X   Z    +X    -X    +/-X   Z
----------------------- ----------------------- -----------------------
          A                       B                       C
```

dbcal_16.dat

```
73.01 73.58 73.30 73.23 73.74 73.91 73.82 73.49 75.33 75.29 75.31 74.79  C0
72.71 73.36 73.04 73.03 74.38 74.54 74.46 74.29 75.31 75.29 75.30 74.82   .
72.64 73.04 72.84 72.90 74.54 74.63 74.59 74.46 74.85 74.80 74.83 74.48   .
72.48 72.76 72.62 72.77 74.49 74.52 74.51 74.44 74.50 74.48 74.49 74.21
72.22 72.57 72.40 72.54 74.26 74.28 74.27 74.20 74.10 74.03 74.07 73.86
72.02 72.37 72.20 72.29 73.87 73.76 73.81 73.77 73.71 73.54 73.63 73.48
71.83 72.25 72.04 72.17 73.40 73.34 73.37 73.37 73.41 73.32 73.37 73.31
71.68 71.94 71.81 71.94 72.76 72.76 72.76 72.76 73.05 73.02 73.04 72.98
71.42 71.68 71.55 71.72 72.25 72.26 72.25 72.25 72.74 72.75 72.75 72.76
71.49 71.46 71.48 71.61 71.86 71.87 71.86 71.86 72.59 72.58 72.59 72.65
71.46 71.49 71.48 71.58 71.28 71.27 71.28 71.26 72.51 72.42 72.47 72.62
71.48 71.52 71.50 71.53 70.66 70.67 70.67 70.66 72.36 72.44 72.40 72.54
71.65 71.47 71.56 71.49 70.11 70.08 70.10 70.10 72.49 72.46 72.48 72.55
71.61 71.56 71.59 71.47 69.61 69.64 69.63 69.61 72.33 72.29 72.31 72.47
71.32 71.10 71.21 71.07 69.10 69.07 69.09 69.10 71.44 71.47 71.45 71.60   .
69.69 69.56 69.63 69.59 67.91 67.84 67.87 67.96 69.73 69.85 69.79 69.85 C15
 +X    -X    +/-X   Z    +X    -X    +/-X   Z    +X    -X    +/-X   Z
----------------------- ----------------------- -----------------------
          A                       B                       C
```

dbcal_32.dat

```
75.39 76.01 75.71 75.63 75.34 75.58 75.46 75.18 77.09 77.10 77.09 76.57 C0
75.39 75.92 75.66 75.61 75.92 76.04 75.98 75.72 77.25 77.16 77.21 76.75  .
75.24 75.91 75.57 75.55 76.18 76.33 76.26 76.04 77.21 77.15 77.18 76.73  .
75.15 75.77 75.42 75.46 76.36 76.54 76.45 76.29 77.03 77.06 77.05 76.63
75.11 75.57 75.28 75.32 76.56 76.65 76.61 76.46 76.88 76.87 76.88 76.49
75.03 75.39 75.18 75.23 76.55 76.64 76.59 76.47 76.67 76.59 76.63 76.28
74.92 75.20 75.06 75.14 76.50 76.49 76.50 76.42 76.42 76.35 76.38 76.06
74.92 75.20 75.06 75.12 76.36 76.45 76.40 76.33 76.12 76.16 76.14 75.87
74.80 75.11 74.96 75.06 76.29 76.29 76.29 76.20 75.94 75.89 75.91 75.69
74.63 75.03 74.83 74.94 76.07 76.12 76.10 76.05 75.73 75.63 75.68 75.46
74.52 74.88 74.71 74.84 75.90 75.85 75.88 75.84 75.55 75.38 75.47 75.28
74.41 74.76 74.59 74.74 75.74 75.55 75.65 75.61 75.31 75.17 75.23 75.15
74.33 74.75 74.54 74.70 75.48 75.33 75.40 75.39 75.16 75.08 75.12 75.03
74.24 74.67 74.46 74.62 75.17 75.19 75.18 75.18 75.00 74.92 74.96 74.89
74.15 74.45 74.30 74.47 75.01 75.00 75.01 74.99 74.85 74.82 74.83 74.77
74.03 74.25 74.14 74.32 74.80 74.82 74.81 74.82 74.72 74.68 74.70 74.65
73.97 74.22 74.09 74.27 74.50 74.52 74.51 74.51 74.57 74.59 74.58 74.55
73.83 74.11 73.97 74.14 74.17 74.18 74.17 74.16 74.57 74.58 74.57 74.58
```

```
73.89 73.89 73.89 74.04 73.92 73.92 73.92 73.91 74.37 74.42 74.40 74.44
73.93 73.87 73.90 74.02 73.63 73.65 73.64 73.64 74.36 74.30 74.33 74.40
73.90 73.96 73.93 74.04 73.33 73.35 73.34 73.33 74.37 74.22 74.29 74.41
73.88 73.88 73.88 73.97 73.09 73.06 73.08 73.08 74.26 74.24 74.25 74.42
73.86 73.86 73.86 73.92 72.72 72.76 72.74 72.74 74.24 74.25 74.24 74.39
73.84 73.91 73.88 73.88 72.52 72.49 72.50 72.51 74.17 74.30 74.24 74.39
74.06 73.81 73.94 73.93 72.24 72.23 72.23 72.23 74.25 74.28 74.27 74.42
74.07 73.97 74.02 73.96 72.07 72.02 72.05 72.04 74.28 74.20 74.24 74.41
74.21 74.08 74.14 74.02 71.87 71.89 71.88 71.86 74.12 74.17 74.14 74.30
74.03 74.05 74.04 73.92 71.62 71.65 71.64 71.63 73.96 73.85 73.91 74.09
73.98 73.72 73.85 73.70 71.27 71.29 71.28 71.29 73.56 73.54 73.55 73.70
73.59 73.41 73.50 73.37 70.87 70.79 70.83 70.86 72.89 72.98 72.93 73.05
72.67 72.54 72.61 72.54 70.19 70.19 70.19 70.28 72.01 72.10 72.06 72.15   .
71.60 71.47 71.54 71.53 69.33 69.19 69.24 69.39 70.75 70.91 70.83 70.93 C31
 +X    -X    +/-X   Z    +X    -X    +/-X   Z    +X    -X    +/-X   Z
---------------------- ---------------------- ----------------------
           A                      B                      C
```

dbcalhf.dat

```
68.23  68.23  72.16  72.11  75.14  75.12  77.26  77.36  C0
  0      0    72.10  72.19  75.48  75.39  78.14  78.00  C1
  0      0      0      0    75.65  75.70  77.69  77.57  C2
  0      0      0      0    74.81  75.00  78.15  78.05  C3
  0      0      0      0      0      0    78.22  78.23  C4
  0      0      0      0      0      0    77.90  77.96  C5
  0      0      0      0      0      0    77.54  77.62  C6
  0      0      0      0      0      0    76.99  77.27  C7
  X      Z      X      Z      X      Z      X      Z
------------  ------------  ------------  ------------
      1             2             4             8
```

phase8_abc.dat

A			B			C			
+X	-X	+/-X	+X	-X	+/-X	+X	-X	+/-X	
2.30	-177.23	2.53	1.61	-176.08	2.77	3.52	-176.30	3.61	C0
1.65	-176.81	2.42	1.57	-176.51	2.53	3.63	-176.35	3.64	C1
1.01	-176.68	2.17	1.61	-176.73	2.44	3.83	-176.20	3.81	C2
0.43	-176.73	1.85	1.86	-176.86	2.50	3.90	-176.46	3.72	C3
0.02	-176.90	1.56	2.19	-176.74	2.72	3.55	-176.71	3.42	C4
-0.09	-177.01	1.45	2.70	-176.54	3.08	3.06	-177.37	2.84	C5
0.65	-176.30	2.17	3.48	-175.91	3.78	2.57	-177.82	2.38	C6
2.78	-174.35	4.22	4.92	-174.52	5.20	2.20	-178.22	1.99	C7

phase16_abc.dat

A			B			C			
+X	-X	+/-X	+X	-X	+/-X	+X	-X	+/-X	
2.46	-177.33	2.57	1.59	-176.06	2.77	3.50	-176.35	3.58	C0
2.14	-177.13	2.50	1.64	-176.10	2.77	3.54	-176.25	3.65	C1
1.82	-176.88	2.47	1.59	-176.40	2.60	3.57	-176.29	3.64	.
1.48	-176.74	2.37	1.54	-176.63	2.46	3.70	-176.40	3.65	.
1.17	-176.65	2.26	1.57	-176.65	2.46	3.78	-176.13	3.83	
0.85	-176.70	2.07	1.65	-176.82	2.42	3.88	-176.28	3.80	
0.55	-176.68	1.94	1.78	-176.84	2.47	3.93	-176.43	3.75	
0.31	-176.78	1.76	1.94	-176.88	2.53	3.87	-176.49	3.69	
0.10	-176.86	1.62	2.09	-176.76	2.67	3.66	-176.56	3.55	
-0.07	-176.94	1.50	2.28	-176.72	2.78	3.45	-176.85	3.30	
-0.14	-177.03	1.42	2.54	-176.66	2.94	3.21	-177.26	2.98	
-0.05	-177.00	1.47	2.87	-176.43	3.22	2.90	-177.49	2.71	
0.28	-176.64	1.82	3.23	-176.15	3.54	2.65	-177.65	2.50	
1.02	-175.96	2.53	3.74	-175.68	4.03	2.49	-177.98	2.25	
2.20	-174.85	3.68	4.52	-174.91	4.81	2.29	-178.12	2.09	.
3.36	-173.85	4.76	5.32	-174.14	5.59	2.10	-178.32	1.89	C15

phase32_abc.dat

A			B			C			
+X	-X	+/-X	+X	-X	+/-X	+X	-X	+/-X	
2.53	-177.39	2.57	1.56	-176.09	2.74	3.49	-176.34	3.57	C0
2.40	-177.27	2.56	1.62	-176.03	2.80	3.51	-176.35	3.58	C1
2.21	-177.20	2.50	1.65	-176.06	2.80	3.54	-176.25	3.64	.
2.07	-177.06	2.50	1.63	-176.15	2.74	3.54	-176.24	3.65	.
1.92	-176.95	2.49	1.62	-176.32	2.65	3.55	-176.22	3.67	
1.72	-176.82	2.45	1.55	-176.47	2.54	3.60	-176.36	3.62	
1.57	-176.73	2.42	1.54	-176.64	2.45	3.67	-176.41	3.63	
1.39	-176.75	2.32	1.54	-176.62	2.46	3.72	-176.39	3.67	
1.26	-176.68	2.29	1.56	-176.61	2.48	3.75	-176.19	3.78	
1.09	-176.63	2.23	1.59	-176.68	2.45	3.82	-176.08	3.87	
0.93	-176.71	2.11	1.61	-176.72	2.44	3.84	-176.18	3.83	
0.77	-176.69	2.04	1.69	-176.91	2.39	3.92	-176.37	3.77	
0.61	-176.63	1.99	1.74	-176.86	2.44	3.91	-176.44	3.74	
0.49	-176.72	1.88	1.81	-176.82	2.49	3.94	-176.43	3.76	
0.37	-176.77	1.80	1.89	-176.86	2.51	3.93	-176.48	3.73	
0.25	-176.80	1.73	2.00	-176.90	2.55	3.82	-176.51	3.66	
0.15	-176.82	1.67	2.06	-176.76	2.65	3.67	-176.53	3.57	
0.05	-176.91	1.57	2.12	-176.75	2.69	3.65	-176.59	3.53	
0.04	-176.90	1.53	2.23	-176.75	2.74	3.49	-176.80	3.35	

0.09	-176.98	1.46	2.34	-176.69	2.82	3.41	-176.91	3.25	
0.13	-177.06	1.41	2.48	-176.68	2.90	3.29	-177.15	3.07	
0.15	-176.99	1.43	2.60	-176.64	2.98	3.13	-177.36	2.88	
0.10	-177.01	1.45	2.79	-176.51	3.14	2.97	-177.47	2.75	
0.00	-177.00	1.50	2.95	-176.35	3.30	2.83	-177.51	2.66	
0.15	-176.77	1.69	3.12	-176.26	3.43	2.70	-177.57	2.57	
0.41	-176.51	1.95	3.34	-176.05	3.65	2.60	-177.74	2.43	
0.76	-176.18	2.29	3.55	-175.85	3.85	2.53	-177.90	2.32	
1.28	-175.74	2.77	3.93	-175.51	4.21	2.44	-178.07	2.19	
1.86	-175.16	3.35	4.31	-175.14	4.59	2.34	-178.07	2.14	
2.54	-174.54	4.00	4.73	-174.67	5.03	2.23	-178.17	2.03	.
3.12	-174.15	4.49	5.22	-174.29	5.46	2.15	-178.29	1.93	.
3.61	-173.56	5.02	5.43	-173.98	5.72	2.06	-178.34	1.86	C31

phase_hf1.dat

Attenuator OFF			Attenuator ON				
+X	-X	+/-X	+X	-X	+/-X		
11.96	-167.00	12.48	11.65	-167.00	12.32	f0	0
11.96	-167.00	12.48	11.65	-167.00	12.32	f1	25
12.49	-166.40	13.05	12.15	-166.53	12.81	f2	50
13.02	-165.79	13.62	12.65	-166.05	13.30	f3	75
			:				
			:				
			:				
14.00	-165.18	14.41	10.41	-171.23	9.59	f171	4275
13.90	-165.22	14.34	10.46	-171.23	9.62	f172	4300

phase_hf2.dat

Attenuator OFF			Attenuator ON				
+X	-X	+/-X	+X	-X	+/-X		
11.96	-167.00	12.48	11.65	-167.00	12.32	f0	25
13.02	-165.79	13.62	12.65	-166.05	13.30	f1	75
15.53	-161.39	17.07	14.45	-160.64	16.91	f2	125
16.53	-163.47	16.53	16.47	-163.48	16.49	f3	175
			:				
			:				
			:				
17.74	-148.37	24.68	25.80	-144.89	30.46	f171	4275
17.93	-148.00	24.96	25.90	-144.76	30.56	f172	4300

phase1248_hf.dat

1f	*2f*	*4f*	*8f*
0.00	-.84	-1.51	-2.19
0	.48	-0.34	-0.74
0	0	0.34	-1.04
0	0	0.97	0.25
0	0	0	0.46
0	0	0	0.31
0	0	0	0.80
0	0	0	1.56

Matlab Programs.

a1hf2find.m

```
disp('lire file e:\cassini\calmv1\flucthf.021')
readdata

f=fstarth2:fsteph2:fstarth2+(nstepsh2-1)*fsteph2;
x=f*pi/40000;
dbsx=20*log10(sin(x)./x);
dbv0=-74.3+dbsx;
save dbv0

agcx=mean(agch21');
agcpx=agcx(1:2:end);
agcmx=agcx(2:2:end);
agcpmx=mean([agcpx;agcmx]);
agcz=mean(agch22');
agcz=(agcz(1:2:end)+agcz(2:2:end))/2;

a1pxoff = 40*[log10(10.^(agcpx/96.76)+1)]-dbv0+30+26;
a1mxoff = 40*[log10(10.^(agcmx/96.76)+1)]-dbv0+30+26;
a1pmxoff = 40*[log10(10.^(agcpmx/96.76)+1)]-dbv0+30+26;
a1zoff = 40*[log10(10.^(agcz/94.81)+1)]-dbv0+30+26;

a1hf2new=[a1pxoff' a1mxoff' a1pmxoff' a1zoff'];
save a1hf2new.dat -ascii a1hf2new

disp('lire file e:\cassini\calmv1\flucthf.022')
readdata

agcx=mean(agch21');
agcpx=agcx(1:2:end);
agcmx=agcx(2:2:end);
agcpmx=mean([agcpx;agcmx]);
agcz=mean(agch22');
agcz=(agcz(1:2:end)+agcz(2:2:end))/2;
load dbv0
load a1hf2new.dat

a1pxon = 40*[log10(10.^(agcpx/96.76)+1)]-dbv0+6+26;
a1mxon = 40*[log10(10.^(agcmx/96.76)+1)]-dbv0+6+26;
a1pmxon = 40*[log10(10.^(agcpmx/96.76)+1)]-dbv0+6+26;
a1zon = 40*[log10(10.^(agcz/94.81)+1)]-dbv0+6+26;

a1hf2new=[a1hf2new a1pxon' a1mxon' a1pmxon' a1zon'];
a1hf2new=[a1hf2new;a1hf2new(321,:)];
save a1hf2new.dat -ascii a1hf2new
```

a1hf1find.m

```
load a1hf2new.dat
k=1:86;
a1hf1new(2*k,:)=a1hf2new(k,:);
a1hf1new(2*k+1,:)=(a1hf2new(k,:)+a1hf2new(k+1,:))/2;
a1hf1new(1,:)=a1hf1new(2,:); % cas 0 Hz
save a1hf1new.dat -ascii a1hf1new
```

dbcal_2.m

```
disp('lire file 32filabc.002')
readdata
autoa1=reshape(autoa1,32,110);
autoa2=reshape(autoa2,32,110);
autob1=reshape(autob1,32,110);
autob2=reshape(autob2,32,110);
autoc1=reshape(autoc1,32,110);
autoc2=reshape(autoc2,32,110);
 a=mean(autoa1');
 b=mean(autob1');
 c=mean(autoc1');
 ax32=ntodb(a);
 bx32=ntodb(b);
 cx32=ntodb(c);
 a=mean(autoa2');
 b=mean(autob2');
 c=mean(autoc2');
 az32=ntodb(a);
 bz32=ntodb(b);
 cz32=ntodb(c);
 abc32=[ax32' az32';bx32' bz32';cx32' cz32'];
 plot(abc32);pause
 save abc32

disp('lire file 16filabc.001')
readdata
autoa1=reshape(autoa1,16,100);
autoa2=reshape(autoa2,16,100);
autob1=reshape(autob1,16,100);
autob2=reshape(autob2,16,100);
autoc1=reshape(autoc1,16,100);
autoc2=reshape(autoc2,16,100);
 a=mean(autoa1');
 b=mean(autob1');
 c=mean(autoc1');
 ax16=ntodb(a);
 bx16=ntodb(b);
 cx16=ntodb(c);
 a=mean(autoa2');
 b=mean(autob2');
 c=mean(autoc2');
 az16=ntodb(a);
 bz16=ntodb(b);
 cz16=ntodb(c);
 abc16=[ax16' az16';bx16' bz16';cx16' cz16'];
 plot(abc16);pause
save abc16

disp('lire file 8filtabc.001')
readdata
autoa1=reshape(autoa1,8,100);
autoa2=reshape(autoa2,8,100);
autob1=reshape(autob1,8,100);
autob2=reshape(autob2,8,100);
autoc1=reshape(autoc1,8,100);
autoc2=reshape(autoc2,8,100);
 a=mean(autoa1');
 b=mean(autob1');
 c=mean(autoc1');
 ax8=ntodb(a);
 bx8=ntodb(b);
```

```
 cx8=ntodb(c);
 a=mean(autoa2');
 b=mean(autob2');
 c=mean(autoc2');
 az8=ntodb(a);
 bz8=ntodb(b);
 cz8=ntodb(c);
 abc8=[ax8' az8';bx8' bz8';cx8' cz8'];
 plot(abc8);pause
 save abc8

load abc32
load abc16

ax32=abc32(1:32,1);
az32=abc32(1:32,2);
bx32=abc32(33:64,1);
bz32=abc32(33:64,2);
cx32=abc32(65:96,1);
cz32=abc32(65:96,2);

ax16=abc16(1:16,1);
az16=abc16(1:16,2);
bx16=abc16(17:31,1);
bz16=abc16(17:31,2);
cx16=abc16(32:48,1);
cz16=abc16(32:48,2);
```

phaseabc.m

```
%Determination of phase shift between +X and -X inputs in ABC bands
%with and without internal attenuator.          - 3.12.99

disp('lire e:\cassini\calmv1\llgcr20.020')
readdata

[ang,mag]=phasemag(crosscr,crossci);
ang=reshape(ang,32,512);
angp=ang(:,1:2:512);
angm=ang(:,2:2:512);
angcp=mean(angp(:,40:70)');
angcm=mean(angm(:,40:70)');

save temp1 angcp angcm

disp('lire e:\cassini\calmv1\llgbr20.020')
readdata

[ang,mag]=phasemag(crossbr,crossbi);
ang=reshape(ang,32,512);
angm=ang(:,2:2:512);
angp=ang(:,1:2:512);
angbm=mean(angm(:,40:70)');
angbp=mean(angp(:,40:70)');

save temp angbp angbm

disp('lire e:\cassini\calmv1\llgar20.020')
readdata

[ang,mag]=phasemag(crossar,crossai);
ang=reshape(ang,32,512);
```

```
angp=ang(:,1:2:512);
angm=ang(:,2:2:512);
angam=mean(angm(:,40:70)');
angap=mean(angp(:,40:70)');

load temp
load temp1

angapm=mean([angap;angam+180]);
angbpm=mean([angbp;angbm+180]);
angcpm=mean([angcp;angcm+180]);

phase32_abc_new=[angap' angam' angapm' angbp' angbm' angbpm' angcp' angcm'
angcpm'];

fid=fopen('phase32_abc_new.dat','w')
fprintf(fid,'%8.2f%10.2f%8.2f%8.2f%10.2f%8.2f%8.2f%10.2f%8.2f\r\n',phase32_
abc_new')
fclose(fid)

phase16_abc_new=(phase32_abc_new(1:2:32,:)+phase32_abc_new(2:2:32,:))/2;
phase8_abc_new=(phase16_abc_new(1:2:16,:)+phase16_abc_new(2:2:16,:))/2;

fid=fopen('phase16_abc_new.dat','w')
fprintf(fid,'%8.2f%10.2f%8.2f%8.2f%10.2f%8.2f%8.2f%10.2f%8.2f\r\n',phase16_
abc_new')
fclose(fid)

fid=fopen('phase8_abc_new.dat','w')
fprintf(fid,'%8.2f%10.2f%8.2f%8.2f%10.2f%8.2f%8.2f%10.2f%8.2f\r\n',phase8_a
bc_new')
fclose(fid)
```

phase_hf_fit.m

```
load phase_hf1.dat
load phase_hf2.dat

hf1tofit=phase_hf1(7:172,:);
%hf2tofit=phase_hf2(4:322,:);
hf2tofit=phase_hf2(4:200,:);

coefpoff=polyfit([1:166]',hf1tofit(:,1),7);
coefmoff=polyfit([1:166]',hf1tofit(:,2),7);
coefpmoff=polyfit([1:166]',hf1tofit(:,3),7);
coefpon=polyfit([1:166]',hf1tofit(:,4),7);
coefmon=polyfit([1:166]',hf1tofit(:,5),7);
coefpmon=polyfit([1:166]',hf1tofit(:,6),7);

poff=polyval(coefpoff,1:166)';
moff=polyval(coefmoff,1:166)';
pmoff=polyval(coefpmoff,1:166)';
pon=polyval(coefpon,1:166)';
mon=polyval(coefmon,1:166)';
pmon=polyval(coefpmon,1:166)';

all=[poff moff pmoff pon mon pmon];
phase_hf1_new=[phase_hf1(1:6,:);all];

coefpoff=polyfit([1:197]',hf2tofit(:,1),9);
coefmoff=polyfit([1:197]',hf2tofit(:,2),9);
coefpmoff=polyfit([1:197]',hf2tofit(:,3),9);
```

```
coefpon=polyfit([1:197]',hf2tofit(:,4),9);
coefmon=polyfit([1:197]',hf2tofit(:,5),9);
coefpmon=polyfit([1:197]',hf2tofit(:,6),9);

poff=polyval(coefpoff,1:197)';
moff=polyval(coefmoff,1:197)';
pmoff=polyval(coefpmoff,1:197)';
pon=polyval(coefpon,1:197)';
mon=polyval(coefmon,1:197)';
pmon=polyval(coefpmon,1:197)';

all=[poff moff pmoff pon mon pmon];
phase_hf2_new=[phase_hf2(1:3,:);all];

hf2tofit=phase_hf2(201:322,:);

coefpoff=polyfit([1:122]',hf2tofit(:,1),9);
coefmoff=polyfit([1:122]',hf2tofit(:,2),9);
coefpmoff=polyfit([1:122]',hf2tofit(:,3),9);
coefpon=polyfit([1:122]',hf2tofit(:,4),9);
coefmon=polyfit([1:122]',hf2tofit(:,5),9);
coefpmon=polyfit([1:122]',hf2tofit(:,6),9);

poff=polyval(coefpoff,1:122)';
moff=polyval(coefmoff,1:122)';
pmoff=polyval(coefpmoff,1:122)';
pon=polyval(coefpon,1:122)';
mon=polyval(coefmon,1:122)';
pmon=polyval(coefpmon,1:122)';

all=[poff moff pmoff pon mon pmon];
phase_hf2_new=[phase_hf2_new;all];
```

readdata.m

(too long)

physique.m

```
%dbvolt.m -> physique.m       16.12.99
%
% conversion of auto/agc results from readdata in dBvolts.
% READDATA or READNORMAL must have run before.

load a123.dat

if att,
   a123(:,1)=a123(:,4);
end

if banda | bandb | bandc,
   if nchanabc==8, load dbcal_08.dat; dbcal=dbcal_08; end
   if nchanabc==16, load dbcal_16.dat; dbcal=dbcal_16; end
   if nchanabc==32, load dbcal_32.dat; dbcal=dbcal_32; end
end
if bandh1 | bandh2, load dbcalhf.dat; end

if bandh1, load a1hf1.dat; end
if bandh2, load a1hf2.dat; end
```

```
dba1=[];dba2=[];dbb1=[];dbb2=[];dbc1=[];dbc2=[];
dbh11=[];dbh12=[];dbh21=[];dbh22=[];
if ~exist('npktnormal'), npktnormal=npacket; end % compatibility
READDATA/READNORMAL

if banda & nagca1,
    a=a123(1,:);
    x1=-a(1)+40*(log10(10.^((agca1(:)-a(3))./a(2))+1));
    agca1=reshape(agca1,nagca1,npktnormal);
    autoa1=reshape(autoa1,nchanabc,nautoa1*npktnormal/nchanabc);
    nn=nautoa1*npktnormal/nchanabc;
    for j=1:nchanabc,
       if dfabc,
          dba1(j,1:2:nn)=ntodb(autoa1(j,1:2:nn))-dbcal(j,1)+x1(1:2:nn)';
          dba1(j,2:2:nn)=ntodb(autoa1(j,2:2:nn))-dbcal(j,2)+x1(1:2:nn)';
       else
          dba1(j,:)=ntodb(autoa1(j,:))-dbcal(j,3)+x1';
       end
   end
    dba1=reshape(dba1,nautoa1,npktnormal);
    autoa1=reshape(autoa1,nautoa1,npktnormal);
end
if banda & nagca2,
    a=a123(2,:);
    x2=-a(1)+40*(log10(10.^((agca2(:)-a(3))./a(2))+1));
    agca2=reshape(agca2,nagca2,npktnormal);
    autoa2=reshape(autoa2,nchanabc,nautoa2*npktnormal/nchanabc);
    for j=1:nchanabc,
      dba2(j,:)=ntodb(autoa2(j,:))-dbcal(j,4)+x2';
    end
    dba2=reshape(dba2,nautoa2,npktnormal);
    autoa2=reshape(autoa2,nautoa2,npktnormal);
end

if bandb & nagcb1,
   a=a123(3,:);
   x1=-a(1)+40*(log10(10.^((agcb1(:)-a(3))./a(2))+1));
   agcb1=reshape(agcb1,nagcb1,npktnormal);
   autob1=reshape(autob1,nchanabc,nautob1*npktnormal/nchanabc);
   nn=nautob1*npktnormal/nchanabc;
   for j=1:nchanabc,
      if dfabc,
         dbb1(j,1:2:nn)=ntodb(autob1(j,1:2:nn))-dbcal(j,5)+x1(1:2:nn)';
         dbb1(j,2:2:nn)=ntodb(autob1(j,2:2:nn))-dbcal(j,6)+x1(1:2:nn)';
      else
         dbb1(j,:)=ntodb(autob1(j,:))-dbcal(j,7)+x1';
      end
   end
   dbb1=reshape(dbb1,nautob1,npktnormal);
   autob1=reshape(autob1,nautob1,npktnormal);
end
if bandb & nagcb2,
   a=a123(4,:);
   x2=-a(1)+40*(log10(10.^((agcb2(:)-a(3))./a(2))+1));
   agcb2=reshape(agcb2,nagcb2,npktnormal);
   autob2=reshape(autob2,nchanabc,nautob2*npktnormal/nchanabc);
   for j=1:nchanabc,
      dbb2(j,:)=ntodb(autob2(j,:))-dbcal(j,8)+x2';
   end
   dbb2=reshape(dbb2,nautob2,npktnormal);
   autob2=reshape(autob2,nautob2,npktnormal);
end

if bandc & nagcc1,
```

```
   a=a123(5,:);
   x1=-a(1)+40*(log10(10.^((agcc1(:)-a(3))./a(2))+1));
   agcc1=reshape(agcc1,nagcc1,npktnormal);
   autoc1=reshape(autoc1,nchanabc,nautoc1*npktnormal/nchanabc);
   nn=nautoc1*npktnormal/nchanabc;
   for j=1:nchanabc,
      if dfabc,
         dbc1(j,1:2:nn)=ntodb(autoc1(j,1:2:nn))-dbcal(j,9)+x1(1:2:nn)';
         dbc1(j,2:2:nn)=ntodb(autoc1(j,2:2:nn))-dbcal(j,10)+x1(1:2:nn)';
      else
         dbc1(j,:)=ntodb(autoc1(j,:))-dbcal(j,11)+x1';
      end
   end
   dbc1=reshape(dbc1,nautoc1,npktnormal);
   autoc1=reshape(autoc1,nautoc1,npktnormal);
end
if bandc & nagcc2,
   a=a123(6,:);
   x2=-a(1)+40*(log10(10.^((agcc2(:)-a(3))./a(2))+1));
   agcc2=reshape(agcc2,nagcc2,npktnormal);
   autoc2=reshape(autoc2,nchanabc,nautoc2*npktnormal/nchanabc);
   for j=1:nchanabc,
       dbc2(j,:)=ntodb(autoc2(j,:))-dbcal(j,12)+x2';
   end
   dbc2=reshape(dbc2,nautoc2,npktnormal);
   autoc2=reshape(autoc2,nautoc2,npktnormal);
end

if bandh1,
   nstart=fstarth1/25;
   dstep=fsteph1/25;
   nstop=nstart+(nstepsh1-1)*dstep;
   freqh1=fstarth1:fsteph1:(fstarth1+fsteph1*(nstepsh1-1));

   if nagch11,
     dbcal=dbcalhf(1:nchanh1,1+2*floor(3.6*log10(nchanh1)));
     a2=a123(7,2);
     a3=a123(7,3);
     agch11=reshape(agch11,nagch11/rch1/rcall,npktnormal*rch1*rcall);
     k=anth11+att*4;
     x1=agch11;
     for j=1:nagch11/rch1/rcall,
        if dfh1,
           k=j+2-2*floor((j+1)/2)+att*4;
        end
        n=nstart+1+floor((j-1)/(1+dfh1))*dstep;
        x1(j,:)=-a1hf1(n,k) ...
               +40*(log10(10.^((agch11(j,:)-a3)./a2)+1));
     end
     if nautoh11,
       dbh11=ntodb(autoh11);
       dbh11=reshape(dbh11,nchanh1,nagch11*npktnormal);
       dbh11=dbh11-repmat(dbcal,1,nagch11*npktnormal);
       dbh11=dbh11+repmat(x1(:)',nchanh1,1);
       if dfh1,
         dbh11=reshape(dbh11,2*nchanh1,nagch11*npktnormal/2);
         dbh11=[reshape(dbh11(1:nchanh1,:),1,nautoh11*npktnormal/2); ...

reshape(dbh11(nchanh1+1:nchanh1*2,:),1,nautoh11*npktnormal/2)];
       end

dbh11=reshape(dbh11,max(nagch11,nautoh11)/rch1/rcall,npktnormal*rch1*rcall)
;
     else,
```

```
      dbh11=zeros(1,nagch11*npktnormal);
      dbh11=dbh11+x1(:)';
      dbh11=reshape(dbh11,nagch11/rch1/rcall,npktnormal*rch1*rcall);
    end
  end

  if nagch12,
    dbcal=dbcalhf(1:nchanh1,2+2*floor(3.6*log10(nchanh1)));
    a2=a123(8,2);
    a3=a123(8,3);
    agch12=reshape(agch12,nagch12/rch1/rcall,npktnormal*rch1*rcall);
    x2=agch12;
    for j=1:nagch12/rch1/rcall,
       n=nstart+1+floor((j-1)/(1+dfh1))*dstep;
       x2(j,:)=-a1hf1(n,4*(att+1)) ...
          +40*(log10(10.^((agch12(j,:)-a3)./a2)+1));
    end
    if nautoh12,
      dbh12=ntodb(autoh12);
      dbh12=reshape(dbh12,nchanh1,nagch12*npktnormal);
      dbh12=dbh12-repmat(dbcal,1,nagch12*npktnormal);
      dbh12=dbh12+repmat(x1(:)',nchanh1,1);
      if dfh1,
        dbh12=reshape(dbh12,2*nchanh1,nagch12*npktnormal/2);
        dbh12=[reshape(dbh12(1:nchanh1,:),1,nautoh12*npktnormal/2); ...

reshape(dbh12(nchanh1+1:nchanh1*2,:),1,nautoh12*npktnormal/2)];
      end

dbh12=reshape(dbh12,max(nagch12,nautoh12)/rch1/rcall,npktnormal*rch1*rcall)
;
    else,
      dbh12=zeros(1,nagch12*npktnormal);
      dbh12=dbh12+x1(:)';
      dbh12=reshape(dbh12,nagch12/rch1/rcall,npktnormal*rch1*rcall);
    end
  end
 end

 if bandh2,
   nstart=(fstarth2-25)/50;
   dstep=fsteph2/50;
   nstop=nstart+(nstepsh2-1)*dstep;
   freqh2=fstarth2:fsteph2:(fstarth2+fsteph2*(nstepsh2-1));

   if nagch21,
     dbcal=dbcalhf(1:nchanh2,1+2*floor(3.6*log10(nchanh2)));
     a2=a123(7,2);
     a3=a123(7,3);
     agch21=reshape(agch21,nagch21/rch2/rcall,npktnormal*rch2*rcall);
     k=anth21+att*4;
     x1=agch21;
     for j=1:nagch21/rch2/rcall,
       if dfh2,
         k=j+2-2*floor((j+1)/2)+att*4;
       end
       n=min(nstart+1+floor((j-1)/(1+dfh2))*dstep,322);
       x1(j,:)=-a1hf2(n,k) ...
           +40*(log10(10.^((agch21(j,:)-a3)./a2)+1));
     end

     if nautoh21,
       dbh21=ntodb(autoh21);
       dbh21=reshape(dbh21,nchanh2,nagch21*npktnormal);
```

```
        dbh21=dbh21-repmat(dbcal,1,nagch21*npktnormal);
        dbh21=dbh21+repmat(x1(:)',nchanh2,1);
        if dfh1,
          dbh21=reshape(dbh21,2*nchanh2,nagch21*npktnormal/2);
          dbh21=[reshape(dbh21(1:nchanh2,:),1,nautoh21*npktnormal/2); ...

reshape(dbh21(nchanh2+1:nchanh2*2,:),1,nautoh21*npktnormal/2)];
        end

dbh21=reshape(dbh21,max(nagch21,nautoh21)/rch2/rcall,npktnormal*rch1*rcall)
;
      else,
        dbh21=zeros(1,nagch21*npktnormal);
        dbh21=dbh21+x1(:)';
        dbh21=reshape(dbh21,nagch21/rch2/rcall,npktnormal*rch2*rcall);
      end

    end

    if nagch22,
      dbcal=dbcalhf(1:nchanh2,2+2*floor(3.6*log10(nchanh2)));
      a2=a123(8,2);
      a3=a123(8,3);
      agch22=reshape(agch22,nagch22/rch2/rcall,npktnormal*rch2*rcall);
      x2=agch22;
      for j=1:nagch22/rch2/rcall,
        n=min(nstart+1+floor((j-1)/(1+dfh2))*dstep,322);
        x2(j,:)=-a1hf2(n,4*(att+1)) ...
             +40*(log10(10.^((agch22(j,:)-a3)./a2)+1));
      end
      if nautoh22,
        dbh22=ntodb(autoh22);
        dbh22=reshape(dbh22,nchanh2,nagch22*npktnormal);
        dbh22=dbh22-repmat(dbcal,1,nagch22*npktnormal);
        dbh22=dbh22+repmat(x1(:)',nchanh2,1);
        if dfh1,
          dbh22=reshape(dbh22,2*nchanh2,nagch22*npktnormal/2);
          dbh22=[reshape(dbh22(1:nchanh2,:),1,nautoh22*npktnormal/2); ...

reshape(dbh22(nchanh2+1:nchanh1*2,:),1,nautoh22*npktnormal/2)];
        end

dbh22=reshape(dbh22,max(nagch22,nautoh22)/rch2/rcall,npktnormal*rch2*rcall)
;
      else,
        dbh22=zeros(1,nagch22*npktnormal);
        dbh22=dbh22+x1(:)';
        dbh22=reshape(dbh22,nagch22/rch2/rcall,npktnormal*rch2*rcall);
      end
    end
 end
```

phasemag.m

```
function [phase,mag] = phasemag(crossr,crossi)

% phasemag.m -- 27.09.99
% Transforms cross reals and imaginaries Kronos
% in phase (degrees) and magnitude.

er=fix(abs(crossr)/8);
ei=fix(abs(crossi)/8);
```

```
mr=abs(crossr)-er*8;
mi=abs(crossi)-ei*8;
nr=2.^er.*(mr+8);
ni=2.^ei.*(mi+8);
nr=nr.*sign(crossr);
ni=ni.*sign(crossi);
phase=atan2(ni,nr)*180/pi;
nri=sqrt(nr.^2+ni.^2);

 siz=size(crossr);
 e=zeros(siz);
 for j=1:32,
    nrimag=nri>16;
    e=e+nrimag;
    nri=nri-nri.*nrimag/2;
 end

m=nri-8;
mag=e*8+m;
return
```

correl_phase.m

```
function [ph,tauxr,tauxi] = corr_ph(auto1,auto2,crossr,crossi)
%
%function [ph,tauxr,tauxi] = corr_ph(auto1,auto2,crossr,crossi)
%calculates the phase shift (in degrees) and cross-correlation ratios

lx=crossr;
ly=crossi;
ex=fix(abs(lx)/8);
ey=fix(abs(ly)/8);
mx=abs(lx)-ex*8;
my=abs(ly)-ey*8;
nx=2.^ex.*(mx+8);
ny=2.^ey.*(my+8);
nx=nx.*sign(lx);
ny=ny.*sign(ly);
ph=atan2(ny,nx)*180/pi;

lx=auto1;
ly=auto2;
ex=fix(abs(lx)/8);
ey=fix(abs(ly)/8);
mx=abs(lx)-ex*8;
my=abs(ly)-ey*8;
nxa=2.^ex.*(mx+8);
nya=2.^ey.*(my+8);
tauxr=nx./sqrt(nxa.*nya);
tauxi=ny./sqrt(nxa.*nya);
```

fixsign.m

```
% fixsign.m  --  27.09.99
% to be called after READDATA to correct signs of cross-correlations.

nca=ncrossa;
ncab=nca+ncrossb;
ncabc=ncab+ncrossc;
ncabch1=ncabc+ncrossh1;
```

```
ncabch12=ncabc+ncrossh2;

x1=flipud(reshape(xi,8,npacket*nsign));
x2=flipud(reshape(xr,8,npacket*nsign));
x=[x1;x2];
x=reshape(x,nsign*16,npacket);

if ncrossa,
   crossar=abs(crossar).*x(2:2:2*nca,:);
   crossai=abs(crossai).*x(1:2:2*nca,:);
end
if ncrossb,
   crossbr=abs(crossbr).*x(2*nca+2:2:2*(ncab),:);
   crossbi=abs(crossbi).*x(2*nca+1:2:2*(ncab),:);
end
if ncrossc,
   crosscr=abs(crosscr).*x(2*ncab+2:2:2*ncabc,:);
   crossci=abs(crossci).*x(2*ncab+1:2:2*ncabc,:);
end
if ncrossh1,
   crossh1r=abs(crossh1r).*x(2*ncabc+2:2:2*ncabch1,:);
   crossh1i=abs(crossh1i).*x(2*ncabc+1:2:2*ncabch1,:);
end
if ncrossh2,
   crossh2r=abs(crossh2r).*x(2*ncabch1+2:2:2*ncabch12,:);
   crossh2i=abs(crossh2i).*x(2*ncabch1+1:2:2*ncabch12,:);
end
```

ntodb.m

```
function [db] = ntodb(counts)
% ntodb.m -- 27.09.99

e=fix(counts/8);
m=counts-8*e;
db=10*log10(2 .^e .*(m+8));
```

fitlogeq.m

```
function err = fitlogeq(a)

%  FITLOGEQ(a) returns the residuals between the input log response points
%  and the computed response curve with current values of coefficients
%  A1, A2, A3, A4.  It is called by FITLOG as an argument of FMINS.

global data plothandle err nx1 nx2 z

t = data(:,1);
y = data(:,2);

z=a(2).*log10((10.^((a(1)-t)/10)+10.^(-a(4)/10)).^.25-1)+a(3);

set(plothandle,'ydata',z)
drawnow
err = norm(z(nx1:nx2)-y(nx1:nx2));
```

fitlog.m

```
function err = fitlog(data)

% Fit of log response ...
% equation in FITLOGEQ.M

% function to call
%     -> data must be of the form [n,2] where the first column contains
%        attenuations and the second one the telemetry points to be fitted.

% Derived from "FITDEMO Nonlinear curve fit with simplex algorithm".

close
figure

global data

%  Let's plot the data.

t = data(:,1);
y = data(:,2);
axis([0 130 0 260])
hold on
plot(t,y,'c+','EraseMode','none')
title('Loi Log')
xlabel('dB attenuation')
ylabel('points télémesure')

siz=prod(size(data))/2;
xmin=data(1,1);xmax=data(siz,1);
disp('cliquez sur le premier point pour le fit')
[x1,y1]=ginput(1);
disp('cliquez sur le dernier point pour le fit')
[x2,y2]=ginput(1);
if x1<xmin, x1=xmin; end
if x2>xmax, x2=xmax; end
nx1=ceil(siz*(x1-xmin)/(xmax-xmin))+1;
nx2=floor(siz*(x2-xmin)/(xmax-xmin));
%data=data(nx1:nx2,:);

plot(t,y,'c+',t(nx1:nx2),y(nx1:nx2),'rx','EraseMode','none')
title('Loi Log')
xlabel('dB attenuation')
ylabel('points télémesure')

global plothandle err nx1 nx2 z
plothandle = plot(t,y,'y-','EraseMode','xor');

a0 = [100 100 0 -20]';
trace = 0;
tol = .1;
a = fmins('fitlogeq',a0,[trace tol]);

hold off
echo off
s = ['a = fmins(''fitlogeq'',[100 100 0  -20]'',[0 .1]);'];
uicontrol('Units','normal','Position',[.15 .01 .1
.06],'String','Again','callback',s)

t1=sprintf('A1 = %6.2f',a(1));
t2=sprintf('A2 = %6.2f',a(2));
t3=sprintf('A3 = %6.2f',a(3));
t4=sprintf('A4 = %6.2f',a(4));
terr=sprintf('erreur = %6.2f',err);
text(60,235,t1);
```

```
text(60,220,t2);
text(60,205,t3);
text(60,190,t4);
text(60,165,terr);

disp('End')
```

llogntox.m

```
function [x]=llogntox(n,a)

% x = a1 - 40*[log10(10^((n-a3)/a2)+1)]

% n == points de telemesure
% x == entree deduite en dB (a V0 pres)

x = a(1) - 40*[log10(10.^((n-a(3))/a(2))+1)];
```

llogxton.m

```
function [n]=llogxton(x,a)

% x == entree en dB
% n == points de telemesure

n=a(2).*log10((10.^((a(1)-x)/10)+10.^(-a(4)/10)).^.25-1)+a(3);
```

Various files.

dbcal32.txt

```
» readdata
which data file? fluctabc.004
bench1 =
old
Analysis data
Bands A  B  C
ABC integrate  time = 1.000 sec
    no. of channels =    32
    direction finding ON
    internal attenuator OFF
  90 packets
» axp=mean(autoa1(1:32,:)');
» bxp=mean(autob1(1:32,:)');
» cxp=mean(autoc1(1:32,:)');
» cxm=mean(autoc1(33:64,:)');
» bxm=mean(autob1(33:64,:)');
» axm=mean(autoa1(33:64,:)');
» axp=ntodb(axp);
» bxp=ntodb(bxp);
» cxp=ntodb(cxp);
» cxm=ntodb(cxm);
» bxm=ntodb(bxm);
» axm=ntodb(axm);
» hold off
» plot([axp bxp cxp],'r')
» hold on
» plot([axm bxm cxm],'b')
» title('dBcals deduced from file fluctabc.004 - + & - Ex')
» ylabel('dB')
» print -dpsc ___1.ps

» ax=mean(reshape(autoa1,32,180)');
» bx=mean(reshape(autob1,32,180)');
» cx=mean(reshape(autoc1,32,180)');
» cz=mean(reshape(autoc2,32,180)');
» bz=mean(reshape(autob2,32,180)');
» az=mean(reshape(autoa2,32,180)');
» ax=ntodb(ax);
» bx=ntodb(bx);
» cx=ntodb(cx);
» cz=ntodb(cz);
» bz=ntodb(bz);
» az=ntodb(az);
» dbcal=[axp' axm' ax' az'
         bxp' bxm' bx' bz'
         cxp' cxm' cx' cz']
dbcal =
   75.3941   76.0089   75.7124   75.6301
   75.3941   75.9166   75.6632   75.6107
   75.2363   75.9062   75.5744   75.5463
   75.1506   75.7690   75.4203   75.4579
                :
                :
                :
   70.7538   70.9125   70.8339   70.9269
```

dbcal.txt

```
» readdata
which data file? llgar20.020
bench1 =
old
Analysis data
Bands A                          repeat count ALL =     1
ABC integrate  time = 1.000 sec
    no. of channels =    32
    antenna 1 -> +/-Ex              autos ON
    antenna 2 -> +Ez                cross ON
    direction finding ON            repeat count =     4
    internal attenuator OFF
  64 packets

» physique
» size(dba1)
   256    64
» d1=reshape(dba1,64,256);
» d2=reshape(d1',4,256*16);
» d2=mean(d2);
» d3=reshape(d2,64,64);
» d3=d3';
» d4=reshape(d3,32,128);
» dpx=d4(:,1:2:128);
» dmx=d4(:,2:2:128);
» plot(mean(dpx(:,1:35)'-dmx(:,1:35)'))

» title('mean(dpx(:,1:35)''-dmx(:,1:35)''')

» x=1:32;
» y=mean(dpx(:,1:35)'-dmx(:,1:35)');
» c=polyfit(x,y,5);
» y1=polyval(c,x);
» plot(x,y,x,y1)
» title('diff. dBcal32 bande A - (+X)-(-X) - file llgar20.020')
» ylabel('dB');xlabel('canaux');grid on

» yy=[y' y1'];
» save dbcal_diff_A.dat -ascii yy
»
» load dbcal_32.dat
» size(dbcal_32)
    96     2
» dpxc_32=dbcal_32(1:32,1);
» dmxc_32=dpxc_32+y1';
» dpmxc_32=(dpxc_32+dmxc_32)/2;
» coeffs_c_32=[dpxc_32 dmxc_32 dpmxc_32 dbcal_32(1:32,2)];
» save dbcoeffs_a_32.dat -ascii coeffs_c_32
» plot([dpxc_32 dmxc_32 dpmxc_32])
» ylabel('dB');xlabel('canaux');grid on
» title('dBcal +X, -X, +/-X, Bande A, 32 canaux')

» load dbcal_16.dat
» size(dbcal_16)
    48     2
» dpxc_16=dbcal_16(1:16,1);
» yb=(y1(1:2:32)+y1(2:2:32))/2;
» dmxc_16=dpxc_16+yb';
» dpmxc_16=(dpxc_16+dmxc_16)/2;
» coeffs_c_16=[dpxc_16 dmxc_16 dpmxc_16 dbcal_16(1:16,2)];
» save dbcoeffs_a_16.dat -ascii coeffs_c_16
```

```
» plot([dpxc_16 dmxc_16 dpmxc_16])
» ylabel('dB');xlabel('canaux');grid on
» title('dBcal +X, -X, +/-X, Bande A, 16 canaux')

» load dbcal_08.dat
» size(dbcal_08)
     8     6
» dpxc_08=dbcal_08(:,1);
» yc=(yb(1:2:16)+yb(2:2:16))/2;
» dmxc_08=dpxc_08+yc';
» dpmxc_08=(dpxc_08+dmxc_08)/2;
» coeffs_c_08=[dpxc_08 dmxc_08 dpmxc_08 dbcal_08(:,4)];
» save dbcoeffs_a_08.dat -ascii coeffs_c_08
» plot([dpxc_08 dmxc_08 dpmxc_08])
» ylabel('dB');xlabel('canaux');grid on
» title('dBcal +X, -X, +/-X, Bande A, 08 canaux')

» readdata
which data file? llgbr20.020
bench1 =
old
Analysis data
Bands    B                      repeat count ALL =     1
ABC integrate  time = 1.000 sec
    no. of channels =    32
    antenna 1 -> +/-Ex              autos ON
    antenna 2 -> +Ez                cross ON
    direction finding ON            repeat count =     4
attenuateur interne OFF
  64 packets

» physique
» d1=reshape(dbb1,64,256);
» d2=reshape(d1',4,256*16);
» d2=mean(d2);
» d3=reshape(d2,64,64);
» d3=d3';
» d4=reshape(d3,32,128);
» dpx=d4(:,1:2:128);
» dmx=d4(:,2:2:128);
» y=mean(dpx(:,4:34)'-dmx(:,4:34)');
» x=1:32;
» plot(x,y)
» plot(dpx'-dmx')
» c=polyfit(x,y,5);
» y1=polyval(c,x);
» plot(x,y,x,y1)
» ylabel('dB');xlabel('canaux');grid on
» title('diff. dBcal32 bande B - (+X)-(-X) - file llgbr20.020')
» yy=[y' y1'];
» save dbcal_diff_B.dat -ascii yy

» load dbcal_32.dat
» size(dbcal_32)
    32     6
» dpxc_32=dbcal_32(:,2);
» dmxc_32=dpxc_32+y1';
» dpmxc_32=(dpxc_32+dmxc_32)/2;
» coeffs_c_32=[dpxc_32 dmxc_32 dpmxc_32 dbcal_32(:,5)];
» save dbcoeffs_b_32.dat -ascii coeffs_c_32
» plot([dpxc_32 dmxc_32 dpmxc_32])
» ylabel('dB');xlabel('canaux');grid on
» title('dBcal +X, -X, +/-X, Bande B, 32 canaux')
```

```
» load dbcal_16.dat
» size(dbcal_16)
    16     6
» dpxc_16=dbcal_16(:,2);
» yb=(y1(1:2:32)+y1(2:2:32))/2;
» dmxc_16=dpxc_16+yb';
» dpmxc_16=(dpxc_16+dmxc_16)/2;
» coeffs_c_16=[dpxc_16 dmxc_16 dpmxc_16 dbcal_16(1:16,5)];
» save dbcoeffs_b_16.dat -ascii coeffs_c_16
» plot([dpxc_16 dmxc_16 dpmxc_16])
» ylabel('dB');xlabel('canaux');grid on
» title('dBcal +X, -X, +/-X, Bande B, 16 canaux')

» load dbcal_08.dat
» size(dbcal_08)
     8     6
» dpxc_08=dbcal_08(:,1);
» yc=(yb(1:2:16)+yb(2:2:16))/2;
» dmxc_08=dpxc_08+yc';
» dpmxc_08=(dpxc_08+dmxc_08)/2;
» coeffs_c_08=[dpxc_08 dmxc_08 dpmxc_08 dbcal_08(:,5)];
» save dbcoeffs_b_08.dat -ascii coeffs_c_08
» plot([dpxc_08 dmxc_08 dpmxc_08])
» ylabel('dB');xlabel('canaux');grid on
» title('dBcal +X, -X, +/-X, Bande B, 8 canaux')
»
» readdata
which data file? llgcr20.020
bench1 =
old
Analysis data
Bands       C                    repeat count ALL =     1
ABC integrate  time = 1.000 sec
    no. of channels =    32
    antenna 1 -> +/-Ex              autos ON
    antenna 2 -> +Ez                cross ON
    direction finding ON            repeat count =     4
attenuateur interne OFF
  64 packets
» d1=reshape(dbc1,64,256);
??? Undefined function or variable 'dbc1'.

» physique
» d1=reshape(dbc1,64,256);
» d2=reshape(d1',4,256*16);
» d2=mean(d2);
» d3=reshape(d2,64,64);
» d3=d3';
» d4=reshape(d3,32,128);
» dpx=d4(:,1:2:128);
» dmx=d4(:,2:2:128);
» plot(dpx'-dmx')
» plot(dpx(1:32,:)'-dmx(1:32,:)')
» plot(dpx(:,1:32)'-dmx(:,1:32)')
» y=mean(dpx(:,1:32)'-dmx(:,1:32)');
» x=1:32;
» c=polyfit(x,y,5);
» y1=polyval(c,x);
» plot(x,y,x,y1)
» ylabel('dB');xlabel('canaux');grid on
» title('diff. dBcal32 bande C - (+X)-(-X) - file llgcr20.020')

» load dbcal_32.dat
» dpxc_32=dbcal_32(:,3);
```

```
» dmxc_32=dpxc_32+y1';
» dpmxc_32=(dpxc_32+dmxc_32)/2;
» coeffs_c_32=[dpxc_32 dmxc_32 dpmxc_32 dbcal_32(:,6)];
» save dbcoeffs_c_32.dat -ascii coeffs_c_32
» plot([dpxc_32 dmxc_32 dpmxc_32])
» ylabel('dB');xlabel('canaux');grid on
» title('dBcal +X, -X, +/-X, Bande C, 32 canaux')

» load dbcal_16.dat
» dpxc_16=dbcal_16(:,3);
» yb=(y1(1:2:32)+y1(2:2:32))/2;
» dmxc_16=dpxc_16+yb';
» dpmxc_16=(dpxc_16+dmxc_16)/2;
» coeffs_c_16=[dpxc_16 dmxc_16 dpmxc_16 dbcal_16(1:16,6)];
» save dbcoeffs_c_16.dat -ascii coeffs_c_16
» plot([dpxc_16 dmxc_16 dpmxc_16])
» ylabel('dB');xlabel('canaux');grid on
» title('dBcal +X, -X, +/-X, Bande C, 16 canaux')

» load dbcal_08.dat
» yc=(yb(1:2:16)+yb(2:2:16))/2;
» dpxc_08=dbcal_08(:,3);
» dmxc_08=dpxc_08+yc';
» dpmxc_08=(dpxc_08+dmxc_08)/2;
» coeffs_c_08=[dpxc_08 dmxc_08 dpmxc_08 dbcal_08(:,6)];
» save dbcoeffs_c_08.dat -ascii coeffs_c_08
» plot([dpxc_08 dmxc_08 dpmxc_08])
» ylabel('dB');xlabel('canaux');grid on
» title('dBcal +X, -X, +/-X, Bande C, 8 canaux')
```

dbcal_2.txt

```
» dbcal_2 --> continuation of processing described in dbcal32.txt

readdata
which data file? 32filabc.002
bench1 =
old
Analysis data
Bands A  B  C                    repeat count ALL =    10
ABC integrate  time = 1.000 sec
    no. of channels =    32
    antenna 1 -> +/-Ex              autos ON
    antenna 2 -> +Ez                cross ON
    direction finding OFF           repeat count =     1
    internal attenuator ON
  11 packets

readdata
which data file? 16filabc.001
bench1 =
old
Analysis data
Bands A  B  C                    repeat count ALL =   100
ABC integrate  time = 1.000 sec
    no. of channels =    16
    antenna 1 -> +/-Ex              autos ON
    antenna 2 -> +Ez                cross ON
    direction finding OFF           repeat count =     1
    internal attenuator ON
   1 packets
```

```
readdata
which data file? 8filtabc.001
bench1 =
old
Analysis data
Bands A  B  C                    repeat count ALL =   100
ABC integrate  time = 1.000 sec
    no. of channels =     8
    antenna 1 -> +/-Ex              autos ON
    antenna 2 -> +Ez                cross ON
    direction finding OFF           repeat count =     1
    internal attenuator ON
   1 packets

--> continuation of processing done in dbcal_2.m

» plot([[ax32;bx32;cx32] dbcal32(:,1)])
» ylabel('dB');xlabel('canaux');grid on
» title('[[ax32;bx32;cx32] dbcal32(:,1)]')
» x32=[ax32;bx32;cx32];
» z32=[az32;bz32;cz32];
» deltax32=x32-dbcal32(:,1);
» deltaz32=z32-dbcal32(:,4);
» plot([deltax32 deltaz32])
» ylabel('dB');xlabel('canaux');grid on
» title('[deltax32 deltaz32]')

» diffp_m32=dbcal32(:,1)-dbcal32(:,2);
» plot(diffp_m32)
» ylabel('dB');xlabel('canaux');grid on
» title('diffp_m32=dbcal32(:,1)-dbcal32(:,2)')

» dbcal16=zeros(48,4);
» dbcal8=zeros(24,4);

» x16=[ax16;bx16;cx16];
» z16=[az16;bz16;cz16];
» x8=[ax8';bx8';cx8'];
» z8=[az8';bz8';cz8'];
» deltax16=(deltax32(1:2:96)+deltax32(2:2:96))/2;
» deltaz16=(deltaz32(1:2:96)+deltaz32(2:2:96))/2;
» deltax8 = (deltax16(1:2:48)+deltax16(2:2:48))/2;
» deltaz8 = (deltaz16(1:2:48)+deltaz16(2:2:48))/2;
» diffp_m16=(diffp_m32(1:2:96)+diffp_m32(2:2:96))/2;
» diffp_m8 = (diffp_m16(1:2:48)+diffp_m16(2:2:48))/2;
» dbcal16(:,1)=x16-deltax16;
» dbcal16(:,2)=x16-deltax16-diffp_m16;
» dbcal16(:,3)=x16-deltax16-diffp_m16/2;
» dbcal16(:,4)=z16-deltaz16;
» dbcal8(:,1)=x8-deltax8;
» dbcal8(:,2)=x8-deltax8-diffp_m8;
» dbcal8(:,2)=x8-deltax8-diffp_m8/2;
» dbcal8(:,2)=x8-deltax8-diffp_m8;
» dbcal8(:,3)=x8-deltax8-diffp_m8/2;
» dbcal8(:,4)=z8-deltaz8;
»
» dbcal_32=[dbcal32(1:32,:) dbcal32(33:64,:) dbcal32(65:96,:)];
» dbcal_16=[dbcal16(1:16,:) dbcal16(17:32,:) dbcal16(33:48,:)];
» dbcal_08=[dbcal8(1:8,:)     dbcal8(9:16,:)     dbcal8(17:24,:)];
» dbcal_32=round(dbcal_32*100)/100;
» dbcal_16=round(dbcal_16*100)/100;
» dbcal_08=round(dbcal_08*100)/100;
» save dbcal_32.dat -ascii dbcal_32
» save dbcal_16.dat -ascii dbcal_16
```

```
» save dbcal_08.dat -ascii dbcal_08
```

correction_sinx_x_abc.txt

```
Calculation of the correction to apply to Vo in log response calibrations
of ABC receivers due to the sin(x)/x shape of the spectrum of noise
generators.

» fca=40;
» fcb=180;
» fcc=800;

» fra=3.6:.02:3.6*4.5;
» frb=4.5*fra;
» frc=4.5*frb;

» arga=pi*fra/fca;
» argb=pi*frb/fcb;
» argc=pi*frc/fcc;

» pa=(sin(arga)./arga).^2;
» pb=(sin(argb)./argb).^2;
» pc=(sin(argc)./argc).^2;

» meana=10*log10(.02*sum(pa)/3.6/3.5)
meana = -0.9686
» meanb=10*log10(.02*sum(pb)/3.6/3.5)
meanb = -0.9686
» meanc=10*log10(.02*sum(pc)/3.6/3.5)
meanc = -0.9927

% calculation of average level of noise generators.

» dbv0a=10*log10(1.86^2/2/fca/1000)+meana
dbv0a = -44.6093
» dbv0b=10*log10(1.86^2/2/fcb/1000)+meanb
dbv0b = -51.1414
» dbv0c=10*log10(1.835^2/2/fcc/1000)+meanc
dbv0c = -57.7611
```

integration_times.txt

== discussion of acquisition and computation times for each configuration.

```
Calculation of ABC measurement times
====================================

» ncycles=ones(3,1)*[81 18 4]   % sampling rate in multiples of 200 ns
    81    18     4
    81    18     4
    81    18     4

» scale=[1128;513;245]; % of files iscale(8,16,32).dat, canal 0
» nn=230;

» q=(2*256*(nn-1)./scale+1)/2 % == onboard  calculations
   52.4716
  114.7768
  239.7816
```

```
» ntaps=floor(q*ones(1,3))    % filter lengths (canal 0)
    52    52    52
   114   114   114
   239   239   239
» nsamples=2*ntaps;

» tacq=.0002*ncycles.*nsamples
       A         B         C
    1.6848    0.3744    0.0832  |  8
    3.6936    0.8208    0.1824  | 16
    7.7436    1.7208    0.3824  | 32

» ttotal=[2.532 1.2214 .936;5.572 2.879 2.246;13.476 7.452 6.119]
    2.5320    1.2214    0.9360   % measured by P. Fedou
    5.5720    2.8790    2.2460
   13.4760    7.4520    6.1190

 » tcalcul=ttotal-tacq           % == quite homogeneous (except B16)
    0.8472    0.8470    0.8528
    1.8784    2.0582    2.0636
    5.7324    5.7312    5.7366


 » nblocks=[407 873 1164;179 367 478;76 140 172] % of file blocks.dat,
         407         873        1164                values for 1 sec
         179         367         478
          76         140         172

» nblocks.*ttotal/1000
    1.0305    1.0663    1.0895   % =~ 1 sec.
    0.9974    1.0566    1.0736
    1.0242    1.0433    1.0525
```

idem for HF

============

```
» scale=[512;1024;2047]; % of file hfscale.dat
    512
    1024
    2047

» nn=80;
» q=(2*256*(nn-1)./scale+1)/2
   40.0000
   20.2500
   10.3798

» ntap=floor(q);
» ntaps=flipud([80;ntap])
    10
    20
    40
    80
» nsamples=2*ntaps;

» tacq=.0002*ncycles.*nsamples

    0.0680
    0.1360
    0.2720
    0.5440
```

```
» ttotal=[.2472;.4178;.8102;1.7761]
    0.2472
    0.4178
    0.8102
    1.7761

» tcalcul=ttotal-tacq
    0.1792
    0.2818
    0.5382
    1.2321
```

corr_integrate_times.txt

» load blocks.tmp = *number of analyses averaged by the ADSP as a function of the band number of filters, and integration time.*

```
» abc=blocks(1:36);hf=blocks(37:56);

» abc=reshape(abc,3,12)

  51   102   204   407   109   218   436   873   145   291   582  1164   8f
  22    45    90   179    46    92   183   367    60   119   239   478  16f
   9    19    38    76    17    35    70   140    21    43    86   172  32f
.125  .25   .5     1    .125  .25   .5     1    .125  .25   .5     1   sec
 --------------------   --------------------   --------------------
          A                      B                      C

» abcnn=reshape(abc',4,9)

  51     109     145      22      46      60       9      17      21  .125s
 102     218     291      45      92     119      19      35      43   .25
 204     436     582      90     183     239      38      70      86    .5
 407     873    1164     179     367     478      76     140     172     1
  A       B       C       A       B       C       A       B       C
 --------------------   --------------------   --------------------
          8f                     16f                    32f
```

Normalize wrt … 1 sec, ideally ratios of 2 :

```
» abcnn(1,:)=abcnn(1,:)*8;
» abcnn(2,:)=abcnn(2,:)*4;
» abcnn(3,:)=abcnn(3,:)*2;
» abcnn

 408     872    1160     176     368     480      72     136     168
 408     872    1164     180     368     476      76     140     172
 408     872    1164     180     366     478      76     140     172
 407     873    1164     179     367     478      76     140     172
```

Compare with ideal matrix :

```
» norm=ones(4,1)*abcnn(4,:)

 407     873    1164     179     367     478      76     140     172
 407     873    1164     179     367     478      76     140     172
 407     873    1164     179     367     478      76     140     172
 407     873    1164     179     367     478      76     140     172

» abcn=abcnn./norm

1.0025  0.9989  0.9966  0.9832  1.0027  1.0042  0.9474  0.9714  0.9767
```

```
1.0025  0.9989  1.0000  1.0056  1.0027  0.9958  1.0000  1.0000  1.0000
1.0025  0.9989  1.0000  1.0056  0.9973  1.0000  1.0000  1.0000  1.0000
1.0000  1.0000  1.0000  1.0000  1.0000  1.0000  1.0000  1.0000  1.0000


» dbabc=10*log10(abcn);
» dbabc=reshape(dbabc,12,3)';
» dbabc=reshape(dbabc,3,4,3)
dbabc(:,:,1) =
    0.0107    0.0107    0.0107         0   A- 8
   -0.0734    0.0242    0.0242         0   A-16
   -0.2348         0         0         0   A-32
dbabc(:,:,2) =
   -0.0050   -0.0050   -0.0050         0   B- 8
    0.0118    0.0118   -0.0118         0   B-16
   -0.1259         0         0         0   B-32
dbabc(:,:,3) =
   -0.0149         0         0         0   C- 8
    0.0181   -0.0182         0         0   C-16
   -0.1022         0         0         0   C-32
   » -----     -----     -----     -----
     .125s      .25s       .5s        1s
```

idem for HF
==========

```
» hf=reshape(hf,4,5)
    41    85   171   345   692   1f
    25    50   102   205   412   2f
    13    26    53   106   213   4f
     6    12    24    48    96   8f
    10    20    40    80   160  ms
```

Normalize wrt … 80 msec, ideally ratios of 2 :

```
» test=[8 4 2 1 .5];
» test=ones(4,1)*test
    8.0000    4.0000    2.0000    1.0000    0.5000
    8.0000    4.0000    2.0000    1.0000    0.5000
    8.0000    4.0000    2.0000    1.0000    0.5000
    8.0000    4.0000    2.0000    1.0000    0.5000
» hfn=hf.*test
  328.0000  340.0000  342.0000  345.0000  346.0000
  200.0000  200.0000  204.0000  205.0000  206.0000
  104.0000  104.0000  106.0000  106.0000  106.5000
   48.0000   48.0000   48.0000   48.0000   48.0000
```

Compare with ideal matrix :

```
» norm=hfn(:,4)*ones(1,5)
   345   345   345   345   345
   205   205   205   205   205
   106   106   106   106   106
    48    48    48    48    48

» dbhf=10*log10(hfn./norm)
   -0.2195   -0.0634   -0.0379         0    0.0126  1 filt.
   -0.1072   -0.1072   -0.0212         0    0.0211  2  "
   -0.0827   -0.0827         0         0    0.0204  4  "
         0         0         0         0         0  8  "
     -----     -----     -----     -----     -----
      10ms      20ms      40ms      80ms     160ms
```

"worst case error" equals case 10 ms, 1 filter == -.22 dB

But... results of trials on files flucthf.001 to flucthf.010...

```
» a1=[157.1 156.8 156.7 156.8 156.6];
» a2=[167.9 167.8 167.7 167.6 167.5];
» a3=[175.4 175.9 176.1 176.0 175.9];
» a4=[183.9 184.3 182.2 182.2 182.2];
» d1=(ntodb(a1)-ntodb(a1(4)));
» d2=(ntodb(a2)-ntodb(a2(4)));
» d3=(ntodb(a3)-ntodb(a3(4)));
» d4=(ntodb(a4)-ntodb(a4(4)));

» [d1;d2;d3;d4]
    0.1006         0   -0.0341         0   -0.0684  1
    0.0827    0.0553    0.0278         0   -0.0279  2
   -0.1660   -0.0272    0.0540         0   -0.0272  4
    0.4911    0.6782         0         0         0  8
»    -----     -----     -----     -----     -----
      10ms      20ms      40ms      80ms     160ms
```

These results are not in very good agreement with theoretical predictions above, but probably the tests were not well controlled and long enough to reach the required accuracy.

Files newcode

used for data decompression (meander)

newcode1.dat	newcode2.dat	newcode3.dat
040f	0000	0000
0508	0000	0000
0511	040a	0000
0000	0000	0000
0514	0000	0000
0502	0502	0000
050b	050a	0407
0000	0000	0000
040c	040f	0000
0505	0505	0404
050e	0407	0305
0000	0000	0000
0000	0000	0000
0000	0000	0000
0000	0000	0000
0000	0000	0000
040d	0000	0000
0506	0506	0000
050f	0408	0400
0000	0000	0000
0512	040b	0000
0500	0500	0306
0509	0508	0405
0000	0000	0000
0515	040d	0000
0503	0503	0402

050c	050b	0408
0000	0000	0000
0000	0000	0000
0000	0000	0000
0000	0000	0000
0000	0000	0000
040e	0000	0000
0507	0507	0000
0510	0409	0307
0000	0000	0000
0513	040c	0000
0501	0501	0401
050a	0509	0406
0000	0000	0000
040b	040e	0000
0504	0504	0403
050d	0406	0409
0000	0000	0000

IDL programs.

The programs involved in data calibration (from raw auto and cross values to physical units) are "cal.pro", which calls the routines "agc_db.pro" and "auto_db.pro" and uses the save_set "constants.xdr". This save set is built with the program "read_constants.pro" and the above data tables "a….dat" and "dbcal….dat".

help_cal.pro

```
pro HELP_CAL
  print,'Function CAL, agc, auto, bande, ant, freq, nfilters, filter'
  print,'Function AGC_dB, agc, a1, a2, a3'
  print,'Function AUTO_dB, auto'
return
end
```

cal.pro

```
Function CAL, agc, auto, bande, ant, freq, nfilters, filter      ;, att

; Conversion of [tables of] couples (agc,auto) or (agc,cross) into values
; in physical units (dB / Volts.Hz^-1/2)

; band = 0-4 (A,B,C,H1,H2)
; ant = 0-3 (+X,-X,D,Z)
; freq = frequency (kHz), H1 & H2 only; =0 pour ABC
; nfilters = 1,2,4,8,16,32 (filters/band)
; filter = 1-32 (# of filter in the band)
; att = 0-1 (Off,On)

  common KRONOSCAL, a1h1,a1h2,ai,dbcal_abc,dbcal_h

  if n_elements(ai) eq 0 then restore,'constants.xdr'
  ncal=n_elements(agc)
  if n_elements(att) eq 0 then att=intarr(ncal)
  a123=fltarr(3,ncal)
  iant=byte(ant/3)
  for i=0L,ncal-1L do a123(*,i)=ai(*,iant(i),bande(i),att(i))
  ifreq=freq
  test=where(bande eq 3)
  if test(0) ne -1 then begin
      testfreq=where(bande eq 3 and ifreq gt 4300)
      if testfreq(0) ne -1 then ifreq(testfreq)=4300
      ntest=n_elements(test)
      for i=0L,ntest-1L do a123(0,test(i))= $
            a1h1(ant(test(i)),fix(ifreq(test(i))/25),att(test(i)))
  endif
  test=where(bande eq 4)
  if test(0) ne -1 then begin
        testfreq=where(bande eq 4 and ifreq gt 16075)
        if testfreq(0) ne -1 then ifreq(testfreq)=16075
        ntest=n_elements(test)
        for i=0L,ntest-1L do a123(0,test(i))= $
                a1h2(ant(test(i)),fix((ifreq(test(i))-25)/50),att(test(i)))
  endif

  dBcal=fltarr(ncal)
```

```
  test=where(bande le 2)
  ntest=n_elements(test)
  if test(0) ne -1 then for i=0L,ntest-1L do dBcal(test(i))= $
      dBcal_abc(filter(test(i)),ant(test(i)),bande(test(i)), $
      fix(alog(nfilters(test(i))*1.)/alog(2.)+0.5)-3)
  test=where(bande gt 2)
  ntest=n_elements(test)
  if test(0) ne -1 then for i=0L,ntest-1L do dBcal(test(i))= $
      dBcal_h(filter(test(i)),iant(test(i)), $
      fix(alog(nfilters(test(i))*1.)/alog(2.)+0.5))

  dB=fltarr(ncal)
  test=where(agc ne 255)
  if test(0) ne -1 then $
      dB(test)=AGC_dB(agc(test),a123(0,test),a123(1,test),a123(2,test))
  test=where(auto ne 255)
  if test(0) ne -1 then $
        dB(test)=dB(test)+AUTO_dB(auto(test))-dBcal(test)

  test=where((agc ne 255 or auto ne 255) and ant ne 2)
  if test(0) ne -1 then dB(test)=dB(test)+3.          ; +3 dB in monopole

  return, dB

; dB = 0 si agc = auto = 0
end
```

agc_db.pro

```
Function AGC_dB, agc, a1, a2, a3
  dB = -a1 + 40.*alog10( 1. + 10.^((agc-a3)/a2) )
  return, dB
end
```

auto_db.pro

```
Function AUTO_dB, auto
  dB = 10.*alog10( (8.+(auto and '07'x)) *2.^(ishft(auto and 'f8'x, -3)) )
  return, dB
end
```

read_constants.pro

```
; READ_CONSTANTS.pro

; reads a_i & dB_cal values from files db_cal.dat, a1hf1.dat & a1hf2.dat

  buf=[     166.37,73.20,-0.01,     $      ; A band, Ex, Att Off
      164.84,73.16, 3.21,     $      ; A band, Ez,     "
      168.48,85.61, 0.08,     $      ; B band, Ex,     "
      168.70,85.03, 1.31,     $      ; B band, Ez,     "
      168.43,82.58, 0.01,     $      ; C band, Ex,     "
      169.46,82.30, 0.00,     $      ; C band, Ez,     "
        0.  ,94.81, 0.  ,     $      ; H1 band, Ex,    "
          0.  ,96.76, 0.  ,   $      ; H1 band, Ez,    "
          0.  ,94.81, 0.  ,   $        ; H2 band, Ex   H2 = H1
```

```
          0.  ,96.76, 0.  ]              ; H2 band, Ez
  ai=fltarr(3,2,5,2)          ; a123, Ex/z, 5 bands, att off/on
  ai(*,*,*,0)=reform(buf,3,2,5)
  ai(*,*,*,1)=ai(*,*,*,0)

ai(0,*,*,1)=reform([136.27,134.84,138.38,138.70,138.33,139.46,0,0,0,0],2,5)

  a1h1=fltarr(4,173,2)        ; +x/-x/+-x/z, 0,25,50...4300 kHz, att off/on
  a1h2=fltarr(4,322,2)        ; +x/-x/+-x/z, 25,75...16075 kHz, att off/on
  buf=fltarr(8)

  openr,u,'a1hf1.dat',/get_lun
  for i=0,172 do begin
    readf,u,buf
    a1h1(*,i,0)=buf(0:3) & a1h1(*,i,1)=buf(4:7)
  endfor
  close,u & free_lun,u

  openr,u,'a1hf2.dat',/get_lun
  for i=0,321 do begin
    readf,u,buf
    a1h2(*,i,0)=buf(0:3) & a1h2(*,i,1)=buf(4:7)
  endfor
  close,u & free_lun,u

  dbcal_abc=fltarr(32,4,3,3)  ; #filt, +x/-x/+-x/z, ABC, 8/16/32
  buf=fltarr(12)

  openr,u,'dbcal_08.dat',/get_lun
  for i=0,7 do begin
    readf,u,buf
    dbcal_abc(i,*,0,0)=buf(0:3) & dbcal_abc(i,*,1,0)=buf(4:7)
    dbcal_abc(i,*,2,0)=buf(8:11)
  endfor
  close,u & free_lun,u

  openr,u,'dbcal_16.dat',/get_lun
  for i=0,15 do begin
    readf,u,buf
    dbcal_abc(i,*,0,1)=buf(0:3) & dbcal_abc(i,*,1,1)=buf(4:7)
    dbcal_abc(i,*,2,1)=buf(8:11)
  endfor
  close,u & free_lun,u

  openr,u,'dbcal_32.dat',/get_lun
  for i=0,31 do begin
    readf,u,buf
    dbcal_abc(i,*,0,2)=buf(0:3) & dbcal_abc(i,*,1,2)=buf(4:7)
    dbcal_abc(i,*,2,2)=buf(8:11)
  endfor
  close,u & free_lun,u

  dbcal_h=fltarr(8,2,4)       ; #filt, x/z, 1/2/4/8
  buf=fltarr(8)

  openr,u,'dbcalhf.dat',/get_lun
  for i=0,7 do begin
    readf,u,buf
    dbcal_h(i,*,*)=buf
  endfor
  close,u & free_lun,u

save,a1h1,a1h2,ai,dbcal_abc,dbcal_h,file='constants.xdr',/xdr,/verb
```

```
; A1H1            FLOAT = Array(4, 173, 2)
;                        +x/-x/+-x/z, 0,25,50...4300 kHz, att off/on
; A1H2            FLOAT = Array(4, 322, 2)
;                        +x/-x/+-x/z, 25,75...16075 kHz, att off/on
; AI        FLOAT = Array(3, 2, 5, 2)
;                        a123, Ex/z, 5 bands, att off/on
; DBCAL_ABC FLOAT = Array(32, 4, 3, 3)
;                        #filt, +x/-x/+-x/z, ABC, 8/16/32
; DBCAL_H   FLOAT = Array(8, 2, 4)
;                        #filt, x/z, 1/2/4/8

end
```

constants.xdr

```
IDL> restore,'constants.xdr'
IDL> help
A1H1            FLOAT     = Array[4, 173, 2]
A1H2            FLOAT     = Array[4, 322, 2]
AI              FLOAT     = Array[3, 2, 5, 2]
DBCAL_ABC       FLOAT     = Array[32, 4, 3, 3]
DBCAL_H         FLOAT     = Array[8, 2, 4]
```

The program "prep_df.pro" below is an example of reading and calibrating data in direction-finding mode, including calibration of phases. The part in *italics* is simply the loading and selection of raw data. The following part performs the calibration of amplitudes by calling "cal.pro", and than correction of phases using the save_set "phases.xdr". This save set is built with the program "read_phases.pro" and the above data tables "phase….dat".

prep_df.pro

```
pro PREP_DF, aaaajjj, hd, hf, bande, vv,xts,xf,msec

; reads "analysis" data (Kronos ~NewBench) from a list of files
; (from 'liste.scratch'), calibrate, and fills the array VV
; = VV*[+X,Z,-X,Z]  Re,Im(VV*)[+X,Z]  Re,Im(VV*)[-X,Z]
; af full temporal resolution, with corrected phases
; xts & xf = time (sec) and frequency (kHz)
; msec = integration time of measurements
; band : A=0, B=1, C=2, H1=3, H2=4

; do first (in the program directory)
; dir/out=liste.scratch/col=1/nohead/notrail [dir_Kronos]       (VMS)
; ls -1 /dir/sous_dir/dir_Kronos/* > liste.scratch              (Unix)

  common KRONOSCAL, a1h1,a1h2,ai,dbcal_abc,dbcal_h   ; ,v0

  LIT_HFR_LISTE, aaaajjj, hd, hf, bande, bande, z

  print & print,'selection of DF data ...'
  test=where(z.bande eq bande and z.df gt 10 and z.agc1 ne 255b and $
      z.agc2 ne 255b and z.auto1 ne 255b and z.auto2 ne 255b and $
      z.cross1 ne -999 and z.cross2 ne -999)
  if test(0) ne -1 then z=z(test) else stop
```

```
  help,z

; preparation tableaux xts & xf

  nz = n_elements(z)
  xts = dblarr(nz) & xf=fltarr(nz)
  for i=0L,nz-1L do
xts(i)=total(transpose(z(i).time)#[3600.0,60.0,1.0,0.01])
  if bande le 2 then begin
    nfilt=z(0).filters & freq_ABC,nfilt,freq
    for i=0L,nz-1L do begin
      if z(i).filters ne nfilt then begin
      nfilt=z(i).filters & freq_ABC,nfilt,freq
      endif
      xf(i)=freq(bande*nfilt+z(i).filter)
    endfor
  endif else xf=z.channel+25*z.filter/z.filters

; remplissage tableau data (vv)

  df1=where(z.df eq 11) & ndf=n_elements(df1) & df2=lonarr(ndf)
  for i=0L,ndf-1L do begin
    ii=df1(i) & i1=min([ii+1L,nz-1L]) & i2=min([ii+z(ii).filters,nz-1L])
    jj=where(xf(i1:i2) eq xf(ii) and xts(i1:i2) eq xts(ii) $
      and z(i1:i2).df eq 12)
    jj=jj(0) & if jj ne -1 then jj=jj+i1
    df2(i)=jj
  endfor
  test=where(df2 ne -1)
  if n_elements(test) lt ndf then if test(0) ne -1 then begin
      df1=df1(test) & df2=df2(test) & ndf=n_elements(df1)
  endif
  z1=z(df1) & z2=z(df2)
  xf=xf(df1) & xts=xts(df1) & msec=z1.msec*10

  vv=fltarr(ndf,8)
; VV*[+X,Z,-X,Z]  Re,Im(VV*)[+X,Z]  Re,Im(VV*)[-X,Z]
  restore,'phases.xdr'

; AXX+
  buf=cal(z1.agc1,z1.auto1,z1.bande,z1.df-
11b,z1.channel,z1.filters,z1.filter)
  vv(*,0)=10.^(buf/10.)

; AZZ(+)
  buf=cal(z1.agc2,z1.auto2,z1.bande,z1.df-
8b,z1.channel,z1.filters,z1.filter)
  vv(*,1)=10.^(buf/10.)

; AXX-
  buf=cal(z2.agc1,z2.auto1,z2.bande,z2.df-
11b,z2.channel,z2.filters,z2.filter)
  vv(*,2)=10.^(buf/10.)

; AZZ(-)
  buf=cal(z2.agc2,z2.auto2,z2.bande,z2.df-
9b,z2.channel,z2.filters,z2.filter)
  vv(*,3)=10.^(buf/10.)

; Re(+XZ) & Im(+XZ)
  ax=10.^(auto_db(z1.auto1)/10.) & az=10.^(auto_db(z1.auto2)/10.)
  cr=z1.cross1 & cr=cr/abs(cr)*(10.^(auto_db(abs(cr))/10.))
  ci=z1.cross2 & ci=ci/abs(ci)*(10.^(auto_db(abs(ci))/10.))
  cr=cr/sqrt(ax*az)
```

```
  ci=ci/sqrt(ax*az)
  cm=sqrt(cr^2+ci^2)
  thph=atan(ci,cr)*!radeg
  ph=fltarr(ndf)  &  att=intarr(ndf)      ; hyp. = sans attenuation
  if bande le 2 then for i=0L,ndf-1L do ph(i)=phases_abc(z1(i).filter, $
      (z1(i).df mod 10)-1b,z1(i).bande, $
      fix(alog(z1(i).filters*1.)/alog(2.)+0.5)-3)
  if bande eq 3 then begin
    freq=z1.channel
    test=where(freq gt 4300)
    if test(0) ne -1 then freq(test)=4300
    for i=0L,ndf-1L do ph(i)=ph_h1((z1(i).df mod 10)-1b,fix(freq(i)/25),0)+
$
        phases_h(z1(i).filter,fix(alog(z1(i).filters*1.)/alog(2.)+0.5))
  endif
  if bande eq 4 then begin
    freq=z1.channel
    test=where(freq gt 16075)
    if test(0) ne -1 then freq(test)=16075
    for i=0L,ndf-1L do $
      ph(i)=ph_h2((z1(i).df mod 10)-1b,fix((freq(i)-25)/50),0)+ $
        phases_h(z1(i).filter,fix(alog(z1(i).filters*1.)/alog(2.)+0.5))
  endif
  th=(thph-ph)/!radeg
  cr=cm*cos(th)
  ci=cm*sin(th)

; Re(+XZ)
  vv(*,4)=cr
; Im(+XZ)
  vv(*,5)=ci

; Re(-XZ) & Im(-XZ)
  ax=10.^(auto_db(z2.auto1)/10.) & az=10.^(auto_db(z2.auto2)/10.)
  cr=z2.cross1 & cr=cr/abs(cr)*(10.^(auto_db(abs(cr))/10.))
  ci=z2.cross2 & ci=ci/abs(ci)*(10.^(auto_db(abs(ci))/10.))
  cr=cr/sqrt(ax*az)
  ci=ci/sqrt(ax*az)
  cm=sqrt(cr^2+ci^2)
  thph=atan(ci,cr)*!radeg
  ph=fltarr(ndf)  &  att=intarr(ndf)      ; hyp. = sans attenuation
  if bande le 2 then for i=0L,ndf-1L do ph(i)=phases_abc(z2(i).filter, $
      (z2(i).df mod 10)-1b,z2(i).bande, $
      fix(alog(z2(i).filters*1.)/alog(2.)+0.5)-3)
  if bande eq 3 then begin
    freq=z2.channel
    test=where(freq gt 4300)
    if test(0) ne -1 then freq(test)=4300
    for i=0L,ndf-1L do ph(i)=ph_h1((z2(i).df mod 10)-1b,fix(freq(i)/25),0)+
$
        phases_h(z2(i).filter,fix(alog(z2(i).filters*1.)/alog(2.)+0.5))
  endif
  if bande eq 4 then begin
    freq=z2.channel
    test=where(freq gt 16075)
    if test(0) ne -1 then freq(test)=16075
    for i=0L,ndf-1L $
      do ph(i)=ph_h2((z2(i).df mod 10)-1b,fix((freq(i)-25)/50),0)+ $
        phases_h(z2(i).filter,fix(alog(z2(i).filters*1.)/alog(2.)+0.5))
  endif
  th=(thph-ph)/!radeg
  cr=cm*cos(th)
  ci=cm*sin(th)
```

```
; Re(-XZ)
  vv(*,6)=cr
; Im(-XZ)
  vv(*,7)=ci

  help, vv,xts,xf,msec
return
end
```

read_phases.pro

```
; READ_PHASES.pro

; reads phases values from files phase8/16/32_abc.dat,
;   phase_hf1/2.dat & phase1248_hf.dat

  ph_h1=fltarr(3,173,2) ; +x/-x/+-x(ref=z), 0,25,50...4300 kHz, att off/on
  ph_h2=fltarr(3,322,2) ; +x/-x/+-x(ref=z), 25,75...16075 kHz, att off/on
  buf=fltarr(6)

  openr,u,'phase_hf1.dat',/get_lun
  for i=0,172 do begin
    readf,u,buf
    ph_h1(*,i,0)=buf(0:2) & ph_h1(*,i,1)=buf(3:5)
  endfor
  close,u & free_lun,u

  openr,u,'phase_hf2.dat',/get_lun
  for i=0,321 do begin
    readf,u,buf
    ph_h2(*,i,0)=buf(0:2) & ph_h2(*,i,1)=buf(3:5)
  endfor
  close,u & free_lun,u

  phases_abc=fltarr(32,3,3,3) ; #filt, +x/-x/+-x(ref=z), ABC, 8/16/32
  buf=fltarr(9)

  openr,u,'phase8_abc.dat',/get_lun
  for i=0,7 do begin
    readf,u,buf
    phases_abc(i,*,0,0)=buf(0:2) & phases_abc(i,*,1,0)=buf(3:5)
    phases_abc(i,*,2,0)=buf(6:8)
  endfor
  close,u & free_lun,u

  openr,u,'phase16_abc.dat',/get_lun
  for i=0,15 do begin
    readf,u,buf
    phases_abc(i,*,0,1)=buf(0:2) & phases_abc(i,*,1,1)=buf(3:5)
    phases_abc(i,*,2,1)=buf(6:8)
  endfor
  close,u & free_lun,u

  openr,u,'phase32_abc.dat',/get_lun
  for i=0,31 do begin
    readf,u,buf
    phases_abc(i,*,0,2)=buf(0:2) & phases_abc(i,*,1,2)=buf(3:5)
    phases_abc(i,*,2,2)=buf(6:8)
  endfor
  close,u & free_lun,u
```

```
  phases_h=fltarr(8,4)        ; #filt, 1/2/4/8
  buf=fltarr(4)

  openr,u,'phase1248_hf.dat',/get_lun
  for i=0,7 do begin
    readf,u,buf
    phases_h(i,*)=buf
  endfor
  close,u & free_lun,u

save,ph_h1,ph_h2,phases_abc,phases_h,file='phases.xdr',/xdr,/verb

; PH_H1           FLOAT     = Array(3, 173, 2)
;                           +x/-x/+-x(ref=z), 0,25,50...4300 kHz, att off/on
; PH_H2           FLOAT     = Array(3, 322, 2)
;                           +x/-x/+-x(ref=z), 25,75...16075 kHz, att off/on
; PHASES_ABC      FLOAT     = Array(32, 3, 3, 3)
;                           #filt, +x/-x/+-x(ref=z), ABC, 8/16/32
; PHASES_H        FLOAT     = Array(8, 4)
;                           #filt, 1/2/4/8

end
```

phases.xdr

```
IDL> restore,'phases.xdr'
IDL> help
PHASES_ABC      FLOAT     = Array[32, 3, 3, 3]
PHASES_H        FLOAT     = Array[8, 4]
PH_H1           FLOAT     = Array[3, 173, 2]
PH_H2           FLOAT     = Array[3, 322, 2]
```

12.1 WBR Subsystem Description

This section of the RPWS Calibration Document describes the Wideband Receiver (WBR), extending the description contained in the Section 3 instrument overview. The WBR subsystem provides very high frequency/time resolution electric and magnetic field measurements for a selection of frequency passbands, and is similar to the wideband receivers previously designed for the Voyager, Galileo, Polar and Cluster missions.

12.1.1 General WBR Characteristics

The WBR processes signals from one of the electric or magnetic sensors, or from the Langmuir Probe, as selected by instrument command A block diagram of the WBR subsystem is shown in Figure 12.1.1.1.

Input signals for the WBR are chosen via an analog antenna selection switch located at the receiver input. The output of this switch goes to a 50 Hz to 80 kHz bandpass filter which sets the bandwidth of the input waveform. To provide the capability for obtaining waveforms at frequencies above 80 kHz, the HFR is utilized to down-convert higher frequency signals into a 50 kHz to 75 kHz bandpass (HF input in Figure 12.1.1.1).

To allow the WBR to accommodate the large (>100 dB) dynamic range of input signals, a set of gain amplifiers are used to regulate signal amplitudes in the receiver in steps of 10 dB over a range of 0 dB to 70 dB. The output from the gain select amplifiers then goes to a 50 Hz to 10 kHz and a 1 kHz to 80 kHz bandpass filter. A switch determines which filter output is sent to the HRP for 8-bit sampling, and also to a peak detector. The peak detector creates a voltage that is used by an automatic gain control (AGC) implemented in software.

Figure 12.1.1.1
RPWS WIDEBAND RECEIVER (WBR)

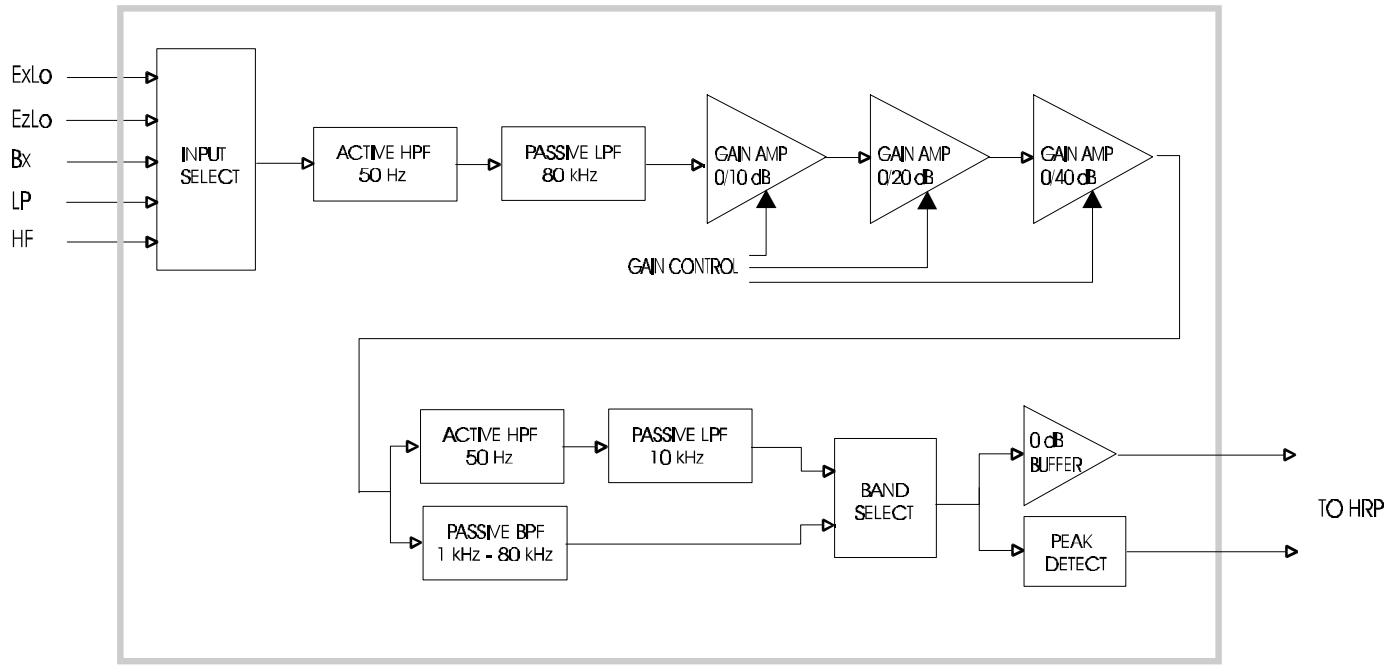

12.1.2 Receiver Inputs

The WBR subsystem has the capability of processing signals from one of the electric or magnetic field sensors, or from the Langmuir Probe. The WBR is provided with the following signal inputs:

Sensor Designation	Description
ExLo	10 meter electric antennas. The HFR can provide for the ExLo input either the dipole configuration (default); or either the Ex+ or Ex- as a monopole
EzLo	10 meter electric antenna (monopole)
HF	High frequency electric field signals are down-converted by the HFR into a 50 kHz to 75 kHz band. This mode requires that the WBR 1 kHz to 80 kHz output passband be selected. The possible frequency bands for conversion are any between 150 kHz and 4.125 MHz, and any band except those centered at multiples of 50 kHz between 4.125 and 16 MHZ. It should be noted that HF input signals have been through the HFR AGC, and thus are kept at a fairly constant amplitude. Also, proper use of the HF input mode restricts the WBR band select to the 1 kHz to 80 kHz passband.
Bx	Magnetic search coil antenna with axis aligned with spacecraft x-axis
LP	Langmuir Probe

12.1.3 Output Passbands

The bandwidth of the WBR output waveform is determined by one of two bandpass filters selected by the HRP. The bandwidths of the WBR output waveform and associated sampling rates are:

Filter	Sampling Rate
50 Hz - 10 kHz	36 μs
1 kHz - 80 kHz	4.5 μs

12.1.4 Gain Select

The gain select stage of the WBR employs three switchable amplifiers (0/10 dB, 0/20 dB, and 0/40 dB) which may be commanded via the HRP to provide gain combinations of 0 dB to 70 dB in 10 dB increments.

Additionally, the WBR has the capability of auto-ranging through the gain steps via an automatic gain control (AGC) loop. The automatic gain select function is controlled by the HRP and allows the WBR to respond to large changes in signal intensity. In this operational mode, the signal from the output bandpass filter (50 Hz to 10 kHz or 1 kHz to 80 kHz) goes through a peak detector stage as shown in the block diagram. The output from the peak detect, after sampling, is then compared in software to a pair of reference amplitudes, and the gain state is either increased by one step (10 dB) or decreased by one step accordingly for the next set of contiguous samples. In order to avoid excessive toggling between gain steps, a threshold must be exceeded in either direction, thereby introducing hysteresis in the AGC loop. The gain update rate is adjustable, with dwell times of 0.25 seconds or greater possible, depending on output data mode. The autoranging gain capability allows the WBR to respond to large changes in input signal levels so as to maximize the signal-to-noise ratio and to avoid saturation of the receiver.

12.1.5 Receiver Output

The output signal from the WBR is routed to the HRP to be sampled (8 bits), and packed into WBD mini-packets before being transmitted to the ground. To increase the amount of wideband waveform data which can be transmitted with the available telemetry, the output of the WBR is usually compressed.

12.1.6 Control

WBR control functions which determine instrument modes are managed by the HRP. The WBR receives the following control inputs:

Function
Antenna Select
Band Select
Gain Select
Gain Time Constant

12.1.7 Power

The WBR is provided with four power supply lines. The regulated supply voltages and measured average current loads are as follows:

+12 V	5.5 mA
−12 V	6.9 mA
+ 6 V	39.0 mA
− 6 V	39.0 mA

The total power requirement for the WBR is 313 mW.

12.2 Converting WBR Telemetry Values to Physical Units

In this section, the procedure for obtaining calibrated data values for the Wideband Receiver is described.

1. First a snapshot consisting of 2^N raw WBR data samples is obtained. These data samples are 8-bit unsigned values (0-255).

2. The DC component is obtained by averaging the 2^N samples. The DC component is subtracted from the 2^N samples, because the receiver is an AC-coupled system and the DC-component is not related to any sensor measurement. Furthermore, removal of the DC offset is needed for the next step.

3. The proper counts-to-$volts_{rms}$ factor is now applied to the data. This is the amplitude in counts of a sine wave in the middle of the pass-band which would be measured by the WBR if a 1 $Volt_{rms}$ signal were injected into the Eu differential amplifier and the WBR had no gain amplifier turned on. The 2^N samples are all divided by this factor. Throughout the calibrations, another way this is expressed is the decibels below a maximum amplitude sine wave; for 8-bit data, which can range 0 through 255, this is dB below a sine wave of amplitude 127.5 counts (or 255 counts peak-to-peak) and it is referred to as dBmax. This factor depends upon the filter mode:

Translation Mode	Filter	counts/V_{rms}	dBmax
Baseband	10 kHz	264.25	+6.33
Baseband	80 kHz	267.31	+6.43

4. Next the WBR gain amplifier value must be divided out. The gain can vary from 0 dB through 70 dB in steps of 10 dB. If the gain is G, then the 2^N samples should all be divided by $10^{G/20}$.

5. Next a Hanning window can be applied to the 2^N samples. For a Hanning window the coherent gain is 0.5 (see "Digital Filter Design Handbook" by Fred J. Taylor). Therefore the 2^N samples must then be multiplied by 2. The equation for a Hanning window is $H_i=0.5*(1-\cos(2*P*i/(2^N-1)))$ for i=0, 2^N-1.

6. An FFT should be performed on the 2^N samples. The FFT output must be normalized using whatever normalization factors are necessary to give the amplitude of a sine wave when real and imaginary parts are squared, summed and the square root taken. The normalization factors may be different for different FFT implementations. The phase information from the FFT is not useful, so the magnitudes can now be calculated by squaring the real and imaginary parts, summing them and taking the square root. This yields $volts_{rms}$ in each FFT bin. This is the voltage difference Vdiff between the Ex+ and Ex- antennas at the frequency corresponding to that FFT bin.

7. Once the voltage Vdiff is found, the sensor-dependent conversion factor must be used to adjust the voltage. The voltage difference between the Ex+ antenna and the Ex- antenna is given the symbol VDEx. Since the voltage difference Vdiff calculated in steps 1 through 6 is for the voltage difference between Ex+ and Ex-, no conversion is necessary for VDEx. VDEx is equal to Vdiff. The voltage between the Ex+ antenna and spacecraft ground is given the symbol VEx+. The voltage between the Ex- antenna and spacecraft ground is given the symbol VEx-. The voltage between the Ez antenna and spacecraft ground is given the symbol VEz. The voltage out of the Bx magnetic preamp is given the symbol Vbxpa. Figure 12.2.1 shows the location of these voltages. The conversion factors and their symbols are listed below. The conversion factors convert the Vdiff values to the voltage at the various sensors.

Symbol	Factor	
CF+ex	1.0	Conversion factor for a monopole using the the Ex+ antenna
CF-ex	1.0	Conversion factor for a monopole using the the Ex- antenna
CFez	1.0	Conversion factor for the Ez antenna
CFbx	24.0	Conversion factor for the Bx Search Coil

The formulas for converting the Vdiff value to the sensor input voltage are:

VDEx	=	Vdiff	(units are V_{rms})
VEx+	=	(CF+ex)*(Vdiff)	
VEx-	=	(CF-ex)*(Vdiff)	
VEz	=	(Cfez)*(Vdiff)	
Vbxpa	=	(Cfbx)*(Vdiff)	

8. Now the sensor-dependent calibrations must be applied. For the Bx Search Coil, the voltage at the output of the Search Coil preamplifier must be converted to nanotesla. See Table 7.1.1 in the section about the Magnetic Search Coils for the frequency-dependent conversion factors. For a particular frequency let this conversion factor be given the symbol CBxnt; for example, Table 7.1.1 shows that at 1000 Hz the Bx Search Coil's response is 147.8 mV/nT, so CBxnt is 0.1478. To convert from voltage at the output of the Bx Search Coil preamplifier, VBxpa must be divided by CBxnt. This is shown in the following equation:

$$NTBx = VBxpa / CBxnt \qquad (\text{units are } nT_{rms})$$

NTBx is the field detected by the Bx Search Coil. At this point we have meaningful physical units. For the electric antennas we have voltage measured at the antenna elements. For the magnetic sensor we have the magnetic field in nanotesla at the sensor. Next the magnitude of the electric field for the electric antennas can be obtained. The voltages at the antennas are divided by the effective antenna length, producing units of

volts per meter. Here the effective antenna lengths are defined as the physical distances between the geometric centers of the antennas for the Ex dipole, and the geometric center for the Ez antenna and also for the individual monopole configurations of Ex+ and Ex-. The effective length for the Ex+ to Ex- dipole antenna configuration is given the symbol Lexdelta. The Ex+ monopole effective length is given the symbol L+Ex. The Ex- monopole effective length is given the symbol L-Ex. The Ez monopole effective length is given the symbol LEz. For a more detailed discussion of the effective lengths of the electric antennas, see Section 5.

Effective Antenna Lengths in Meters for various mode configurations

Antenna	Effective Length (meters)	Configuration
LExdelta	8.66	dipole
L+Ex	5.00	monopole
L-Ex	5.00	monopole
LEz	5.00	monopole

The electric field on the Ex dipole is represented by VMExdelta, the electric field on the Ex+ monopole by VM+Ex, the electric field on the Ex- monopole by VM-Ex, and the electric field on the Ez monopole by VMEz. The following equations show the method for calculating the electric field on the antenna in volts per meter. These equations do not include effects due to stray capacitive divider effects between the antennas and the spacecraft.

VMExdelta = (VDEx) / (LExdelta)
VM+Ex = (VEx+) / (L+Ex)
VM-Ex = (VEx-) / (L-Ex)
VMEz = (VEz) / (LEz)

9. Finally, to obtain power spectral density, one must square the value and divide by the bandwidth, which depends upon the type of window function used before performing the FFT. If no window function is used, then the equivalent noise bandwidth is the FFT bin width, which is the sample frequency divided by the number of samples ($f_S/2^N$). If the Hanning window suggested above is used, then the equivalent noise bandwidth is 1.5 times the FFT bin width (again see “Digital Filter Design Handbook” by Fred J. Taylor).

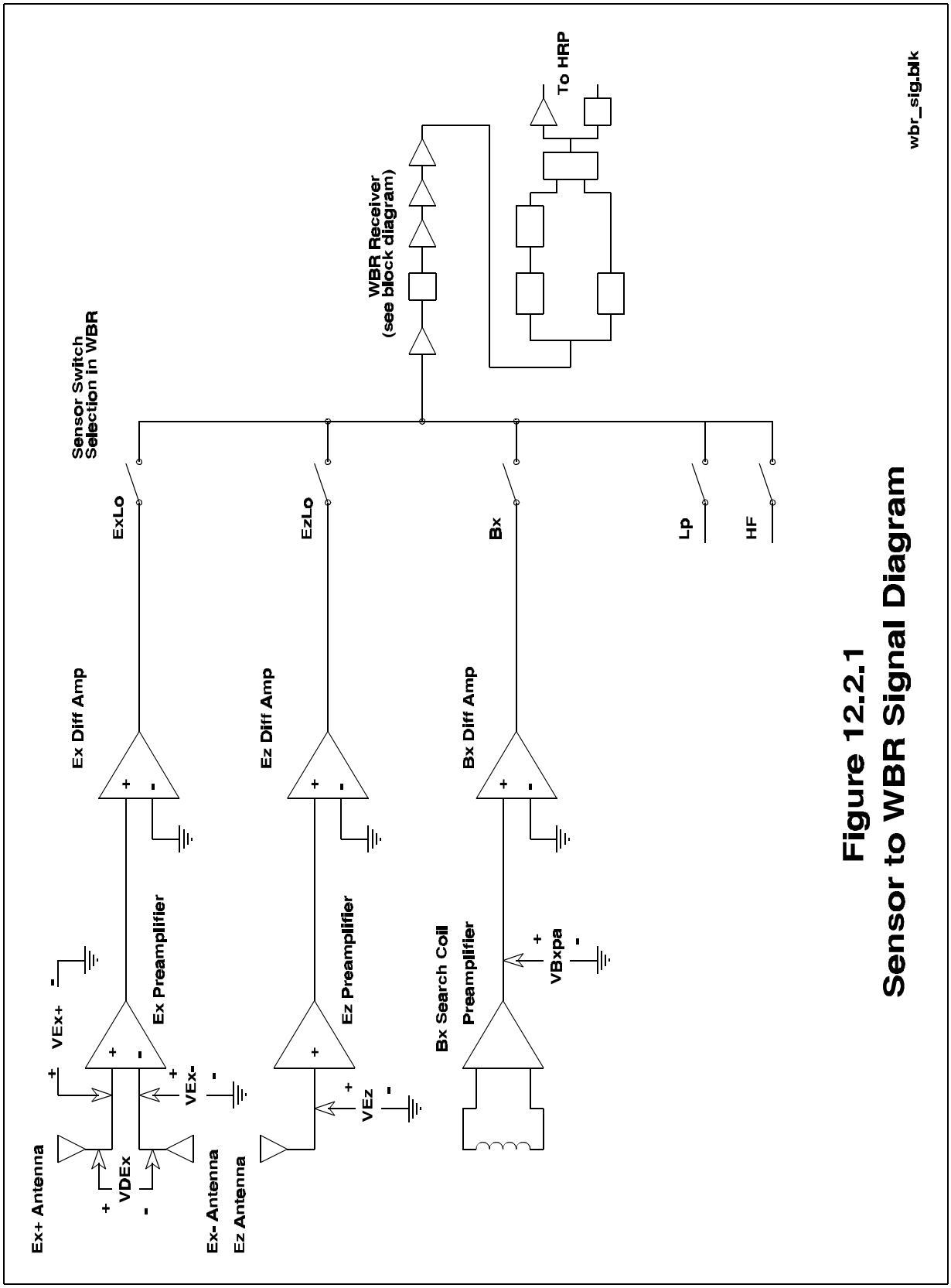

Figure 12.2.1
Sensor to WBR Signal Diagram

As an illustration of how to obtain calibrated values from WBR telemetry, let us look at some real data:

Example 1: SCET 1997-October-25-UT06:34:25 (SCLK 4AE3F190.1)

After electric antenna deployment, a broad-band emission is examined. The WBR was in 10-kHz mode with 60 dB of gain and connected to the Ex dipole. A waveform of length 2048 was captured. Following the recipe for obtaining calibrated values, the DC component is computed and subtracted from all 2048 samples. Since the filter mode is 10-kHz, all 2048 samples are then divided by 264.25 counts per V_{rms}, and also divided by the gain amplifier factor, $10^{60/20}$ (or 1000). A Hanning window is applied to the data and then all windowed values are multiplied by 2 to offset the Hanning window's coherent gain. An FFT is performed on the data, and after normalizing, the magnitudes of the resulting 1024 components are computed by squaring the real and imaginary parts of the complex outputs, summing them, and taking the square root. The broad-band emission under examination extends from about 1 kHz to 3 KHz and is about 10 to 20 dB above the Ex dipole's noise floor. The peak amplitude occurs at frequency 2835 Hz, and this peak amplitude is Vdiff at 2.835 kHz:

$$\text{Vdiff} = 1.33\text{x}10^{-5}\ V_{rms}.$$

Since the sensor is the Ex dipole, we know that the voltage VDEx is the same as Vdiff. So the electric field strength can be calculated directly:

$$\begin{aligned} \text{VMExdelta} &= (\text{VDEx}) / (\text{LExdelta}) \\ &= 1.33\text{x}10^{-5} / 8.66 \\ &= 1.54\text{x}10^{-6}\ V_{rms}/\text{meter}. \end{aligned}$$

Finally, to determine the electric field power spectral density, we must square this value and divide by the equivalent noise bandwidth. Since we have 10-kHz mode, the sample frequency is given by

$$\begin{aligned} F_s &= 1. / 36.\text{x}10^{-6} \\ &= 27778\ \text{Hz} \end{aligned}$$

and since the sample set size is 2048, the FFT bin size is given by

$$\begin{aligned} Df &= F_s / 2048 \\ &= 27778 / 2048 \\ &= 13.563\ \text{Hz}. \end{aligned}$$

But since a Hanning window was applied to the data, the equivalent noise bandwidth is given by

$$\begin{aligned} ENBW &= 1.5 * Df \\ &= 20.345 \text{ Hz.} \end{aligned}$$

So the power spectral density at 2.8 kHz is given by

$$\begin{aligned} PSD &= (VMExdelta)^2 / ENBW \\ &= (1.54 \times 10^{-6})^2 / 20.345 \\ &= 1.17 \times 10^{-13} \ V_{rms}^2 / meter^2 \text{ Hz.} \end{aligned}$$

Example 2. SCET 1996-July-31-UT18:52:32 (SCLK 31FFAB70.1)

During unit level testing the Bx Search Coil was stimulated with a 1 kHz tone at 0.5 V_{rms}, which should have produced a magnetic field of 0.5 nT_{rms}. The WBR was in 80-kHz mode with 30 dB of gain. A waveform of length 2048 was captured. The raw data shows a sine wave with maximum value of 152 and a minimum value of 109, giving an initial estimate of 43 counts peak-to-peak for the sine wave. Following the recipe for obtaining calibrated values, the DC component is computed and found to be 130.35 counts. This value is subtracted from all 2048 samples. A Hanning window is applied to the data and then all windowed values are multiplied by 2 to offset the Hanning window's coherent gain. An FFT is performed on the data, and after normalizing, the magnitudes of the resulting 1024 components are computed by squaring the real and imaginary parts of the complex outputs, summing them, and taking the square root. The peak amplitude occurs in the 9th FFT bin, corresponding to frequency 977 Hz, and this peak amplitude is 19.46 counts (note that this is close to our initial estimate of 21.5 counts for the amplitude). Dividing this by the calibration factor of 267.31 counts/V_{rms} and also by the gain factor of $10^{G/20}$, we obtain Vdiff at 1 kHz:

$$\begin{aligned} Vdiff &= 19.46 / (267.31 * 10^{30/20}) \\ &= 19.46 / (267.31 * 31.62) \\ &= 2.30 \times 10^{-3} \ V_{rms} \end{aligned}$$

Since the sensor is the Bx Search Coil, we now want to know what the voltage VBxpa from the Search Coil preamplifier is. It is:

$$\begin{aligned} Vbxpa &= (CFbx)*(Vdiff) \\ &= 24 * 2.30 \times 10^{-3} \ V_{rms} \\ &= 55.25 \ mV_{rms} \end{aligned}$$

Now referring to the Search Coil calibration in Table 7.1.1, we find that at 1000 Hz the Bx Search Coil's response CBxnt is 147.8 mV/nT. So we find that the magnetic field strength NTBx is

$$\begin{aligned} NTBx &= VBxpa / CBxnt \qquad (\text{units are } nT_{rms}) \\ &= 55.25 / 147.8 \ nT_{rms} \\ &= 0.374 \ nT_{rms} \end{aligned}$$

This is probably more correct than the 0.5 nT_{rms} presumed value, since the MFR also gives a similar answer. In this case, it makes little sense to calculate spectral density since the signal is a tone.

12.3 WBR-Specific Calibration Tests and Results

12.3.1 WBR Frequency Responses

In this section, frequency response calibration data for the wideband receiver are presented. Transfer functions for each of the filters and translation modes is shown. Figure 12.3.1.1 illustrates the stimulus configuration used for the WBR frequency responses. The oscillator output is attenuated by a fixed amount and a balancing transformer is used to drive the Ex+/- inputs differentially.

During the calibrations, the HP workstation commands the oscillator to step in frequency. For each frequency step, a waveform is captured and telemetered to the spacecraft stimulator. An FFT is performed on the data after removing the DC component. The peak amplitude is chosen from the frequency-domain result, and the peak frequency (which should be very close to the stimulus frequency) is chosen. The amplitude is calculated by a simple time domain rms average and then is adjusted by $2^{1/2}/2$ to give the amplitude of the sine wave in WBR counts. This rms calculation yields a value very close to the FFT result at the peak frequency, but does not suffer from the "scallop loss" effect of the FFT results, which are sensitive to the proximity of the frequency to the center of an FFT bin. For further discussion on this effect, see Section 12.3.2, where the FFT amplitudes of the peak frequencies are presented for the gain calibrations. Finally, the amplitude is expressed in dBmax, i.e., 0 dB corresponds to a sine wave of amplitude 127.5 counts.

Although the frequency response could be used to adjust the calibrations of the WBR data, it is recommended that this not be done, since the noise floor becomes accentuated outside the pass-band. Instead, one should simply note from the frequency response tests that the filters are flat to within a dB or less in the pass-band. And data should be ignored if it is outside the 3-dB points. From the frequency response curves, those 3-dB points are approximately:

Translation Mode	Filter	3-dB points
Baseband	80 kHz	0.80 - 75 kHz
Baseband	10 kHz	0.06 - 10.65 kHz

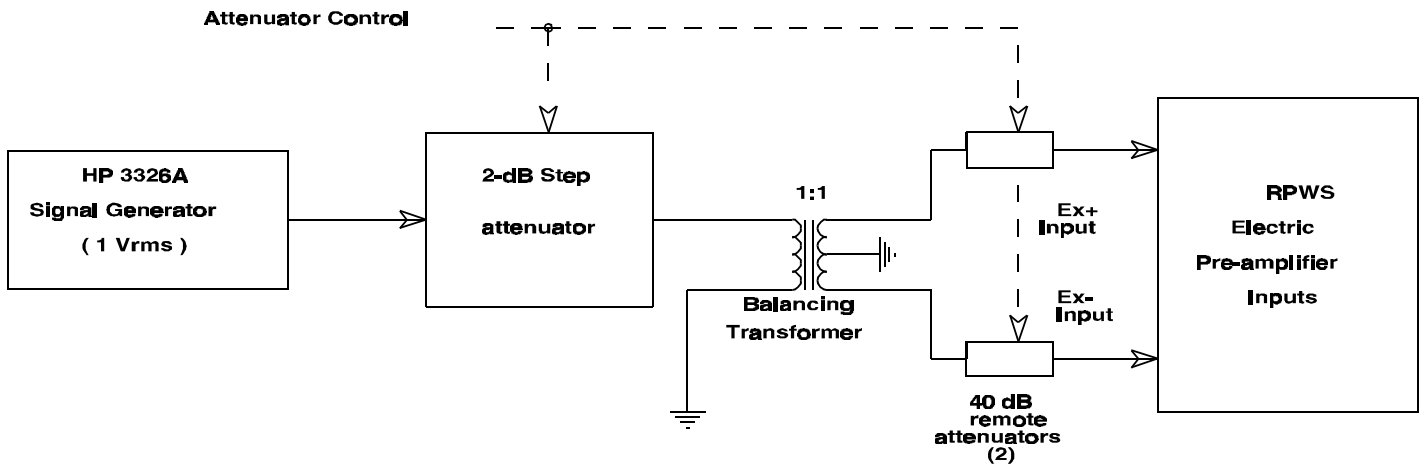

Figure 12.3.1.1

WBR Frequency Response Calibration Stimulus Configuration

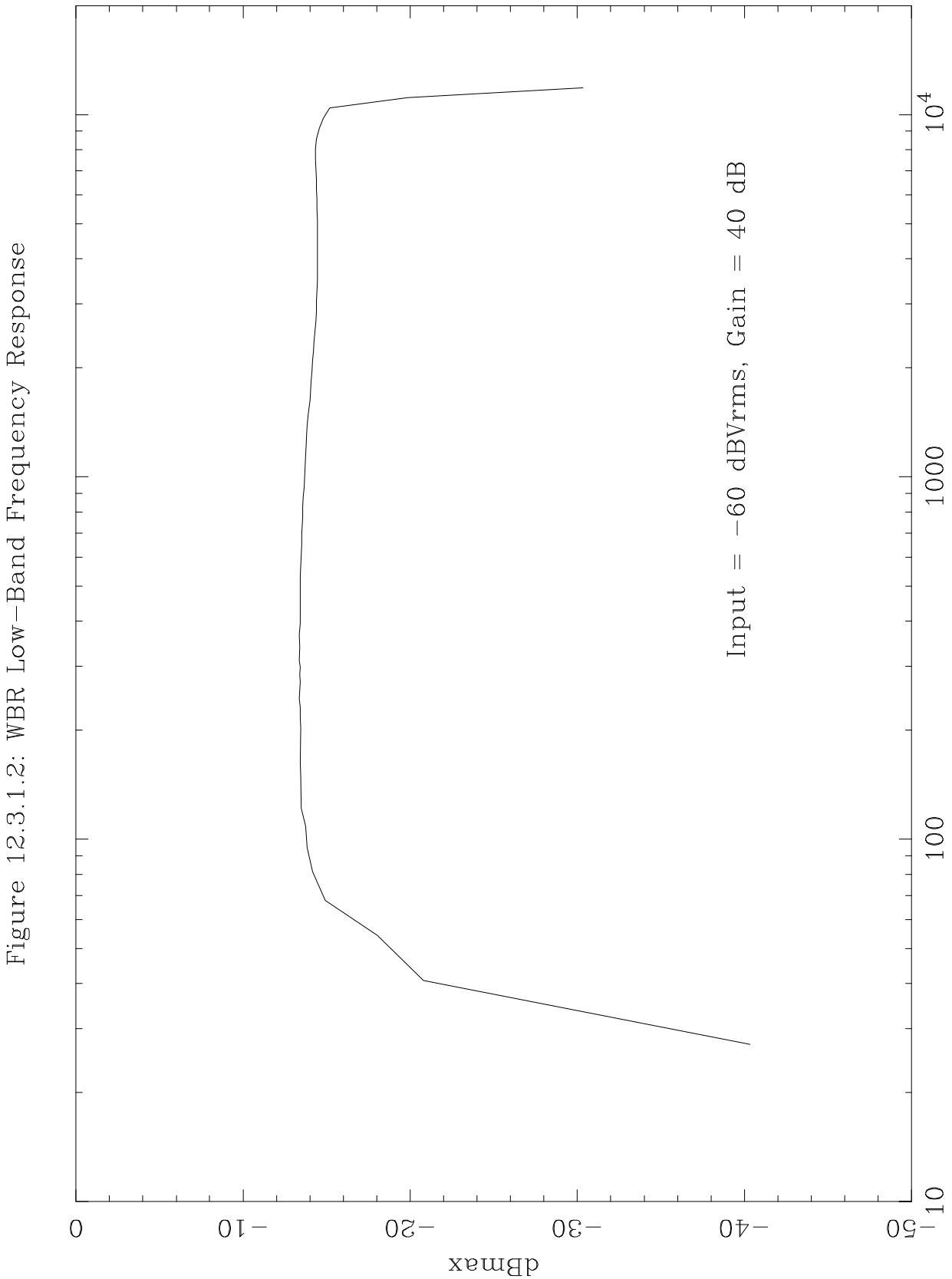

Figure 12.3.1.2: WBR Low−Band Frequency Response

Table 12.3.1.1 WBR 10 kHz Mode Frequency Response

Frequency (Hz)	Amplitude (dBmax)	Frequency (Hz)	Amplitude (dBmax)
27.13	-40.33	1152.89	-13.74
40.69	-20.79	1220.70	-13.77
54.25	-18.04	1315.65	-13.81
67.82	-14.91	1383.46	-13.84
81.38	-14.15	1478.41	-13.90
94.94	-13.82	1627.60	-13.99
108.51	-13.74	1722.55	-14.03
122.07	-13.48	1831.05	-14.07
149.20	-13.45	1966.69	-14.12
162.76	-13.41	2088.76	-14.16
203.45	-13.46	2224.39	-14.21
217.01	-13.41	2360.03	-14.25
230.58	-13.43	2522.79	-14.30
244.14	-13.37	2699.11	-14.35
271.27	-13.41	2861.87	-14.38
284.83	-13.40	3051.76	-14.40
298.39	-13.41	3255.21	-14.42
311.96	-13.36	3472.22	-14.44
339.08	-13.39	3702.80	-14.45
366.21	-13.37	3960.50	-14.45
393.34	-13.41	4218.21	-14.44
406.90	-13.41	4503.04	-14.44
434.03	-13.43	4801.43	-14.43
461.15	-13.42	5126.95	-14.43
501.84	-13.42	5466.04	-14.42
528.97	-13.43	5832.25	-14.41
569.66	-13.46	6212.02	-14.40
610.35	-13.49	6618.92	-14.40
651.04	-13.50	7066.51	-14.37
691.73	-13.52	7541.23	-14.34
732.42	-13.53	8043.08	-14.33
773.11	-13.55	8558.49	-14.38
827.37	-13.58	9168.84	-14.56
881.62	-13.61	9752.06	-14.81
935.87	-13.64	10430.23	-15.17
1003.69	-13.67	11121.96	-19.87
1071.51	-13.71	11840.82	-30.33

Figure 12.3.1.3: WBR High-Band Frequency Response

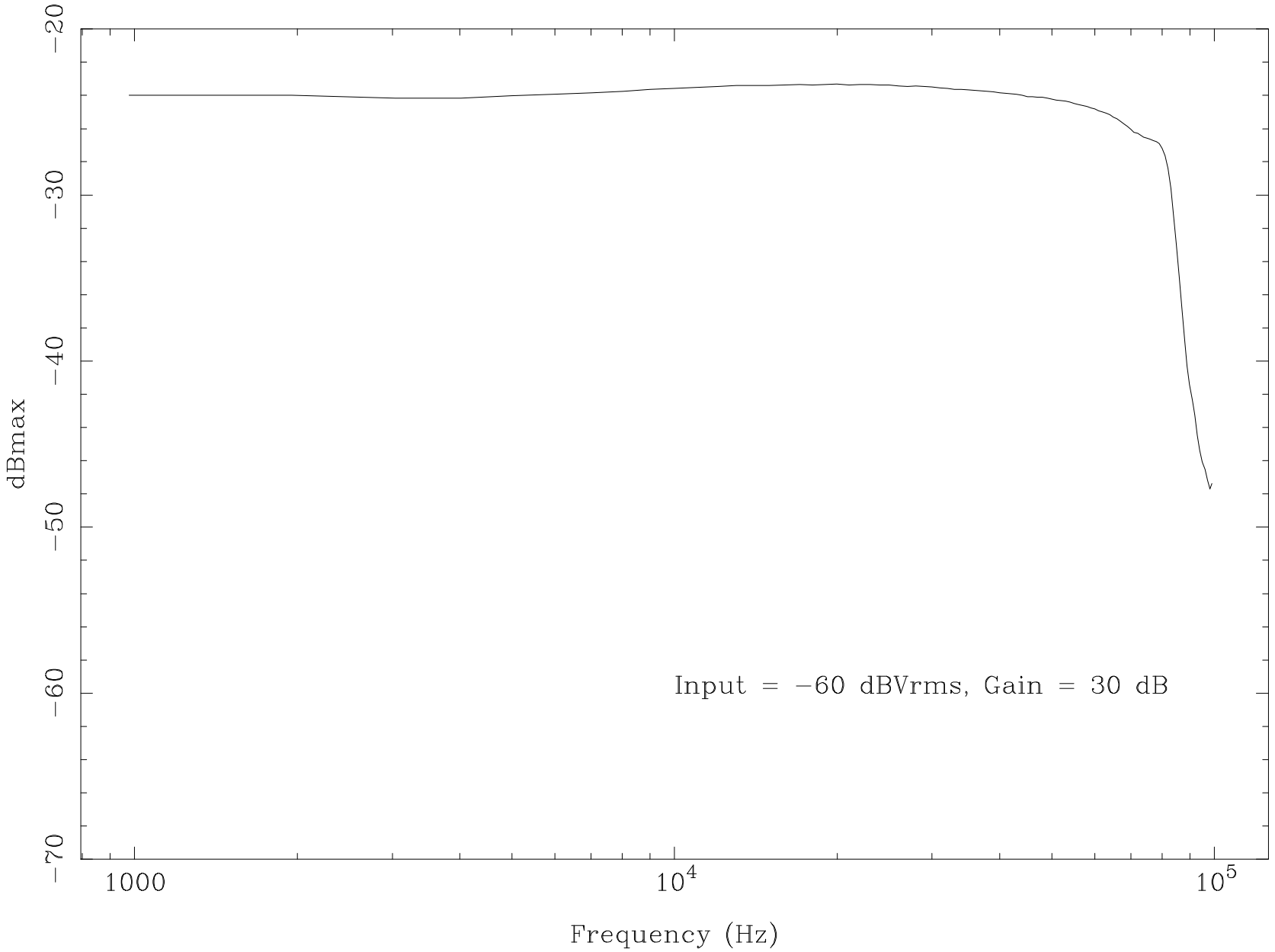

Table 12.3.1.2 WBR 80 kHz Mode Frequency Response

Frequency (Hz)	Amplitude (dBmax)	Frequency (Hz)	Amplitude (dBmax)
976.56	-23.99	50998.26	-24.27
1953.12	-24.00	51974.83	-24.32
3038.19	-24.16	52951.39	-24.34
4014.76	-24.15	54036.46	-24.41
4991.32	-24.03	55013.02	-24.49
5967.88	-23.93	55989.58	-24.54
7052.95	-23.83	56966.15	-24.59
8029.51	-23.76	58051.22	-24.66
9006.08	-23.64	59027.78	-24.75
9982.64	-23.57	60004.34	-24.81
10959.20	-23.51	60980.90	-24.93
12044.27	-23.47	61957.47	-24.99
13020.83	-23.41	63042.53	-25.08
13997.40	-23.39	64019.10	-25.18
14973.96	-23.39	64995.66	-25.31
15950.52	-23.38	65972.22	-25.40
17035.59	-23.35	66948.78	-25.54
18012.15	-23.37	68033.85	-25.73
18988.72	-23.34	69010.42	-25.88
19965.28	-23.31	69986.98	-26.05
21050.35	-23.38	70963.54	-26.21
22026.91	-23.35	72048.61	-26.29
23003.47	-23.35	73025.17	-26.39
23980.03	-23.38	74001.74	-26.51
24956.60	-23.38	74978.30	-26.58
26041.67	-23.42	75954.86	-26.64
27018.23	-23.45	77039.93	-26.72
27994.79	-23.44	78016.49	-26.77
28971.35	-23.47	78993.06	-26.89
29947.92	-23.50	79969.62	-27.19
31032.99	-23.55	81054.69	-27.62
32009.55	-23.58	82031.25	-28.39
32986.11	-23.63	83007.81	-29.60
33962.67	-23.63	83984.38	-31.14
35047.74	-23.67	84960.94	-32.95
36024.31	-23.69	86046.01	-34.92
37000.87	-23.71	87022.57	-36.65
37977.43	-23.77	87999.13	-38.69
38953.99	-23.79	88975.69	-40.29
40039.06	-23.84	89952.26	-41.40
41015.62	-23.87	91037.33	-42.34
41992.19	-23.90	92013.89	-43.25
42968.75	-23.94	92990.45	-44.47
44053.82	-23.99	93967.01	-45.37
45030.38	-24.06	94943.58	-46.05
46006.94	-24.06	95052.08	-46.15
46983.51	-24.10	96028.65	-46.53
47960.07	-24.10	97005.21	-47.18
49045.14	-24.17	97981.77	-47.69
50021.70	-24.22	98958.33	-47.37

12.3.2 WBR Gain Calibration

In this section, the amplitude calibrations for the wideband receiver are presented. Data at selected stimulus frequencies are shown for all filters and translation modes. The stimulus configuration used for the WBR gain calibration is similar to that used for the WBR frequency response tests; see Figure 12.3.2.1. The GSE workstation is used to command the oscillator and programmable attenuators. The attenuator is converted to a differential signal using a balancing transformer. The Ex+ and Ex- inputs are driven differentially. The WBR amplitude response to any of the other sensors may be determined by applying the appropriate sensor and differential amplifier curves to the data here.

The procedure used for the performance of the calibrations is as follows. A command is sent to the oscillator and attenuator to set the desired setting. A waveform is captured by the WBR and telemetered to the spacecraft simulator. An FFT is performed on the WBR capture and both the time and frequency domains are plotted. The amplitude of the the signal at the stimulus frequency is shown on each plot, where the amplitude is given in dB below maximum signal detectable. Throughout the amplitude calibrations, this is expressed is the decibels below a maximum amplitude sine wave; for 8-bit data, which can range 0 through 255, this is dB below a sine wave of amplitude 127.5 counts and it referred to as dBmax. This can be converted to the amplitude in counts of a sine wave in the middle of the pass-band which would be measured by the WBR if a 1 $Volt_{rms}$ signal were injected into the Eu differential amplifier and the WBR had no gain amplifier turned on. The results for the 10-kHz WBR mode are presented in Table 12.3.2.1 and for the 80-kHz WBR mode in Table 12.3.2.2. These results are also presented in graphical form in Figures 12.3.2.1 and 12.3.2.2.

The amplitude calibrations show that the gain amplifiers are very accurate. At any fixed frequency, the variations in the gain are on the order of 1 dB. Furthermore, the variations across the frequency pass-band are mostly due to the "scallop loss" for a Hanning window. The scallop loss is defined as the ratio of coherent gain for a tone located half a bin from an FFT sample point to the coherent gain for a tone at the FFT sample point (see "Digital Filter Design Handbook" by Fred J. Taylor). For a Hanning window the scallop loss is 1.42 dB. White noise does not exhibit the scallop loss evident when using tones; the response is flatter like that shown in Section 12.3.1. Because of these considerations, a single conversion factor can be used for each filter mode. The calibration factors will be given for a frequency in the middle of the pass-band. For the 10 kHz mode this is 1 kHz; for the 80 kHz mode this is 10 kHz. If frequency-dependent variations are to be removed, then the calibration factors can be adjusted across the pass-band using the frequency response data of Section 12.3.1. The conversion factors which should be used are:

Translation Mode	Filter	counts/V_{rms}	dBmax
Baseband	10 kHz	264.25	+6.33
Baseband	80 kHz	267.31	+6.43

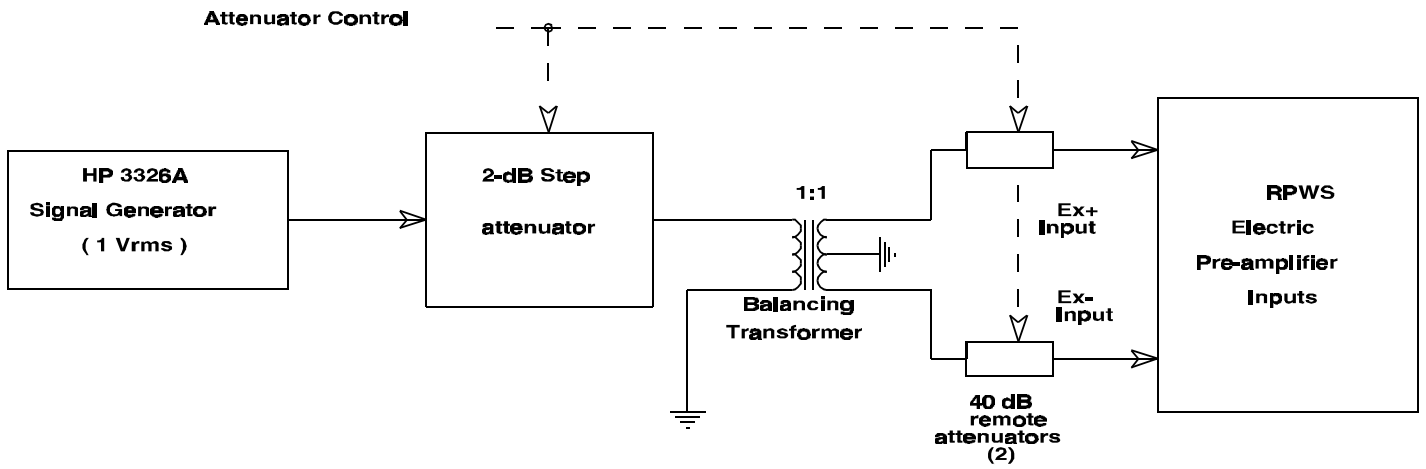

Figure 12.3.2.1

WBR Gain Calibration Stimulus Configuration

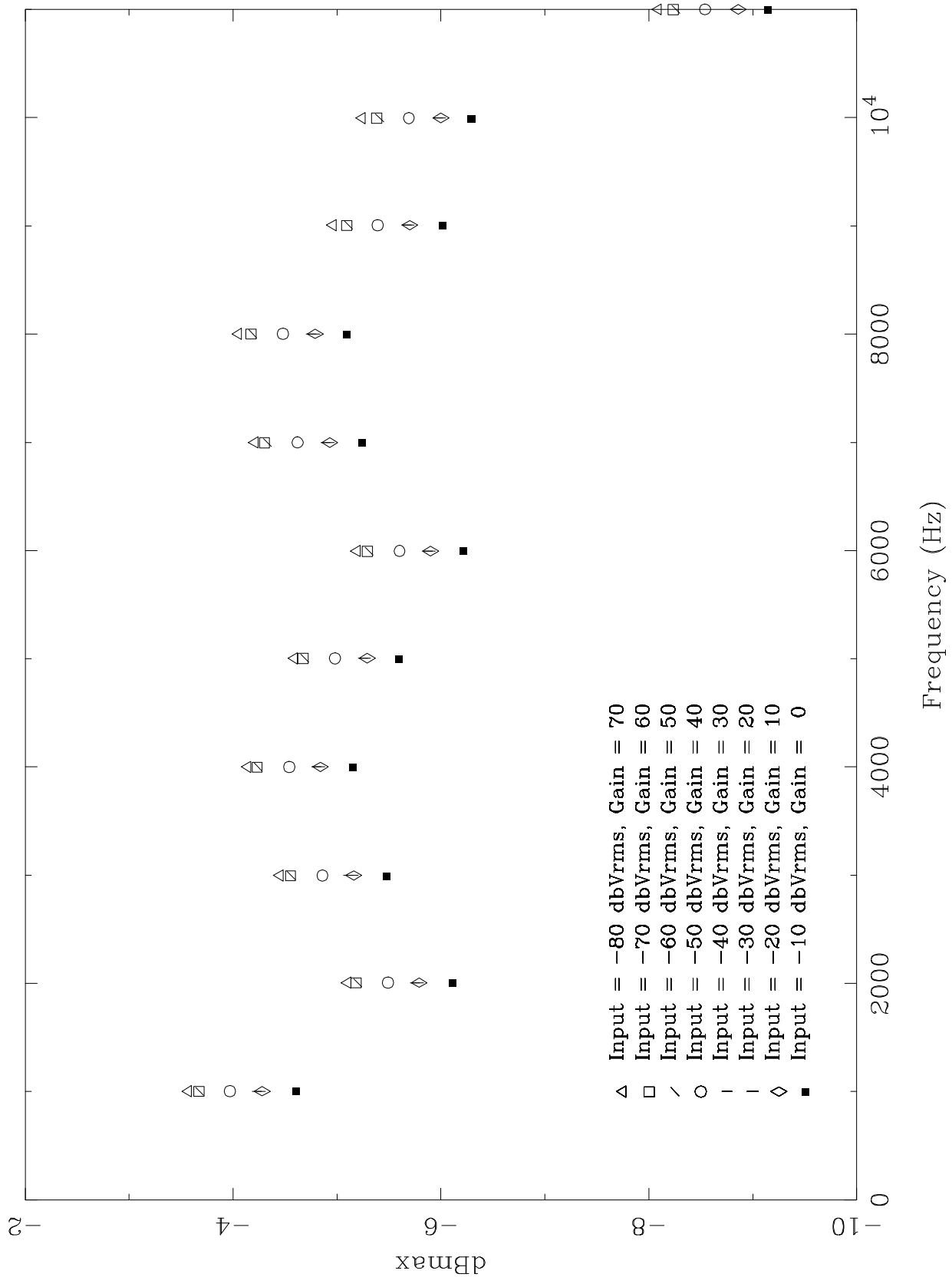
Figure 12.3.2.2: WBR Low−Band Amplitude Response
dBmax
−2
−4
−6
−8
−10
0
2000
4000
6000
8000
10^4
Frequency (Hz)
Input = −80 dbVrms, Gain = 70
Input = −70 dbVrms, Gain = 60
Input = −60 dbVrms, Gain = 50
Input = −50 dbVrms, Gain = 40
Input = −40 dbVrms, Gain = 30
Input = −30 dbVrms, Gain = 20
Input = −20 dbVrms, Gain = 10
Input = −10 dbVrms, Gain = 0

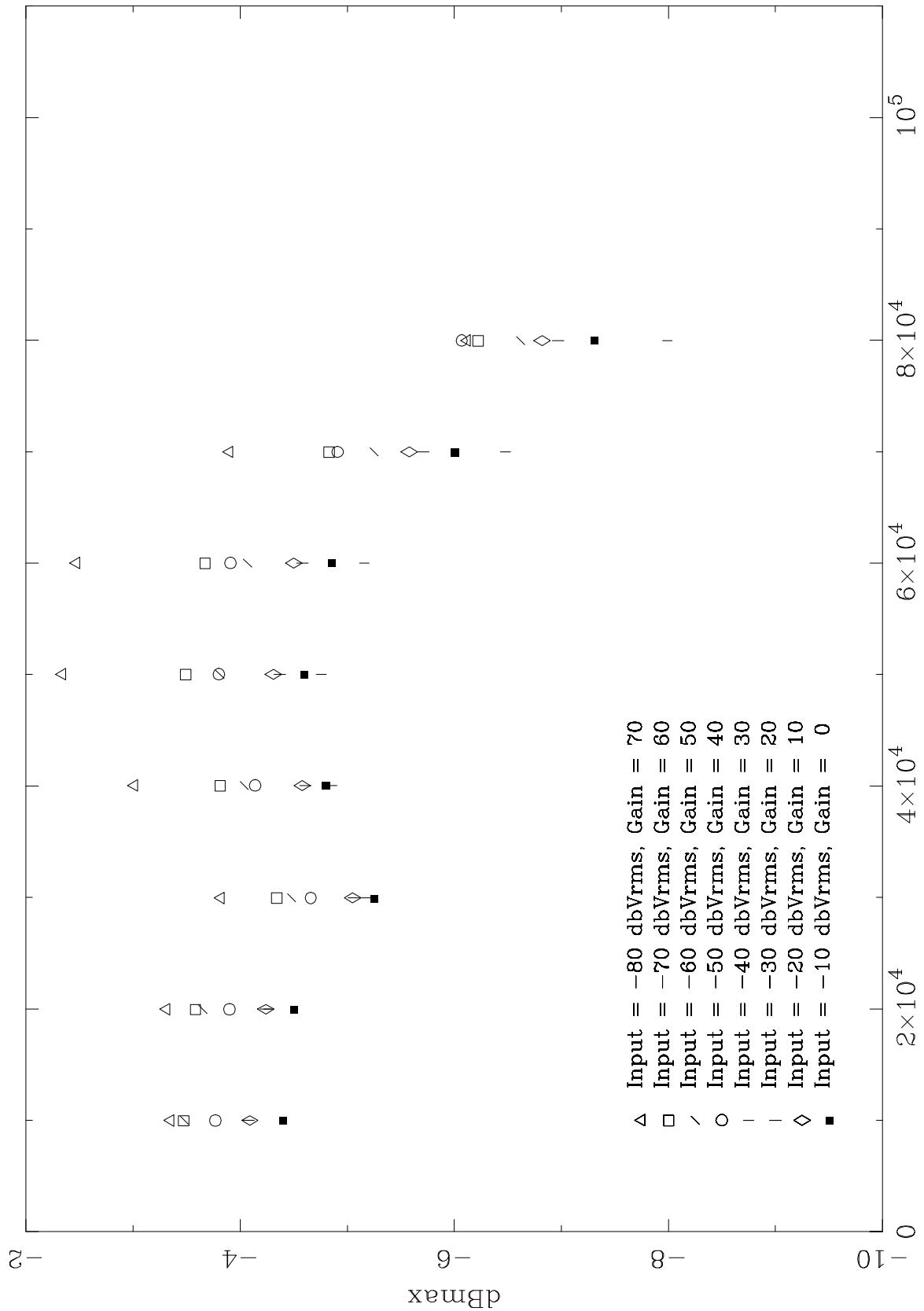
Figure 12.3.2.3: WBR High−Band Amplitude Response
dBmax
−2
−4
−6
−8
−10
0
2×10^4
4×10^4
6×10^4
8×10^4
10^5
Frequency (Hz)
Input = −80 dbVrms, Gain = 70
Input = −70 dbVrms, Gain = 60
Input = −60 dbVrms, Gain = 50
Input = −50 dbVrms, Gain = 40
Input = −40 dbVrms, Gain = 30
Input = −30 dbVrms, Gain = 20
Input = −20 dbVrms, Gain = 10
Input = −10 dbVrms, Gain = 0

Table 12.3.2.1: WBR Low-Band Gain Calibration vs. Frequency
(Entries are in units of dBmax).

Freq. (kHz)	Gain 0dB	Gain 10dB	Gain 20dB	Gain 30dB	Gain 40dB	Gain 50dB	Gain 60dB	Gain 70dB
1	-4.60	-4.28	-4.26	-4.23	-3.97	-3.68	-3.67	-3.57
2	-6.11	-5.79	-5.78	-5.75	-5.49	-5.20	-5.18	-5.10
3	-5.47	-5.16	-5.15	-5.11	-4.86	-4.56	-4.55	-4.45
4	-5.15	-4.84	-4.83	-4.80	-4.54	-4.24	-4.23	-4.14
5	-5.59	-5.29	-5.27	-5.25	-4.98	-4.69	-4.67	-4.59
6	-6.21	-5.90	-5.89	-5.87	-5.60	-5.31	-5.29	-5.19
7	-5.24	-4.93	-4.92	-4.89	-4.62	-4.33	-4.30	-4.21
8	-5.09	-4.79	-4.78	-4.75	-4.48	-4.19	-4.17	-4.05
9	-6.01	-5.70	-5.69	-5.67	-5.39	-5.11	-5.09	-4.96
10	-6.29	-6.00	-5.99	-5.97	-5.69	-5.41	-5.38	-5.24
11	-9.14	-8.86	-8.85	-8.83	-8.54	-8.26	-8.23	-8.09
12	-23.93	-23.51	-23.50	-23.53	-23.20	-22.96	-22.92	-22.79
13	-41.67	-40.71	-40.27	-39.92	-39.73	-39.20	-39.23	**

**No data was acquired at this setting

Table 12.3.2.2: WBR High-Band Gain Calibration vs. Frequency
(Entries are in units of dBmax)

Freq. (kHz)	Gain 0dB	Gain 10dB	Gain 20dB	Gain 30dB	Gain 40dB	Gain 50dB	Gain 60dB	Gain 70dB
10	-4.40	-4.09	-4.08	-4.06	-3.77	-3.48	-3.47	-3.35
20	-4.50	-4.24	-4.24	-4.27	-3.90	-3.65	-3.58	-3.31
30	-5.25	-5.05	-5.06	-5.18	-4.66	-4.48	-4.34	-3.82
40	-4.80	-4.58	-4.61	-4.86	-4.14	-4.04	-3.81	-3.01
50	-4.59	-4.31	-4.37	-4.76	-3.80	-3.81	-3.49	-2.34
60	-4.85	-4.50	-4.58	-5.16	-3.91	-4.07	-3.67	-2.47
70	-6.00	-5.58	-5.71	-6.48	-4.91	-5.25	-4.83	-3.90
80	-7.31	-6.82	-6.97	-7.99	-6.07	-6.62	-6.22	-6.12
90	-23.82	-23.23	-23.39	-24.76	-22.46	-23.23	-22.94	-23.82
100	-41.92	-41.86	-42.02	-43.55	-41.85	-42.93	**	**

** No data was acquired at this setting

12.3.3 <u>WBR AGC Characteristics</u>

Tests were conducted to characterize the response of the Wideband Receiver Automatic Gain Control (AGC) hardware. This corresponds to the "Peak Detect" section of Figure 12.1.1.1. The WBR software reads an 8-bit value provided by this hardware, and can make automatic gain decisions based upon the value it reads. As stated in Section 12.1.4, if the software AGC function has been enabled, then the output from the peak detect is compared to a pair of reference amplitudes, and the gain state is either increased by 1 step (10 dB) or decreased by one step accordingly for the next set of contiguous samples. The pair of reference amplitudes can be reprogrammed, so it is necessary to understand what the response of the peak detect hardware is. For the first three tests, see the test configuration block diagram of Figure 12.3.3.1.

The first test was performed during Spacecraft Thermal Vacuum testing, on February 3, 1997. The Spacecraft was at room temperature. The WBR was configured in the 10-kHz mode, the input sensor was the Ex dipole, and the WBR gain was fixed at 0 dB gain (i.e., the AGC software was disabled and the WBR was in "manual" gain mode). The input frequency was 526.5 Hz (this is the "drive" frequency for MFR step 16), and the input voltage was varied in steps of 2 dB. The results are plotted in Figure 12.3.3.2 and given as AGC data number versus dBmax (the decibels below a maximum amplitude sine wave measured by the WBR) in Table 12.3.3.1.

Table 12.3.3.1 WBR 10 kHz mode: AGC vs. dBmax

dBmax	AGC	dBmax	AGC	dBmax	AGC	dBmax	AGC
-0.6	209	-8.8	86	-20.6	32	-32.4	24
-0.8	201	-10.6	71	-22.6	29	-35.2	24
-1.6	186	-12.7	59	-24.6	27	-36.3	24
-2.8	163	-14.7	49	-26.6	26	-41.0	23
-4.7	132	-16.7	42	-28.5	25		
-6.7	106	-18.6	37	-30.4	24		

Clipping in the WBR data and harmonic distortion occurred at dBmax values greater than -2.8, so the useful range of the AGC extends from data numbers 163 to 24. This corresponds to about 30 dB of signal range.

The second test was performed during Unit Level Thermal Vacuum testing, on August 19, 1996. The unit was at +75 degrees C. The WBR was configured in the 10-kHz mode, the input sensor was the Ex dipole, and the WBR gain was fixed at 40 dB gain (i.e., the AGC software was disabled and the WBR was in "manual" gain mode). The input frequency was 5 kHz, and the input voltage was attenuated at various levels. The results are plotted in Figure 12.3.3.3 and given as AGC data number versus dBmax, the decibels below a maximum amplitude sine wave measured by the WBR, in Table 12.3.3.2.

Table 12.3.3.2 WBR 10 kHz mode: AGC vs. dBmax

dBmax	AGC	dBmax	AGC	dBmax	AGC	dBmax	AGC
-0.1	218	-13.0	59	-24.9	30	-36.2	27
-3.0	159	-14.9	50	-27.0	28	-39.7	26
-5.0	129	-17.1	42	-29.9	27	-42.2	26
-7.2	103	-20.0	35	-32.6	27		
-10.1	77	-22.9	31	-34.9	27		

Again, clipping in the WBR data and harmonic distortion occurred at dBmax value -0.1, so the useful range of the AGC extends from data numbers 159 to 26. Notice the similarity to the first test, where a different gain setting and different signal amplitudes and frequency were used. The likely reason for the higher AGC values at the low end of the curve here is the temperature: at +75 degrees C, the bottom value has raised slightly. For gain-setting decisions, the room temperature test is the better calibration.

The third test was also performed during Spacecraft Thermal Vacuum testing, on February 3, 1997. The Spacecraft was at room temperature. The WBR was configured in the 80-kHz mode, the input sensor was the Ex dipole, and the WBR gain was set to several gains, including 30, 40, and 50 dB gain. The input frequency was 20 kHz, and the input voltage was attenuated to various levels. The results are plotted in Figure 12.3.3.4 and given as AGC data number versus dBmax, the decibels below a maximum amplitude sine wave measured by the WBR, in Table 12.3.3.3.

Table 12.3.3.3 WBR 80 kHz mode: AGC vs. dBmax

dBmax	AGC	dBmax	AGC	dBmax	AGC	dBmax	AGC
-11.7	64	-14.0	53	-16.0	44	-22.1	30
-12.0	63	-14.0	52	-18.0	38	-23.1	29
-12.9	58	-15.0	48	-20.0	33	-24.0	28
-13.0	57	-15.7	45	-21.0	32	-25.0	27

Although a variety of gain states are combined in this data set, notice that the dBmax relative scale is insensitive to this. And notice that this AGC response is very close to the response of the WBR 10-kHz mode to a 526 Hz tone. This indicates that the same gain control window points can probably be used for both the low-band and high-band modes.

The fourth test was performed on August 7, 1996 during unit level testing at room temperature. During a white noise response test for the MFR Band 3, data was also acquired by the WBR. The WBR was configured in the 10-kHz mode, the input sensor was the Ex dipole, and the WBR gain was set to 70 dB gain. For the stimulus configuration see Figure 10.3.3.2.3 in the MFR section. With white noise as the input, the signal voltage was stepped in 2-dB intervals. The results are plotted in Figure 12.3.3.5 and given as AGC data number versus dBmax in Table 12.3.3.4.

Table 12.3.3.4 WBR 10 kHz mode: AGC vs. dBmax

dBmax	AGC	dBmax	AGC	dBmax	AGC	dBmax	AGC
-1	238	-7	99	-17	37	-26	26
-2	179	-8	83	-19	34	-28	25
-3	152	-10	69	-20	33	-30	24
-4	124	-12	58	-21	30		
-5	122	-14	49	-23	28		
-6	102	-16	42	-24	27		

To compare to the sine wave data of the previous tests, the random noise signal was processed as follows: an RMS average was calculated for the time series and the result was multiplied by • 2. This result can then be converted to the dBmax value, which is rounded to the nearest dB. The reason that the higher values of dBmax do not step by 2 dB is because there was clipping of the input signal at 70 dB gain. Notice that this AGC response is very close to the response of the WBR 10-kHz mode to tones.

The final conclusions for the WBR AGC response are as follows. One commonly used rule of thumb in setting the gain is that 10 dB of "headroom" is desired for random noise spikes. This determines the upper set point, and corresponds to about 70 on the AGC response curve. The other rule of thumb is that the window formed by the upper and lower set points must be wider than one gain step, which is 10 dB. The wider the window is, the larger the hysteresis produced. To get a window which is 14 dB wide with the upper end of the window at 10 dB headroom, the lower threshold would be set at AGC value 27. These values can be changed a little, but there is not much adjustment possible because of the limited range of the AGC peak detector.

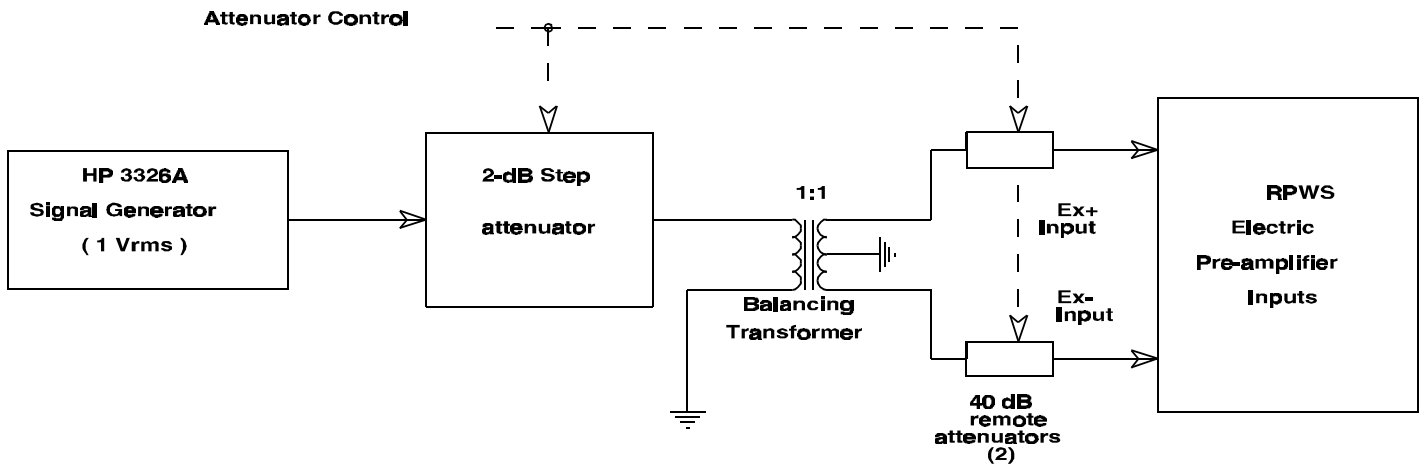

Figure 12.3.3.1

WBR AGC Characteristics Calibration

Stimulus Configuration

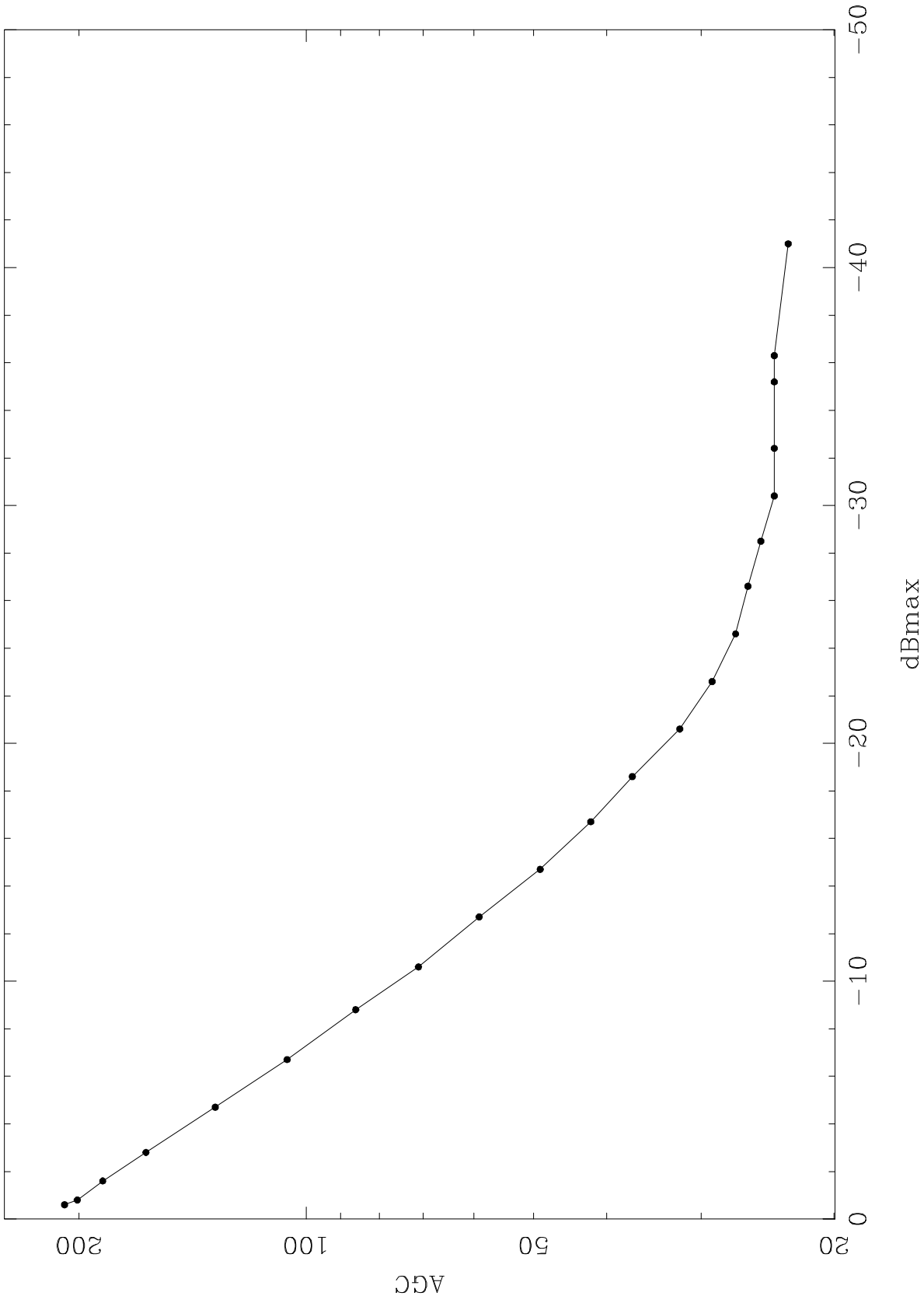

Figure 12.3.3.2: WBR Low−Band AGC Response at 526 Hz

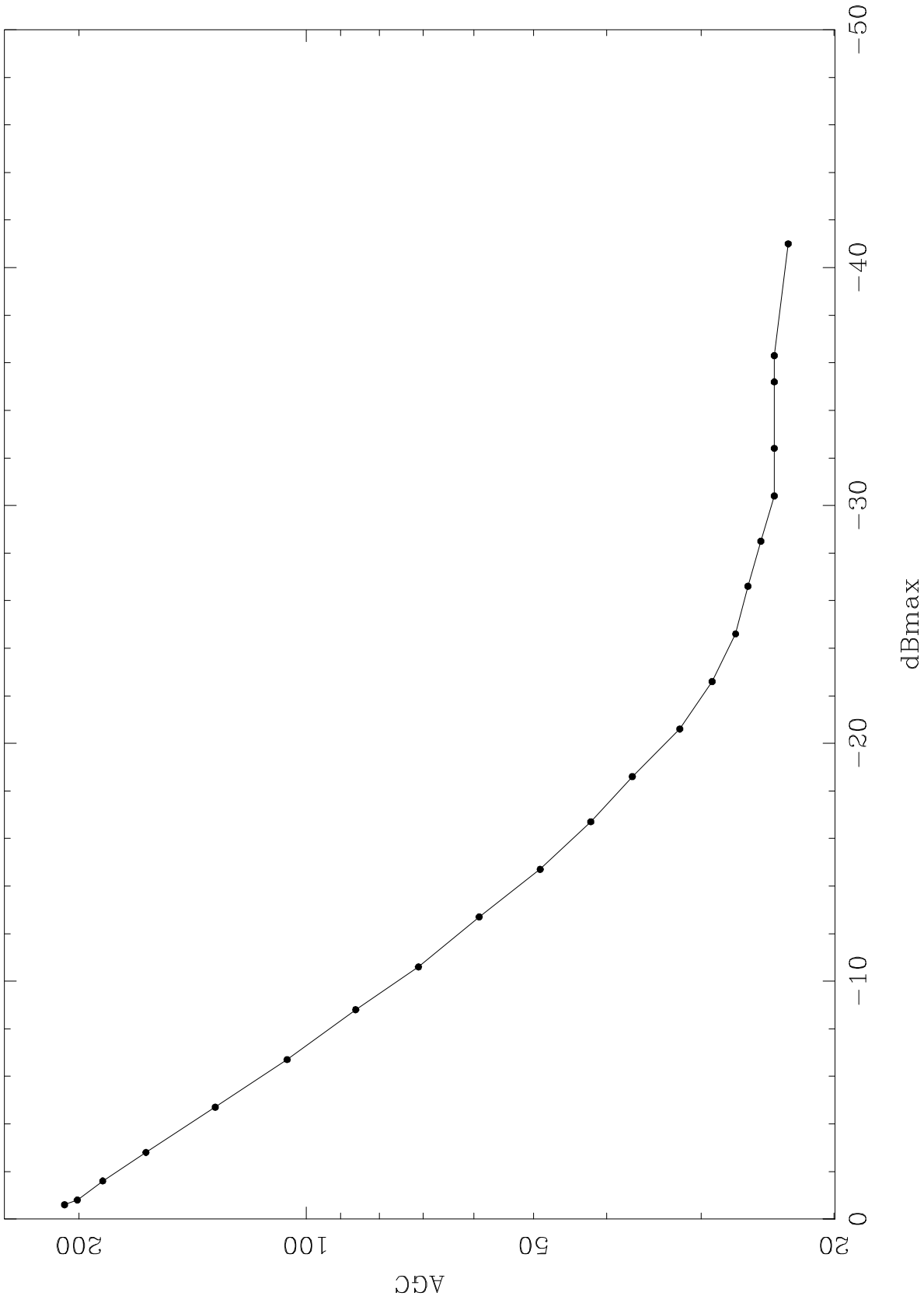

Figure 12.3.3.3: WBR Low-Band AGC Response at 5 KHz

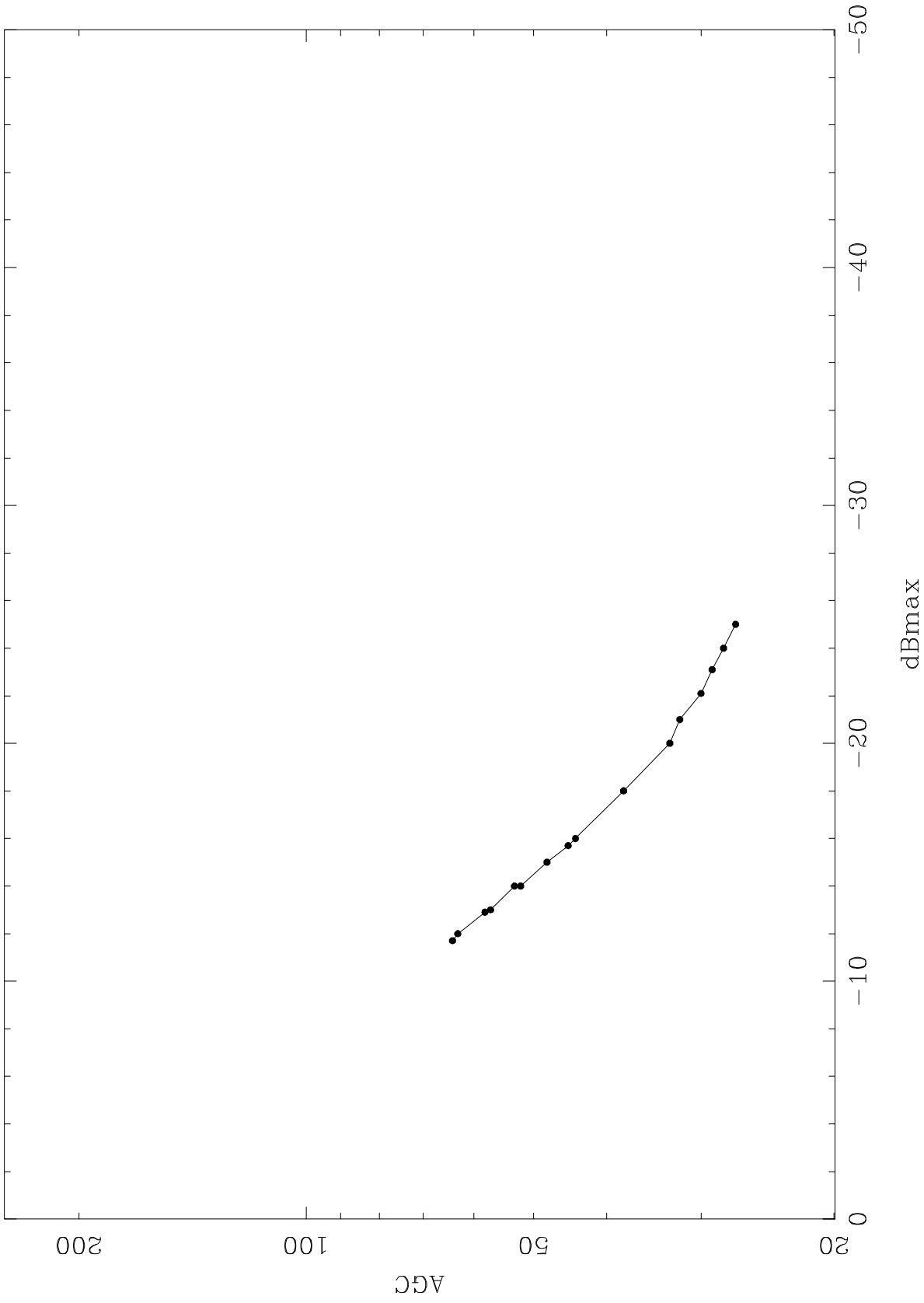

Figure 12.3.3.4: WBR High-Band AGC Response at 20 KHz

Figure 12.3.3.5: WBR Low-Band AGC Response to White Noise

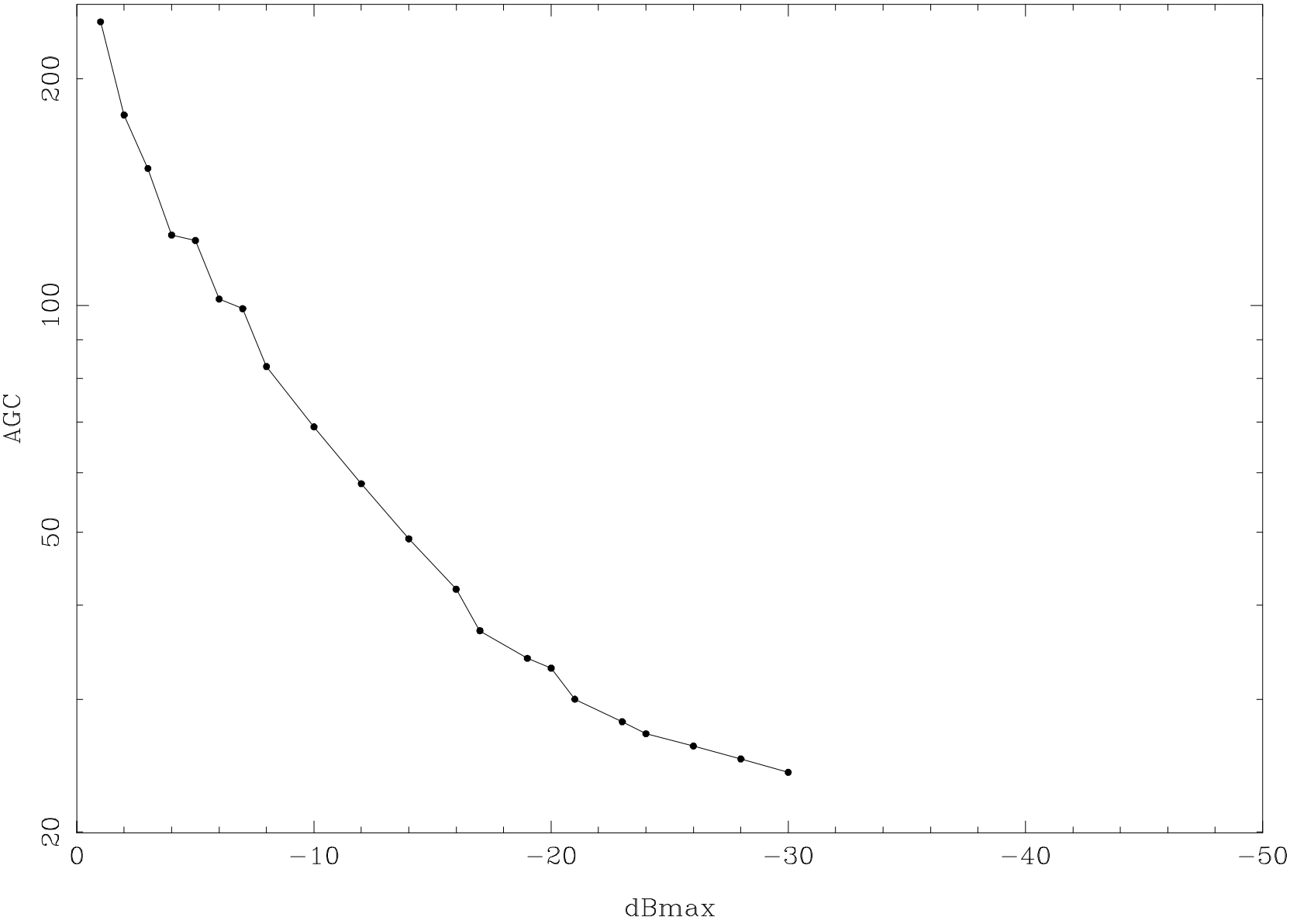

12.3.4 WBR Random Noise Response

Tests were conducted to characterize the response of the Wideband Receiver to random noise. These bench tests were performed on July 28-29, 1996, at +40 degrees C. Two test configurations were used, one for the 10 kHz WBR mode and one for the 80 kHz WBR mode. These configurations are shown in Figures 12.3.4.1 and 12.3.4.2. The GSE was connected to the instrument Ex+ and Ex- inputs. The noise spectral density was measured using the HP8535 Spectrum Analyzer, and graphs showing the frequency spectrum for the two GSE configurations are shown in Figures 12.3.4.3 and 12.3.4.4. Also a measure of the total power was made using a true RMS meter, and an estimate of the noise spectral density was obtained by using that and the signal bandwidth. For each of the WBR modes, 100 spectra were averaged and the average spectra are shown in Figures 12.3.4.5 through 12.3.4.8. Using an estimate of the average level for each plot, an estimate of the noise spectral density was done using the calibration procedure described in Section 12.2. Note that the FFT size for all of these tests is 2048 samples, and a Hanning window was applied to the data. The results are summarized for the 10-kHz mode in Table 12.3.4.1.

Table 12.3.4.1 WBR 10 kHz mode: White Noise Response

RMS voltage (V_{rms})	1.00	1.00	1.00	1.00
Bandwidth (kHz)	20	20	20	20
Attenuation (dB)	30	20	10	00
Est. PSD ($dBV/Hz^{1/2}$)	-73	-63	-53	-43
HP8535 SD ($dBV/Hz^{1/2}$)	-74	-64	-54	-44
Avg. WBR PSD ($dBV/Hz^{1/2}$)	-75	-65	-56	-52

Notice the large discrepancy for the test at 0 dB attenuation: the HP8535 spectrum analyzer measured -44 $dBV/Hz^{1/2}$, while the WBR measured -52 $dBV/Hz^{1/2}$. The reason for this discrepancy is that the data was clipped, so a low estimate of the power results. This overloading is apparently just starting to occur at the 10 dB attenuation setting, where the WBR estimate is 1 dB lower relative to the tests at higher attenuations. Those tests at 20 and 30 dB attenuation are both within 1 dB of the HP8535 estimate. The scatter in the data seems to indicate that these are reasonable answers.

The results for the 80-kHz mode are summarized in Table 12.3.4.2.

Table 12.3.4.2 WBR 10 kHz mode: White Noise Response

RMS voltage (V_{rms})	1.00
Bandwidth (MHz)	2
Attenuation (dB)	10
Est. PSD (dBV/Hz$^{1/2}$)	-73
HP8535 SD (dBV/Hz$^{1/2}$)	-71
Ave. WBR PSD (dBV/Hz$^{1/2}$)	-72

Notice that for the 80 kHz test, there was an interference tone present. It is thought that the 32 kHz interference originates from the Noise Generator. Nevertheless, it does not interfere with the test. The HP8535 measured the spectral density at 50 kHz, avoiding the noise line, and the WBR PSD estimate is within one dB of that.

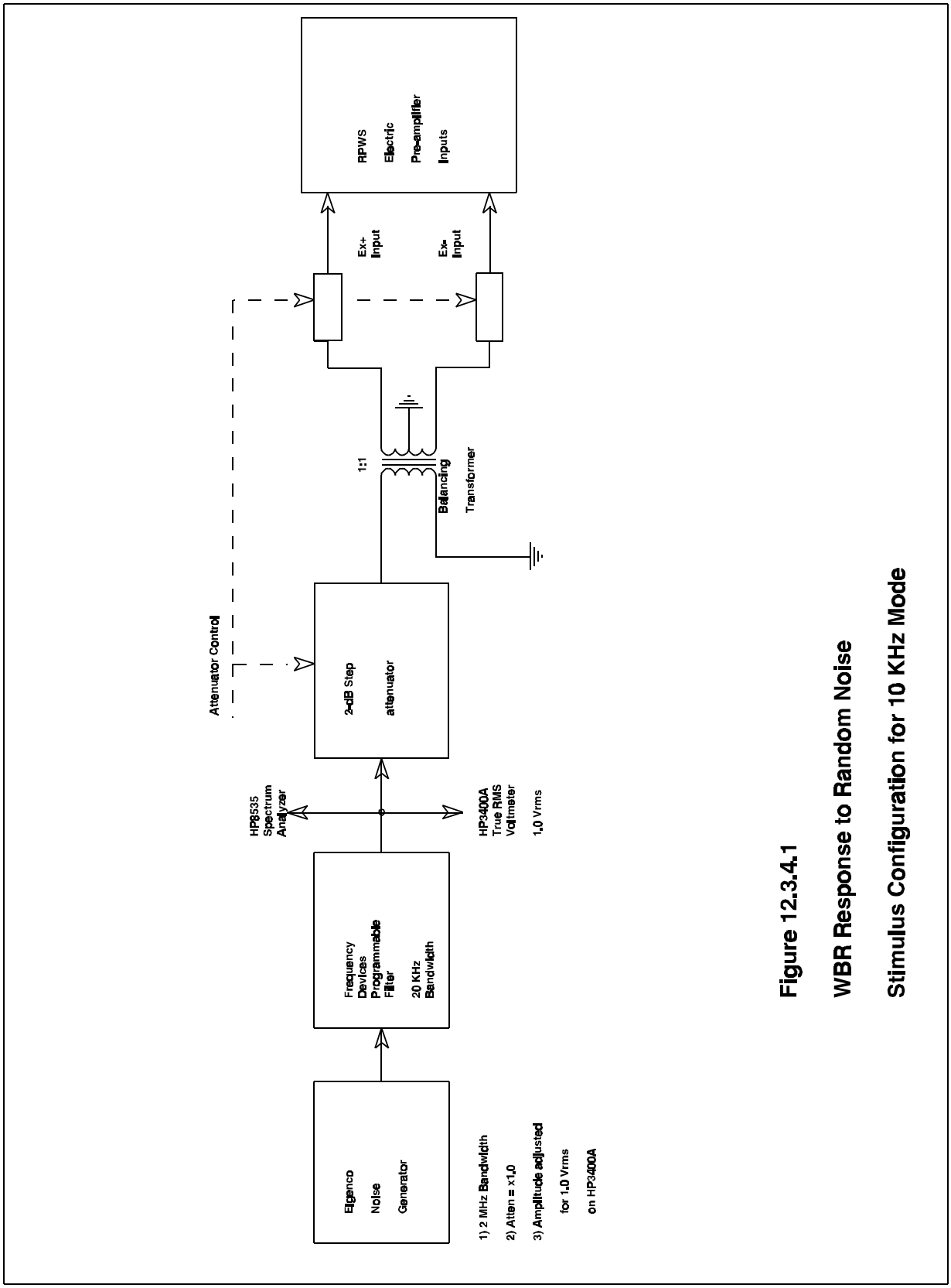

Figure 12.3.4.1

WBR Response to Random Noise

Stimulus Configuration for 10 KHz Mode

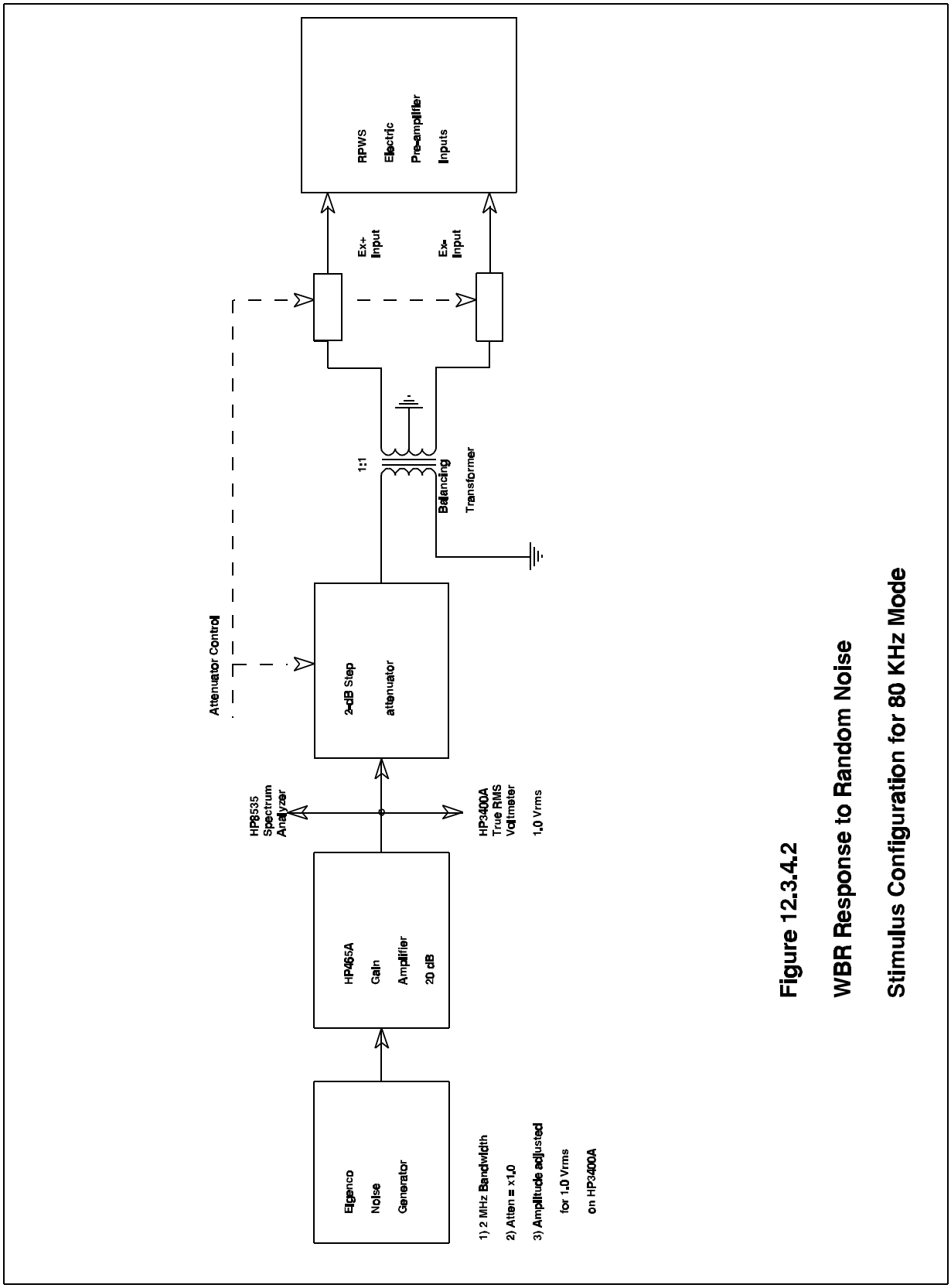

Figure 12.3.4.2

WBR Response to Random Noise

Stimulus Configuration for 80 KHz Mode

Figure 12.3.4.3: HP8535 Spectrum Analyzer Display
WBR 10 KHz Mode White Noise Test

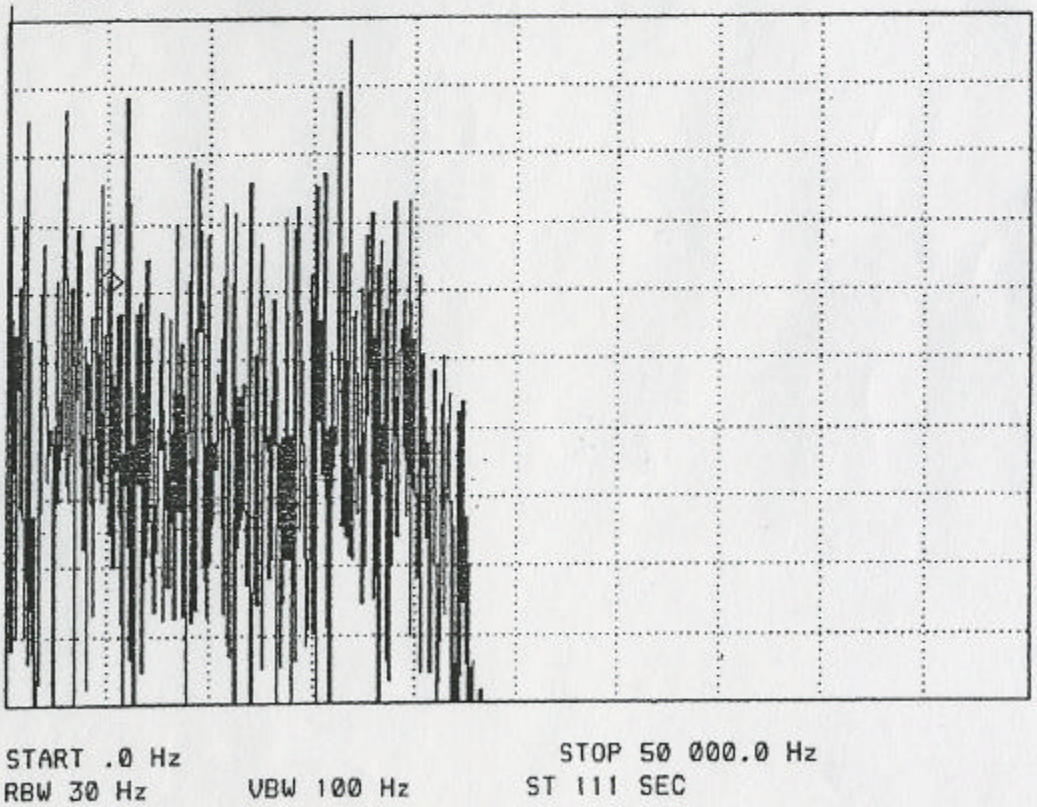

Figure 12.3.4.4: HP8535 Spectrum Analyzer Display
WBR 80 KHz Mode White Noise Test

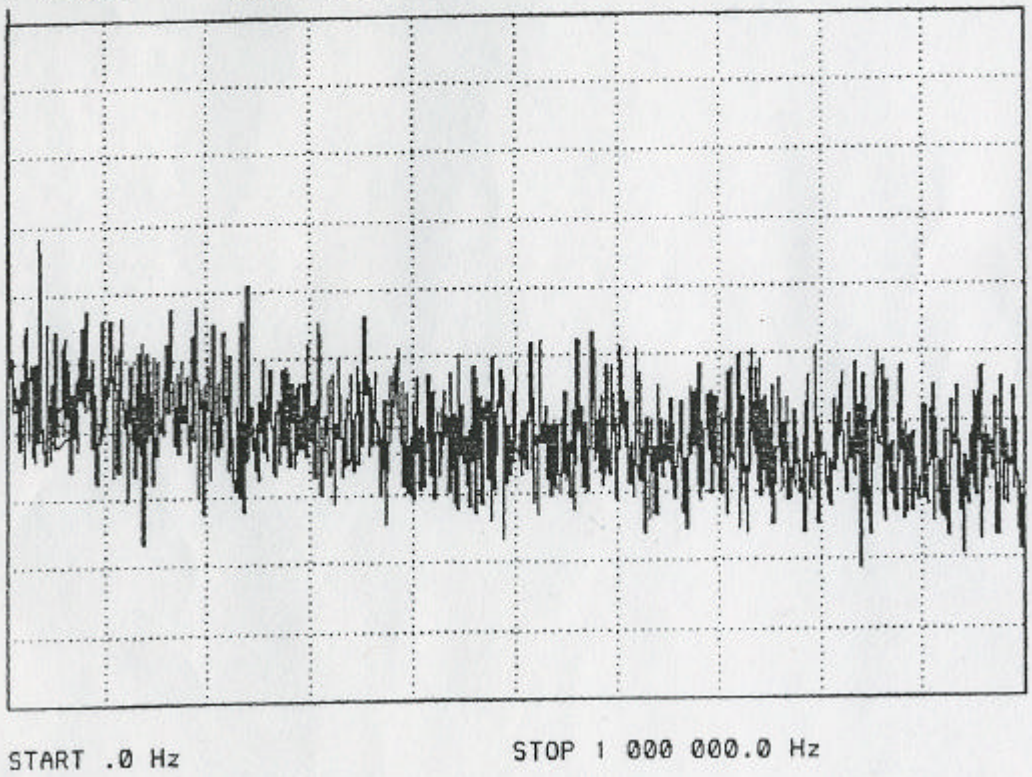

Figure 12.3.4.5: WBR Low-Band White Noise Response

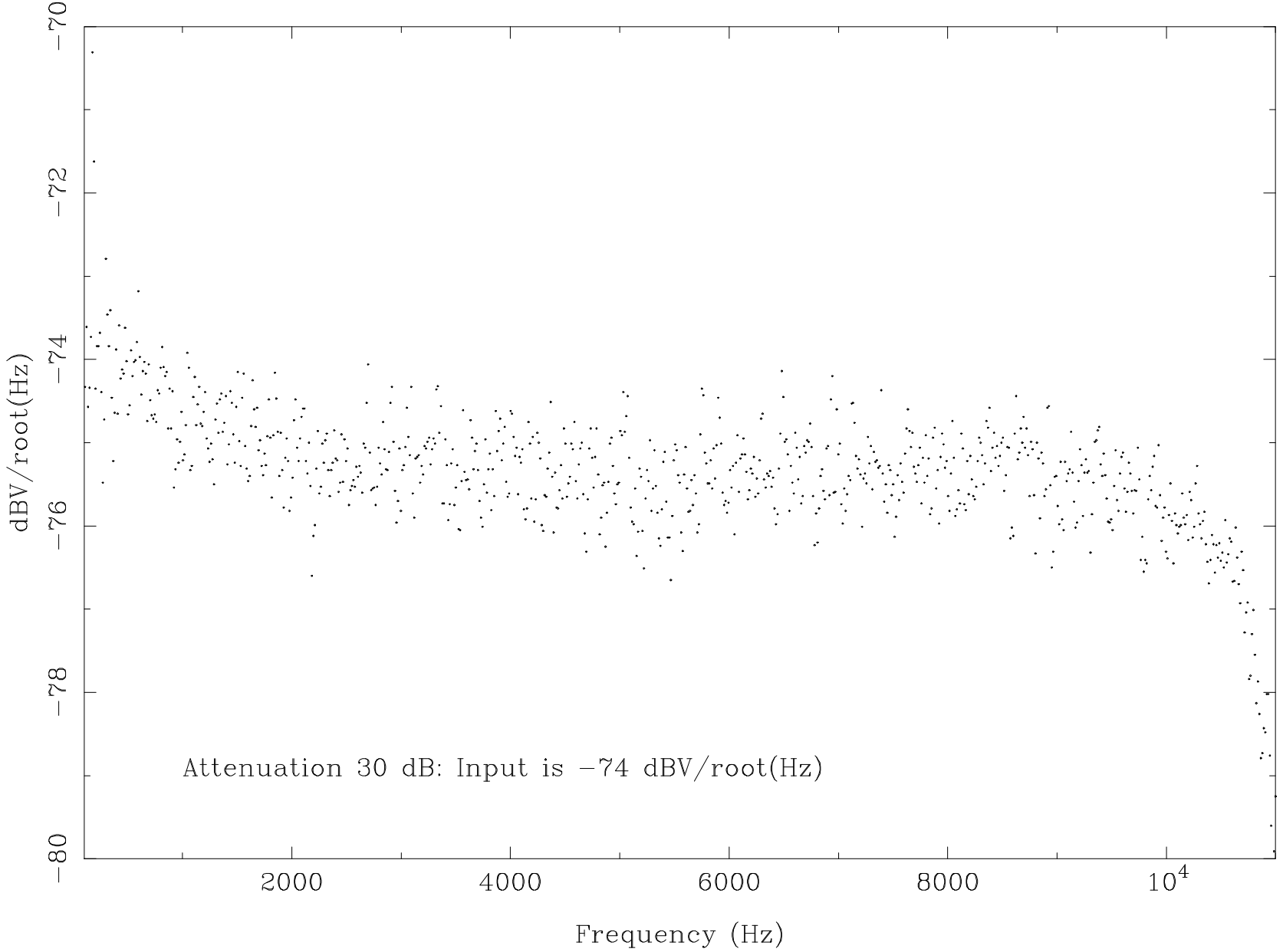

Figure 12.3.4.6: WBR Low-Band White Noise Response

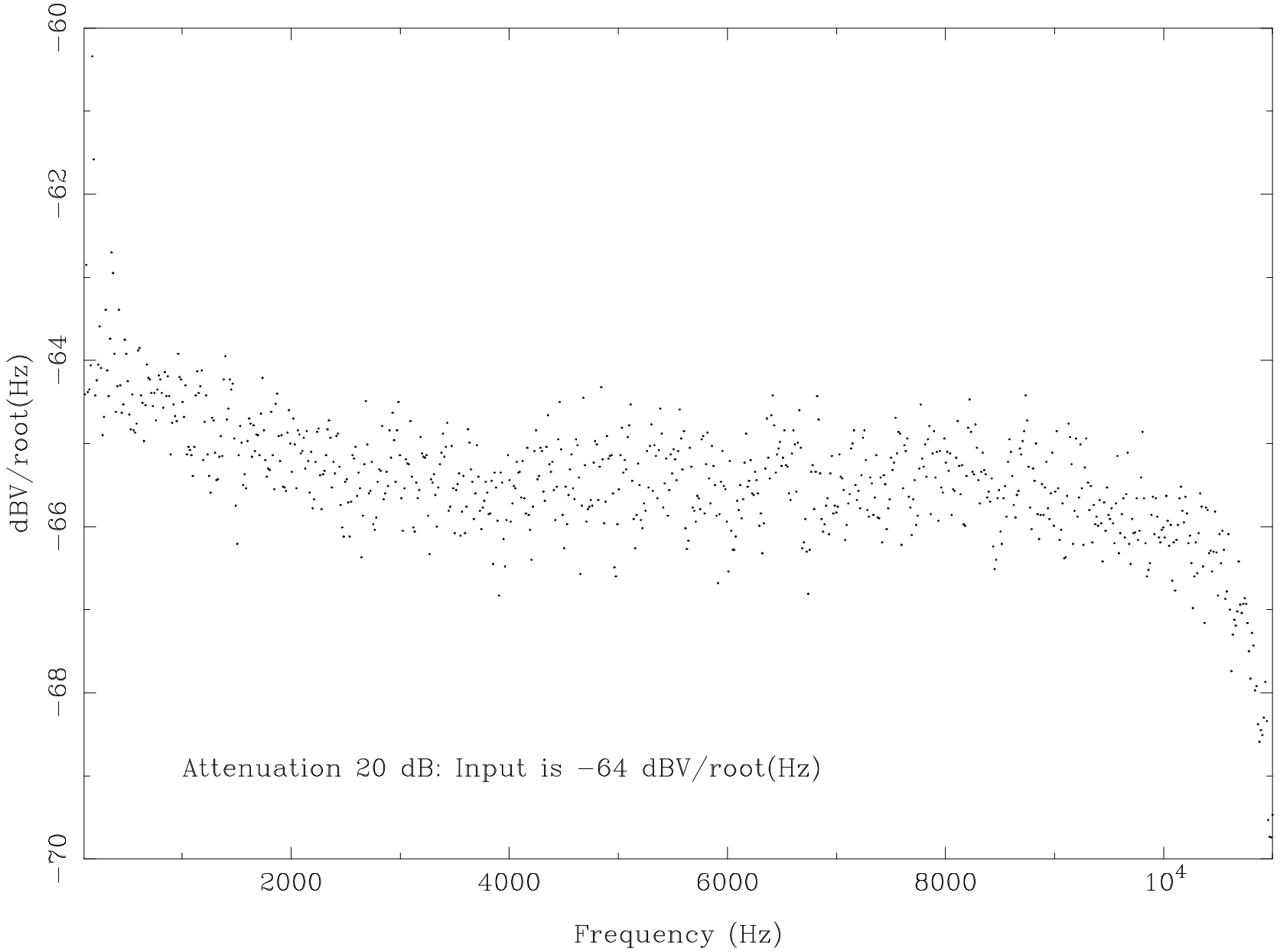

Figure 12.3.4.7: WBR Low-Band White Noise Response

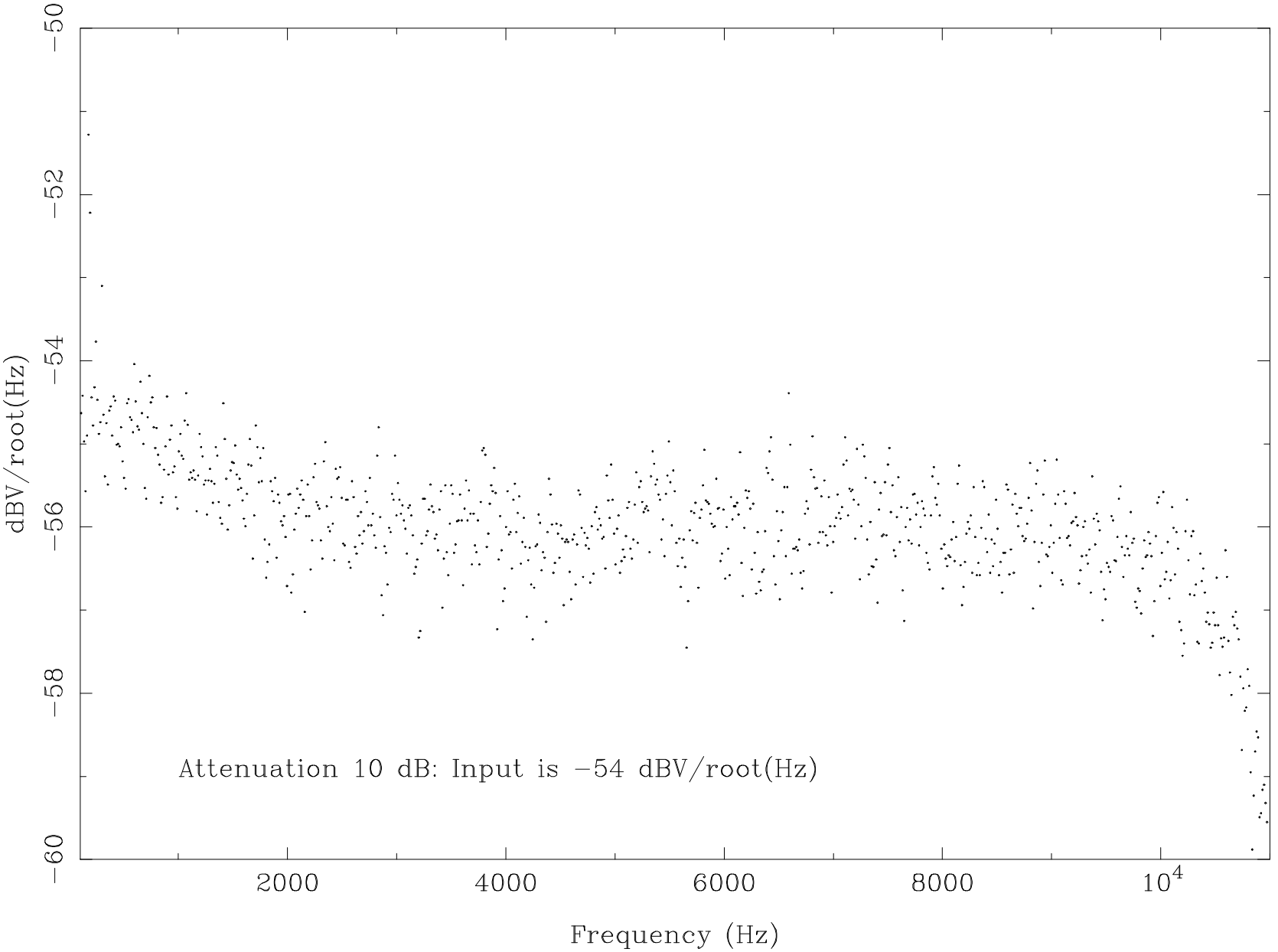

Figure 12.3.4.8: WBR Low-Band White Noise Response

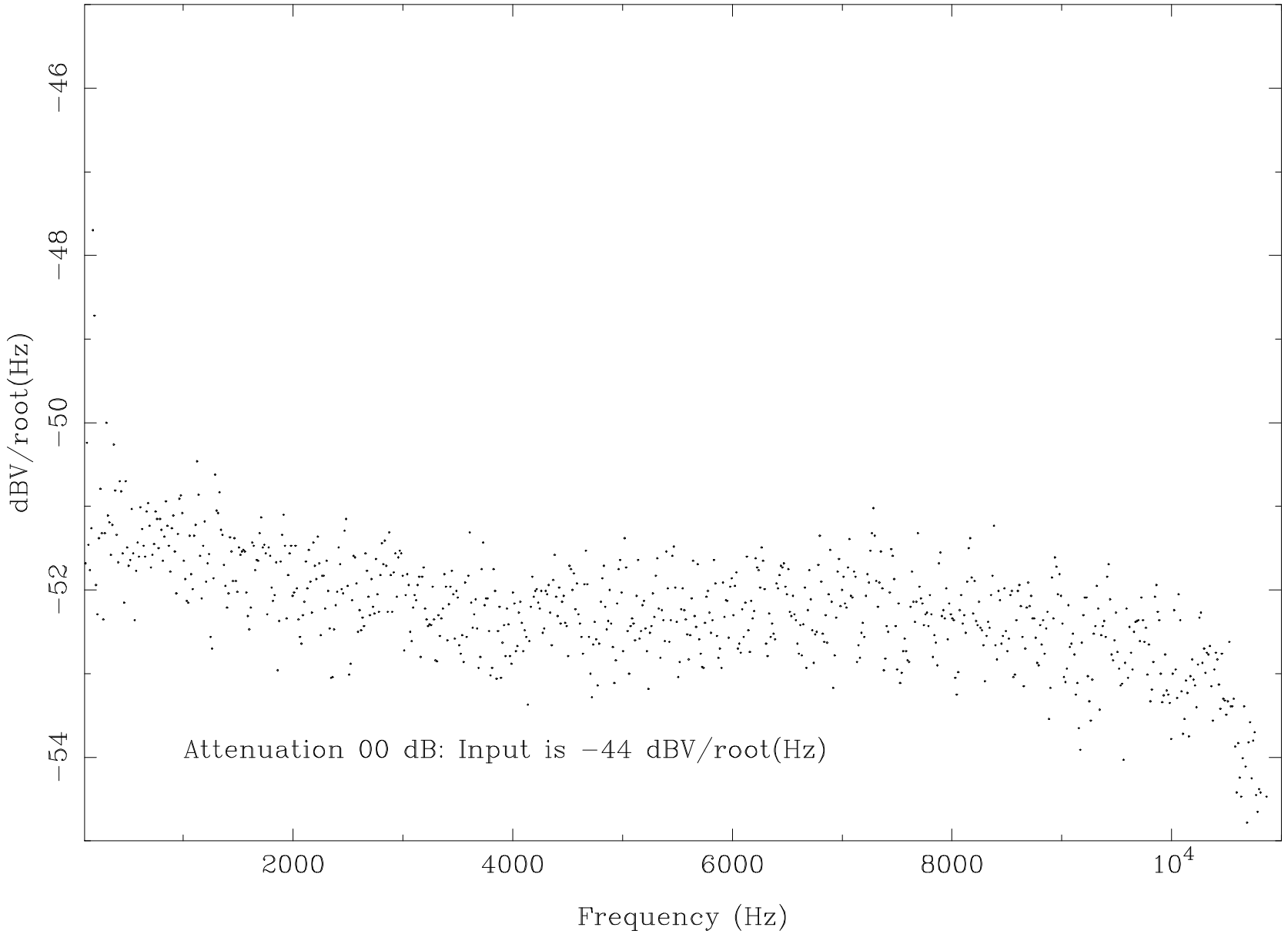

Figure 12.3.4.9: WBR High-Band White Noise Response

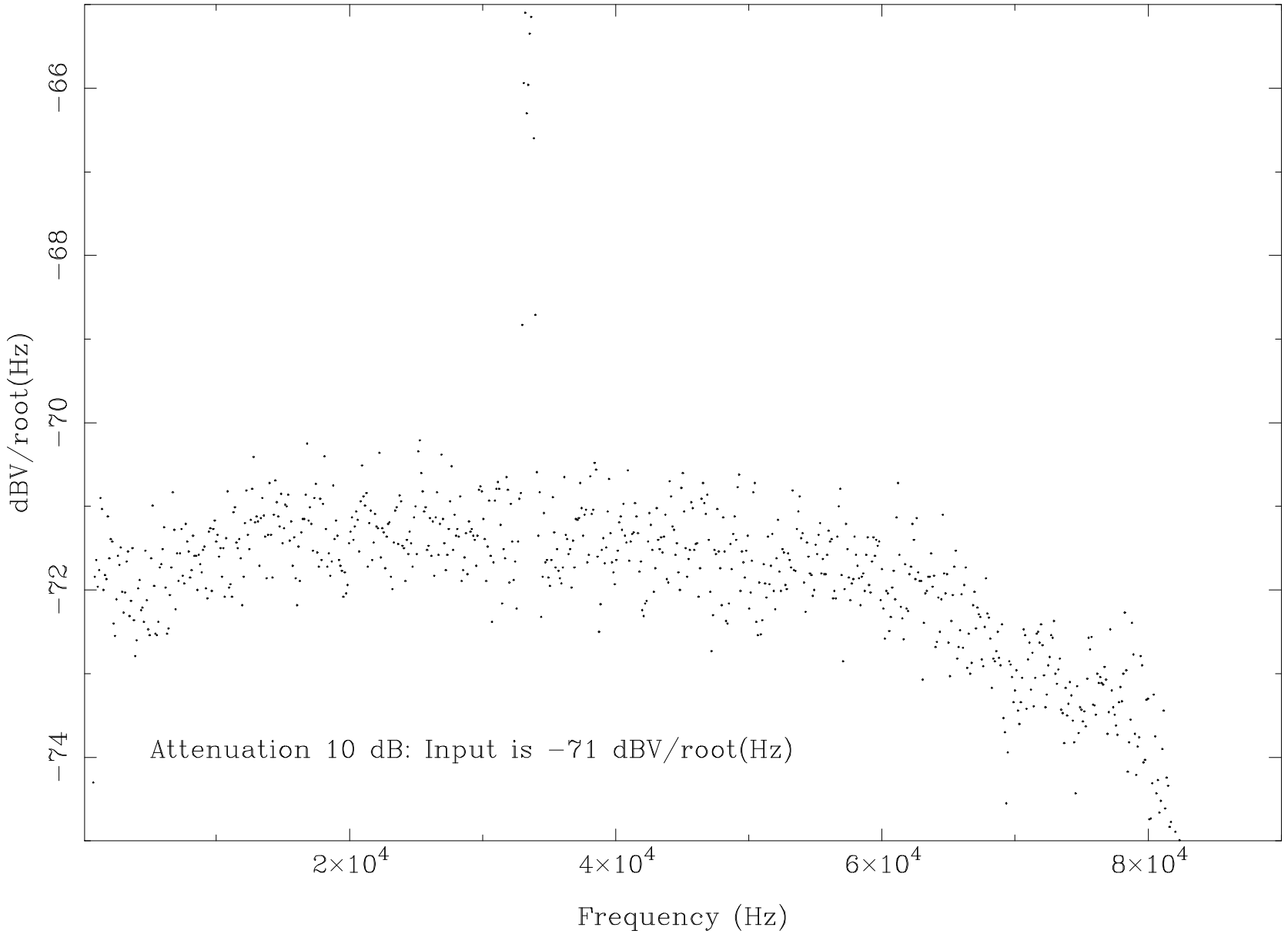

12.4 WBR Noise Levels

In this section, the in-flight receiver noise floors are detailed for the commonly used modes. These modes will include:

Translation Mode	Filter	Antenna
Baseband	80 kHz	Ex dipole
Baseband	80 kHz	Ez monopole
Baseband	10 kHz	Ex dipole

When flight data is acquired for other sensors, those sensors' noise levels will be added to this document.

For the 80 kHz, Ex dipole configuration, see Figure 12.4.1. The data plotted in red (the lower noise level) was acquired just prior to antenna deployment, from the following data times, which are referred to as Spacecraft Event Times (SCET):

Start SCET	Stop SCET	# Spectra Averaged
1997-Oct-25-00:20:09	1997-Oct-25-00:30:01	75

One can see the low-end roll-off, with the cutoff frequency of about 800 Hz. There is no apparent 1/f noise, so the WBR rather than the pre-amps appears to set the noise floor. There are many noise lines, some caused by the MFR and some by the HFR.

In Figure 12.4.1, the data plotted in green was taken after the electric antennas were deployed, from the following data times:

Start SCET	Stop SCET	# Spectra Averaged
1997-Oct-25-04:15:05	1997-Oct-25-04:21:37	50

In this data, one sees the shot noise at about 10 dB higher than the pre-deployment noise level for frequencies up to about 10 kHz. But above that, the internal noise lines are comparable to or even greater than the antenna shot noise. Some of the noise lines have now disappeared below the shot noise floor.

Figure 12.4.1: WBR High-Band In-Flight Ex Noise Floor

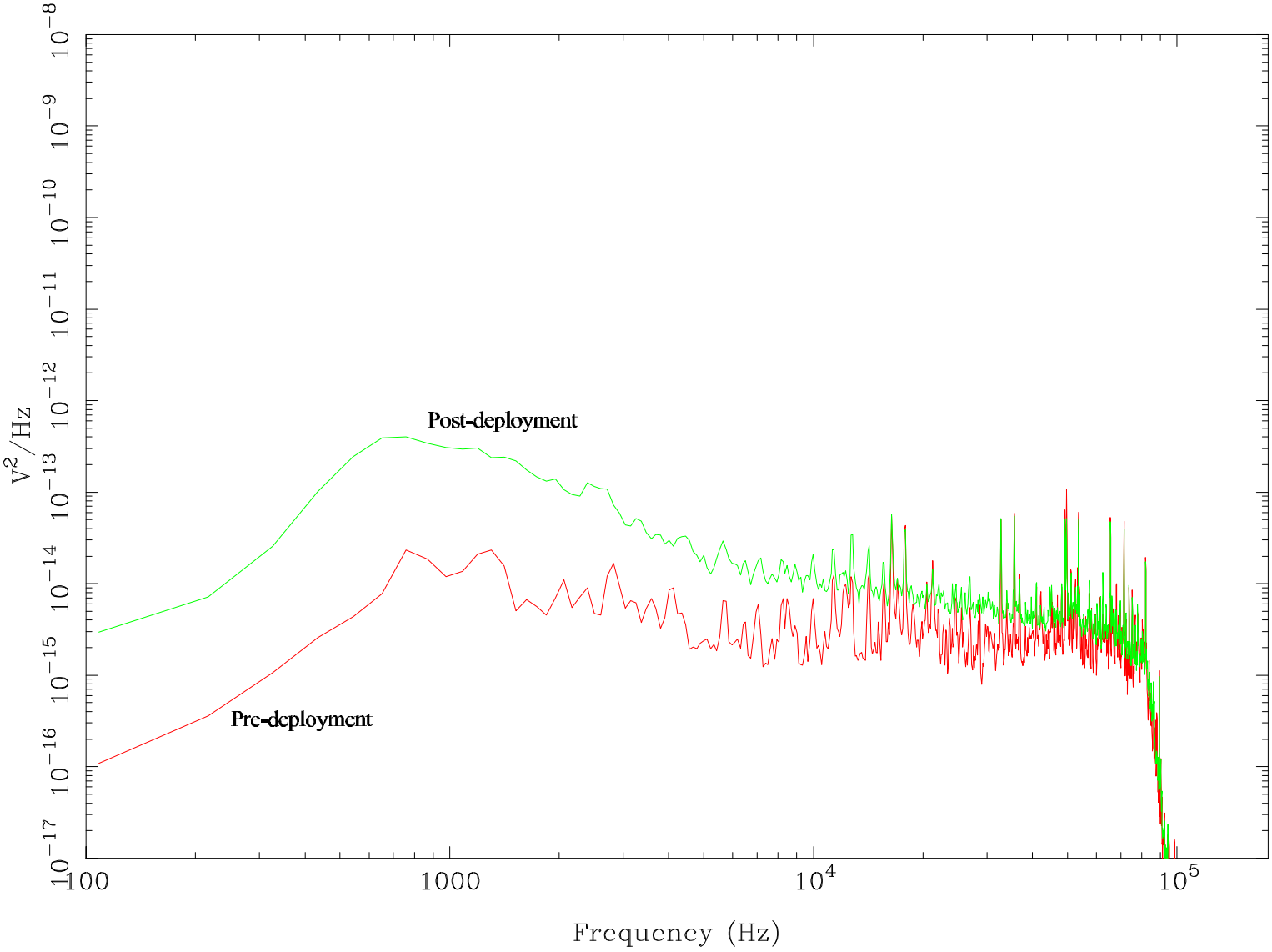

For the 80 kHz, Ez dipole configuration, see Figure 12.4.2. The data plotted in red (the lower noise level) was acquired just prior to antenna deployment, from the following data times:

Start SCET	Stop SCET	# Spectra Averaged
1997-Oct-25-00:15:05	1997-Oct-25-00:19:53	37

There are many noise lines, and these are exacerbated by the lack of common mode rejection.

In Figure 12.4.2, the data plotted in green was taken after the electric antennas were deployed, from the following data times:

Start SCET	Stop SCET	# Spectra Averaged
1997-Oct-25-04:10:09	1997-Oct-25-04:14:57	37

In this data, one sees the shot noise a few dB higher than the pre-deployment noise level for frequencies up to about 10 kHz. But above that, the internal noise lines are comparable to or even greater than the antenna shot noise. Some of the noise lines have now disappeared below the shot noise floor, but some, like that around 1200 Hz, are no better.

Figure 12.4.2: WBR High-Band In-Flight Ez Noise Floor

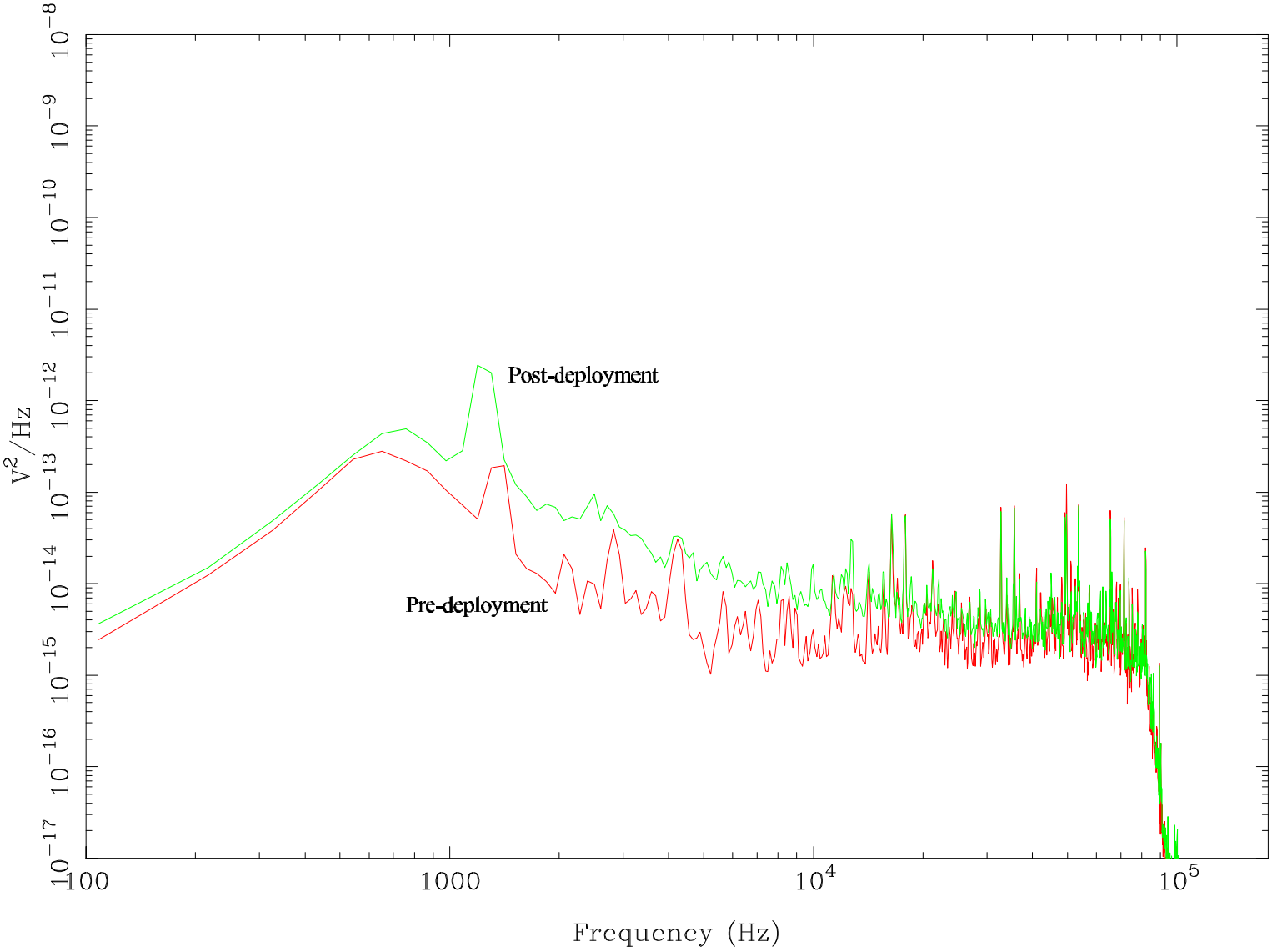

For the 10 kHz, Ex dipole configuration, see Figure 12.4.3. The data plotted in red (the lower noise level) was acquired just prior to antenna deployment, from the following data times:

Start SCET	Stop SCET	# Spectra Averaged
1997-Oct-25-00:30:09	1997-Oct-25-00:40:01	71

The noise level here is set primarily by the Ex preamps. One can see the low-end roll-off, with the cutoff frequency of about 60 Hz, followed by 1/f noise for most of the spectrum. At the high end the WBR itself appears to set the noise level, and there are many noise lines, some caused by the MFR and some by the HFR.

For the 10 kHz, Ex dipole configuration, see Figure 12.4.3. The data plotted in red (the lower noise level) was acquired just prior to antenna deployment, from the following data times:

Start SCET	Stop SCET	# Spectra Averaged
1997-Oct-25-00:30:09	1997-Oct-25-00:40:01	71

The noise level here is set primarily by the Ex preamps. One can see the low-end roll-off, with the cutoff frequency of about 60 Hz, followed by 1/f noise for most of the spectrum. At the high end the WBR itself appears to set the noise level, and there are many noise lines, some caused by the MFR and some by the HFR.

In Figure 12.4.3, the data plotted in green was taken after the electric antennas were deployed, from the following data times:

Start SCET	Stop SCET	# Spectra Averaged
1997-Oct-25-06:08:01	1997-Oct-25-06:17:45	74

In this data, one sees the shot noise at about 20 dB higher than the pre-deployment noise level. Also some of the noise lines have now disappeared because of the higher noise floor.

Figure 12.4.3: WBR Low-Band In-Flight Ex Noise Floor

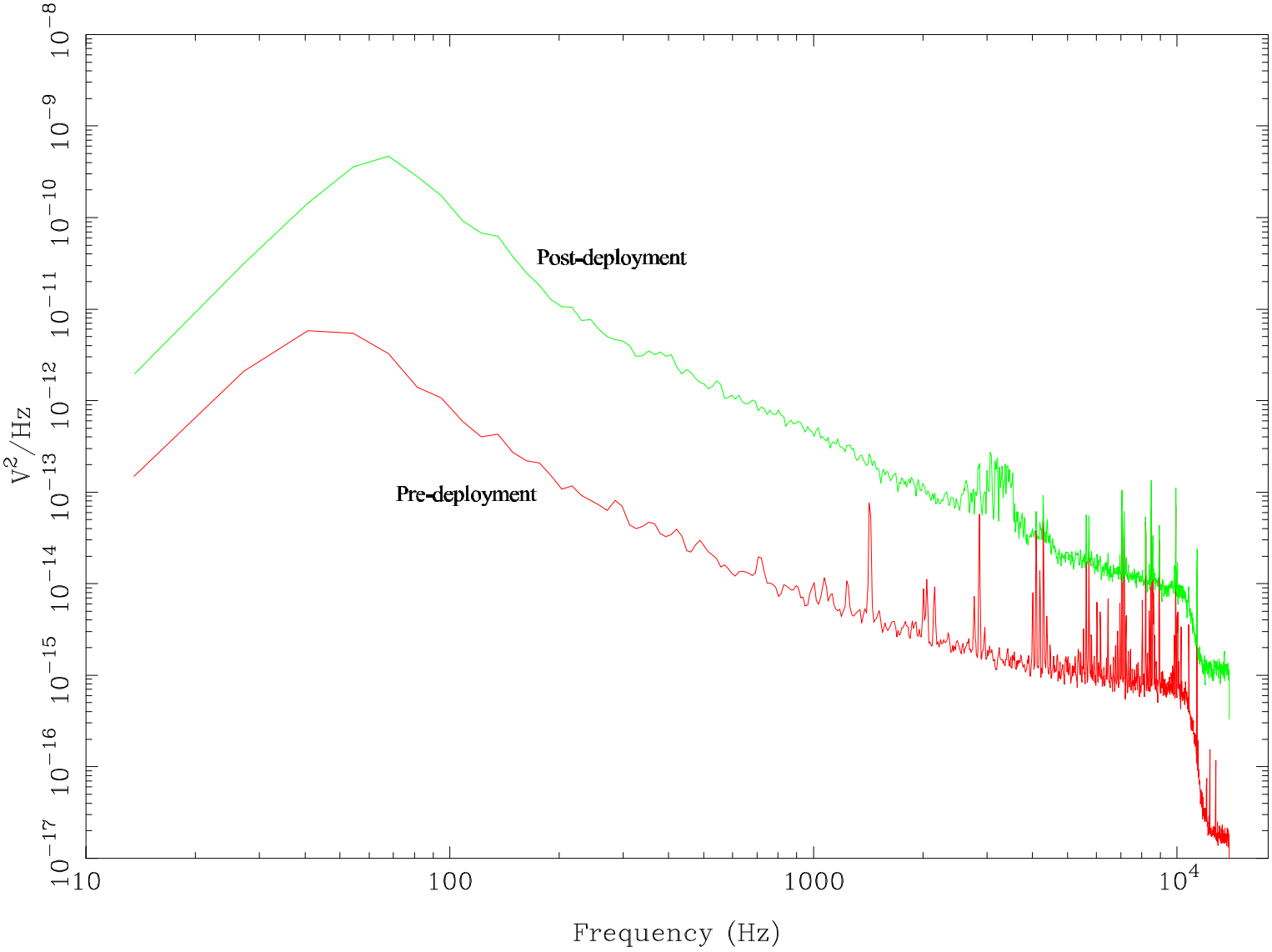

13.0 Waveform Receiver (WFR)

13.1 WFR Subsystem Description

This section of the RPWS Calibration Document describes the five-channel Waveform Receiver (WFR), extending the description contained in the Section 3 instrument overview. The WFR subsystem provides simultaneous measurements of plasma wave signals from up to five separate sensors. The purpose of this receiver is to provide high resolution spectral measurements down to ~1 Hz and to provide simultaneous waveform information from five sensors for the purpose of determining the polarization and propagation vector of the low frequency plasma waves and radio emissions. When utilizing the Langmuir Probes, the WFR can provide $\Delta n/n$ waveforms, including time delay measurements between the different sensors. During data analysis on the ground, signal processing routines will analyze the five-component measurements, providing cross-correlation products which may be used to deduce the wave normal, Poynting, and polarization vectors. The WFR is similar to waveform receivers previously designed for the Polar spacecraft.

13.2.1 General WFR Characteristics

The WFR consists of five parallel analog input channels, with each channel dedicated to an electric, magnetic, and/or a Langmuir sensor. The five channel inputs are coupled directly to the differential amplifiers of the electric antennas [EXLO (dipole) and EZLO(monopole)], the magnetic search coil antennas (BX, BY, and BZ), and Langmuir Probe (LMR+, LMR-, and LMR). It should be noted that the HFR can provide to the EXLO input of the WFR either the Ex+ or Ex- monopole electric antenna, and that the LMR+ and LMR- are the Ex+ and Ex- antenna elements used as a Langmuir Probe. The first channel of the WFR can select between EXLO and LMR+; the second can select between EZLO and LMR-; the third can select between BX and LMR; and the fourth and fifth are always connected to the BY and BZ, respectively. Signals from the five antennas are routed directly to a gain select stage which provides commandable gains of 0, 10, 20, or 30 dB for each receiver channel. The first two channels have independent gain settings, but the last three channels share the same gain control lines. The gain increments are provided by programmable gain amplifiers which are similar to those used for gain control in the WBR. During operations, the gain state for each receiver channel is selected by the HRP in response to appropriate spacecraft commands. The output of the programmable gain amplifiers goes to a 27 Hz lowpass filter and a 3 Hz to 2.5 kHz bandpass filter (a 3 Hz highpass filter and a 2.5 kHz lowpass filter). The desired frequency range sent to the A/D driver is selected by spacecraft command. The output from the A/D driver goes to the HRP. On the HRP, the signals are then sampled simultaneously by sample-and-hold circuits and routed to multiplexers to 12-bit analog to-digital converters. The WFR can also be commanded to measure one, two, three or four channels. These special modes allow greater resolution for special observations. The WFR provides the Low-Frequency Digital Receiver (LFDR) one or two channels of low frequency (1 to 27 Hz) data.

13.1.2 Frequency Response

The frequency response of the WFR is determined by the low frequency cutoff of the sensor's differential amplifiers (~1 Hz), and by the filters which follow the gain control stage of each of the five receiver channels. The 2.5 kHz lowpass filters are of the passive type, but the 27 Hz lowpass filters and the 3 Hz highpass fitters are active. The bandwidth of the WFR is selected by the HRP (WFRBND command) in response to the appropriate spacecraft command. Listed below are the filter commands:

Back End Filter	WFRBND	Sampling Rate
27 Hz LPF	1	10 ms
3 Hz - 2.5 kHz	0	140 μμs

13.1.3 Phase Response

Since the primary purpose of the WFR is to provide cross-correlations between the five measured wave components, each receiver channel must have a known phase response. To this purpose, it is specified that all five lowpass passive filters are matched in phase response, and are determined to be phase-stable within a 1% (~3°) margin within 1 Hz to 2.5 kHz.

13.1.4 Gain Select

The gain select stage of each channel of the WFR employs a variable gain amplifier which may be selected to provide gains of 0, 10, 20, and 30 dB. The first two channels have independent gain settings, but the last three channels share the same gain control lines. The gain is selected by the HPR (WFG command) in response to the appropriate spacecraft command.

13.1.5 Receiver Inputs

The selection of the sensor signal inputs for the first three channels of the WFR is determined by the HRP (WFRSEN command) in response to the appropriate spacecraft command. The WFR will have the capability of processing signals from the following sensors:

Command	Setting	Sensor	Channel
WFRSEN0	0	LMR+	0
WFRSEN0	1	EXLO	0
WFRSEN1	0	LMR-	1
WFRSEN1	1	EZLO	1
WFRSEN2	0	BX	2
WFRSEN2	1	LMR	2
		BY	3
		BZ	4

13.1.6 Power

The WFR is provided with four power supply lines. The regulated supply voltages and expected average current loads are as followed:

+12 V	3.6 mA
−12 V	3.8 mA
+ 6 V	28 mA
− 6 V	34 mA

The total power requirement for the WFR is expected to be 461 mW.

413.1.7 Receiver Output

The output signal from the WFR A/D drivers goes to the HRP to be processed before being transmitted to the ground. See the Data Processing Unit sections for a detailed discussion of this processing.

13.2.1 Conversion of Data Numbers to Science Units

This section describes the procedure for obtaining a calibrated data value from a WFR raw measurement.

1. First a snapshot consisting of 2^N raw WFR data samples is obtained. These data samples are 12-bit unsigned values (0-4095).

2. The DC component is obtained by averaging the 2^N samples. The DC component is subtracted from the 2^N samples, because the receiver is an AC coupled system and the DC component is not related to any sensor measurement. Furthermore, removal of the DC offset is needed for the next step.

3. The proper counts-to-volts rms factor is now applied to the data. This is the amplitude in counts of a sine wave in the middle of the pass-band which would be measured by the WFR if a 1 volt rms signal were injected into the Ex antenna inputs and the WFR had no gain amplifiers turned on. The 2^N samples are all divided by this factor. Throughtout the calibrations, another way this is expressed is the decibels below a maximum sine wave; for 12 bit data, which can range from 0 to 4095, this is dB below a sine wave amplitude of 2047.5 counts (or 4095 counts peak-to-peak) and it is referred to as dB max. This factor depends upon the filter mode and gain. The conversion factors are given in section 13.3.2 in tables 13.3.2.1 and 13.3.2.2.

4. Next the WFR gain amplifier value must be divided out. The gain can vary from 0 dB through 30 dB in steps of 10 dB. If the gain is G, then the 2^N samples should all be divided by $10^{G/20}$.

5. Next a Hanning window can be applied to the 2^N samples. For a Hanning window the coherent gain is 0.5 (see "Digital Filter Design Handbook" by Fred J. Taylor). Therefore the 2^N samples must then be multiplied by 2. The equation for a Hanning window is $H_i = 0.5*(1-\cos(2*\prod*i/(2^N -1)))$ for $i = 0, 2^N -1$.

6. A FFT should be performed on the 2^N samples. The FFT output must be normalized using whatever normalization factors are necessary to give the amplitude of a sine wave when real and imaginary parts are squared, summed and the square root is taken. The normalization factors may be different for different FFT implementations. The phase information for the FFT is not useful, so the magnitudes can now be calculated by squaring the real and imaginary parts, summing and then taking the square root. This yields volts rms in each FFT bin. This is the voltage difference Vdiff betweeen the Ex+ and Ex- antennas at the frequency corresponding to that FFT bin.

7. Once the voltage Vdiff is found, the sensor-dependent conversion factor must be used to adjust the voltage. The voltage difference between the Ex+ and Ex- antennas is given the symbol VDEx. Since the voltage difference Vdiff calculated in steps 1 through 6 is for the voltage difference between the Ex+ and Ex- antennas, no conversion is necessary for VDEx. VDEx is equal to Vdiff. The voltage between the Ez antenna and spacecraft ground is given the symbol VEz. The voltages at the outputs of the Bx, By and Bz magnetic preamps are given the

symbols VBxpa, VBypa and VBzpa respectively. Figure 13.2.1 shows the location of each of these voltages.

The conversion factors and their symbols are listed below. The conversion factors convert the Vdiff values to the voltage at the various sensors.

Symbol	Factor	
CFez	1.0	Conversion factor for the Ez antenna
CFbx	24.0	Conversion factor for the Bx Search Coil
CFby	24.0	Conversion factor for the By Search Coil
CFbz	24.0	Conversion factor for the Bz Search Coil

The formulas for converting the Vdiff value to the sensor input voltage are shown below.

VDEx	=	Vdiff	(units are volts rms.)
VEz	=	(CFez)*(Vdiff)	
VBxpa	=	(CFbx)*(Vdiff)	
VBypa	=	(CFby)*(Vidff)	
VBzpa	=	(CFbz)*(Vdiff)	

For the electric sensors there may be frequency dependent adjustments necessary because of the interaction of the antenna with the plasma, but these are dependent upon the plasma impedance. If the user wishes to adjust for these effects, see Section 6.0.

8. Now the sensor-dependent calibrations must be applied. For the Bx, By and Bz Search Coils, the voltage at the output of the Search Coil preamplifiers must be converted to nanotesla. See tables 7.1.1 through 7.1.3 in the section about the Magnetic Search Coils for the frequency-dependent conversion factors. For a particular frequency let this conversion factor be given the symbol CBxnt; for example, Table 13.2.1.8.2 shows that at 1000 Hz the Bx Search Coil's response is 147.8 mV/nT, so CBxnt is 0.1478. To convert from voltage at the output of the Bx, By and Bz Search Coil preamplifiers, VBxpa, VBypa and VBzpa must be divided by CBxnt, CBynt or CBznt respectively. This is shown in the following equations:

NTBx	=	VBxpa/CBxnt	(units are nT rms)
NTBy	=	VBypa/CBynt	
NTBz	=	VBzpa/CBynt	

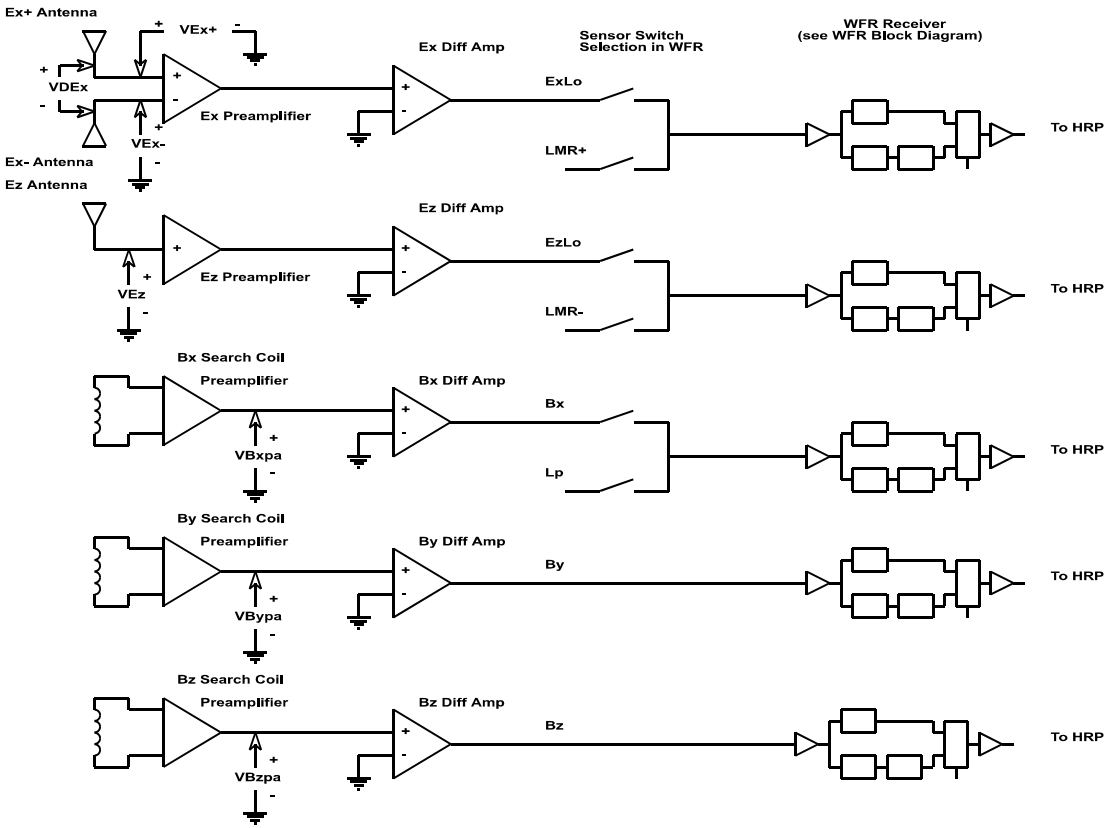

Figure 13.2.1
Sensor to WFR Signal Diagram

wfr_sig.blk

NTBx, NTBy and NTBz are the fields detected by the Bx, By and Bz Search Coils. At this point we have meaningful physical units. For the electric antennas we have voltage measured at the antenna elements. For the magnetic senors we have the magnetic field in nanotesla at the sensors. Next the magnitude of the electric field for the electric antennas can be obtained. The voltages at the antennas are divided by the effective antenna length, producing units of volts per meter. Here the effective antenna lengths are defined as the physical distances between the geometric centers of the antennas for the Ex dipole and the geometric center for the Ez antenna. The effective length of the Ex+ to Ex- dipole antenna configuration is given the symbol LExdelta. The Ez monopole effective length is given the symbol LEz. For a more detailed discussion of the effective lengths of the electric antennas, see Section 5.

Effective Antenna Lengths in Meters for various mode configurations

Antenna	Effective Length (meters)	Configuration
LExdelta	9.26	dipole
LEz	5.00	monopole

The electric field on the Ex dipole is represented by VMExdelta, and the electric field on the Ez monopole by VMEz. The following equations show the method for calculating the electric field on the antenna in volts per meter. These equations show the method for calculating the electric field on the antenna in volts per meter. These equations do not include effects due to stray capacitive divider effects between the antennas and the spacecraft.

VMExdelta = (VDEx)/(LExdetlta)
VMEz = (VEz)/(LEz)

9. Finally, to obtain the power spectral density, one must square the value and divide by the bandwidth, which depends upon the type of window function used before performing the FFT. If no window function is used, then the equivalent noise bandwidth is the FFT bin width, which is the sample frequency divided by the number of samples ($fs/2^N$). If the Hanning window suggested above is used, then the equivalent noise bandwidth is 1.5 times the FFT bin width (again see "Digital Filter Handbook" by Fred Taylor).

13.2.2 Examples of Conversions from Data Numbers to Science Units

As an illustration of how to obtain calibrated values from WFR telemetry, let us look at some real data:

Example 1:	CDS Time	1997-298 T05:17:28.000	(SCLK 4AE3DF87 FC30)
	SCET	1997-298 T05:17:27.000	(SCLK 4AE3DF86 FC30)

After the electric antenna deployment, a broad band emission is examined. The WFR mode was cycling between the 40 Hz band and the 2.5 kHz band with 30 dB gain. Lets look at the 2.5kHz Ex dipole data for this example. A waveform of length 512 samples was captured. Following the recipe for obtaining calibrated values, the DC component is computed and subtracted form all the 512 samples. Since the filter mode is 2.5kHz, all 512 samples are then divided by 6136 which has units of counts per volts rms. Then the samples are multiplied by the gain factor, $10^{60/20}$ (or 1000). A Hanning window is applied to the data and then all windowed values are multiplied by 2 to offset the Hanning window's coherent gain. A FFT is performed on the data, and after normalizing, the parts of the complex outputs, summing them, and taking the square root. The broad-band emission under examination extends from about 600 Hz to 1700Hz. The peak amplitude occurs at frequency 1060.27 Hz. This peak amplitude is Vdiff at 1060.27Hz.

$$\text{Vdiff} = 6.58\text{x}10^{-5}\ \text{Vrms}$$

Since the sensor is the Ex dipole, we know that the voltage VDEx is the same as Vdiff. So the electric field strength can be calculated directly:

$$\begin{aligned} \text{VMExdelta} &= (\text{VDEx})/(\text{LExdelta}) \\ &= 6.58\text{x}10^{-5}\ /9.26 \\ &= 7.11\text{x}10^{-6}\ \text{Vrms/meter} \end{aligned}$$

Finally, to determine the electric field power spectral density, we must square this value and divide by the equivalent noise bandwidth. Since we have the 2.5 kHz mode, the sample frequecny is given by:

$$\begin{aligned} \text{Fs} &= 1.0/1.4\text{x}10^{-4} \\ &= 7142.9\ \text{Hz} \end{aligned}$$

and since the sample set size is 512, the FFT bin size is given by

$$\begin{aligned} \Delta\text{f} &= F_s / 512 \\ &= 7142.9 / 512 \\ &= 13.95\ \text{Hz} \end{aligned}$$

But since a Hanning window was applied to the data, the equivalent noise bandwidth is given by:

ENBW	=	1.5 * Δf	
	=	20.93	Hz

So the power spectral density at 1590.4 Hz is given by

PSD	=	$(\text{VMExdelta})^2$ /ENBW	
	=	$(7.11 \times 10^{-6})^2$ / 20.93	
	=	2.42×10^{-12}	Vrms^2 / meter^2 Hz

Example 2.	Unix Time	1996-214 T01:07:34	(SCLK 32000356 1AB0)
	SCET	1996-214 T01:07:24.250 Epoch 0	(SCLK 3200034C 1A60)

During unit level testing the Bx Search Coil was stimulated with a 1 kHz tone at 0.5 Vrms. This should have produced a magnetic field of 0.5nT(rms). The WFR was in the 2.5 kHz mode with 30 dB of gain. A waveform of length 512 was captured. The raw data shows a sine wave with a maximum value of 2555 and a minimum value of 1538, giving an initial estimate of 1017 counts peak-to-peak for the sine wave. Following the recipe for obtaining calibrated values, the DC component is computed and found to be 2051.01 counts. This value is subtracted form all 512 samples. A Hanning window is applied to the data and then all windowed values are multiplied by 2 to offset the Hanning window's coherent gain. A FFT is performed on the data, and after normalizing, the magnitudes of the resulting 256 components are computed by squaring the real and imaginary parts of the complex outputs, summing them, and taking the square root. The peak amplitude occurs at the frequency of 1004.46 Hz, and this peak amplitude is 496.1 counts. (note that this is close to our initial estimate of 508.5 counts peak for the amplitude). Dividing this by the calibration factor of 6136 counts peak / Vrms and also by the gain factor of $10^{G/20}$, we obtain Vdiff at 1 kHz:

Vdiff	=	$496.83 / (6136 * 10^{30/20})$
	=	351.31 / (6136* 31.62)
	=	2.56×10^{-3} Vrms

Since the sensor is the Bx Search Coil, we now want to know what the voltage VBxpa from the Search Coil preamplifier is:

VBxpa	=	(CFbx) *(Vdiff)
	=	$24 * 2.56 \times 10^{-3}$ Vrms
	=	61.44 mVrms

Now referring to the Search Coil calibration in Table 7.1.1, we find that at 1000 Hz the Bx Search Coil's response CBxnt is 147.8 mV / nT. So we find that the magetic field strength NTBx is:

NTBx	=	VBxpa / CBxnt	(units are nT rms)
	=	61.44 / 147.8	nT rms
	=	0.416	nT rms

This value agrees well with the WBR example 2 in section 12.2. As in section 12.2 it makes little sense to calculate the spectral density since the signal is a tone.

13.3.1 WFR Frequency Response

In this section the frequency response calibration data for the waveform receiver are presented. Transfer functions for each of filters is shown. Figure 13.3.1.1 illustrates the stimulus configuration used for the WFR frequency responses. The oscillator output is attenuated by a fixed amount and a balancing transformer is used to drive the Ex+ and Ex- inputs differentially.

During the calibrations, the HP workstation commands the oscillator to step in frequency. For each frequency step, a waveform is captured and telemetered to the spacecraft simulator. A FFT is performed on the data after removing the DC component. The peak amplitude is chosen from the frequency domain result, and the peak frequency (which should be very close to the stimulus frequency) is chosen. The amplitude is calculated by simple time domain rms average and then is adjusted by square root of two divided by two to give the amplitude of the sine wave in WFR counts. This rms calculation yields a value very close to the FFT result at the peak frequency, but does not suffer from the "scallop loss" effect of the FFT results, which are sensitive to the proximity of the frequency to the center of a FFT bin. For further discussion on this effect, see Section 12.3.2, where the FFT amplitudes of the peak frequencies are presented for the WBR gain calibrations. Finally, the amplitude is expressed in counts peak out per volts rms input.

Although the frequency response could be used to adjust the calibrations of the WFR data, it is recommended that this not be done, since the noise floor becomes accentuated outside the pass-band. Only frequencies inside the pass-band should be adjusted. And data should be ignored if it is outside the 3-dB points. From the frequency response curves, those 3-dB points are approximately:

Filter	Gain	3-dB points
40 Hz	0 dB	2.2 Hz - 26.8 Hz
40 Hz	10 dB	2.5 Hz - 26.8 Hz
40Hz	20 dB	4.5 Hz - 26.8 Hz
40 Hz	30 dB	9.3 Hz - 26.8 Hz
2.5 kHz	0 dB	3 Hz* - 2.56 kHz
2.5 kHz	10 dB	3 Hz* - 2.56 kHz
2.5 kHz	20 dB	5 Hz - 2.56 kHz
2.5 kHz	30 dB	9 Hz - 2.56 kHz

The two 3-dB points in the table above marked with * are extrapolated values calculated from board level test data which show 3-dB break points of 3 Hz for the high pass filter in the 2.5 kHz filter band.

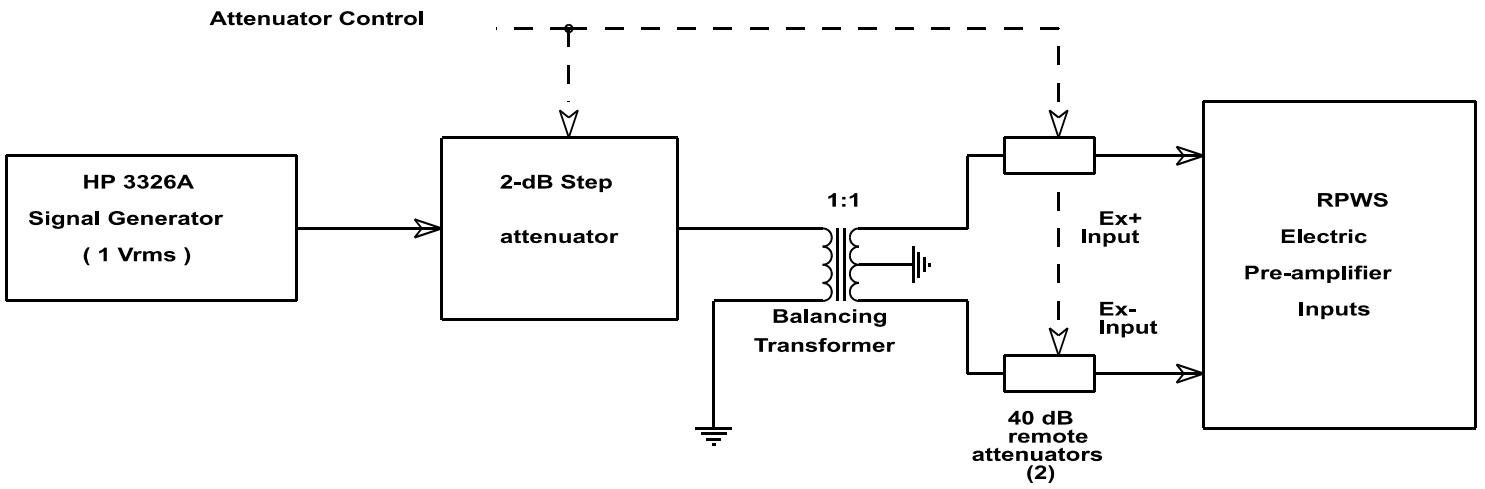

Figure 13.3.1.1

WFR Frequency Response Calibration Stimulus Configuration

wfr_frq.blk

Figure 13.3.1.2 WFR Frequency Response

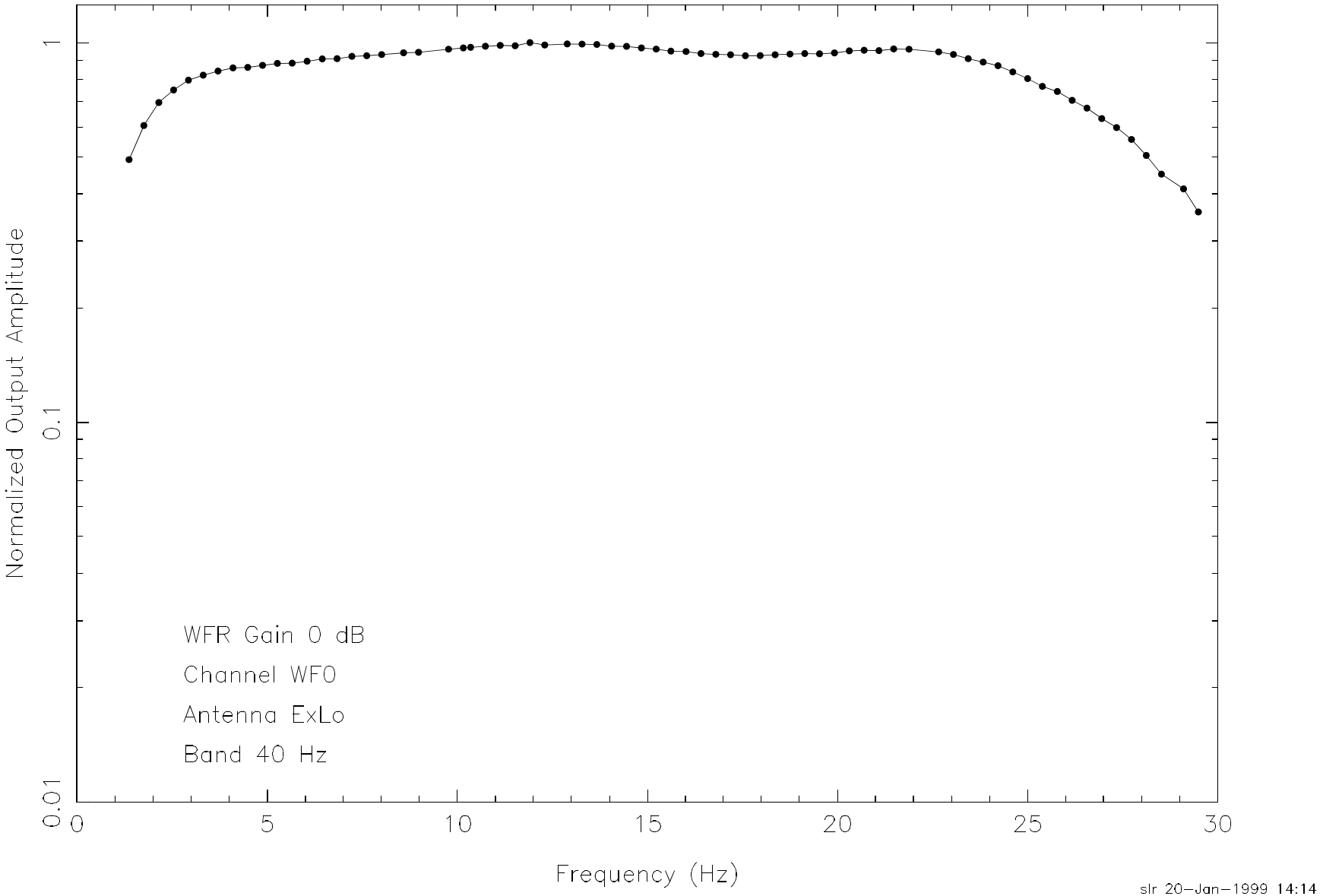

Figure 13.3.1.3 WFR Frequency Response

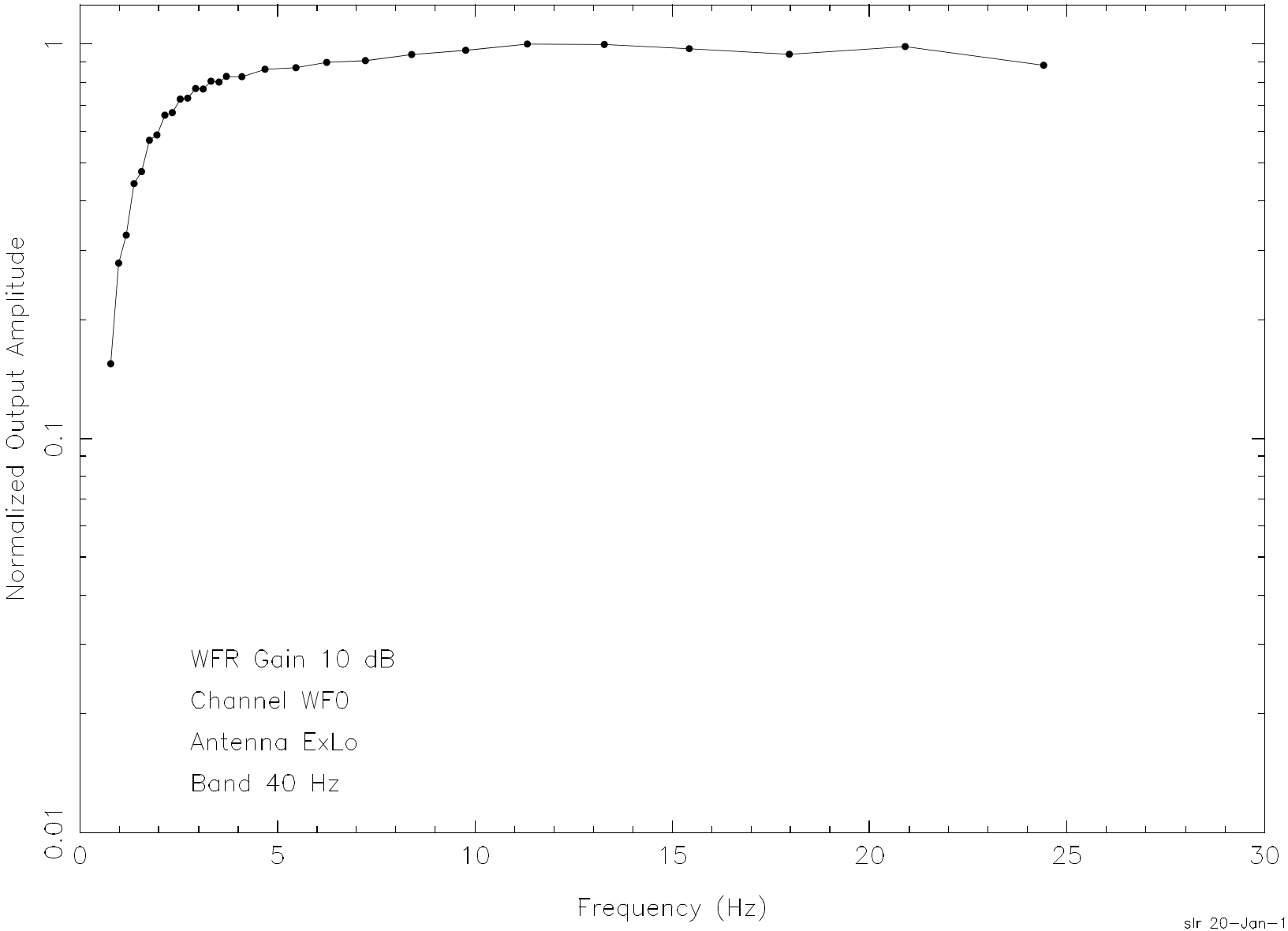

Figure 13.3.1.4 WFR Frequency Response

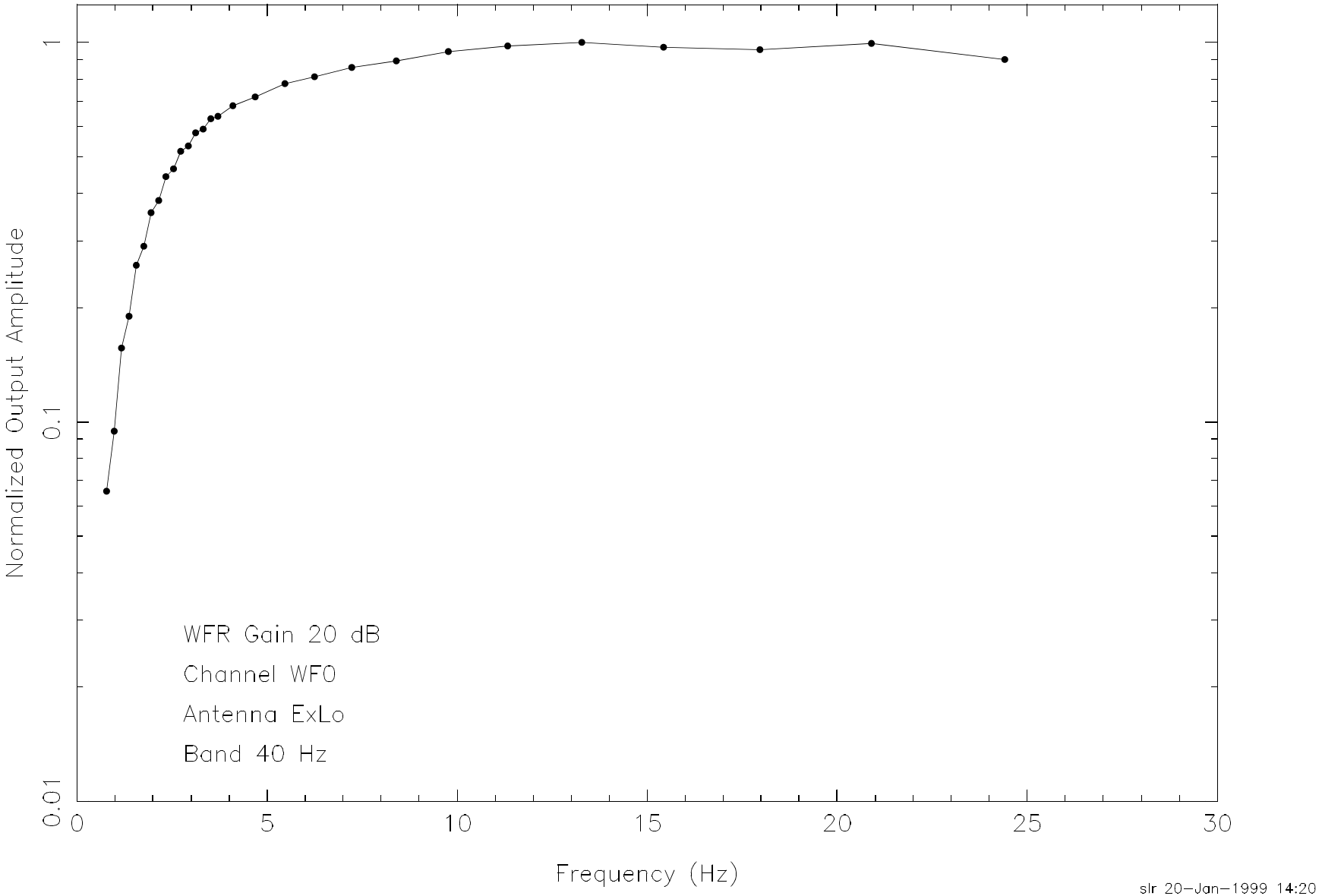

WFR Low Band Frequency Response

Room Temperature
File T960729.U06
Band 40 Hz
Antenna ExLo
WFR Gain 30 dB

Frequency	Normalized Output
0.9800000	0.0294155
1.3700000	0.0640782
1.7600000	0.1047824
2.1500001	0.1459476
2.5400000	0.1898210
2.9300001	0.2300148
3.3199999	0.2672539
3.7100000	0.3044979
4.0999999	0.3394885
4.4899998	0.3729623
4.8800001	0.4052884
5.2700000	0.4372225
5.6599998	0.4682141
6.0500002	0.4966799
6.4499998	0.5227515
6.8400002	0.5518564
7.2300000	0.5781877
7.6199999	0.6031932
8.0100002	0.6282924
8.3999996	0.6524822
8.7900000	0.6784075
9.1800003	0.7024354
9.5699997	0.7261289
9.9600000	0.7504578
10.3500004	0.7714002
10.7399998	0.7934631
11.1300001	0.8117408
11.5200005	0.8298280
11.9099998	0.8457571
12.3000002	0.8591852
12.8900003	0.8711307
13.2799997	0.8812733
13.6700001	0.8883258
14.2600002	0.8979663
14.6499996	0.8998978
15.0400000	0.9029118
16.2099991	0.9079832

16.7999992	0.9101573
17.1900005	0.9135265
17.5799999	0.9177758
17.9699993	0.9229839
18.3600006	0.9283523
18.7500000	0.9369215
19.1399994	0.9445062
19.5300007	0.9558038
19.9200001	0.9645656
20.3099995	0.9751027
20.7000008	0.9835373
21.0900002	0.9917958
21.4799995	0.9973176
21.8799992	1.0000000
22.2700005	0.9981878
22.6599998	0.9952689
23.0499992	0.9849772
23.4400005	0.9690644
23.8299999	0.9503459
24.2199993	0.9266265
24.6100006	0.8988805
25.0000000	0.8697878
25.3899994	0.8384596
25.7800007	0.8056284
26.1700001	0.7724604
26.5599995	0.7349731
26.9500008	0.6967620
27.3400002	0.6542301
27.7299995	0.6101620
28.1200008	0.5622446
28.5200005	0.5118249
28.9099998	0.4599399
29.2999992	0.4087435
29.6900005	0.3594084
29.8799992	0.3353098

Figure 13.3.1.6 WFR Frequency Response

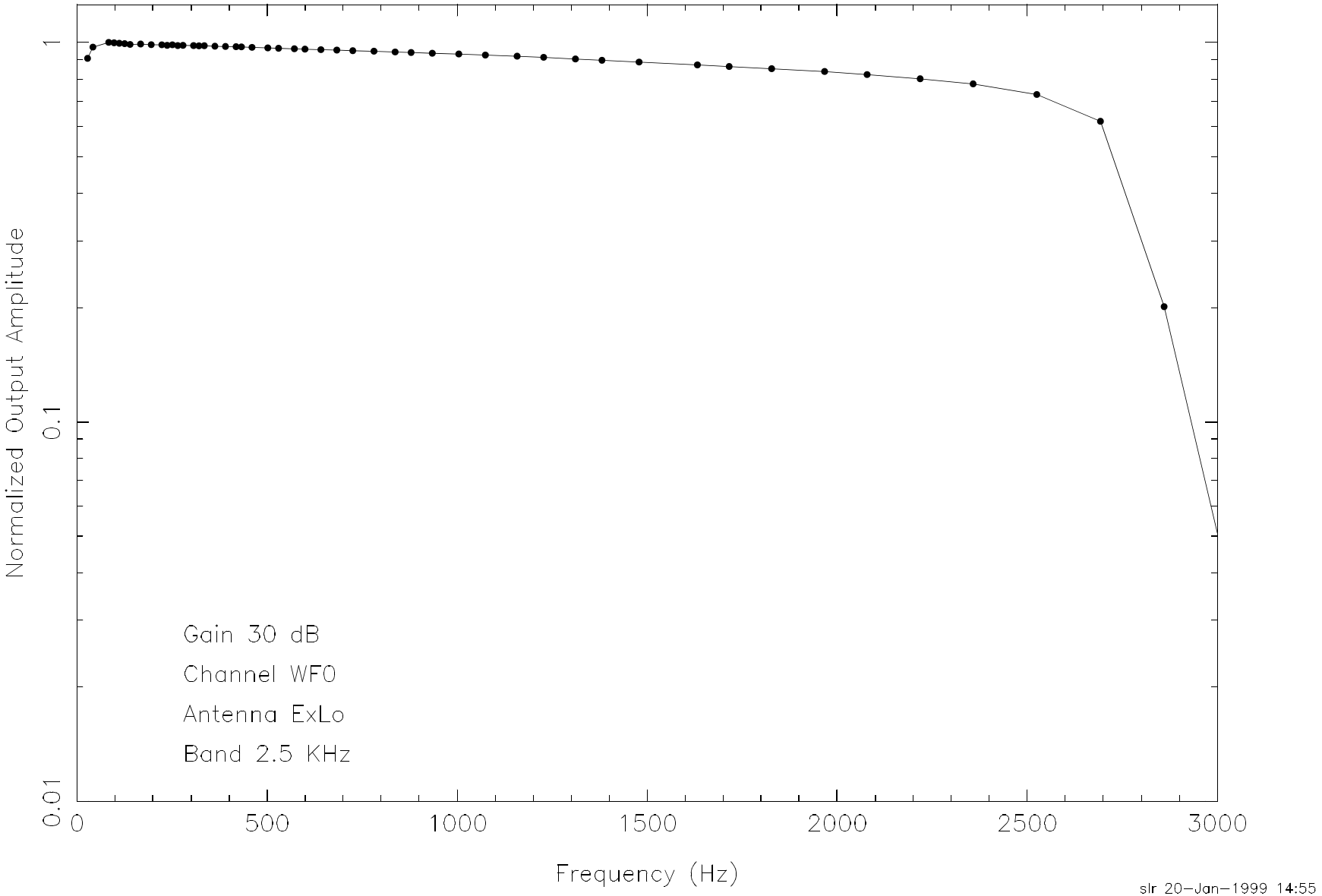

WFR High Band Frequency Response

Room Temperature
File T960705.U04
Band 2.5 KHz
Antenna ExLo
Gain 30 dB

Frequency	Normalized Output
27.900	0.9078102
41.850	0.9715824
83.710	1.0000000
97.660	0.9980220
111.610	0.9945238
125.560	0.9921464
139.510	0.9879963
167.410	0.9900233
195.310	0.9865163
223.210	0.9853725
237.170	0.9822952
251.120	0.9850758
265.070	0.9804959
279.020	0.9824361
306.920	0.9804398
320.870	0.9791099
334.820	0.9801606
362.720	0.9770414
390.620	0.9757941
418.530	0.9741844
432.480	0.9729114
460.380	0.9701056
502.230	0.9672104
530.130	0.9652461
571.990	0.9616783
599.890	0.9594510
641.740	0.9564958
683.590	0.9546308
725.450	0.9508037
781.250	0.9476834
837.050	0.9437379
878.910	0.9404175
934.710	0.9360785
1004.460	0.9317712
1074.220	0.9264954
1157.920	0.9194059
1227.680	0.9133144

1311.380	0.9042442
1381.140	0.8973154
1478.790	0.8873913
1632.250	0.8724679
1715.960	0.8639951
1827.570	0.8525341
1967.080	0.8378108
2078.680	0.8227733
2218.190	0.8015717
2357.700	0.7770430
2525.110	0.7287361
2692.520	0.6192870
2859.930	0.2011404
3055.250	0.0295593

13.3.2 WFR Gain Calibration

In this section, the amplitude calibrations for the waveform receiver are presented. The gain calibrations were done at a limited number of frequencies in the pass band of the filters in the receiver. One stimulus frequency in each of the two bands was chosen for this calibration. The stimulus configuration used for the WFR gain calibration is shown in Figure 13.3.2.1.

The procedure used for the performance of the calibrations is as follows. A command is sent to the oscillator and attenuator to set the desired setting. A waveform is captured by the WFR and telemetered to the spacecraft simulator. An FFT is performed on the WFR capture to determine the frequency. Also the waveform is analyzed in the time domain to determine the rms amplitude in counts rms.

The results are shown in Table 13.3.2.1 for the 40 Hz WFR mode and Table 13.3.2.2 for the 2.5 kHz WFR mode.

Table 13.3.2.1 WFR Low-Band 40 Hz Gain Calibration (@ 24.4 Hz)

WFR Gain Setting (dB)	Output Amplitude of Stimulus(dB)	Counts (rms) @ Stimulus amplitude & WFR Gain	Counts / Volt normalized to WFR gain = 0 dB	Counts peak output per Volt rms input normalized to WFR Gain = 0 dB
0	-60 dB	4.286	4286.77	6062.41
10	- 60 dB	14.012	4430.91	6266.26
20	-60 dB	43.972	4397.16	6218.52
30	-60 dB	128.926	4076.98	5765.72

Table 13.3.2.2 WFR High-Band 2.5 KHz Gain Calibration (@ 1.0 KHz)

WFR Gain Setting (dB)	Output Amplitude of Stimulus(dB)	Counts (rms) @ Stimulus amplitude & WFR Gain	Counts / Volt normalized to WFR gain = 0 dB	Counts peak output per Volt rms input normalized to WFR Gain = 0 dB
0	-20 dB	423.727	4237.27	5992.40
10	-40 dB	135.875	4296.74	6076.51
20	-40 dB	431.357	4313.57	6100.31
30	-30 dB	142.541	4507.53	6374.61

The amplitude calibrations show that the gain amplifiers have small variations in gain from the desired gain change for each filter band. At the frequency that the calibrations were performed, the variations in the gain are less than 1 dB. The gains were calculated by performing a time domain calculation of the amplitude rather than using the amplitude result from the FFT. This eliminates the “scallop loss” mentioned in section 12.3.2. Because of the small variations due to gain settings a single conversion factor can be used for each filter band. These average gain

conversion factors are shown in Table 13.3.2.3.

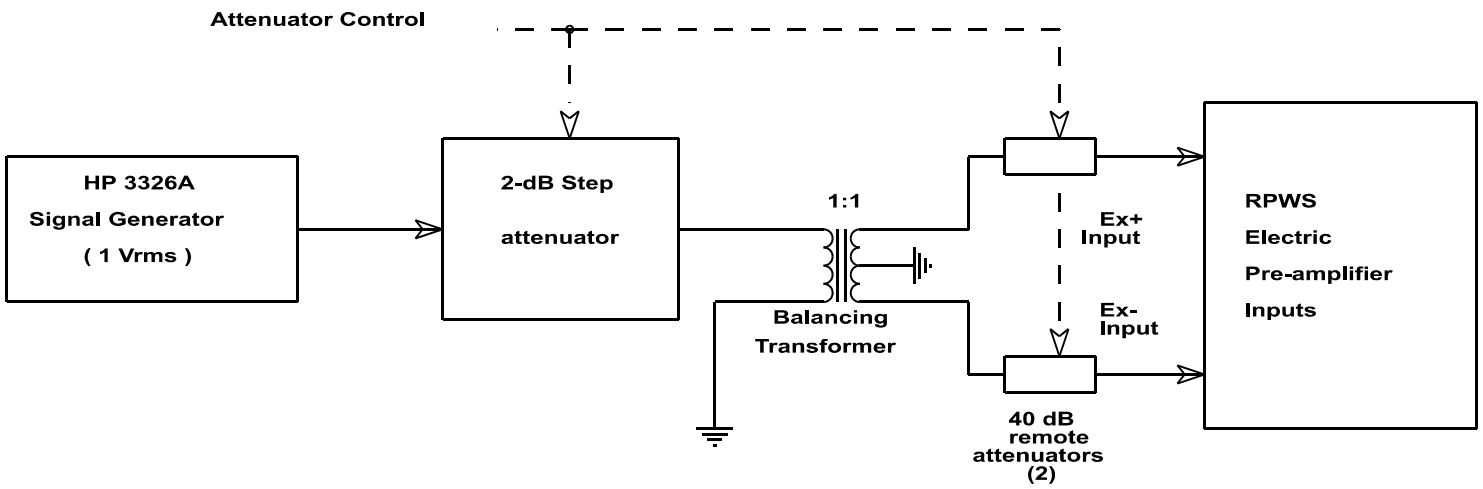

Figure 13.3.2.1

WFR Gain Calibration Stimulus Configuration

wfr_gain.blk

Table 13.3.2.3 WFR Average Gain Conversion Factors

WFR Filter	Counts / Volt normalized to WFR gain = 0 dB	Counts peak output per Volt rms input normalized to WFR Gain = 0 dB
40 Hz	4298	6078
2.5 kHz	4339	6136

13.3.3 WFR Random Noise Response

Tests were conducted to characterize the response of the Waveform Receiver to random noise. These bench tests were performed on July 28-29, 1996. The 40 Hz band response was performed at +28 degrees C and the 2.5 kHz band response was performed at +40 degrees C. Two test configurations were used. These test configurations are shown in Figures 13.3.3.1 and 13.3.3.2. The stimulus was connected to the instrument Ex+ and Ex- inputs. The noise spectral density was measured using the HP3585A Spectrum Analyzer, and the graphs showing the frequency spectrum for the two stimulus configurations are shown in Figure 13.3.3.3 and 13.3.3.4. Also a measure of the total power was made using a true RMS meter, and an estimate of the noise spectral density was obtained by using that and the signal bandwidth. For each of the WFR modes approximately spectra were averaged. The average spectra for the 40 Hz band are shown in Figures 13.3.3.5 through 13.3.3.8. The average spectra for the 2.5 kHz band are shown in Figures 13.3.3.9 through 13.3.3.12. Using an estimate of the average level for each plot, an estimate of the noise spectral density was done using the calibration procedure described in Section 13.2. Note that the FFT size for all of these tests is 512 samples, and a Hanning window was applied to the data. The results are summarized for the 40 Hz mode in Table 13.3.3.1.

Table 13.3.3.1 WFR 40 Hz Mode: White Noise Response (WFR Gain = 0 dB)

RMS voltage (V_{rms})	1.00	1.00	1.00	1.00
Bandwidth (Hz)	200	200	200	200
Attenuation(dB)	30	20	10	0
Est. PSD ($dBV/Hz^{1/2}$)	-53	-43	-33	-23
HP3585 SD ($dBV/Hz^{1/2}$)	-54	-44	-34	-24
Avg. WFR PSD ($dBV/Hz^{1/2}$)	-53	-43	-35	-33

Notice the large discrepancy for the test at 0 dB attenuation. The HP3585 spectrum analyzer measured -24 $dBV/Hz^{1/2}$, while the WFR measured -33 $dBV/Hz^{1/2}$. The reason for this discrepancy is that the data was clipped , so a low estimate of the power results. This overloading is apparently just starting to occur at the 10dB attenuation setting, where the WFR estimate is 1 dB lower relative to the tests at the higher attenuations. Those tests at 20 and 30 dB attenuation are both within 1 dB of the HP3585 estimate. The scatter in the data seems to indicate that these are reasonable answers.

Notice that for the 40 Hz test, there was an interference tone present. This 180 Hz tone is a harmonic of the 60 Hz power line and is being input through the stimulus. Nevertheless, it does not interfere with the test. The HP3585 measured the spectral density at 90 Hz, avoiding the noise line, and the WFR PSD estimate is within one dB of that.

The results for the 2.5 kHz filter mode are summarized in Table 13.3.3.2.

Table 13.3.3.2 WFR 2.5 kHz Mode: White Noise Response (WFR Gain - 0 dB)

RMS voltage (V_{rms})	1.00	1.00	1.00	1.00
Bandwidth (kHz)	20	20	20	20
Attenuation(dB)	30	20	10	0
Est. PSD (dBV/$Hz^{1/2}$)	-73	-63	-53	-43
HP3585 SD (dBV/$Hz^{1/2}$)	-74	-64	-54	-44
Avg. WFR PSD (dBV/$Hz^{1/2}$)	-74	-64	-55	-51

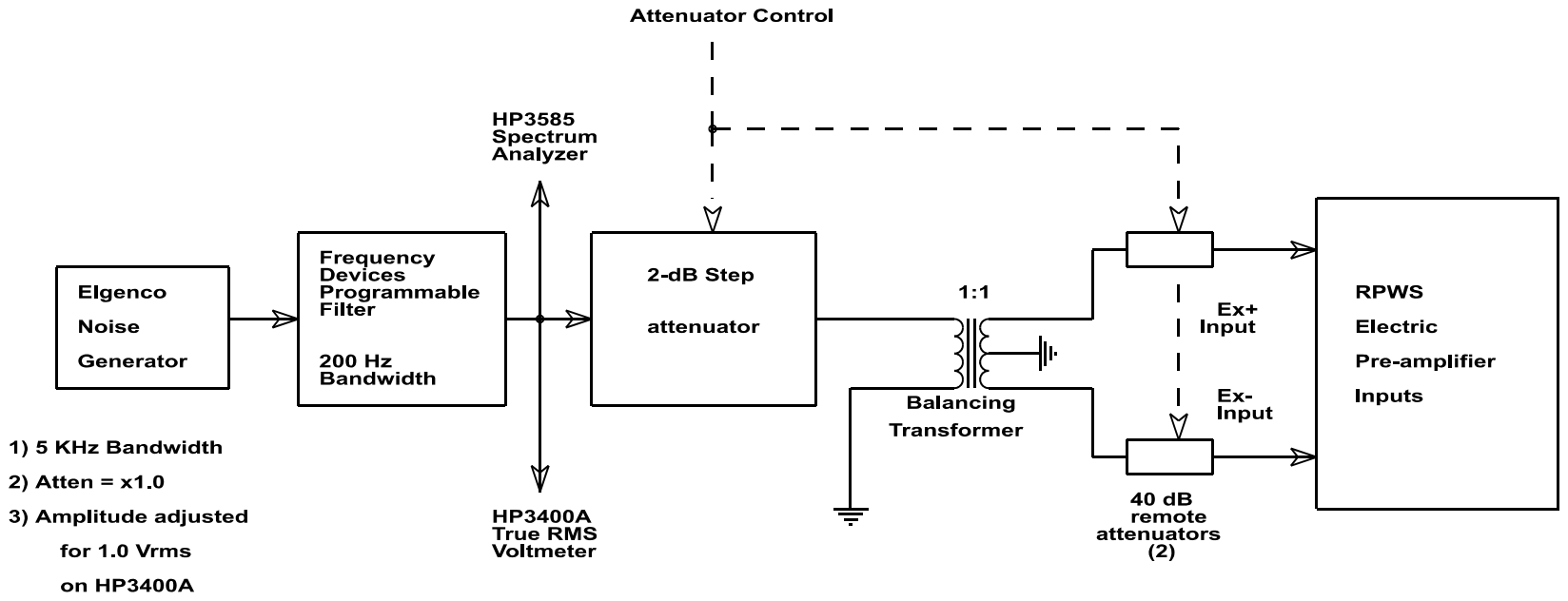

Figure 13.3.3.1

WFR Response to Random Noise
Stimulus Configuration for 40 Hz Mode

wfrlnois.blk

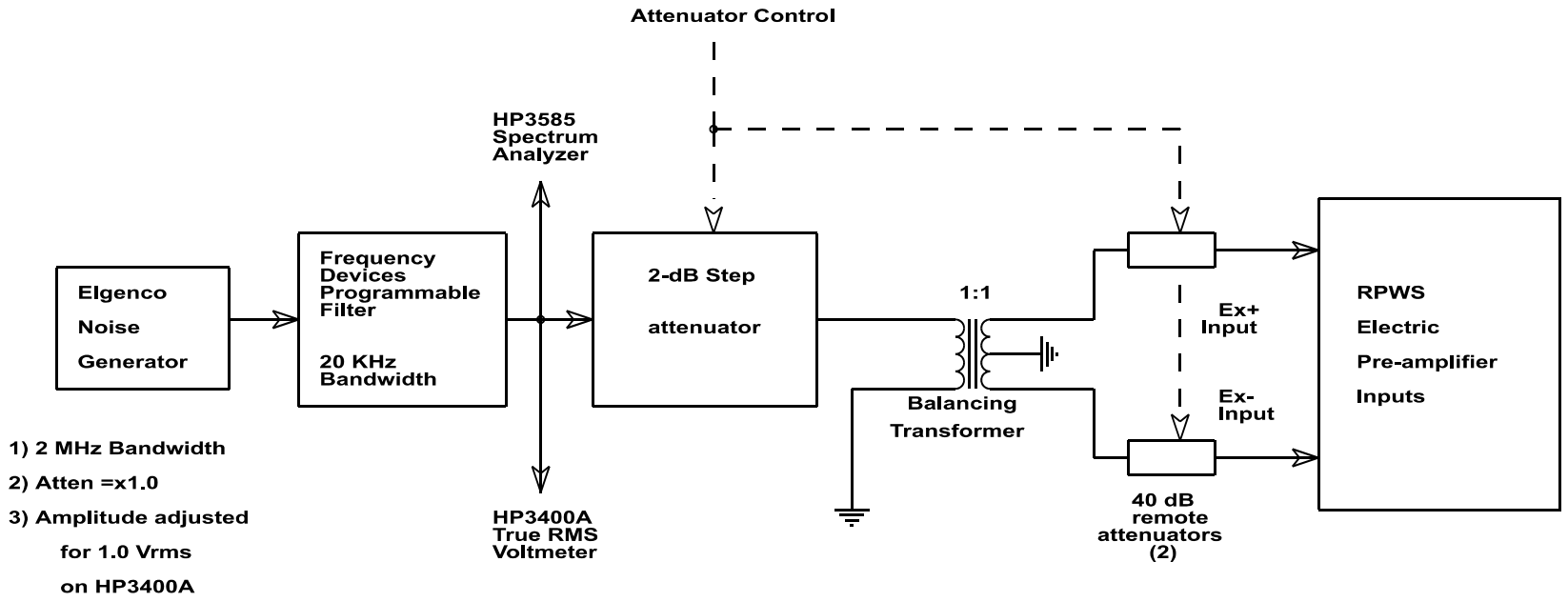

Figure 13.3.3.2

WFR Response to Random Noise
Stimulus Configuration for 2.5 KHz Mode

wfrhnois.blk

Figure 13.3.3.3: HP3585 Spectrum Analyzer Display
WFR 40 Hz Mode White Noise Test

REF 12.0 dBv MARKER 90.0 Hz
5 dBv/DIV RANGE 12.0 dBv -24.5 dBv (1 Hz)

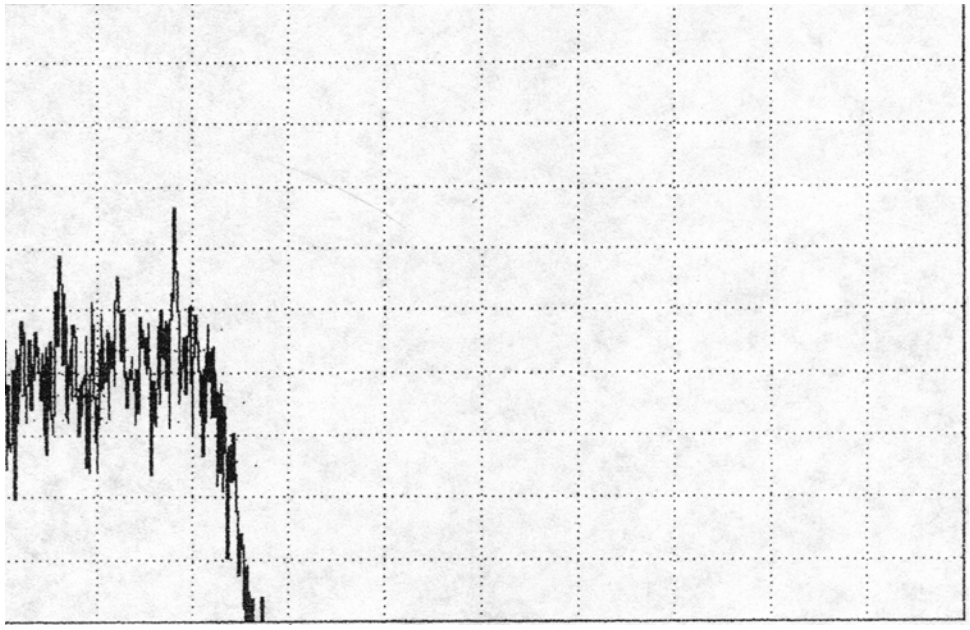

START .0 Hz STOP 1 000 Hz
RBW 3 Hz VBW 10 Hz ST 222 SEC

Figure 13.3.3.4: HP3585 Spectrum Analyzer Display
WFR 2.5 kHz Mode White Noise Test

REF -18.0 dBv MARKER 5 000.0 Hz
1 dB/DIV RANGE 12.0 dBv -44.2 dBv (1 Hz)

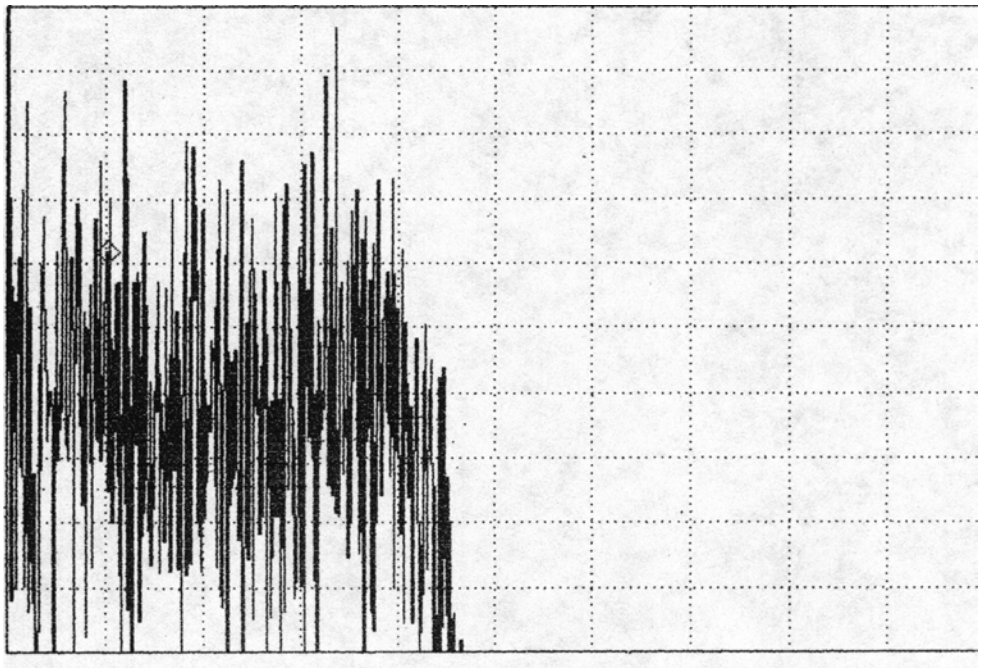

START .0 Hz STOP 50 000.0 Hz
RBW 30 Hz VBW 100 Hz ST 111 SEC

Figure 13.3.3.5 WFR Random Noise Response

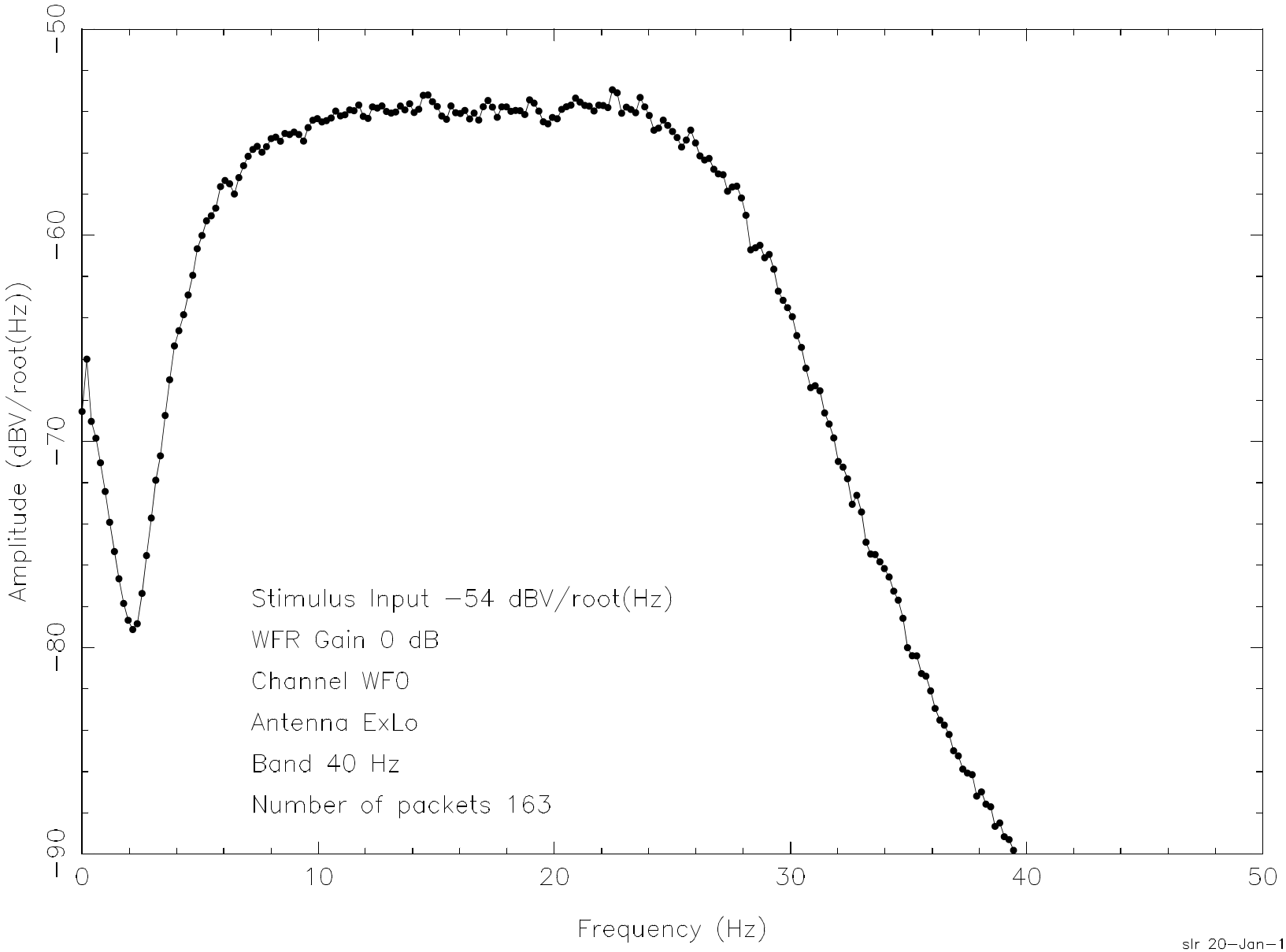

Figure 13.3.3.6 WFR Random Noise Response

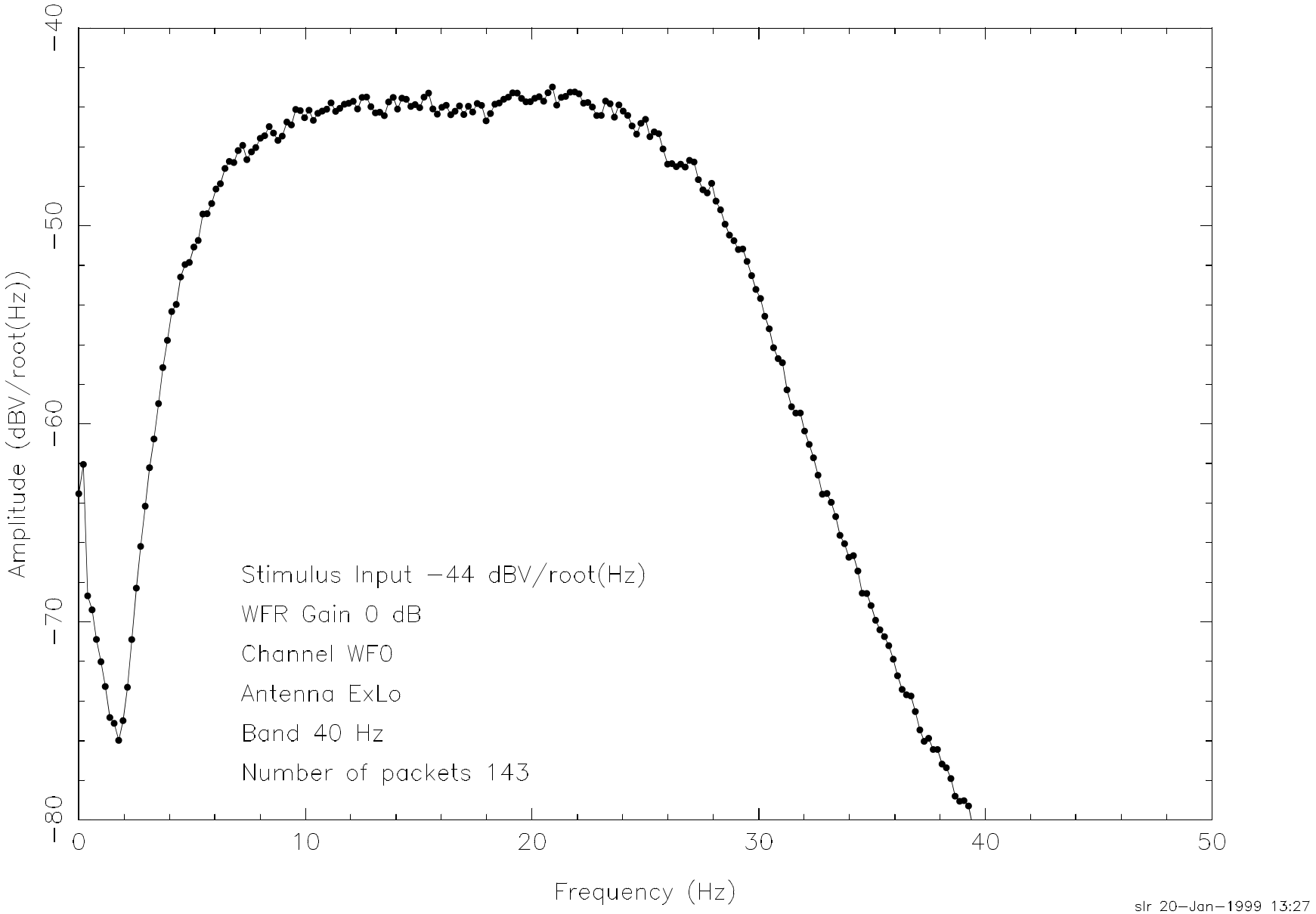

Figure 13.3.3.7 WFR Random Noise Response

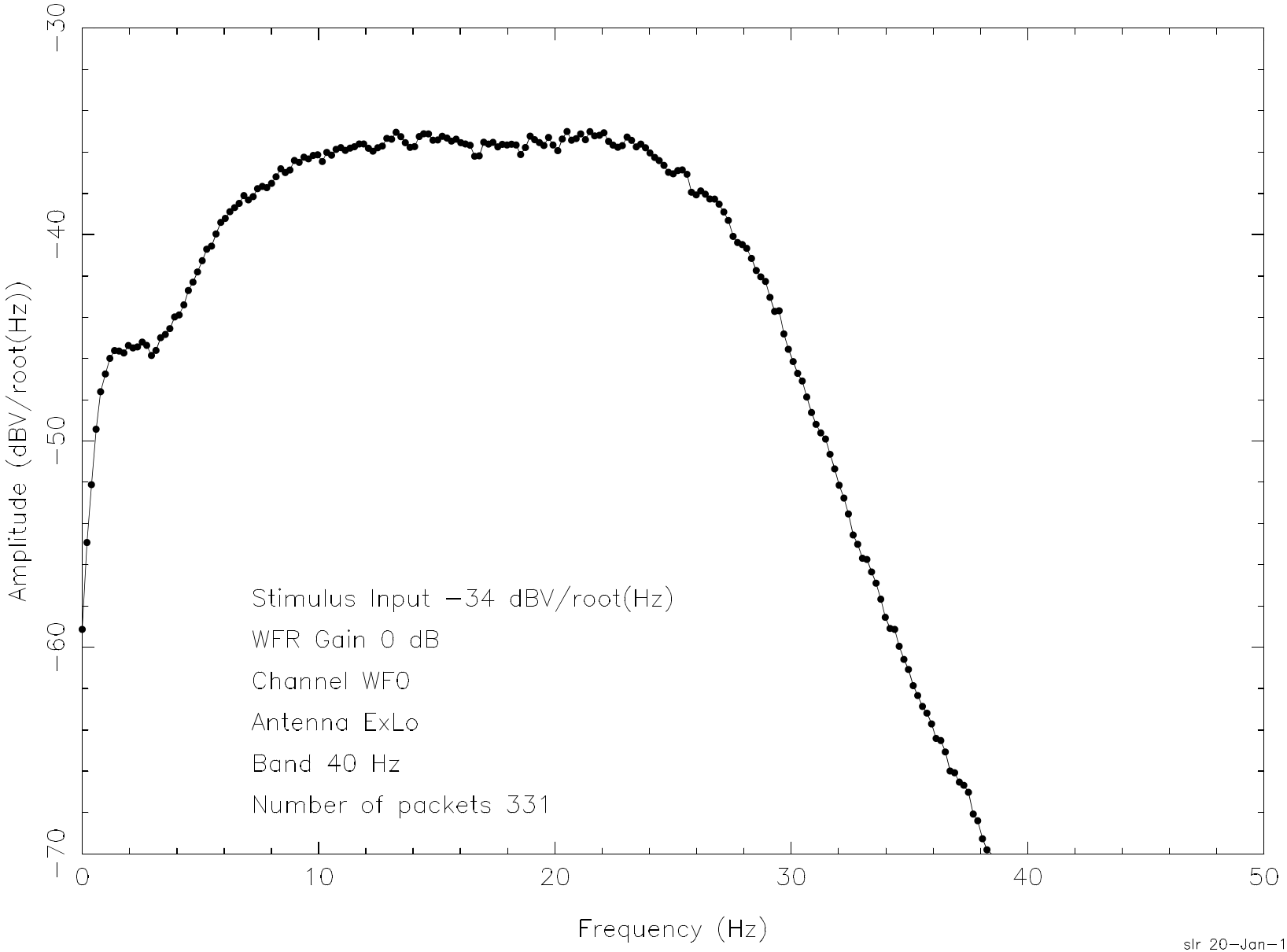

Figure 13.3.3.8 WFR Random Noise Response

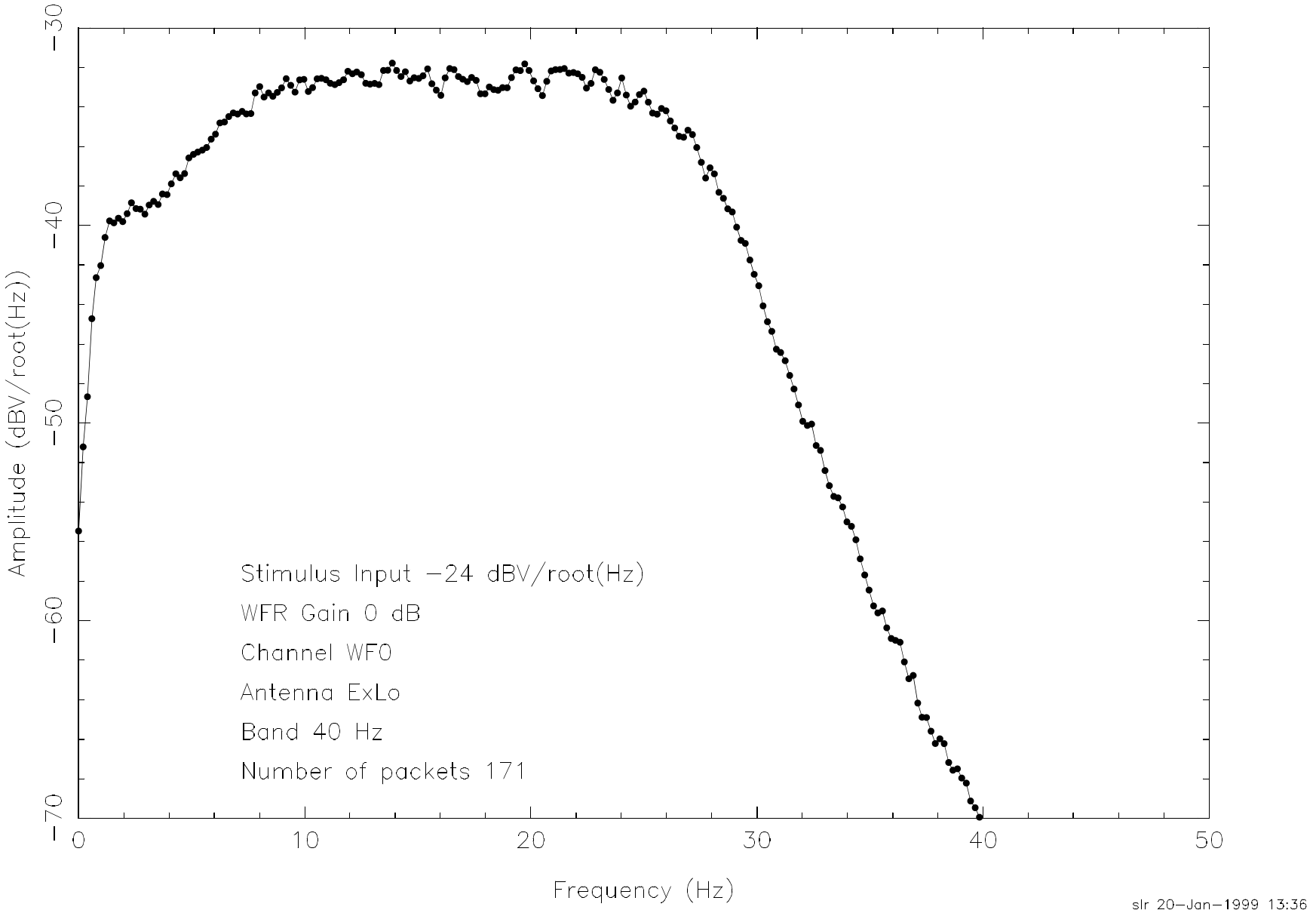

Figure 13.3.3.9 WFR Random Noise Response

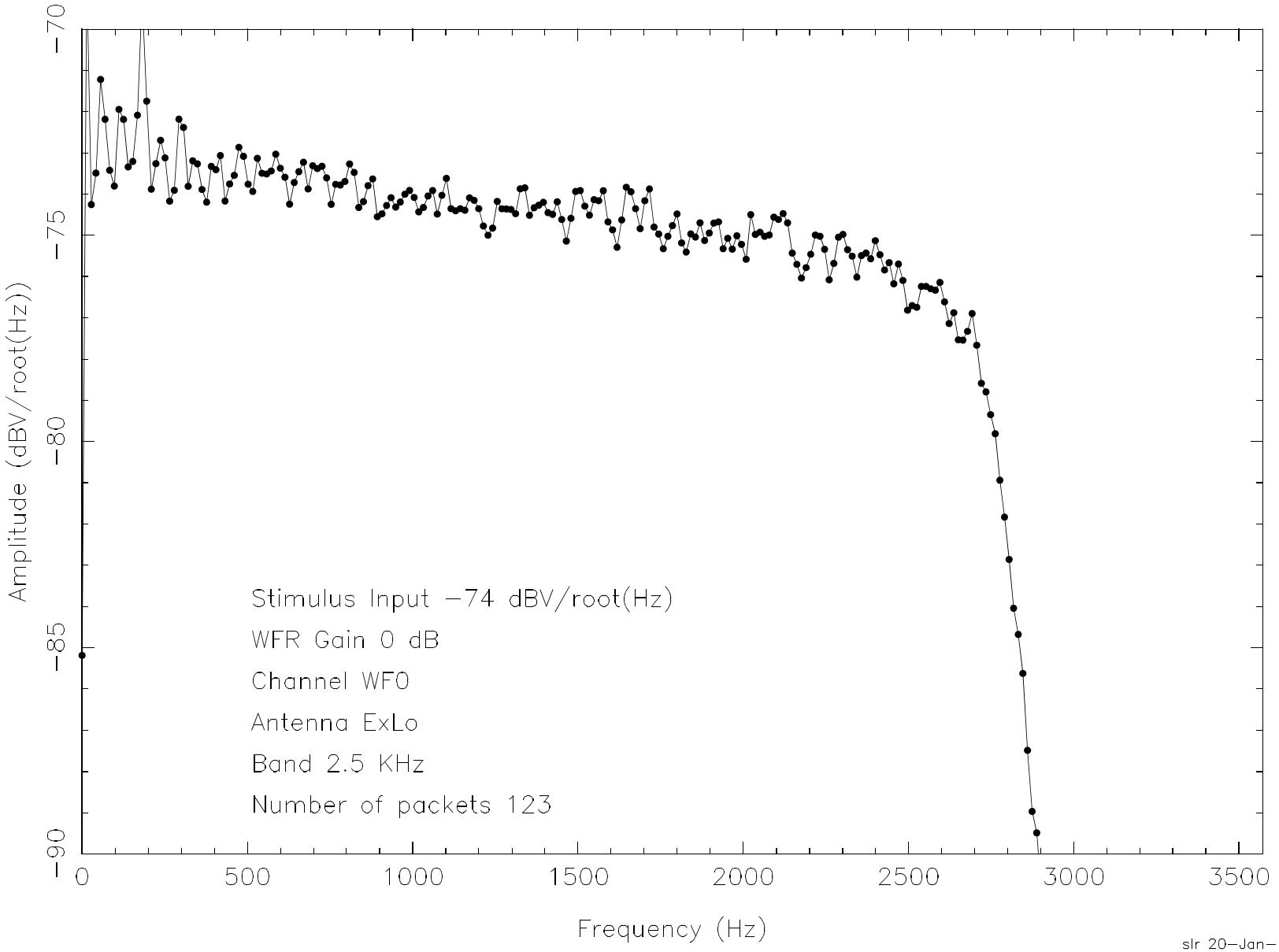

Figure 13.3.3.10 WFR Random Noise Response

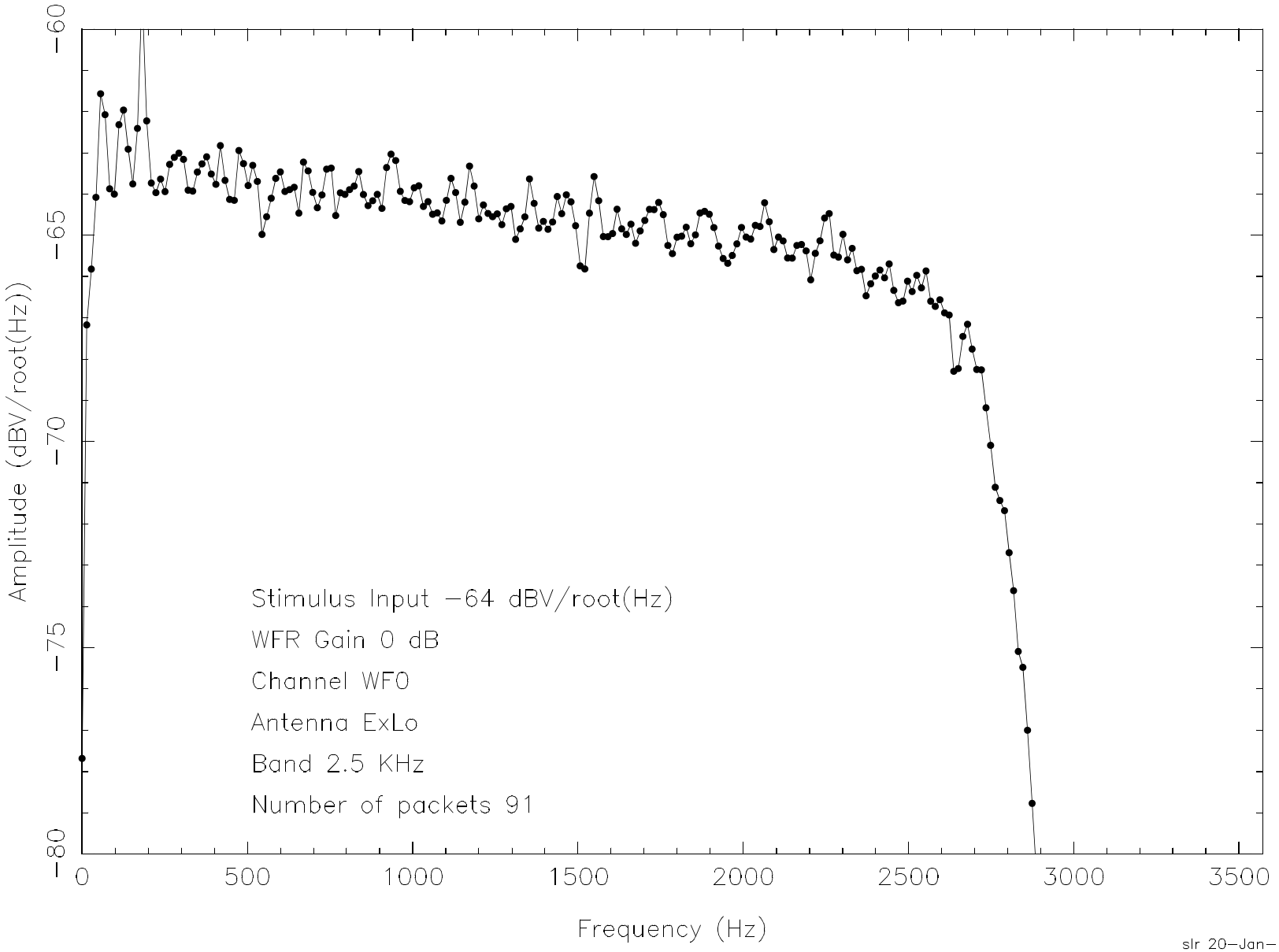

Figure 13.3.3.11 WFR Random Noise Response

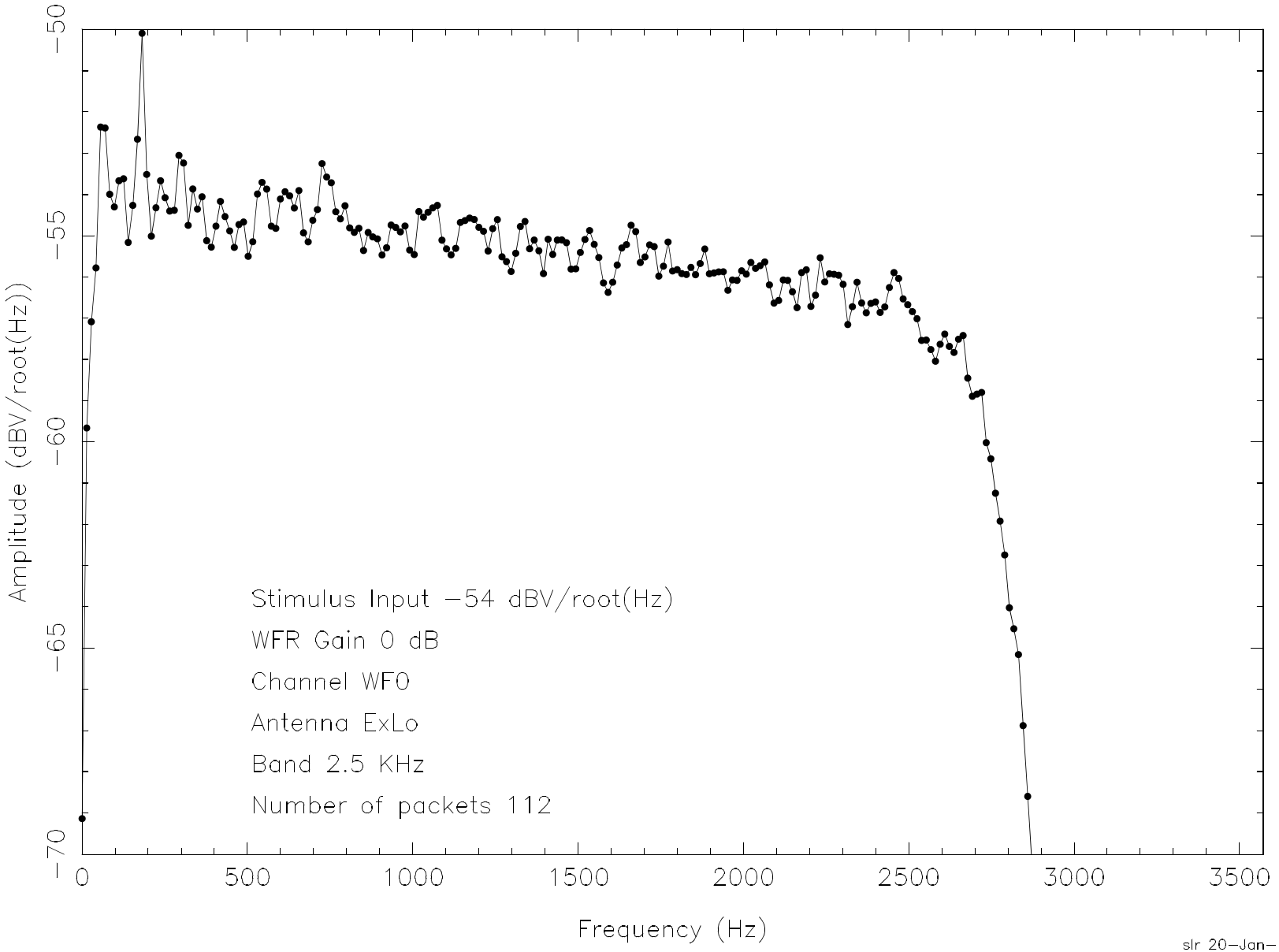

Figure 13.3.3.12 WFR Random Noise Response

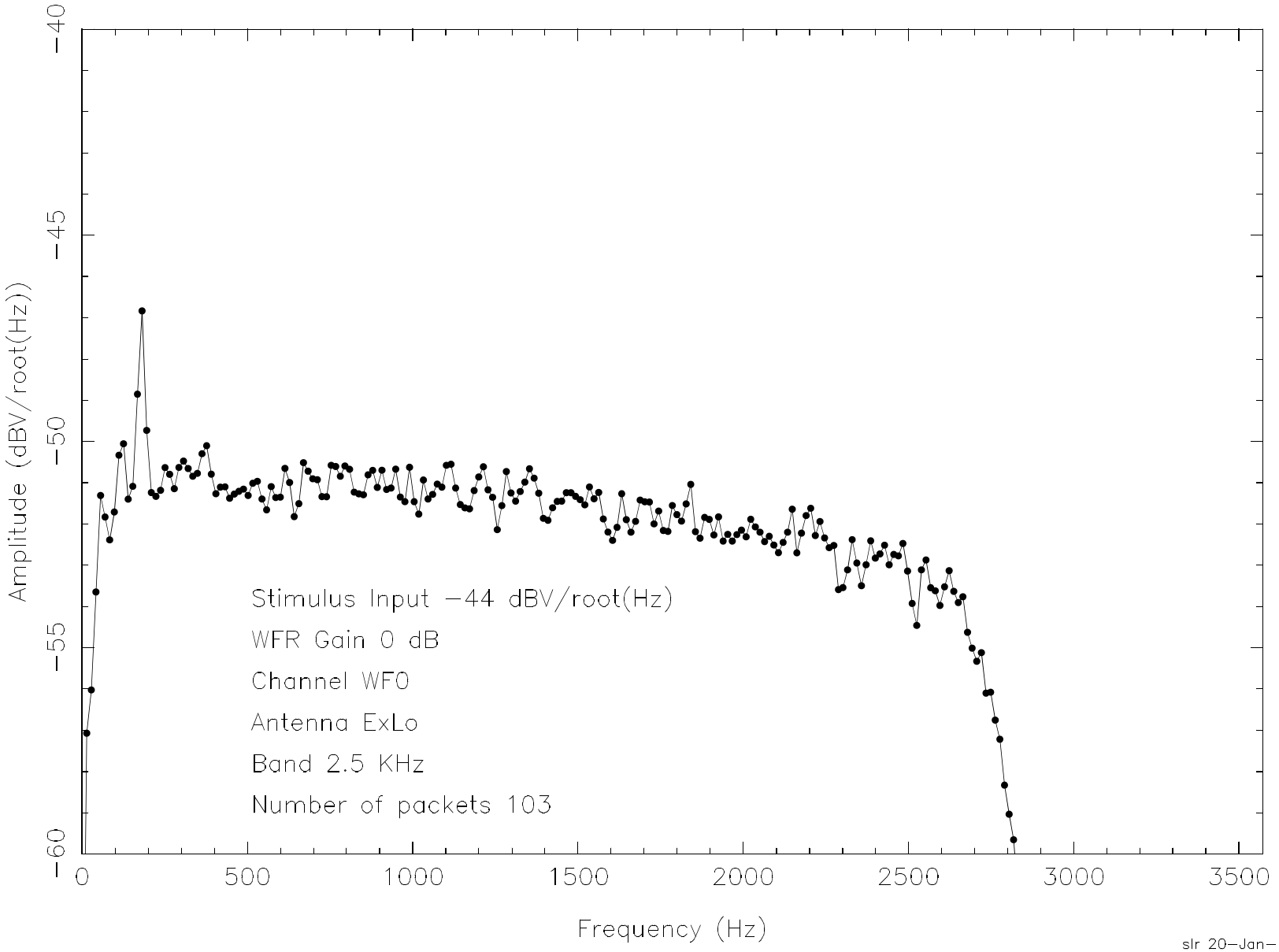

13.3.4 WFR Noise Levels

In this section, the in-flight receiver noise floors are detailed for the commonly used modes. The figure numbers of the in-flight noise floors for these modes are shown in Table 13.3.4.1.

Table 13.3.4.1 List of Figures Showing In-Flight Noise Floors

Figure	Sensor	Band	Gain	Comment
13.3.4.1	Ex	2.5kHz	30dB	Antenna Retracted
13.3.4.2	Ex	2.5kHz	30dB	Antenna Extended
13.3.4.3	Ez	2.5kHz	30dB	Antenna Retracted
13.3.4.4	Ez	2.5kHz	30dB	Antenna Extended
13.3.4.5	Bx	2.5kHz	30dB	
13.3.4.6	By	2.5kHz	30dB	
13.3.4.7	Bz	2.5kHz	30dB	
13.3.4.8	Ex	40Hz	30dB	Antenna Extended
13.3.4.9	Ez	40Hz	30dB	Antenna Extended
13.3.4.10	Bx	40Hz	30dB	
13.3.4.11	By	40Hz	30dB	
13.3.4.12	Bz	40Hz	30dB	

Figure 13.3.4.1 WFR Ex In Flight Noise Levels (Antennas Retracted)

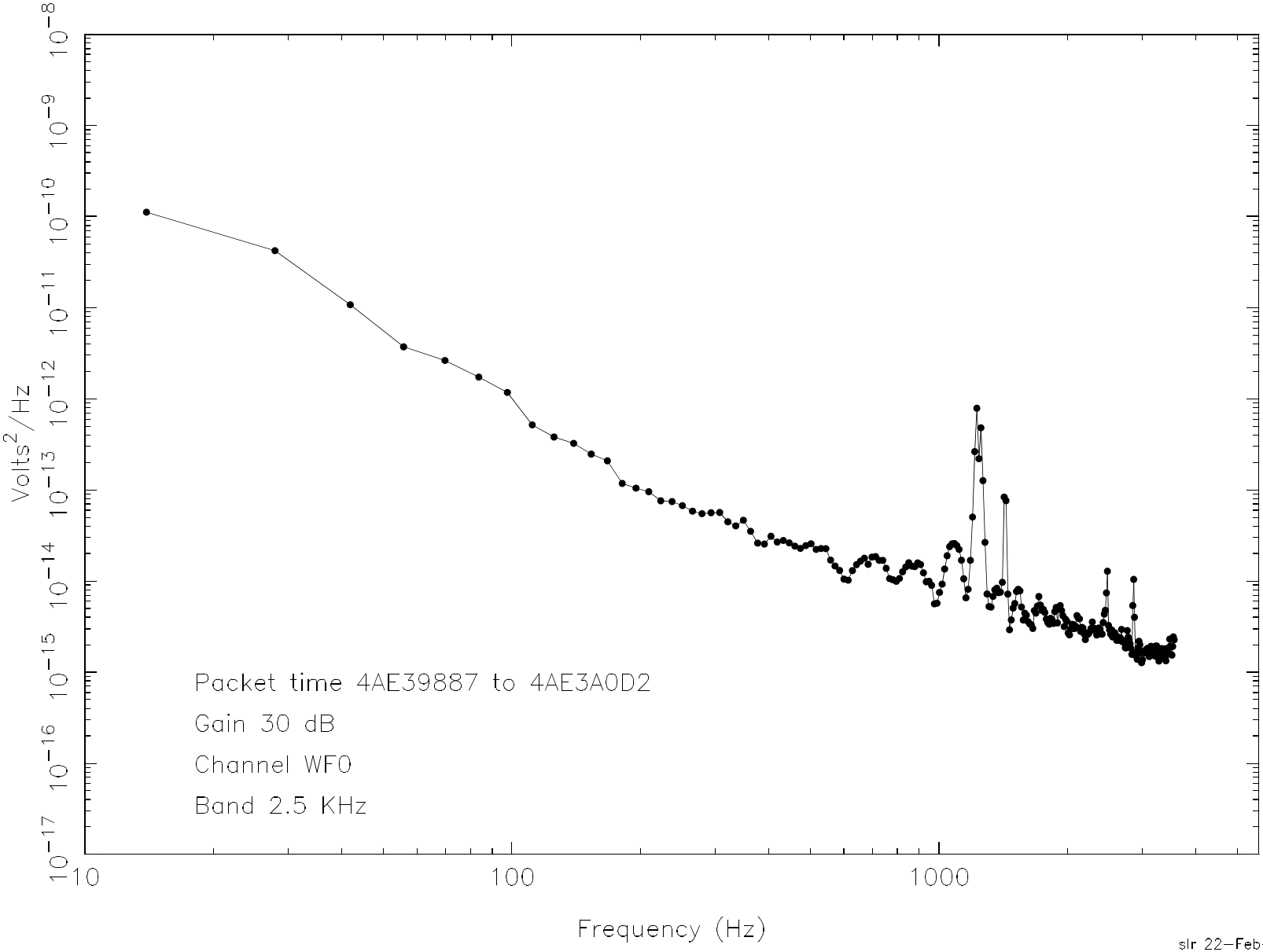

Figure 13.3.4.2 WFR Ex In Flight Noise Level (Antennas Extended)

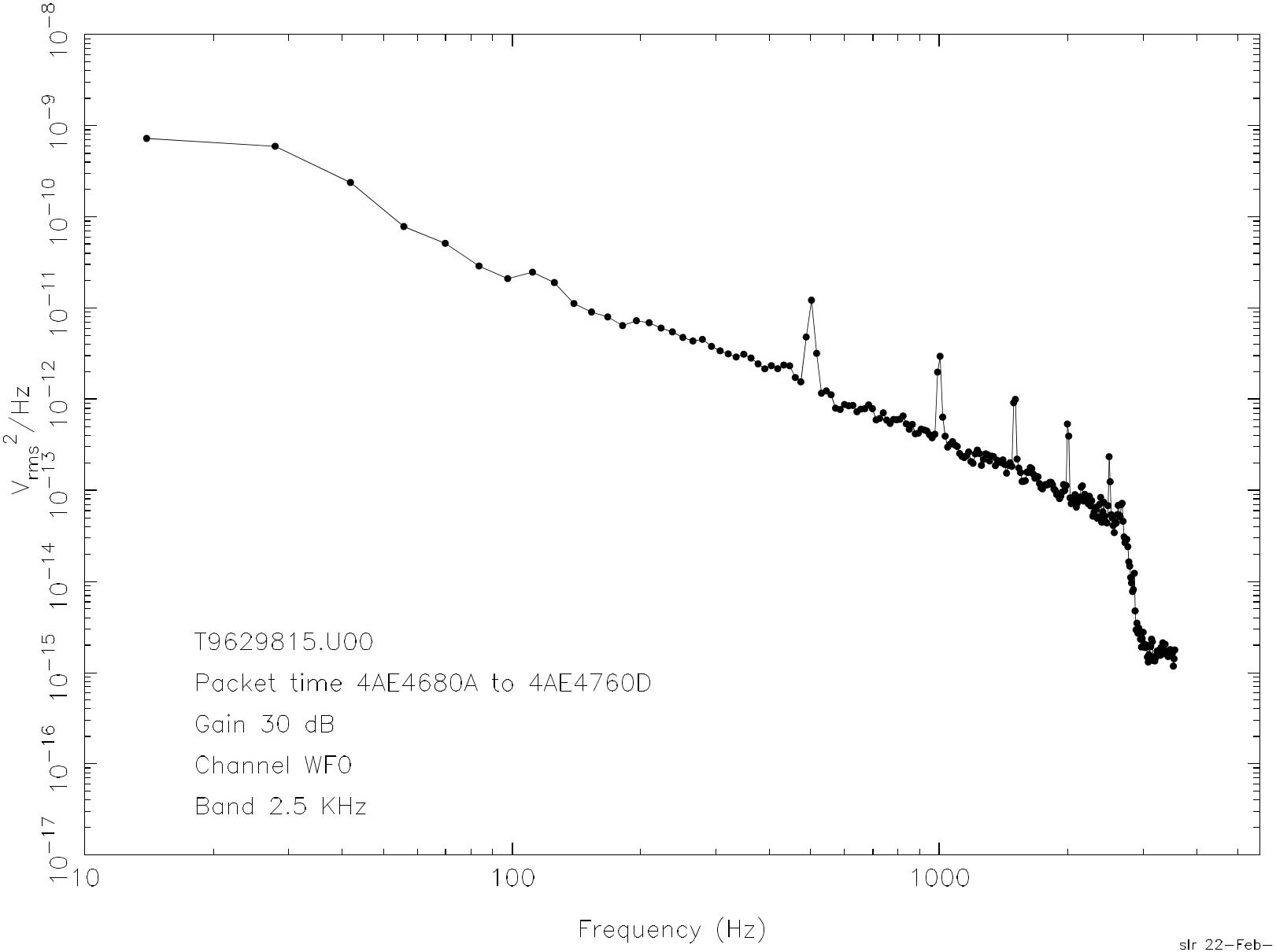

slr 22-Feb-1999 11:24

Figure 13.3.4.3 WFR Ez In Flight Noise Level (Antenna Retracted)

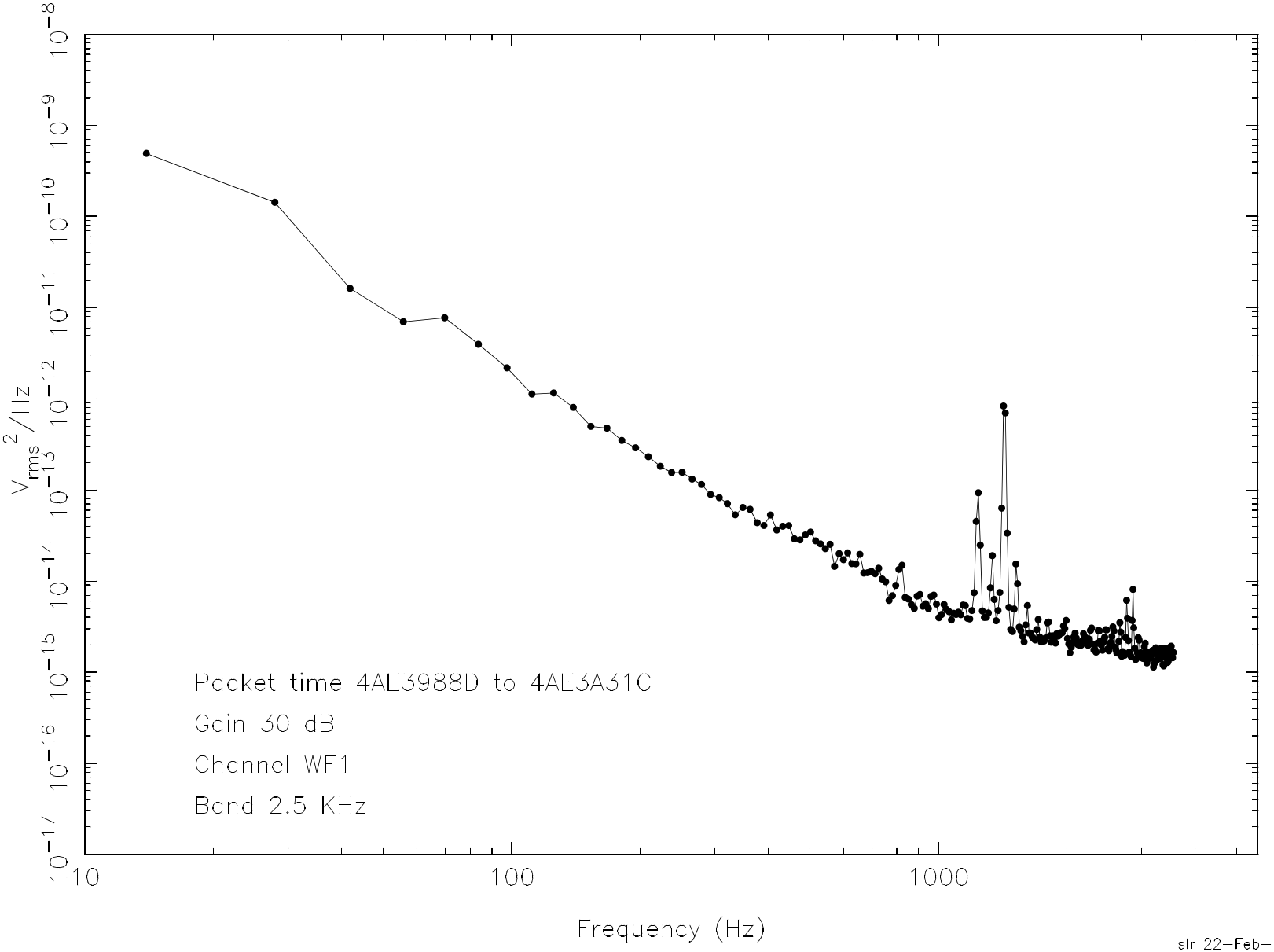

slr 22-Feb-1999 11:32

Figure 13.3.4.4 WFR Ez In Flight Noise Level (Antenna Extended)

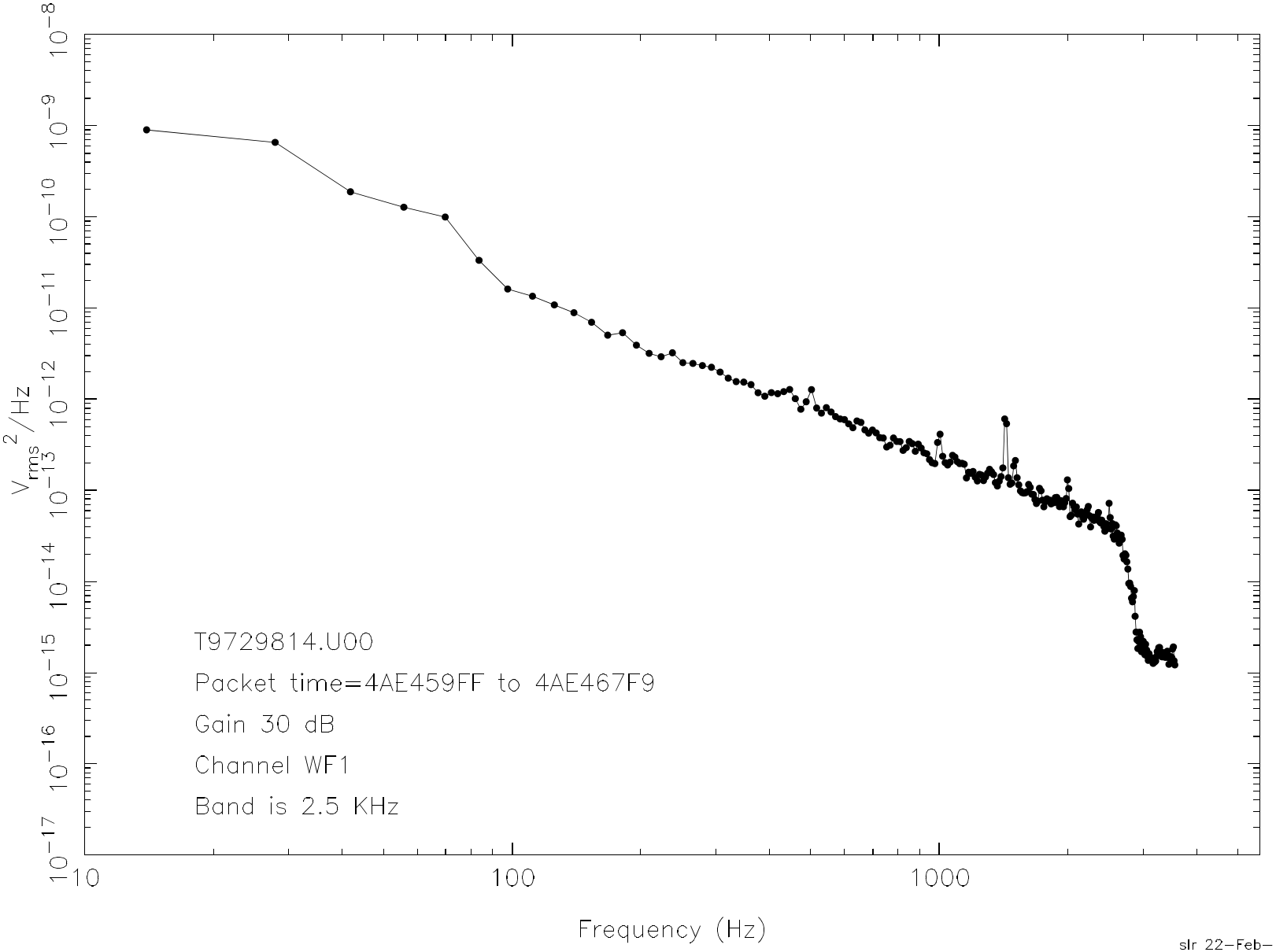

slr 22-Feb-1999 11:34

Figure 13.3.4.5 WFR Bx In Flight Noise Level

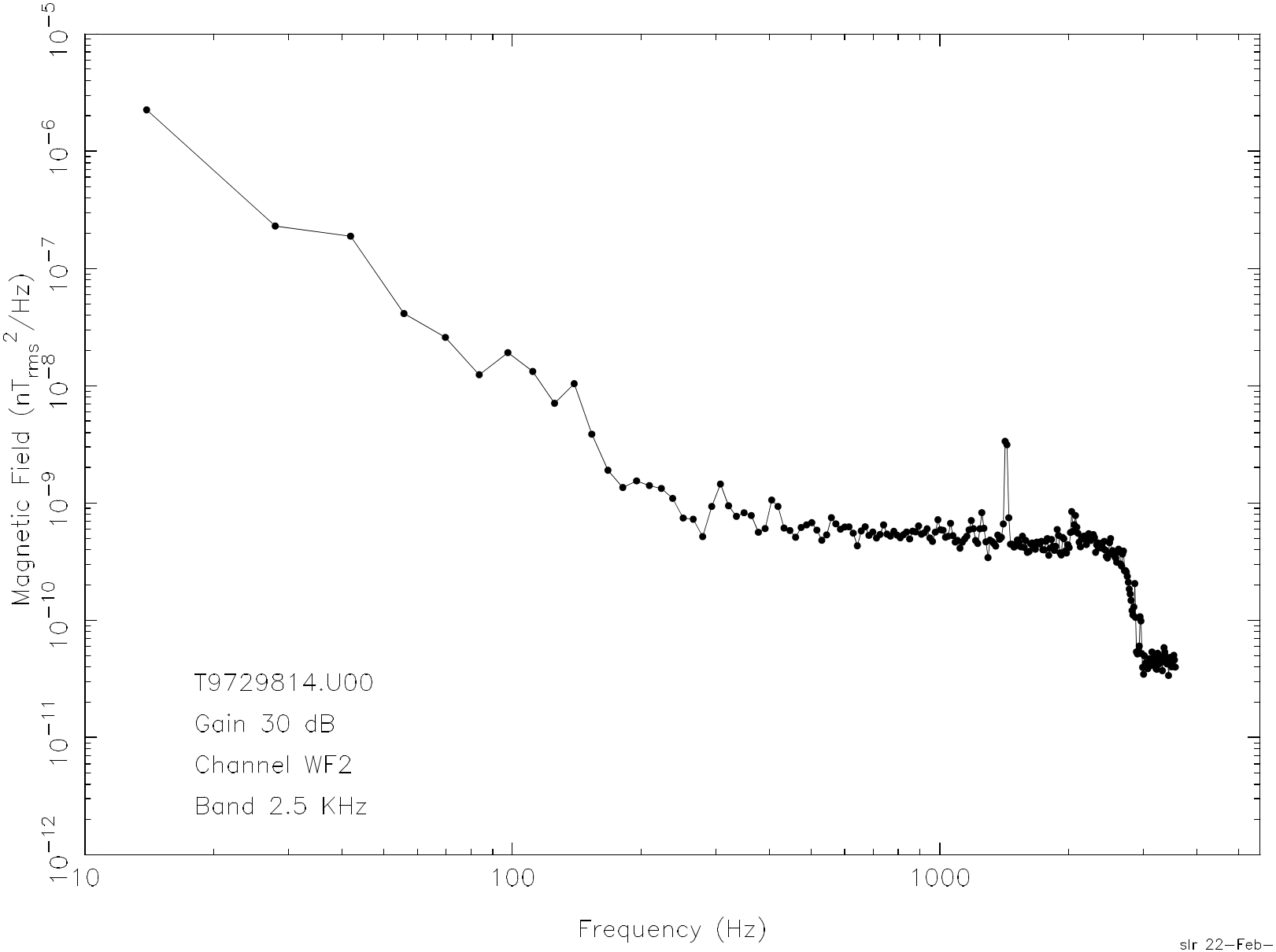

slr 22-Feb-1999 11:45

Figure 13.3.4.6 WFR By In Flight Noise Level

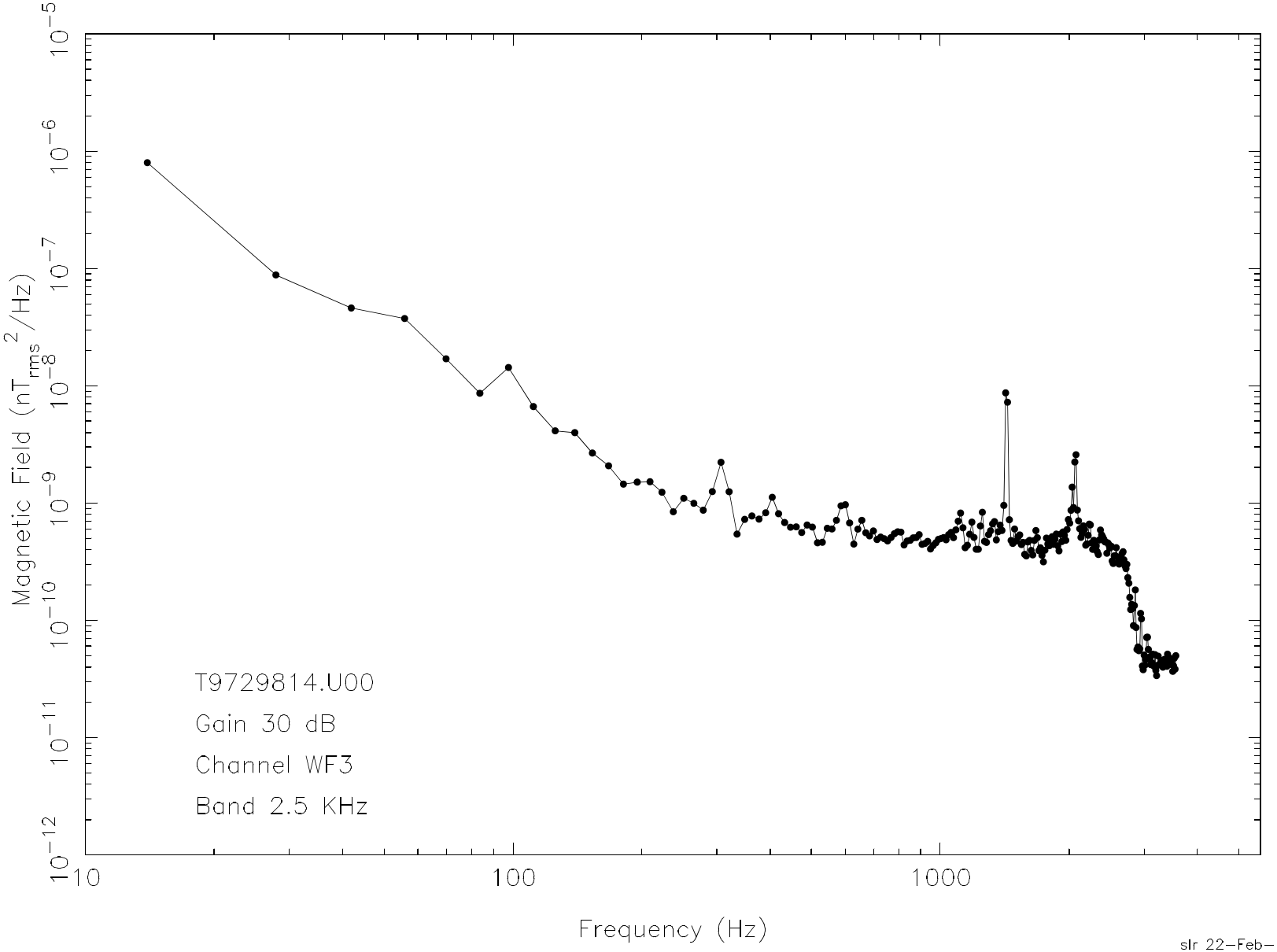

slr 22-Feb-1999 11:49

Figure 13.3.4.7 WFR Bz In Flight Noise Levels

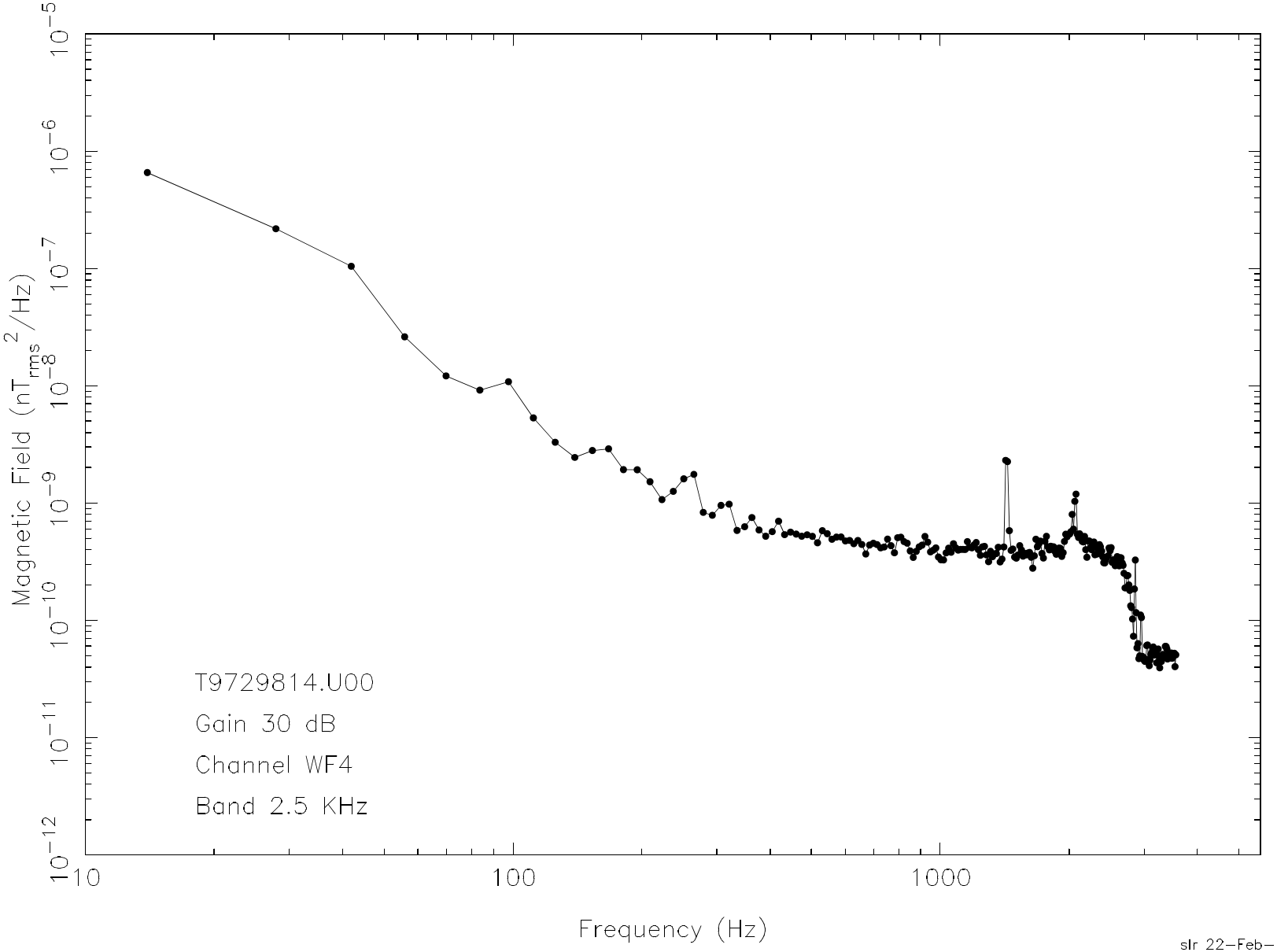

Figure 13.3.4.8 WFR Ex In Flight Noise Level

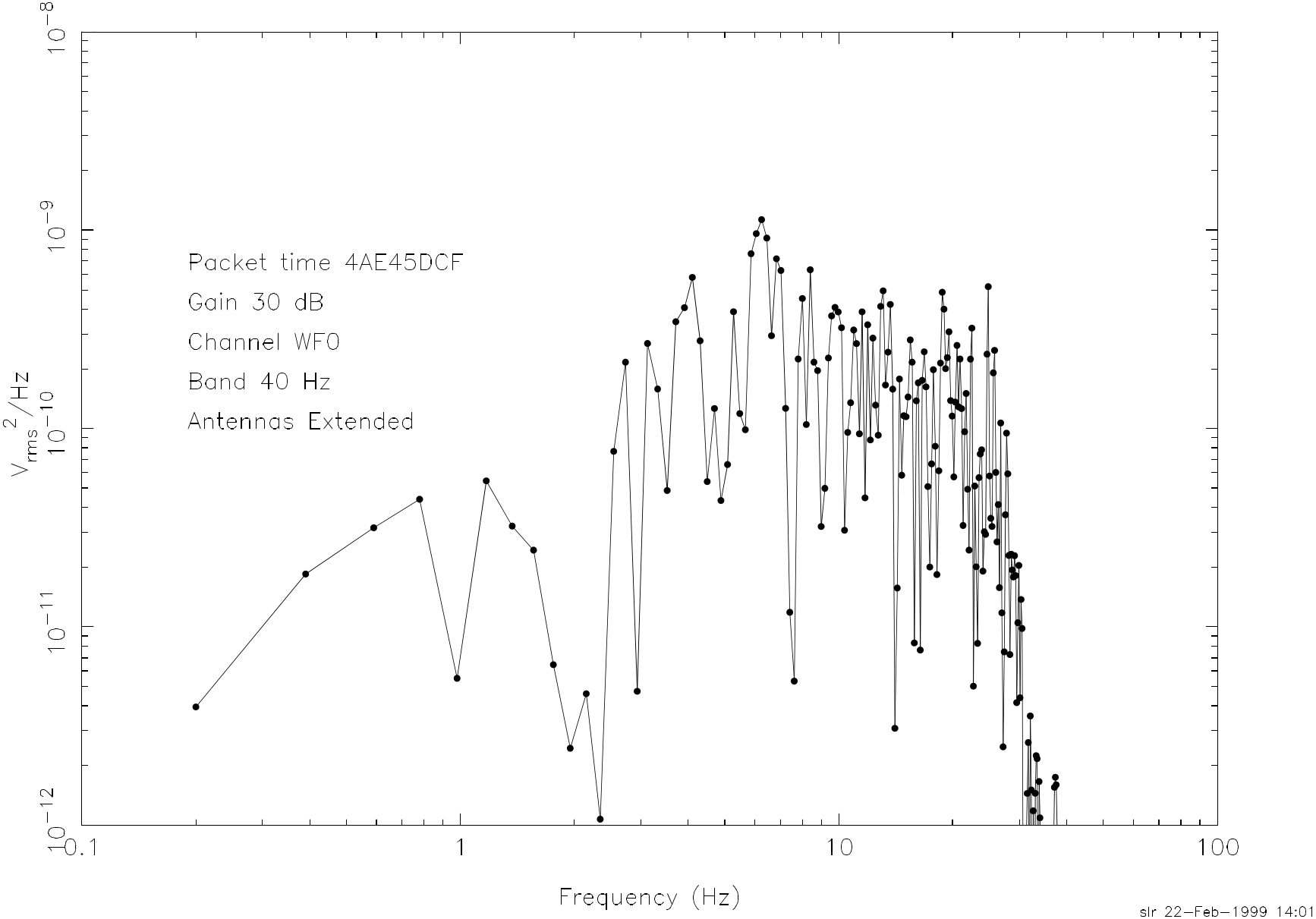

Figure 13.3.4.9 WFR Ez In Flight Noise Level

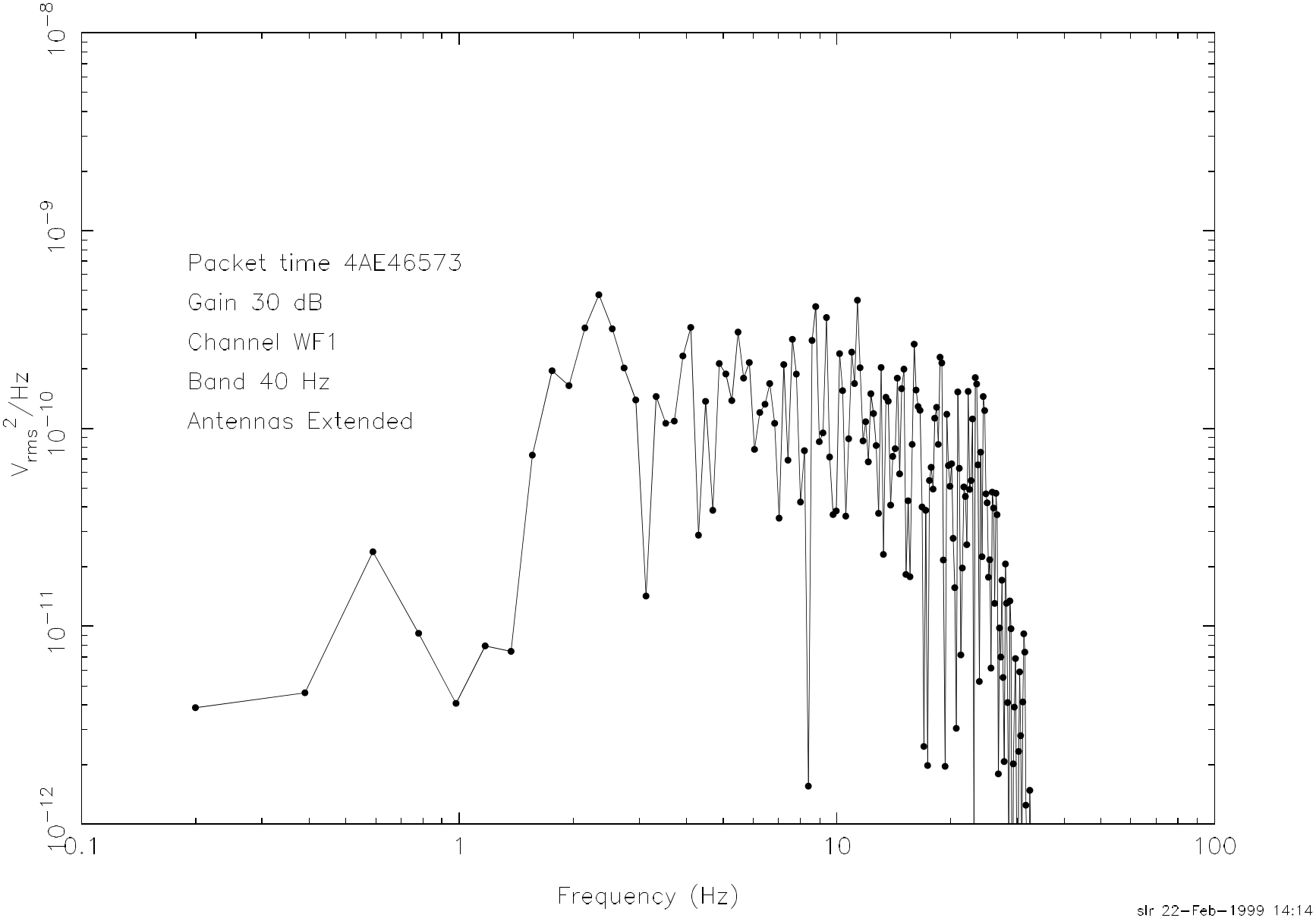

Figure 13.3.4.10 WFR Bx In Flight Noise Level

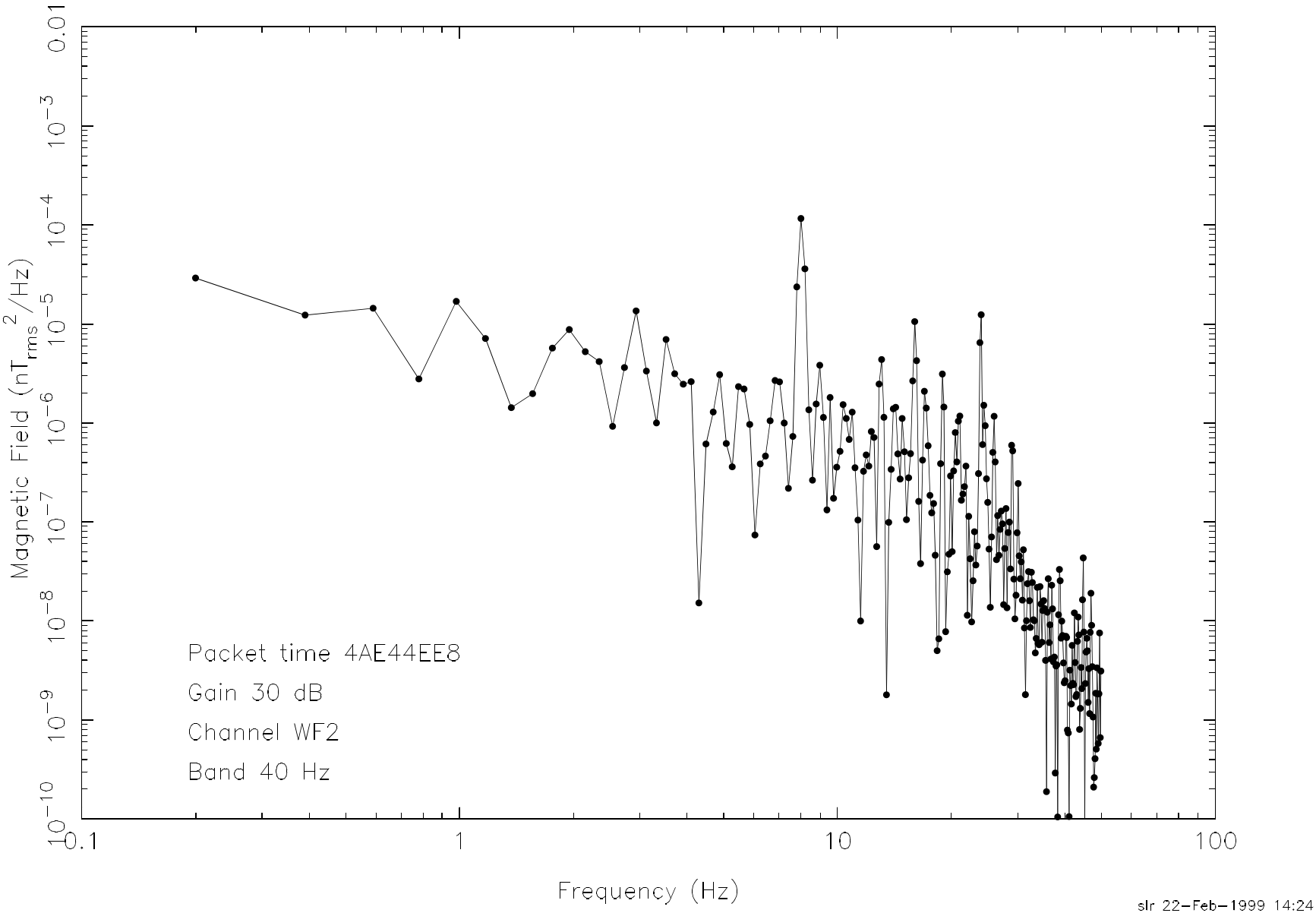

Figure 13.3.4.11 WFR By In Flight Noise Level

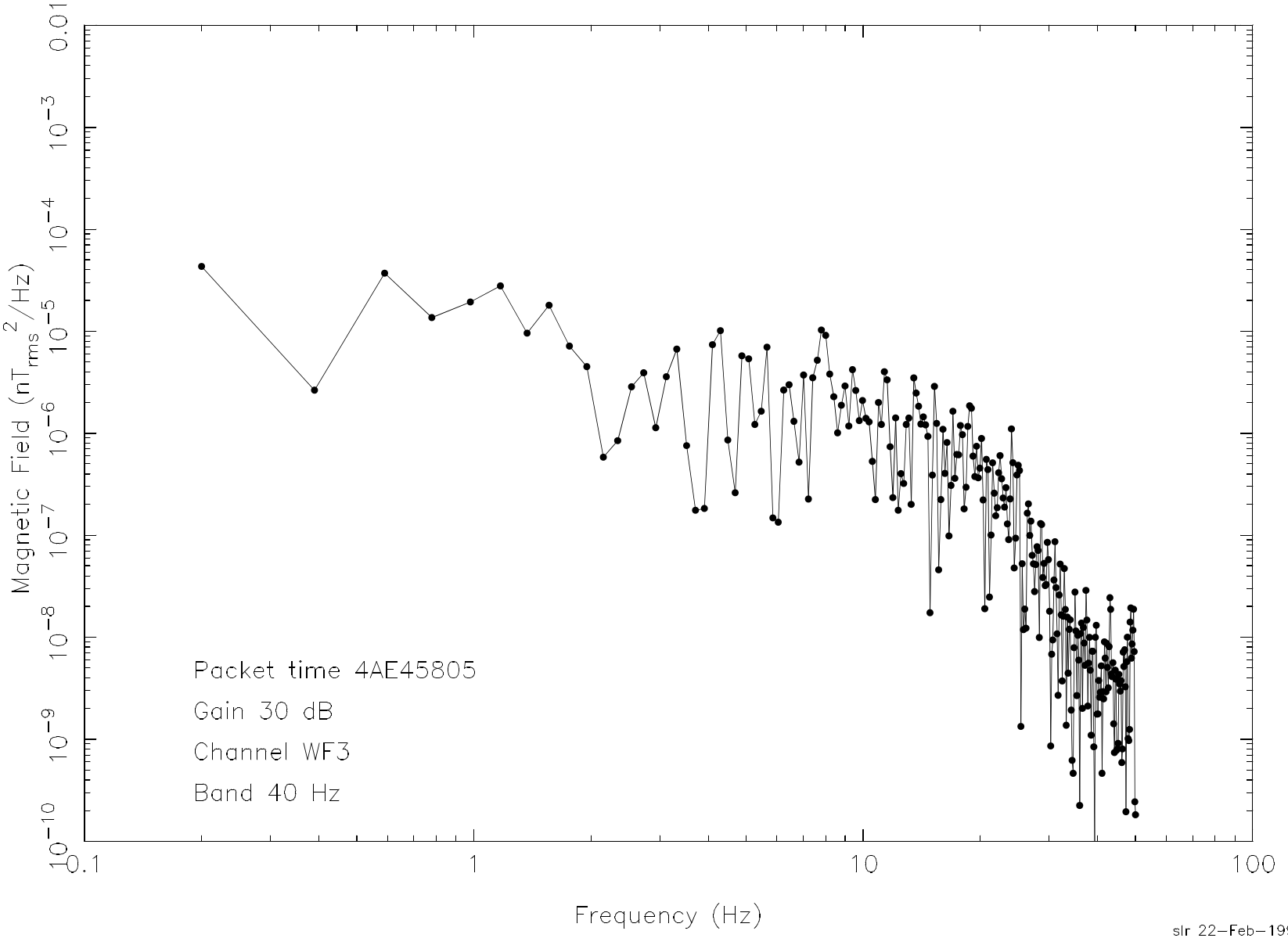

Figure 13.3.4.12 WFR Bz In Flight Noise Level

